DR-166

CONF-751006-P2

FUNDAMENTAL ASPECTS OF RADIATION DAMAGE IN METALS

Proceedings of an International Conference held at Gatlinburg Tennessee, U. S. A., October 6-10, 1975

Volume II

NOTICE

PORTIONS OF THIS REPORT ARE ILLEGIBLE. It has been reproduced from the best available copy to permit the broadest possible availability.

Sponsored by

U. S. ENERGY RESEARCH AND DEVELOPMENT ADMINISTRATION
NATIONAL SCIENCE FOUNDATION
OAK RIDGE NATIONAL LABORATORY

DISTRIBUTION OF THIS DOCUMENT IS UNLIMITED

DISCLAIMER

This report was prepared as an account of work sponsored by an agency of the United States Government. Neither the United States Government nor any agency Thereof, nor any of their employees, makes any warranty, express or implied, or assumes any legal liability or responsibility for the accuracy, completeness, or usefulness of any information, apparatus, product, or process disclosed, or represents that its use would not infringe privately owned rights. Reference herein to any specific commercial product, process, or service by trade name, trademark, manufacturer, or otherwise does not necessarily constitute or imply its endorsement, recommendation, or favoring by the United States Government or any agency thereof. The views and opinions of authors expressed herein do not necessarily state or reflect those of the United States Government or any agency thereof.

DISCLAIMER

Portions of this document may be illegible in electronic image products. Images are produced from the best available original document.

NOTICE

This report was prepared as an account of work sponsored by the United States Government. Neither the United States nor the United States Energy Research and Development Administration, nor any of their employees, nor any of their contractors, subcontractors, or their employees, makes any warranty, express or implied, or assumes any legal liability or responsibility for the accuracy, completeness or usefulness of any information, apparatus, product or process disclosed, or represents that its use would not infringe privately owned rights.

This report has been reproduced directly from the best available copy.

Available from the National Technical Information Service, U. S. Department of Commerce, Springfield, Virginia 22161

Price: Paper Copy $16.25 (domestic)
$18.75 (foreign)
Microfiche $2.25 (domestic)
$3.75 (foreign)

CONF-751006-P2
Distribution Category UC-25

FUNDAMENTAL ASPECTS OF RADIATION DAMAGE IN METALS

PROCEEDINGS OF AN INTERNATIONAL CONFERENCE HELD AT GATLINBURG, TENNESSEE, U.S.A., OCTOBER 6-10, 1975

Mark T. Robinson and F. W. Young, Jr., Editors

VOLUME II

NOTICE
This report was prepared as an account of work sponsored by the United States Government. Neither the United States nor the United States Energy Research and Development Administration, nor any of their employees, nor any of their contractors, subcontractors, or their employees, makes any warranty, express or implied, or assumes any legal liability or responsibility for the accuracy, completeness or usefulness of any information, apparatus, product or process disclosed, or represents that its use would not infringe privately owned rights.

Sponsored by

U. S. ENERGY RESEARCH AND DEVELOPMENT ADMINISTRATION
NATIONAL SCIENCE FOUNDATION
OAK RIDGE NATIONAL LABORATORY

DISTRIBUTION OF THIS DOCUMENT IS UNLIMITED

TABLE OF CONTENTS

VOLUME I

Preface iii

Table of Contents v

The Theory of Radiation Induced Defect Production, *M. T. Robinson* . . 1

Effect of Thermal Vibrations on the Displacement Energy Threshold, *J. R. Beeler, Jr., and M. F. Beeler* 21

Collision Cascades in Iron for Energies up to 5 MeV, *J. R. Beeler, Jr., and M. F. Beeler* 28

Atomic Displacement Distributions for Light Energetic Atoms Incident on Heavy Atom Targets, *D. K. Brice* 35

The Production of Frenkel Defects in Metals, *P. Lucasson* 42

A Study of Low-Temperature Electron-Irradiated Chromium, *M. Biget, P. Vajda, F. Maury, A. Lucasson, and P. Lucasson* 66

Determination of Threshold Displacement Energies by High Voltage Electron Microscopy, *T. E. Mitchell, G. Das, and E. A. Kenik* . . . 73

Defect Production Rate, in Aluminum and Some Dilute Aluminum Alloys, During Neutron Irradiation at 4.6 K, *O. Dimitrov, C. Dimitrov, P. Rosner, and K. Böning* 80

Hall Effect Measurements of Frenkel Defect Clustering in Aluminum During High-Dose Reactor Irradiation at 4.6 K, *K. Böning, W. Mauer, K. Pfändner, and P. Rosner* 88

Depth Distribution of Damage in Copper Irradiated with MeV, Ni and He Ions, *J. Narayan, T. S. Noggle, and O. S. Oen* 90

Transmission Electron Microscopy of Point Defect Clusters in Metals Produced by Energetic Heavy Ions, *M. Wilkens* 98

Displacement Cascades in an Ordered Alloy Cu_3Au as Revealed by Transmission Electron Microscopy, *M. L. Jenkins, K.-H. Katerbau, and M. Wilkens* 113

Ni Ion Damage in Cu and Nb, *J. B. Roberto and J. Narayan* 120

Energetic Displacement Cascades at Elevated Temperature, *K. L. Merkle and R. S. Averback* 127

Study of Clusters in Ion Irradiated Gold, *M. O. Ruault, B. Jouffrey, J. Chaumont, and H. Bernas* 134

The Study of Defect Saturation in Copper with Fission Fragments, *R. C. Birtcher, T. H. Blewitt, B. S. Brown, and T. L. Scott* . . . 138

Defect Distributions in Self-Ion Irradiated Gold by the Channeling Technique, *P. P. Pronko* 145

Replacement Collision Sequences in Metals, *T. H. Blewitt, M. A. Kirk, and T. L. Scott* 152

Fission Neutron Sputtering of Gold, *M. A. Kirk and R. A. Conner, Jr.* 171

Stacking Fault Tetrahedra in Au Created as a Consequence of Dynamic Vacancy Injection During Sub-Threshold Irradiation in the HVM, *D. Cherns, F. J. Minter, and R. S. Nelson* 178

Self-Interstitials in Metals, *P. H. Dederichs* 187

Core-Overlap Interactions in Metals, *R. Benedek* 207

Dynamics of the [100] Dumbbell Interstitial in Copper, *R. M. Nicklow, R. R. Coltman, Jr., F. W. Young, Jr., and R. F. Wood* 214

Change of Phonon Dispersion by Interstitials in fcc-Metals, *H. R. Schober, P. H. Dederichs, and V. K. Tewary* 220

Theory of the Change of Elastic Constants by Interstitials, *N. Breuer, P. H. Dederichs, C. Lehmann, G. Leibfried, and A. Scholz* 227

Irradiation Induced Diaelastic Modulus Change in Al and Cu, *L. E. Rehn, K.-H. Robrock, and V. Spirić* 234

Elastic After Effect Measurements of Point Defect Relaxations in Electron Irradiated Aluminum, *V. Spirić, K.-H. Robrock, and L. E. Rehn* 240

Investigation of Interstitials in Metals by Means of Elastoresistivity, *J. von Stebut and A. Sechard* 247

Theory of Polarization Induced Eleastic Interaction of Point Defects, *H. Trinkaus* 254

Determination of Point Defects Symmetry in A Cubic Lattice by Magnetic Relaxation, *W. Chambron, J. Verdone, and P. Moser* 261

Study of Irradiation Induced Point Defects by Diffuse Scattering, *H.-G. Haubold* 268

Diffuse X-Ray Scattering from Copper After Neutron Irradiation at 4.6 K, *B. von Guérard and J. Peisl* 287

X-Ray Investigation of Interstitials and Interstitial Clusters after Low Temperature Electron Irradiation and Thermal Annealing of Gold, *P. Ehrhart and E. Segura* 295

Interstitials and Interstitial Clusters in BCC and HCP Metals Investigated by Huang Diffuse Scattering, *P. Ehrhart* 302

Annealing Behaviour of Copper after Low Temperature Neutron Irradiation, *B. von Guérard and J. Peisl* 309

The Use of the Backscattering-Channeling Method to Investigate Interactions between Solute Atoms and Irradiation-Induced Defects in Metals, *M. L. Swanson, L. M. Howe, and A. F. Quenneville* 316

Model for the Dose Dependence of the Substitutional Fraction of Heavy Ions Implanted in Ferromagnetics, *J. Odeurs, R. Coussement, and H. Pattyn* 325

Self-Interstitials in Nickel, *W. Schüle, E. Lessmann, and R. Scholz* . 333

Vacancies and Self-Interstitials in Copper-Gold Alloys, *G. Oleownik and W. Schüle* 341

Mössbauer Studies of Interstitials in F.C.C. Metals, *G. Vogl and W. Mansel* 349

Experimental Studies on Self-Interstitials in BCC Metals, *S. Okuda.* . 361

The Study of Stages I to IV of Irradiated or Quenched Tungsten and Tungsten Alloys by Field-Ion Microscopy, *D. N. Seidman, K. L. Wilson, and C. H. Nielsen* 373

Interstitials in Pure Metals, *J. S. Koehler* 397

Very Low Temperature Electron Irradiation and Annealing of Gold and Lead, *R. C. Birtcher, W. Hertz, G. Fritsch, and J. E. Watson* . . . 405

Recovery of Pure Lead after Electron Irradiation at 4.7 K and below 3 K, *H. Schroeder, R. Lennartz, and U. Dedek* 411

Annealing Experiments on Platinum Single Crystals, *P. Jung and T. Schober* 418

Recombination and Transformation of Frenkel Defects in Platinum by Subthreshold Irradiation, *P. Jung* 424

Low Temperature Recovery of Radiation Damage in Vanadium, *C. E. Klabunde, R. R. Coltman, Jr., and J. M. Williams* 431

The Low-Temperature Recovery of Electron-Irradiated Tungsten, *F. Dausinger and H. Schultz* 438

Recovery in Stages I and II of Thermal and Fission Neutron Irradiated Molybdenum, *R. R. Coltman, Jr., C. E. Klabunde, and J. K. Redman* . 445

The Effect of Pre-Irradiation Treatment on Stage I Energy Release in Platinum, *J. J. Jackson* 452

The Resistivity Recovery of Niobium and Tantalum Following 3 MeV-Electron Irradiation at 4.5 K, *K. H. Faber, J. Schweikhardt, and H. Schultz* 459

Defects in High Purity Iron after 27 K-Electron Irradiation, *H. E. Schaefer, D. Butteweg, and W. Dander* 463

Interpretation of Defect Reactions in Irradiated Metals by the One Interstitial Model, *W. Schilling, P. Ehrhart, and K. Sonnenberg*. . 470

The Interpretation of Radiation Damage in Metals, *A. Seeger* 493

Kinetic Spectrometry in Copper and Copper Alloys, *A. Sosin* 518

Effective Diffusion Constant in Crystals with Traps, *K. Schroeder* . . 525

Computer Simulation of Interstitial Diffusion in Tungsten, *M. W. Guinan, R. N. Stuart, and R. J. Borg* 532

Kinetics of Bimolecular Diffusion Limited Reactions for Different Dimensionalities of Diffusion, with Application to Recovery of Irradiated Cadmium and Crowdion-Crowdion Interactions, *U. Gösele and A. Seeger* 539

Isothermal and Isochronal Recovery between 40 K and 80 K in Cu and CuAu after Thermal Neutron Irradiation, *J. Aspeling, K. Isebeck, and C.S.B. Piani* 545

Interpretation of the Experiments by Isebeck, Aspeling and Piani (IAP), *A. Seeger, W. Frank, and J. Aspeling* 553

The Influence of Divacancies on the Stage III Recovery in Cu, *G. Antesberger, K. Sonnenberg, P. Wienhold, R. R. Coltman, Jr., C. E. Klabunde, J. M. Williams, and R. L. Chaplin* 561

Effect of Hydrostatic Pressure on Stage III Recovery in Irradiated and Cold Worked Molybdenum, *H. E. Kissinger, J. L. Brimhall, and E. P. Simonen* 568

Determination of Single Interstitial and Single Vacancy Migration Temperature by Electron Damage Rate Experiments at Different Temperatures in Cu, Ag, Au, Mo, Re, *G. Antesberger, H. Schroeder, K. Sonnenberg, and U. Dedek* 575

Defect Interactions above Stage I, *H. Wollenberger* 582

Interstitial Trapping and Detrapping in Electron Irradiated Dilute Aluminum Alloys, *F. Dworschak, R. Lennartz, Th. Monsau, and H. Wollenberger* 601

Influence of the Nature of the Addition Element on the Recovery of Dilute Binary Aluminum Alloys, Neutron-Irradiated at Low Temperature, *C. Dimitrov* 608

Damage Production in Plastically Deformed Copper by Electron Irradiation above Stage I, *F. Dworschak, H. P. Meurer, and H. Wollenberger* 615

Effect of Impurities on Recovery Stages in Electron-Irradiated Gold, *K. Nakata, K. Ikeuchi, H. Hirano, K. Furukawa, and J. Takamura* . . 622

Dose Dependence and Annealing of Electrical Resistivity and Internal Friction of Nitrogen Doped Iron after Neutron Irradiation at 400 K, *U. Merbold, M. Weller, and J. Diehl* 629

A Study of Low Temperature Fission Neutron Damage in B_2 Type Fe-Al Ordered Alloys, *J. P. Rivière and J. Grilhé* 636

Cyclotron Irradiation of Cu_3Au Alloys at Low Temperatures, *H. Sakairi, E. Yagi, A. Koyama, T. Karasawa, and R. R. Hasiguti* 643

The Nature of Defect Clusters in Electron-Irradiated Copper, *S. M. Ohr* 650

VOLUME II

Table of Contents iii

Evidence for Vacancy Migration in Stage III for Copper, *G. Antesberger, K. Sonnenberg, P. Wienhold, R. R. Coltman, Jr., C. E. Klabunde, and J. M. Williams* 657

Interactions Between Radiation Defects and Interstitial Impurities in B.C.C. Metals, *J. Diehl* 663

Studies on Radiation-Induced Point Defects in Metals by Means of High-Voltage Electron Microscopy, *K. Urban* 675

Electron Radiation Damage of Metals and Nature of Point Defects by High Voltage Electron Microscopy, *M. Kiritani* 695

In-Situ Electron Irradiation of Aluminum in a 200 kv Electron Microscope, *H. Fischer, C. Gomez, M. Rühle, and J. Diehl* 715

Oriented Stacking Fault Tetrahedra in Electron Irradiated Gold, *M. O. Ruault, A. Rocher, L. Kubin, and B. Jouffrey* 722

Irradiation Damage Structures Generated in Metals and Alloys During Irradiation at Elevated Temperatures, *B. L. Eyre* 729

Theory of the Nucleation Growth and Annealing of Interstitial Dislocation Loops, *M. R. Hayns* 764

The Nucleation of Point Defect Agglomerates, *L. M. Brown and R. M. Mayer* 775

Irradiation Growth in Zirconium and Its Alloys, *G.J.C. Carpenter and D. O. Northwood* 782

An Experimental Study of Dislocation Loop Nucleation, *J. Y. Bounaud and J. Leteurtre* 790

Effect of Alloying Elements and Irradiation Temperature on Dislocation Loops of Electron Bombarded Niobium, *N. Igata, F. Watari, and H. Murakami* 797

Defect Annealing and Clustering in the Elastic Interaction Force Field, *M. H. Yoo, W. H. Butler, and L. K. Mansur* 804

Segregation of Point Defects by Internal Stress Fields, *W. G. Wolfer* 812

X-Ray Studies of Irradiation Induced Dislocation Loops in Metals, *B. C. Larson* 820

Investigation of Interstitial Clusters in Copper by Measurements of the Huang Diffuse Scattering, *P. Ehrhart and U. Schlagheck* 839

Measurements of Conduction Electron Scattering in Neutron-Irradiated Copper by the De Haas-Van Alphen Effect, *Y. K. Chang, A. J. Arko, G. W. Crabtree, J. B. Ketterson, L. R. Windmiller, R. J. Higgins, and F. W. Young, Jr.* 846

Voids, Dislocation Loops and Grain Boundaries as Sinks for Point Defects, *R. W. Balluffi* 852

Point Defect Annealing Near Voids, *R. A. Johnson and J. H. Fikus* . . 875

Interactions Between Dislocations and Point Defects, *N. Sumida, H. Fujita, K. Takemoto, and A. Sawada* 882

Long-Range Interaction Between Radiation-Induced Point Defects and Dislocations, *M. Kiritani, H. Takata, N. Yoshida, and Y. Maehara* . 889

Some Considerations in the Splitting of Interstitial Frank Loops Formed by Irradiation, *K. Seshan, J. Grilhé, and J. Washburn* . . . 896

Climb of Prismatic Loops in Cu-Al Alloys During Irradiation in the HVEM, *T. Kosel and J. Washburn* 903

The Behaviour of Collision Cascades at Elevated Temperatures in Copper and Molybdenum Crystals, *C. A. English, B. L. Eyre, J. Summers, and H. Wadley* 910

The Effect of Solute Atoms on Collision Cascades in Copper and Molybdenum Irradiated with Self-Ions, *C. A. English, B. L. Eyre, H. Wadley, and A. Y. Stathopoulos* 918

High Temperature Neutron Irradiation Damage in Molybdenum, *J. Bentley, B. L. Eyre, and M. H. Loretto* 925

Dislocation-Defect Interactions and Mechanical Properties of Crystals, *A. V. Granato* 932

Effect of Irradiation Point Defects on the Internal Friction Peaks of Cold Worked Copper, *P. Moser, C. Minier, and J. Lauzier* 957

Point Defect Dislocation Pinning in Irradiated Copper, *C. Minier, J. Lauzier, and S. L. Seiffert* 963

Stage III Dislocation Pinning in Silver Resulting from Gamma Irradiation, *R. A. Van Konynenburg and M. W. Guinan* 970

Effects of Low Temperature Neutron Irradiation on the Mechanical Properties of Iron Single Crystals, *K. Kitajima, H. Abe, S. Takamura, and S. Okuda* 977

Mechanical Effects of Electron Irradiation in Iron Single Crystals, *M. Meshii and A. Sato* 984

Radiation Embrittlement of Metals and Alloys, *M. S. Wechsler* 991

The Influence of Oxygen Impurity Atoms on Defect Clusters and Radiation Hardening in Neutron-Irradiated Vanadium, *R. Bajaj and M. S. Wechsler* 1010

Deformation Characteristics of High Purity Neutron Irradiated Vanadium, *J. Bressers and R. J. Arsenault* 1018

Theory of Diffusion and Trapping of Hydrogen and Helium in Metals: A Review, *W. D. Wilson* 1025

Radiation Enhanced Diffusion and the Effectiveness of 14-MeV Neutrons, *G. J. Dienes* 1045

Radiation Annealing in Ag and Au Due to Energetic Displacement Cascades, *R. S. Averback and K. L. Merkle* 1048

Enhanced Atomic Mobility Due to Low Dose Neutron Irradiation as Measured in a Ag-30 At.% Zn Alloy by Zener Relaxation Methods, *M. Halbwachs, J. Hillairet, H. Gonzalez, and J. Cost* 1055

13

Enhanced Diffusion of Zn in Al Under Ne Irradiation, *S. M. Myers* . . 1063

Kinetics of Interstitialcy Diffusion in Electron Irradiated Cu-Ni Alloys, *R. Poerschke and H. Wollenberger* 1070

Self-Diffusion in Silver Under Electron Irradiation, *S. J. Rothman, N. Q. Lam, L. J. Nowicki, and C. A. Beck* 1077

Phase Instability in Crystals Under Irradiation, *G. Martin* 1084

Effects of Heavy-Ion Irradiation on the Morphology of γ/γ' Alloys, *D. I. Potter and H. A. Hoff* 1092

Effect of Electron Irradiation on Precipitation of Carbon & Nitrogen in Alpha Iron, *T. Takeyama and H. Takahashi* 1100

Positron Annihilation in Perfect and Imperfect Metals: A Brief Review, *A. N. Goland* 1107

Direct Evidence for Vacancy Clustering in Electron Irradiated Copper by Positron Annihilation, *S. Mantl and W. Triftshäuser* 1122

Vacancy Migration and Void Formation During the Annealing of Electron Irradiated Molybdenum, *M. Eldrup, O. E. Mogensen, and J. H. Evans* 1127

Investigations of Neutron Irradiated Iron by Positron Annihilation and Internal Friction Measurements, *M. Weller, W. Triftshäuser, and J. Diehl* 1136

Annealing of Dislocation Loops in Neutron-Irradiated Copper Investigated by Positron Annihilation, *W. B. Gauster, S. Mantl, T. Schober, and W. Triftshäuser* 1143

Critical Current Changes in Nb_3Sn Irradiated with Fast Neutrons at 6 K, *B. S. Brown, R. C. Birtcher, T. H. Blewitt, and D. G. Wozniak* 1150

Neutron Irradiation Damage on the Superconducting Properties in Vanadium and Nb-Ti Alloys, *H. Tsubakihara, S. Katoh, M. Nishimoto, and T. Okada* 1155

The Effects of Reactor Neutron, 14-MeV Neutron and Energetic-Charged-Particle Irradiations on the Critical Current in Nb_3Sn, *D. M. Parkin and C. L. Snead, Jr.* 1162

Studies of Void Formation in Pure Metals, *J. M. Lanore, L. Glowinski, A. Risbet, P. Regnier, J. L. Flament, V. Levy, and Y. Adda* . . . 1169

Evaluation of Time-Dependent Void Nucleation Theory Under Ion Bombardment Conditions, *J. A. Sprague, K. C. Russell, and Y. H. Choi* 1181

Effect of Be Doping on Void Swelling in Nickel, *P. R. Okamoto, A. Taylor, and H. Wiedersich* 1188

The Dependence of Swelling on Void Surface Reaction Rate Constants, *E. P. Simonen and J. L. Brimhall* 1196

The Effect of Solute Content and Precipitate Distribution on Fast Neutron Damage in Aluminum-Copper Alloys, *R. W. Carpenter and J. C. Ogle* 1203

Suppression of Void Formation in Nickel by a Dynamic Trapping Mechanism, *S. M. Sorensen, Jr., and C. W. Chen* 1213

The Origin and Stability of Defect Structures: The Void Lattice and Similar Phenomena, *A. M. Stoneham* 1221

Stability of Void Lattices Under Irradiation: A Kinetic Model, *P. Benoist and G. Martin* 1236

Void Ordering in O-Doped Nb and Nb-1 At. % Zr Induced by $^{58}Ni^{+}$ Bombardment, *B. A. Loomis, A. Taylor, and S. B. Gerber* 1245

Elastic Interactions Between "Voids" Induced by Solute Segregation, *F. V. Nolfi, Jr.* 1252

Irradiation Creep and Effects of Stress on Swelling, *R. Bullough* . . 1261

The Growth of Grain Boundary Cavities Under Applied Stress and Irradiation, *J. F. Mancuso, F. H. Huang, and C. Y. Li* 1279

Radiation Damage Simulation Experiments in Zirconium, *D. Faulkner and M. P. Puls* 1287

Author Index 1296

EVIDENCE FOR VACANCY MIGRATION IN STAGE III FOR COPPER

G. Antesberger[+], K. Sonnenberg[+], P. Wienhold[+]
R.R. Coltman[++], C.E. Klabunde[++], J.M. Williams[++]
[+]Institut für Festkörperforschung der Kernforschungsanlage Jülich
D 517 Jülich, Germany
[++]Oak Ridge National Laboratory, Oak Ridge, Tennessee

ABSTRACT

Specimens doped with interstitial clusters and single vacancies have been annealed isochronally through the temperature range of stage III. Combining this annealing with a test irradiation after each annealing step we have studied reactions of mobile single test interstitials with the doping defects. These reactions provide information about the variation of the doping defect structure during annealing. The experimental results suggests that vacancy clusters are formed in stage III.

In the last two years many experimental results have been obtained which strongly suggest that vacancies become mobile already in stage III. In some cases these results are based on the observation that vacancy clusters are formed in stage III. The purpose of the present work was to study such clustering reactions in stage III by employing recovery and damage production measurements.

High purity Cu specimens (RRR = 10^4) have been doped by an e^- irradiation at 4 K to different doses followed by an annealing treatment, at $T_d^{(A)}$=100 K and $T_d^{(B)}$=400 K, respectively (Fig. 1). Fig. 2 schematically shows the doping structure present after the 100 K anneal. This structure is characterized by interstitial clusters[1] and single vacancies, since there is general agreement that vacancies are immobile below stage III. After an annealing treatment at 400 K the doping defects consist of interstitial and vacancy clusters (Fig. 3)[2]. Again there is agreement that single vacancies cannot survive an annealing temperature $T_d^{(B)}$= 400 K. The 2-interstitial model, e.g., assumes that vacancy migration occurs around 350 K ("stage IV") in Cu, while in the 1-interstitial model the vacancies become mobile already in stage III.

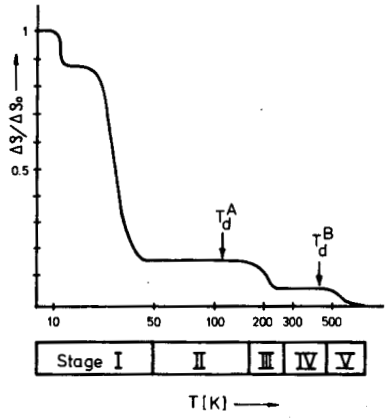


Fig. 1. Schematical recovery curve of Copper after irradiation

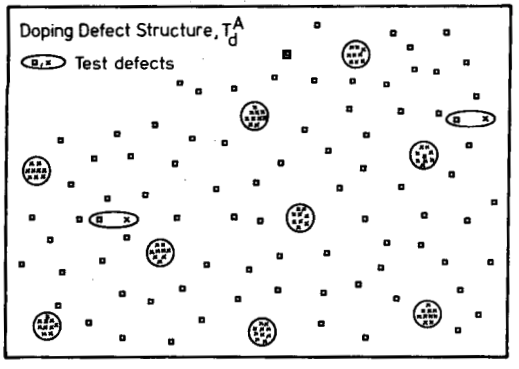


Fig. 2. Schematical doping defect structure after an e^- irradiation at 4 K plus an annealing treatment at $T_d \approx 100$ K. The test defects are generated by a subsequent test irradiation at 4 K.

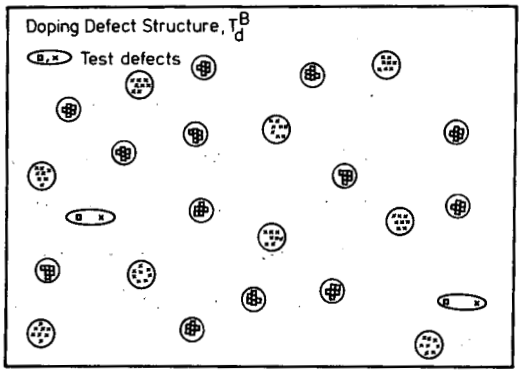


Fig. 3. Schematical doping defect structure after an e^- irradiation at 4 K plus an annealing treatment at $T_d \approx 400$ K. The test defects are generated by a subsequent test irradiation at 4 K.

The doped specimens have then been irradiated with a small testdose at 4 K followed by an anneal at about T = 65 K > $T_{Stage\ I}$ to measure the fractional amount of testdefects, $r_I = \Delta\rho/\Delta\rho_o$, remaining above stage I. At 65 K the test interstitials are highly mobile and perform the following reactions.

1) close pair recombination
2) correlated recombination; $R_{\square}$
3) (A) recombination with single vacancies; $R_{\square}$
   (B) annihilation at vacancy clusters; $R_{\square}^{cl}$
4) association with interstitial clusters; R_i^{cl}
5) uncorrelated recombination; $R_{\square}$
6) agglomeration with other single interstitial; R_i

$R_{\square}$, R_i, $R_{\square}^{cl}$, R_i^{cl} are the reaction radii defining the interaction between free migrating single interstitials and single vacancies, single interstitials, vacancy and interstitial clusters. R_i^{cl}, $R_{\square}^{cl}$ are normalized to the number of interstitials (vacancies) present in the interstitial (vacancy) clusters. Since the doping concentration in this work was always much higher than the test defect concentration, reaction 5) and 6) may be neglected here. In this case r_I is mainly determined by the branching ratio for the reaction of the mobile interstitials with interstitial clusters 4) on the one hand and with single vacancies 3)(A) or vacancy clusters 3)(B) on the other hand. r_I is given by

$$r_I = (1-f_{c.p.})\,(1-f_{corr.})\,\frac{R_i^{cl}}{R_i^{cl} + \begin{cases} R_{\square} & \text{for structure A} \\ R_{\square}^{cl} & \text{for structure B} \end{cases}} \qquad (1)$$

where $f_{corr.}$ and $f_{c.p.}$ are the fractions of F.D. which recombine correlated or as close pairs. $f_{c.p.}$ is known from pure specimens[3]. Unfortunately $f_{corr.}$ depends weakly on the doping defect concentration, since interstitials which normally recombine correlated can be trapped at interstitial clusters. For this reason it is difficult to determine quantitatively the reaction radii R_i^{cl}, $R_{\square}^{cl}$ from Eq. (1).

For a doping structure (A) the measured values of r_I are between 5 and 9 %. (This result is consistent with earlier measurements[4].) The higher

of these r_I values correspond to higher doping concentration indicating that an influence of the doping defects on the correlated recombination may be effective. This means that the low values are probably more representative for the determination of, e.g., R_i^{cl} from Eq. (1). Taking r_I = 5 % the ratio $R_i^{cl}/R_\square$ is about 1/4 which means that the efficiency per interstitial in an interstitial cluster for attracting a free migrating interstitial is about 4 times smaller than that of a single vacancy. (A similar result has been obtained from damage production rate measurements as a function of dose[5].)

For specimens doped with interstitial- and vacancy clusters - as schematically shown in Fig. 3 - r_I values between 25 and 30 % have been measured. Since the main difference between doping structure A and B is the different structure of the vacancies, it is very likely that the large difference (about a factor 5) between the r_I values comparing structure A and B must be attributed to the different vacancy structures. This means that vacancies after being clustered are not longer very effective for reacting with free migrating interstitials. In other terms $R_\square^{cl} << R_\square$. (The same result has been already observed by H. Wollenberger et al measuring the damage production at stage II temperatures for radiation doped specimens annealed below and above stage III[6].)

If the above interpretation is correct it should be possible to determine the temperature where vacancy clustering occurs by varying the annealing temperature T_d of the doping defects. This has been achieved by an isochronal annealing treatment of the doping defects between 100 and 400 K. After each annealing step the specimens received a very small test irradiation at 4 K to measure r_I. Fig. 4 shows the annealing curves of the doping defects together with r_I as a function of the annealing temperature, $T_d^{(N)}$. In another experiment we have measured the damage production at 70 K, $d\rho/d\phi/_{70\ K}$, after each isochronal annealing step of the doping defects; $d\rho/d\phi/_{70\ K}$ should provide similar informations as r_I since it essentially is determined also by the branching ratio $R_i^{cl}/(R_i^{cl} + R_\square)$ and $R_i^{cl}/(R_i^{cl} + R_\square^{cl})$, respectively. The results of $d\rho/d\phi/_{70\ K}$ as a function of $T_d^{(N)}$ are shown in Fig. 5.

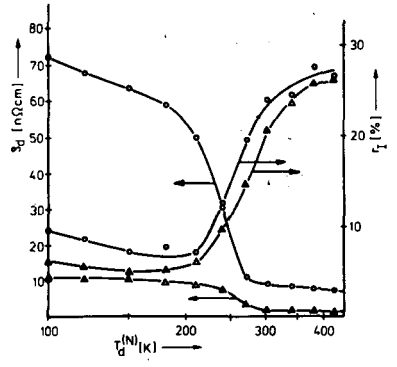


Fig. 4. Isochronal recovery curves in stage III region of Cu and the fractional remaining test defect concentration above stage I, r_I, as a function of the annealing temperature of the doping defects.

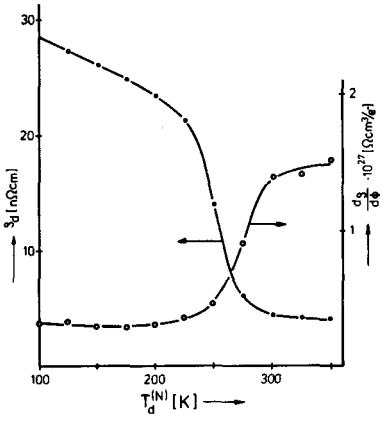


Fig. 5. Isochronal recovery curve in stage III region of Cu and the damage production rate at T_{irr} = 70 K. $d\rho/d\phi/_{70\ K}$ as a function of the doping defects.

Both for $d\rho/d\phi/_{70\ K}$ as well as for r_I a drastic increase is observed when the doping defects are annealed through stage III. In other words the transition from the low values of r_I and $d\rho/d\phi/_{70\ K}$ to the high values occurs in stage III which means that the vacancies must cluster in stage III.

It is not possible to explain the experimental result by a change in the structure of the interstitial type defects in the doped samples: There is evidence[1] that the growth of interstitial clusters which has been observed in stage II continues also in stage III. Since no increase of r_I and $d\rho/d\phi/_{70\ K}$ has been observed in stage II the continuing growth of interstitial clusters in stage III cannot be responsible for the drastic increase of r_I and $d\rho/d\phi/_{70\ K}$ in this stage. Intuitively the specific ability of defects to attract other interstitials (expressed by R^{cl}) should rather decrease instead of increase upon clustering. In the 2-interstitial model one would therefore rather expect a further reduction of r_I and $d\rho/d\phi/_{70\ K}$ upon annealing through stage III since only interstitial- and no vacancy clustering should occur in this stage.

During the isochronal annealing of the doping defects their concentration inevitably is reduced in stage III. In order to investigate to what extent the observed increase of r_I and $d\rho/d\phi/_{70\ K}$ might be attributed to this doping defect reduction we have performed the experiment for different initial defect concentrations. This is shown in Fig. 4. Although the initial defect concentration has a small influence on r_I this effect certainly cannot account for the drastic increase of r_I in stage III. Our contrary r_I is lower for lower doping defect concentration, which is probably due to an influence of the doping defects to the correlated recombination.

CONCLUSION

The drastic increase of r_I and $d\rho/d\phi/_{70\ K}$ in stage III can be explained easily by clustering of vacancies in this stage. The present experiment therefore gives further evidence for vacancy migration in stage III.

ACKNOWLEDGEMENTS

The authors wish to thank Prof. Dr. W. Schilling, Dr. F. W. Young and Dr. T. S. Noggle for many clarifying discussions and for carefully reading the manuscript.

REFERENCES

1. P. Ehrhart and U. Schlagheck, J. Phys. F 4, 1589 (1974)
2. M. Ohr, to be published
3. D. M. Parkin, Ph. D. Thesis University of Utah 1970
4. R. M. Walker, Proc. of the Intern. School of Physics "E. Fermi", ed. D. S. Billington (Academic Press, New York, 1962)
5. D. E. Becker, F. Dworschak, and H. Wollenberger, phys. stat. sol.(b) 47, 171 (1971)
6. F. Dworschak, H. Schuster, H. Wollenberger, and J. Wurm, phys. stat. sol. 29, 81 (1968)

INTERACTIONS BETWEEN RADIATION DEFECTS AND INTERSTITIAL IMPURITIES IN B.C.C. METALS

J. Diehl
Max-Planck-Institut für Metallforschung, Institut für Werkstoffwissenschaften, Stuttgart, Germany

ABSTRACT

From several features of radiation damage in b.c.c. metals containing small concentrations of interstitial impurity atoms a number of different reactions between foreign interstitial atoms and radiation induced defects can be deduced. Based mainly on neutron irradiation experiments on niobium and iron with nitrogen or carbon concentrations of 10 to 1000 at.ppm the following reactions are discussed: trapping of focusing collision sequences during low temperature irradiation; detrapping and/or delayed diffusion of self-interstitials during annealing; formation of complexes or radiation induced precipitates due to mobile interstitial impurities upon annealing or irradiation at elevated temperatures.

INTRODUCTION

In b.c.c. metals mostly small amounts of interstitial impurity atoms such as carbon, nitrogen or oxygen are present. Even if their concentrations are that low that if they were substitutional impurities the effects on radiation damage would be rather small or negligible, these interstitial impurity atoms can give rise to remarkable effects in the irradiation behaviour of this group of metals. Apparently there are strong interactions between interstitial impurity atoms and different kinds of intrinsic point defects as they are generated by energetic particle irradiations. Since this is so, quite a number of systematic studies have been carried out on the influence of such interstitial foreign atoms (IFA) on radiation effects in b.c.c. metals during the last ten to fifteen years. It can not be the task of this paper to give a comprehensive review of all this work. It is only attempted here to outline the main types of reactions which

can occur under different irradiation and post irradiation treatments according to the present state of knowledge. The paper will be further restricted by concentrating on rather small IFA-concentrations, for which in general the IFA would remain in random solid solution under identical treatments without irradiation. Consequently the wide and important field of the influence of irradiation on the formation and redissolution of second phase precipitates, as it was studied in Fe-C and Fe-N already ten years ago by Damask[1] and Stanley[2], will be left out almost completely.

In order to react with each other, IFA and radiation induced defects have to meet. Therefore, the mobililty of the possible reaction partners, or the temperature, plays a decisive rôle in the selection of reaction processes. Several cases can be distinguished: (i) Low temperature irradiation at which neither irradiation induced defects nor IFA are mobile by thermally activated migration. (ii) Annealing after low temperature irradiation, during which intrinsic defects become mobile, while IFA are still immobile. (iii) Irradiations at intermediate temperatures, at which IFA are immobile but some of the radiation induced defects are mobile during irradiation. (iv) Annealing to temperatures at which IFA become mobile after irradiation at lower temperatures. (v) Irradiation at elevated temperatures, at which IFA are mobile during irradiation.*

This report is subdivided according to the range of irradiation and/or annealing temperatures, listed above. For each case one or a few experimental examples are briefly discussed, most of which are results of work recently carried out in the laboratory of the author by using reactor neutron irradiations.

---

* It should be mentioned that the classification given above is incomplete because it does not include a clear distinction between temperature ranges, in which self-interstitials, vacancies and multiples of these elementary intrinsic defects are mobile; this originates mainly from the lack of reliable knowledge on some of the mobilities, especially of that of the single vacancy (cf.[3,4,5]). Furthermore, it has to be admitted that case (v) comprises at least two important subcases: The one, treated here, at which the irradiation temperature is close to that at which IFA become mobile, and the case of real high temperature irradiation, under which it is certain that vacancies are readily mobile as well as the IFA.

LOW TEMPERATURE IRRADIATION

Defect Production. -- The damage rate at low temperature, measured e.g. by the increase of the electrical resistivity, is enhanced by the presence of IFA, as observed by several authors[6-9]. This is demonstrated in Fig. 1, in which resistivity measurements of Keil et al.[9] on purified Nb and Nb with 40 and 850 at.ppm nitrogen are shown. The damage rates $d\Delta\rho/d\Phi t$ measured during neutron irradiation at 20 K are plotted in the usual way versus the total radiation induced resistivity increase $\Delta\rho$ (total damage). The decrease of the damage rate with the total damage is usually interpreted by the spontaneous recombination of newly produced vacancies and interstitials with already existing (anti)defects[10]. Generally speaking, these recombinations seem to be partly suppressed by the presence of IFA, resulting in an enhanced effective defect production. Since at the irradiation temperature no thermally activated long range migration of radiation defects or IFA is expected, it has to be assumed that dynamical processes are of importance here.

In ref.[9] the observations of Fig. 1 are interpreted in the following way: A rather large fraction $\eta \simeq 0{,}4$ of the self-interstitial atoms is generated during irradiation by means of focusing collision sequences (f.c.s.) along closed packed lattice directions propagating in average over a rather large

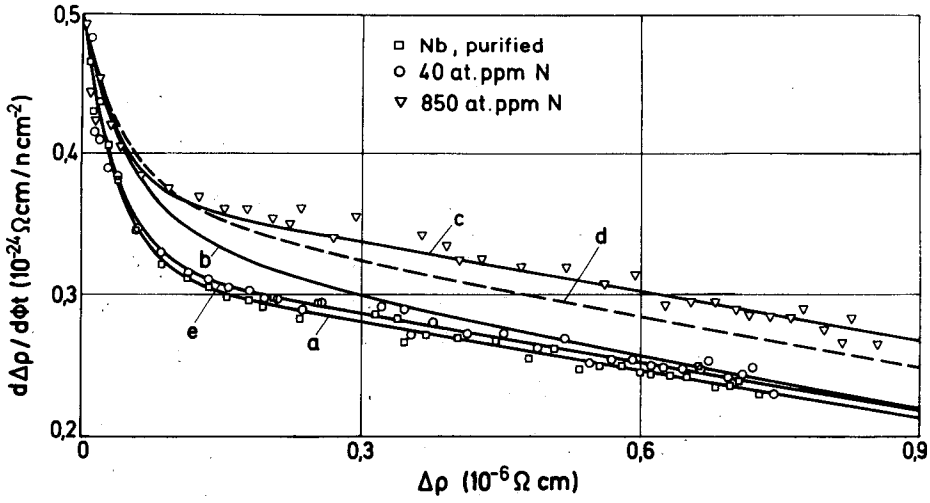


Fig. 1. Damage rate versus resistivity increase of n-irradiated purified and N-doped Nb. Curves a - d are computer fitted, see[9] and text.

distance. Trapping of a f.c.s. at a vacancy (with trapping cross section σ_V) leads to annihilation of a Frenkel pair. Such capturing of f.c.s. at vacancies, being much more effective than the spontaneous recombination of interstitials produced in random directions, is regarded to cause the strong initial and non-linear decrease of the curves in Fig. 1. Trapping of f.c.s. at IFA (and at self-interstitials) competes with the capture at vacancies. In this way, if IFA are present, self interstitials (trapped at IFA) are retained, which otherwise would fall into vacancies (which are also retained). The experimental curves can be accounted for quantitatively, if it is assumed in addition that in the neighbourhood of an IFA the probability for the production of long range f.c.s. is reduced. Using these assumptions, curves a, c and e in Fig. 1 were fitted to the data. From the fitting parameters it turns out that the capture cross section of IFA for f.c.s., σ_F, is very small as compared to that of vacancies. The strong suppression of recombination at small total damage can be accounted for by $\sigma_F/\sigma_V \simeq 0.04$.

The concept that f.c.s. and their capture at IFA is of importance for the damage at low temperatures is supported by internal friction measurements on Fe, doped with N or C, after low temperature reactor irradiation[11]. An internal friction peak (labelled I_E) appearing at $\simeq$ 120 K was assigned to the reorientation of free <110>-self-interstitials[12]. This peak, measured immediately after low temperature irradiation (so that thermal migration of the interstitials over larger distances is unlikely), was found to be the smaller the more N or C the Fe samples contain. The rapid decrease of this damping peak with IFA-content (at constant neutron dose) again can be explained by the capture of f.c.s. at IFA, since the self-interstitials coming to rest at the capturing IFA will be unable to reorientate in the same manner as if they were free interstitials.

In summing up this section it can be stated that most likely in b.c.c. metals containing IFA, self-interstitial-IFA pairs are formed during low temperature irradiation in appreciable numbers, already at rather small doses. At higher doses probably larger agglomerates can be built up with the same basic mechanism by multiple capture of f.c.s. at IFA.

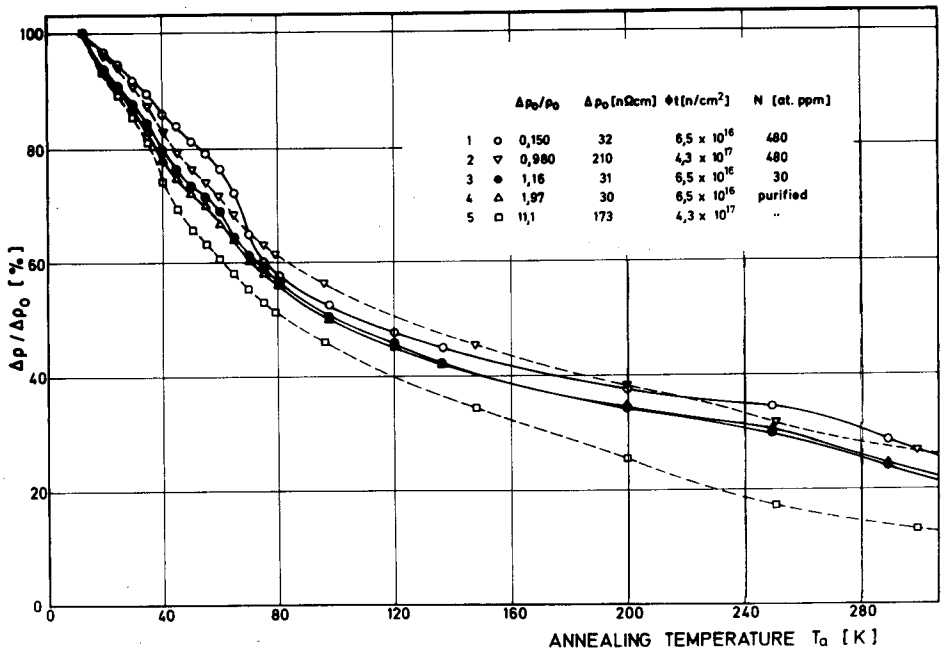


Fig. 2. Isochronal annealing curves of purified and N-doped Nb after n-irradiation at 13 K.

Annealing up to Room Temperature. -- An overall impression about the influence of dose and IFA content on the annealing behaviour in the temperature range in which IFA remain immobile, can be obtained from Fig. 2, which shows isochronal annealing curves of the residual resistivity of Nb with three IFA-concentrations and two neutron doses.[13] As it was observed also by other authors (e.g.[7]), quite generally there is less annealing in doped samples than in purified ones and the differences become more pronounced with increasing dose. It seems to be a characteristic feature of the annealing of b.c.c. metals (also after electron irradiation, see e.g.[14]) that most of the annealing occurs more or less continuously with some distinct

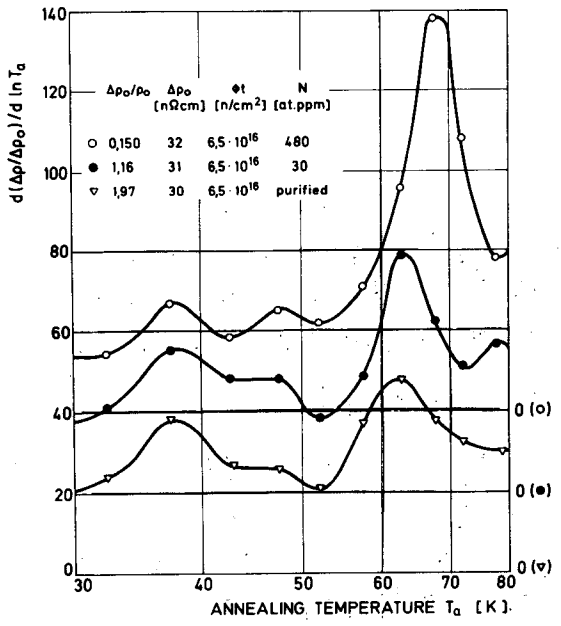


Fig. 3. Differentiated annealing curves from Fig. 2.

but small annealing stages superimposed on this relatively high "background ".

Since there doesn't exist a reliable interpretation of the background-annealing we will focus our attention here only to the temperature range 30 to 80 K, in which a fine-structure is clearly resolvable in the curves of Fig. 2 as well as in other studies, and in which, in addition, the strongest influence of IFA occurs at small irradiation doses. This is demonstrated more clearly in Fig. 3, in which three differentiated annealing curves are shown for the same dose but different IFA contents. For interpreting these curves we refer to very detailed investigations of Faber et al.[14]. These authors observed in very high purity niobium after a low dose electron irradiation in addition to annealing peaks at 37 K and 43 K, both of which show first order kinetics and can be seen also in Fig. 3 as a distinct peak or as a shoulder, a small annealing peak at 52 K, which shifts to lower temperatures with dose, and which was assigned to the free migration of self-interstitials. This peak is not observed in the less pure samples and the nitrogen doped ones of Fig. 3. But there appears a peak between 60 and 70 K, which increases in heights and shifts to higher temperatures with increasing N content. It is believed, that this peak can be assigned to the annealing out of the self-interstitials retained during irradiation because of the trapping of f.c.s. at IFA. The activation energy for this annealing process should be enhanced as compared to the free migration of the self-interstitials (0.11 eV according to[14]) by the binding energy between interstitials and IFA, if the dissociation is the rate determining s+ep. According to a rough estimate the binding energy would then have to be between 0.05 and 0.10 eV. The shift of the stage to higher temperatures with increasing IFA concentration is thought to be caused by delayed diffusion due to repeated retrapping and detrapping of migrating interstitials at other IFA after dissociation from their original trapping sites according to a mechanism corresponding to that considered by K. Schröder[15] for the diffusion of vacancies in an array of traps.

At higher doses the distinct low temperature annealing stages are less pronounced as compared to the background annealing, and IFA reduce mainly this background. Although it can't be explained in detail, it is thought,

that this originates from multiple capture of self-interstitials at IFA and the corresponding formation of clusters of interstitials already during the low temperature irradiation.

IRRADIATION AT INTERMEDIATE TEMPERATURE

Defect Production. -- Intermediate temperature as defined in the introduction are for most of the b.c.c. metals ambient temperatures of conventional research reactors or temperatures around or slightly above room temperature. For such temperatures, at which most of the radiation defects are mobile, but IFA are immobile, the defect production has not been studied very thoroughly so far. The most informative investigations are those on the dose dependence of irradiation hardening in Nb[16,17], combined with some TEM observations[17,18]. Three dose ranges were observed: Up to about 5.10^{17} n/cm^2 there is a steep rise of the lower yield point with dose, followed by a flat region (saturation), the heights of which is the higher the more IFA are in solution. Depending on IFA concentrations the yield stress increases again more strongly at or above 10^{19} n/cm^2. Some electrical resistivity measurements[19] proove that in the plateau region also the total damage is considerably higher in IFA doped samples than in purified ones. TEM observations show clearly that at equal doses there are more and smaller defect clusters visible in doped samples than in those with smaller IFA content[17]. Furthermore, a quantitative correlation between yield stress and the smaller ones (<70 Å) of the visible defect clusters could be established [16,17]. So, undoubtedly, the defect production is strongly influenced by the presence of IFA. Nevertheless a straightforward explanation of these observations doesn't exist.

Mainly in order to explain radiation hardening, radiation anneal hardening (RAH) of Nb, and other related observations, to be discussed in the following section, the following qualitative model has been developed recently[20]: During n-irradiation rather loosly packed vacancy clusters are formed within the defect cascades. Self-interstitials which are mobile at the considered irradiation temperatures agglomerate at least partly. Thereby IFA increase the density of nucleation sites for these

agglomerates. In this way the number of radiation defects prevented from mutual annihilation is increased and the observed enhancement of defect clusters density due to IFA, as observed in TEM, can be explained. Since upon further annealing most of the IFA, which were in solution before irradiation, show up again in the Snoek-peak of internal friction[1,2,19,21] (cf. next section), either only a small fraction of IFA serve as nucleation sites or the IFA are only loosely bound to the interstitial agglomerates. The plateau region in the yield stress is explained in this model by a predominance of the growth of already existing interstitial agglomerates against a continuation of the formation of new agglomerates. Supposedly the stronger increase of the yield point at high doses is caused by the continuously increased density of vacancy cluster becoming the predominant dislocation obstacles again.

Annealing to elevated temperatures. -- When samples containing IFA are annealed after irradiation into a temperature range in which IFA become thermally mobile, the concentration of IFA in solid solution decreases rapidly (starting close to the pre-irradiation value) according to Snoek-peak and magnetic desaccomodation measurements[1,2,19,21,22]. In the same temperature range (formerly called "stage III"[19,23,24]) an increase of the yield stress occurs (RAH; cf.[25,26]). Since this decrease in IFA-concentration takes place also in cases in which without irradiation no property changes would occur during the same heat treatment, it is conclusive that the mobile IFA react with radiation defects. Mainly three types of reactions were discussed so far: Accelerated precipitation of nitrides, carbides etc. due to an enhanced nucleation rate on radiation induced defects[1,2], trapping of individual IFA at vacancies[1,27] and trapping of IFA at intrinsic defects clustered into dislocation loops[25,28,29]. Which one of these mechanisms predominates and whether also other types of reactions are of importance seems to depend on several parameters, primarily on IFA-concentration and on type and dose of irradiation. It, therefore, is impossible to go into all details of these reactions here. Only a few special cases will be mentioned: As it was shown already in[1,2] acceleration of precipitation plays a decisive rôle in supersaturated solid solutions after neutron irradiation. In recent experiments on Fe with small

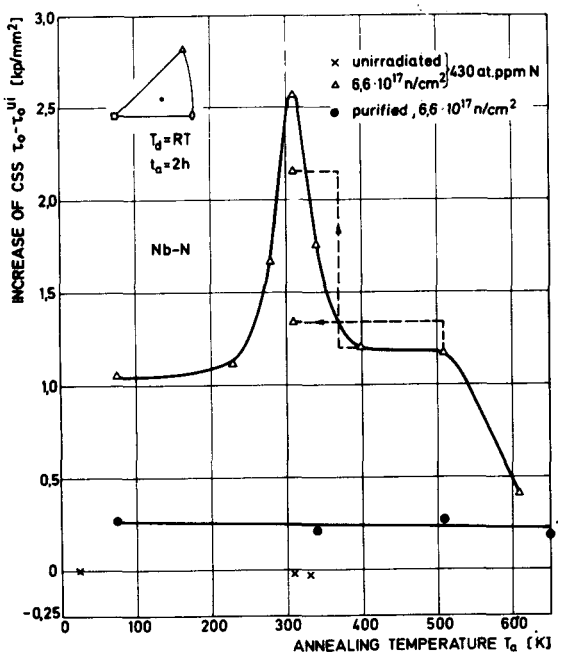


Fig. 4. Isochronal annealing curves of the CSS of n-irradiated Nb-single crystals.

N- and C-concentrations it could be clearly demonstrated by applying internal friction and positron annihilation techniques, that IFA indeed react with vacancies[29], thereby forming "complexes" on an atomistic scale, which give rise to a relaxation maximum in internal friction; they may well be of the configuration predicted theoretically in[30].

RAH has been considered by several authors to be caused by the strengthening of small dislocation loops, present from the previous irradiation by the attachment of IFA (cf. some related papers in[4]). That this picture is oversimplified and that rather complicated defect states may occur can be demonstrated by Fig. 4, in which the increase of the critical shear stress (CSS) of Nb single crystals doped with 430 at.ppm N after n-irradiation at 80°C and isochronal annealing (Δt = 2 h) is shown[20]. The following points will be stressed: Hardening due to irradiation and RAH starting at ≈250°C anneals out in two separated stages. Two types of radiation induced defects (agglomerates) seem to be necessary, in order to explain the data. This turns out from "reversibility" measurements. Annealing to the maximum temperature of RAH after a previous anneal at the beginning and at the end of the CSS level separating the two annealing stages leads to a reappearance of RAH in the first case but not in the second (dashed arrows in Fig. 4). So, the nucleation sites for the attachment of the N-atoms, which cause RAH, must anneal out in the temperature range of the level between 400 and 500°C and can't cause the CSS at this level, which is of approximately the same heights as the one reached during irradiation before annealing. Taking into account further informations, as those mentioned in the last section, it is tentatively proposed[20], that this CSS-level originates from self-interstitial agglom-

erates and that the preferred nucleation sites for the the "precipitation" of N-atoms causing the RAH-peak are vacancy clusters in a thermally less stable configuration than the interstitial agglomerates.

IRRADIATION AT ELEVATED TEMPERATURES

When the irradiation temperature is high enough for IFA to be mobile by thermal migration, complexes and other reaction products between IFA and radiation defects, as discussed before, are formed already during irradiation. In this way the strong IFA dependencies of the increase of the CSS and of the residual electrical resistivity during n-irradiation of Fe containing N or C at $\simeq 130^{\circ}C$ were explained. Since this is partly treated in an other paper at this conference[31], only a few characteristic features will be mentioned here. The reaction products originating under this condition seem in principle to be similar to those generated during annealing after irradiation at lower temperatures. IFA content and irradiation dose are of importance for the details of the reaction processes also in this case. In supersaturated solid solutions again radiation induced precipitates occur, at least at small doses. However, there are indications, that with an increasing supply of intrinsic defects - that means with increasing dose - the IFA are redistributed to form more and smaller IFA-defect complexes[33-35]. Such smaller complexes are predominantly generated at small IFA concentrations and then determine apparently the initial increase of the CSS and of the resistivity. This type of damage production, however, is expected to die out, when all IFA are used up in the complex formation. In this way a levelling off of the CSS damage rate[35,36] is interpreted. There has been found an almost linear relation between the dose at which this type of "saturation" sets in and the IFA-concentration for different sets of experiments, as shown in[31,33]. This indicates that there is kind of a stochiometric relation between radiation induced defects and IFA at the onset of this saturation. Without going into the lengthy details of the corresponding experiments here, the irradiation condition treated in this section can be characterised by the statement, that in agreement with Snoek-peak measurements, the

straight line shown in Fig. 2 of ref.[31] subdivides the IFA-concentration-neutron-dose-diagram into two sections, in one of which IFA are still in solution (small dose range), in the other one all IFA are bound in reaction products with radiation induced defects, so that further damage is only created by newly produced intrinsic defects.

ACKNOWLEDGEMENTS

The author is indepted to his colleagues, who cooperated in the reported investigations and in the preparation of the manuscript, especially to W. Decker, B. Hertel, D. Keil, U. Merbold, M. Schreiner and M. Weller. Part of the work presented here was sponsored by the Gesellschaft für Kernforschung, Karlsruhe.

REFERENCES

1. A.C.Damask, Diffusion in B.C.C. Metals, p.317, ASM, Metals Park, 1965.
2. J.T.Stanley, Diffusion in B.C.C. Metals, p. 349, ASM, Metals Park, 1965.
3. Defects in Refractory Metals (R. de Batist, J.Nihoul, I.Stals, eds.), S.C.K./C.E.N., Mol. 1972.
4. Defects and Defect Clusters in B.C.C. Metals and Their Alloys (R.J. Arsenault, ed.), Nuclear Metallurgy, Vol. 18, 1973.
5. H. Schultz, Scripta.Met. 8, 721 (1974).
6. H.Wagenblast, F.C.Schwerer and J.A.Horak, rad.effects 14, 203 (1972).
7. F.Varva, W.Dönitz and K.Böning, phys.stat.sol.(a) 20, 511 (1973).
8. D.S.Brown, T.H. Blewitt, T.L.Scott and A.C.Klank, J.Nucl.Mat. 52, 215 (1974).
9. D.Keil, W.Decker and J.Diehl, rad. effects, in the press.
10. G. Burger, W. Meissner and W. Schilling, phys.stat.sol. 4, 281 (1964).
11. M. Weller and J. Diehl, Internal Friction and Ultrasonic Attenuation in Crystalline Solids (D. Lenz and K. Lücke, eds.), Vol.I, p. 352, Springer Berlin-Heidelberg-New York, 1975.
12. V.Hivert, P.Pichon, H.Bilger, P.Bichon, J.Verdone, D.Dautreppe and P.Moser, J.Phys.Chem.Solids 31, 1843 (1970).
13. D.Keil, Dr.-Thesis, Univ.Stuttgart, 1973; D.Keil, W.Decker and J.Diehl, to be published.

14. K.Faber, Dr.-Thesis, Univ.Stuttgart, 1973; K.H.Faber, H.Schultz and J.Schweikhardt, this conference.

15. K. Schroeder, this conference.

16. R.P.Tucker and M.S.Wechseler, rad.effects 3, 73 (1970).

17. B.A.Loomis and S.B.Gerber, Acta Met. 21, 165 (1973).

18. R.P.Tucker and S.M.Ohr, Phil.Mag. 16, 643 (1967).

19. J.M.Williams, W.E.Brundage and J.T.Stanley, Met.Sci.J. 2, 100 (1968).

20. M.Schreiner, Dr.-Thesis, Univ.Stuttgart, 1974; M.Schreiner and J.Diehl, to be published.

21. M.Weller and J.Diehl, submitted to Scripta Met.

22. M.Wuttig, J.T.Stanley and H.K.Birnbaum, phys.stat.sol. 27, 701 (1968).

23. A.A.Johnson, Scripta Met. 7, 1 and 15 (1973).

24. M.S.Wechsler, J.M.Williams and J.T.Stanley, Scripta Met. 7, 7 (1973).

25. S.M.Ohr, R.P. Tucker and M.S.Wechsler, phys.stat.sol.(a) 2, 559 (1970).

26. M.S.Wechsler, ref.[3], p. 235.

27. H.Wagenblast and A.C.Damask, J.Phys.Chem.Solids 23,21 (1961).

28. R.Bullough, J.T.Stanley and J.M.Williams, Met.Sci.J. 2, 93 (1968).

29. M.Weller, W.Triftshäuser and J.Diehl, Solid State Comm., in the press; this conference.

30. R.A.Johnson and A.C.Damask, Acta.Met.12, 443 (1964).

31. U.Merbold, M.Weller and J.Diehl, this conference.

32. G.P.Seidel, rad.effects 1, 177 (1969).

33. J.Diehl, U.Merbold, O.Reimold and M.Weller, ref.[4], p.69.

34. A.C.Damask, J.G.Y. Chow, J.J.Kelsch and H.Wagenblast, Phil.Mag.22, 549 (1970).

35. G.P.Seidel, phys.stat.sol. 25, 175 (1968).

36. J.Diehl, G.P.Seidel and M.Weller, Trans.Japan Inst.Met. (Suppl.) 9, 219 (1968).

STUDIES ON RADIATION-INDUCED POINT DEFECTS IN METALS BY MEANS OF HIGH-VOLTAGE ELECTRON MICROSCOPY

K. Urban
Max-Planck-Institut für Metallforschung, Institut für Physik,
D7000 Stuttgart 80, Büsnauer Straße 171, W.-Germany

ABSTRACT

The contributions of in-situ studies in the high-voltage electron microscope (HVEM) to the understanding of radiation damage formation are reviewed. After consideration of some basic features of HVEM studies the experimental results on production and diffusion of point defects and their interaction with dislocations are discussed.

1. INTRODUCTION

Electrons passing through a metal specimen in a HVEM may displace lattice atoms permanently. The appropriate threshold accelerating voltages range from 170 kV for Al to 1500 kV for U. While single atomic defects cannot be resolved in the microscopic image, defect reactions allow us to detect the damage and to perform in-situ studies during irradiation or subsequent treatments. Since its first application[1] 7 years ago this method has proved to be particularly successful in studying the formation and growth of defect clusters which become visible in the microscopic image after some fifty defects have agglomerated. In many cases it is then possible to deduce the nature of the agglomerating defect unambiguously from contrast experiments. Cluster formation can be studied under a variety of experimental conditions regarding e.g. electron energy, specimen orientation or temperature. In the thin foils necessary for electron microscopy surfaces may play an important

role as defect sinks. Their influence has to be taken into account when comparing HVEM results with those of conventional methods. Since most of the results reported here were deduced from observations of clusters a brief account of the formation and growth of clusters as needed in the following sections will be given first.

2. BACKGROUND OF STUDIES ON POINT DEFECTS IN THE HVEM

Defect Production

Usually only a circular spot of some μm in diameter is irradiated in the specimen. Because of the small thickness d of the foils used ($d \lesssim 1$ μm) the displacement rate is uniform throughout the full foil depth. Beam spreading is only some 0.1^{o} (Bragg angle). The displacement rate K (d.p.a./s) calculated from the electron current density j (10^{17} e/scm^2 $\lesssim$ j $\lesssim$ 10^{20} e/scm^2) by

$$K = \sigma \cdot j \qquad (1)$$

(σ-total displacement cross section[2]) is typically $10^{-6} \lesssim K \lesssim 10^{-3}$. K is therefore some orders of magnitude higher than in conventional reactor or v.d.Graaff irradiations. Nevertheless the local temperature rise in the irradiated spot due to electron energy dissipation can be kept negligibly small because of favourable irradiation conditions[3].

Interstitial Dislocation Loop Growth at Low Vacancy Mobility

In the following merely cases of low and high vacancy mobility will be distinguished, since during irradiation vacancies and interstitials can carry out radiation-induced diffusion (see §4) and are therefore never totally immobile.

At temperatures where only interstitials are mobile by thermally activated diffusion the qualitative picture of damage formation is as follows: After starting the irradiation the

interstitial concentration C_I and the vacancy concentration C_V rise initially at equal rate $\propto K$. The interstitials then form clusters and C_I decreases while C_V is increasing further to such an extent that mutual annihilation becomes dominant and cluster nucleation is impeded. Using rate equations the time dependence of C_I, C_V, the concentration of interstitial loops C_L and their radius R have been calculated[4-7]. For di-interstitial and interstitial-impurity complex as nucleus the loop concentration was found to increase initially $\propto t^3$. For the saturation loop density C_L^∞, $C_L^\infty \propto K^{1/2}\exp(E_M^I/2kT)$ and $C_L^\infty \propto K^{1/2}\exp(E_M^I+E^B/2kT)$ were obtained (E_M^I-interstitial migration activation energy; E^B-interstitial-impurity binding energy). The loop radius increases as $R \propto t^{1/3}$.

The $K^{1/2}$ dependence of C_L^∞ has been observed experimentally e.g. in Cu[8], Ni[5,9], Au[6]. In Cu at 55K the initial time dependence of C_L was observed to be $C_L \propto K^{1/2}t$ [10]. The reason for the discrepancy with theory is not yet investigated. Diffusion of interstitials to surface sinks leads to loop denudation at surfaces within a distance w approximately given by[11]

$$w \simeq 2(D_I V_a/4\pi V_c K)^{1/4} \qquad (2)$$

(D_I-interstitial diffusion constant, V_a-atomic volume, V_c-radius of spontaneous recombination volume). w may reach (e.g. in Cu at 300K) about 0.1μm under normal operating conditions.

Interstitial Dislocation Loop Growth at High Vacancy Mobility

The defect concentrations at high temperature develop according to the following picture[6,12-15]: Initially C_I and C_V rise at a rate $\propto K$. After a very short time τ_1 (10^{-2}-10^{-1} s under conditions typical for many experiments) a quasi-steady state between generation and recombination is achieved. After $\tau_2 \simeq s^2/2D_I$ the interstitials as the faster migrating defects "feel" the surface sinks (s-separation from surface; $\tau_2 \gtrsim \tau_1$ for most cases used). C_I then decreases while C_V increases further until a steady state is reached after $\tau_3 \simeq d^2/2\pi^2 D_V$ where the

rate at which defects recombine or go to sinks equals the generation rate (τ_3 may reach some 10^1 to 10^2 s).

The net rate of interstitials arriving at a sink is given by

$$dN_I/dt = k_I D_I \bar{C}_I - k_V D_V \bar{C}_V \qquad (3)$$

($\bar{C}_I$, $\bar{C}_V$-average C_I and C_V values around the sink). k_I and k_V contain the sink efficiency for interstitials and vacancies respectively. As shown in §5 $k_I > k_V$ for dislocation loops, and interstitial loop nucleation is favoured shortly after beginning the irradiation where dN_I/dt is large due to $\bar{C}_I \approx \bar{C}_V$ and $D_I >> D_V$. The subsequent drop in C_I may reduce τ_3 considerably. It also terminates the nucleation phase at an early stage at which surfaces are still dominant sinks. Thus application of Eq.(3) to surface sinks yields for steady state ($dN_I/dt=0$)

$$\gamma^S D_I \bar{C}_I = D_V \bar{C}_V \qquad (4)$$

($\gamma^S = k_I^S/k_V^S$; S-for surface). If surfaces are neutral sinks $\gamma^S=1$. Calculating, again in steady state, dN_I/dt for an interstitial loop using Eqs.(3) and (4) and $D_I C_I = (K V_a D_V/4\pi r_c \gamma^S)^{1/2}$ we obtain

$$\frac{dN_I^{IL}}{dt} = K^{1/2} D_V^{1/2} k_I^{IL} (V_a/4\pi r_c \gamma^S)^{1/2} (1-\gamma^S/\gamma^{IL}) \qquad (5)$$

(IL-for interstitial loop). This shows that, at high temperatures, the interstitial loop growth rate depends on the vacancy diffusion constant only. The $K^{1/2}$ law was confirmed experimentally e.g. for Ni[9] and Cu[8]. At the foil surfaces defect-denuded layers are formed whose width is given approximately by an equation as Eq.(2) with D_I replaced by D_V[15]. The denuded layer width may exceed 0.1µm (e.g. in Cu at high temperatures) under normal operating conditions.

3. EXPERIMENTS ON DEFECT PRODUCTION

Threshold Energy for Displacement

It is a good approximation (especially for low-temperature irradiations) to assume a well defined threshold energy $E_d(\vartheta,\varphi)$

for displacement of an atom moving after a collision with an electron in a direction with spherical coordinates ϑ and φ. The entirety of the $E_d(\vartheta,\varphi)$ when plotted as radius vectors in a spherical coordinate system forms the threshold energy surface. The determination of this surface is the subject of investigations mainly applying resistivity measurements[16,17]. However for technical reasons the angular resolution is limited to about 5°. In the HVEM studies on $E_d(\vartheta,\varphi)$ can be carried out with an order of magnitude higher resolution by observing e.g. the defect cluster growth as function of electron energy for different crystal orientations. E_d-studies were carried out at room temperature in Cu[1], Ni[5,18], Co[19] (s. table). With exception of [5] it was attempted to deduce E_d directly from the minimum electron energy producing visible cluster formation for a certain irradiation direction $\underline{e}$. The threshold values $\hat{E}_d(\underline{e})$ determined this way are in general not identical with $E_d(\underline{e})$ since if at some angular distance θ from $\underline{e}$ $E_d(\theta)<E_m\cos^2\theta$ displacements will occur along this direction (E_m-maximum transferred energy for a given electron energy). In Cu, where no lattice direction is separated by more than 25° from directions for which E_d=19eV (minimum E_d determined in[17]), E_d calculated using the above considerations is in excellent agreement with the values determined in[1]. For Ni a more sophisticated method was used. σ was deduced from the total electron dose that yields a certain total dislocation loop area. A plot of the thus obtained σ-values versus electron energy gave the $\hat{E}_d$-values listed in the table. Then the σ-curves were fitted by a model which expands the E_d in a certain direction along the first order cubic harmonics using the E_d-values along the main crystallographic directions as free parameters[20]. Best fit was obtained by the values listed in the table.

The HVEM measurements have not yet reached the precision of conventional studies. On the one hand $\hat{E}_d$ was only determined for very few orientations. On the other hand at the tempera-

tures used interstitial atoms are highly mobile giving rise to loop denuded regions at foil surfaces. With decreasing K it is the overlapping of the denuded zones of the two foil surfaces which limits the formation of visible damage when the threshold energy is approached. Thus results may depend on foil thickness and investigations in the range of low K are impeded. As will be seen below the value of the method can be greatly improved by working at low specimen temperatures.

An interesting feature of the damage rate curves obtained by resistivity measurements are tails extending to very low energies. For these tails, which have been found in e.g. Cu[16], Au[16], Pt[17], mainly two explanations were developed. (i) Displacement of heavy host atoms be light impurity atoms which have gained energy in a collision with an electron. In such a double-collision process the energy transferred to a host atom may be greater than in a direct collision[16]. (ii) Existence of cones of small angular width in the crystal containing "soft" directions with low E_d which cannot be resolved by conventional methods[21]. The last concept is favoured by recent high-sensitivity dislocation pinning experiments in Cu in which E_d was found to be as low as 9eV[22] in contrast to the 19eV determined by the resistivity method[17]. Two HVEM results also indicate that low $\hat{E}_d$-values are not associated with a double-collision process. In Pb the threshold for visible cluster formation at 50K was determined as 7.5eV[14] in contrast to 11.5eV found in a conventional study[23]. In Al at 300K $\hat{E}_d$=14eV was found[24] while conventional methods yielded 16eV[25]. Although it was claimed in[24] that the displacements were involving impurities it can easily be shown for both cases that the observed defect cluster formation is due to an intrinsic effect. Even when anticipating relatively high light impurity contents (100ppm) calculation of the double-collision process yields defect concentrations more than three orders of magnitude lower than those stored in the observed dislocation loops.

Effect of Electron Channelling on Production Rate

Electrons passing through a crystal can be described by a superposition of Bloch waves. Each Bloch wave is localized in a different part of the lattice potential. The electron currents associated with the various Bloch waves can to a good approximation be regarded to be independent of each other. Due to a low cross section of atoms for displacement only electron currents close to the atomic nuclei can produce displacements.

The fractional intensity excited in each Bloch wave when the electrons enter the crystal at the upper surface depends sensitively on crystal orientation. When the electrons propagate into the crystal inelastic scattering occurs (electron-electron, electron-phonon) leading to transitions to other Bloch states. This loss in amplitude is especially great for waves localized near the atom positions. Such waves are said to channel less well than waves localized between the atom positions. If therefore a crystal is suitably orientated that a Bloch wave localized near the atom positions has especially high amplitude a high displacement rate is expected near the upper surface. But due to bad channelling this wave quickly looses intensity which reduces the displacement rate to some average value. Suitable orientations are those where the electrons enter the crystal parallel to a set of low order index lattice planes. According to theory[26,27] the damage rate enhancement over the average value should not exceed a factor of 4 being negligible at crystal depths higher than about 0.2μm and deviations from the exact symmetry position of some 0.1^{o}. Thin foil experiments at room temperature in the HVEM gave striking evidence on the electron channelling effect[26]. But due to dislocation loop denudation at surfaces no quantitative check of the theories was possible. Current work[10] on Cu is carried out at 55K where loop denudation at surfaces is negligible. Fig.1a shows a plot of loop density versus distance from entrance surface for two cases. In one the beam is

exactly parallel to the (100) lattice planes but tilted in the other case off this symmetry position. In the first case the loop density is enhanced at the entrance surface by a factor of about 5 over the average value reached at a depth of about 0.2μm. Remembering that under the irradiation conditions used (§2) the loop density is proportional to $K^{1/2}$ an enhancement of the damage rate in the symmetry position by a factor of 25 is deduced. A similar result is obtained in a sample oriented for the (111) symmetry position (Fig.1b). The high enhancement factors observed are not accounted for by the wave channelling theory. More work is required in which not only the probability of scattering but also that of displacement should be considered.

Replacement Collision Sequences (see also §5)

An interstitial created in an ordered binary alloy by irradiation may recombine with a vacancy so that the local order is either restored or destroyed. Besides recombination which may lead to the local destruction of order, disorder may be produced with high efficiency by replacement collision sequences along crystallographic directions where lattice sites are occupied alternately by the alloying elements. This was shown in an experiment on ordered Ni_3Mn[28].

Prior to irradiation in the HVEM the used samples were deformed in tension to create superdislocations consisting of two dislocations of the same sign enclosing an anti-phase boundary. The equilibrium separation is determined by an attractive force due to the boundary energy and an elastic repulsive force. The separation is proportional to S^{-2}, where S is the parameter of long-range order. Measuring the separation before and after an irradiation with 1200kV electrons in (110), $(3\bar{1}\bar{8})$ and $(3\bar{5}2)$ oriented samples (Fig.2) a decrease in order from S=1 before irradiation to $S_{110}\approx 0.6$, $S_{3\bar{1}\bar{8}}\approx 0.8$, $S_{3\bar{5}2}\approx 0.9$ was deduced. For a simple displacement process, however, S is only expected to decrease to about 0.9 and the observed aniso-

tropy cannot be explained, even if a reasonable orientation dependence of E_d is taken into account. The authors then calculated the scattering cross sections for displacements into cones of 10^o angular width around the relevant <110> directions for each irradiation case. An excellent fit to the measured data could be obtained using a maximum length of replacement collision sequences along <110> directions of about 50 atomic distances.

4. EXPERIMENTS ON DIFFUSION PROPERTIES OF POINT DEFECTS

Radiation-Induced Diffusion

In Ni[29] and Cu[30] dislocation loops form during irradiation at temperatures as low as 8K (Fig.3), i.e., well below stage $I_{D,E}$ temperatures where long-range interstitial migration sets in. In Cu[30] and Pb[14] stacking-fault tetrahedra (SFT) were observed to form during irradiation at temperatures down to 100K (Cu) and 35K (Pb). The SFT are presumably of vacancy type since SFT formed by clustering of interstitial atoms have never been observed. Thermal equilibrium experiments show that thermally activated vacancy motion can be excluded at the mentioned low temperatures.

The nature of the defect migration responsible for cluster formation at temperatures too low for thermally activated diffusion could be determined experimentally in lead[14]. One of these experiments may be described here. Two spots of the same sample were irradiated at 58K with 630 keV electrons. Such irradiation produces stable defect pairs which results in the formation of interstitial loops and at a later stage, due to preferential loss of interstitials to surfaces (§5), in the growth of vacancy SFT. After this had been achieved one of the spots received a sub-threshold irradiation with 390keV electrons which are not able to produce stable defect pairs. During this treatment the SFT density and size grew (Fig.4).

Subsequently the sample was warmed-up to room temperature where vacancies can migrate by thermal activation. This resulted in the spot not re-irradiated at the low temperature in formation of a high density of SFT (Fig.5a) while in the sub-threshold re-irradiated spot only little change occurred (Fig. 5b). This shows that free vacancies present in the sample after above-threshold irradiation can migrate and cluster already at low temperature under irradiation with electrons of sub-threshold energy.

The energy to carry out jumps can be transferred in sub-threshold collisions either directly to defects or their immediate vicinity . In addition the formation of unstable but temporarily existing defect pairs near an interstitial or a vacancy may lead to site exchanges over more than one atomic distance[14]. The energies involved are of the order of magnitude of the migration activation energies for thermal diffusion and are rather frequently transferred since in Coulomb scattering the collision cross section increases rapidly with decreasing atom recoil energy.

In Cu the electron threshold dose to form visible clusters (2nm-3nm in size) at 8K is 2.5×10^{20} e/cm^2 (650keV). For observation of SFT at 140K a threshold dose of 4×10^{21} e/cm^2 (650keV) is necessary. From the cluster densities observed at the low temperature (up to about 10^{18} cm^{-3}) a cross section for radiation-induced defect jumps of 10^4-10^5 b can be estimated. As outlined in §5 SFT can grow in thin foils due to preferential loss of interstitials at surfaces. The threshold dose for SFT is therefore not typical of radiation-induced vacancy mobility but reflects the loss of interstitials at surfaces.

The introduction of very high concentrations of immobile interstitials and/or vacancies may lead to clustering of both defect types due to statistical processes. This has been studied by numerical methods[31]. However, while in Fig.3b

clusters containing some 100 defects are visible at a density of about 3×10^{17} cm^{-3} the calculations for comparable irradiation conditions yield merely a small amount of di-interstitials or di-vacancies inside the capture volume of an observed cluster. This means that although agglomeration by the statistical effect at the high defect concentrations used in HVEM experiments cannot be completely excluded, the growth of clusters to the observed sizes cannot be explained this way.

Deduction of Activation Energies for Thermally Activated Diffusion from Interstitial Loop Growth

As shown in §2 theoretical expressions for the saturation concentration of interstitial loops C_L^∞ have been developed for the case where vacancies can be considered to be practically immobile. From a plot of observed C_L^∞-values versus irradiation temperature it should be possible to deduce E_M^I and in addition E_B if varying impurity contents are used. This method was applied to Ni doped with Si[9], and to Fe[7] and Au[6]. It requires that loop denudation at foil surfaces is taken into account carefully[32]. The reliability of the theory for the evaluation of data provided, the described method can be an interesting supplement to conventional ones in that it is capable to deduce effective migration energies for clustering which may be especially important for technological applications.

At high temperatures where also vacancies are mobile by thermally activated diffusion the time-independent loop growth rate (§2) in a sample which is sufficiently thick to neglect surface effects is proportional to $\exp(E_M^V/2kT)$[18]. This relation was used to estimate the effective vacancy migration energy from the observed temperature dependence of the growth rate[8]. The obtained values are smaller than those determined by conventional methods which presumably reflects a di-vacancy contribution to D_V. This is understandable if one considers the high defect concentrations used in the HVEM.

Dislocation Loop Growth During Annealing of Low-Temperature Irradiated Cu

By observing the growth of dislocation loops during in-situ anneal of a sample after low-temperature irradiation one may be able to contribute information for the understanding of annealing stages, in particular of stage III. Such a study is currently carried out on Cu[33]. Samples were irradiated at 10K to a total dose of 7×10^{19} e/cm^2 (650keV) which is too low to form visible clusters. During stepwise annealing dislocation loops become first visible at 50K. These loops, although not analyzed yet, are likely to be of interstitial type. Annealing further the loops become continuously larger (Fig.6a). The loop density increases up to about 150K and drops between 200K and 250K to a value of about 30% of that at 200K (Fig.6b). No gradual shrinking could be observed and the loops surviving the drop in density continued to grow. Stereo pictures revealed that about 50% of the vanishing loops lie within 20nm thick layers at foil surfaces. The drop in density is therefore attributed to loop glide. It is presumed that loops are primarily formed as Frank loops which, due to image force interaction with surfaces, undergo a shear into glissile loops. At $T \gtrsim 200K$ the loops near surfaces reach the critical size for this shear. Subsequently they may, as frequently observed, slip out of the foil. Frank loops lying deeper in the foil experience smaller image forces due to the s^{-4} dependence of the latter (s-distance from surface). They therefore have a larger critical size and remain stable under the given conditions. Image force interaction has its parallel in loop-loop interactions in bulk material. It may therefore be presumed that loop glide processes also play a role in other experiments leading e.g. to coalescence of loops under suitable conditions. Contrast analysis was performed at 180K, 240K and 300K[34] and yielded for the ratio of interstitial to vacancy

loops 4:1, 8:1 and 13:1 respectively*. So far the observations have not yielded any evidence for onset of vacancy migration in stage III.

5. EXPERIMENTS ON THE INTERACTION OF POINT DEFECTS WITH SINKS

Interstitial and Vacancy Cluster Growth

It was already mentioned (§2) that the sink efficiency ratio $\gamma>1$ for dislocation loops, i.e. interstitials are there absorbed preferentially. The reason for this lies in the elastic interaction of point defects with dislocations. The case of an edge dislocation will be treated here. For an edge dislocation the energy due to first order size interaction is given by $U=A\sin\theta/r$ (Fig.7) where A is proportional to the volume misfit of the defect and therefore large and positive for interstitials and small and negative for vacancies. Thus interstitials are separated from vacancies in the stress field of an edge dislocation. Interstitials experience a large attractive (repulsive) force at the dilatation (compression) side of the dislocation while opposite smaller forces act on vacancies. The different size of the elastic interaction energy allows interstitial dislocation loop growth under steady state conditions.

Under suitable conditions also vacancy cluster (VC) growth can take place. We have to introduce a sink with $\gamma>\gamma^{VC}$ which determines $\bar{C}_I$ and $\bar{C}_V$ in the vicinity of the cluster. Taking into account that due to self-screening a small loop has at some distance a smaller stress field than a larger loop or a

---

* It should be mentioned, that some rare ion damage events, normally leading to vacancy clusters, cannot be excluded in HVEM irradiations.

straight dislocation one can expect that the former can grow in the stress field of the larger loop. A preferred place for nucleation would be the compression field of the larger loop because of the interstitial denudation existing there. This was verified in an experiment in Ni[15]: Large interstitial Frank loops were created by irradiation at a temperature too high for vacancy cluster nucleation. After re-irradiation at a lower temperature vacancy loops formed as expected at the inner periphery, i.e. at the compression side of the edge dislocations. If due to local stresses a Frank loop is converted into a glissile one which glides out of the foil the vacancy loops left behind shrink during further irradiation according to Eq.(5). Similar observations were made on quenched-in vacancy loops[7].

From observations in thin foils of Cu[30,33], Au[35,6], Pb[14] it was deduced that interstitials are also absorbed preferentially at free surfaces[14]. In low-temperature irradiated Pb, for example, interstitial loops grow temporarily according to the relations given in §2 but shrink again in a later stage while vacancy SFT grow (due to radiation-induced diffusion). Two processes may be responsible for preferential loss of interstitials at surfaces: (i) Interaction of defects with surfaces via image forces. This should, due to the larger stress field of the interstitial, be greater for interstitials than for vacancies. (ii) Long-range propagation of interstitials by replacement collision sequences in the defect creation event. If such a sequence is terminated at the surface only a vacancy is created in the sample by a collision event.

Using a similar equation as Eq.(3) and Eq.(4) we get for the net rate of vacancies arriving at a stacking-fault tetrahedron

$$dN_V/dt = D_V\bar{C}_V k_V(1 - \gamma^{VC}/\gamma^S) \qquad (6)$$

and growth if $\gamma^S > \gamma^{VC}$. Elastic interaction of defects with surfaces is certainly weaker than with a SFT stair-rod dislocation. Therefore only replacement collision sequences can

create enough interstitial denudation to get a positive growth rate since they cause different creation rates for vacancies and interstitials*. γ^{VC} increases during growth of the SFT from nearly 1 (due to self-screening of the very small cluster) to the γ of a single stair rod dislocation. According to Eq.(6) growth ends when $\gamma^{VC}=\gamma^{S}$. This allows to express γ^{S} in terms of the sink efficiency ratio of a SFT of the limiting size.

The Stacking-Fault Tetrahedron Lattice

Recent HVEM work showed that in Au[35] and Cu[36,30] SFT form arrays along <100> directions resulting under suitable conditions in the formation of a SFT lattice. To clarify nucleation and growth in this lattice an investigation was carried out in Cu. There are the most important observations: (i) SFT grow with high ordering tendency in thin foils where no dislocations as interstitial absorbing sinks are present (Fig.8). (ii) In very thick foils SFT only grow near loops and show little or no ordering tendency. (iii) SFT belonging to a certain arrangement form one after the other. (iv) SFT reach a maximum size which depends on irradiation conditions (~20nm) and then no longer grow. The following model is able to explain these observations: The SFT grow in thin foils due to a preferential loss of interstitials at surfaces. Far away from the surfaces (in thick foils) this effect cannot supply sufficient interstitial denudation and SFT only grow near dislocations. The foil surfaces provide only a limited interstitial denudation. Therefore nucleation is favoured in places where additional denudation due to dislocation-point defect interaction occurs. This is the case near a SFT nucleated and grown earlier. As illustrated in Fig.9 the stair-rod edge dislocations create at

---

* To stay within the formalism of §2 γ^{S} is taken to be > 1 but is now a correction factor to fulfil Eq.(4) near the surface.

their compression side due to elastic interaction a zone of low interstitial concentration. The concentration is lowest in a plane perpendicular to the Burgers vector containing the dislocation line. This favours nucleation and growth of SFT in rows extending along <100> directions. The interstitial screening effect can however only occur after the elder tetrahedron has reached a certain minimum size which explains that the SFT grow one after the other. As observed the inter-tetrahedron distance should be in the order of magnitude of the SFT diameter. Otherwise the effects of the 6 stair-rod dislocations of a SFT would partly cancel out.

REFERENCES

1. M. J. Makin, Phil. Mag. 18, 637 (1968).
2. O. S. Oen, ORNL Report 4897 (1973).
3. S. B. Fisher, Rad. Eff. 14, 171 (1972).
4. L. M. Brown, A. Kelley, R. M. Mayer, Phil. Mag. 19, 721 (1969).
5. A. Bourret, phys. stat. sol. (a) 4, 813 (1971).
6. N. Yoshida, M. Kiritani, J. Phys. Soc. Japan 35, 1418 (1973).
7. N. Yoshida, M. Kiritani, F. E. FUJITA, J. Phys. Soc. Japan, in press.
8. M. Kiritani, N. Yoshida, H. Takata, Y. Maehara, J. Phys. Soc. Japan 38, 1677 (1975).
9. M. K. Hossain, L. M. Brown, in High-Voltage Electron Microscopy, p. 360, Academic Press: London, New York, 1974.
10. N. Yoshida, K. Urban, to be published.
11. M. J. Makin, Phil. Mag. 20, 1133 (1969).
12. J. V. Sharp, AERE Report 6267 (1969).
13. S. J. Rothman, N. Q. Lam, R. Sizmann, H. Bisswanger, Rad. Eff. 20, 223 (1973).
14. K. Urban, A. Seeger, Phil. Mag. 30, 1395 (1974).
15. K. Urban, M. Wilkens, in Electron Microscopy and Structure of Materials, p. 929, Univ. Cal. Press, 1972.
16. W. Bauer, A. Sosin, J. Appl. Phys. 35, 703 (1964).
17. P. Jung, R. L. Chaplin, H. J. Fenzl, K. Reichelt, P. Wombacher, Phys. Rev. B8, 553 (1973).
18. K. Urban, phys. stat. sol. (a) 4, 761 (1971); K. Urban, M. Wilkens, phys. stat. sol. (a) 6, 173 (1971).
19. B. L. Howe, Phil. Mag. 22, 965 (1970).

20. R. V. Jan, A. Seeger, phys. stat. sol. 3, 465 (1963).
21. H. Wollenberger, J. Wurm, phys. stat. sol. 9, 601 (1965).
22. K. Lücke, G. Roth, H. Wollenberger, Ch. Zeckau, unpublished.
23. H. Schroeder, Thesis T. H. Aachen (1974).
24. A. Wolfenden, Rad. Eff. 21, 197 (1974).
25. H. M. Simpson, R. L. Chaplin, Phys. Rev. 185, 958 (1969).
26. L. E. Thomas, Rad. Eff. 5, 183 (1970).
27. P. A. Doyle, Phil. Mag. 29, 537 (1974).
28. A. Cordier, A. Degeith, F. Garat, F. Reynaud, Rad. Eff. 17, 127 (1973).
29. K. Urban, phys. stat. sol. (b) 49, K1 (1972).
30. K. Urban, W. Jäger, phys. stat. sol. (b) 68, K1 (1975).
31. G. Lück, R. Sizmann, phys. stat. sol. 6, 263 (1964).
32. M. J. Goringe, Rad. Eff. 10, 169 (1971).
33. W. Jäger, K. Urban, Proc. Int. Congr. HVEM Toulouse 1975, in press.
34. W. Jäger, to be published.
35. M. O. Ruault, B. Jouffrey, Appl. Phys. Let. 25, 265 (1974).
36. N. Yoshida, M. Kiritani, J. Phys. Soc. Japan 38, 1220 (1975).

Table. Results of HVEM experiments to determine displacement threshold energies

$\acute{E}_d$ - values (eV)

	<110>	<100>	<111>
Cu[1]	19	22	27
Ni[5]	23	31	28
Ni[18]		23	
Co[19] (fcc)	23	30	
(hcp)	23 <1120>	30 <1010>	33 <0001>

E_d - values (eV)

	<110>	<100>	<111>
Ni[5]	21	38	>60

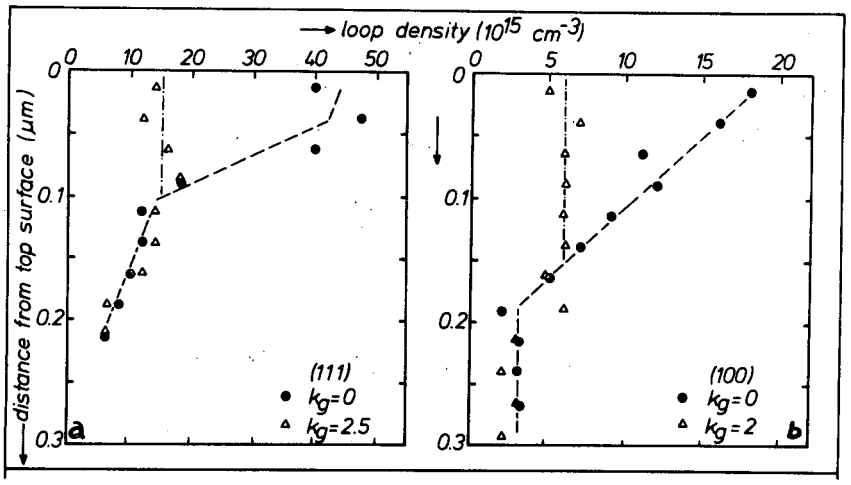


Fig.1 Loop depth distribution in Cu irradiated with 650keV electrons at 55K. Beam ● parallel, ▲ tilted 0.7°(a),0.75°(b)

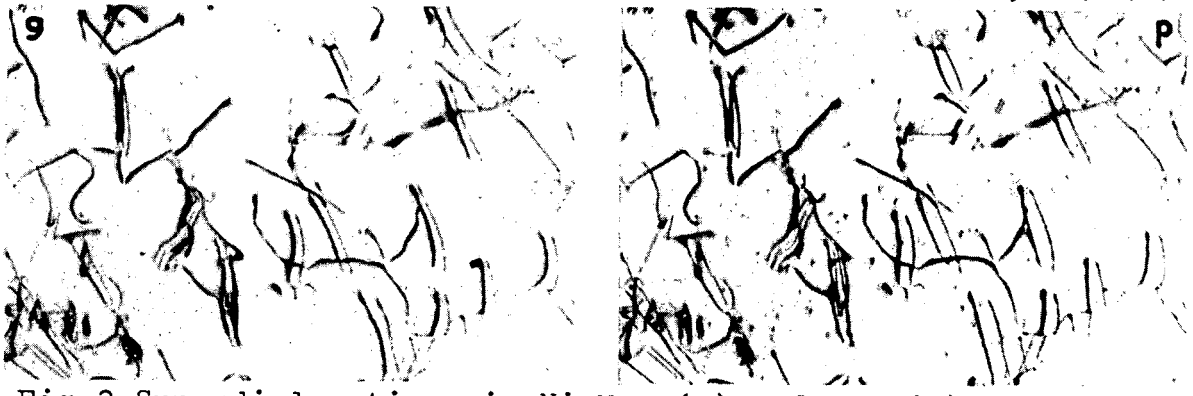


Fig.2 Superdislocations in Ni_3Mn; (a) before, (b) after irradiation with 1.2MV electrons (∥ to <138>).From[28].

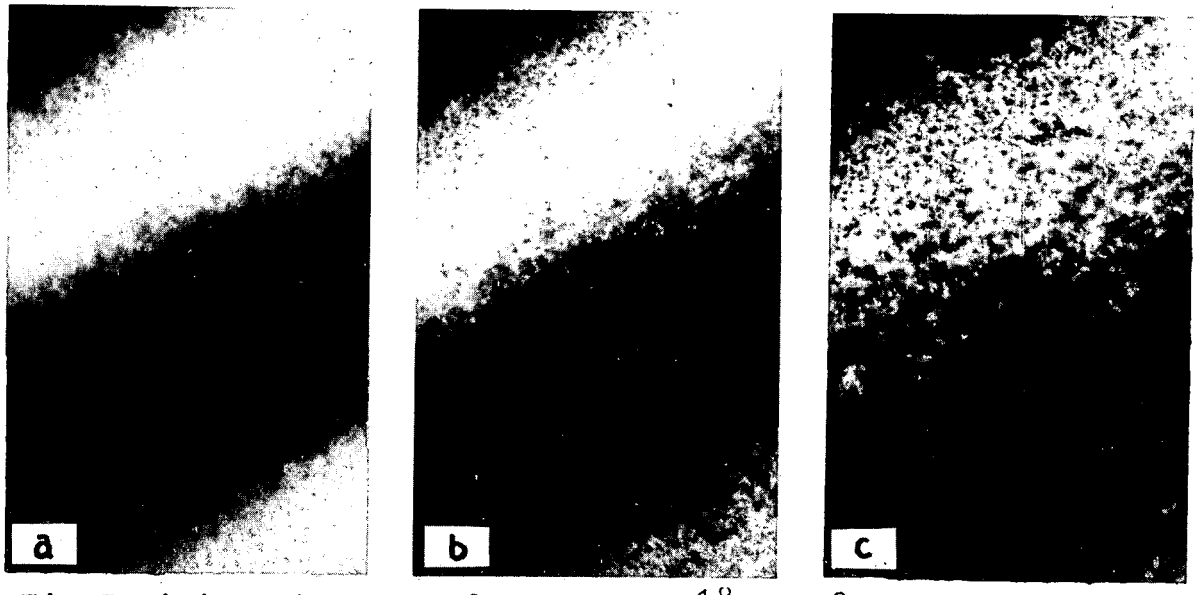


Fig.3 Ni irradiated at 8K with $4x10^{18}$e/scm^2. After 105s (a), 220s(b), 300s(c).

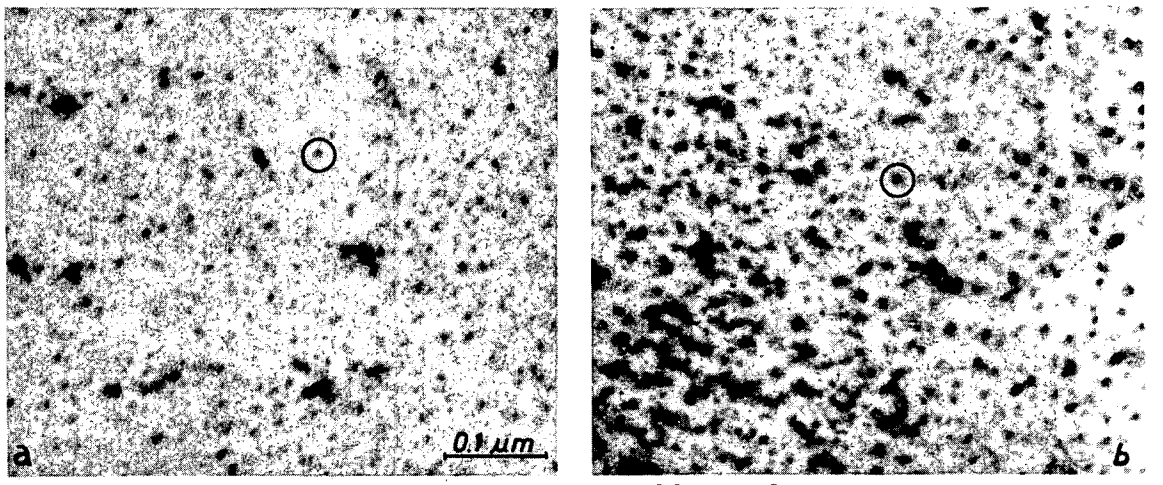


Fig.4 Pb pre-irradiated with $2x10^{22}e/cm^2$(630keV) at 58K. (a)before,(b)after sub-threshold irrad.w.$2x10^{22}e/cm^2$ (390keV)

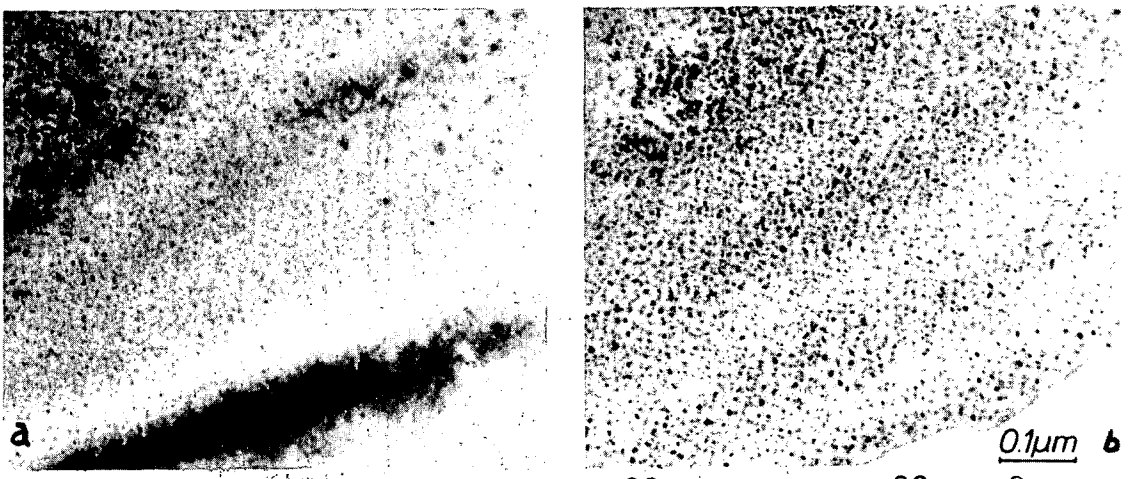


Fig.5a Pb pre-irradiated with 10^{22}(**right**)-$3x10^{22}e/cm^2$ (left side) (630keV) at 58K. (a) at 58K, (b) at 300K.

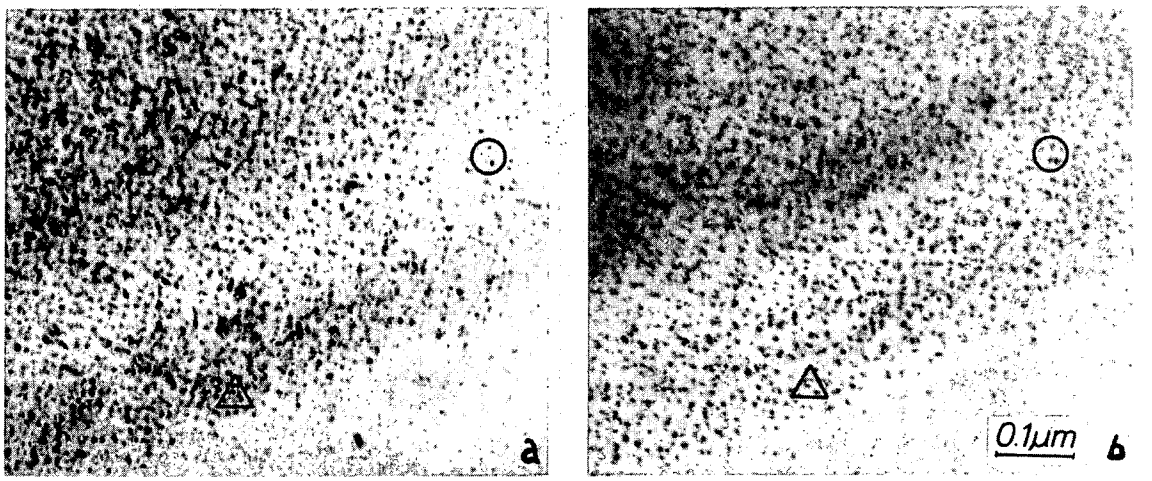


Fig.5b Same sample as in Fig.4 at (a) 58K, (b) 300K.

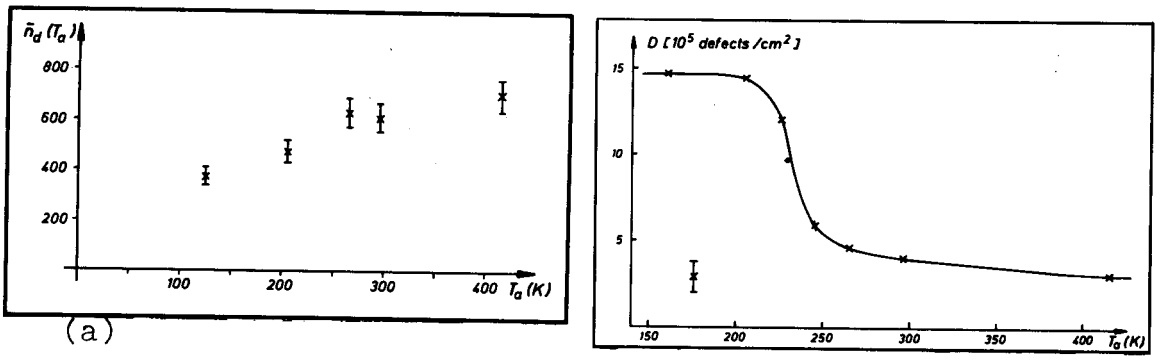


Fig.6 Annealing of 10K-irradiated Cu: Mean number of interstitials per loop (a) and loop density (b) at the indicated annealing temperature.

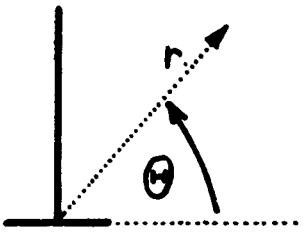


Fig. 7

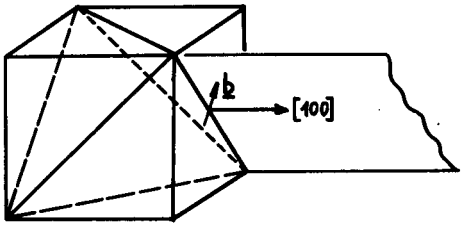


Fig. 9

(see text)

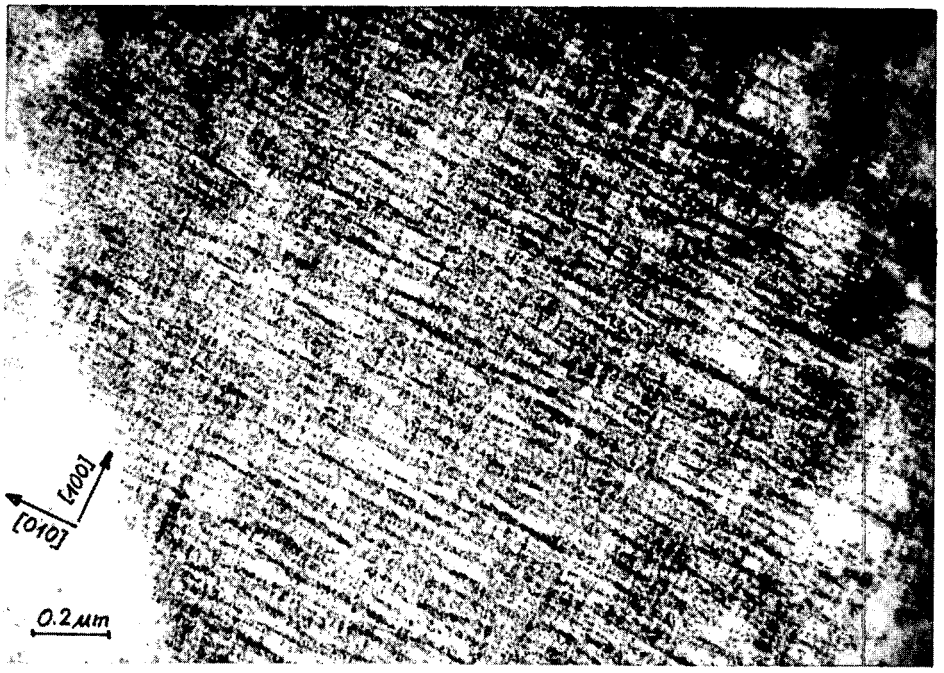


Fig.8 Stacking-fault tetrahedron lattice formed in Cu irradiated at 300K with 5×10^{19} e/scm^2 (1MeV) for about 30min.

ELECTRON RADIATION DAMAGE OF METALS AND NATURE OF POINT DEFECTS BY HIGH VOLTAGE ELECTRON MICROSCOPY*

M. Kiritani
Department of Material Physics
Faculty of Engineering Science, Osaka University
Toyonaka, Osaka, Japan

ABSTRACT

The formation of point defect clusters by electron irradiation in a variety of metals (Al, Au, Cu, Fe, Ni, Mo, Pt, W) in a wide range of temperatures 10-1000 K are observed. A unified explanation is given for their nucleation and growth from the view point of the migration and interaction of point defects. The effect of free surfaces and other permanent sinks are examined.

Analysis of the systematic variation of the nucleation of interstitial clustered defects lead to confirm the free migration of interstitials with fairly small activation energies. Their apparent values obtained from the impurity sensitive nucleation at medium temperatures are 0.08 (Al), 0.19 (Au), 0.26 (Fe), 0.18 (Mo) and 0.21 eV (W), and their values obtained from low temperature irradiation are 0.03 (Al), 0.04 (Au) and 0.05 eV (Mo). The trapping of interstitials by foreign atoms and heterogeneous effect on nucleation of interstitial clusters are discussed.

The observed linear growth behaviour of interstitial type dislocation loops at high temperatures is found to be controlled by the migrational nature of vacancies. A method for obtaining the activation energy for vacancy motion is presented. Conditions for vacancy cluster formation are investigated.

A variety of phenomena related to the electron radiation induced diffusion of point defects has been observed. The mechanism of the induced diffusion is quantitatively discussed, and the extent of the effect was found to be similar between vacancies and interstitials. More effect is expected for heavier elements from medium energy electrons.

The existence of the directional flow of interstitials along the dilatation strain field gradient is demonstrated.

---

*A review of works by the author with N. Yoshida (presently at Max-Planck-Institute, Stüttgart), H. Takata (Osaka University, Osaka) and Y. Maehara (Sumitomo Metal Ind. Ltd., Amagasaki).

INTRODUCTION

Recently developed high voltage electron microscopy is now serving as a powerful method to study the elementary process of radiation damage and to disclose a wide variety of phenomena related to the aggregation process of radiation induced point defects. In this paper efforts will be made to obtain systematic knowledge of radiation induced defect sturctures organizing the difference and similarity of phenomena occuring in a variety of metals over a wide range of irradiation conditions. From the analysis of the observed variation of the defect structure development, the problems concerning the fundamental properties of point defects, especially of interstitial atoms, will be elucidated.

EXPERIMENTAL TECHNIQUES

Microscopy and Specimen Temperature Controll

A high voltage electron microscope HU-2000 with its maximum acceleration voltage of 3000 kV was used for the introduction of damage structures and for observations. The irradiation intensity was measured with a Faraday cage located between the projection lens and the fluorescent screen, and its range used was from 10^{17} up to 5×10^{19} electrons/cm^2.sec.

With heating and cooling stages with universal tilting devices, specimens could be heated up to 1000 K and cooled down to 7 K. The temperature of a specimen was measured with a fine thermocouple spot-welded on a metal block which is united with the specimen. Although it was easy to maintain the measured temperature within one degree of each desired one, the another importance is the extent of the local heating of a specimen by the electron beam. The extent of the local heating measured with the local difference of the speed of known thermally activated process, in a thermally good conductive metals, was several to 20 degres depending on the irradiation condition.

Specimens

Purity and treatment before the preparation of electron microscope specimens are as follows. The data in the parentheses are the source of

each material, nominal purity and in some metals the measured value of the ratio of the resistivlity at room temperature to that at liquid helium temperature. Aluminum (Sumitomo Chemicals,99.994% and Zone-refined, 13000) was annealed in air at 600°C. Rolled sheets of gold (Johnson Mathey Chemicals, 99.999% and Sumitomo Metal Mining, oxidation purified by Takamura's Lab., Kyoto Univ., 6000) was annealed in air at 800°C. Sheets of copper (JMC, 99.999%), sheets of nickel (JMC,99.998%) and sheets of platinum (JMC, 99.998%) were annealed in vaccum of 10^{-6} Torr at 700, 1000 and 1200°C, respectively. Molybdenum (Material Research Corp., 99.992%, 1700 and Kimura's Lab., Tohoku Univ., >8000) was treated in hydrogen at 1000°C. Tungsten (MRC, 99.97%) was annealed at 1300°C in vaccum of 10^{-8} Torr. Iron rod (JMC, 99.999%) was cold rolled and decarburized at 700°C. For three metals, Al, Au and Mo, two different purities were compared. The first and the second in the above list of each metal are lower and higher purity, respectively, and will be denoted by (L) and (H) in the text when needed.

All the microscope specimens were prepared by electrolytic polishing. Efforts were made to have smoothly tapered specimen edges at which quantitative experiments could easily be performed.

GENERAL MORPHOLOGY AND NATURE OF DEFECTS

At high temperatures, at which vacancies move thermally very fast, dislocation loops of interstitial type which successively nucleated during irradiation develop into well defined shape. In face-centered cubic metals the loops are faulted type on (111) planes, and they are often unfaulted and glide out of specimen during irradiation. The basic shape is hexagonal surrounded by [110] directions, and sometimes exhibit roundish shape depending on the irradiation condition. Multiple layer loops are often observed, and the second loop tends to be triangular reflecting the difference in the core structure of dislocations. In body-centered cubic metals, no such general rule on the morphology was found; the loops in iron are on (100) planes, whereas the loops in molybdenum are on (111) planes. No vacancy type defect was observed at these high temperatures.

At medium temperatures, at which vacancies move but not violently, the interstitial type defects become to have complicated shape by the absorption of vacancies. They are often segmented into many pieces during their growth. The another cause for the complication of the shape comes from the directional interaction of an edge dislocation to interstitial atoms. At these medium temperatures vacancies can form their own clusters especially when they are accumulated by the local consumption of interstitials. For example, in a very thin foil and in a specimen with high density of dislocations, no interstitial cluster formation takes place and gradual formation of vacancy clusters are observed.

At low temperatures, at which thermal motion of vacancies are entirely prohibited, primarily formed defects are high density of interstitial type and accumulated vacancies in later stage of irradiation sometimes destroy the interstitial type defects and form their own clusters by radiation induced diffusion.

NUCLEATION OF INTERSTITIAL CLUSTERS

Nucleation Time

At low temperatures at which vacancies do not thermally move fast, the nucleation of interstitial clusters ceases within a very short period at the beginning of irradiation. At elevated temperatures at which vacancies can move thermally fast, continuous nucleation during irradiation was observed. At intermediate temperatures between the above two some clusters nucleate at the beginning of irradiation and additional clusters appear continuously during the contiuned irradiation. Figure 1 is a typical example of these three cases observed in molybdenum and Fig. 2 is the collected result for various metals.

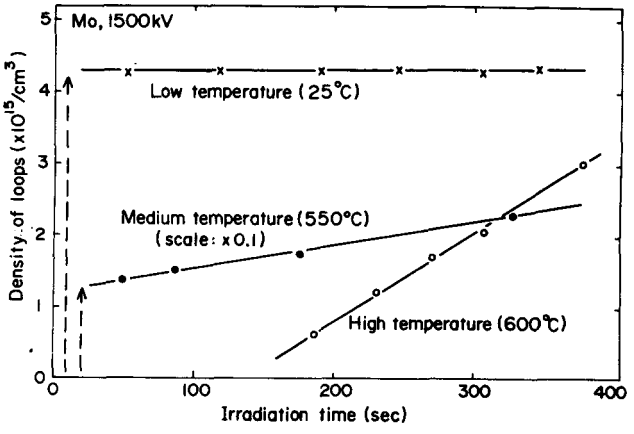


Fig. 1 Three characteristics of the interstitial cluster nucleation in molybdenum.

Here the idea and method for acquisition of density data used in this paper should shortly be described. The always existing defect free layers along the specimen surfaces could be eliminated by adopting, as the volume density of defect clusters, the gradient of the linear part in the counted areal density of the defects against the increase of the specimen thickness. This method might be called 'Thickness gradient method'.

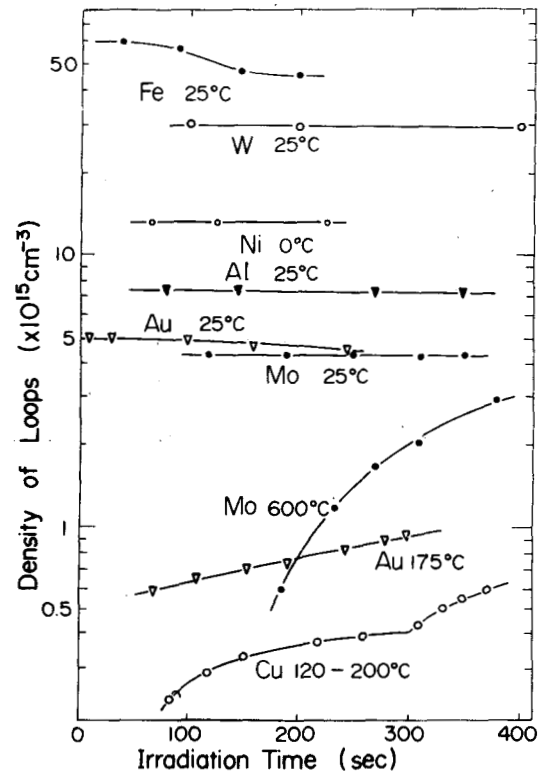


Fig. 2 Variations of the number of interstitial clusters during steady irradiation.

Low Temperatures

At low temperatures at which vacancies can hardly move, the variation of interstitial concentration under steady irradiation of the point defect pair production rate P is approximated by

$$dC_I/dt = P(1-C_V)(1-Z_{IV}C_V) - Z_{IV}M_IC_VC_I - Z_{II}M_IC_I^2 - Z_{IL}M_I\sqrt{C_LC_{IL}} - M_IC_SC_I, \quad (1)$$

where M_I is the interstitial mobility and Z's are the site numbers of spontaneous reaction of each process. The formation rate of interstitial clusters C_{IC} is given by the third term when di-interstitials are adopted as the nucleus. The forth term is the rate of the absorption of interstitials to the interstitial loops, where C_L is the concentration of interstitials which have already been absorbed to the loops. The last term is the escape of the interstitials to permanent sinks C_S such as specimen surfaces. The corresponding variation of vacancies is simply given by

$$dC_V/dt = P(1-C_V)(1-Z_{IV}C_V) - Z_{IV}M_IC_VC_I. \quad (2)$$

At the beginning of the irradiation, interstitials and vacancies increase together by the same amount linearly with the irradiation time. In a very thin foil, the interstitials soon begin to escape to the foil surfaces and keep a constant level for a certain period and start to decrease, when vacancies become more effective than surfaces, whereas the vacancies still increase as shown in a computer simulation of Fig. 3. This interstitial level in a thin foil is usually not high enough to nucleate observable clustered defects. In thick foils on the other hand, the escape to the surface does not become effective and the accumulating vacancies become dominant sinks for interstitials. Then interstitial concentration begins to decrease while vacancies still continue to increase. In the later stage of irradiation, the decrease of the interstitial concentration is accelerated by the annihilation to the growing interstitial loops. The analytical approximation is summerized in Fig. 4 for three cases of permanent sink density, namely corresponding to thick, medium and thin foil cases. The observed early cessation of the interstitial cluster nucleation is well understood from the existence of the appreciable concentration of interstitial atoms only at the beginning of the irradiation.

The width of the defect free zones at the edge of the tapered specimen increases with increasing temperature as typically shown in Fig. 5 for gold. When we consider that the observed density of defect clusters deviates from the linear relation with the specimen thickness when the interstitials do not raise to peaks in Figs. 3 and 4, the criterion for

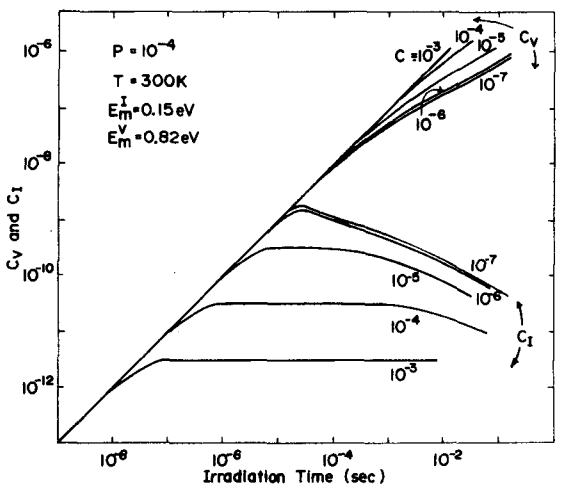


Fig. 3 A computer simulation of point defect concentrations for various foil thickness.

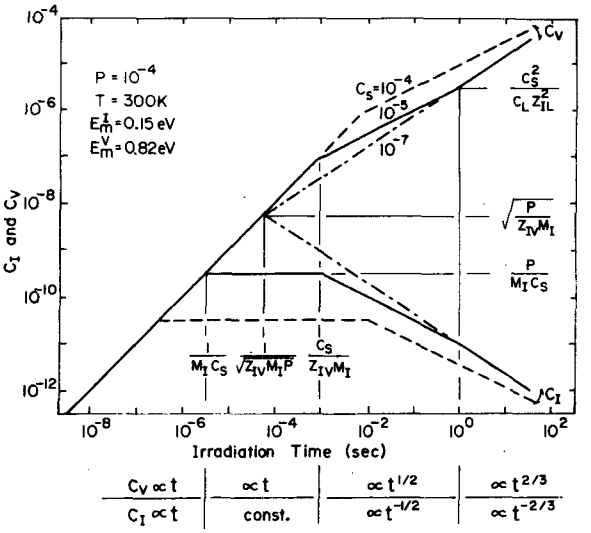


Fig. 4 Schematic deagram of the point defect concentration variations

the formation is obtained as $1/M_I C_S = C_S/Z_{IV}P$. The sink efficiency C_S of specimen surfaces are proportional to the square root of the foil thickness, and consequently the critical thickness for the formation of defect clusters becomes proportional to the one-forth power of the migrational activation energy of interstitials. Thus obtained value of migration activation energy of interstitials in gold was 0.12 eV as in Fig.5.

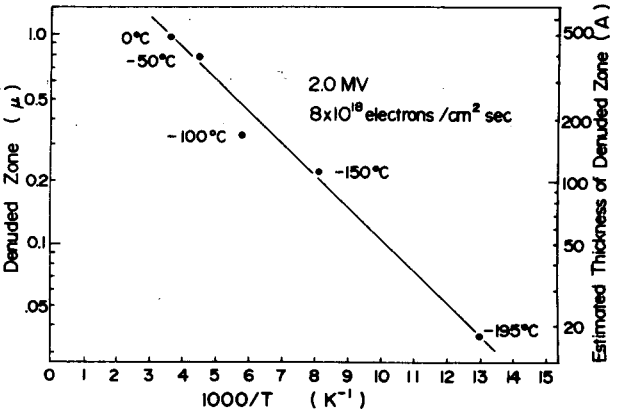


Fig. 5 Variation of the defect free zone thickness with irradiation temperature in gold.

When the di-interstitial is adopted as the stable nucleus of an interstitial cluster, the density of interstitial clusters which are nucleated through the above maximum is obtained by integrating the third term in Eq.(1) as

$$C_{IC} = \alpha P^{1/2} M_I^{-1/2}, \qquad (3)$$

where α is the constant of the order of unity which is determined by the combination of geometrical factors of reactions. Here the interstitial cluster density is proportional to the square root of the production rate P of point defects, which have been observed as a common rule in the irradiation intensity dependence in Fig. 6.

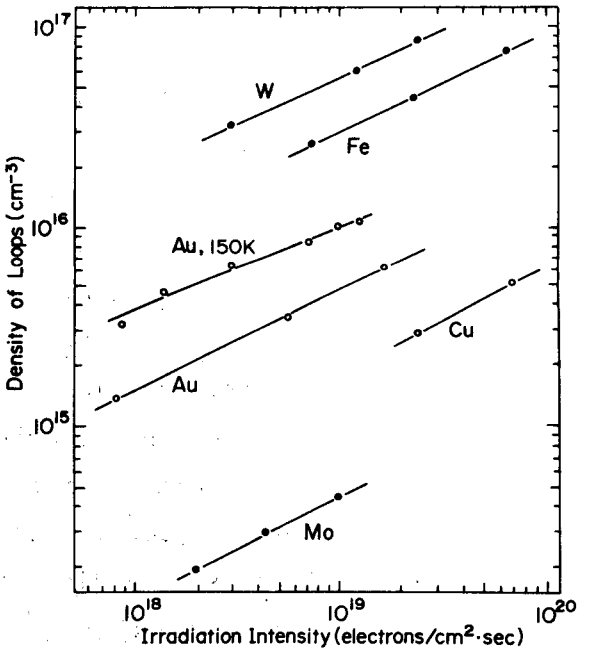


Fig. 6 Irradiation intensity dependence of interstitial cluster density. At room temperature, when not indicated otherwise.

The inverse proportionality relationship of the cluster density to the square root of the interstitial mobility M_I tells that the apparent activation energy in the experimentally obtained relation

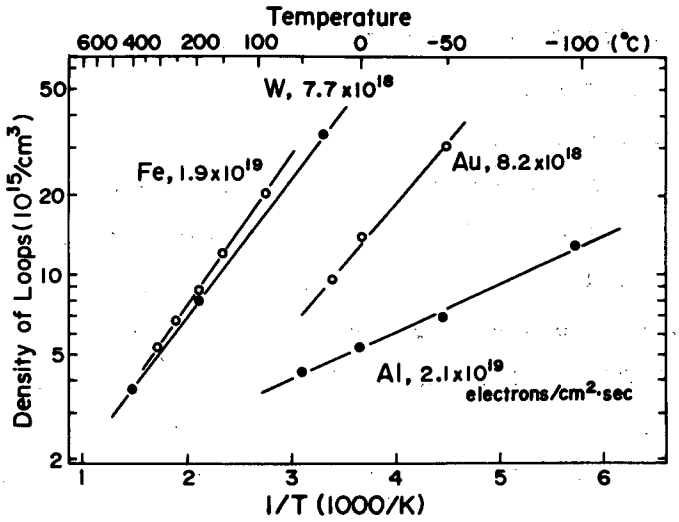


Fig. 7 Irradiation temperature dependence of interstitial cluster density at medium temperatures.

between the interstitial cluster density and irradiation temperature as in Fig. 7 is the half of the free migration activation energy of interstitial atoms. The energies thus obtained in Al, Au, Fe, Mo and W are 0.08, 0.19, 0.26, 0.18 and 0.21 eV, respectively. These values of the migration energy are fairly small, and the interstitials can migrate freely even at some lower temperatures.

Considering the purity of metals used in the present experiments, the obtained activation energy may correspond to the apparent activation energy of the migration of interstitial atoms through the trapping and detrapping by impurity atoms, which is typically the activation energy to release an interstitial atom from the impurity. Furthermore, the trapping of interstitials by impurities accelerate the interstitial cluster nucleation, and after an elaborate analysis, the temperature dependent part M_I in Eq. (3) was found to be simply replaced by M_B/C_{IM}, where C_{IM} is

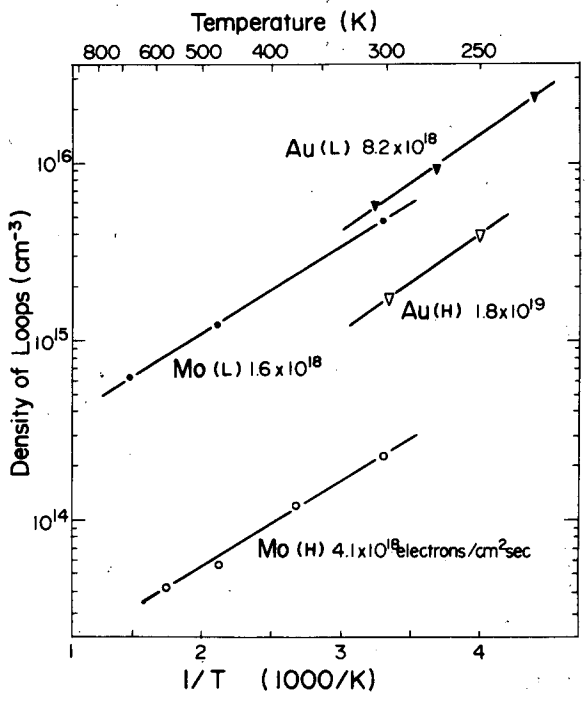


Fig. 8 Comparison of temperature dependence of the cluster formation between two purities.

the effective impurity concentration and M_B is the rate of release of interstitials from impurity atoms. One example which supports this thought is presented in Fig. 8 which compares the temperature dependence between two purities each of molybdenum and gold. The slope in the figure are quite similar between the two purities but the absolute values are quite different between the two for both metals. This tells us that the effective speed of migration of interstitials are different between the two purities because of the different number of trapping centers, but the temperature dependence of the migration speed is the same reflecting the same activation energy to make release the interstitials from impurities. Here it can be said at least that the intrinsic values of the free migration activation energies of interstitials are smaller than the above obtained values.

Medium and High Temperatures

When vacancies are mobile, they prevent the initial increase of interstitial concentration as is demonstrated in the simulation curves in Fig. 9, which is obtained by introducing the terms of reactions by vacancy motion into Eqs. (1) and (2). Vacancies soon become to maintain the balance with interstitial atoms, $M_V C_V = M_I C_I$. During this steady state of point defect concentrations, the observed continuous constant rate nucleation is thought to take place. At medium temperatures, the initial maximum of the interstitial concentration is still enough to afford to nucleate some clusters at the beginning of irradiation and continuous nucleation is followed.

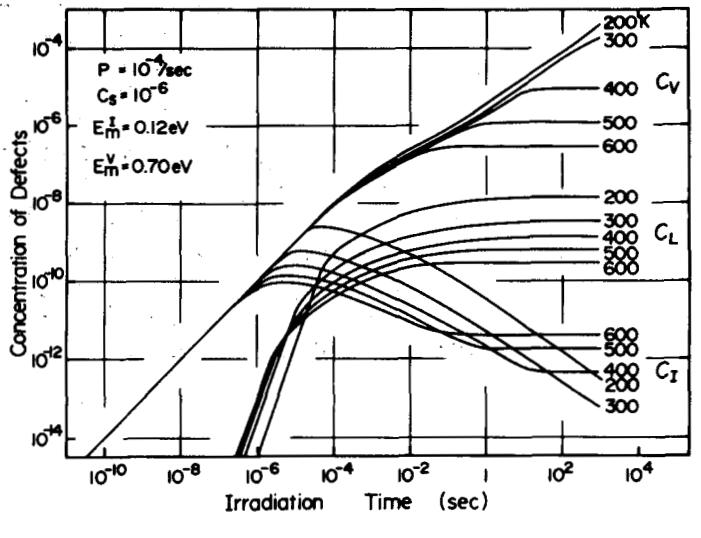


Fig. 9 A computer simulation of variations of point defect concentrations at various elevated temperatures.

Very Low Temperatures

Although the density of the clusters becomes extremely high at low temperatures and the accurate data is difficult to be obtained, the results shown in Fig. 10 show at least a large temperature dependence down to the lowest temperature examined. This result confirms the existence of the temperature dependent motion of interstitial atoms at such low temperatures. The case of iron which shows no variation under about 100 K is rather exceptional, and it agrees both with the high stage I recovery temperature of low temperature irradiated iron and also agrees with the large activation energy 0.26 eV obtained in the preceeding section. Electron radiation induced diffusion might be the main process to carry out the cluster formation at low temperatures in iron.

The density variation of defect clusters plotted against the reciplocal of the absolute temperature is again informative. Figure 11 is the result of three series of experiments on molybdenum, only one of which was carried out down to the temperature very close to that of liquid helium. Above 250 K three have the same slope of apparent energy of 0.09eV. The difference in the absolute value between the two series of high purity is due to the difference in the irradiation intensity. Much higher density in less pure specimen above 250 K was already discussed. The density does not vary between 250 K and 200 K, and again increases with a smaller slope of apparent energy of 0.025 eV.

The existence of the temperature region with no variation of the interstitial cluster density and the slow increase below these temperaturs

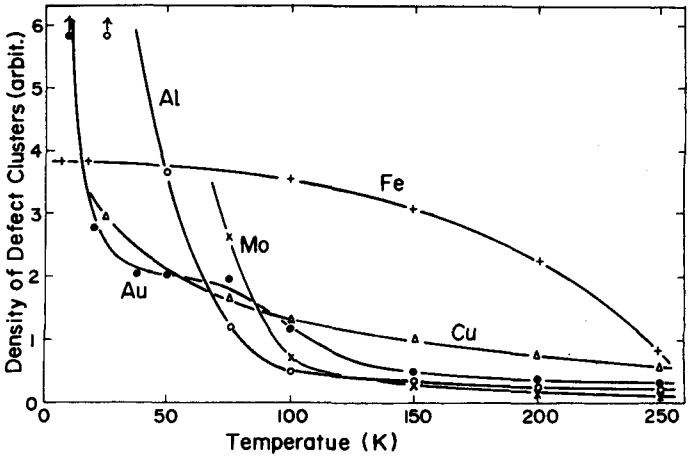


Fig. 10 Variations of interstitial cluster density in low temperature irradiated metals.

have been observed also for gold and aluminum and seems to be rather general. The result on gold in Fig. 12 indicates the no variation temperatures between 150 K to 200 K and the slope of about 0.02 eV. The corresponding values observed for aluminum was 100 K to 150 K and 0.015 eV.

The number of interstitial clusters formed with the aid of impurities increases with the decreasing specimen temperature, but it can not exceed the number of effective impurities and the density is thought to saturate to this level, and this saturation phenomena may correspond to the no variation region in the above experimental observations. At further low temperatures, the cluster density again increases by the slowing down of interstitial motion. Here the slope at very low temperature side still does not give the half of the migrational activation energy, because the high temperature side of this low temperature region is lifted to larger value by the effect of impurities. This means the value obtained from the apparent slope is the lower limit of the intrinsic values. Thus obtained lower limiting values of the migrational activation energy are 0.03eV for aluminum, 0.04 eV for gold, and 0.05 eV for molybdenum. Their higher limits obtained were 0.08, 0.19 and 0.18 eV, respectively. Of course the

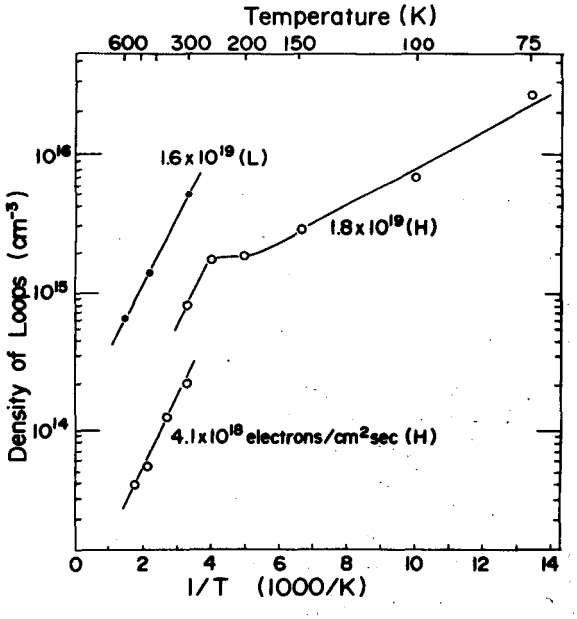


Fig. 11 Irradiation temperature dependence of interstitial cluster density in molybdenum at low temperatures.

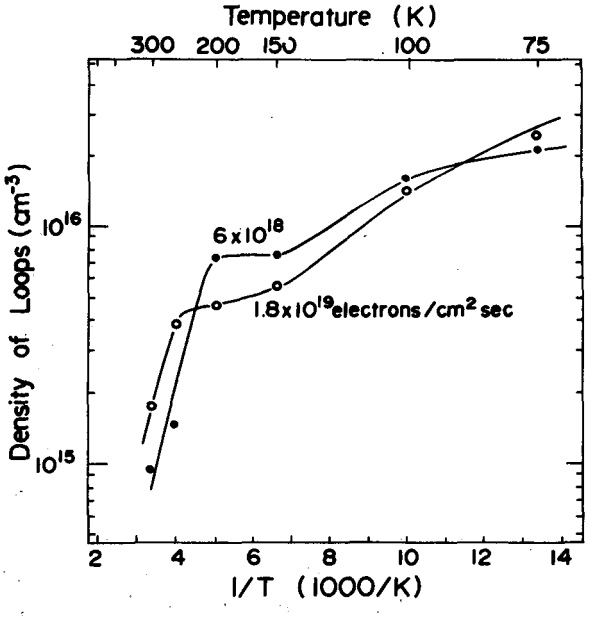


Fig. 12 Irradiation temperature dependence of interstitial cluster density in gold at low temperatures.

possibility of the very low temperature side to be still impurity sensitive with smaller bindings is not eliminated. Actually another temperature invariant nucleation has been observed for gold at temperature ranges between 35 K to 75 K. The value as small as 0.01 eV was obtained from the temperature dependence below 35 K.

GROWTH OF INTERSTITIAL CLUSTERS

Observed Characteristics

At high temperatures interstitial type dislocation loops grow into a well defined shape with smooth perimeters, and they grow linearly with the irradiation time. At intermediate temperatures, the loops become irregular in shape, partly because of the reaction of vacancies and partly because of the directional interaction between dislocations and point defects. At low temperatures, the growth speed of loops continuously slows down, typically the size increases with the cube root of the irradiation time. The examples of these characteristic natures of the loop growth are given in Fig. 13. The temperature at which each characteristic growth was observed was plotted against the migration activation energy of vacancies in Fig. 14, and the estimated jump frequencies around the border of the characteristic growth are also shown. The lower limit temperatures for the linear growth were found to be closely related to the vacancy mobility, namely the temperature of more than 100 jumps/sec of vacancy is required.

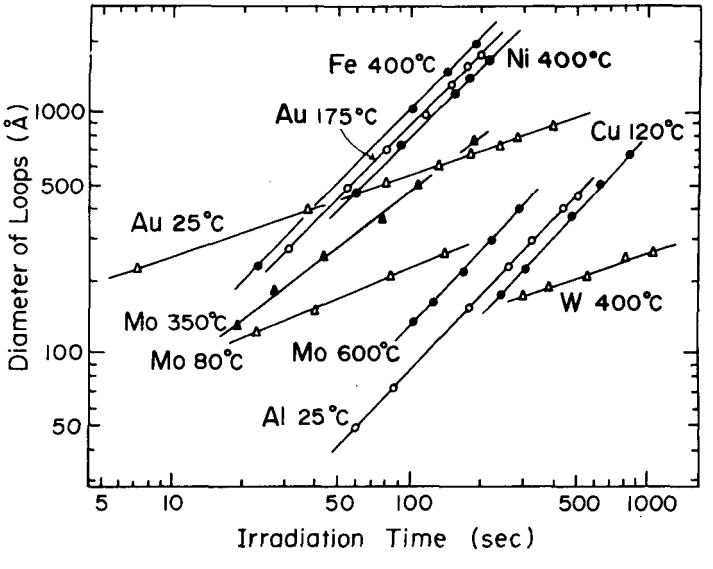


Fig. 13 Growth behaviour of interstitial type dislocation loops under steady irradiation in various metals at various temperatures.

Low Temperatures

As slready explained the concentration of interstitial atoms continuously decreases during constant irradiation at vacancy immobile temperatures, typically proportionally to $t^{-2/3}$, when the growing loops act as comparative effective sinks as the accumulating vacancies. The size of interstitial loops all of which nucleated at the beginning of the irradiation will be proportional to the integral of the interstitial concentration, namely proportional to the one-third power of the irradiation time. This growth rule was clearly observed in Fig. 13 for comparatively low temperature irradiation.

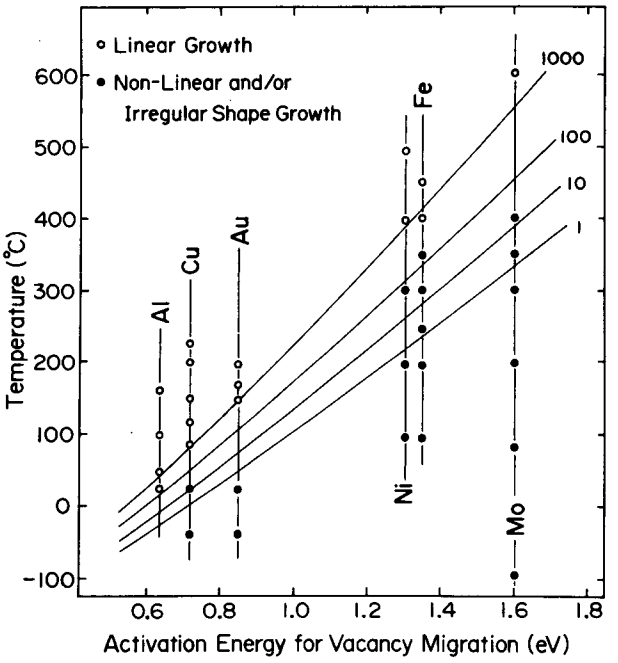


Fig. 14 Observed characteristic growth of dislocation loops classified with the mobility of vacancies. The numbers are the jump rates of vacancies.

High Temperatures

When vacancies have appreciable mobility, vacancies and interstitials soon become to maintain the mutual balance as already explained; the equality of the product of the concentration and mobility of each point defect will be established. Therefore the loops do not grow nor shrink, if the relation of interstitials to the loop dislocation is exactly the same as that of vacancies. As in the further discussion in another paper by the present author in this conference, intersitial atoms have a long range attractive interaction to an edge dislocation and consequently interstitials are absorbed in excess of vacancies, resulting the loop growth with a speed proportional to the saturated level of

$$M_I C_I = M_V C_V = Z_{IV}^{-1/2} P^{1/2} M_V^{1/2}. \qquad (4)$$

Here it should be noticed that the growth speed of interstitial clusters does not depend on the interstitial mobility M_I.

The square root dependence of the growth speed on the point defect production rate P in Eq. (4) was experimentally observed as the irradiation intensity dependence. Figure 15 is an example of the observed temperature dependence of the growth speed in copper for several loops situated at positions of different thickness of a specimen foil. The apparent activation energy obtained from the slope of the straight lines in the figure should correspond to the half of the activation energy of vacancy migration. The value 0.6 eV for copper seems to be a little too small for single vacancies. Further consideration which takes the role of divacancies into account brings the experimentally obtained value to the mathematical average value of the activation energies of single and divacancies.

The above saturation levels are for the thick foil in which the point defects of one kind operate as dominant sinks for the other kind of point defects. In a thinner foil in which the surface acts as dominant sinks, the saturation level is given by

$$M_I C_I = M_V V_V = P/C_S \qquad (5)$$

which has no temperature dependence. The border between the situations expressed by Eq. (4) and Eq. (5) is given by the critical thickness $h^* = a(M_I/4Z_{IV}P)^{1/4}$ where a is the atomic distance. The observed results in Fig. 15 show the temperature independent growth at thinner part at higher temperatures in good agreement with this thickness criterion.

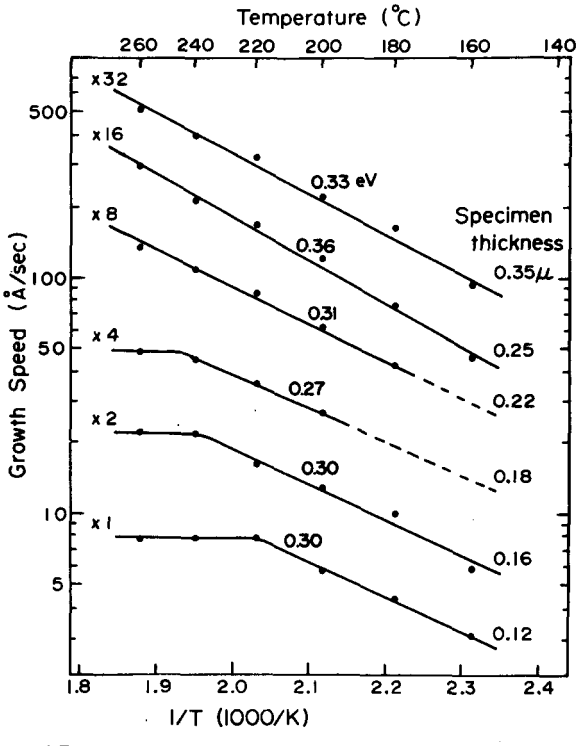


Fig. 15 Temperature dependence of the growth speed of loops in copper. 2000 kV, 1.6×10^{19} electrons/cm^2·sec.

FORMATION OF VACANCY CLUSTERS

As has been explained, vacancies have hidden important roles both in the nucleation and growth of interstitial type defects. Generally the accumulated vacancies work in the direction to suppress the nucleation and growth of interstitial clusters. These accumulated vacancies reveals themselves as their own clusters under some conditions.

When a high density of tangled dislocations is preliminarily introduced in a specimen by deformation, in some metals the damage structure development completely skips the stage of interstitial cluster formation, as the result of very effective disappearance of interstitials to dislocations. A typical example of the result of the local consumption of interstitials is shown for copper in Fig. 16. The growth path of interstitial loops is generally the place for preferential vacancy accumulation and often serves the sites for vacancy cluster formation.

Generally at the edge of an wedge shaped specimen, there exists interstitial loop free part due to the prompt escape of interstitials to the specimen surfaces. This thin part is one of the favoured place for vacancy cluster formation. Figure 17 is an example of nickel irradiated at 75°C.

Even in the case in which no clear vacancy clusters are observed during the irradiation, clear development of the clusters is observed after stopping the irradiation. An example of the shrinkage of interstitial loops and formation of vacancy clusters after irradiation was

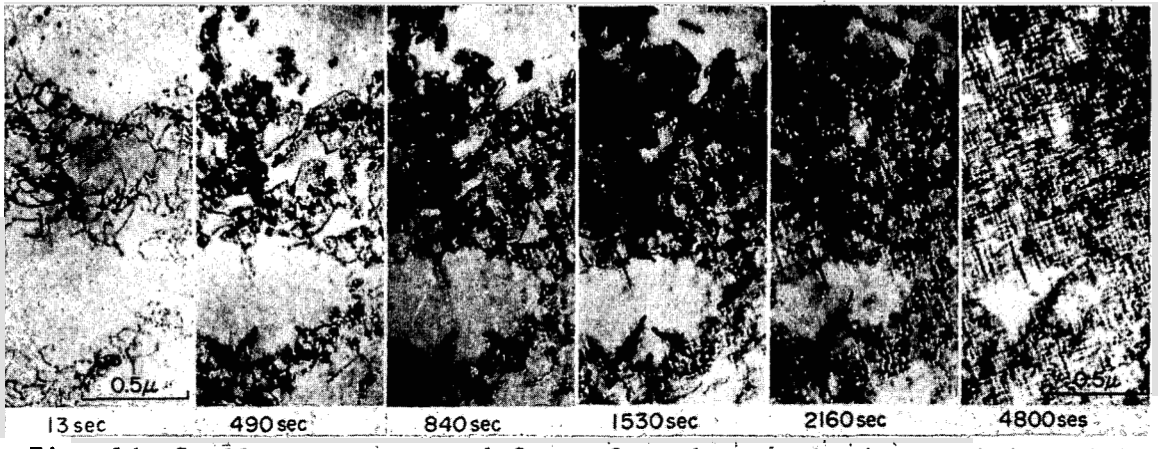


Fig. 16 Small vacancy type defects formed near the interstitial sinks in copper at room temperature. They develop into regular arrangement along [100]. 2000 keV, 1×10^{19} electrons/cm^2·sec.

presented in Fig. 18 for gold. The reason for the suppression of vacancy cluster formation during irradiation may be in the continuous destruction of small vacancy clusters by the absorption of interstitial atoms.

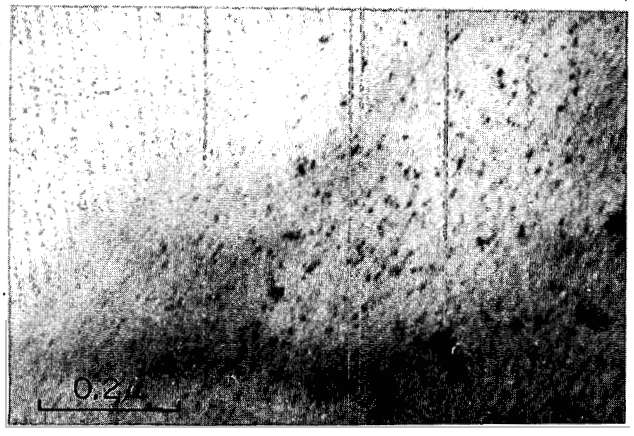


Fig. 17 Small vacancy clusters formed at thin part of nickel irradiated at 75°C. 2000 keV, $1x10^{19}$e./cm^2.sec, for 610 sec.

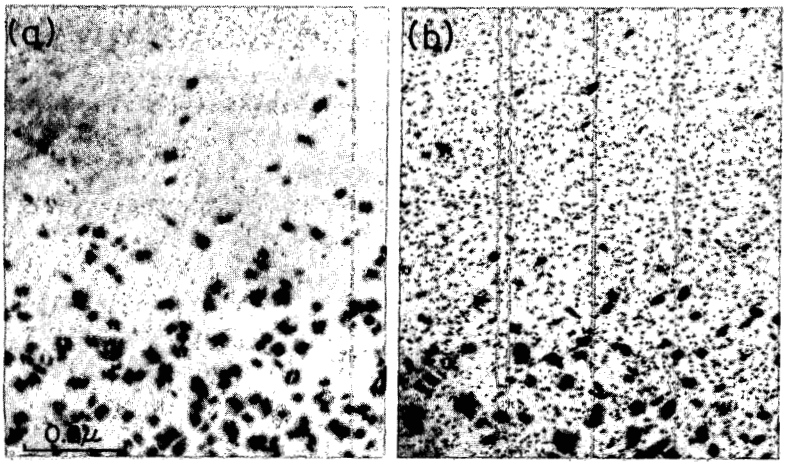


Fig. 18 Interstitial type defects in gold at room temperature, 2000 keV, $2x10^{19}$ e./cm^2·sec, 230 sec (a). Vacancy type defects, 600 sec after irradiation (b).

ELECTRON RADIATION INDUCED DIFFUSION

Displacements of point defects by the collision of electrons to atoms result in a quite similar phenomena as those by thermally activated diffusion of point defects. **The visible effect of the sub-threshold irradiation** in HVEM experiment was reported by Urban and Seeger (Phil. Mag. 30, 1395 (1974)). **It should be clarified how much extent of the effect of so called** radiation induced diffusion is included in the present experiment and discussions.

Experimental Coordination of Radiation Induced Diffusion

The phenomena which occur even when the irradiation experiment is carried out at low enough temperatures to stop completely the thermally

activated motion of point defects is obviously those by radiation induced effects. An example is the formation of small vacancy clusters at low temperatures at the interstitial cluster free part of thin specimen foil.

Figure 19 shows these clusters formed in gold at 250 K. The formation of these small clusters become detectable at around 200 K and becomes pronounced towards the room temperature at which vacancies in gold can thermally move. The same kind of vacancy reaction in platinum is shown in Fig. 20. In this case the vacancy acted to eliminate once formed interstitial clusters rather than their own cluster formation. This phenomenon was hardly detected at room temperature and becomes pronounced toward the vacancy mobile temperatures. The variation of the vacancy cluster formation in nickel has also the similar tendency as in gold and platinum.

Although the above results may suggest the existence of an appreciable temperature dependence of the radiation induced diffusion of vacancies, more detailed experiment should be carried out to eliminate the possibility of less accumulation of vacancies at lower temperatures. Another difficulty preventing the final conclusion for the temperature dependence is the overlapping effect of the thermal motion at higher temperatures.

A gold specimen was irradiated with the over-threshold electrons of 2000 keV at the lowest temperature achieved below 10 K, and was successi-

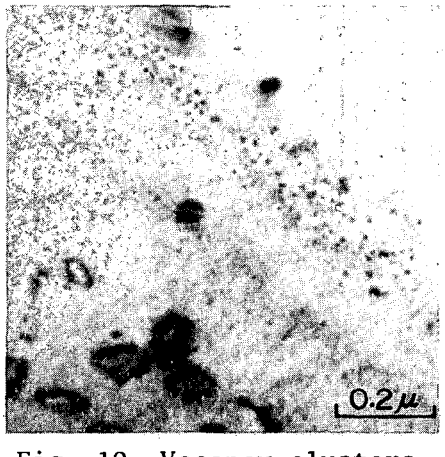


Fig. 19 Vacancy clusters formed at low temperature 250 K in gold. 2×10^{19} e./cm^2.sec, for 210 sec.

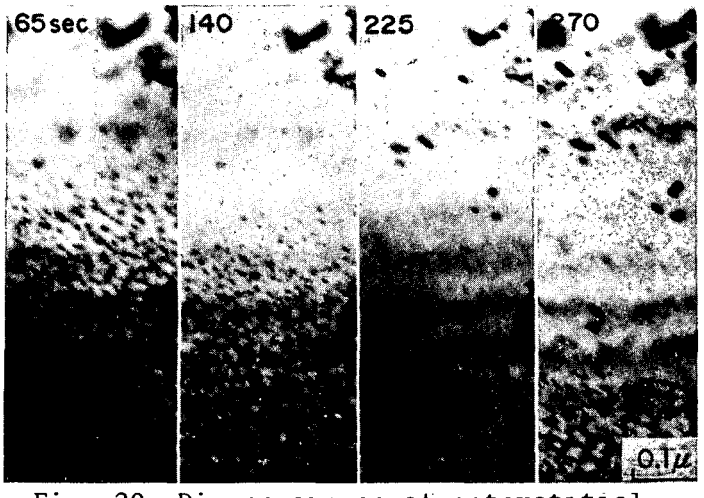


Fig. 20 Disappearance of interstitial clusters during irradiation of Pt. 2000 keV, 1.5×10^{19} e./cm^2·sec, at 200°C.

vely heated stepwisely and observed with the sub-threshold electrons of 1000 keV. Figure 21 is the result of observation at each temperature. The specimen was illuminated for several minutes at each step. The interstitial clusters started to disappear at around 200 K, which is much lower than the temperature for vacancy thermal motion. Finally almost completely disappeared, and small vacancy clusters revealed themselves. Another series of experiment, in which the illumination by 1000 keV electrons was continued at 200 K, showed that about 30 minutes is required for the completion of vacancy process. The radiation induced jump frequencies of a vacancy estimated from the time required for the process and the size and density of vacancy clusters was several jumps/sec for the irradiation intensity of 1×10^{19} electrons/$cm^2 \cdot sec$.

The large temperature dependence of the interstitial cluster nucleation at medium low temperatures are granted as the result of their thermally activated motion. The low dependence of the nucleation at lower temperatures could of cause be doubted to be resulted from the temperature dependence of the radiation induced motion of interstitial atoms. However, the large variation which still exists at very low temperatures as in Fig. 10 is difficult to be expected from the induced motion only. This point is still open for discussion.

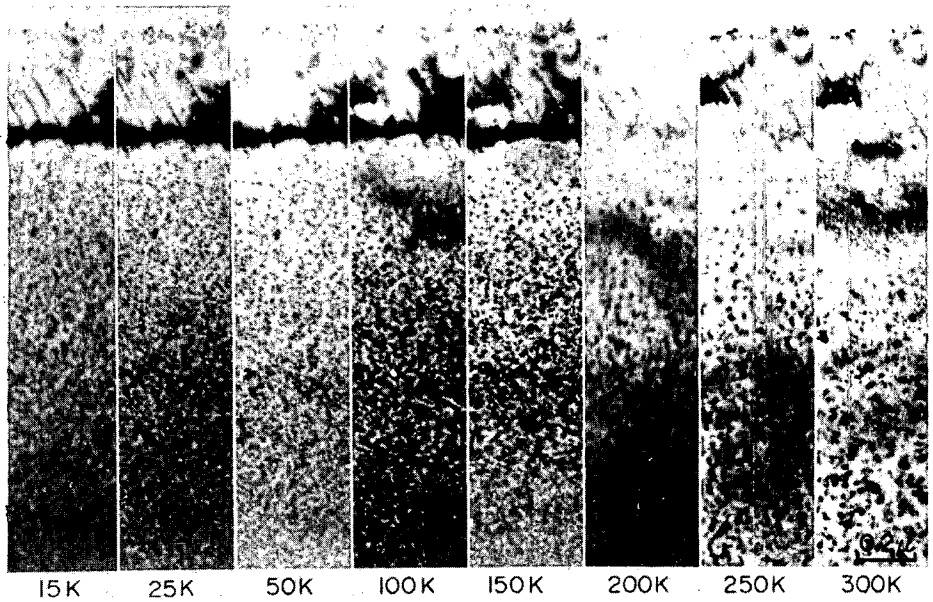


Fig. 21 Observation of the annealing of irradiated gold (2000 keV, 1.2×10^{19} e./$cm^2 \cdot sec$, 15 sec) with 1000 keV electrons. Annealed for 5 minutes at each temperature.

Theoretical Estimation of Radiation Induced Diffusion

The differential cross-sections of electron scattering which transfer the energy to an atom were multiplied by the number of the affected atoms, which is approximated by dividing the transfered energy by the migration activation energy of each point defect, and integrated over all the ranges of transfered energy. The effective number of jumps of a point defect could be obtained as the product of irradiation intensity and these total cross section by multiplying the number of atoms which results the displacement of a point defect. Typical examples of the number of displacements induced by 2000 keV electrons of 1×10^{19} electrons/cm^2·sec are listed in Table 1. The representative value is 1 jump/sec both for vacancy and interstitial atom. This direct process of induced effect is found to be generally larger for heavier metals.

The variation of the collision cross-section to induce point defect migration with the electron energy was calculated. Figure 22 is the example of the variation of collision cross-section to induce the vacancy migration for various metals. An intersting characteristics is the existence of the maximum of the effect, several times larger than that by 2000 keV electrons, at the medium acceleration voltage of the present state of high voltage electron microscopy.

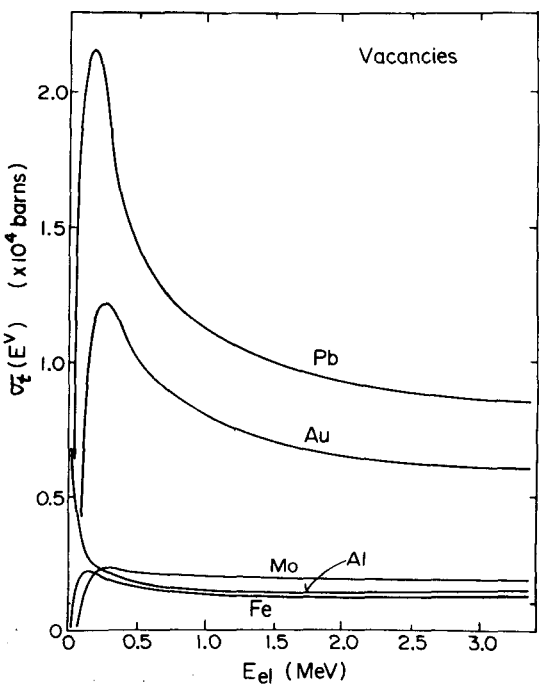


Fig. 22 Electron energy dependence of the total collision cross-section to induce the radiation induced motion of vacancies.

Table 1 Number of jumps (sec^{-1}) of a point defect by 2000 keV electron radiation of 1 x 10^{19} electrons/cm^2·sec.

Metal	Al	Fe	Cu	Mo	Au	Pb
Vacancies	0.51	0.27	0.75	0.35	2.1	3.4
Interstitials		0.44		1.0	2.0	

The ccoperative effect of the radiation induced diffusion with the thermal vibration of atoms was examined, but no pronounced temperature dependence was found. The effect of a large energy recoil was considered as the effect of local thermal heating, and the effect was also found to be much smaller than the above direct processes.

LONG RANGE INTERACTION BETWEEN POINT DEFECTS AND DISLOCATIONS

The necessity of the attractive interaction between the interstitial atoms and an edge dislocation was shortly mentioned to explain the interstitial type dislocation loop growth at high temperatures. The mechanism of this attractive interaction can be understood from the directional flow of interstitials along the gradient of the dilatation strain field. Microscopic evidences for this strong long range interaction will be presented in another paper in the present conference.

ACKNOWLEDGEMENTS

The author is grateful to Professors H. Fujita and F. E. Fujita for their continuous encouragements. He is also grateful to Messrs. K. Yoshida, M. Komatsu and T. Sakata for their help in operating the microscope.

REFERENCES

1) M. Kiritani and N. Yoshida, Crystal Lattice Defects 4, 83 (1973).
2) M. Kiritani, N. Yoshida and H. Takata, J. Phys. Soc. Japan 35, 306 (1973)
3) N. Yoshida and M. Kiritani, J. Phys. Soc. Japan 25, 1418 (1973).
4) M. Kiritani and N. Yoshida, J. Phys. Soc. Japan 36, 613 (1974).
5) M. Kiritani, N. Yoshida and H. Takata, J. Phys. Soc. Japan 36, 720 (1974).
6) Y. Maehara and M. Kiritani, Japan. J. appl. Phys. 14, 559 (1975).
7) M. Kiritani, N. Yoshida, H. Takata and Y. Maehara, J. Phys. Soc. Japan 38, 1677 (1975).
8) N. Yoshida, M. Kiritani, F. E. Fujita, J. Phys. Soc. Japan 39, 170 (1975).

IN-SITU ELECTRON IRRADIATION OF ALUMINIUM IN A 200 KV ELECTRON MICROSCOPE

H. Fischer, C. Gomez, M. Rühle, and J. Diehl
Max-Planck-Institut für Metallforschung,
Institut für Werkstoffwissenschaften,
Stuttgart, Germany

ABSTRACT

Polished aluminium foils were irradiated with electrons in a 200 kV electron microscope at temperatures between 150 K and 500 K. The radiation-induced defect clusters were analysed by means of TEM. Emphasis was put on the determination of the distribution of the defect clusters inside the foil. After irradiation at 150 K and 450 K the defect clusters are distributed homogeneously inside the foil. However, after room temperature (RT) irradiation nearly all defect clusters were situated in layers (thickness ~900 Å) near both foil surfaces. - The observations can be explained with the assumption that during the RT-irradiation a vacancy type defect (di-vacancy) has the highest mobility.

INTRODUCTION

In the literature several papers are published concerning in-situ irradiation of aluminium in an electron microscope (voltage $\geq$200 kV)[1-4]. The different authors obtained different and sometimes even contradictory results regarding the size, size distribution and the nature of the defects. Since the differences can not be explained[1-4] the experiments were repeated in this work. The experimental conditions were carefully controlled and the analysis of the radiation induced defects was performed as described by Wilkens[5]. Special emphasis was put on the determination of the depth distribution of the defects inside the foil.

EXPERIMENTAL DETAILS

Aluminium foils of different purity were annealed at 500°C and then polished electrolytically. The foils were irradiated with 200 kV electrons in a JEM 200A electron microscope. The beam current was measured with a Faraday cage, and could be varied between 1 and 20 A/cm^2. The irradiation temperature was adjustable between room temperature and 800 K. Low temperature irradiations (T_{irr}=150 K) were performed in a Hitachi HU 650 microscope at 300 kV. The beam current was 0.17 A/cm^2. - The Al foil was orientated in such a way that the direction of incidence of the electron beam was always parallel to [013] . The (200) reflection was dynamically excited.

EXPERIMENTAL RESULTS

In Fig.1 micrographs of Al irradiated at 150 K, 300 K and 450 K are shown.

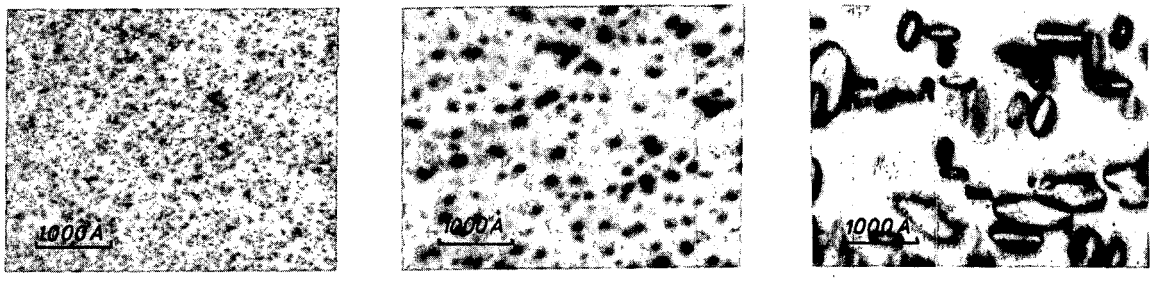


Fig.1.a. Fig.1.b. Fig.1.c.

Fig.1. 99.9999% Al irradiated with electrons.
Fig.1.a.: T_{irr}=150 K, $7 \cdot 10^{21}$ el/cm^2; Fig.1.b.: T_{irr}=300 K, $6 \cdot 10^{22}$ el/cm^2; Fig.1.c.: T_{irr}=450 K, $4 \cdot 10^{22}$ el/cm^2.

After room temperature (RT) irradiation with doses greater than $1.5 \cdot 10^{22}$ electrons/cm^2, small defect clusters were observable (black spots). The number density of defects (per unit area) was counted as a function of the foil thickness for a constant electron dose. After RT irradiation the

number density per unit area increased linearly up to a foil thickness of ~2000 Å. For thicker foils the density stayed nearly constant. In order to explain these observations the depth distribution of the defect clusters inside the foil was measured using the stereo technique[5,6]. In Fig.2 results are represented for 3 different foil thicknesses. Fig.2 shows that the distribution of the defect clusters inside the foil is not homogeneous. For foils with thicknesses smaller than ~2000 Å, the distribution curve shows one broad maximum (Fig.1.a.) whereas for larger foil thicknesses nearly all defect clusters are located in two layers

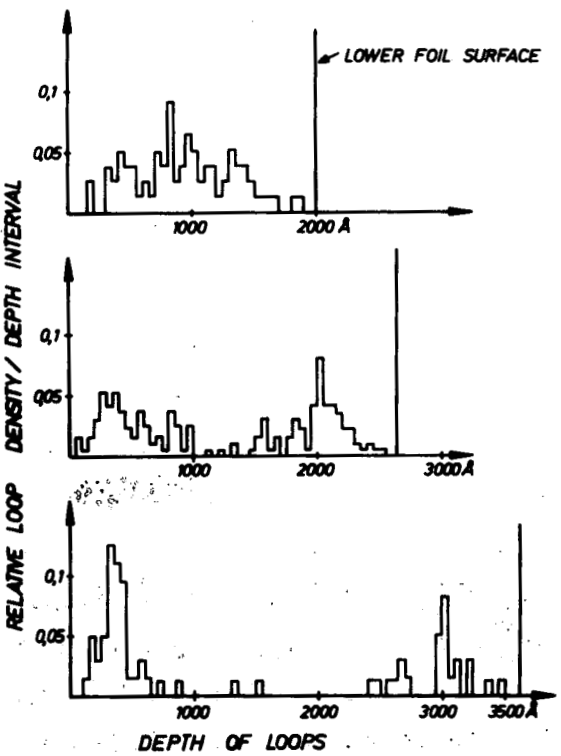


Fig.2.a.

Fig.2.b.

Fig.2.c.

Fig.2. Distribution of defect clusters inside an electron-irradiated foil of Al. RT irradiation. Direction of incidence [013]; g=(200) is exactly excited. Irradiation dose $5 \cdot 10^{22}$ el/cm^2. Foil thicknesses: Fig.2.a.: 2000 Å, Fig.2.b.: 2600 Å, Fig.2.c.: 3600 Å.

near both foil surfaces. The thicknesses of the layers after RT irradiation are about 900 Å. The distribution of defect clusters inside the foil was found to be independent of the purity of the material and of the different electron doses.

After irradiations at temperatures between RT and 400 K, besides the non-resolvable defect clusters large resolvable dislocation loops are also observed. In this range of irradiation temperatures, the thicknesses of the defect free layers near the surfaces as well as the thicknesses of the layers containing the defects increase. After irradiations at temperatures between 400 K and 500 K, only resolvable dislocation loops are observed which are homogeneously distributed in the foil. For $T_{irr} \gtrsim 500$ K no visible defect clusters are formed.

After irradiation at $T_{irr}=150$ K with $7 \cdot 10^{21}$ a high density of small black spots is observed. Stereo micrographs reveal that the black spots are distributed homogeneously throughout the foil.

The dependence of the defect density on the electron dose was independent of the electron flux for $T_{irr}=RT$.

The defect clusters formed after RT-irradiation showed, under dynamical imaging conditions, black-white constrast. From the properties of the contrast figures[5,6] it was determined that nearly all defects are Frank dislocation loops with a Burgers vector 1/3 ⟨111⟩. By quantitative evaluation of the stereo micrographs it can be concluded that in 99.9999% Al specimens nearly all defects are of the interstitial type, while in 99.99% Al specimens both interstitial and vacancy type defects are formed with about the same frequency. After irradiation at 400 K Frank dislocation loops and perfect dislocation loops are detected. The nature of the resolvable loops was determined by using the method described by Föll and Wilkens[7]. All the loops

in 99.9999% Al are formed by interstitial atoms.- The nature of the small black spots formed after irradiation at 150 K could not be analysed due to the very high density of defects.

DISCUSSION

Shirashi et al[2] and Kiritani et al[3] observed in electron-irradiated materials after RT irradiation large resolvable dislocation loops. In our observations those large loops are only formed if $T_{irr} > RT$. In Al an increase of T_{irr} during the RT irradiation can easily occur if the thermal contact between the specimen and the specimen holder is not good. Therefore, we assume that during the irradiation experiments of Shirashi et al[2] and Kiritani et al[3] the temperature of the specimen was raised.

In the following we discuss only the distribution of the defect clusters inside the foil for different irradiation temperatures, in a qualitative manner.-Our studies have shown (c.f. Fig.2) that after RT irradiation nearly all defect clusters are located in layers near both surfaces. These observations can either be artifacts caused by experimental conditions or effects caused by properties of the point defects created during the electron irradiation. Both aspects will be discussed.

Mackintosh and Brown[8] showed that during electropolishing of Al, the impurity atoms directly beneath the surface are displaced towards the center of the foil. After polishing, a high concentration of impurity atoms is then located near the polished surfaces. The impurity atoms could act in our irradiation experiments as nuclei for the interstitial clusters. To test the influence of the impurity atoms on the nucleation of the interstitial clusters, we annealed polished specimens at 500°C. At this temperature the impurity atoms should be mobile and should then

be distributed homogeneously inside the foil. After irradiation of the annealed specimens we again observed defects only near the surfaces. Therefore, we can conclude that impurities concentrated beneath the polished surface are of no importance in our observations.

On Al foils there is an unavoidable oxide layer of ~50 Å thickness present, which could prevent point defects from diffusing out of the foil. However, theoretical estimations show that this effect extends just over distances of ~200 Å. Therefore, we feel sure that the observed layer structure is due to specific properties of point defects in Al. If we assume that the most mobile atomic defect at RT is of a vacancy type, we can conclude that more vacancy type defects diffuse out of the foil than interstitials. The higher concentration of interstitials near the surfaces leads then to the preferred clustering of interstitials.

At room temperature both interstitials and single vacancies are expected to be mobile with about the same migration energy. However, there will also be a high concentration of di-vacancies in the irradiated specimens. The migration energy of the di-vacancies is always lower than that of single vacancies. Since divacancies are able to escape more easily to the foil surface, we can assume that they are responsible for the unequal concentration of remaining point defects within layers near the surfaces, and the subsequent clustering of interstitial atoms. An estimation of the thickness of the layer with a reduced vacancy concentration (Foreman[9]) is in agreement with the observations. At elevated temperatures, di-vacancies dissociate into single vacancies. The result will be a balanced distribution of single vacancies and interstitials throughout the foil. Therefore, we get a homogeneous distribution of large loops similar to those observed by Urban[10]. At the irradiation temperature of 150 K no di-vacancies are formed since

the vacancies are not mobile. Therefore, the defects must also be distributed homogeneously inside the foil (Urban[10]). With these considerations, the observations can be explained qualitatively. A quantitative evaluation will be published elsewhere[11].

REFERENCES

1. M. J. Makin, Phil. Mag. 18, 637 (1968).
2. K. Shirashi, A. Hishinuma, Y. Katano, T. Taoka, J. Phys. Soc. Japan 32, 964 (1972).
3. M. Kiritani, N. Yoshida, H. Takata, J. Phys. Soc. Japan 36, 720 (1974).
4. J. H. Chen, P. Rao, P. S. Ho, Rad. Eff. 18, 157 (1973).
5. M. Wilkens, Modern Diffraction and Imaging Techniques in Material Science, p. 233, North Holland, Amsterdam-London, 1970.
6. M. Rühle, Radiation Induced Voids in Metals, USAEC, p. 255 (1972).
7. H. Föll, M. Wilkens, Phys. stat. sol. (b), (1975), in the press.
8. W. D. Mackintosh, F. Brown, Applications of Ion Beams to Metals, p. 111 (1973), Plenum Press, New York and London.
9. A. J. E. Foreman, Rad. Eff. 14, 175 (1972).
10. K. Urban, phys. stat. sol. (a) 4, 761 (1971).
11. H. Fischer, C. Gomez, M. Rühle, to be published.

ORIENTED STACKING FAULT TETRAHEDRA IN ELECTRON IRRADIATED GOLD

M.O. Ruault, A. Rocher, L. Kubin, B. Jouffrey
Laboratoire d'Optique Electronique du C.N.R.S.
31055 TOULOUSE CEDEX, FRANCE

ABSTRACT

The partial alignment of stacking fault tetrahedra in gold is investigated "in situ" during electron irradiation. The influence of thickness, purity and orientation of the sample with respect to the electron beam is investigated. The characteristics of the pseudo-arrays are determined by further examinations using 100 keV electron microscopy and laser optical diffraction analysis. The experimental results are in reasonable agreement with a model assuming an elastic interaction between stacking fault tetrahedra.

The formation of regular void arrays by heavy particle irradiation has been described in most the b.c.c. metals (see for example [1] to [4], but only in few f.c.c. metals [3-5], Al.[5-6-7]). Recently, high voltage microscopy allowed "in situ" electron irradiation of many metals and arrays of stacking fault tetrahedra (S.F.T.) in gold [8-9] and copper [10] or vacancy clusters in copper [11] have been observed. An extensive review of results on that field is given in ref [12].

EXPERIMENTAL CONDITIONS FOR THE APPEARANCE OF PSEUDO-ARRAYS OF S.F.T.

"In situ" electron irradiation of pure gold has been carried out in the 3 MV Electron Microscope of Toulouse. The electron energies, in our experiments, are 2.5 and 3 MV, the flux varying from $\sim 2 \times 10^{17}$ to $\sim 3 \times 10^{19}$ e $cm^{-2}s^{-1}$. The impurity content varies from sample to sample from 1 to 100 ppm.

For high doses (> 5 x 10^{21} to 5 x 10^{22} e/cm^2), we observe a periodic, but imperfect, alignment of vacancy stacking fault tetrahedra (S.F.T.'s) [8-11] (see for example fig. 1-2).

The lowest dose necessary to initiate the pseudo-arrays (Table 1) is a function of the impurity content and of the orientation of the sample during irradiation. There is no observable effect of the irradiation flux on this threshold dose.

Orientation of the sample \ Impurity Content	1 ppm	10 ppm	100 ppm
(100)	5 x 10^{21}	8 x 10^{21}	1 to 3 x 10^{22}
(110)	8 x 10^{21} to 10^{22}		
(111)	1 to 2 x 10^{22}		

Table 1 : Experimental values of the lowest doses (e/cm^2) necessary to initiate the pseudo-arrays.

The arrays appear first in the thinnest parts of the sample and around the sinks for interstitials (like stacking faults, grain-boundaries, interstitial loops which appear in earlier stage...). With further irradiation, the arrays appear over the whole irradiated zone.

CHARACTERISTICS OF PSEUDO-ARRAYS

Further observations and quantitative measurements have been performed through low voltage electron microscopy (including stereoscopic method) and optical diffractometry.

(100) Sample irradiation

The arrays appear along <100> directions (fig. 1) with an angular dispersion of about 30°. The average distance D between S.F.T.'s is between 160 and 180 Å with a standard deviation ΔD from sample to sample which varies from 50 Å to 100 Å. The ratio of D to the average image size, d, is generally $\frac{D}{d} \sim 2$. We have noted, for unknown reasons, that

one sample had an average distance D ∿ 115 Å and a ratio $\frac{D}{d} \sim 3$.

One can observe one to three superimposed plane arrays of S.F.T.'s when the thickness increases up to 1000 Å. It is difficult to determine from experimental results whether S.F.T. chains are formed along the [100] normal to the foil plane, since these chains should not consist of more than three S.F.T.'s.

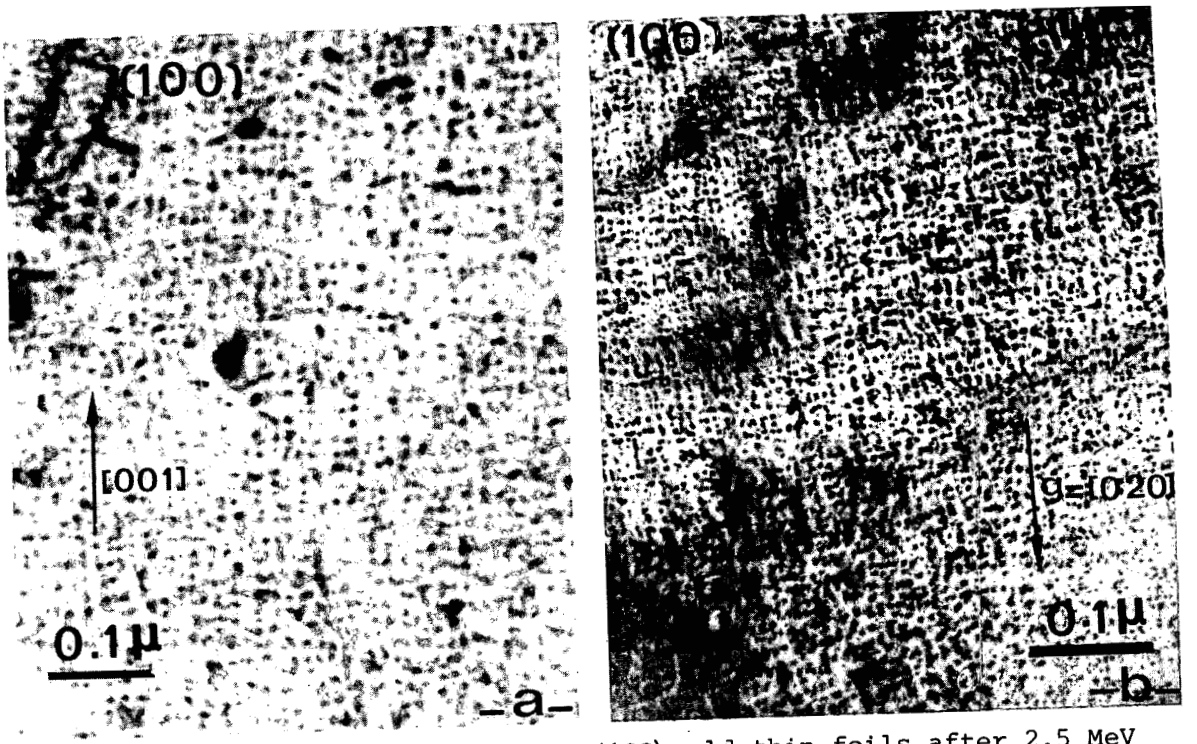


Fig. 1 : S.F.T.'s pseudo-lattice in (100) gold thin foils after 2.5 MeV electron irradiation. a - in thick zones (> 1500 Å), dose 6.3×10^{22} electrons/cm^2, b - in thin zones, dose 4.4×10^{22} electrons/cm^2.

(011) Sample irradiation

Only [100] arrays are observed in the thinnest parts (fig. 2, 3_d) in the thicker parts arrays along $[0\bar{1}1]$ are observed (fig. $2\text{-}3_b$). The projection of these arrays on {112}, {013}, {001} and {111} planes was investigated by using tilting experiments of the sample foil, so as to determine their crystallographic direction in space. These directions have been identified as being [010] and [001], at 45° of the foil plane (fig. 3_a-_c). For instance, in fig. 3_b (foil plane {112} the alignment is

observed along the three projections of the <100> directions.

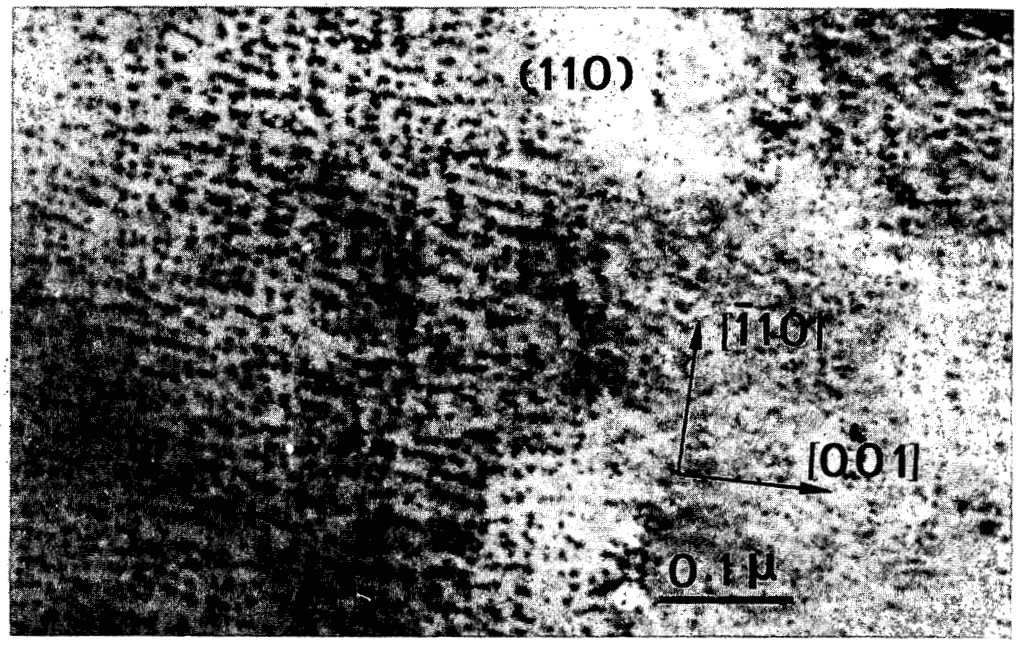


Fig. 2 : S.F.T's arrays in a (011) gold thin foil after 2.5 MeV electron irradiation. Dose : 5×10^{22} electrons/cm^2. Note only one direction of alignment in thin zones .

The measured value of D is about 130 Å with $\Delta D \sim 70$ Å and the ratio $\frac{D}{d}$ is 1.5 to 2.

We noticed that chains aligned along [010] or [001] are shorter than 100 chains which lie in the foil plane. For a thickness $\sim$ 1000 Å, in a (011) irradiated sample, there is place for 5 to 7 S.F.T.'s to align along [010] or [001], which corresponds to experimental measurements or micrographs such as fig. 3_b.

(111) Sample irradiation

We have also observed an alignment along <211> (fig. 4_a). <211> is the projection of <100> into the foil plane. Further experiments show that these "arrays" are also of <100> type (fig. 4_{b-c}). The measured value of D is about 80 Å and the ratio $\frac{D}{d} \sim 1.7$. The alignment is less good than for (100) and (110) sample irradiation.

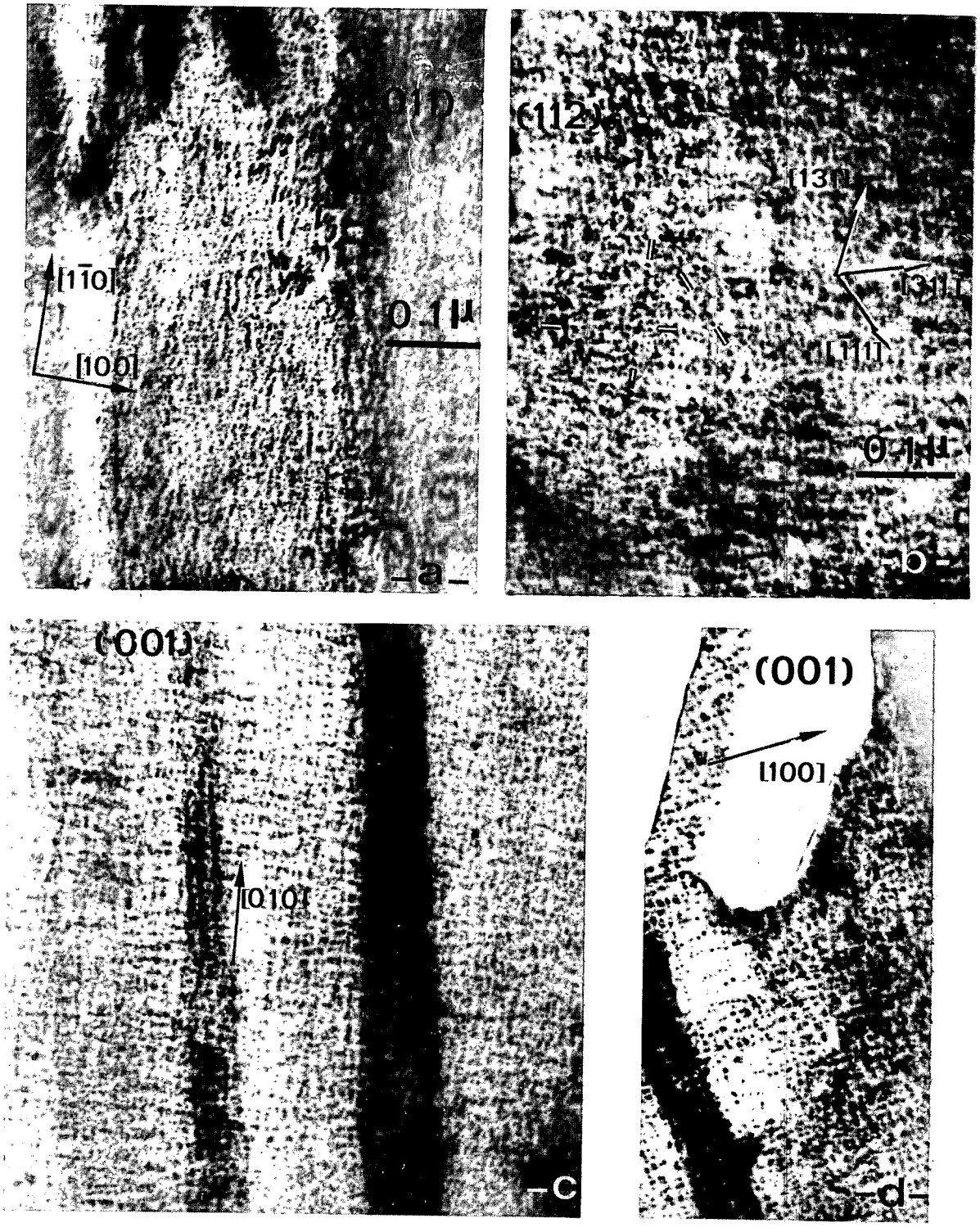


Fig. 3 - (01$\bar{1}$) gold foil irradiated with 3 MeV electrons. Dose : 6 x 10^{22} electrons/cm^2. Projection of <100> arrays along : a - (011), b - (112), c - (001), d - (001) : note alignment only along [100] in thinnest parts.

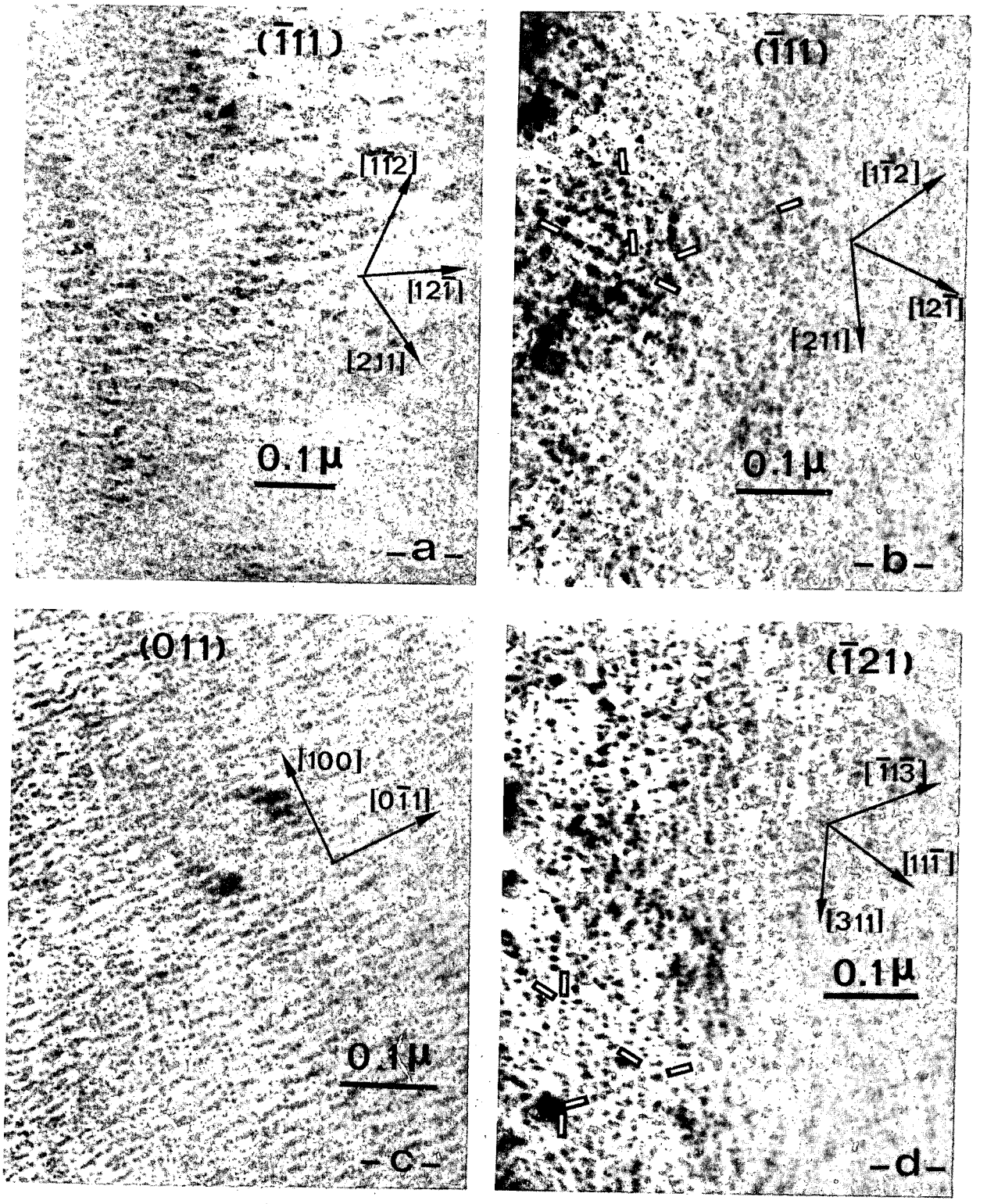


Fig. 4 - $(\bar{1}11)$ gold foils irradiated with 2.5 MeV electrons.
a - dose 1.7 x 10^{22} e/cm^2 ; $(\bar{1}11)$.
Dose : 2.5 x 10^{22} e/cm^2 b - $(\bar{1}11)$, c - (011), d - $(\bar{1}21)$.

DISCUSSION

Experiments show that a regular lattice cannot actually been formed, but only short and discontinuous chains aligned along the <100> directions. The previous calculations devoted to lattice voids (see for example [13-14-15]) supposed that if the voids are spherical in shape, elastic anisotropy is responsible for the whole interaction energy [13]. For the other cases, ("faceted voids") the interaction energy does not vanish in an isotropic medium. This is also the case of S.F.T.'s. An explanation for the alignment can be obtained assuming only an elastic interaction between S.F.T.'s. These calculations have been performed within the framework of linear isotropic elasticity [16] by computing the elastic interaction energy between the stair-rod dislocations of the S.F.T.'s. In agreement with experimental results, an energy minimum is found along the <100> directions. Other crystallographic directions only exhibit monotonical variation of the interaction energy versus the distance between the S.F.T.'s. The theoretical values of D/d at equilibrium distance are in reasonable agreement with the values reported above.

REFERENCE

1. B.L. Eyre and J.H. Evans, in Voids in Reactor Materials, p. 323 (ed. Pugh S.F., D.I.R. Norris, M.H. Loretto), British Nuclear Energy Society, Los Angeles, 1971.
2. F.W. Wiffen, Conference on radiation induced voids in metals, p.386,ed. J.W. Corbett and L.C. Ianiello, Albany US. AEC, Washington D.C., 1971.
3. G.L. Kulcinski, J.L. Brimhall and H.E. Kissinger, J. Nucl. Mater. 40 166, (1971).
4. V.K. Sikka and J. Moteff, Cryst. Lattice defects, 3, 113, (1972).
5. D.J. Mazey, S. Francis and J.A. Hudson, J. Nucl. Mater. 47, 137 (1973).
6. J.O. Stiegler and K. Farrel, Scripta. Met. 8, 651, (1974).
7. A. Risbet and V. Levy, J. Nucl. Mater, 50, 116 (1974).
8. M.O. Ruault, B. Jouffrey, J. Chaumont and H. Bernas, J. Phys. Supp. 34, C 5, 21, (1973).
9. M.O. Ruault and B. Jouffrey, Appl. Phys. Letters, 25, 265, (1974).
10. K. Urban, 4e Int. Conf. on H.V.E.M. (1-4 sept. 1975, Toulouse, France).
11. M. Kiritani, N. Yoshida, H. Takata and Y. Machara, 8e Int. Congress on Electron Microscopy, p. 444 (ed. J.V. Sanders, D.J. Goodchild) Aust. Acad. of Science, Canberra, 1974.
12. M.O. Ruault, Thesis (University of Orsay, 1975).
13. A.M. Stoneham, J. Phys., F, 1, 778, (1971).
14. V.L. Tewary and R. Bullough, J. Phys., F, 2, 69, (1972).
15. V.K. Tewary, J. Phys., F, 3, 1275, (1973).
16. L. Kubin, M.O. Ruault, A. Rocher and B. Jouffrey, submmited to Phil. Mag.

IRRADIATION DAMAGE STRUCTURES GENERATED IN METALS AND ALLOYS DURING IRRADIATION AT ELEVATED TEMPERATURES

B.L. Eyre
Metallurgy Division, A.E.R.E., Harwell, Oxfordshire, England

ABSTRACT

Irradiation of metals and alloys at elevated temperature generally results in at least part of the surviving vacancy component of the damage structure aggregating to form voids while the interstitials aggregate to form planar defects. The result of these processes is to change the external dimensions of the irradiated material and, because of the practical importance of this to the behaviour of core components in reactors, elevated temperature damage structures have been extensively studied in a wide range of materials. A large proportion of the work has been based on transmission electron microscopy (TEM) but this has been supplemented by dimensional and density measurements and more recently by the use of physical techniques such as neutron and X-ray scattering and positron annihilation. The paper aims to highlight the experimental results, particularly from TEM, that have contributed to our understanding of elevated temperature irradiation damage. We consider in particular how the survival and clustering of vacancy and interstitial defects are influenced by the major irradiation and materials variables. In discussing these aspects the results from fcc metals and alloys are compared and contrasted with those from materials having a bcc structure.

INTRODUCTION

An increasing amount of work has been carried out in recent years on the damage structures of metals and alloys irradiated at elevated temperatures. Much of the practical impetus for this has come from the materials development programmes for fast reactors and, more recently, thermo nuclear reactors. Emphasis has, therefore, been placed on determining the void swelling characteristics of commercial alloys irradiated to comparatively high doses, i.e. > 1 displacement per atom (d.p.a.). The results from these studies have exposed the complex relationships existing between void swelling characteristics and the principal irradiation and material variables. This has led, in recent

years, to more systematic studies of how void swelling is influenced by material composition and structure, the aim being to identify swelling resistant alloys.

In parallel with the experimental work, a considerable effort has also been directed to developing a theoretical understanding of void swelling. Success has been achieved in identifying the fundamentally important roles that (a) dislocations play in acting as biased sinks for interstitials[1,2] and (b) displacement cascades play in the development of the vacancy component of the structure[3]. The models are able to predict the main features of how void swelling varies with the more important irradiation variables such as dose, dose rate, temperature and recoil energy. However, they do not include, in any precise manner, the complex effects that basic material parameters such as composition, structure and stacking fault energy have on the damage structure. It has become clear that to gain further insight into these aspects requires a more detailed experimental picture of how the damage structure as a whole (including dislocation components and re-distribution of pre-existing structural features such as precipitates as well as voids) evolve during irradiation. Our aim in this paper is to consider the experimental work on void swelling in the light of what is understood about the other components of the damage structure. We begin, therefore, by summarising the observations concerning the formation and subsequent development of interstitial and vacancy planar defects at elevated temperatures.

HIGH TEMPERATURE DAMAGE STRUCTURES

Nucleation and Growth of Interstitial Clusters

In terms of cluster geometry the aggregation of interstitials is comparatively simple since all of the evidence shows that they plate out on close packed planes to form dislocation loops. In fcc metals the nucleation plane is $\{111\}$ and the loops are faulted with $\underline{b} = 1/3\ \langle 111\rangle$ whereas in bcc metals the planes are $\{110\}$ and the loops are again faulted with $\underline{b} = a/2\ \langle 110\rangle$ although these shear over to a perfect configuration with $\underline{b} = a/2\ \langle 111\rangle$ at an early stage[4]. Theoretical treatments of interstitial loop nucleation[5,6] have in general assumed that the minimum stable loop nucleus is a di interstitial. In pure crystals these

are assumed to form homogeneously and under steady state conditions, the equilibrium concentration of loops on completion of the nucleation stage, C_L^i, varies with temperature and dose rate as follows -

$$C_L^i = C_o^i K^{\frac{1}{2}} \exp^{-E_m^i/2kT} \quad (1)$$

where K is the defect production rate and C_o^i contains the necessary geometrical constants representing the capture cross sections for loss of interstitials by recombination, at fixed sinks such as grain boundaries and dislocation lines and at the loop embryos themselves. In the case of crystals containing impurities which trap interstitials with a binding energy E_b, Eq. (1) must be modified to take into account the reduced interstitial mobility, i.e.

$$C_L^i \alpha C_o^i K^{\frac{1}{2}} \exp - (E_m^i + E_b)/2kT \quad (2)$$

Although many observations of interstitial loops in metals have been reported, there has been little systematic work on the variation in loop numbers with temperature which can be analysed to give activation parameters. Considering first the results from fcc metals, Kiritani[5] has studied the temperature dependence of C_L^i in electron irradiated aluminium and gold over temperature ranges where the vacancy mobility is expected to be much less than interstitial mobility. Analysis of the results to obtain E_m^i gave values of $\sim$0.1 eV and $\sim$0.19 for aluminium and gold respectively which are consistent with an interstitial that is mobile in Stage I, although they may include some impurity trapping. An important consequence of having a low E_m^i is that the nucleation stage is completed at an early stage in the irradiation, although the defect production rate also affects both the number of loops and the rate at which saturation in C_L^i is achieved. Since no comparable studies have been made of the temperature dependence of C_L^i in neutron or ion irradiated pure fcc metals, it is not possible to reach any definitive conclusion regarding the influence of recoil energy and hence, damage processes, on interstitial loop nucleation. It is expected that the distribution of interstitials is reasonably uniform even when displacement cascades are produced and thus the nucleation of interstitial loops during neutron or ion irradiation should be qualitatively the same as during electron irradiation.

With regard to the role played by impurities, it is commonly observed that their presence leads to a finer loop distribution suggesting that they promote heterogeneous nucleation. However, no systematic studies have been made of the influence of specific impurities on the temperature dependence of C_L^i in metals. Some data has been obtained from solution treated stainless steels neutron irradiated at temperatures within the void swelling regime. Interpretation of the results is made difficult by the uncertainties in the irradiation temperatures, the large amount of scatter in the data and the intersection of loops to form network segments, particularly at the higher temperatures which leads to an under estimate of C_L^i. Arrhenius plots of the data from neutron irradiated 304 and 316 [7,8,9] are presented in Fig. 1. It can be seen that there are two families of points which can be approximately fitted to two straight lines having different slopes. The points lying on the shallower line are from 304 and 316 steels irradiated to lower doses and temperatures, i.e. 1-2 x 10^{22} n.cm^{-2} and <530°C, whereas the steeper line fits the higher dose and temperature data from 316. The effective activation energies calculated from the two slopes are ~1.6 eV and 2.6 eV respectively. It is considered that the line showing the lower slope is more valid since the loop numbers are less likely to be distorted by intersections. Williams[10] is currently making a more precise study of the temperature dependence of C_L^i in ion irradiated stainless steels in which temperature, irradiation and material conditions are all closely controlled. The aim is to explore the influence of irradiation conditions, helium gas content and metallurgical condition, i.e.

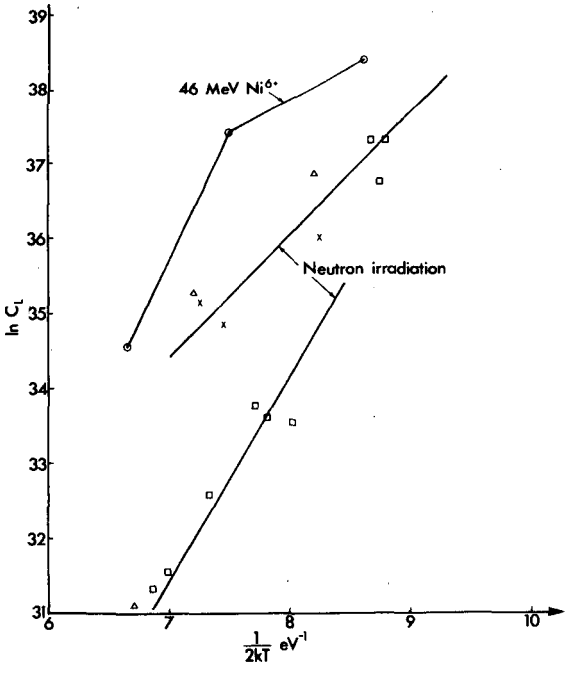


Fig. 1. Plots of ln C_L^i versus $\frac{1}{2}kT$ for interstitial loops in 46 MeV Ni^{6+} irradiated 316[10] and neutron irradiated 316 and 304 steels[21,23].

heat treatment and composition, on interstitial loop nucleation and relate this to the void swelling characteristics of the steel. A set of his data obtained from 46 MeV Ni^{6+} irradiated solution treated 316 steel pre-injected with 10 atom ppm helium is included in Fig. 1. Comparison with the reactor data shows that the number of loops is higher in the ion irradiated material at all temperatures and this can be attributed to the higher dose rate. Again, the points do not lie on a single line and in this case the measured C_L^i values were not distorted significantly by loop-loop intersections. Clearly no physical significance can be placed on activation energies derived from the results but they serve to demonstrate the large effect alloying is having on loop nucleation. Comparison with Kiritani's results suggests that interstitial mobility is reduced very considerably, presumably as a result of trapping at solutes. In this context it is interesting to note that Bloom et als[8] data from 304 steel shows that the times to complete nucleation are considerably longer than those observed by Kiritani. While this can be partly accounted for by the difference in dose rate, it is also consistent with a large difference in effective interstitial mobility.

With regard to the survival of interstitial loops during irradiation, the rate equation defining their growth or shrinkage rate is of the form -

$$\left(\frac{dr_L}{dt}\right)_i = \frac{1}{b}\left\{Z_i D_i c_i - D_v c_v + D_v c_v^e \exp - \left[\frac{(F_{el} + \gamma_{SF})\, b^2}{kT}\right]\right\} \quad (3)$$

where c_i and c_v are the interstitial and vacancy concentrations respectively, D_i and D_v are their diffusivities, F_{el} is the elastic energy of the loop, $\underline{b}$ is its Burgers vector, γ_{SF} is its stacking fault energy if faulted and Z_i is the bias term defining the preferential attraction the dislocation bounding the loop has for interstitials point defects. Values for c_i and c_v are obtained by solving rate equations containing the point defect generation rate, loss rates at sinks and recombination rates. The important point to emerge from Eq.(3) is that interstitial loops are basically stable defects which, in the presence of neutral sinks, can undergo continuous growth during irradiation. At low temperatures this growth is bias driven, i.e. $Z_i D_i c_i > D_v c_v$, whereas at higher temperatures, when $D_v c_v^e$ becomes significant, growth by vacancy emission makes

an increasingly important contribution. Evidence from fcc metals shows that the interstitial loops mostly remain faulted during growth, even in the high stacking fault energy metals such as nickel, until they intersect with another loop or other defects when they unfault. The important practical consequence of this is that the interstitial loops remain evenly distributed and that the network formed by the intersection of loops is a function of the scale on which the loops are originally nucleated.

Turning to bcc metals, the experimental evidence, obtained mainly from molybdenum, shows that the nucleation and growth of interstitial loops differs fundamentally from that in fcc metals. More specifically, because the loops shear over to a glissile configuration at an early stage in their formation, they are able to move by glide. It has been observed that with increasing irradiation dose at temperatures > 200°C loops having identical Burgers vectors eventually glide together as a result of the elastic interaction between loops. Thus, the loops are able to aggregate to form rafts and the spacing between these is strongly influenced both by impurity content and irradiation temperature because of their effect on the loop glide stress[11]. Moreover, at the higher temperatures the loop movement gains an additional degree of freedom because of self climb and those in the rafts can coalesce leading eventually to network formation. These effects of impurities and temperature on the development of the interstitial components of the structure are illustrated very well by Bentley et al's[12] results from molybdenum and TZM. The important practical consequence of loops coalescing by glide and climb is that they coarsen into a network at much lower homolagous temperatures than if the loops are sessile as in the fcc metals. We shall return to discuss the implications of this to the void swelling characteristics later.

Nucleation and Growth of Vacancy Clusters

(a) Vacancy loops

It has been established from studies of both quenched and irradiated metals that vacancies can aggregate to form planar defects or voids and in this respect their clustering behaviour is different to that of

interstitials. In irradiated metals it has been established that in general voids only form at elevated temperatures. With regard to vacancy loops, the rate equation defining their growth or shrinkage is given by

$$\left(\frac{dr_L}{dt}\right)_v = \frac{1}{b}\left[D_v c_v - Z_i D_i c_i - D_v c_v^e \exp\frac{(F_{el} + \gamma_{SF})b^2}{kT}\right] \qquad (4)$$

It can be seen that in contrast to interstitial loops, vacancy loops are basically unstable defects during irradiation undergoing bias driven shrinkage at low temperatures when $Z_i D_i c_i > D_v c_v$ and shrinkage by thermal vacancy emission at elevated temperatures when $D_v c_v^e$ becomes appreciable. An important consequence of this is that vacancy loops are unlikely to form when point defect generation is uniform such as during electron irradiation. Exceptions to this general behaviour can occur in the vicinity of dislocations where the preferred drift of interstitials to the dislocation cores leads to a localised inbalance in the vacancy and interstitial concentrations which allows vacancy loops to form and grow[13]. However, once a dislocation climbs away from adjacent vacancy loops, they become preferred sinks for interstitials and shrink. Thus, vacancy loop formation is unlikely to play any significant role in the development of damage structures during electron irradiation, irrespective of temperature.

A basically different situation exists during irradiation with neutrons or heavy ions. In this case the recoil energies are mostly $\gg$ 1 KeV[14] and they generate displacement cascades in which the interstitials are transported athermally away from the cascade centres by focussed collision sequences leaving a region in which the vacancy super-saturation can be very high. TEM studies of a number of fcc and bcc metals following ion irradiation have shown that such vacancy rich regions can collapse with high efficiency to form loops[15].

We wish to emphasise two aspects of vacancy loop formation that are relevant to the void swelling characteristics of metals and alloys. The first concerns the temperature range over which they form during irradiation and the effect this has on void formation and growth. The second concerns the influence impurities have on point defect survival in

cascades and therefore on the efficiency of vacancy retention in collapsed cascades. These are both aspects that are being studied in detail at Harwell and some of the results are being presented by English et al [16,17] at this Conference. With regard to the effect of temperature, calculations using Eq. (4) show that at low temperatures the vacancy loops formed by cascade collapse will undergo slow bias driven shrinkage. Thus we expect C_L^v to increase with dose initially and eventually saturate when the loss rate due to shrinkage balances the generation rate. At temperatures where $D_v c_v^e$ becomes appreciable, shrinkage due to thermal emission is dominant and the loss rate increases rapidly with increasing temperature. This pattern of behaviour has been confirmed by our observations in self ion irradiated copper in which the temperature range for thermal emission controlled shrinkage to become dominant is 0.4 - 0.5 T_m (see Fig. 1 in reference 16). This compares with the approximate lower threshold temperature for void formation of 0.35 T_m in neutron irradiated copper [18] and $\sim$0.5 T_m in ion irradiated copper [19]. It is clear, therefore, that in this case there is an overlap in the temperature ranges within which the two types of vacancy clusters can form and we have to consider how this affects the development of the damage structure, particularly at elevated temperatures.

We have not yet completed any systematic studies of how alloying affects cascade collapse in fcc metals but on going to a considerably more complex alloy such as an austenitic stainless steel, it is found [20] that the numbers and sizes of visible vacancy defects are much lower than in copper. Nevertheless, more recent work by Williams [10] has shown that there is no appreciable change in the defect yield and cascade efficiency in stainless steel at least up to 400°C. This is illustrated qualitatively by the weak beam micrographs presented in Fig. 2a and b which were obtained from solution treated and aged 316 steel irradiated with 80 KeV Cr^+ at room temperature and 400°C. The lower threshold temperature for void formation in heavy ion irradiated stainless steels is $\gtrsim$ 450°C [21] which suggests that account must again be taken of the effect that vacancy loops have on void swelling. The lower defect yield and cascade efficiency in stainless steel, i.e. $\sim$0.1 and 0.1 → 0.2, respectively

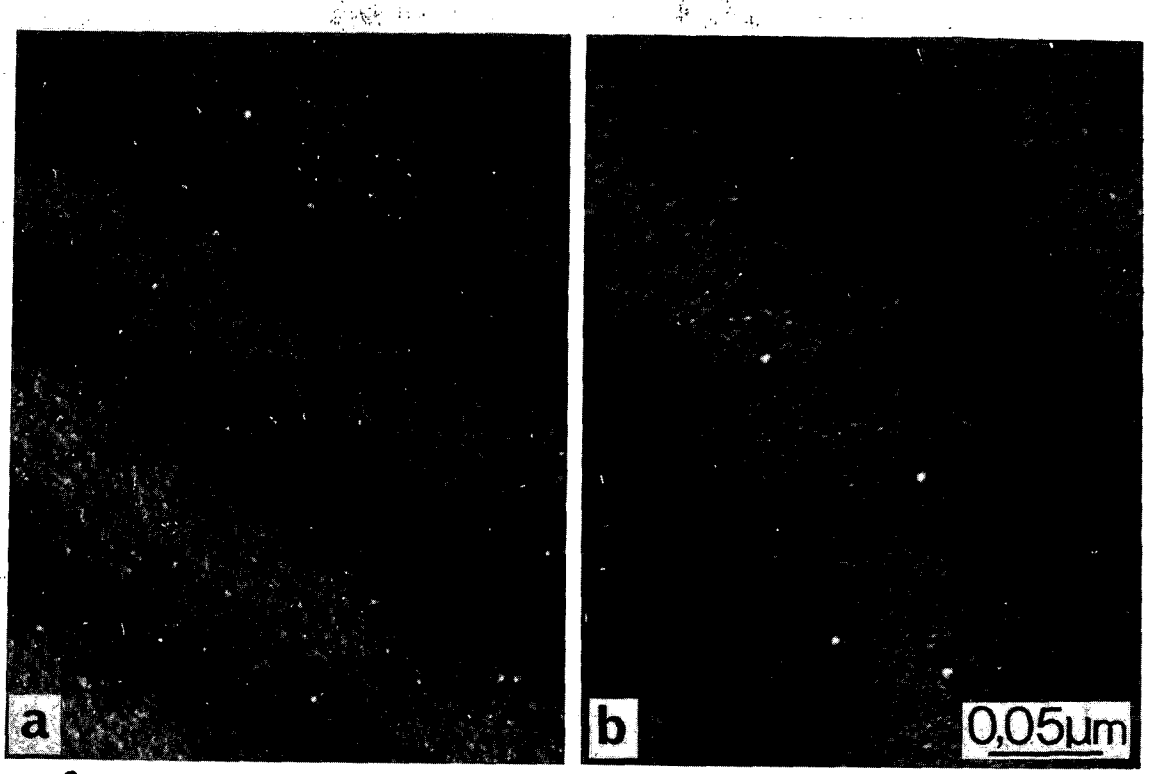


Fig. 2. Weak beam micrographs of solution treated 316 irradiated with 80 KeV Cr^+ to a dose of 10^{13} ions cm^{-2} at (a) room temperature and (b) 400°C. The micrographs were taken in g - 2g combination with 200 being the imaging reflection.

compared with copper, i.e. $\sim$0.5 and $\sim$1.0 respectively, is considered to be due to the effect solute atoms have in promoting recombination within the cascades. Williams most recent results suggest that carbon in solution is particularly effective in this respect. A possible explanation is that the solute atoms defocus replacement collision sequences thus reducing the separation of interstitials from the vacancy rich centres of the cascades. Clearly this has the important practical consequence of reducing the production rate of point defects that can take part in the various clustering processes.

Before concluding our discussion of vacancy loop formation in fcc metals, it should be emphasised that little evidence has been obtained from neutron irradiated specimens. It has been established that vacancy loops form in pure fcc metals such as copper neutron irradiated at $< 100°C$ [22] but the influence of purity and irradiation temperature have not been studied systematically. In the particular case of stainless

steel, weak beam micrographs obtained from solution treated 316 irradiated to 2 x 10^{22} n.cm^{-2} at temperatures in the range 430 - 500°C [9] reveals a population of small defects < 50 Å in diameter in addition to large faulted interstitial loops, voids and small three dimensional precipitates. Although their nature has not been positively determined yet, their size and distribution is consistent with them being small collapsed vacancy defects.

Considering now the evidence regarding vacancy loop formation in irradiated bcc metals, we find once again that the observed behaviour differs significantly from that in fcc metals. Results from room temperature ion irradiated tungsten and molybdenum show that the vacancy rich cascade centres collapse to form vacancy loops although, because of their high stacking energy, they shear over at an early stage to a glissile configuration [23,24]. The defect yield and cascade efficiencies in high purity molybdenum are not very different to the observed values for copper. More systematic studies of the influence exerted by impurities have demonstrated that low levels of interstitial impurities can have a large effect in reducing both defect yield and cascade efficiency [24]. Where the bcc metals differ very considerably from fcc metals, is in the effect temperature has on vacancy loop formation. Results obtained from both self ion [16] and neutron irradiated molybdenum [12] show that the vacancy loop concentration decreases at much lower temperatures than can be explained by a simple vacancy emission model. This behaviour is not understood but it appears to be a consequence of the cascades not collapsing to form loops. More specifically, the very high stacking fault energy characteristic of bcc metals may result in the cascades collapsing to form voids rather than loops or in the vacancies migrating away from the cascade centres at quite modest temperatures. It has been established in neutron irradiated molybdenum [12] that the vacancies are not lost by recombination or to dislocations and grain boundaries since the vacancy loop population is replaced by a high concentration of voids.

(b) Voids

Before discussing the experimental observations of voids in detail

we need to summarise the principal theoretical relationships that provide us with a framework for analysing the data. An important parameter is the activation energy for forming a critical sized nucleus since this governs the temperature dependence of the void concentration, C_V. During irradiation the crystal is driven into a highly irreversible state and it is therefore not valid to apply classical nucleation theory involving an equilibrium activation energy, ΔG^o. The procedure adopted is to define an effective activation energy for forming a nucleus of critical size, r_v^{crit}, containing n_v^{crit} vacancies and n_g gas atoms, $\Delta G' (n_v^{crit} n_g)$ [25,26]. The nucleation rate, J, is then given by -

$$J (n_v^{crit} n_g) = Z D_v c_v N_o \exp -\frac{\Delta G' (n_v^{crit} n_g)}{kT} \quad (5)$$

where Z is the Zeldovich factor. Thus, the void concentration on completion of the nucleation stage is -

$$C_V = \int_{t=0}^{t\ nucl} J (n_v^{crit} n_g)\, dt \quad (6)$$

The rate equation defining void growth rate can be written as follows [27] -

$$\frac{dr_v}{dt} = \frac{1}{r_v} \left\{ D_v c_v - D_i c_i - D_v c_v^e \exp\left[\left(\frac{2\gamma}{r_v} - p_g \right) \frac{b^3}{kT} \right] \right\} \quad (7)$$

We can therefore obtain a value for r_v^{crit}, important to void nucleation, by setting $dr_v/dt = 0$. Approximate solutions have been obtained for two limiting cases [28]. Firstly, at low temperatures when c_v and c_i are largely governed by mutual recombination r_v^{crit} is approximately given by -

$$r_v^{crit} \simeq \frac{D_v c_v^e 2\gamma b^3}{Kkt (Z_i - 1) \left[\frac{D_i D_v}{\alpha K} \right]^{\frac{1}{2}}} \quad (8)$$

where α is a recombination constant. At higher temperatures, when

thermal vacancy emission plays an important role, r_v^{crit} is approximately given by -

$$r_v^{crit} = \frac{D_v c_v^e \rho_d 2\pi\gamma}{Kkt\,(Z_i-1) - 8\pi\gamma b^3 D_v C_v} \tag{9}$$

where ρ_d is the total dislocation density.

Considering more specifically void growth rates, two temperature regimes can be defined. Within the lower temperature range, when the thermal emission term in Eq. 7 is small, void growth is bias driven. Bullough and Perrin[27] have obtained solutions for three limiting cases as defined by sink strengths. The first is when the dislocation spacing is only slightly greater than the void spacing. Then

$$\bar{r}_v^3 = \frac{1}{\rho_d^{1/2}}\left[\frac{1}{Z_v} - \frac{1}{Z_i}\right]^{3/2}(Kt)^{3/2} \tag{10}$$

The second case is when we have a very high dislocation density and therefore the dislocation sink strength, k_d^2, dominates, i.e.

$$\bar{r}_v^3 = \frac{1}{\rho_d^{3/2}}\left[\frac{1}{Z_v^{1/2}} - \frac{1}{Z_i^{1/2}}\right]^3 (Kt)^3 \tag{11}$$

The third case is when the void spacing is less than the dislocation spacing and void sink strength $k_v^2 > k_d^2$ -

$$\bar{r}_v^3 = \left[\frac{1}{16\pi^2 C_v^2}(Z_i - Z_v)\rho_d\right]^{3/4} (Kt)^{3/4} \tag{12}$$

At higher temperatures when the thermal emission term becomes dominant, whether voids grow or shrink depends on the sign of $(2\gamma/r_v - P_g)$. During neutron irradiation when He gas is being continuously created, a flux of gas atoms can arrive at the voids. In this situation we can get gas driven swelling when r_v^3 can again follow a $(Kt)^{3/2}$ law[29].

Turning now to a consideration of the experimental observations of void formation and growth, we shall again follow the procedure of first discussing fcc metals and then comparing and contrasting their behaviour with what has been observed in bcc metals. The discussion of fcc metals will largely centre around the results from the austenitic alloys ranging from 18/8 type stainless steels to nickel based alloys. Void nucleation and growth in pure fcc and cph metals are being discussed at this conference by Levy et al[30].

It has been established that the principal variables influencing void swelling in austenitic alloys are irradiation temperature and dose and material composition and structure. An important variable bridging these two groups is gas content since it can include both irradiation induced He and H production due to (n-α) and (n-p) reactions and residual gases such as O_2 and N_2. A convenient framework for the present discussion therefore is to consider void nucleation and growth in terms of the influence exerted by these variables. A comparison of the simulation and reactor results shows that these effects are sensitive to dose rate and recoil energy and we include these aspects in the discussion. It should be stressed at the outset that many of the critical experiments required to understand the mechanisms involved, particularly in void nucleation, have not been carried out. Nevertheless, emphasis will be placed on discussing those aspects about which some physical understanding has been achieved.

In considering the influence of irradiation variables on void swelling parameters, results from solution treated (S.T.) 316 (see Table 1 at end of paper) provides a useful basis since it has been studied extensively using a range of irradiation techniques. In order to evaluate void nucleation parameters defined in Eq. 5 it is necessary to determine nucleation rates at early times as a function of temperature. Unfortunately, much of the experimental data is from specimens irradiated to comparatively high doses, i.e. >1 dpa, when C_v has frequently saturated. In fact, a comparison of results from electron, heavy ion and neutron irradiation experiments on S.T. 316 suggests that the dose for C_v to saturate is strongly influenced by recoil energy. More specifically,

the saturation dose, $(Kt)_{sat}$, is often <1 dpa in HVM irradiated specimens, although it can be influenced by composition[31]. In reactor irradiation $(Kt)_{sat}$ appears to be 10-20 dpa[7,9] although no systematic studies have been made of the dose dependence of C_v at a given temperature. In heavy ion irradiation experiments C_v goes through a maximum at about 10-20 dpa in 22 MeV C^{++} irradiation[21] and at 40-60 dpa in 5 MeV Ni ion irradiation[21,32]. Recoil energy also influences the lower threshold temperature for the formation of visible voids. In S.T. 316 this is typically 450-500°C for heavy ion irradiation, 300-350°C for reactor irradiation whereas, voids have been observed[33] down to 200°C in 1 MeV electron irradiated S.T. FV548 (see Table 1).

The increase in both incubation dose and threshold temperature to form visible voids as recoil energy increases can be accounted for by cascade collapse to form vacancy loops. This process results in a significant fraction of the vacancies being effectively trapped until thermal emission temperatures are reached. At the dose rates typically encountered in heavy ion irradiation experiments the temperature for rapid evaporation of vacancies from loops is >0.4 Tm which, in the case of stainless steels, is >420-450°C. Thus, we can explaine the large increase in threshold temperature for void formation on going from electron to heavy ion irradiation. The increase in $(Kt)_{sat}$ in the latter case is considered to be due, in part at least, to an incubation period which is related to the thermal vacancy emission rate from the loops. In order to obtain bias driven void growth it is necessary to approach a dynamic steady state whereby the loss rate of vacancies by cascade collapse is matched by vacancy emission from the loops. Thus, the incubation period is related to the time required to achieve this condition.

Arrhenius plots of the void concentration data from neutron,[7,9,34] electron[31,35] and heavy ion irradiated[36,21,32] S.T. 316 are presented in Fig. 3 and three main features can be identified. Firstly, all sets of data can be fitted to straight lines having a common slope and they therefore yield a common activation energy of 1.0 - 1.1 eV. Secondly, whereas the heavy ion data is from specimens preinjected with 10-15 atom ppm He the electron irradiation data is from He free specimens. Thirdly,

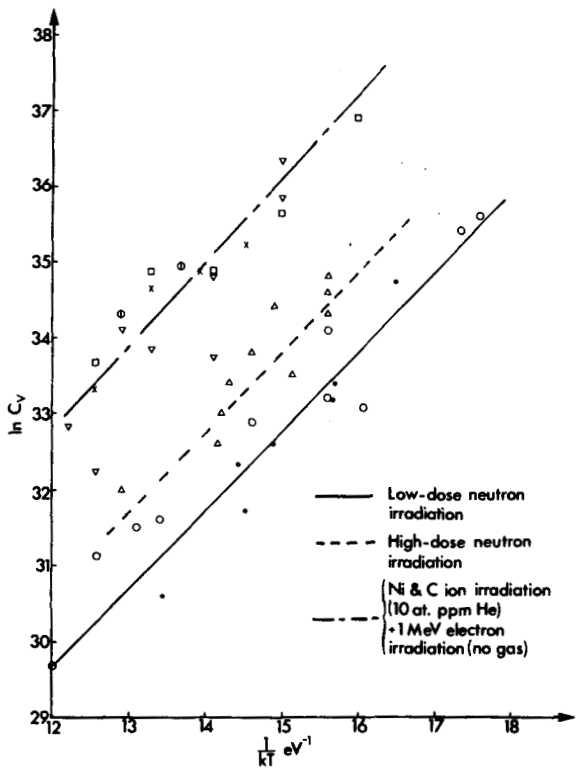


Fig. 3. Arrhenius plots of C_V versus T for S.T. 316 following low and high dose neutron irradiation, heavy ion irradiation (with He preinjection) and 1 MeV electron irradiation (no He).

an increase in dose rate from 10^{-6} dpa sec^{-1} (reactor) to 10^{-3} - 10^{-4} dpa sec^{-1} (accelerators and HVM) increases C_V by a factor of 20-30. The first two features suggest that in 316 steel the activation energy for forming a void nucleus is dominated by the surface energy term rather than any terms related to recoil energy, dose rate or presence of He. The third feature suggests that dose rate does have an effect on the pre-exponential terms in Eqs. (5) and (6). However, this aspect of the results cannot be interpreted in any simple manner because the HVM data are from He free specimens. We shall see later that He preinjection is an important variable in determining C_V in both electron and heavy irradiated specimens. A further feature not shown in Fig. 3 is that C_V decreases sharply between 650 and 700°C in Ni ion irradiated 316 and 321 steels[21]. Calculations[33] of r_v^{crit} using Eqs. (8) and (9) show that it increases sharply over this temperature range which would lead to an increase in $\Delta G'$.

A majority of the data regarding isothermal void growth and swelling rates during irradiation have come from simulation experiments. Plots of $(\bar{r}_v)^3$ against dose for S.T. 316 following 1 MeV electron irradiation at 500 and 600°C[31,35] and Ni ion irradiation at 535 and 625°C[21,32] are presented in Figs. 4a and 4b. Relating the temperature to peak swelling temperatures, T_p, 500 and 525°C are both well below T_p, 600°C is 50-100°C

below T_p in electron irradiated 316 whereas 625°C is close to T_p in 5 MeV Ni^+ irradiated 316. We also include in Fig. 4b two points corresponding to S.T. 316 neutron irradiated at the peak swelling temperature of 450°C to 6 and 16 dpa[9]. Both sets of HVM and accelerator data show that the dose dependence of void volume can be fitted to a relationship of the form $(\bar{r}_v)^3 = A(Kt)^n$ with n remaining constant up to a critical dose. The values of n over this initial period, the dose and mean void radius at which breakaway occurs, $(Kt)_b$ and $(\bar{r}_v)_b$ respectively, and the coefficient A are summarised in Table 2.

TABLE 2

Irradiation	Temperature °C	n	$(Kt)_b$ dpa	$(\bar{r}_v)_b$ Å	A
1 MeV e^-	500	2.2	>10	114	5.32×10^{-21}
1 MeV e^-	600	2.7	8	270	4.39×10^{-19}
46 MeV Ni^{6+}	525	2.2	>50	170	1.42×10^{-21}
5 MeV Ni^+	625	2.5	>200	>580	1.44×10^{-21}
neutrons	450	2.0	>16	>138	2.18×10^{-20}

Figs. 4a and b and the sumary of the data in Table 2 expose a number of features which provide some insight into the physical processes influencing void growth rate. Firstly, the value of n at low doses lies between 2 and 3 and appears to be virtually independent of recoil energy. On the other hand, it does increase markedly with temperature from 2.1 to 2.6 Thus, the observed values of n fall between the exponents in Eqs. (10) and (11), i.e. between $^3/_2$ and 3, suggesting that over the dose range in question the dislocation component of the structure is the dominant sink. This is consistent with the build-up in dislocation structure occurring more rapidly than the void component as is commonly observed experimentally. The increase in n between 500 and 600-625°C is also consistent with C_v being lower at the higher temperature (Fig. 3). Secondly, the decrease in n at the higher doses towards the value of $^3/_2$ predicted when dislocation and void spacings are similar is again

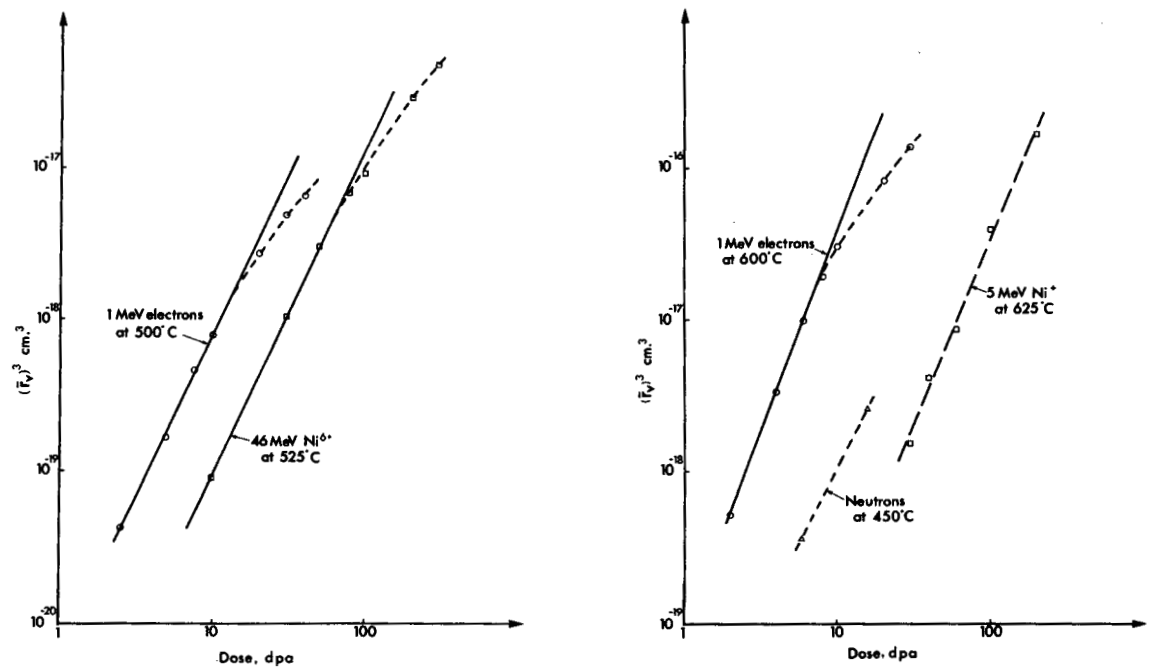


Fig. 4. Plots of $(\bar{r}_v)^3$ versus dose for S.T. 316. (a) 1 MeV electron and 46 MeV Ni^{6+} irradiation at 500 and 525°C respectively and (b) 1 MeV electron, 5 MeV Ni^{6+} and neutron irradiation at 600, 625 and 450°C respectively.

consistent with the later build-up of the void component of the structure. It is interesting to note that $(Kt)_b$ increases markedly with recoil energy and this is expected in view of the large increase in the dose for C_V to saturate. Thirdly, the coefficient A, which in terms of Eq. (10) and (11) is proportional to $1/\rho_d^{3/2}$, is very sensitive to recoil energy. It also appears to be independent of temperature in the heavy ion irradiated material but is strongly dependent on temperature in the electron irradiated material. This is consistent with the dislocation density being both significantly higher and temperature independent in the heavy ion irradiated material. The ratios of ρ_d between heavy ion and electron irradiated specimens calculated from the values of A are as follows :-

$$\frac{(\rho_d\ 525)\ \text{Ni}}{(\rho_d\ 500)\ \text{electrons}} \sim 2.5 \qquad \frac{(\rho_d\ 625)\ \text{Ni}}{(\rho_d\ 600)\ \text{electrons}} \sim 45 \qquad \frac{(\rho_d\ 500)\ \text{electrons}}{(\rho_d\ 600)\ \text{electrons}} \sim 20$$

The consistently higher dislocation density in the heavy ion irradiated material could in part be a consequence of the contribution made by a vacancy loop population.

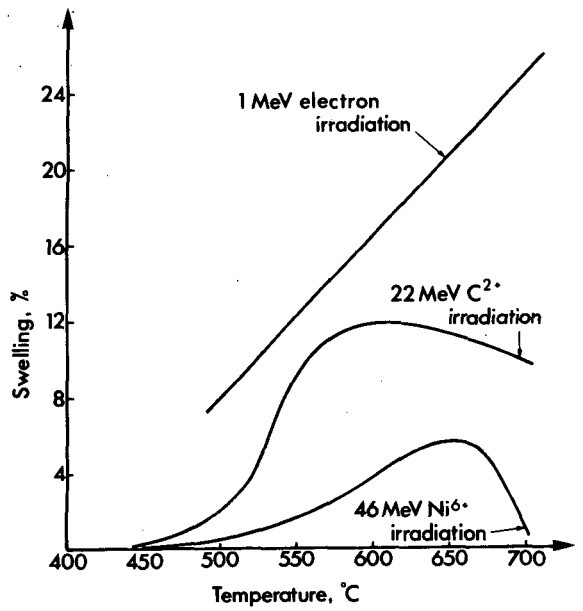


Fig. 5. Swelling versus temperature curves for electron and heavy ion irradiated S.T. 316.

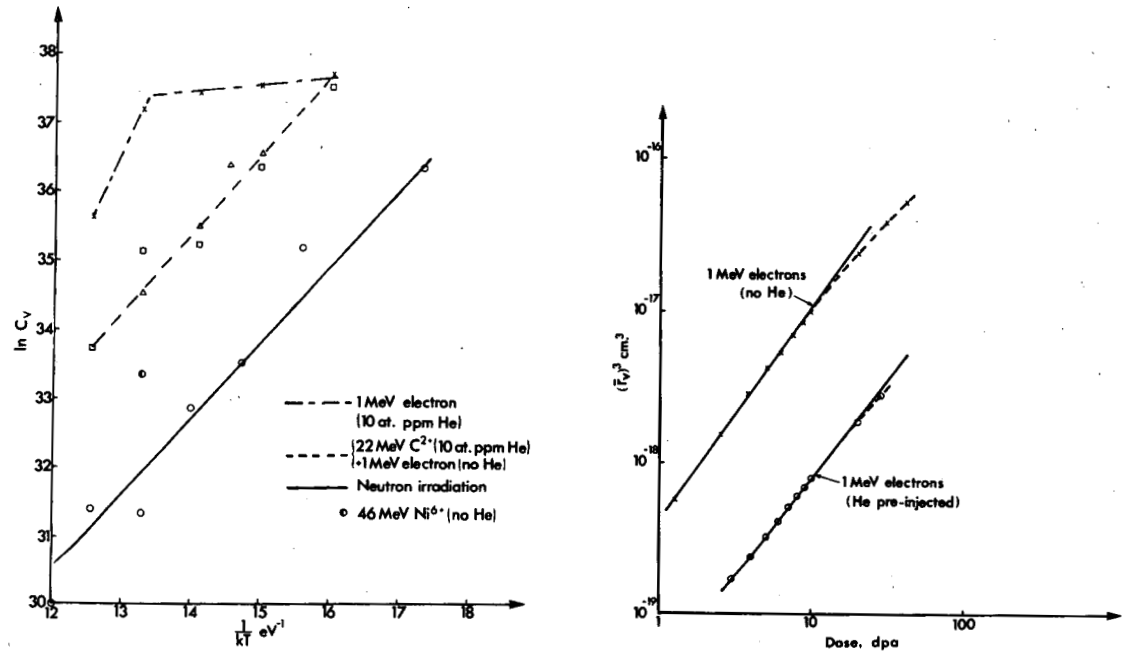
To conclude the discussion of the influence of irradiation variables on void swelling in stainless steels, we present swelling versus temperature curves for S.T. 316 irradiated with 1 MeV electrons (no He)[31], 22 MeV C^{++} (He preinjected)[36] and 46 MeV Ni^{6+} (He preinjected)[21] in Fig. 5. The results reflect very clearly the large effect recoil energy has on both void nucleation and growth. We believe that this can be accounted for by cascade collapse into vacancy loops and this has recently been put on a quantitative basis in a modified rate theory of void swelling[3].

During neutron irradiation He and H are created continuously as a result of (n-α) and (n-p) reactions and O_2, N_2 and H are frequently present as solute atoms in metals and alloys. Thus, an important aspect of the void swelling problem is the effects these gases have on void nucleation and growth. Experiments aimed at investigating the effects of He preinjection have shown that it invariably results in an increase in C_v during subsequent neutron, heavy ion or 1 MeV electron irradiation. In the case of neutron irradiation, it has been shown[37] that preinjecting type 304 steel (see Table 1) with 20 at ppm He results in C_v being increased by a factor of ~ 2 during subsequent neutron irradiation at 390°C. In heavy ion irradiated specimens He preinjection has an even larger effect. In unstabilised steels such as S.T. 316 preinjection of 10-15 at ppm He increases C_v by about an order of magnitude during subsequent irradiation with C or Ni

ions at 600 or 625°C[38,32]. The behaviour in stabilised steels is rather more complex. For example, voids were not observed in 22 MeV C^{++} irradiated type 321 steel (see Table 1) which did not contain He whereas in specimens preinjected with 10 at ppm He, C_v was similar to that for preinjected 316[38]. The significant feature of type 321 steel is that it is hyperstoichiometric with respect to the Ti : C ratio and Ti has a strong affinity for the residual gases O_2 and N_2. These results therefore imply that in the absence of He uncombined residual gases are necessary for void nucleation.

The most complete information on the influence exerted by He has been obtained from S.T. FV548 (see Table 1) in which the temperature dependence of C_v and the void growth rates have been measured in He preinjected[33] and He free[33,39] specimens during subsequent 1 MeV electron irradiation. Arrhenius plots of C_v versus temperature for these two cases are presented in Fig. 6a. This Figure also includes data from 22 MeV C^{++} irradiated specimens preinjected with 10 at ppm He[40] and reactor irradiated pin cladding[41]. It can be seen that a common line can be drawn through the points from electron irradiated He free and C^{++} ion irradiated He preinjected specimens. Moreover, the slope of the line is close to that for the reactor irradiation results yielding an effective formation energy of 1.1 - 1.15 eV. In this respect, therefore, the results are in good agreement with those from S.T. 316 (Fig. 3). However, on preinjecting FV548 with 10 ppm He we observed during subsequent electron irradiation that C_v is virtually independent of temperature up to 550-600°C above which it decreases sharply. Moreover, C_v in the He preinjected specimens is considerably higher than in the He free specimens over most of the temperature range.

The interpretation of these observations has been discussed in some detail by Williams and Eyre[33]. They proposed that the He atoms diffuse interstitially to form a cluster population during room temperature preinjection. Because of the low recoil energies, this population is not changed significantly during subsequent electron irradiation, and at low temperatures, when r_v^{crit} is small as calculated from Eq. (8), all of the He clusters act as supercritical void nuclei. The critical radius remains small, i.e. < 2 Å, up to 550-600°C and thus C_v is expected to



(a) (b)

Fig. 6a. Arrhenius plots of C_v versus Temperature for S.T. FV548 following neutron irradiation, electron irradiation with He preinjection and electron irradiation with no He preinjection. Fig. 6b. Plots of $(\bar{r}_v)^3$ versus dose for S.T. FV548 electron irradiated at 600°C with and without He preinjection.

remain independent of electron irradiation temperature over this range. At 600°C and above r_v^{crit} (as calculated from Eq. (9)) increases sharply so that an increasingly small fraction of the He atom clusters act as a supercritical nucleus and thus C_v is expected to decrease. There is, therefore, good agreement between predicted and observed behaviour. It is interesting to note that the proposed model predicts that if the He level is increased, resulting in the He cluster population moving to larger sizes, C_v at 650°C should increase. Also, if He preinjection is carried out at the same temperature as the subsequent electron irradiation we expect C_v to decrease with increasing temperature over the whole range. Recent unpublished work by Arkell and Williams show that both of these predictions are supported by experimental observations.

With regard to the He preinjected C^{++} ion irradiated specimens

Williams and Eyre[33] concluded that because of the high recoil energies the pre-existing He atom clusters are destroyed as a result of resolution. The similarity in the slope of the Arrhenius plots of C_v versus temperature for ion irradiation (+ He), electron irradiation (no He) and neutron irradiation suggests that in all these cases the rate controlling parameter is the effective free energy for forming a critical sized void nucleus. Moreover, because the effect He preinjection has in increasing C_v in ion irradiated FV548 (and 316) (see Fig. 5a), we conclude that it increases the pre-exponential terms in the nucleation equation.

The effect of the He preinjection on void growth rates in electron irradiated FV548 is shown by Fib. 6b in which $(\bar{r}_v)^3$ is plotted against dose. The general form of the curves is similar to those for electron irradiated 316 (Figs. 4a and b) with exponent, n, remaining constant up to ~10 dpa and then decreasing. However, the values of n are considerably lower than for 316 electron irradiated at 600°C, being 1.7 and 1.3 for He free and He preinjected specimens respectively. This is consistent with the appreciably higher void concentrations in both sets of FV548 specimens. Moreover, reduction in n with He preinjection is consistent with the increase in C_v. On the other hand, the coefficient A is reduced by about an order of magnitude by the addition of He from 3×10^{-19} to 3×10^{-20} which corresponds to an increase in ρ_d by a factor of 4-5.

The effect preinjected He has on overall swelling in electron irradiated FV548 is shown by the swelling versus temperature curves in Fig. 7. We see that He preinjection has a marked effect in reducing swelling even though C_v is increased. This is in marked contrast to heavy ion irradiated 316 in which He preinjection increases void swelling in direct proportion to the increase in C_v[32].

Broadening the discussion to include other compositional effects on void swelling, we need to recognise that these may be complicated due to the role radiation stimulated diffusion and resolution may play in redistributing solute atoms and precipitates[42]. Thus, recoil energy will again be an important factor in governing the effects. There is a considerable amount of evidence to show that composition has a large influence on void swelling, but there have been few systematic investigations of specific

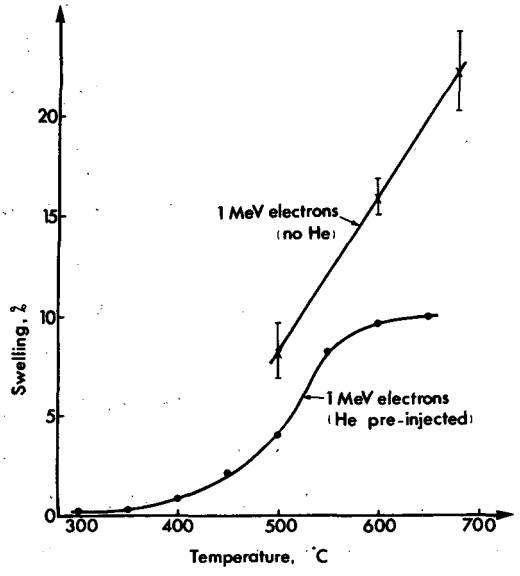


Fig. 7. Swelling versus temperature curves for 1 MeV electron irradiated FV548 with and without He preinjection.

elements. In austenitic steels the element that has been most thoroughly studied is carbon[35,39] and related to these are the comparisons that have been made between stabilised and unstabilised steels[34,43,44]. A comparison has also been made between the swelling behaviour of a high purity and a commercial purity type 316 steel following reactor irradiation[45]. Lastly, Johnston and co-workers[46] have made a systematic study of how swelling varies with major alloy element content and particularly nickel.

Considering first the results related to carbon level and distribution, two series of experiments have been carried out using 1 MeV electron irradiation. In the first it was found that increasing the carbon level from .02 to 1.0 wt% in solution treated 316 resulted in an increase in C_v at 500, 600 and 650°C in He free specimens.[35] Arrhenius plots of the data indicate that it is the pre-exponential terms rather than $\Delta G'$ that is changed. The dose dependence of mean void diameter showed considerable scatter, particularly in the 0.02 wt% carbon alloy but there was a general tendency for void growth to be less in the higher carbon containing alloys. Plots of $(\bar{r}_v)^3$ versus dose at 600°C gave exponent, n, approaching 3 at low doses in all of the alloys but the coefficient A decreased with increasing carbon content the amount being consistent with a decrease in ρ_d by a factor of up to 16 on going from 1.0 wt% carbon to 0.02 wt% carbon. The important practical consequence of increasing carbon content is that the reduction in void growth rate more than counteracts the increase in C_v and therefore void swelling is reduced. It is

emphasised that specimens were slow cooled following solution treatment and therefore most of the carbon was probably precipitated as $M_{23}C_6$. Thus, in the higher carbon specimens the depletion of chromium in the matrix was appreciable and it is feasible that the 1 wt% alloy could have partially transformed to martensite. Consequently the observed changes in C_v, void growth and swelling cannot be interpreted simply in terms of differences in soluble or precipitated carbon in the austenite.

In the second series of experiments[39] FV548 specimens of a given carbon content were subjected to solution treatment at temperatures in the range 1050-1300°C to vary the carbon level in solution. Subsequent electron irradiation of He free specimens did not reveal any systematic differences in C_v. However, the void growth rates were reduced very considerably by increasing the solution treatment temperature. Analysis of the void growth rates shows that increasing the solution treatment temperature does not have any significant effect on n, but it results in A being decreased by about an order of magnitude which is consistent with ρ_d being increased by a factor of 4 or 5. Thus, in this respect, the increase in carbon in solution in FV548 has qualitatively the same effect as increasing the total carbon content in 316. Clearly, the reduction in void growth rate with increasing solution treatment temperature, while C_v remains approximately constant, leads to a reduction in swelling[39].

It appears, therefore, that whereas carbon in solution does not significantly influence void nucleation, carbide precipitates may promote nucleation. Further evidence on this is obtained from observations of voids in ion and neutron irradiated unstabilised[41] and stabilised steels[43,44] in which there appears to be an association between voids and $M_{23}C_6$ precipitates. However, in the case of neutron irradiated 316 at least, this association is only apparent at temperatures >500°C when the precipitates are comparatively large; at lower temperatures when they are in the form of finely distributed spherical particles <200 Å dia there is no correlation between voids and precipitates[9]. Moreover, in FV548 irradiated with 22 MeV C^{++} NbC is precipitated on a fine scale and there is no association between precipitates and voids[40]. This observation suggests that precipitate coherence with the matrix may be an important

factor in deciding whether they act as nucleation sites for voids since, on the one hand $M_{23}C_6$ remains reasonably coherent with the matrix irrespective of size, whereas NbC becomes incoherent at an early stage of its development.

Leitnaker et al[45] have compared C_v, r_v and void swelling in a so-called high purity steel designated HPS (see Table 1) and a commercial purity 316 following neutron irradiation at 500 and 600°C. An important feature of the results is that C_v is appreciably higher in HPS and the limited data indicates that this increase cannot be accounted for by any change in $\Delta G'$. Comparison of Leitnaker et al's results with those discussed earlier (Fig. 3) suggests that void nucleation was not completed in their commercial purity 316 specimens and this accounts in part for the lower C_v. A second important feature of the results is that void diameters are also significantly larger in the HPS. Clearly the combined effect of increasing both C_v and r_v is to also increase the swelling in the high purity steel.

Relating the observed changes in void parameters to compositional differences, our earlier discussion indicates that a reduction in carbon level will not result in an increase in C_v but it could be an important factor in causing a higher void growth rate. Of the other elements that are reduced in the HPS, Leitnaker et al concludes that Mn probably does not have a significant affect on void nucleation and growth which leave Si and/or the trace elements S, P and N. Evidence has been obtained[35] to show that increasing the Si level in commercial purity 316 causes a reduction in void growth rate.

Turning now to the question of how changes in the major alloy elements influence void swelling characteristics, a number of observations have been reported which indicate that nickel plays an important role. For example, type 304 steel which has 8% nickel swells at a higher rate than the higher nickel containing steels such as type 316[47] and there is a range of evidence to show that the high nickel containing alloys such as PE16 swell much less than the austenitic stainless steels[48]. In a recent paper Johnston et al[46] reported preliminary results from a systematic series of experiments aimed primarily at determining the influence of nickel on the swelling of austenitic alloys. They investigated both a

range of commercial alloys and a range of synthesised pure Fe-Cr-Ni alloys. The irradiations were carried out on the preinjected specimens with 5 MeV Ni^{++}, generally to one dose, 140 dpa, and at one temperature, 625°C. Thus, the conclusions on how nickel influences void nucleation and growth are limited at this stage. Nevertheless, the results exposed some interesting trends, particularly on how C_V and $\bar{d}_v$ varies with nickel content. The early work on PE16[48] and other high nickel containing alloys indicated that void nucleation is suppressed in these alloys compared with the traditional austenitic steels. The effect is confirmed by Johnston's results from the range of commercial alloys and this is illustrated by Fig. 8a. It can be seen that C_V decreases with increasing Ni content to a minimum value of $\sim 10^{13}$ cm^{-3} at 40-50 wt% Ni and then increases to $>10^{15}$ cm^{-3} in pure nickel.

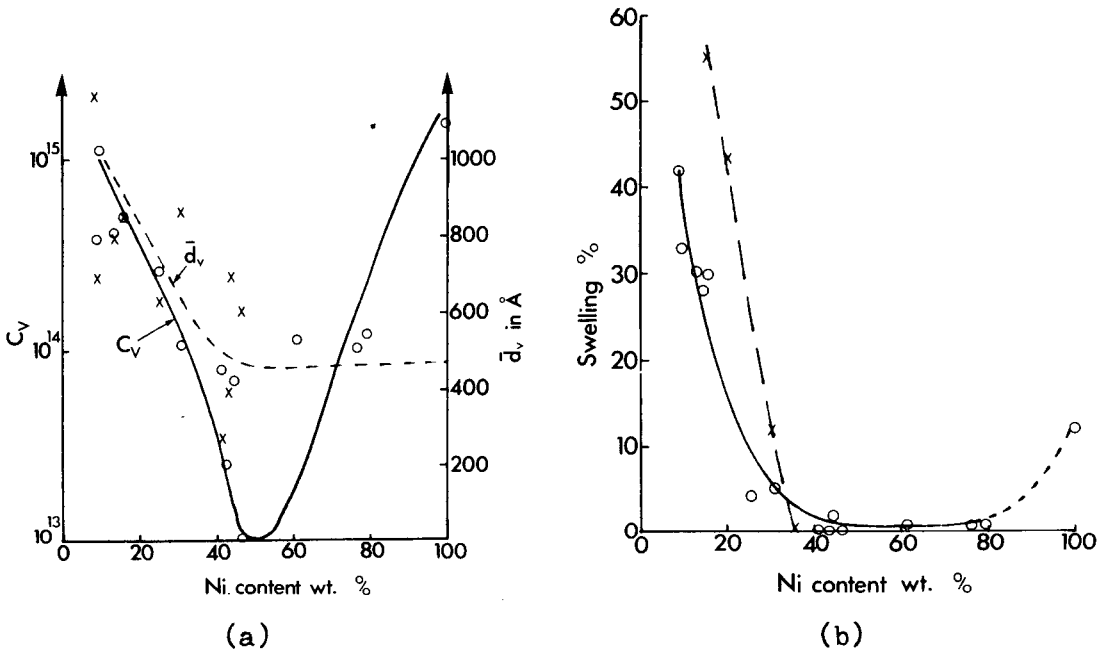


Fig. 8a and b. Plots of the variation in C_V, $\bar{d}_v$ and void swelling with increasing Ni content in a series of commercial alloys and pure Fe-Cr-Ni alloys following irradiation with 5 MeV Ni^+ to 140 dpa at 625°C.

Also included in Fig. 8a is a plot of $\bar{d}_v$ and we see that it also decreases with increasing Ni content to a minimum value of 400-500 Å at 40-50 wt% Ni, but it remains fairly constant on going to higher nickel contents. It is emphasised that elements other than Ni are also changing on going from one alloy to another precluding any interpretation of the trends shown in

Fig. 8a simply in terms of Ni content. It will be interesting to obtain similar plots of the data from the pure Fe-Cr-Ni alloys. In fact, Johnston et al have compared the volume swelling in the commercial and pure alloys. Their results are shown in Fig. 8b in which it can be seen that swelling achieves a minimum at 40 wt% nickel above which it increases. Comparison of Figs. 8a and b show that up to 40 wt% nickel the decrease in volume swelling is due to a decrease in both C_v and $\bar{d}_v$ whereas the increase in higher nickel alloys is due principally to the increase in C_v.

Further examples of void nucleation being suppressed by alloying additions have been observed in a series of heavy ion irradiation experiments on He preinjected binary nickel alloys containing Al, Cu, Fe or Cr [49-51]. Invariably irradiation at 525°C led to void nucleation being completely suppressed or to C_v being lower than in pure Ni and in most cases this led to a reduction in swelling. It was proposed that the main role of the solute additions was to trap He atoms, thus inhibiting them from acting as nucleation sites for voids. A further possibility is that the solute atoms segregate to vacancy loops, formed as a result of cascade collapse, thereby suppressing vacancy emission. A particularly interesting feature of the results is that irradiation of Ni - 27 atom% Cr alloy at >650°C resulted in higher swelling than in pure Ni. This is again consistent with segregation to vacancy loops effectively increasing the thermal emission temperature by adding a binding energy to the vacancy formation energy. Clearly, the effectsof solutes on the vacancy component of the damage structure need to be explored more thoroughly.

To conclude our discussion of fcc metals, we consider briefly the effect prior cold work (C.W.) has on void swelling. Most of the evidence has been obtained from stainless steels and it has been generally observed that >10-20% C.W. has the effect of reducing swelling and shifting the swelling peak to a higher temperature. Results from neutron and 22 MeV C^{++} ion irradiated 316 and 321 steels in the S.T. and 20% C.W. conditions has shown that C.W. has no significant effect on C_v but it increases the incubation period prior to the onset of void growth[36,41,52]. Johnston et al's[32] observations on 20% C.W. 316 show that once the dose for void growth rate has been exceeded the swelling rate is the same as that for

S.T. material. It has also been observed that at temperatures >600°C the C.W. structure recovers, at least in unstabilised steels such as 316 and 304, and the difference in swelling rates between S.T. and C.W. materials is reduced[53]. The mechanism by which C.W. suppress void swelling is not understood in detail but it is generally thought that when the dislocation density is high the dislocation segments act as the dominant sink for vacancies and interstitials. It has also been suggested that the dislocations delay void nucleation by trapping He and/or residual gas atoms.

Turning now to consider briefly the situation in bcc metals, it is emphasised that much less work has been reported on their void swelling characteristics than for the austenitic alloys. On the other hand, much more is known about how the other components of the damage structure, i.e. interstitial and vacancy loops, develop during irradiation over a wide temperature range. Most of the studies of damage in bcc metals, including voids, have been carried out on neutron irradiated molybdenum and TZM and we shall limit ourselves to discussing these cases.

Considering first the evidence regarding void nucleation in neutron irradiated Mo and TZM[54-57] there are three main features that distinguish them from austenitic alloys. Firstly, the threshold dose for the formation of visible voids is low, i.e. down to $<10^{20}$ n.cm^{-2} or $<<1$ dpa[12,56,58]. Secondly, the temperature range over which voids are observed is much wider extending from 330°C[12] to 1300°C[56], i.e. 0.2 Tm to 0.55 Tm. Thirdly, at temperatures up to 7-800°C C_V is both much higher and weakly dependent on temperature, ranging from 10^{17} cm^{-3} at 450°C to 5×10^{16} at 700-800°C. Above 800°C C_V decreases exponentially with temperature falling to $\sim 10^{12}$ cm^{-3} at 1300°C[57]. A further important feature that characterises void formation in bcc metals, although it is by no means exclusive to this crystal structure, is that after sufficiently high doses, i.e. >1 dpa, the voids exhibit long range order tending to form a bcc lattice[59,60]. With regard to void growth during neutron irradiation, no systematic studies have been made but comparing results from different experiments indicate that the rate is low over the whole temperature range and volume swelling has rarely been observed to exceed 1%[57].

The limited evidence from heavy ion irradiation experiments on

molybdenum are broadly consistent with the neutron irradiation results[56,61]. As expected C_v is higher at a given temperature because of the higher dose rate, but the insensitivity of C_v to temperature, low void growth and low swelling are again observed. In fact, Evans[61] observed dose dependence of void diameter in molybdenum irradiated with 2 MeV N^+ at 900°C gives an exponent n of ~ 0.75-1.0, which is consistent with the void component being the dominant sink, i.e. $k_v^2 > k_d^2$ (Eq. (12)). A particularly interesting feature of the results is that unlike austenitic steels, the swelling characteristics appear to be insensitive to ion mass and therefore recoil energy. For example, Evans[57] using 2 MeV N^+ and Brimhall et al[56] using 7.5 MeV Ta^{++} obtained almost identical swelling after 100 dpa at 900°C.

By relating the void observations to the observed behaviour of interstitial and vacancy loops we can build up a self consistent picture of how the damage structure develops in molybdenum during irradiation. We have seen that the void formation and growth characteristics are fundamentally different to those in austenitic alloys and we believe that a major factor causing this difference is the extremely high stacking fault energy in molybdenum. In particular, it leads to early unfaulting of the interstitial loops and this, in turn, results in the dislocation component of the structure coarsening at an anomalously low temperature compared with fcc metals. Furthermore, it provides a major barrier to the nucleation of faulted vacancy loops in the cascades and at temperatures at which long range vacancy migration can occur, i.e. >200°C, we believe that the vacancies diffuse away and are available to nucleate voids. Thus, the situation is similar to that existing during electron irradiation and in many respects void formation and growth in neutron irradiated molybdenum is similar to that in electron irradiated stainless steels, i.e. low threshold temperature for forming visible voids and a low incubation dose. An important conclusion from the results for molybdenum is that the cascades do not play a particularly important role in the development of the damage structure at elevated temperatures and thus, recoil energy is not an important factor.

A second important feature of the observations is the very high C_v in molybdenum up to quite high temperatures, i.e. 800°C = 0.37 Tm. This

is consistent with the existence of a high vacancy supersaturation which provides a strong driving force for nucleation. Two factors contribute to this high supersaturation. Firstly, the low dislocation density, which is typically 1-2 orders of magnitude lower than in fcc metals at equivalent homologous temperatures and doses, means that the sink density for vacancies is low in the early stages of irradiation. Secondly, we believe that the vacancy migration to formation energy ratio is lower in molybdenum (E_v^m/E_v^f 0.5) than in fcc metals (typically E_v^m/E_v^f 0.8-1.0) which means that the vacancy supersaturation is higher for a given vacancy concentration at equivalent homologous temperatures. The important consequence of having a high C_v combined with a low dislocation density is that the voids are the dominant sink for both vacancies and interstitials resulting in a low void growth rate and low swelling.

CONCLUDING REMARKS

In this paper we have attempted to select particular aspects of the high temperature damage problem on which experimental studies have led to an improvement in our understanding. Naturally, the subject has been dominated by the need to characterise the void swelling characteristics of commercial alloys. However, we have emphasised that to understand the development of any one component of the structure during irradiation we have to take into account its interaction with the other components of the structure. Thus it is necessary to study the damage structure as a whole and there is a need for more comprehensive quantitative and geometrical analysis of high temperature structures, particularly in alloys, following irradiation to low doses.

The present discussion of how damage structures vary with irradiation conditions has pointed to the important role played by recoil energy. A major aspect of this is the collapse of cascades to form vacancy loops and their is a need to obtain a better understanding of the factors affecting the collapse process. Of particular interest is the fundamentally different behaviour between fcc and bcc metals which has important implications to their void swelling characteristics. A second important

aspect concerning recoil energy is its effect on the redistribution of solutes and phases, including gases, as a result of resolution and radiation stimulated diffusion.

A major area that has been neglected experimentally is the nucleation of point defect clusters during irradiation. Although nucleation occurs most rapidly during the early stages, it plays a fundamentally important role in determining the sink distribution throughout irradiation. There is a recognition of the important role played by gases, particularly in the nucleation of voids, but we need to clarify the respective roles played by inert and residual surface active gases.

A particularly important aspect of the nucleation problem is the role played by solutes and second phases. In the final part of the paper we considered how void swelling is related to metallurgical parameters such as composition and C.W. and we showed that progress has been made in isolating the factors that lead to swelling resistance. A general feature highlighted by the results is that swelling resistance requires an imbalance in the sink distribution, i.e. $k_d^2 \gg k_v^2$ as in nickel based alloys and C.W. stainless steels, or $k_v^2 \gg k_d^2$ as in molybdenum and its alloy TZM. Particularly intriguing are the trends observed by Johnston et al[46] in the Fe-Ni-Cr system as a function of nickel content. Harries[62] has discussed the void swelling characteristics of these alloys in terms of their position on the constitution diagram. He concludes that alloys close the $\gamma - \sigma$ phase boundary, e.g. many of the stainless steels, exhibit poor void swelling resistance and suggest that this could be a consequence of sigma phase formation during irradiation, whereas alloy in the centre of γ phase field such as PE16 exhibit good swelling resistance. However, there is need to understand these trends in terms of how they affect the nucleation and growth of the interstitial and vacancy components of the damage structure.

TABLE 1

Typical Compositions of Austenitic Alloys

Element	316	HPS	304	FV548	321	P.E.16
Fe	64.6	65	69	67.5	70	34.1
Cr	17	17.5	18	16.5	18	16.6
Ni	13	14.4	9	12	9.5	<42.3
Mn	1.8	<0.001	1.8	1.4	1.8	0.12
Mo	2	2.8	0.4	1.1	-	3.6
Si	0.7	0.01	0.72	0.4	0.6	0.2
Al	-	-	-	-	-	0.99
Ti	<.02	-	<.02	-	0.33	1.31
Nb	-	-	-	0.9	-	-
V	-	-	-	-	-	-
Ta	-	-	-	-	-	-
C	0.05	0.005	0.07	0.11	0.05	0.06
N	0.03	0.0003	0.03	0.03	0.005	-
S	0.005	0.002	0.005	0.005	0.005	0.004
P	0.02	0.03	0.03	0.01	0.03	0.003
B	0.002	-	-	0.002	-	0.001

REFERENCES

1. R. Bullough, B.L. Eyre and R.C. Perrin, Nucl. Appl. and Tech. 9, 346, (1970).
2. S.D. Harkness and Che-Yu Li, Met. Trans., 2, 1457, (1971).
3. R. Bullough, B.L. Eyre and K. Krishan, Proc. Roy. Soc. (in press).
4. B.L. Eyre and R. Bullough, Phil. Mag., 12, 31, (1965).
5. N. Yoshida and M. Kiritani, J. Phys. Soc. Japan, 35, 1418, (1973).
6. M.R. Hayns, J. Nucl. Matls, 56, 267, (1975).
7. H.R. Brager and J.L. Straaslund, J. Nucl. Matls., 46, 134, (1973).
8. E.E. Bloom, J.O. Steigler and C.J. McHargue, Rad. Effects, 14, 231, (1972).
9. P.J. Barton, D. Stow and B.L. Eyre, Irradiation Behaviour of Fuel Cladding and Core Component Materials. Conference organised by KTG/ BNES, December 1974.
10. T.M. Williams, unpublished work.
11. B.L. Eyre and D.M. Maher, Phil. Mag., 24, 745, (1971).
12. J. Bentley, B.L. Eyre and M.H. Loretto, Proceedings of this Conference.
13. K. Urban, Phys. Stat. Solidi a, 4, 761, (1971).
14. A.D. Marwick, J. Nucl. Matls, 55, 259, (1975).
15. B.L. Eyre, J. Phys. F., Metal Physics, 3, 422, (1973).
16. C.A. English, B.L. Eyre, J. Summers and H. Wadley. Proceedings of this Conference.
17. C.A. English, B.L. Eyre, A. Stathopoulos and H. Wadley. Proceedings of this Conference.
18. M. Labbe and J. Poirier, J. Nucl. Matls., 46, 86, (1973).
19. V. Levy, The Physics of Irradiation Produced Voids. Harwell Report AERE-R 7934 edited by R.S. Nelson (1975).
20. C.A. English, B.L. Eyre, K. Shoiab and T.M. Williams, J. Nucl. Matls. (in press).
21. J.A. Hudson, Void Formation in Solution Treated AISI 316 and 321 Stainless Steels Under 46.5 MeV Ni^{6+} Irradiation, Harwell Report AERE-R 7922, (1975).
22. M.R. Rühle, Phys. Stat. Solidi, 19, 279, (1967).
23. F. Haussermann, M.R. Rühle and M. Wilkens, Phys. Stat. Solidi, 50, 445, (1972).

24. C.A. English, B.L. Eyre and H. Wadley. The Effects of Material Purity and Irradiation Temperature on Vacancy Cluster Damage in Molybdenum Irradiated with Self Ions, Harwell Report AERE-R 8083, (1975).

25. K.C. Russell, Acta. Met., 19, 753, (1971).

26. J.L. Katz, H. Weidersich, J. Chem. Phys., 55, 1414, (1971).

27. R. Bullough R.C. Perrin, Radiation-Induced Voids in Metals. Proceedings of Conference held at Albany, New York, June 1971. Edited by J.W. Corbett and I.C. Ianello, Pub : USAEC, (1972).

28. A.D. Brailsford and R. Bullough, J. Nucl. Matls, 44, 121, (1972).

29. M.R. Hayns and R. Bullough, Radiation Effects and Tritium Technology for Fusion Reactors, Conference held in Gatlinburg, Tennessee, October 1975. Proceedings to be published.

30. V. Levy, J.M. Lanore, L. Glowinski,A. Risbot, P. Regnier, J.L. Flament Y. Adda, Proceedings of this Conference.

31. M.J. Makin and G.P. Walters, Physical Metallurgy of Reactor Materials Proceedings of a Conference held at Berkeley Nuclear Laboratories, Berkeley, U.K.

32. W.G. Johnston, J.H. Rosolowski and A.M. Turkalo, J. Nucl. Matls., 48, 330, (1973).

33. T.M. Williams and B.L. Eyre, J. Nucl. Matls, in press.

34. W.K. Appleby, D.W. Sandusky and V.E. Wolff, Radiation Induced Voids in Metals, Proceedings of Conference held at Albany, New York, June 1971. Edited by J.W. Corbett and I.C. Ianello. Pub : USAEC, (1972).

35. M.J. Makin and G.P. Walters, The Physics of Irradiation Produced Voids. Harwell Report, AERE-R 7934 edited by R.S. Nelson (1975).

36. T.M. Williams, Voids Formed by Irradiation of Reactor Materials, Proceedings edited by S.F. Pugh, M.H. Loretto and I.C. Ianello, Pub : BNES (1972).

37. E.E. Bloom and J.O. Steigler, J. Nucl. Matls., 36, 331, (1970).

38. R.S. Nelson, J.A. Hudson and D.J. Mazey, Voids Formed by Irradiation of Reactor Materials. Proceedings of Conference held at Reading, U.K., March 1971. Proceedings edited by S.F. Pugh, M.H. Loretto and D.I.R. Norris. Pub. by BNES, (1972).

39. M.J. Makin and G.P. Walters, unpublished work.

40. T.M. Williams and D.R. Arkell, unpublished work.

41. C. Cawthorne, E.J. Fulton, J.I. Bramman, G.A.B. Linekar and R.M. Sharpe. Voids Formed by Irradiation of Reactor Materials. Proceedings edited by S.F. Pugh, M.H. Loretto and D.I.R. Norris. Pub. by BNES, (1972).

42. J.A. Hudson, Structural Stability During Irradiation. Harwell Report AERE-R 7943, (1975).

43. K. Ehrlich and N.H. Rackan, Effects of Radiation on Sub-structure and Mechanical Properties of Metals and Alloys. Proceedings of an ASTM symposium held at Los Angelos, Calif., June 1972. ASTM STP, 529,(1973)

44. W.K. Appleby and V.E. Wolff, Effects of Radiation on Sub-structure and Mechanical Properties of Metals and Alloys. Proceedings of an ASTM symposium held at Los Angelos Calif., June 1972, ASTM STP, 529, (1973).

45. J.M. Leitnaker, E.E. Bloom and J.O. Steigler, J. Nucl. Matls., 49, 57, (1973/74).

46. W.G. Johnston, J.H. Rosolowski, A.M. Turkalo and T. Lauritzen, J. Nucl.Matls. 54, 24, (1974).

47. E.E. Bloom, Radiation Induced Voids in Metals, Proceedings of a Conference held at Albany, N.Y., June 1971. Edited by J.W. Corbett and I.C. Ianello. Pub : USAEC, (1972).

48. J.A. Hudson, D.J. Mazey and R.S. Nelson. Voids Formed by Irradiation of Reactor Materials. Proceedings edited by S.F. Pugh, M.H. Loretto and D.I.R. Norris. Pub : BNES, (1972).

49. D.J. Mazey and F. Menzinger. Resistance to Void Formation of Cu-Ni Alloys. Harwell Report AERE-R 7410, (1973).

50. J.A. Hudson, S.J. Francis, D.J. Mazey and R.S. Nelson. Effects of Radiation on Sub-structure and Mechanical Properties of Metals and Alloys. Proceedings of an ASTM symposium held at Los Angelos, Calif., June 1972. ASTM STP, 529, (1973).

51. J.A. Hudson and S. Ashby. The Physics of Irradiation Produced Voids Harwell Report, AERE-R 7934, edited by R.S. Nelson, (1975).

52. G.P. Walters, Voids Formed by Irradiation of Reactor Materials. Proceedings edited by S.F. Pugh, M.H. Loretto and D.I.R. Norris, Pub : BNES, (1972).

53. S.G. McDonald and A. Taylor, Effects of Radiation on Sub-structure and

Mechanical Properties of Metals and Alloys. Proceedings of an ASTM symposium held at Los Angelos, Calif., June 1972. ASTM STP 529, (1973).

54. B.L. Eyre and A.F. Bartlett, J. Nucl. Matls, 47, 143, (1973).
55. F.W. Wiffen, Radiation Induced Voids in Metals. Proceedings of a Conference held at Albany, N.Y., June 1971. Edited by J.W. Corbett and I.C. Ianello. Pub : USAEC, (1972).
56. J.L. Brimhall, E.P. Simonen and H.E. Kissinger, J. Nucl. Matls., 48, 339, (1973).
57. V.K. Sikka and J. Moteff, J. Nucl. Matls., 54, 325, (1974).
58. J.D. Elen, G. Hamburg and A. Mastenbroek, J. Nucl. Matls., 39, 194, (1971).
59. J.H. Evans, Nature, 229, 403, (1971).
60. B.L. Eyre and J.H. Evans. Effects of Radiation on Sub-structure and Mechanical Properties of Metals and Alloys. Proceedings of an ASTM symposium held at Los Angelos, Calif., June 1972. ASTM STP 529, (1973).
61. J.H. Evans, Rad. Effects, 8, 115, (1971).
62. D.R. Harries, The Physics of Irradiation Produced Voids, Harwell Report, AERE-R 7934. Edited by R.S. Nelson, (1975).

THEORY OF THE NUCLEATION GROWTH AND ANNEALING OF INTERSTITIAL DISLOCATION LOOPS

M.R. Hayns
Theoretical Physics Division
AERE Harwell, Oxon OX11 ORA
United Kingdom

ABSTRACT

The nucleation and growth kinetics of interstitial dislocation loops is treated by a rate theory approach which allows aggregates of up to 10^6 atoms to be considered. A binary nucleation model is assumed and its consequences investigated.

Calculations of the loop concentration and size distribution are made for M316 steel, which is of particular interest for fast reactor materials studies. The effects of differing dose rates, to allow comparisons between the HVEM, VEC and reactor conditions and the consequences of cold working are assessed by means of suitable calculations.

The model contains both forward and reverse mechanisms, that is, interstitial and vacancy absorption, and vacancy emission, therefore the dynamics of high temperature annealing experiments may be detailed and the results utilized to analyse the experimental evidence for these conditions.

INTRODUCTION

The precipitation of interstitial dislocation loops from a super-saturated solution of point defects is one of the most important pre-

requisits for void growth in irradiated, solution treated steels, since it provides a biased sink for interstitials. It has been clearly shown that the degree and temperature dependence of void swelling is concerned intimately with the development of the interstitial loop population[1]. Unfortunately the direct observation and measurement of these loops in the alloy steels of interest for reactor applications is very difficult under neutron irradiation conditions, whilst results from simulation experiments in the VEC (Variable Energy Cyclotron) and HVEM (High Voltage Electron Microscope) facilities must be correlated with the neutron irradiation situation in a similar way to void swelling[2] and this requires detailed knowledge of the physical mechanisms governing their nucleation and growth. It is the purpose of this work to present a theoretical model for the nucleation and growth of interstitial loops which is computationally useful but still retains sufficient information to allow a detailed theoretical analysis. It is based upon the well known chemical rate theory method and this has the advantages that it is conceptually simple and that further physical processes which could influence the nucleation and growth behaviour of the loops are readily incorporated into the model. The basic method has already been described in detail[3] and here we shall concentrate upon describing improvements to the original scheme. These are the inclusion of a clustering method similar to that devised by Kiritani[4] which combines rate equations and makes it possible to include large (i.e. containing in excess of 10^6 atoms) loops into the calculation without undue computational effort and the allowance of thermal emission of vacancies from interstitial loops which facilitates the investigation of high temperature effects.

Calculations have been performed with parameters appropriate to M316 stainless steel in both the solution treated and cold-worked conditions for dose rates varying from 5×10^{-3}dpa/sec. (for the HVEM) to 10^{-6}dpa/sec (for neutron irradiation in a fast reactor situation) and for a range of temperatures. We also briefly discuss the high temperature behaviour of the loops by means of calculations which simulate a post-irradiation annealing experiment.

The model is still undergoing development and so several potentially important mechanisms are not included, notably the trapping of point defects at impurity sites and the co-precipitation of vacancy and interstitial loops during heavy ion and neutron irradiated systems. The first of these is currently being investigated and will be incorporated shortly, whilst the second is more difficult with the present formulation of the model[5].

THE THEORETICAL MODEL

The rate theory model has been described in detail previously so here we shall concentrate only upon the modifications necessary to include the thermal emission of vacancies and the grouping scheme. The fundamental assumptions of the theory are that nucleation occurs homogeneously throughout the material, that a di-interstitial pair is a stable immobile nucleus and that the densities of other sinks in the system are low enough to allow the use of continuum defect loss rates to them. The full rate equations for the interstitial loop problem may be written,

$$\frac{dc_v}{dt} = K_T - \alpha c_i c_v - \sum_{n=2}^{M} A_n c_v - D_v \rho_D c_v - D_v \frac{6}{d} c_v \sqrt{g \sum_{n=2}^{M} A_n + \rho_D}, \qquad (1)$$

$$\frac{dc_i}{dt} = K - \alpha c_i c_v - \sum_{n=2}^{M} I_n c_i - D_i \rho_D c_i - D_i \frac{6}{d} c_i \sqrt{g \sum_{n=2}^{M} I_n + \rho_D}, \qquad (2)$$

and

$$\frac{d\bar{C}_j}{dt} = \frac{2\Delta n_{j-1}}{\Delta n_j (\Delta n_j + \Delta n_{j-1})} (I_{j-1} + E_{j-1}) \bar{C}_{j-1} - \frac{2}{(\Delta n_{j+1} + \Delta n_j)} (I_j + E_j) \bar{C}_j \qquad (3)$$

$$- \frac{2}{(\Delta n_j + \Delta n_{j-1})} A_j \bar{C}_j + \frac{2\Delta n_{j+1}}{\Delta n_j (\Delta n_{j+1} + \Delta n_j)} A_{j+1} \bar{C}_{j+1}.$$

Here we have given the rate equations for the vacancy (c_v) and interstitial (c_i) concentrations and one representative equation for the average concentration of loops in the j^{th} group ($\bar{C}_j$) from the remaining set of M-2 equations. Each term in equation 3 is weighted according to the number of single equations which have been condensed into it. The width of the j^{th} equation is $\Delta n_j = n_j - n_{j-1}$ where n_j is the number of atoms in a loop at the upper limit of the j^{th} group. This scheme is very similar to that devised by Kiritani[4]. We retain a number of single equations at the beginning of the hierarchy since they govern the nucleation stage and hence the ultimate total loop concentration; since we know that nucleation is complete very quickly in these conditions we need to retain relatively few ungrouped equations. The form of these equations is readily seen by putting $\Delta n_j = 1$ in equation 3. If we assume that we have k ungrouped equations then the algorithm[6] $\Delta n_j = (n_{j-1}+1)/k$ may be used to provide the group width as a function of the number of atoms in the loops covered by that equation. This provides a convenient computational scheme and ensures that numerical instabilities[7] associated with the transition from grouped to un-grouped equations are minimised. In the calculations to be reported below we have used a value of k=20, which allows loops containing in excess of 5×10^4 atoms to be covered by 100 rate equations and this represents a reasonable compromise between computational effort and accuracy. The quantities I_j are the rate constants for the absorption of interstitials by loops in the j^{th} group, multiplied by the interstitial loop concentration, i.e. in the terminology of reference 3, $I_j = R_j \bar{C}_j$ and the quantity R_j is given by

$$R_j = Z_i D_i \frac{2\Pi}{\Omega} \sqrt{\frac{\bar{n}_j A}{\Pi}} \qquad (4)$$

where Z_i is the bias for interstitials, Ω is the atomic volume, A is the area per atom and is $a^2\sqrt{3}/4$ for {111} loops in an f.C.C. lattice, a is the lattice constant and D_i is given by $D_i = \gamma a^2 \nu_i \exp(-E_m^i/kT)$ where ν_i is the attempt frequency, $\gamma = 1/12$ for f.c.c. structure and E_m^i is the interstitial migration energy. Similarly the quantities A_j are the rate

constants for vacancy absorption and are defined in reference 3 and are similar to R_n, with E_m^i replaced by the vacancy migration energy E_m^v and ν_i replaced by ν_v. The quantities E_j are terms defining the rate of thermal emission of vacancies from the interstitial loops and are defined by $D_v \bar{c}_v$ where $\bar{c}_v$ is the vacancy concentration adjacent to a loop in the $j^{\underline{th}}$ group and is[1]

$$\bar{c}_v = c_v^e \exp\left[-(\gamma_{SF} + F_{e\ell})b^2/kT\right], \tag{5}$$

in the absence of any external stress. Here γ_{SF} is the stacking fault energy, $F_{e\ell}$ the elastic energy, defined by

$$\frac{\mu' b^2}{4\pi(\bar{r}_j+b)} \log\left(\frac{\bar{r}_j+b}{b}\right) \tag{6}$$

where μ' is the effective shear modulus and r_j the mean radius of a loop in the j^{th} group. c_v^e is the equilibrium thermal vacancy concentration ($c_v^e = \exp(-E_m^f/kT)$ and b is the Burgers vector. Equations (1) and (2) contain in addition the continuum grain boundary loss terms for interstitials and vacancies[1]. The quantity α in those equations is the recombination coefficient. The only remaining difference from the earlier equations lies in the generation rate of point defects. K is the rate of production of interstitials by the incident irradiation, whilst K_T is the total production rate of vacancies and now includes the thermal contributions, ie $K_T = K_{TH} + K$, and K_{TH} is given by

$$K_{TH} = D_v \left\{ \sum_{m=2}^{N} E_m \bar{C}_m + \left(\rho_D + \frac{6}{dg}\sqrt{\sum_{m=2}^{M} E_m \bar{C}_m + \rho_D}\right) c_v^e \right\} \tag{7}$$

where the second term in parentheses is the thermal emission rate from network dislocations, present in a quantity of ρ_D cm/cm^3 and from grain boundaries. We have not included the possibility of thermal dissociation of di-interstitial pairs since our earlier work has shown that this is not significant. These equations are integrated numerically using a Harwell library subroutine based upon Gears method[8].

RESULTS OF CALCULATIONS ON M316 STAINLESS STEEL

All of the calculations to be discussed below have been performed using the data set out in table 1 which is representative of M316 stainless steel.

Table 1 Parameters for M316 Stainless Steel

E_m^i (e.v)	E_m^v (e.v)	E_f^v (e.v)	ν_i, ν_v (sec^{-1})	a (cm)	b (cm)	γ_{SF} ($ergs/cm^2$)	μ' ($dynes/cm^2$)	α/D_i (cm^{-2})	d_g (μm)
0.2	1.3	1.6	10^{13}	3.6×10^{-8}	2×10^{-8}	9.4×10^{12}	8.0×10^{11}	1.0×10^{16}	70.0

Evolution of the size distribution:- The approximate solution of the growth equations by means of the hierarchy of rate equations gives a very detailed picture of the evolution of the size distribution of the loop population. With the grouping method this may be followed to sufficient doses to cover loops of observable sizes. As an illustration we show in figure (1) the calculated size distributions for a temperature of 723K, for a typical reactor dose rate of 10^{-6} dpa/sec and for solution treated material ($\rho_D = 10^9 cm/cm^3$). The end of nucleation is achieved in $\sim 4\times10^{-6}$ dpa ie $\sim$ 4 seconds according to the definition of end of nucleation defined previously[3]. At this time the maximum in the distribution occurs for loops containing only 8 atoms, therefore substantiating our use of 20 single equations to cover the nucleation period. After $\sim 2\times10^{-3}$ dpa the maximum occurs at $\sim$ 15,000 atoms, corresponding to a loop radius of $\sim$ 140Å; by 10^{-2} dpa the maximum size has increased to $\sim$ 200Å(30,000 atoms/loop) although for clarity this is not shown in figure 1. These results confirm the very rapid nucleation and growth of interstitial loops already noted previously[3,10].

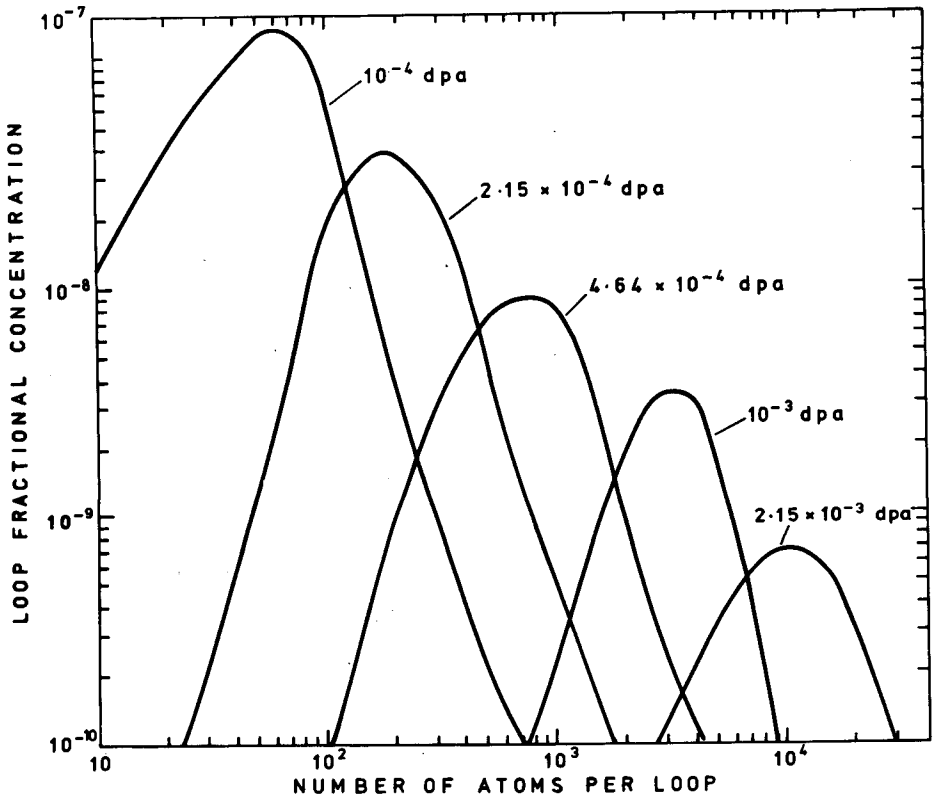


Figure 1. Evolution of the loop size distribution

The temperature dependence of the total loop concentrations:- The temperature dependence of the total loop concentration is shown in figure 2 for various values of the network dislocation density for reactor dose rates. The curves are shown as a function of dose to indicate that in all cases nucleation has been easily achieved in the doses covered by this figure. These results are very similar to those presented previously indicating that the influence on the concentration of loops of the thermal emission of vacancies is small, which is natural since the nucleation period is only concerned with very small loops whose growth rate by thermal emission will be negligible, it is only the subsequent growth stage which will be effected. As expected from

homogeneous nucleation theory the concentration decreases with temperature. The effect of increasing the dose rate

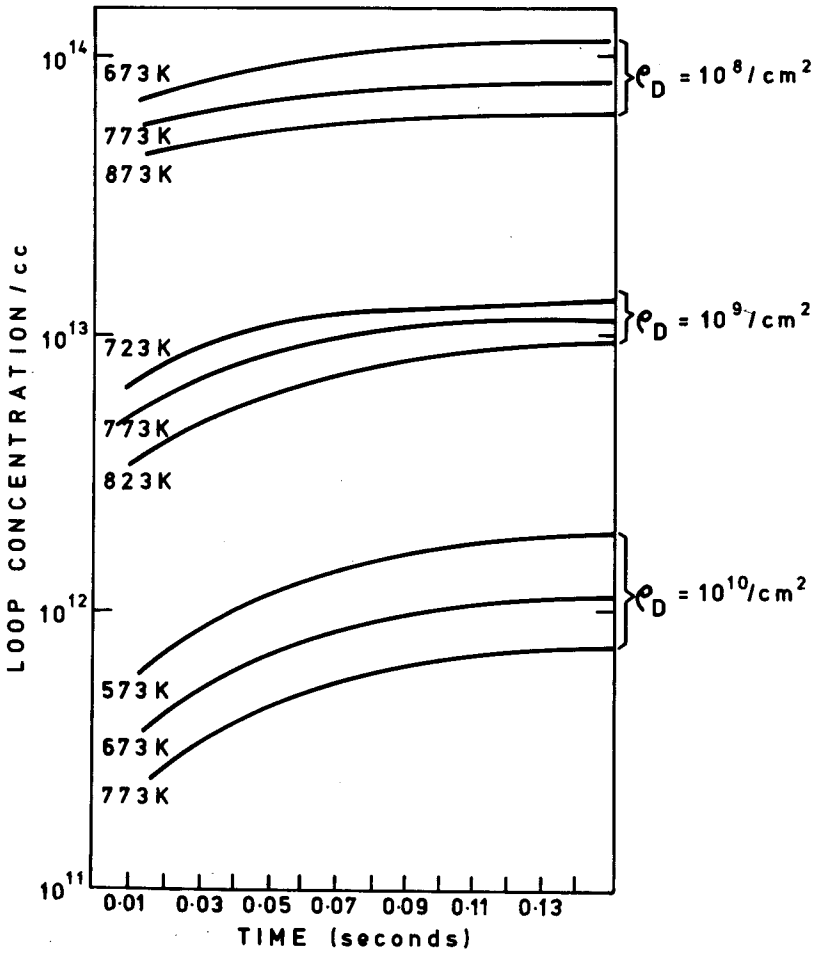


Figure 2. Total loop concentrations for various values of ρ_D

over the value of 10^{-6} for the reactor case is to increase the loop concentrations. For example at 723K, with a dislocation density of 10^8 cm/cm^3 the concentration is increased from $\sim 10^{14}$/cc for the reactor dose rate to $\sim 4\times10^{15}$/cc for a typical VEC dose rate of 10^{-3}dpa/sec and to $\sim 10^{17}$/cm^3 for the HVEM dose rate of 5×10^{-3} dpa/sec. These results may be compared with the values obtained by Bullough, Eyre and Krishan[2] of 2.2×10^{14}/cc, 4.5×10^{15}/cc and 2.2×10^{17}/cc respectively which were

required to fit the void swelling data for solution treated M316.

Annealing of the loop population at high temperatures:- To simulate the behaviour of the interstitial loops during annealing we have made calculations in which the loops were grown "normally" under irradiation (HVEM dose rate) at 873K for 10^{-4}dpa. This is ample time to have completed nucleation and achieved a reasonably sized loop population, the maximum in the population lies at 550 atoms/loop. At this point the computation is arrested, to be restarted with the temperature at 1073K and with no irradiation. We have made no attempt to simulate an experiment in detail by slowly increasing the temperature, although the rate of rise could influence the results quantitatively. Furthermore, in these calculations we have removed the thermal emission terms from grain boundaries. The reasons for this were as follows: the experiments of Mazey and Francis[9] have shown that there is a strong spatial effect in these annealing experiments. The reason is simply that vacancies are emitted freely from grain boundaries and therefore diffuse into the grain, annealing out the loops in passage. The really interesting loop behaviour occurs at the centre of the grain where there is sufficient time for the loop population to emitt and absorb vacancies according to their size and hence change the size distribution. Consequently by ignoring grain boundary emission we are considering in effect an infinitely large grain and this allows a detailed discussion of the growth process. The continuum grain boundary sink term does not allow for the spatial screening of the loops and they are consequently rapidly annealed and this term is retained. We are now proceeding with spatially dependent calculations along the lines of those already discussed for the problem of the denuded layer[10] in thin film electron microscopy. In figure 3 we show the calculated loop size distributions during a 1073K anneal The distribution is seen to move to larger loop sizes as the larger loops grow by vacancy emission and the smaller loop shrink because the external vacancy concentration is increased by the emission from both the larger loops and the dislocation network, although we have kept the latter to a minimum here by using $\rho_D=10^8 cm/cm^2$. This behaviour is qualitatively in keeping with the observations of Mazey and Francis[9].

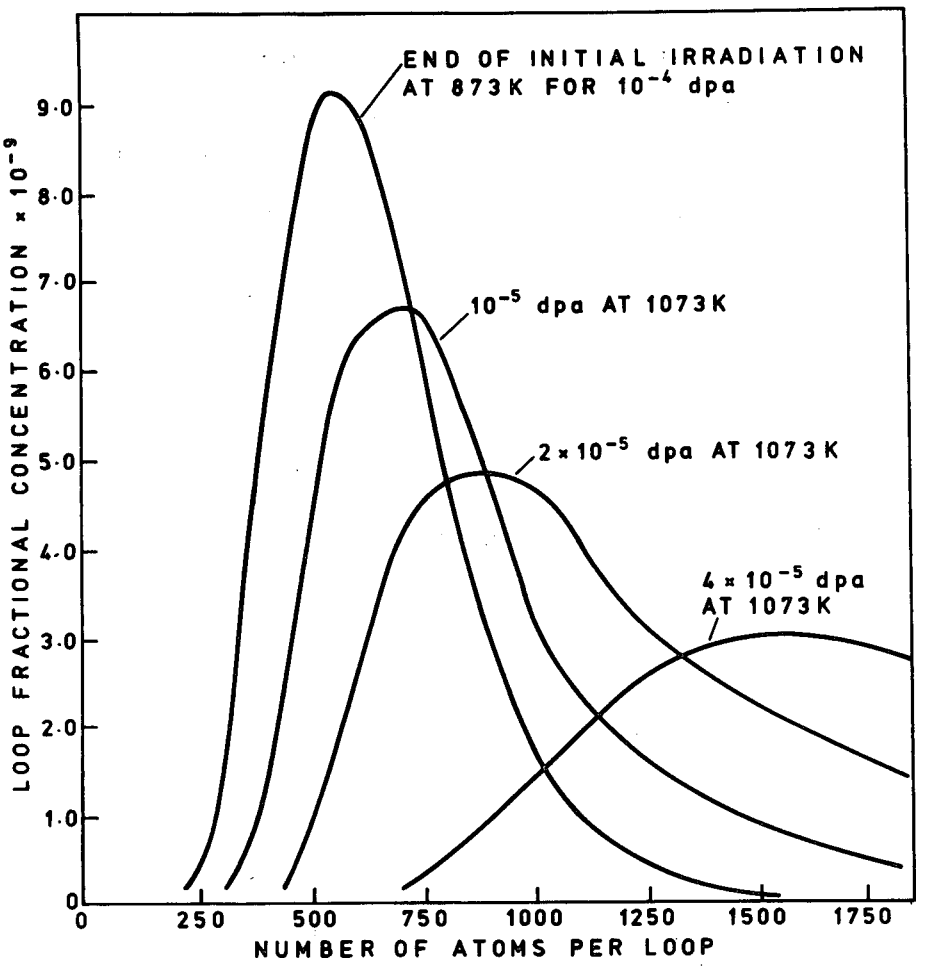


Figure 3. Evolution of the loop size distribution during 1073K anneal. The timescales in this figure are calculated using a virtual dose rate of 5×10^{-3}d.p.a/sec

Unfortunately there is not sufficient space here to discuss the details of the competing physical mechanisms which occur during such an anneal, however, by including a detailed description of the loop distribution function, this model is capable of revealing fascinating information on the loops behaviour.

CONCLUSIONS

The rate theory model for the homogenous nucleation and subsequent growth of interstitial dislocation loops in irradiated materials has been extended to include the thermal emission of vacancies from the loops.

A technique for compressing the number of rate equations to be solved has also been investigated which allows the growth stage of the loops well into the observable domain to be computed. Explicit calculations for conditions appropriate to M316 stainless steel in both neutron irradiation and simulation environments show that quantatively reasonable results are obtained for the total loop concentration whilst the model contains sufficient detailed physical mechanisms to allow the study of the competitive growth of different sized loops during a simulated annealing experiment.

REFERENCES

1. A.D. Brailsford and R. Bullough, J.Nucl.Mat. 44, 121 1972
2. R. Bullough, B.L. Eyre and K. Krishan, Proc.Ro.Soc. to be published 1975 Harwell Res.Rep. R-7952 1975
3. M.R. Hayns, J.Nucl.Mat. 56, 267 1975
4. M. Kiritani, J.Phys.Soc. Japan 35, 1, 95 1973
   and M. Kiritani and N. Yoshida, J.Phys.Soc.Japan 35, 3, 83 1973
5. K.C. Russell and R.W. Powell, Acta.Met. 21 187 1973
6. M.R. Hayns, unpublished work
7. M. Koiwa, J.Phys.Soc.Japan 37, 6, 1532 1974
8. C.W. Gear, Numerical Integration of Stiff Ordinary Differential Equations" Report No. COO-1469-0051, Dept of Computer Science Univ. of Illinois.
9. D.J. Mazey and S. Francis "Consultants Symposium on the Physics of Irradiation Produced Voids" Harwell Res.Rep. AERE R7934, 257 1974
10. M.R. Hayns and R.C. Perrin "Consultants Symposium on the Physics of Irradiation Produced Voids" Harwell Res. Rep. AERE R7934, 188 1974.

THE NUCLEATION OF POINT DEFECT AGGLOMERATES

L.M. Brown, Cavendish Laboratory, Cambridge and
R.M. Mayer, Atomic Energy Board, Pretoria,
South Africa

ABSTRACT

A theory of the agglomeration of point defects into dislocation loops and voids is formulated. A critical comparison between theory and experiment is made for nickel and copper irradiated in a high voltage electron microscope.

INTRODUCTION

Bombarding particles such as X-rays, γ-rays, electrons and neutrons can displace atoms from their lattice sites. We shall limit ourselves in this paper to cases in which the spacing between successive displacements is much greater than the interatomic spacing, so there is no 'spike' formation.

CLUSTERING PROCESS

The great majority of the displaced atoms ('interstitials') and vacancies will recombine provided that one or both species are mobile. A small proportion of the remainder will cluster to form a two defect cluster. The fate of the divacancy which is mobile and the larger vacancy and interstitial atom clusters which are immobile are all similar. They can grow by trapping a like type defect or shrink by trapping a defect of opposite character. In the absence of spike formation, the increasing sink density suppresses nucleation of new clusters, so most nucleation occurs within a fairly well-defined time and

subsequent irradiation produces only growth or shrinkage.

The interstitial loop is the only type of interstitial cluster that has been observed in the electron microscope. It consists of a two dimensional (i.e. one atom thick) cluster of interstitial atoms sandwiched between two layer planes of atoms. A vacancy loop is composed of a cluster of vacancies within a layer plane. We assume that two interstitials form a stable nucleus of an interstitial loop and five vacancies the nucleus of a vacancy loop.

We suppose that the small vacancy atom complex which acts as a nucleus for a vacancy loop can also act as a void nucleus if it traps a mobile gas atom. This is in accordance with the suggestion of Shimomura and Yoshida[1] for the void nucleus in quenched Aℓ and the generally accepted conclusion that gas is necessary to nucleate a void.

We consider the single vacancy to act as a shallow trap for a vacancy thereby decreasing its mobility, but not as a suitable defect for forming a void nucleus. The presence of the di-, tri- and tetra-vacancies have been ignored as they are less numerous than the vacancy defects considered already.

Chemical rate equations have been formulated to describe the variation of the different defect species with time and the set of differential equations have been numerically integrated on the computer[2]. To illustrate the results we calculate the cluster concentrations for two fcc metals, copper and nickel, which have been extensively studied in the high voltage electron microscope.

INTERSTITIAL LOOPS

Calculations based on these rate equations confirm our earlier findings[3] and those of Hossain and Brown[4] that the

interstitial loop concentration approaches its maximum value after a very short nucleation time and that thereafter the loop density saturates. Neither the mobility of the vacancy and divacancy nor the presence of gas atoms nor the preferential drift of interstitials over vacancies to dislocations affect this result. The interstitial loop concentration is described by an equation of the form

$$NLI = K\ (G/V_i \Omega) \qquad (1)$$

where G is the defect generation rate, V_i the interstitial atom velocity, Ω the mutual capture cross-section and K a numerical constant of the order one.

Equation (1) has been verified by a number of experiments[4,5,6] from which it is also possible to derive the migration energy of an interstitial E_{mi}:

Metal	Cu[4,5]	Ni[4]	Au[6]	Mg[4]	Fe[6]	Aℓ[6]
E_{mi} (eV)	0.12	0.21	0.19	0.06	0.26	0.08

The values obtained by Kiritani and Yoshida[6] may require adjustment because of impurity and foil-thickness effects. These values of the migration energy correlate with the activation energy of recovery peak 1 E of low temperature irradiated Ni, Cu and Aℓ.

VACANCY LOOPS

The calculations show that if there is no preferential drift of interstitials over vacancies to sinks, it is not possible to grow vacancy loops or voids (unless the vacancy is more mobile than the interstitial). In other words, the interstitial flux (concentration times velocity) always exceeds the vacancy flux, the two becoming nearly equal after a long irradiation time.[11]

If the interstitials are preferentially attracted to dislocation loops, it becomes possible to grow neutral sinks such as voids but of course even more difficult to grow vacancy loops. Thus the void nucleation and growth is strongly dependent on Z, the ratio of the cross-section of a dislocation loop for interstitial absorption to that for vacancy absorption.

Some vacancy loops have been observed after electron irradiation in high voltage electron microscopes. These loops could only grow if there was an excess of vacancies over interstitials, such as occurs by the escape of interstitials to the foil surfaces. Goringe[7] has indicated how one can correct for the presence of the surfaces in estimating the defect retention in thin foils.

VOIDS

Voids will be nucleated as soon as the vacancies cluster since the gas atoms are in general more mobile than the vacancies. There will be no void growth until the vacancy flux exceeds the interstitial flux into the void nucleus ('incubation time'). For 1 ppm of inert gas injected into Ni or Cu, and for Z = 1.4, calculations show that the incubation time at 420 C and 250 C respectively is so long that each gas atom nucleates one void (fig. 1). Such a high concentration of voids is not observed experimentally.

The void growth is initially very rapid and then increases as the time to the one-fourth power. This gives an increase of void volume fraction (swelling) with time to the three-quarters power whilst a linear dependence has been observed[8].

CONCLUSIONS

1) We have extended our original model[3] to include the possibility of void nucleation and the mobility of the vacancy, di-vacancy and gas atoms. Unlike the case of the interstitial loops, there are no analytical solutions for the concentration and growth of the vacancy agglomerates. However, the calculations can be performed rapidly on a computer (a typical run of 10^7 seconds irradiation time takes only three minutes) and it is our intention to make the programme freely available[2].

2) The overall agreement between theory and experiment for interstitial and vacancy loops is good over a very wide range of irradiation conditions. Bourret[9] has shown how equation (1) needs to be modified at very high temperatures.

3) For voids, the theory gives a good qualitative account of the experimental results obtained by electron irradiation. The void concentration depends on the presence of gas, and void growth displays an incubation time as is observed. The theory predicts too high a void concentration because it does not take into account the clustering of the mobile gas atoms. This will markedly reduce the void concentration and improve the agreement with experiment.

4) Because the simple theory produces such good agreement with experiment, it seems possible to extend it to try to produce a computer programme which will predict the swelling behaviour of materials in a fast neutron environment[10].

We wish to acknowledge the work of Mr. P.B. Kruger in writing the computer programme.

REFERENCES

1. Y. Shimomura and S. Yoshida, J. Phys. Soc. Japan 22 319 (1967)
2. P.B. Kruger and R.M. Mayer, to be published.
3. L.M. Brown, A. Kelly and R.M. Mayer, Phil. Mag. 19 721-40 (1969)
4. M.K. Hossain and L.M. Brown in High Voltage Electron Microscopy (ed P.R. Swann, Academic Press) 360-364 (1974)
5. M.S. Spring, M. Ipohorski and M.J. Goringe, Radiat. Eff. 11 251-9 (1971)
6. M. Kiritani and N. Yoshida, J. Phys. Soc. Japan 36 613 (1974)
7. M.J. Goringe, Radiat. Eff. 10 169 (1971)
8. D.I.R. Norris, Radiat. Eff. 15 1-22 (1972)
9. A. Bourret, Phys. Stat. Solidi A4 813
10. R.M. Mayer and L.M. Brown, Proc. Int. Conf. Radiation Effects and Tritium Technology for Fusion Reactors, Gatlinburg, Tenn., in press (1975)
11. M.K. Hossain, Ph.D. thesis, University of Cambridge, 1974

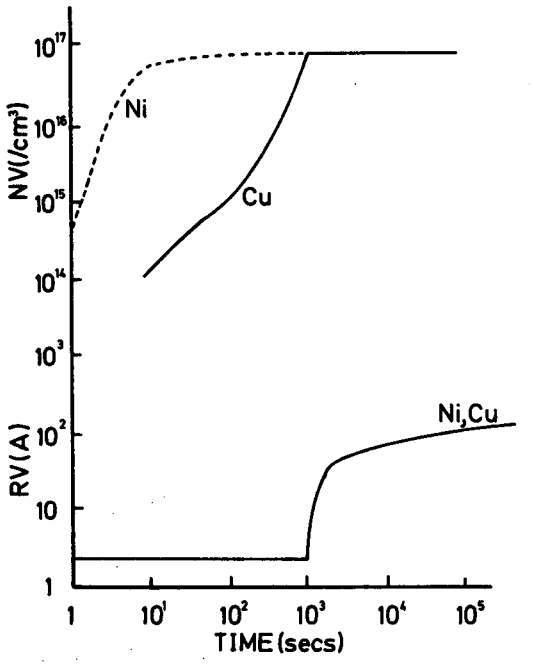


Fig. 1 Void concentration and radius versus time for Ni and Cu irradiated with electrons to give a displacement rate of 1 x 10^{20} atoms/sec. Pre-injected with 1 ppm helium gas. Irradiation temperatures Cu - 250 C; Ni - 400 C.

IRRADIATION GROWTH IN ZIRCONIUM AND ITS ALLOYS

G.J.C. Carpenter and D.O. Northwood
Atomic Energy of Canada Limited
Chalk River Nuclear Laboratories
Chalk River, Ontario, Canada

ABSTRACT

Observations of neutron irradiation damage in zirconium and its alloys using transmission electron microscopy show that the mechanism of radiation growth is quite different from that in uranium.

INTRODUCTION

Dilute zirconium alloys are used as core structural components in natural uranium reactors where high neutron efficiency is essential. The alloys appear to be resistant to void swelling during irradiation[1] but are subject to another source of dimensional change, radiation growth which is a shape change at constant volume in the absence of an applied stress.

Radiation growth in metallic uranium has been extensively studied and the theory proposed by Buckley[2] has won wide acceptance as being best able to account for the growth phenomena observed experimentally. The model was also applied to other anisotropic metals, including zirconium. The principle requirement of the theory is that the metal should have both crystallographic and thermal expansion anisotropy. An incoming neutron that initiates an energetic primary knock-on collision, creates a cascade of displaced atoms (the displacement spike) and a high localised generation of heat (the thermal spike). Since the thermal expansion coefficient is greatest along the c-axis direction in zirconium, the displacement spike will experience compressive stresses along this direction. This favours the collapse of vacancy clusters into dislocation loops with Burgers vectors having a large component parallel to the c-axis direction.

The interstitials were believed to condense as loops with a-type Burgers vectors i.e. a/3 $\langle 11\bar{2}0 \rangle$. The mechanism is equivalent to a transfer of atoms from the basal planes to the prism planes.

Applying this model to uranium, Buckley accounted satisfactorily for the observed dimensional changes and a later study using transmission electron microscopy[3] (TEM) provided further evidence in support of the theory. For zirconium, however, some recent observations using TEM[4-12] have been at variance with the model. Here, we report the results of further studies and compare them to other observations in the published literature.

EXPERIMENTAL

Thin foils for transmission microscopy were prepared using a jet polishing technique[13] and examined in a Philips EM 300G electron microscope at 100 kV. The following materials were examined:

(1) crystal bar zirconium, Zircaloy-2, Zr-2.5 wt% Nb and Zr-1.15 wt% Cr-0.1 wt% Fe, all in the annealed condition (1 h at 1025-1075 K) irradiated at approximately 575 K in either the NRX reactor (flux $\sim 10^{17}$ n.m.$^{-2}$ s^{-1}, E > 1 MeV) or the NRU reactor ($\sim 3 \times 10^{17}$ n.m.$^{-2}$ s^{-1}) at the Chalk River Nuclear Laboratories.

(2) Crystal bar zirconium and Zircaloy-2, both furnace cooled after 30 min. at 975 K and irradiated at about 675 and 875 K in sodium in the EBR-2 reactor (flux = 9.7×10^{17} n.m.$^{-2}$, E > 1 MeV) at Idaho Falls. The temperatures were estimated from gamma heating data.

Details of the irradiation conditions of previously published experiments are summarised in Table 1. Complete information regarding the irradiation facility, flux, etc., and full details of the contrast experiments can be found in the appropriate references.

RESULTS OF TEM EXPERIMENTS

The results of the present contrast experiments are summarised in Table 1 together with those published previously. A considerable amount of

data on the Burgers vectors of the dislocation loops is now available. The information on the character of the loops (vacancy or interstitial) is rather small and limited to unalloyed zirconium. The Burgers vector determinations of the present study were made using the $\underline{g}.\underline{b} = 0$ criterion for invisibility and are illustrated using zirconium irradiated at 675 K in Figure 1. As in the majority of the experiments listed in Table 1, only dislocation loops with Burgers vectors of the type a/3 $\langle 11\bar{2}0 \rangle$ were present. It should be emphasised that our experience at CRNL indicates that complete extinction of the dislocation images is normally obtained provided a good two-beam condition is set up with a reflection giving $\underline{g}.\underline{b} = 0$. This is in line with the low anisotropy of elastic constant at room temperature in zirconium[14].

DISCUSSION

Although most of the results in Table 1 indicate that only loops with a-type Burgers vectors are present in irradiated zirconium and its alloys, there are a number of studies in which loops with c-axis components were claimed to be present[15-18]. Since this question is crucial to a discussion of the mechanism of irradiation growth, the evidence must be examined more critically.

The contrast analysis carried out by Riley and Grundy[15] was necessarily limited by the lack of a high angle goniometer stage. Thus, although they observed what appeared to be evidence of c-component loops, it was not possible to prove this by detailed contrast analysis. The weak images shown in Figure 4 of ref.(15) for example, show considerably more residual contrast than we normally obtain for a true $\underline{g}.\underline{b} = 0$ condition. Kelly[19] has pointed out that such images could be obtained from loops for which $\underline{g}.\underline{b} = 1$, which often gives rise to weak images under conditions of large deviation from the Bragg orientation[20].

It is difficult to assess the validity of the conclusion of Gelles and Harbottle[16] that c-component loops were formed. However, we must question the relevance to neutron irradiation growth of their observations of electron irradiated material, since, according to Buckley's[2] model,

vacancy loops are formed on the basal planes due to the forces generated in the thermal spike region. In electron irradiation there are no collision cascades or thermal spikes. The driving force necessary to form the vacancy loops on basal planes is therefore missing.

Lee and coworkers[17,18] stated that loops with a c-axis component were present in Zircaloy-2 after irradiation with neutrons[18] or nickel ions[17,18], based on the observation that some damage remained in contrast using 0002 reflections. While it is clearly difficult to critically assess such experiments in the published literature, there are some features that raise questions about this conclusion. Experiments using nickel ions may be severely complicated by the presence of the implanted nickel which diffuses extremely rapidly[21]. Since it is only slightly soluble in the α-phase, it is possible that nickel precipitation complicated the contrast analysis. Also, Figure 6 of reference 17 shows evidence for strong contributions of reflections in addition to 0002 and Figure 3b of reference 18 is not convincing as evidence for c-component damage. The asymmetrical strain fields are characteristic of defects situated very close to the surface and are probably due to surface precipitation of hydrogen picked up during elec-electropolishing[13,22]. Finally, zirconium specimens are normally coated with a thin oxide film that gives rise to strong, granular contrast using $\underline{g}$ = 0002, (Fig.5 in ref.18). When the irradiation-induced defects are small the diffraction conditions must be carefully controlled to minimise the contribution of the oxide film[4].

The nucleation of loops with a c-axis component is also unlikely on theoretical grounds. Piercy's[23] calculations indicated that the contribution of the local stress caused by anisotropic thermal expansion in the thermal spike was small compared to the other energy terms irvolved. Perfect dislocation loops with $\underline{b}$'s of the type a/3 $\langle 11\bar{2}0\rangle$ were favoured since no stacking fault energy has to be provided. Examination of a hard sphere model indicates that the formation of perfect prismatic loops should occur readily by direct condensation of point defects on $\{11\bar{2}0\}$ planes. This can be seen from Fig.2, which shows that a pair of $(11\bar{2}0)$ planes are quite similar to a close packed plane with zig-zag corrugations parallel to [0001]. Further confirmation for the lowest energy loop configuration

comes from quenching experiments using Zircaloy-2 and Zr-Al alloys[24], where vacancy character loops were produced by quenching and ageing, all with b's of the type a/3 <11$\bar{2}$0>.

CONCLUSIONS

On the basis of most of the experimental evidence we believe that the theory used by Buckley to account for radiation growth in uranium cannot be applied to α-zirconium irradiated with neutrons. It appears that insufficient stress can be generated by anisotropic expansion in the thermal spike to provide the large energy needed to nucleate dislocation loops with Burgers vectors having a c-axis component. In addition, the displacement events under neutron irradiation may not be sufficiently energetic (compared to fission fragment damage in uranium) to give a high enough local vacancy concentration for direct collapse to a dislocation loop. From the existing experimental data we cannot rule out the possibility that fission fragment damage may result in radiation growth by Buckley's mechanism in zirconium.

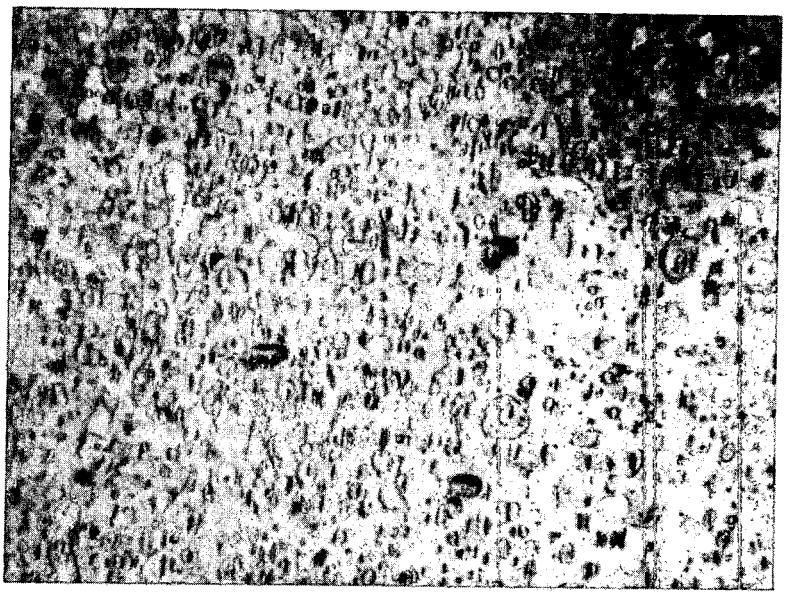
An alternative, qualitative model to account for growth in neutron-irradiated zirconium has been presented elsewhere[4]. Calculations are in progress to assess the validity of the model.

REFERENCES

1. A. Wolfenden, and K. Farrell, Scripta. Met. 6, 127, (1972).
2. S.N. Buckley, Properties of Reactor Materials and Effects of Radiation Damage, Ed. D.J. Littler, p.413, Butterworths, London, 1962.
3. B. Hudson, Phil. Mag., 10, 949, (1964).
4. D.O. Northwood, V. Fidleris, R.W. Gilbert and G.J.C. Carpenter, Dislocation Loop Generation and Irradiation Growth in a Zirconium Single Crystal, To be published.
5. T.D. Gulden and I.M. Bernstein, Phil. Mag. 14, 1087 (1966).
6. P.M. Kelly and R.G. Blake, Phil. Mag. 28, 415 (1973).

7. R.G. Blake, A. Jostsons and P.M. Kelly, Proc. Eighth Int. Congress on Electron Microscopy, Canberra, Vol.1, p.610, 1974.
8. D.O. Northwood, and R.W. Gilbert, J. Nucl. Mater. 51, 271, (1974).
9. G.J.C. Carpenter and D.O. Northwood, J. Nucl. Mater. 56, 260, (1975).
10. D.O. Northwood, Proc. 2nd AGM Microscopical Society of Canada, p.2, Imperial Press, Toronto, 1975.
11. C.D. Williams and C.E. Ells, Phil. Mag. 18 763 (1968).
12. D. Faulkner, and R.C. Styles, Proc. Thirty-First Annual EMSA Meeting, p.152, Claitors Publishing Division, Baton Rouge, 1973.
13. D.O. Northwood and R.W. Gilbert, J. Aust. Inst. Metals, 18, 158(1973).
14. D.O. Northwood, I.M. London and L.E. Bahen, J. Nucl. Mater. 55, 299, (1975).
15. A. Riley and P.J. Grundy, Phys. Stat. Sol. (a) 14, 239, (1972).
16. D.S. Gelles and J.E. Harbottle. Electron Irradiation Damage in Zirconium, Berkeley Nuclear Labs. (U.K.) Report RD/B/N2973 (April 1974).
17. D. Lee, E.F. Koch and J.H. Rosolowski, J. Nucl. Mater. 50, 162(1974).
18. R.B. Adamson, W.L. Bell and D. Lee, Zirconium in Nuclear Applications, ASTM, STP-551, p.215, ASTM, Philadelphia, 1974.
19. P.M. Kelly, Private Communication.
20. D.E. Barry and D.M. Maher, Phil. Mag. 21, 1255, (1970).
21. G.M. Hood and R.J. Schultz, Phil. Mag. 26, 329 (1972).
22. A.J. Bedford and D.R. Miller, J. Aust. Inst. Metals, 17, 120(1972).
23. G.R. Piercy, J. Nucl. Mater., 26, 18 (1968).
24. G.J.C. Carpenter and J.F. Watters, Acta Met. 21, 1207 (1973).

(a)



(b)

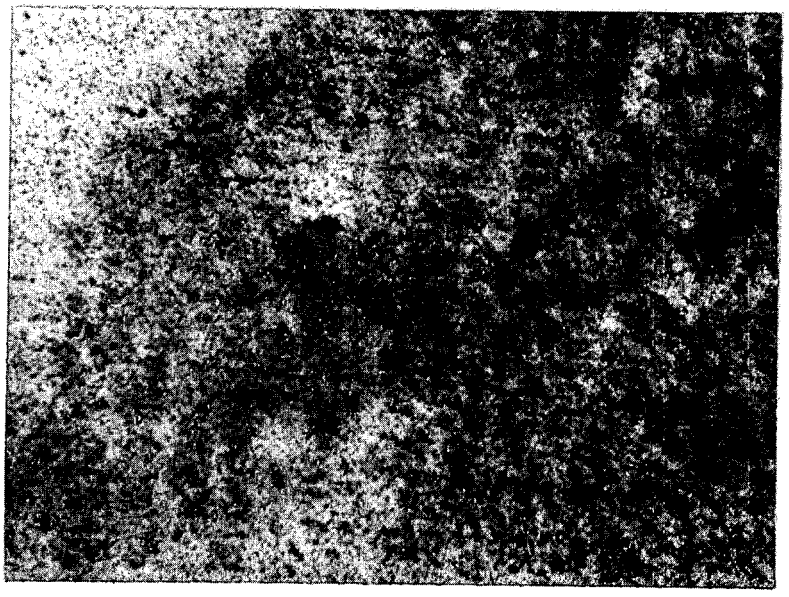


Fig.1 Transmission micrographs of zirconium irradiated to 7.4×10^{24} n/m^2 at 675K: (a) Dislocation loops in contrast, $\underline{g} = 1\bar{1}03$ (b) all loops out of contrast, $\underline{g} = 0002$. Magnification 29,000x.

TABLE 1

CHARACTERIZATION OF DAMAGE IN IRRADIATED ZIRCONIUM ALLOYS

Irradiation Conditions				Character of Damage		
Alloy	Type of Irrad.	Temp. K	Fluence	Burgers Vector	Vacancy Intersitial	Ref.
Zirconium	Neutron	473	8×10^{23} n.m.$^{-2}$	a/3 <11$\bar{2}$0>	---	4
"	Neutron	523	1.8×10^{24} n.m.$^{-2}$	a/3 <11$\bar{2}$0>	45% I/55% V	4
"	Kr + ions	R.T.	10^{13} ions/cm^2	a/3 <11$\bar{2}$0>	I	5
"	Neutron	473 & 673	10^{24} n.m.$^{-2}$	a/3 <11$\bar{2}$0> plus 1/3<11$\bar{2}$3>?	-	15
"	Neutron	675	7.4×10^{24} n.m.$^{-2}$	a/3 <11$\bar{2}$0>	-	This work
"	1 MeV e$^-$	570-873	up to 4.8 dpa	a/3<11$\bar{2}$0> + ∿ 5% non-basal	-	16
"	Neutron	R.T.	1.4×10^{24} n.m.$^{-2}$ (+ anneal)	a/3 <11$\bar{2}$0>	67% V/33% I	6
"	Neutron	573	3×10^{23} n.m.$^{-2}$	a/3 <11$\bar{2}$0>	-	6
"	Neutron	573	8×10^{23} n.m.$^{-2}$	a/3 <11$\bar{2}$0>	-	This work
"	Neutron	573-673	up to 7×10^{23} n.m.$^{-2}$	a/3 <11$\bar{2}$0>	V + I (relative proportions not given)	7
Zircaloy-2	5 MeV Ni++	573-873	7-87 dpa	a/3 <11$\bar{2}$0>	-	17, 18
"	Neutron	563-600	$0.7 - 2.5 \times 10^{25}$ n.m.$^{-2}$	a/3 <11$\bar{2}$0> + some evidence for c-component	-	18
"	1 MeV e$^-$	570-873	up to 4.8 dpa	a/3 <11$\bar{2}$0>+ ≈ 5% non-basal	-	16
"	Neutron	573 & 673	10^{24} n.m.$^{-2}$	a/3 <11$\bar{2}$0>plus 1/3 <11$\bar{2}$3>	-	15
"	Neutron	575	1.5×10^{24} n.m.$^{-2}$	a/3 <11$\bar{2}$0>	-	8
"	Neutron	∿575	$4 \times 10^{23} - 10^{26}$ n.m.$^{-2}$	a/3 <11$\bar{2}$0>	-	9,10
"	Neutron	∿875	7.4×10^{24} n.m.$^{-2}$	a/3 <11$\bar{2}$0>	-	This work
Zr-2.5 wt% Nb	Neutron	573	3×10^{24} n.m.$^{-2}$	a/3 <11$\bar{2}$0>	-	11
	Neutron	653-663	1.24×10^{25} n.m.$^{-2}$	a/3 <11$\bar{2}$0>	-	12
	Neutron	∿575	8×10^{23} & 3×10^{24} n.m.$^{-2}$	a/3 <11$\bar{2}$0>	-	This work
Zr-1.15 wt% Cr - 0.1 wt% Fe	Neutron	∿570	1.7×10^{24} n.m.$^{-2}$	a/3 <11$\bar{2}$0>	-	This work

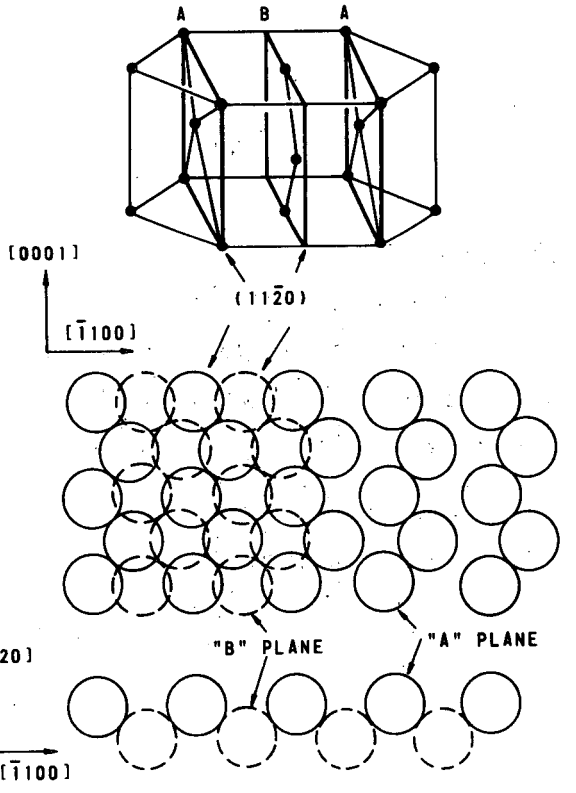


Fig.2 Illustration of the similarity of {11$\bar{2}$0} planes in the h.c.p. lattice to close packed planes.

AN EXPERIMENTAL STUDY OF DISLOCATION LOOP NUCLEATION

J.Y. Bounaud and J. Leteurtre
Section d'Etude des Solides Irradiés
Centre d'études nucléaires de Fontenay-aux-Roses (92260) - France

ABSTRACT

The nucleation of dislocation loops is experimentally studied by observing the **separation of the Burgers vector of** dislocation loops nucleated in copper whiskers irradiated in flexion by fission fragments at room temperature. The demixion of Burgers vectors is observed by the dimensional effects of dislocation loops : after irradiation, the applied stress is removed ; the whisker shows a residual strain that is due to loops because, after an annealing treatment to evaporate dislocation loops, each whisker recovers its initial straight shape. Everywhere along the whisker, the radius of curvature is measured and plotted vs the max. applied stress. Estimations of the interstitial and vacancy dislocation loop nuclei are derived.

INTRODUCTION

Estimations of the dislocation loop nuclei sizes have been recently proposed, thanks to computer aided simulations of annealing experiments [1, 2]. These very interesting simulations have however to cope with a great number of unknown parameters, i.e. the binding energies of all polyvacancies either intrinsic or associated with impurity atoms, since most of the experimental work has accumulated the evidence of great complexity of dislocation loop nucleation often governed by impurities [3, 4].

Our study aims an other way of investigation of dislocation loop nucleation, using a perturbation by an applied stress field, i.e. a well known perturbation directly connected to the nucleus size of dislocation loops [5].

EXPERIMENTS

We chosed to irradiate under stress whiskers because they elastically support stresses up to about $\mu/50$, where μ is the shear modulus of the material ; they have perfectly crystallographic shapes ; and, because whiskers are initially dislocation free, one single phenomenom can be studied : the dislocation climb creep is completely suppressed if the irradiation dose is low enough, and thus the radiation induced dislocation loops have not grown enough so as to interact and form a dislocation network. Copper was chosen for several reasons, i.e. it has the face-centred cubic structure ; its dislocation loops are imperfect with $\frac{1}{3}$ <111> Burgers vectors (the dislocation loop planes are well defined) ; copper whisker making by the Brenner method is easy.

These whiskers were strained on a very simple flexion device shown on fig. 1. Each whisker is bent up to the desired bending distance. A micrograph of the elastically bent whisker helps to :

i) verify that the bending is pure (without stretching),

ii) measure the diameter d of the whisker,

iii) measure the radius of curvature R and thus compute the applied stress everywhere in the whisker. According to [6], the only important component of the stress tensor is σ_{zz}, where z is parallel to the whisker axis ; all the other components are vanishingly small if the diameter d of the whisker (1 - 5 μ) is small compared to the radius of curvature R (~ 1 mm).

Whiskers bent by this flexion device have been irradiated by fission fragments thanks to a uranium foil held close by the whisker. The irradiations were performed in the nuclear reactor Triton, Fontenay-aux-Roses, at room temperature. Simultaneously copper foils,6 μ thick, have been very carefully annealed near the melting point and then irradiated by fission fragments in the same conditions than for whiskers. After irradiation, these foils are thinned down by electropolishing with phosphoric acid and observed by transmission electron microscopy at 100 keV.

EXPERIMENTAL RESULTS

The irradiation effects are shown on fig. 2 : well resolved but non-overlapping dislocation loops are observed. The concentration of defects clustered into dislocation loops has been estimated to be about 3×10^{-3}/at.

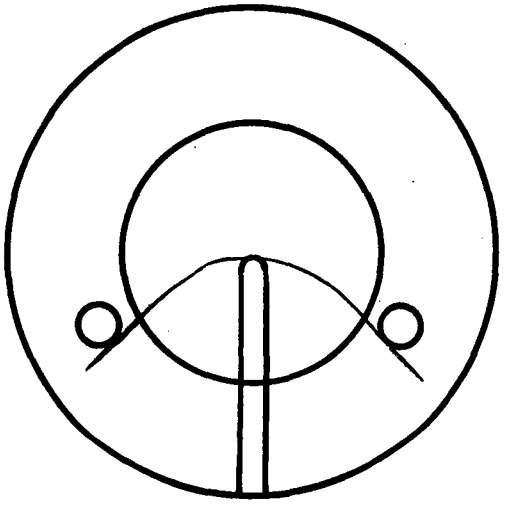


Fig. 1. Diagram of the experimental agencement for whisker irradiations.

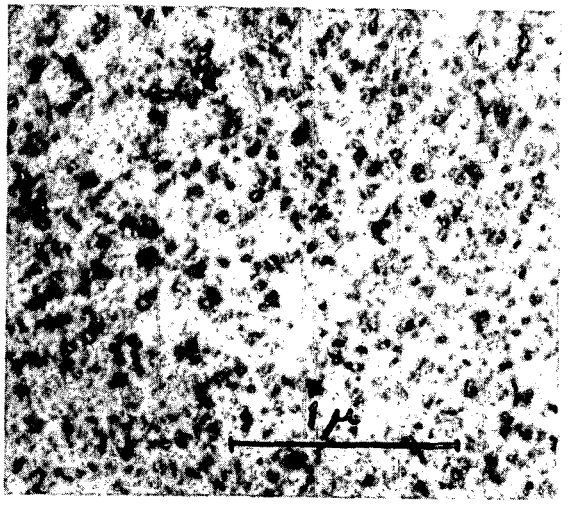


Fig. 2. Radiation damage in copper for the chosen fission fragment dose.

On the other hand, after irradiation, whiskers are unstrained and observed in the stress free state. Only results concerning <110> whiskers are reported here. Fig. 3b shows what has happened : the whisker shape, that was initially straight, has become bent after its irradiation under the applied stress (fig. 3a). After irradiation, the whisker, still quite elastic, keeps a memory of its imposed shape under irradiation. This memory effect results from the observed dislocation loops, as clearly proved by fig. 3c showing the straight shape of the whisker recovered after an annealing treatment of 1 hour at 400°C, which is enough to evaporate the dislocation loops in copper.

Measurements in each point of a whisker of radii of curvature R and ρ before and after the irradiation respectively allow the determinations of the applied stress (σ) and residual length changes of the specimen ($\Delta\ell/\ell$). The results of several experiments are gathered in fig. 4.

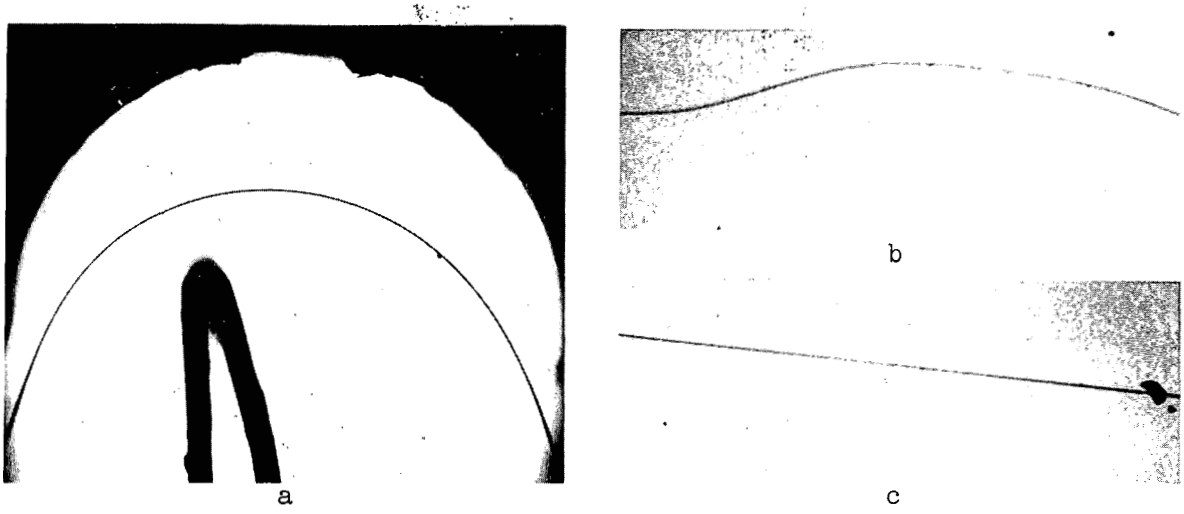


Fig. 3. Before irradiation, the whisker is bent by the flexion device (a). After irradiation, the applied stress is removed (b) ; the whisker shows a residual strain. After an annealing treatment, the whisker recovers its initial straight shape (c).

DISCUSSION

These experiments have proved that the dislocation loops are affected by the applied stress. One knows [7] that the applied stress modifies only very little the growth of the various dislocation loops but affects directly their nucleation probabilities.

In [110] whiskers, only $\frac{1}{3}[111]$ and $\frac{1}{3}[11\bar{1}]$ dislocation loops induce length changes, the two other Burgers vectors being perpendicular to the whisker axis and thus without any effect on the whisker curvature. As the [111] and $[11\bar{1}]$ directions are equally inclined with respect to the direction [110] of the applied uniaxial stress σ, the nucleation probabilities of $\frac{1}{3}[111]$ and $\frac{1}{3}[11\bar{1}]$ interstitial and vacancy loops are respectively [5, 8] :

$$p_i = 0.5 \times \left[1 + \exp\left(-\frac{N_i a^3 \sigma}{6\,kT}\right)\right]^{-1} \qquad (1)$$

and

$$p_v = 0.5 \times \left[1 + \exp\left(+\frac{N_v a^3 \sigma}{6\,kT}\right)\right]^{-1} \qquad (2)$$

where N_i and N_v are the numbers of interstitial atoms and vacancies in both dislocation loop nuclei, a is the lattice parameter of copper, k and T being the Boltzmann constant and temperature. The length change due to vacancy and interstitial dislocation loops in concentration C is [8] :

$$\Delta\ell/\ell = \frac{4}{3} (p_i - p_v) C . \qquad (3)$$

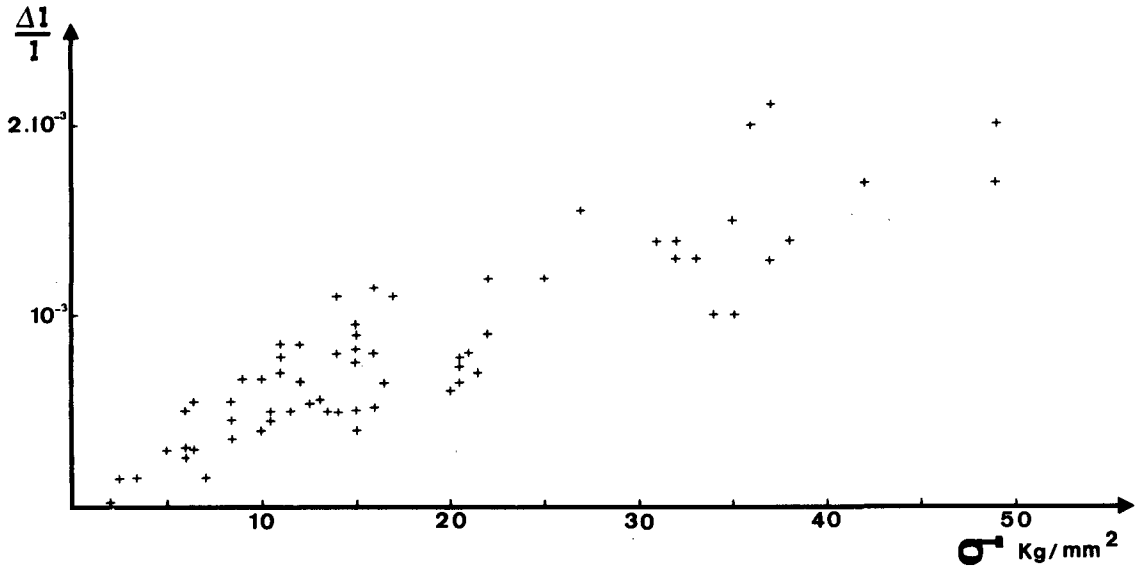


Fig. 4. Measurements of radii of curvature R and ρ before (fig. 3a) and after (fig. 3b) irradiation allow calculations of the applied stress and length changes.

Let us notice that for small stresses, $\Delta\ell/\ell$ can be approximated by :

$$\Delta\ell/\ell \simeq \frac{a^3}{36k} . C . \frac{N_i + N_v}{T} . \sigma \qquad (4)$$

C is known from electron microscopic observations. From the slope of the experimental curve $\Delta\ell/\ell$ vs σ near the origin of coordinates, one finds

$$1{,}3 \times 10^{-2} < \frac{N_i + N_v}{T} < 2{,}7 \times 10^{-2} \qquad (5)$$

T is the temperature of the material where and when the loops have been nucleated, i.e. within displacement cascades. In copper irradiated by fission fragments, the thermal spike amplitude is expected to be 100°C

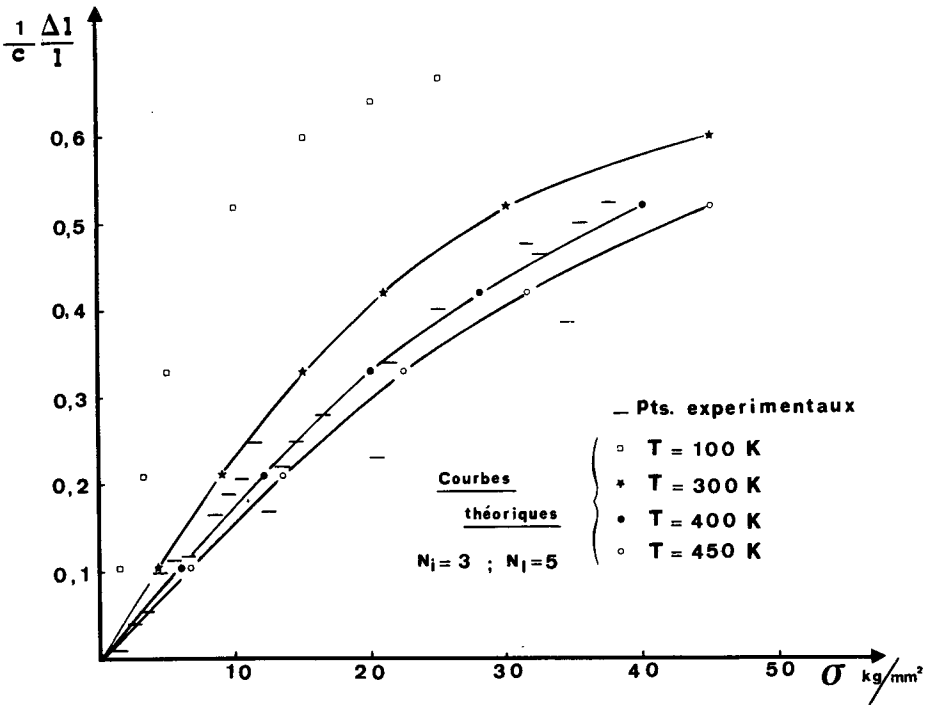


Fig. 5. Theoretical curve computed with $N_i = 3$, $N_V = 5$.

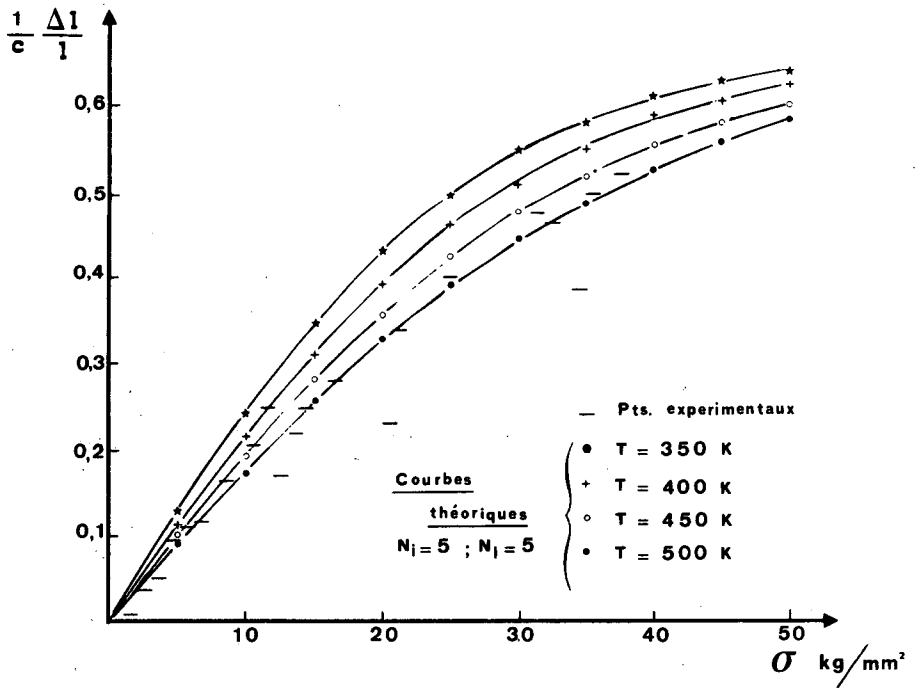


Fig. 6. Theoretical curve computed with $N_i = 5$, $N_V = 5$.

or 200°C [9]. For our room temperature irradiation, T might thus be 400 K or 500 K. Then (5) gives that $(N_i + N_v)$ should be between 6 and 16 in copper.

If however all experimental points are considered, fig. 5 shows that they fit correctly the theoretical curve computed with T = 400 K, $N_i = 3$ and $N_v = 5$.

An other possibility (fig. 6) could be T = 500 K, $N_i = 5$ and $N_v = 5$.

CONCLUSION

The nucleation of dislocation loops has been experimentally studied by observing the demixion of Burgers vectors of dislocation loops nucleated under an applied stress field. This approach allows a determination of the size of the nuclei of both type of dislocation loops.

Experiments are going on with electron irradiations which do not induce displacement cascades.

REFERENCES

1. J.M. Lanore, Note CEA-N-1567 (1972).
2. M. Kiritani, J. Phys. Soc. Jap. 35, 95 (1973).
3. R.E. Smallman and K.H. Westmacott, Mat. Sci. Eng. 9, 249 (1972).
4. A.A. Hussein and R.A. Dodd, Phil. Mag. 24, 1441 (1971).
5. J. Leteurtre, J.L. Pouchou and L. Zuppiroli, Phil. Mag. 27, 1323 (1973).
6. L. Landau and E. Lifchitz, Theorie de l'élasticité, Ed. Mir, Moscou (1967).
7. A.D. Brailsford and R. Bullough, Phil. Mag. 27, 49 (1973).
8. J.Y. Bounaud, Thesis Orsay (1973) ; Note CEA-N-1664 (1973).
9. R.S. Nelson, Phil. Mag. 11, 219 (1965).

EFFECT OF ALLOYING ELEMENTS AND IRRADIATION TEMPERATURE ON DISLOCATION LOOPS OF ELECTRON BOMBARDED NIOBIUM

N. Igata, F. Watari and H. Murakami
Department of Metallurgy and Materials Science,
University of Tokyo, 7-3-1, Hongo, Bunkyoku,
Tokyo, 113, Japan

ABSTRACT

Outgassed niobium, niobium containing interstitial alloying atoms, niobium-zirconium and niobium-molybdenum alloys were electron irradiated and observed in situ under a high voltage electron microscope between 10K and 573K. The logarithmic density of dislocation loops was proportional to reciprocal irradiation temperature. Below 77K loop density was saturated. The loop radius grew in proportion to one-third power of time at the lower temperature and first power at high temperature. Interstitial alloying atoms decreased the mobility of self-interstitials and vacancies, and increased loop density in proportion to the square root of their content and decreased loop growth. For substitutional alloying atoms it is necessary to consider the interaction effect with interstitial alloying atoms.

INTRODUCTION

A high voltage electron microscope (HVEM) is a powerfull means for simulation experiment of radiation damage because defect production rate is high and in situ observation is possible. The objective of this study is to observe the damage process of niobium and niobium alloys between 10K and 573K under a HVEM in situ and to investigate the effect of alloying elements and irradiation temperature on nucleation and growth of dislocation loops.

EXPERIMENTAL PROCEDURE

The chemical compositions of used materials are summarized in Table 1. The electron irradiation and the in situ observation were made using JEM 1250. Accelerating voltage was 1000kV. Beam intensity was 4.8×10^{18} e/cm^2·sec which was approximately equivalent to 10^{-3}dpa/sec. Both liquid helium stage and hot stage were used in vacuum of 10^{-7}torr.

EXPERIMENTAL RESULTS

1) Effect of Irradiation Temperature on Density of Dislocation Loops

The density of secondary defects did not change throughout irradiation after incubation time. Secondary defects were identified to be interstitial dislocation loops on $\{111\}$ planes with $\frac{a}{2}\langle 111\rangle$ Burgers vector.

Fig.1 shows dislocation loops formed between 10K and 550K in specimens B, D and J. The density of dislocation loops increased as irradiation temperature became lower. The logarithm of loop density was plotted against reciprocal irradiation temperature in Fig.2. Clearly there was difference between above and below room temperature. Above room temperature the relation was of Arrhenius type. Below room temperature range there was little temperature dependence.

2) Effect of Interstitial Alloying Atoms on Loop Density

As shown in Fig.1, loop density became larger with the increase of interstitial alloying atoms. Fig.3 reveals that loop density increases in proportion to the square root of interstitial alloying atoms above room temperature. Below room temperature there seemed to be less dependence on interstitial alloying atoms.

3) Effect of Substitutional Alloying Atoms on Loop Density

Figs.1 and 2 show that the loop density in very dilute niobium-zirconium alloy was lower than that of pure niobium

containing about the same content of interstitial alloying atoms. As substitutional alloying atoms increased further, loop density increased again. This behavior was similar also in the case of niobium-molybdenum alloy.

4) Effect of Irradiation Temperature on Growth of Dislocation Loops

Fig.4 shows the growth of dislocation loops at various temperature. Growth rate was larger at higher temperature. Loop diameter grew in proportion to t^n where t is time and n is exponent. The value of n changed gradually from 1/3 to 1 as irradiation temperature increased.

5) Effect of Interstitial and Substitutional Alloying Atoms on Growth of Dislocation Loops

Figs.5 and 6 show the growth behavior of dislocation loops in changing alloying atom content. Interstitial alloying atoms lowered the growth rate. Substitutional element (molybdenum) accelerated in very dilute alloys and lowered the growth rate in higher content. Zirconium showed almost the same effect as molybdenum.

DISCUSSION

1) Formulation of Loop Density

Makin[1] deduced the equation for loop density in high purity materials. If there are alloying atoms, the jump frequency of self-interstitials, ν_i, is represented as

$$\nu_i = \nu_0 \exp(-E_m/kT) / \left\{1-wC+wC\cdot\exp(B/kT)\right\} , \qquad (1)$$

where ν_0 is frequency factor, E_m is migration energy of self-interstitials, w is factor containing coordination number and entropy change, C is concentration of alloying atoms, and B is binding energy between self-interstitials

and alloying atoms. Then the loop density, N, is shown in the next equation,

$$N = \left[\frac{K \left\{ 1-wC+wC \cdot \exp(B/kT) \right\} \exp(E_m/kT)}{\nu_o v'(4z+\sqrt{2}z_1)} \right]^{1/2}, \qquad (2)$$

where K is defect production rate, v' is atomic volume, z is number of atoms within the self-interstitial-vacancy mutual recombination volume, and z_1 is number of atoms within interstitial-interstitial combination volume. The effect of vacancy migration on loop density was estimated to be negligible and Eq.(2) was valid when the mobility of vacancies was much less than that of interstitials.

2) Formulation of Growth of Dislocation Loops

When vacancies are immobile, Makin[1] showed the loop radius r, as follows,

$$r \propto K^{1/6} \nu_i^{1/6} t^{1/3}. \qquad (3)$$

When alloying atoms are contained, ν_i should be revised by Eq.(1). When vacancy is mobile and steady state is attained, loop radius is expressed in the next equation,

$$r = \frac{(v')^{3/2}}{a^2} \left[z' \left(\frac{S_v}{zS_i} \right)^{1/2} - z'' \left(\frac{S_i}{zS_v} \right)^{1/2} \right] K^{1/2} \nu_v^{1/2} t, \qquad (4)$$

where a is interatomic distance, z' and z'' are number of atoms per one atomic site along dislocation line within self-interstitial-dislocation and vacancy-dislocation capture volume, S_i and S_v are sink density for single interstitials and vacancies, and ν_v is jump frequency of vacancies.

3) Effect of Irradiation Temperature and Alloying Atoms on Loop Density

Eq.(2) predicts that the logarithmic loop density should be proportional to reciprocal irradiation temperature. This relation is applicable to the region above room temperature. From the slope of this figure, (E_m+B) was estimated to be about 0.15eV. For the effect of interstitial alloying atoms, the loop density is proportional to the square root of the concentration as predicted by Eq.(2). The result shown in Fig.2 shows this relation.

In ordet to interpret the effect of substitutional alloying atoms, it is necessary to consider not only the binding effect against self-interstitials as expressed by Eq.(1) but also the interaction between substitutional and interstitial alloying atoms, for example scavenging effect.

At 77K and 10K there seems to be the saturation of loop density. Self-interstitials seem to migrate in long range.

4) Effect of Irradiation Temperature and Alloying Atoms on the Growth of Dislocation Loops

As for the effect of irradiation temperature, Eq.(3) shows the exponent n=1/3 at vacancy immobile stage, Eq.(4) shows n=1 at vacancy mobile (steady state) stage and Fig.4 can be interpreted by those equations. At the same time, ν_i and ν_v, accordingly the coeffecient to t^n in Eqs.(3) and (4) increase with temperature in each stage (Fig.4). Alloying atoms raise steady state stage (n=1) to higher temperature and also decreased ν_i, ν_v and the coeffecient. This is shown in Figs.5 and 6.

REFERENCE

1. M. J. Makin, Phil. Mag. 19, 1133 (1969).

No. of specimen		Interstitial Impurity (wt. ppm)			
		O	N	C	H
A	MRC-Nb 99.95% up	-	-	-	-
B		30	17	10	1.5
C		71	5.9	trace	1.6
D		530	11	90	1.3
E		2700	18	80	1.3
F		3100	75	80	5.4
G	Nb-0.15%Mo	64	22	-	-
H	Nb-1.00%Mo	80	25	-	-
I	Nb-4.95%Mo	87	16	-	-
J	Nb-0.14%Zr	110	24	-	-

Table 1. Content of interstitial and substitutional alloying atoms.

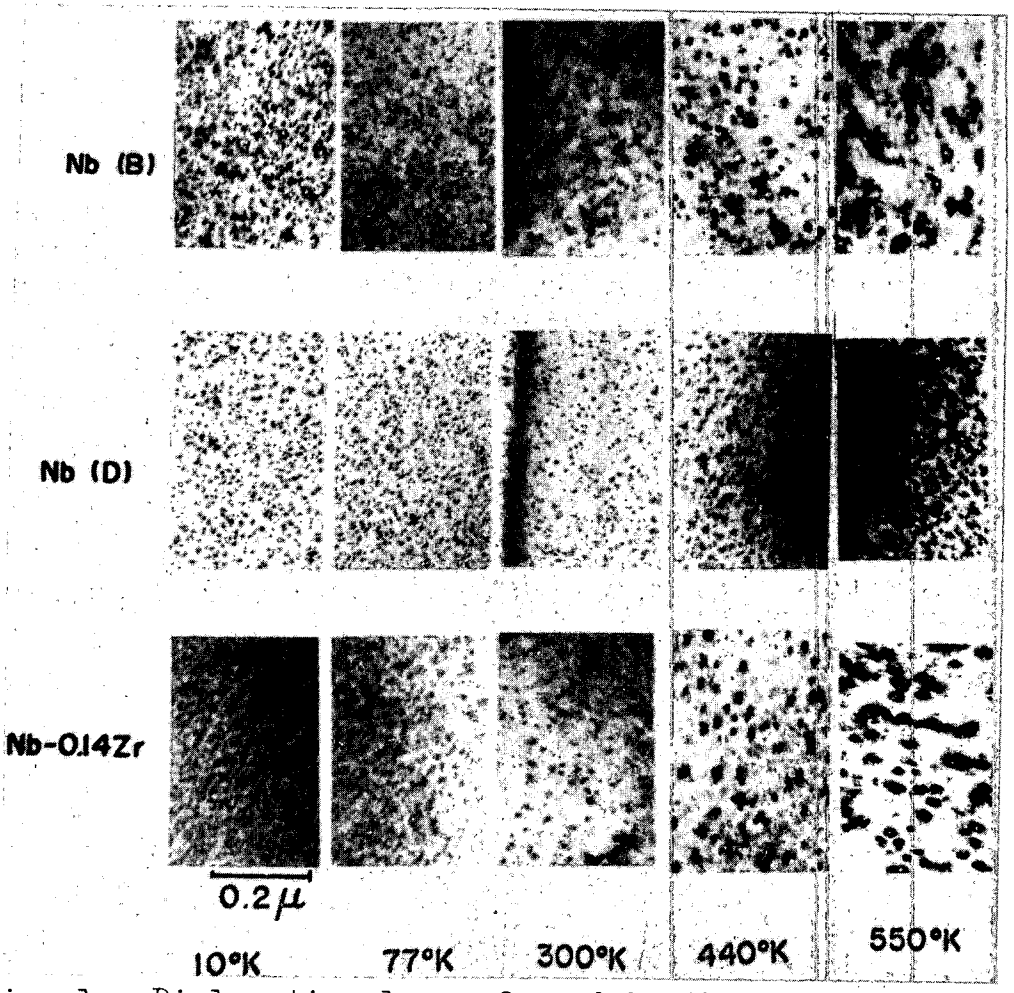


Fig. 1. Dislocation loops formed by the irradiation at various temperature. (Total dose:$8.6 \times 10^{21} e/cm^2$ at 10K and 77K, $2.3 \times 10^{21} e/cm^2$ at above 300K)

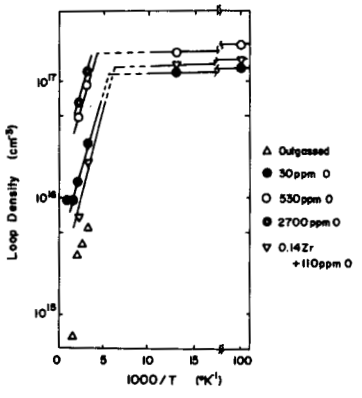


Fig.2. Dislocation loop density vs reciprocal irradiation temperature.

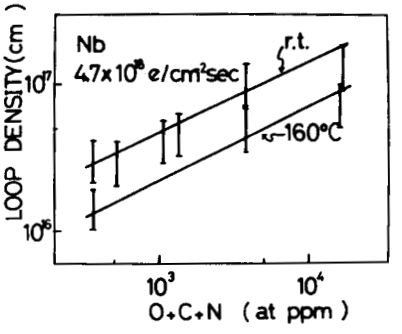


Fig.3. Dependence of loop density on interstitial alloying atom content.

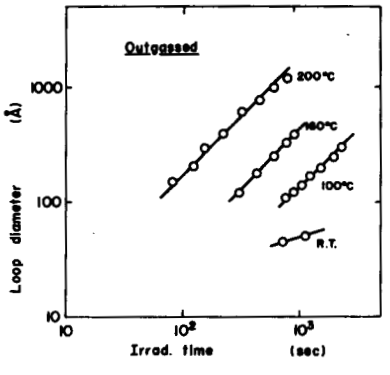


Fig.4. Growth of dislocation loops at various temperature in Nb(A).

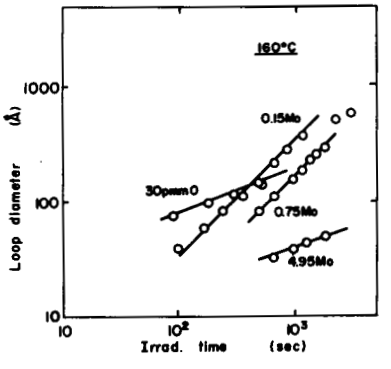


Fig.5. Effect of interstitial alloying atoms on growth of dislocation loops.

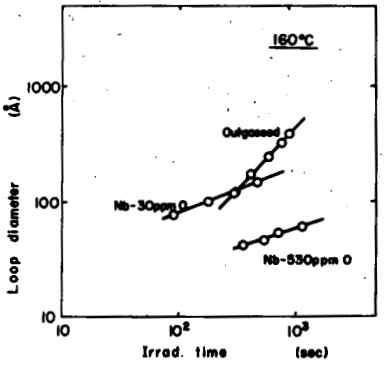


Fig.6. Effect of substitutional alloying atoms on growth of dislocation loops.

DEFECT ANNEALING AND CLUSTERING IN THE ELASTIC INTERACTION FORCE FIELD*

M. H. Yoo, W. H. Butler, and L. K. Mansur
Metals and Ceramics Division
Oak Ridge National Laboratory
Oak Ridge, Tennessee 37830

ABSTRACT

The effective capture radius for recombination and the bias factors of Frank loops for point defects have been calculated by a numerical solution of the steady-state diffusion equation. Employing these results we have obtained from the general rate equations the steady-state diffusion profiles of vacancies and interstitials in bounded media, namely the half-space and the foil. Effects of spatial variation of defect production, thermal emission of vacancies, bias factors of sinks, and the image interaction of point defects with free surfaces on the defect diffusion profiles are described.

INTRODUCTION

In order to develop a model for the formation of a given type of defect cluster, it is important to understand the influence exerted by defect clusters of other types on the point defect concentrations. For instance, for void nucleation, it is necessary to know the influence of dislocation loops, precipitates, dislocations, and other internal sinks. In radiation damage studies by high-voltage electron microscopy and ion bombardment, the effects of free surfaces may also be important. The purpose of this paper is to study the effects of defect sinks, both internal and external, and their interaction with point defects on the point defect concentrations during irradiation.

*Research sponsored by the Energy Research and Development Administration under contract with the Union Carbide Corporation.

RATE EQUATIONS

At temperatures where interstitials and vacancies are the important mobile defects, the point defect concentrations during defect clustering and void swelling can be obtained from the following rate equations:

$$\nabla \cdot (D_v \nabla C_v + \frac{D_v C_v}{kT} \nabla U_v) + G_v - \alpha C_v C_i - \sum_j K_v^j C_v = \frac{\partial C_v}{\partial t} \quad ,$$

$$\nabla \cdot (D_i \nabla C_i + \frac{D_i C_i}{kT} \nabla U_i) + G_i - \alpha C_v C_i - \sum_j K_i^j C_i = \frac{\partial C_i}{\partial t} \quad , \tag{1}$$

where the subscripts v and i denote vacancies and interstitials, D's are diffusion coefficients, and C's are fractional point defect concentrations. In each equation, the first term describes the leakage of defects to discrete external sinks such as free surfaces, where U's are the interaction energies between point defects and the discrete sink and kT is Boltzmann's factor. The second term, G, is the defect generation rate. The third term is for the annihilation rate by recombination with $\alpha = 4\pi r_c (D_i + D_v)/\Omega$, where r_c is the effective capture radius of recombination and Ω is the atomic volume. Finally, the last term includes all the internal sinks of various types, approximated as continuum sinks, each of which is characterized by the point defect loss rate[1], $K_{v,i}^j$. If loss of point defects to internal spherical sinks is controlled by diffusion, then $K_{v,i}^j = 4\pi r_{v,i}^j D_{v,i} N_{v,i}^j$, where the $r_{v,i}^j$ are the effective capture radii and $N_{v,i}^j$ are the number densities of a sink of j type for point defects, respectively.

EFFECTIVE CAPTURE RADIUS

The effective capture radius of a sink for point defects may be defined as[2]

$$r_c = -\frac{1}{4\pi D(C_2 - C_1)} \int_S \underset{\sim}{J} \cdot d\underset{\sim}{S} \quad , \tag{2}$$

the integral being taken over a surface enclosing the sink with the flux of point defects to the sink,

$$\underset{\sim}{J} = -\left(D\nabla C + \frac{DC}{kT}\nabla U\right) \quad . \tag{3}$$

One must take the appropriate values, C_1 and C_2, at r_1 and r_2, the inner and outer boundaries of the diffusion field. Assuming that D is isotropic and independent of concentration and position, the steady-state defect concentration is obtained by a numerical method and r_c is calculated from Eq. (2).[3] The radius of the recombination volume based on the size-effect interaction between a vacancy and an interstitial due to the first-order elastic anisotropy of the medium has been calculated, and the essential conclusions are as follows: in the case of Al for $T > 0.1\ T_m$ (T_m is the absolute melting temperature) r_c is temperature independent and equivalent to r_1, whereas in the case of Ni and Nb the temperature dependence of r_c is appreciable for $T > 0.2\ T_m$ and is very pronounced for $T < 0.2\ T_m$. This result is consistent with that of Schroeder[4] who estimated the effective capture radius by a variational method. At ambient temperature and above, however, the temperature dependence of the recombination rate is due primarily to that of the diffusion coefficients and the inner cut-off radius.

BIAS FACTOR

The so-called "bias factor"[5,6] is obtained directly from the calculated capture radii by $Z = r_c/r_c'$, where r_c' is the capture radius calculated from Eq. (2) with the same boundary conditions as for r_c but without the drift term in Eq. (3). An example of the calculated results is given in Fig. 1. The calculation is based on the infinitesimal loop approximation in an isotropic elastic medium and the "local equilibrium" defect concentration at $r_1 = 2R$, where R is the loop radius, as the inner boundary value, C_1. The bias factor for vacancies is close to unity because of their presumably small relaxation volume, $|\delta_v| \leq 0.4$. With the assumed range of $\delta_i = 1.4$ to 2.2 the bias factor for interstitials is found

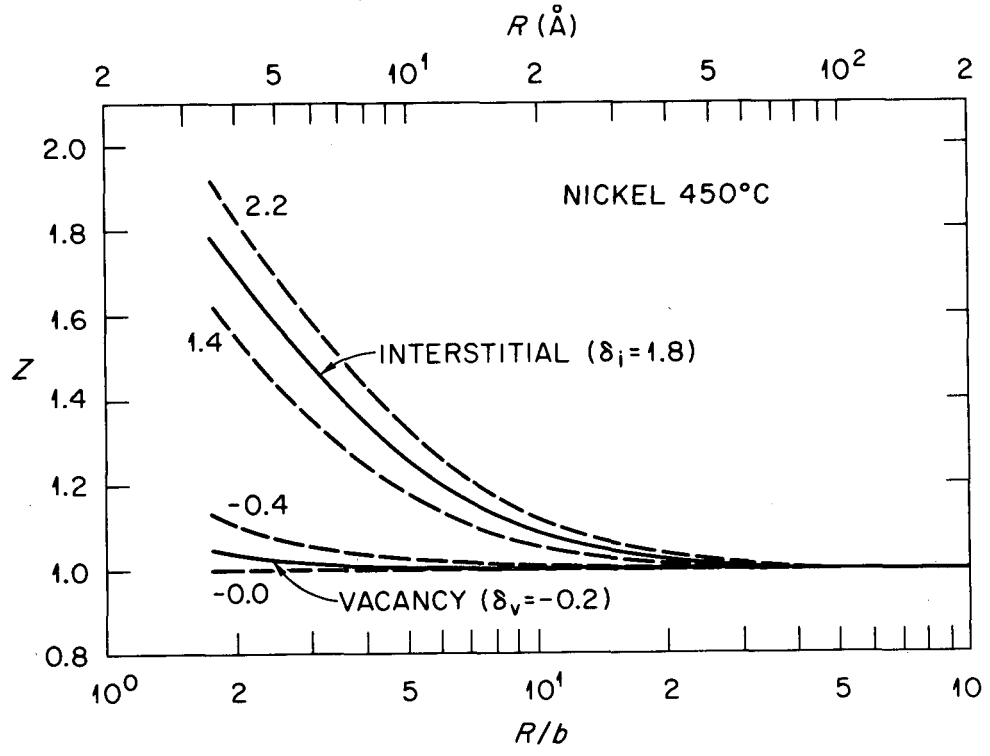


Fig. 1. Bias Factor of a Faulted Frank Type Loop for Point Defects vs. Loop Radius R. b is the Burgers vector strength and $\delta = \Delta V/\Omega$ is the relaxation parameter. The dashed curves give assumed ranges of δ.

to increase markedly as R decreases, e.g., $Z \doteq 1.8$ at $R = 2b$. A similar result was reported by Wolfer and Ashkin who used a perturbation method for their calculation.[6] This pronounced increase in Z for small R is due to the divergent nature of the elastic interaction taken up to $r_1 = 2R$ as R approaches 2b. Such a trend is consistent with the estimated value of Z for a pair of interstitials. For large loop radii, however, Z approaches unity as $R > 50b$, not the greater than unity values obtained for straight edge dislocations.[7] This result may seem odd at first in view of the fact that portion of the large loop would resemble a straight dislocation. However, since the defect production takes place outside of the region that encloses the dislocation loop in the present model, the comparison of the present result with those for straight dislocations cannot be made directly. The result given in Fig. 1 has been found consistent with the recent result of a finite dislocation loop,[8] the main difference being that Z approaches unity at larger loop size, $R > 1000b$, in the latter case.

DEFECT DIFFUSION PROFILES

One dimensional forms of the rate equations, Eq. (1), with x the depth penetration from the free surface have been solved for the steady-state diffusion profiles of point defects by a numerical integration method similar to one used earlier.[3] R and K's are related to the calculated effective capture radii as discussed previously. The following defect parameters are used for Ni: the pre-exponential factor and the migration energy of $D_0(cm^2/sec)$ = 0.19 and 0.008, $E_m(eV)$ = 1.0 and 0.15 for vacancy and interstitial, respectively, and the vacancy formation entropy and enthalpy of S_f = 1.5 k and E_f = 1.39 eV. If the drift flow to the surface, the thermal vacancy emission from the surface, and the differential bias factors of internal sinks are neglected, then the rate equations become equivalent and they are amenable to analytic solutions.[9] The solid curves shown in Fig. 2 illustrate analytic solutions, where

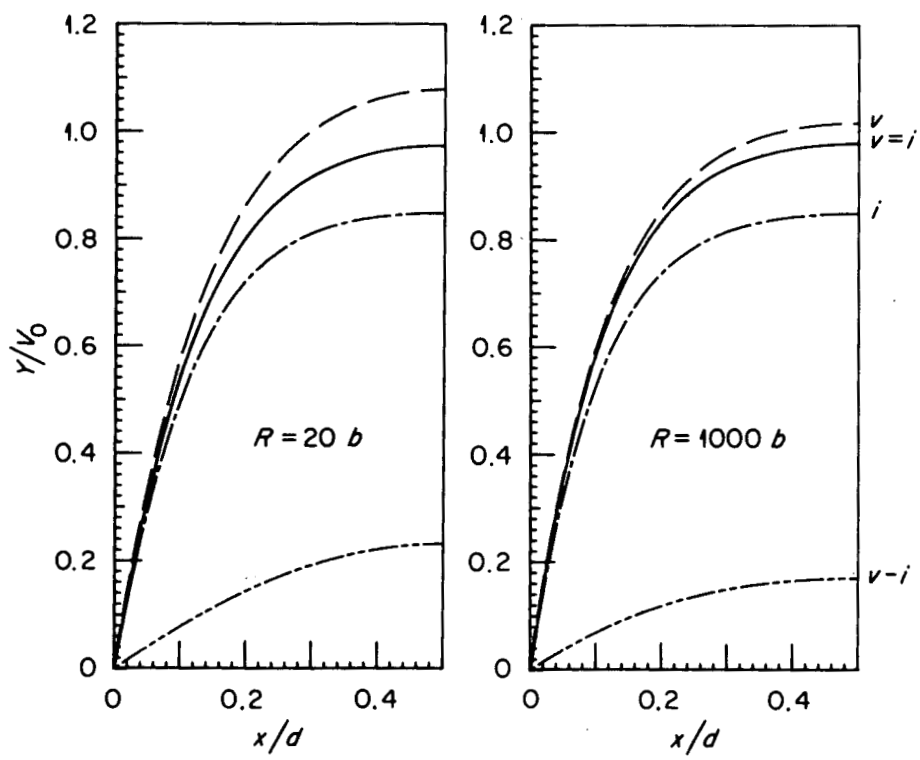


Fig. 2. Diffusion Profiles of Point Defects, $Y = D_v C_v$ or $D_i C_i$, in a Ni Foil of Thickness d = 0.5 μm at T = 450°C under $G = {}^{v}10^{-4}$ dpa/sec. Loop number density is $N = 10^{14}$ cm^{-3}. R is the loop radius.

$V_0 = 3.9 \times 10^{-15}$ cm^2/sec. When the calculated bias factors of finite dislocation loops are included, the diffusion profiles of vacancies is raised appreciably from that of interstitial as shown also in Fig. 2. This result implies that during electron irradiation by a high voltage microscope the region that contains many "small" and "isolated" dislocation loops would develop a high supersaturation of vacancies leading to a strong driving force for void formation.

Thermal emission of vacancies from the surface raises the vacancy profile further from the interstitial profile. In Ni, this effect is found to be neglibible at $T < 0.4\ T_m$ and quite comparable to the effects shown in Fig. 2 at $T \simeq 0.5\ T_m$. The drift term due to the image interaction also raises the vacancy profile with respect to the interstitial profile, but this effect is small on the scale of Fig. 2 at normal irradiation temperature.

Computed profiles of vacancies and interstitials in a semi-infinite medium induced by non-uniform spatial generation during heavy-ion bombardment are shown in Fig. 3. The defect production rate, G, is based on the energy deposition profile that gives a pronounced variation near the surface.[10] The defects are annihilated at the surface and also by recombination. While G increases to its peak at $x = 0.5$ μm and diminishes sharply to zero at $x = 1$ μm, both defect concentration profiles show maxima at $x = 0.6$ μm and decrease rather mildly as x increases. We conclude from the present calculation that the peaks of free defect concentration profiles do not necessarily coincide with that of the energy deposition when internal sinks are not present. All of the effects discussed here must be considered together in order to model an actual irradiation experiment. Additional effects such as coatings covering free surfaces and spatial variation of internal sinks are important in some experiments. Further results will be reported elsewhere.

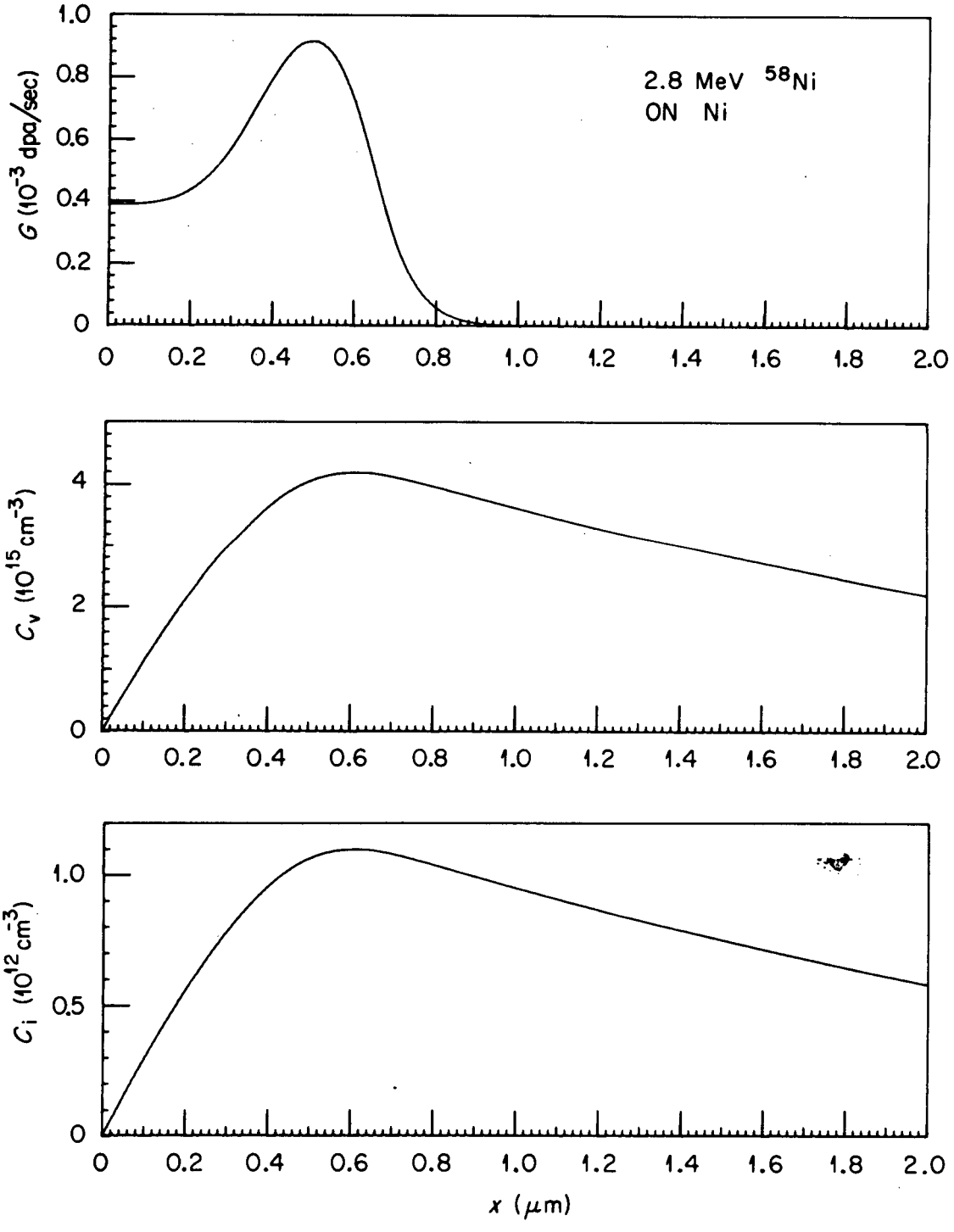


Fig. 3. Defect Concentration Profiles in Ni at T = 590°C (0.5 T_m) During Heavy Ion Bombardment. No defect sinks are included. Thermal equilibrium vacancy concentration is $C_v^e = 3 \times 10^{15}$ cm^{-3}.

REFERENCES

1. L. K. Mansur, P. R. Okamoto, A. Taylor, and Che-Yu Li, Defects and Defect Clusters in B.C.C. Metals and Their Alloys, AIME Nuclear Metallurgy Vol. 18, p. 509, National Bureau of Standards, Gaithersburg, Maryland, 1973.
2. F. S. Ham, J. Appl. Phys. 30, 915 (1959).
3. M. H. Yoo and W. H. Butler, to be published.
4. K. Schroeder, Jülich Report 1083-FF (July 1974).
5. A. D. Brailsford and R. Bullough, J. Nucl. Mater. 44, 121 (1972).
6. W. G. Wolfer and M. Ashkin, J. Appl. Phys. 46, 547 (1975).
7. P. T. Heald, Phil. Mag. 31, 551 (1975).
8. W. A. Coghlan and M. H. Yoo, to be published.
9. N. Q. Lam, S. J. Rothman, and R. Sizmann, Rad. Effects 23, 53 (1974).
10. I. Manning and G. P. Mueller, Computer Phys. Comm. 7, 85 (1974).

SEGREGATION OF POINT DEFECTS BY INTERNAL STRESS FIELDS*

W. G. Wolfer
Metals and Ceramics Division
Oak Ridge National Laboratory
Oak Ridge, Tennessee 37830 USA

ABSTRACT

Internal stress fields from dislocations and voids cause a drift motion of the migrating point defects. This can be expressed by bias factors which are given for voids, dislocation loops and straight edge dislocations. These bias factors provide the basis for theories of void swelling and radiation-induced creep. Their application to both phenomena is briefly discussed.

INTRODUCTION

The formation of voids and dislocation loops as well as the climb of dislocations during high-temperature irradiation requires that the numbers of interstitials and vacancies absorbed at a particular sink are unequal, though they are produced in equal numbers. The cause for this segregation of interstitials and vacancies is the different interaction of point defects with the stress fields of the sinks, and the effect this interaction has on the drift motion of the point defects. This segregation presents one of the cornerstones for our theoretical understanding of void formation and radiation-induced creep. For this reason detailed calculations were performed recently for the stress-induced diffusion of point defects to voids, small dislocation loops,[1] and to edge dislocations. Some of the results of this work and their applications to radiation-induce swelling and creep will be presented in this paper.

*Research sponsored by the Energy Research and Development Administration under contract with the Union Carbide Corporation.

BIAS FACTORS FOR VOIDS

The total interaction energy of point defects with a spherical void is conveniently decomposed into three contributions: the image interaction, and the two induced interactions due to the surface stress and due to external loads.

Moon and Pao[6] give for the image interaction the following expression:

$$E_{im} = -\frac{(1+\nu)^2}{36\pi(1-\nu)} G\Omega\left(\frac{v}{\Omega}\right)^2 \left(\frac{b}{a}\right)^3 \sum_n \frac{n(n-1)(4n^2-1)}{n^2 + n(1-2\nu) + 1 - \nu} \left(\frac{a}{r}\right)^{2n+2} . \quad (1)$$

Here,* a is the void radius and r the distance of the point defect to the void center. The sum in Eq. (1) can be approximated for $a \leq r \leqslant 1.4a$ by $(r/a - 1)^{-3}$; this simple expression is valid for flat surfaces,[4] but it overpredicts the image interaction with a void by a factor of two at $r = 1.4a$, and by a factor of 5 for $4 = 2a$.

Since E_{im} depends only on r the diffusion equation $\nabla \cdot \vec{j} = 0$ can be solved by simple integrations. For radial symmetry, $r^2 j_r = \text{const.}$, and hence

$$j_r = -\exp(-\beta E_{im}) \frac{d}{dr} [DC \exp(\beta E_{im})] = \text{const.}/r^2 .$$

Integration of this equation gives

$$[DC \exp(\beta E_{im})]_a^r = -\text{const.} \int_a^r dr \exp(\beta E_{im})/r^2 ,$$

which determines the constant and hence the current $J^o = 4\pi a^2 j_r(a) = -4\pi \text{ const.}$ The result can be written as

$$J^o = 4\pi a Z^o [DC \exp(\beta E_{im})]_a^A , \quad (2)$$

where C approaches $\overline{C}$** for $A \to \infty$ and the bias factor is given by

---

*For the numerical evaluation the following values are used: Poisson's ratio, $\nu = 0.3$; shear modulus, $G = 10^{12}$ dynes/cm^2; Burgers vector $b = 2.5$ Å; atomic volume, $\Omega = b^3$; relaxation volumes, $v_i = 1.4\ \Omega$ for interstitials, $v_v = -0.2\ \Omega$ for vacancies.

**$\overline{C}$ is the average defect concentration far away from the sinks.

$$Z^{o} = \left[\int_{o}^{1} d\left(\frac{a}{r}\right) \exp\left(\beta E_{im}\right)\right]^{-1} . \qquad (3)$$

This result is valid for any interaction energy that depends only on the radius r and has no positive singularity. The negative singularity E_{im} $(r \to a) \to -\infty$ is of no concern here, since $\exp(\beta E_{im})$ remains finite.

The evaluation of Eq. (3) gives the results shown in Fig. 1 as dashed curves. The bias factors Z^{o} are close to one for large voids, i.e., $a/b \geq 50$, meaning that the capture radius $r_{o} = aZ^{o}$ is close to a. This suggests that we use the result for the flat surface and Schroeder's[5] condition that the capture radius r_{o} is determined by $-E_{im}(r_{o}) \cong kT$. This leads to the approximation

$$Z^{o} \cong 1 + \left[\frac{(1+\nu)^2}{36\pi\,(1-\nu)} \frac{G\Omega}{kT}\right]^{1/3} \left(\frac{v}{\Omega}\right)^{2/3} \frac{b}{a} \qquad (4)$$

which is shown in Fig. 1 by the dotted lines.

Surface tractions induce an additional interaction for small voids. If γ is the surface stress and p the gas pressure in the void, then the leading term of the induced interaction is[6]

$$E = \alpha^{G} \left(p - \frac{2\gamma}{a}\right)^2 \frac{3}{2} \left(\frac{a}{r}\right)^6 \qquad (5)$$

where α^{G} is the shear polarizability of the point defect. External loads add other terms to Eq. (5) as discussed in Ref. 1. If the interaction of Eq. (5) is added to E_{im}, the bias factors are increased for negative shear polarizabilities. The solid lines in Fig. 1 give the total bias factors for $p = 0$, $\gamma = 2000$ ergs/cm^2, $\alpha_{i}^{G} = -150$ eV, and $\alpha_{v}^{G} = -15$ eV.

For small voids the interstitial bias factor becomes rather large, and Wolfer and Yoo[7] have shown that this fact makes void nucleation practically impossible without gases and impurities. The importance of the former is widely recognized, but even large values of p cannot eliminate the image interaction. Thus, it is suggested that impurities are even more important than inert gases for void nucleation. These impurities, invariably present in metals, can be dragged along with the point defects and precipitate on the void surface.[8] Apart from having the obvious effect o reducing the surface energy, the precipitate layer also changes the image interaction. If one models this layer as a shell of different elastic

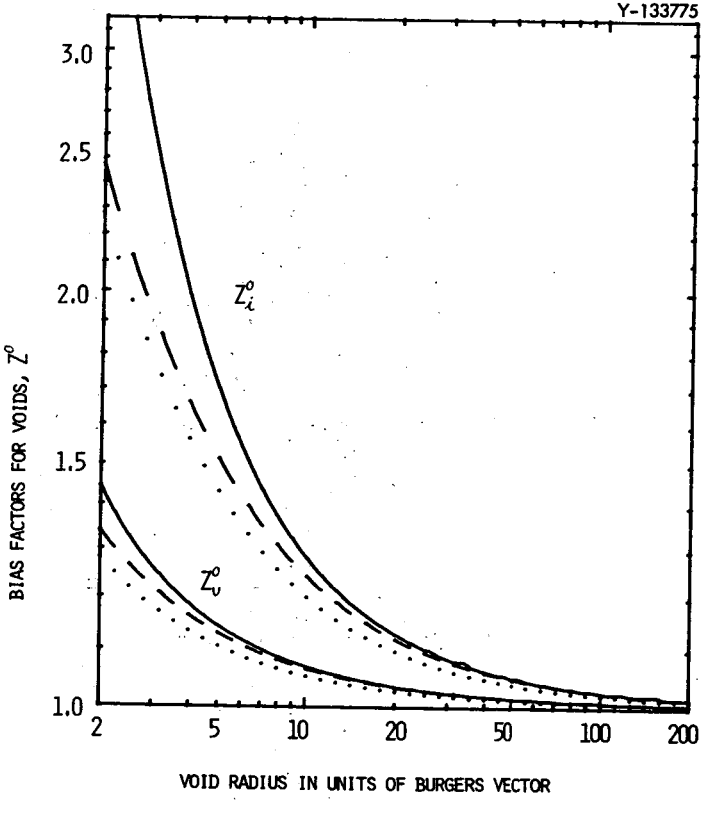


Fig. 1. Bias factors for voids at T = 500°C

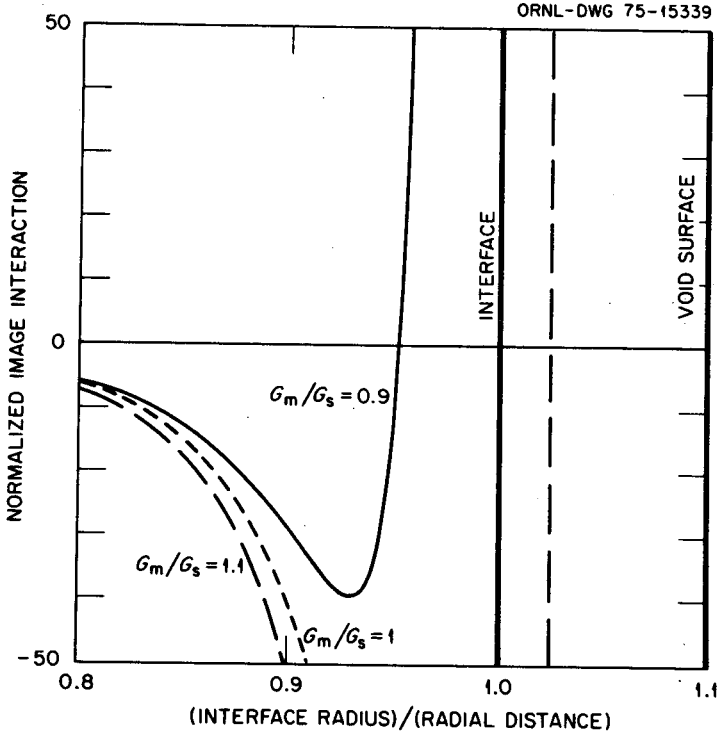


Fig. 2. Image interaction of a center of dilatation with a coated void

material, the image interaction becomes positive just outside or inside the interface, depending on whether the shear modulus G_s of the shell is larger or smaller than the shear modulus G_m of the matrix. An example[9] of this is shown in Fig. 2 together with the result for the uncontaminated void, i.e., $G_m = G_s$. The interaction energy computed with continuum elasticity diverges at the interface $r = r_1$. In reality, however, it exhibits a finite trap and a finite barrier on either side of the interface. If E* is the height and w* the width of this barrier, then an evaluation of Eq. (3) gives the result

$$Z^o = \left[\frac{a}{r_o} + \frac{aw^*}{r_1^2} \exp\ (\beta E^*)\right]^{-1} . \qquad (6)$$

For large barrier energies E*, one obtains then the result that

$$J^o \sim 4\pi r_1^2 \exp\ (-\beta E^*)/w^* . \qquad (7)$$

The effect of a coating on the void surface is therefore twofold. First, since $E^* \sim (v/\Omega)^2$ is larger for interstitials than for vacancies, $Z_i^o/Z_v^o < 1$, and the coated void is no longer biased towards interstitial absorption. Second, the void growth rate is now controlled by surface-reaction ($da^3/dt \sim r_1^2 \sim a^2$) rather than by diffusion ($da^3/dt \sim a$). A surface-reaction controlled kinetics for void growth was suggested earlier by Mansur et al.[10] and shown to be consistent with experimental observations.

BIAS FACTORS FOR DISLOCATIONS

The interaction of point defects with dislocations shows even in isotropic elastic media a complicated angular dependence that cannot be neglected in the calculation of bias factors. It was in fact shown by Wolfer and Ashkin[1,2] that because of the angular dependence, the modulus and size interaction are equally important for the evaluation of the bias. Furthermore, the correct angular dependence is also necessary for the evaluation of the stress-dependent terms of the bias factors which are responsible for a radiation-induced creep deformation.[2,11,12]

For infinitesimal loops, the bias factor* is given by

---

*$K = 3G(1+\nu)/(3-6\nu)$; bulk polarizabilities: $\alpha_i^K = 10$ eV for interstitials, $\alpha_v^K = -15$ eV for vacancies.

$$Z^{\ell} = 1 - \frac{3\beta\alpha^{G}}{128(1-\nu)R} n_i {}'\epsilon_{ij} b_j - \frac{1}{21}\left(\frac{1+\nu}{1-\nu}\right)^2 \frac{\beta\alpha^{G}}{1024R^2} (n_i b_i)^2$$

$$+ \left[\frac{3(1-2\nu)}{32(1-\nu)R}\right]^2 \left\{\frac{3}{7}\left(\frac{2}{7}\beta\nu K\right)^2 + \frac{73}{1155}\beta\alpha^{K} + \frac{C_{\ell}}{10395}\beta\alpha^{G}\right\}\left[b^2 + \frac{1}{3}(n_i b_i)^2\right]. \qquad (8)^*$$

where $C_{\ell} = (-530 - 1460\nu + 1371\nu^2)/(1-2\nu)^2$, $\vec{b}$ is the Burgers vector and $\vec{n}$ the normal vector oriented such that $n_i b_i > 1$ for an interstitial loop and $n_i b_i < 1$ for a vacancy loop. The cut-off radius R was chosen initially to be twice the loop radius because the infinitesimal loop approximation is valid also for finite loops at distances greater than twice the loop radius. However, recent numerical calculation by Coghlan[13] for finite loops have shown that Eq. (8) gives better results if R is equal to the loop radius. Figure 3 shows the bias factors for prismatic loops, i.e., $|n_i b_i| = b$, and for T = 500°C; the dashed curves give the bias factors for the size interaction only. For comparison, the bias factors Z^d for edge dislocations (to be discussed below) are also shown in Fig. 3. It is seen that the loop bias factors fall off rapidly with the loop radius and approach the value of one instead of the values for the straight edge dislocations. There are two reasons why the infinitesimal loop approximation breaks down for R/b > 10 to 20. The obvious reason is that one should use the strain field of a finite loop. However, the more important reason is that the defect production was simulated by prescribing an average defect concentration $\bar{C}$ on the outer boundary surface. This spherical surface encloses the loop entirely. To approach the case of an edge dislocation this outer boundary should become a large torus that surround the dislocation line. Obviously, a continuous transition between the two cases is not possible with the present approach, and it remains an interesting speculation whether or not a minimum exists for the bias factors of finite loops. Nevertheless, the present results show that small loops have large bias factors which decrease initially with loop size.

The stress-induced diffusion of point defects to straight edge dislocations was treated recently[2] by the perturbation method and the following bias factor was found:

---

*$'\epsilon_{ij}$ is the deviatoric strain tensor produced by external loads.

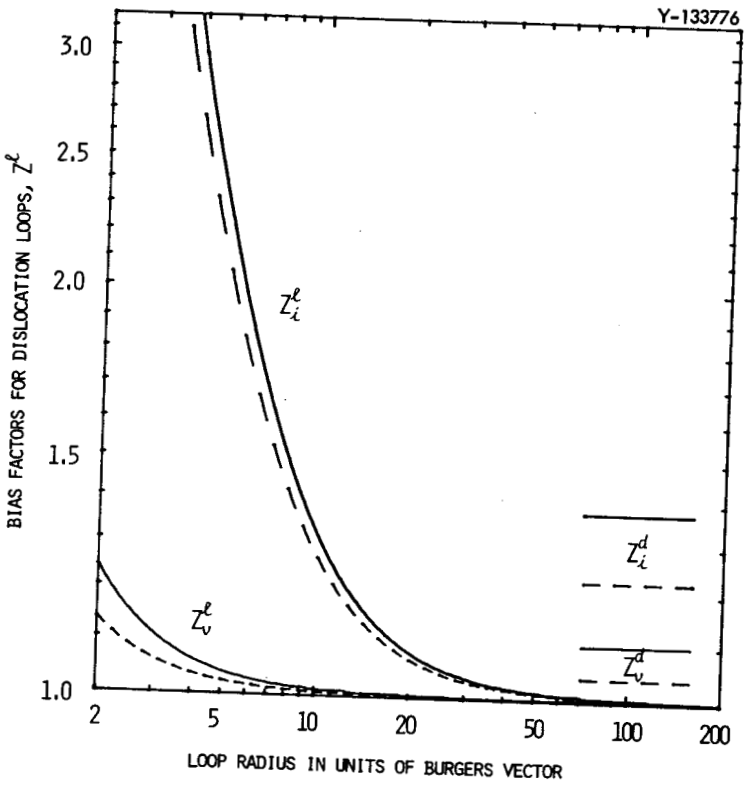


Fig. 3. Bias factors for dislocation loops, Z^{ℓ}, and edge dislocations, Z^d, at a temperature of T = 500°C

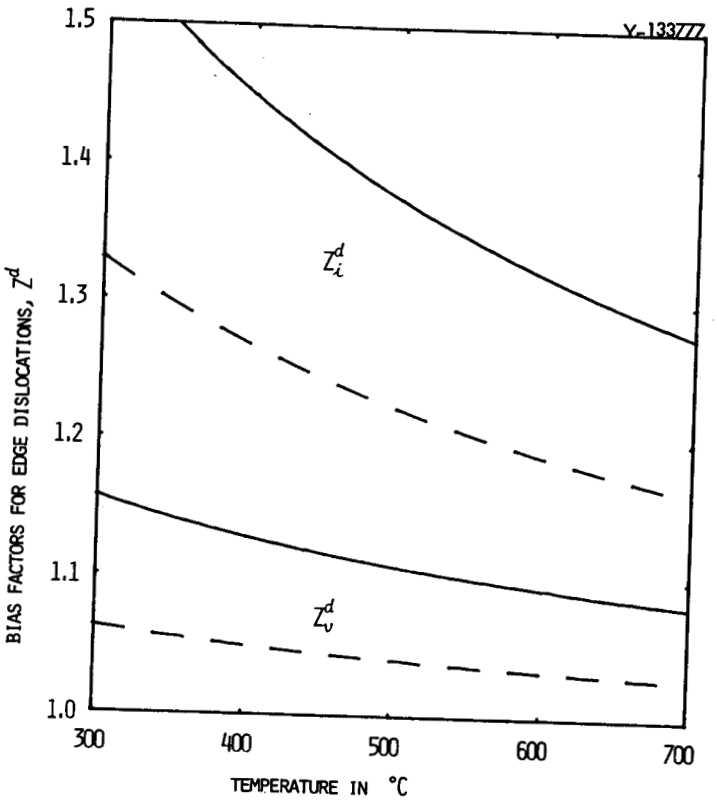


Fig. 4. Bias factors for edge dislocations as a function of temperature

$$Z^d = 1 + (\ell nL/d)^{-1} \left(\frac{b}{8\pi d(1-\nu)}\right)^2 \left\{[\beta\nu K(1-2\nu)]^2 \right.$$
$$- 2\beta\,[(1-2\nu)^2\,\alpha^K + \tfrac{4}{3}\,(1-\nu+\nu^2)\,\alpha^G]$$
$$- [\beta\,(1-2\nu)]^2\,\nu K\alpha^K \epsilon_{ii} \qquad (9)$$
$$\left. + \tfrac{1}{3}\,(1+\nu)\beta^2\nu G\alpha^G\,[2\hat{b}_i\hat{b}_j - (1-4\nu)\hat{\ell}_i\hat{\ell}_j]\;\epsilon_{ij}\right\} \quad .$$

Here, L is the half-distance between dislocations, $\hat{b}_i = b_i/b$, $\hat{\ell}_i$ is the unit line vector, and d is an inner cut-off radius. Using the condition* $\langle \beta\vec{1} \cdot \nabla E\rangle \cong 1$ for the cut-off radius one finds that for an interstitial $d_i \cong 10b$ and for a vacancy $d_v \cong 4b$. Using L = 400b, Eq. (9) gives the bias factors shown in Fig. 4. Again, the dashed curves are obtained with the image interaction only, and they agree with the results obtained from Ham's rigorous solution.[2]

REFERENCES

1. W. G. Wolfer and M. Ashkin, J. Appl. Phys. 46, 547, 4108 (1975).
2. W. G. Wolfer and M. Ashkin, to be published in J. Appl. Phys.
3. F. C. Moon and Y.-H. Pao, J. Appl. Phys. 38, 595 (1967).
4. J. D. Eshelby, Progr. Solid Mech. 2, 89 (1961).
5. K. Schröder, Report Jul-1083-FF (July 1974).
6. W. G. Wolfer and M. Ashkin, Scripta Met. 7, 1175 (1973).
7. W. G. Wolfer and M. H. Yoo, Paper Intern. Conf. on Rad. Effects and Tritium Techn., Gatlinburg, Tenn., Oct. 1975.
8. P. R. Okamoto and H. Wiedersich, J. Nucl. Mater. 53, 336 (1974).
9. W. G. Wolfer and L. K. Mansur, unpublished results.
10. L. K. Mansur, P. R. Okamoto, A. Taylor, and Che-Yu Li, Nucl. Met. 18, ed. by R. J. Arsenault, p. 509.
11. W. G. Wolfer, Scripta Met. 9, 801 (1975).
12. R. Bullough, these proceedings.
13. W. A. Coghlan, private communication.

*Brackets indicate an angular average.

X-RAY STUDIES OF IRRADIATION INDUCED DISLOCATION LOOPS IN METALS

B. C. Larson
Solid State Division, Oak Ridge National Laboratory*
Oak Ridge, Tennessee 37830, U.S.A.

ABSTRACT

Theoretical and experimental progress has resulted in the increased use of x-rays for the study of defects and defect clusters in crystals. In this paper an outline of the theoretical framework associated with Huang, Stokes-Wilson and integral diffuse scattering from dislocation loops is presented, and an account of recent experiments on radiation induced loops is given. These studies include low temperature, ambient temperature and elevated temperature irradiations of metals with electrons, neutrons and accelerated ions, and pertain to the study of the thermal annealing characteristics as well as the as-produced damage structure. The information obtained by x-rays as to the type, size and concentrations of dislocation loops is contrasted with existing electron microscopy, electrical resistivity and lattice parameter data in order to establish correlations and identify areas of disagreement.

INTRODUCTION

The study of defect clusters and dislocation loops by x-ray diffuse scattering has received increased attention in recent years as a result of both theoretical and experimental progress in this field. Although the effects of defect clustering on diffuse scattering had been considered earlier,[1] Krivoglaz[2-4] and later Dederichs[5,6] and Trinkaus[7-9] were instrumental in developing the present form of the theory. This theoretical work facilitated the interpretation of diffuse scattering measurements and stimulated the use of x-ray diffuse scattering for the study[10-17] of loops and defect clusters in both metal and non-metal crystals.

In this paper a brief outline of the theory pertaining to the diffuse scattering near Bragg reflections will be given and the application of this theory to the study of radiation induced loops in metals will be discussed. While differential diffuse scattering measurements have been

*Operated by Union Carbide Corporation for the USERDA.

used to characterize loops during thermal annealing to room temperature after low temperature electron and neutron irradiations, integral diffuse scattering measurements have been applied to ambient temperature and above irradiation and annealing studies. These latter studies have included ion irradiations as well as those of electrons and neutrons.

The results of the diffuse scattering studies will be compared with electron microscopy, electrical resistivity and lattice parameter measurements where possible in order to establish a direct correspondence and identify areas where additional work is needed.

THEORY

The theory of diffuse scattering from lattice defects has been discussed thoroughly in a number of review papers[6,9,16] in the past few years with the result that rather detailed accounts of the underlying assumptions and approximations are available.

Assuming small concentrations of defects distributed randomly throughout a crystal lattice, the scattering cross section per defect is given by

$$\frac{d\sigma}{d\Omega}(\vec{q}) = [r_e f_h e^{-M_h}]^2 \; |A_h(\vec{q})|^2 \qquad (1)$$

where $\vec{q}$ is the vector distance of the scattering vector $\vec{K}$ from the nearest reciprocal lattice vector $\vec{h}$ and r_e is the classical electron radius. f_h is the atomic scattering factor, e^{-M_h} is the thermal Debye-Waller factor and $A_h(\vec{q})$ is the scattering amplitude of the defect. The scattering amplitude is given in terms of lattice sums by

$$A_h(\vec{q}) = \Sigma\, e^{i\vec{K}\cdot\vec{r}_j^{\,d}} + i\vec{K}\cdot\vec{s}(\vec{q}) + \Sigma\, e^{i\vec{K}\cdot\vec{r}_i}(e^{i\vec{K}\cdot\vec{s}_i} - 1 - i\vec{K}\cdot\vec{s}_i) \qquad (2)$$

where $\vec{r}_j^{\,d}$ is the position of the atoms of the defect (dislocation loop) and $\vec{r}_i + \vec{s}_i$ is the position of the i^{th} atom displaced a distance $\vec{s}_i$ from the mean lattice position $\vec{r}_i$. We can recognize the first term as the direct or Laue scattering from the defect, the second term as the Huang scattering which diverges as $q \to o$ and the third term as higher order corrections to the Huang scattering that tends to a constant as $q \to o$. In general, the relative size of q compared to the inverse of the loop radius determines the relative importance of these terms[5] and indeed for

very small q only the Huang term is important. The interference between the Huang and correction terms begin to be important for moderately small $q \sim 1/10R$ where R is the loop radius.

Making use of only the symmetric part of Eq.(2), the reduced cross section, $|A_h(q)|^2$, is given quite accurately by

$$|A_h(\vec{q})|^2_{sym} = |\vec{K}\cdot\vec{s}(\vec{q})|^2 \qquad (3)$$

for $q \lesssim 1/R$. This symmetric part of the scattering is most commonly referred to as the "Huang" scattering. $\vec{s}(\vec{q})$ can be calculated analytically for these small q values, and as a result Eq. (3) can be written in general terms as[6,8,9]

$$|A_h(\vec{q})|^2_{sym} = \frac{h^2}{q^2}(\gamma_1\pi_1 + \gamma_2\pi_2 + \gamma_3\pi_3) \qquad (4)$$

after averaging the cross sections over all equivalent lattice orientations of the dislocation loops. The γ's are functions of the elastic constants, $\vec{h}$ and $\vec{q}$, and the π's are related to the dipole force tensor, P_{nm}. π_1 is proportional to the square of the defect strength $\Delta V = b\pi R^2$ (b = Burgers vector) and π_2 and π_3 are measures of the anisotropy of the defect and are then zero for cubic or isotropic defects. Each of these π's can be determined experimentally by choosing the proper $\vec{h}$ and $\vec{q}$ combinations[13], and as seen from Eq. (4) these are the only unique parameters regarding the defects that are obtainable from the Huang scattering at small q.

The asymmetry in the scattering is important in determining the sign of the distortion (sign of the Burgers vector) around the loop. The magnitude of this antisymmetric scattering is given approximately by

$$|A_h(q)|^2_{anti} \simeq \frac{h}{q}\sqrt{\pi_1\gamma_1}\,\frac{R^3|hb|^{3/2}}{V_c} \qquad (5)$$

and is positive for $\vec{q}$ parallel $\vec{h}$ for interstitial type loops and negative for $\vec{q}$ antiparallel $\vec{h}$ for interstitial loops. The signs are simply reversed for vacancy type loops. V_c is an atomic volume.

For larger $q \gtrsim 1/R$, numerical calculations are required which include the form factor of the loop. Approximate analytical expressions giving the

scattering in this region result in the form [7,6]

$$|A_h(q)|^2_{S-W} \approx \frac{\phi(\vec{q}/q)|\Delta V|h}{4\pi V_c{}^2 q^4} \tag{6}$$

which is sometimes referred to as the Stokes-Wilson (S-W) approximation. $\phi \sim 160$ was found [16] to be reasonable for {111} loops in aluminum, although Eq. (6) can not be expected to be as reliable for $q \gtrsim 1/R$ as Eq. (5) is for $q \lesssim 1/R$.

The scattering resulting from integrating over the Ewald sphere in the region of $\vec{h}$ has been called "integral" diffuse scattering and can be written as [10,11,16]

$$\sigma_{sym}(q_o) = [r_e f_h e^{-M_h}]^2 (\frac{h}{k})^2 2\pi\tau (\frac{b\pi R^2}{V_c})^2 \quad \ell n(e^{1/2}\, \alpha/q_o R) \qquad q_o \leq \alpha/R \tag{7}$$

and

$$\sigma_{sym}(q_o) = [r_e f_h e^{-M_h}]^2 (\frac{h}{k})^2 \quad 2\pi\tau (\frac{b\pi R^2}{V_c})^2 \quad \frac{\alpha^2}{2R^2 q_o{}^2} \qquad q_o \geq \alpha/R \tag{8}$$

k is $2\pi/$(x-ray wavelength) and τ is defined in terms of an average over Eq. (4) but can be approximated as [19,20]

$$2\pi\tau \simeq \frac{8\pi}{15} + \frac{\pi}{15}\left(\frac{3\nu^2+6\nu-1}{(1-\nu)^2}\ \mathrm{Cos}^2\ \theta_B\right) \tag{9}$$

in which ν is Poissons ratio. The parameter α has been estimated [16] as 1 for 111 reflection of copper and 1.3 for the 111 reflection in aluminum from numerical calculations. $q_o = h\Delta\theta \cos\theta_B$ is the minimum q contributing to the integral diffuse scattering at a rocking angle of $\Delta\theta$ off the Bragg angle θ_B as shown in Fig. 1.

For $q_o \gtrsim \alpha/R$ the cross section can be written as[16]

$$\sigma_{sym}(q \gtrsim \alpha/R) = [r_e f_h e^{-M_h}]^2 \left(\frac{h}{k}\right)^2 2\pi\tau \frac{|b|\pi}{V_c} \frac{\alpha^2}{2q_o^2} N_{PD} \qquad (10)$$

where N_{PD} is given by $b\pi R^2/V_c$

and is just the number of point defects in the loop. At large q_o then, $\sigma_{sym}(q_o)$ is directly proportional to the number of point defects contained in the loop independent of the loop size. This is a direct result of the fact that Eq. (6) is proportional to $\Delta V = b\pi R^2$ and is also a direct measure of the point defect concentration stored in loops.

LOW TEMPERATURE IRRADIATION

Electron Irradiation

Huang diffuse scattering studies of 4K electron irradiated aluminum,[13] copper,[17] and gold[21] have been reported in which single interstitials were found in aluminum and copper immediately after irradiation while small defect clusters were found in gold. After annealing to temperatures in the range of 40-200K, however, Ehrhart and Schilling[13] reported the formation of interstitial clusters in aluminum and Ehrhart and Schlagheck[17] reported similar aggregation of point defects in copper. The presence of these clusters was inferred in two ways. The intensity of the diffuse scattering increased considerably after annealing even though the resistivity (being a measure of the total point defect concentration) decreased by 60-70%, indicating that π_1 in Eq. (4) increased and therefore that the strength per defect had increased. In addition, a transition from the Huang scattering law was observed after annealing. Such a transition was not seen in the scattering from the isolated point defects as shown in Fig. 2 and in general can only be seen for strong (cluster) distortion centers.

In addition to the establishment that clusters existed in the samples, it was possible to infer something about the characteristic shape or form of the aggregates by using the observed intensities in various $\vec{q}$ directions to determine the relative sizes of π_1, π_2 and π_3. π_2 and π_3

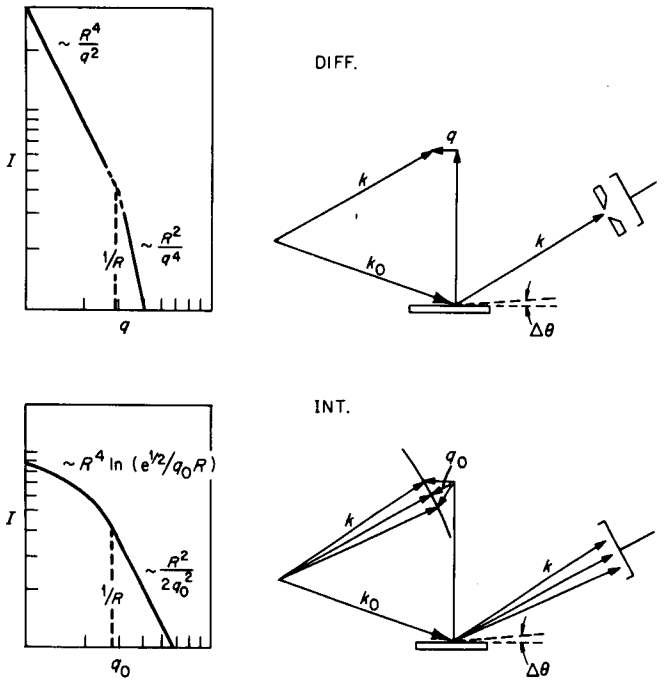


Fig. 1. Differential and integral diffuse scattering geometries

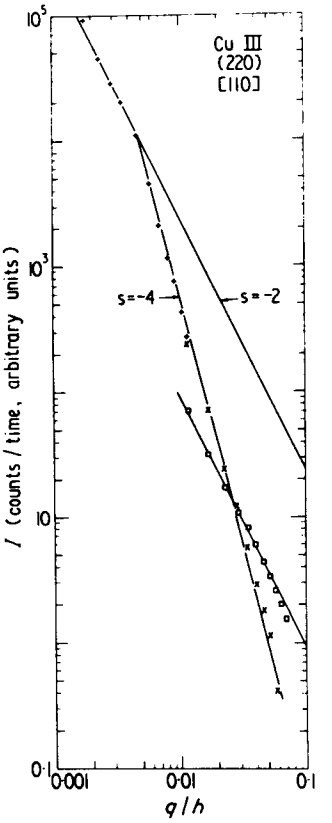


Fig. 2. Huang diffuse scattering from (□) electron irradiated copper at 4K and (+,x) after annealing to 300K.

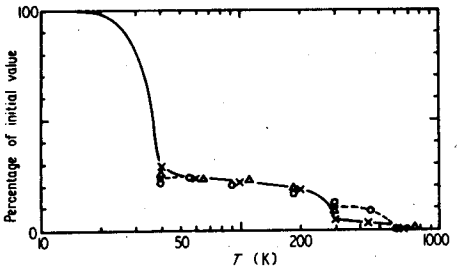


Fig. 3. Electrical resistivity (x) and diffuse scattering (Δ,O) in the q^{-4} Stokes-Wilson region normalized at 60K.

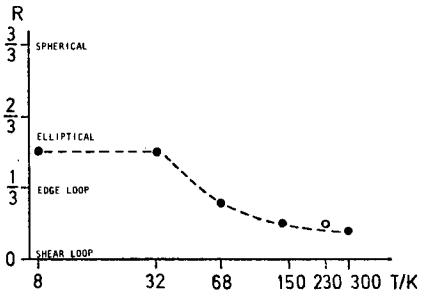


Fig. 4. Ratio of the shear distortion to the total distortion from defects in 4K neutron irradiated copper.

vanish for defects with spherical or cubic symmetry, and therefore the ratios of π_2/π_1 and π_3/π_1 are measures of the anisotropy of the defects. Table 1 shows calculated values of these ratios for various defect configurations in copper and aluminum. These values are to be compared with the measured values of $\pi_2/\pi_1 = 0.02\ (^{+.05}_{-.02})$ and $\pi_3/\pi_1 = 0.05\ (\pm 0.02)$ for aluminum[13] after annealing to 130K; and values of $\pi_2/\pi_1 = 0.008\ (\pm 0.008)$ and $\pi_3/\pi_1 = 0.1\ (\pm 0.05)$ for copper[17] and 200K and $\pi_3/\pi_1 = 0.09\ (\pm 0.02)$ after annealing to 300K. From these measured ratios it is clear that the aggregates are not spherical in nature and, while the uncertainties in the measured values would not allow a clear decision as to the type of loops present, it appears that the measurements are most consistent with loops on {111} planes with either <111> or <110> Burgers vectors.

Table 1. Huang scattering parameters calculated for spherical defects and various types of loops in aluminum and copper.

	Aluminum		Copper	
Defect Type	π_2/π_1	π_3/π_1	π_2/π_1	π_3/π_1
Spherical	0.0	0.0	0.0	0.0
{111} <111>	0.0	0.046	0.0	0.094
{110} <110>	0.012	0.035	0.0036	0.070
{111} <110>	0.012	0.053	0.0036	0.106

The sizes, concentrations and vacancy or interstitial nature of these loops are probably of somewhat larger interest in terms of the understanding of annealing processes. For the case of aluminum ($\Delta\rho_o$ = 192 nΩcm) at 130K, the loops were estimated to contain from 10-20 interstitials under the assumption that a 7 atom loop was the minimum size of loop stable at that temperature and assuming the remainder of the distribution to be exponential like (i.e. $C(o)e^{-R/R_o}$). From the value of q at which the transition from the q^{-2} to q^{-4} dependence of the intensity took place in Fig. 2 Ehrhart and Schlagheck[17] estimated somewhat more than 40 defects per loop after annealing to 300K in the case of copper ($\Delta\rho_o$ = 122 nΩcm).

This number was obtained by equating Eq. (4) and Eq. (6) at the transition q and again assuming an exponential size distribution. Assuming no distribution of sizes, a rather unreasonable value of the order 800-900 defects per loop was obtained.

These results can be compared with size distributions obtained by Larson and Young[20] using integral diffuse scattering measurements made on copper that was electron irradiated ($\Delta\rho_o$ = 132nΩcm). The size distribution was obtained by fitting[16] Eqs. (7,8) to the diffuse scattering and the results are shown in Fig. 5. It can be seen that an average size would correspond to about 10Å radius (~50 defects per loop) which is quite consistent with the results of Ehrhart and Schlagheck. The results of a recent electron microscopy study[22] of similarly irradiated copper ($\Delta\rho_o$ = 130nΩcm) are also indicated in Fig. 5. For radii of 20Å and above the agreement between x-rays and electron microscopy is very good although from 7-15Å there is considerable disagreement.

Although aluminum anneals completely in Stage III and there is no evidence for vacancy clustering, copper retains defects above Stage III as indicated above and there seems to be some evidence of vacancy aggregation during this annealing stage. Ehrhart and Schlagheck[17] reported a significant reduction in the magnitude of the asymmetry in the Huang scattering after annealing from 200-300K. According to Eq. (5), this would result if defects clusters with distortions of opposite sign to those already existing were produced or if a significant reduction in the average size took place. The concommitant observation (Fig. 3) of a much larger annealing fraction of the lattice parameter and electrical resistivity than that for the intensity in the Stokes-Wilson scattering region (which is a measure of the number of point defects in loops independent of the sign of the Burgers vector) was interpreted as even stronger evidence for the clustering of vacancies in Stage III. Isolated vacancies aggregating into loops can be expected to result in a decrease in the lattice parameter since the contraction around a single vacancy is[17] only ~$-0.4V_c$ while the contraction associated with each vacancy in a vacancy loop approaches $-V_c$. Contrarily, the diffuse scattering in the Stokes-Wilson region should sense only the clustered defects and be

insensitive to isolated point defects. The factor of four decrease in the electrical resistivity (and lattice parameter change) compared to less than a factor of two annealing for the diffuse scattering in Fig. 3 was therefore interpreted to be a result of vacancy migration, partial annihilation with interstitial loops and finally the formation of vacancy loops. The interpretation implies that the specific resistivity of point defects in loops is significantly lower than for isolated point defects. There is some independent evidence for this from integral diffuse scattering measurements using Eq. (10) as shown in Table II. This will be discussed later.

Neutron Irradiation

B. von Guérard has reported the observation of some type of interstitial clustering in copper[23] immediately after neutron irradiation to 216 nΩcm at 6K. These clusters did not have the character of loops and were interpreted as resulting from the inhomogeneous nature of cascade damage. However, after annealing to 68K the dominant defects took on the character of edge loops on {111} or {110} planes or possibly unfaulted {111} loops as shown in Fig. 4. Upon further annealing to room temperature the ratio[9] of the edge to shear component of loops showed tendencies toward a larger shear component, indicating a preference for unfaulted {111} loops. Equating Eqs. (4,6) at the effective intersection of the $1/q^2$ and $1/q^4$ scattering laws to determine the loop sizes resulted in radii that varied as a function of annealing from ~18Å at 68K to ~30Å at 230K, and a somewhat broader distribution of sizes varying from 15-40Å observed at room temperature. Without making assumptions about the distribution of sizes, the above size determinations are similar to those observed by Ehrhart and Schlagheck on electron irradiated copper.

During the annealing through Stage III, von Guérard observed the same effects that were observed in electron irradiated copper as regards both the reduction in the magnitude of the asymmetry (Eq. (5)) in the Huang scattering and the more complete annealing of the electrical resistivity and lattice parameter change compared to that of the intensity in the

Stokes-Wilson region. In this neutron irradiated case differences between the annealing rates of the resistivity and diffuse scattering were already evident at 150K, which may indicate a small amount of vacancy reorientation even at these low temperatures.

Size distributions obtained from room temperature integral diffuse scattering measurements[16] made on copper that had been irradiated at low temperature with neutrons ($\Delta\rho_o \approx 100$*; 216nΩcm) as well as with electrons ($\Delta\rho_o = 132$nΩcm) are shown in Fig. 5. As mentioned earlier, these exponential-like size distributions seem to be consistent with the above size estimates of Ehrhart and Schlagheck and also those of von Guérard at room temperature, if it is recognized that the use of Eqs. (4,6) for extracting sizes yields average sizes given by the square root of the ratio of the fourth moment to the second moment. For an exponential size distribution the above value turns out to be $\sqrt{12}$ larger than the average radius.

The similarity in the size distributions in Fig. 5 for electron and neutron irradiations is remarkable. The concentrations are of course lower for electron irradiation due to the larger annealing fraction following electron irradiations; however, the size distribution result seems to imply that the neutron cascade is not of overwhelming influence in determining the cluster nucleation. Rather, some parameter more closely related to the material such as the impurity concentration or defect and cluster mobility may play the decisive role. Scheidler and Roth[24] have observed significant decreases in loop sizes after electron irradiation of copper with higher impurity content.

Further isochronal annealing[16] of the higher dose neutron irradiated samples in Fig. 5 has been carried out. In these studies it was found that the loop size distributions became coarser through the preferential annealing of the smaller loops with a concommitant increase in the numbers of larger loops, as shown in Fig. 6. The detailed annealing characteristics of the various moments of the size distribution are shown in Fig. 7

*Irradiated by T. Blewitt at Argonne National Laboratory

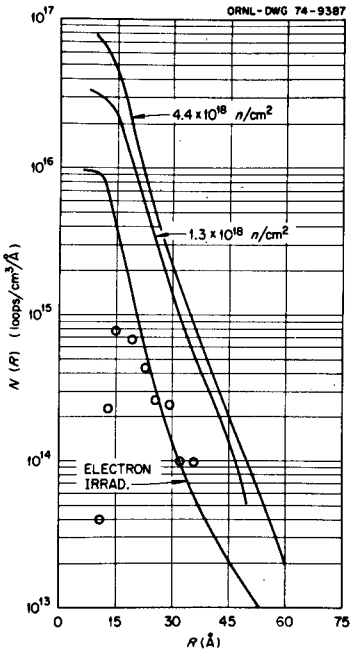


Fig. 5. Loop size distributions for 4K irradiated copper after warming to room temperature. Points (0) electron microscopy measurements.

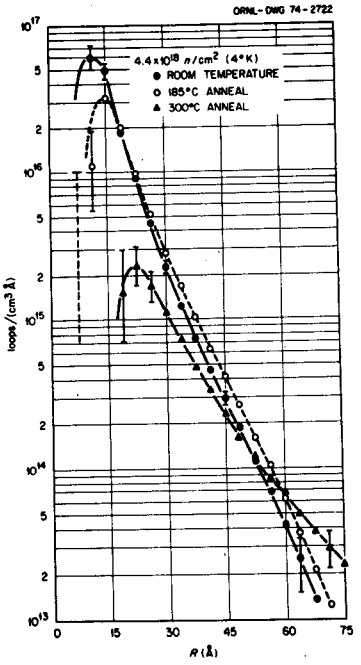


Fig. 6. Size distributions of 4K neutron irradiated copper as a function of annealing temperature.

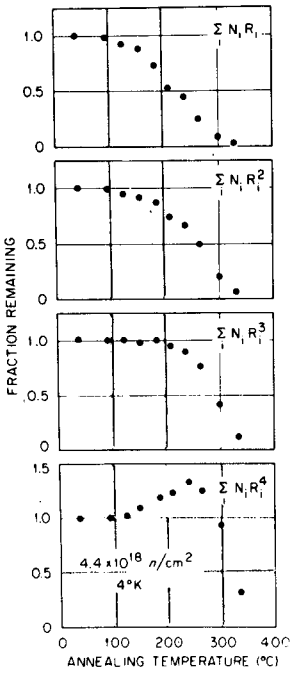


Fig. 7. Annealing characteristics of individual moments of the size distributions from Fig. 6.

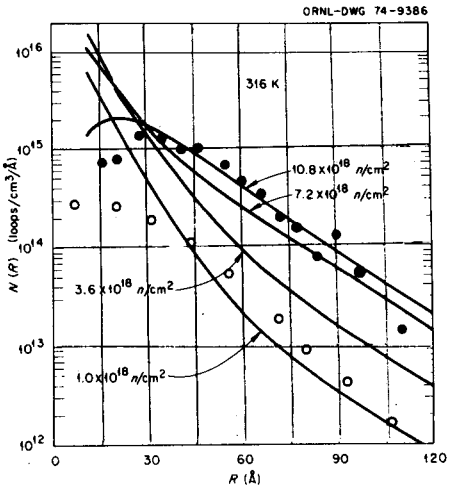


Fig. 8. Loop size distributions for neutron irradiated copper. Points (0) and (•) are for 9×10^{17} n/cm^2 (E > 0.1 MeV) and 10.8×10^{18} n/cm^2 (E > 0.6 MeV) respectively.

for each of the annealing steps used in the above study. It can be seen that the number of point defects (given by $\frac{b\pi}{V_c} \Sigma_i C_i R_i^2$) decreases monotonically, but that the fourth moment increases at about 250°C as a result of the increased numbers of larger loops. These observations are in good qualitative agreement with electron microscope studies of the annealing of dislocation loops in electron irradiated copper reported by Ohr at this conference and those of Rühle et al.[25] for annealing of neutron irradiated copper. Since anomalous x-ray transmission measurements are sensitive to the third and fourth moments of the size distribution of loops, these results may have a bearing on the increased absorption observed[26] at 400K during the annealing of low temperature neutron irradiated copper. That is, a linear combination of the third and fourth moments could result in a maximum below 250°C. In general, these results indicate the use of caution in interpreting defect measurements without considering the possibility of size distribution changes.

Ambient Temperature Irradiations

High resolution Huang diffuse scattering studies of dislocation loops in 316K neutron irradiated copper have been used to study[12] the angular distribution of the diffuse scattering near the Bragg reflection as described by Eqs. (4,5). The measured iso-intensity lines for a dose of $10.8 \times 10^{18} n/cm^2$ were found to be in good agreement with those calculated for perfect loops on {111} planes, using Eq. (4) and considering the elastic anisotropy of copper. The antisymmetrical part resulting from Eq. (5) was also observed to have the expected shape, and it was found to have a sign corresponding to interstitial type loops. Although both vacancy and interstitial loops are known to be present in these samples, the larger loops are mainly interstitial, and due to the R^5 weighting of Eq. (5) the scattering is heavily weighted toward interstitial loops. This fact also seems to explain the observation of perfect loops rather than Frank loops on {111} planes because again many of the larger loops have been observed with electron microscopy[25,27] to be perfect although the smaller ones appear to be overwhelmingly faulted loops.

The above high resolution studies have so far not been used in the determination of the defect concentrations and size distributions of loops due to inadequate statistical accuracy. However, integral diffuse scattering measurements have been used for this purpose and Fig. 8 shows the size distributions and concentrations of loops produced by 316K neutron irradiation of copper in the dose range of 10^{18}-10^{19}n/cm^2 (E > 0.6 MeV). These distributions were obtained through the least squares fitting of Eqs. (7,8) directly to the observed scattering data[20]. The changes in the size distributions correspond to a continual coarsening in the average size of the defects and to a saturation in the number of smaller loops. These changes have been shown to be in good qualitative agreement with lattice parameter change measurements[16] and in quantitative agreement with detailed anomalous transmission measurements[16] made on these crystals. Some electron microscopy[28,29] results are also shown in Fig. 8, which again reveal a systematic disagreement in the loop concentrations at the small sizes, but rather encouraging quantitative and qualitative agreement at the larger sizes.

The x-ray results can be related to electrical resistivity measurements through a comparison of the total number of point defects given by Eq. (10) for x-rays and the electrical resistivity change $\Delta\rho$, assuming 2$\mu\Omega$ cm/at% Frenkel pairs. Such a comparison (at room temperature) has been carried out for copper that had been irradiated at low temperatures as well as for irradiations at reactor ambient temperature, as shown in[30] Table II. In each case the x-ray measurements predict a factor of three more defects than that corresponding to the electrical resistivity. To the extent that Eq. (10) can be considered accurate, this result indicates the resistivity of point defects in dislocation loops to have specific resistivities of a factor of ~3 lower than that for isolated defects. It is interesting to correlate this result with the annealing results of Stage III in copper where a similar relation between x-ray and electrical resistivity seems to emerge. One of the samples in Table II (BSR-2) was isochronally (5 min) annealed through Stage V using 2.5%

steps of $\Delta T/T$. It was found that within the accuracy of the x-ray measurements, the ratio established in Table II remained essentially constant during the annealing.[16]

Table 2. Point defect concentrations at room temperature as measured by x-rays and electrical resistivity.

	BSR-1	BSR-2	FRM	CP-5
Irradiation temperature, °K	316	316	6	8
Dose, neutrons/cm^2	1×10^{18} (E>0.6MeV)	3.6×10^{18} (E>0.6MeV)	4.4×10^{18} (E>0.1MeV)	1.3×10^{18} (fission spectrum)
N_{PD}/cm^3 (x-ray)	1.25×10^{19}	3.9×10^{19}	8.3×10^{19}	5×10^{19}
$\frac{N_{PD}\ (\text{from } \Delta\rho)}{N_{PD}\ (\text{from x-ray})}$	0.31	0.29	0.31	0.30

Higher Temperature Neutron Irradiation

The observation of very large, non-homogeneously distributed dislocation loops and loop tangles after low dose[31] ($\sim10^{18}$n/cm^2) irradiations of copper at 550-650K has been studied by anomalous transmission measurements. The anomalous transmission studies indicated the transition in the cluster character at this dose to be in the temperature range ($\sim$475K) that voids begin to form after much higher doses. Still further work[20] using integral diffuse scattering has provided more insight into the nature of this transition. Fig. 9 shows the size distributions (measured at room temperature) for copper irradiated for 4K to 483K, which indicate a general trend toward larger loop sizes and lower point defect densities with increasing irradiation temperature. The tendency toward a bimodal distribution at 483K in Fig. 9 must be regarded with caution by itself; however, this trend was more pronounced at higher doses and direct electron microscopy observations[32] of a 433K irradiation of 3.6×10^{18}n/cm^2 have shown a well developed bimodal distribution with sizes of $\sim$20Å and $\sim$200Å radius. Although the larger cluster component was quite inhomogeneously distributed, the small component appeared to be homogeneous in the electron micrographs and contained both vacancy and

interstitial type loops. The total point defect concentrations retained in these samples were markedly decreased with increasing irradiation temperature.

ION AND HIGH ENERGY NEUTRON BOMBARDMENT

Initial attempts[33] have been made on the use of x-ray diffuse scattering to investigate Ni ion irradiation damage in copper and niobium. These studies were carried out in conjunction with electron microscopy work so that the depth profiles of the damage were available for the copper. The size distributions and concentrations of loops in copper normalized to that corresponding to the peak near the end of range for 5×10^{12}Ni/cm^2 at 4 MeV and 1.2×10^{13}Ni/cm^2 at 60 MeV were determined by both x-ray and electron microscopy. The systematic discrepancy between x-ray and electron microscope measurements at small sizes was again present; however, with both measuring techniques the size distributions were found to be similar for the two types of irradiations, and as discussed in more detail by Roberto and Narayan at this conference, the total damage scaled closely with the damage energy. With respect to niobium it was found that the fraction of the defects retained compared to those created was a factor of ~5 lower than for copper although the defect size distributions were similar.

Comparisons[34] of fission and 15 MeV neutron damage in copper made using these same techniques have also indicated that the defect density scales with the damage energy for fission neutron doses of 1×10^{18}/cm^2 and 15 MeV neutron doses of 2×10^{17}/cm^2. The size distributions were not markedly changed by the higher energy neutrons.

NUMERICAL CALCULATIONS

For the small -q region analytical approximations corresponding to Eq. (4) seem to be adequate for analysing Huang diffuse scattering. However, for larger q values ($qR \gtrsim 1$) the form factor associated with the loops must be included and the q dependence of Eq. (5) coming from the corrections in Eq. (2) must be considered in order to obtain the most reliable results. This requires numerical calculations making use of precise displacement fields close to the dislocation loop, which are in

principle available for both isotropic and anisotropic materials.[35,36] Such calculations have been carried out[18] for the case of Frank loops on {111} planes in aluminum using a continuum model and assuming elastic isotropy. A typical result for the 222 reflection in aluminum assuming 10Å loops is shown as a function of the variable qR in Fig. 10. The cross section has been multiplied by q^2 so that the q^{-2} Huang scattering law corresponds to zero slope and the q^{-4} Stokes-Wilson scattering region corresponds to a slope of -2 as shown by the solid line. The symmetric part of the scattering (to be compared with Eqs. (3,4)) is shown as the middle dashed line. The shoulder in the region qR ~ 2.5 is worthy of special note as it is a result of the scattering (essentially Bragg) from the compressed region close to the 111 loop of the {111} set. This was demonstrated clearly when the scattering from this particular loop orientation alone was calculated for a plane in reciprocal space. The details of this latter calculation will not be considered here except to mention that the Huang scattering closest to the reciprocal lattice point could be understood analytically and that an intense sattelite peak appeared around qR ~ 2.5 for the 50A radius loop considered. Making use of[6] $\frac{\Delta a}{a} = \frac{-q}{h}$, it was possible to associate the scattering in the region qR ~ 2.5 with the Bragg like scattering from the compressed region (~$\pm$ 2R) perpendicular to the loop plane. $\Delta a/a$ is the relative lattice parameter change due to the compressions.

Since these calculations were performed using a continuum lattice model, the extension of such calculations to the entire Brillouin zone was not reasonable on physical grounds. However, Keating and Goland[38,39] have made use of a discrete lattice model in making calculations throughout several Brillouin zones for loops in BeO and graphite. Similar calculations should be extended to metals also as the possibility of making such diffuse scattering measurements with high precision is already at hand.[40]

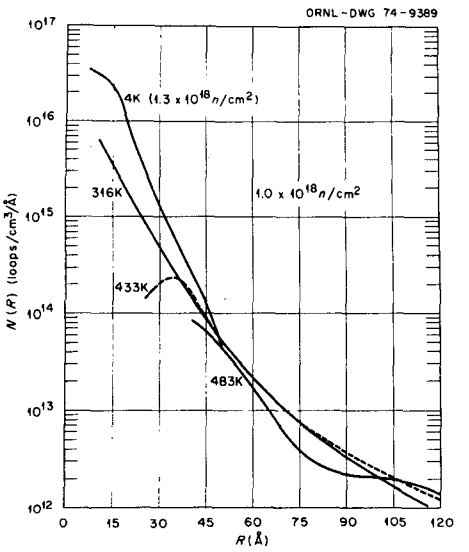


Fig. 9. Dislocation loop size distributions measured at room temperature after neutron irradiation at the indicated temperature.

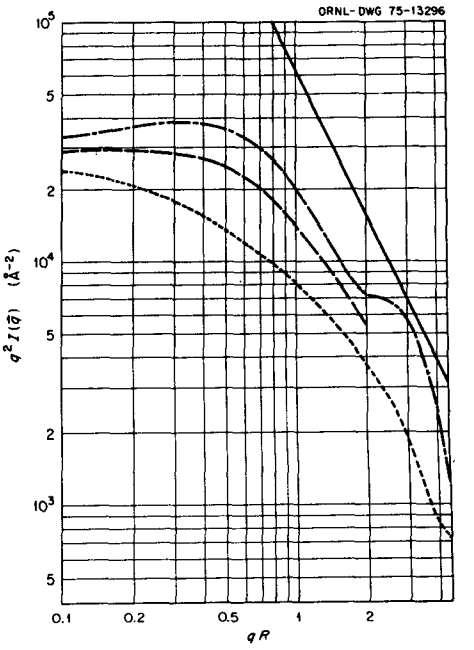


Fig. 10. Calculated diffuse scattering from loops for q parallel (upper), q antiparallel (lower) for the 222 reflection in aluminum. The middle curve is symmetric intensity.

CONCLUSIONS

The use of x-ray diffuse scattering has contributed significantly to the information known about the processes of point defect clustering at low temperatures. X-ray studies have contributed significantly to the understanding of Stage III annealing and have been used for studying loop size distribution changes through Stages IV and V. In addition, work has been reported on the study of dislocation loop size distributions resulting from ambient temperature neutron and ion bombardment and higher temperature neutron irradiations. Comparison of these x-ray studies with electron microscope generated loop size distributions have shown good agreement except in the smaller sizes and correlations with electrical resistivity have demonstrated the possibility of determining the specific resistivity associated with point defects in loops. Calculational efforts have made progress toward the detailed understanding of the scattering in the

Stokes-Wilson region so that continued work in this area and the application of these results to high resolution scattering data should further improve the accuracy of x-ray studies. Further combined electron microscopy and x-ray studies will be necessary in order to resolve the apparent disagreement in the size distributions for the smaller loops.

References

1. W. Cochran and G. Kartha, Acta Cryst. 9, 944 (1956).
2. M. A. Krivoglaz, Phys. Met. Metallogr. 7 (5), 11 (1959).
3. M. A. Krivoglaz, Phys. Met. Metallogr. 9 (5), 1 (1960).
4. M. A. Krivoglaz in Theory of X-ray and Thermal Neutron Scattering by Real Crystals, Plenum Press, New York (1969).
5. P. H. Dederichs, Phys. Rev. B4, 1041 (1971).
6. P. H. Dederichs, J. Phys. F: Metal Phys. 3, 471 (1973).
7. H. Trinkaus. Z. Angew. Phys. 31, 229 (1971).
8. H. Trinkaus, Phys. Stat. Sol. (b), 51, 307 (1972).
9. H. Trinkaus, Phys. Stat. Sol. (b), 54, 209 (1972).
10. J. E. Thomas, T. O. Baldwin and P. H. Dederichs, Phys. Rev. B3, 1167 (1971).
11. B. C. Larson and F. W. Young, Jr., Z. Naturforsch. 28a, 626 (1973).
12. B. C. Larson and W. G. Schmatz, Phys. Rev. 10, 2307 (1974).
13. P. Ehrhart and W. Schilling, Phys. Rev. B8, 2604 (1974).
14. H. Peisl, J. Appl. Cryst., 8, 143 (1975).
15. J. P. Patel, J. Appl Cryst., 8, 186 (1975).
16. B. C. Larson, J. Appl. 8, 150 (1975).
17. P. Ehrhart and U. Schlagheck, J. Phys. F: Metal Phys. 4, 1589 (1974).
18. B. C. Larson and W. Schmatz, unpublished.
19. P. H. Dederichs, Phys. Rev. B1, 1306 (1970).
20. B. C. Larson and F. W. Young, Jr., unpublished.
21. P. Ehrhart and F. Segura, this conference.
22. S. M. Ohr, this conference.
23. B. von Guérard, Thesis, Technical University of Münich, Germany (1974).
24. G. P. Scheidler and G. Roth in Vacancies and Interstitials in Metals, ed. by A. Seeger, D. Schumacher, W. Schilling and J. Diehl, Amsterdam: North Holland, 391 (1968).
25. M. Rühle, F. Häussermann and M. Rapp. Phys. Stat. Sol. 39, 609 (1970).

26. E. E. Gruber, T. H. Blewitt and T. O. Baldwin, J. Appl. Phys. 45, 542 (1974).

27. B. L. Eyre, J. Phys., F: Metal Phys. 3 497 (1973).

28. M. Rühle and J. C. Crump, III, Phys. Stat. Sol. 2, 252 (1971).

29. J. Narayan, Private communication.

30. F. W. Young, Jr. and B. C. Larson, J. Appl. Cryst. 8, 185 (1975).

31. B. C. Larson and F. W. Young, Jr. in Radiation Induced Voids in Metals, ed. by G. W. Corbett and L. C. Iannello, USAEC report CONF-710601, p. 672 (1972).

32. J. Narayan, Private communication.

33. J. B. Roberto and J. Narayan, this conference.

34. J. B. Roberto and J. Narayan, Private communication.

35. S. M. Ohr, J. Appl. Phys. 43, 1361 (1972).

36. S. M. Ohr, Phys. Stat. Sol. (b), 64 317 (1974).

37. B. C. Larson and H. Trinkaus, to be published.

38. D. T. Keating and A. N. Goland, Phys. Rev. B4, 1816 (1971).

39. D. T. Keating and A. N. Goland, Phys. Rev. B10, 1624 (1975).

40. H. -G. Haubold, this conference.

INVESTIGATION OF INTERSTITIAL CLUSTERS IN COPPER BY MEASUREMENTS OF THE HUANG DIFFUSE SCATTERING

P. Ehrhart and U. Schlagheck
Institut für Festkörperforschung der Kernforschungsanlage Jülich
D 517 Jülich, Germany

ABSTRACT

By measuring the Huang scattering on Cu after low temperature electron irradiation and isochronal annealing defects ranging from single interstitials up to dislocation loops that were large enough to be observed in the electron microscope were investigated. The dose dependence of the structure of interstitial defects after low temperature e^--irradiation is discussed. A continuous transition between the single interstitials as observed by diffuse X-ray scattering after electron doses up to 10^{19} e^-/cm^2 and the interstitial clusters observed in the HVM (dose 10^{20} e^-/cm^2) was established. During thermal annealing the formation and stability of small interstitial clusters were investigated. In addition the size distribution of larger clusters is discussed.

INTRODUCTION

This work is a continuation of our earlier investigations of interstitials in Copper[1]. The defect concentration (or irradiation dose) was extended to higher as well as to lower values. At higher concentration there was the interesting question of the connection between our observation of single interstitials up to electron doses of 1×10^{19} e^-/cm^2 and the results of Urban and Jäger[2] who observed defect clusters after about 10^{20} e^-/cm^2 in the HVM. Although there are problems in the exact comparison of electron doses at different energies it was possible to observe the beginning of interstitial clustering after increasing the doses also in our experiments. In addition by studying the annealing of samples irradiated with different doses the condition for interstitial clustering during stage I should be investigated in more detail.

DEFECT STRUCTURES AFTER 5 K IRRADIATION

In the following the diffuse scattering intensity of five copper samples irradiated at 5 K to give electrical resistivity changes of 25, 72, 120, 185 and 220 nΩcm will be compared. The data for the 72 and 120 nΩcm samples were taken from ref. 1. The Huang scattering cross section S is given by[3]

$$S = c\, f^2 \left(\frac{h}{q}\right)^2 \frac{1}{\Omega^2} \left[j^{(1)}\pi^{(1)} + j^{(2)}\pi^{(2)} + j^{(3)}\pi^{(3)} \right] \qquad (1)$$

where $\underline{q} = \underline{k} - \underline{h}$ is the distance of the scattering vector $\underline{k}$ from the nearest reciprocal lattice vector $\underline{h}$, c = defect concentration, f = atomic scattering factor, Ω = atomic volume, $j^{(1)}$, $j^{(2)}$, $j^{(3)}$ are factors which depend on the elastic constants and the directions of $\underline{q}$ and $\underline{h}$. $\pi^{(1)}$, $\pi^{(2)}$, $\pi^{(3)}$ are quadratic expressions of the dipole force tensor P_{ij} of the defects

$$\pi^{(1)} = \frac{1}{3}(\mathrm{Tr}P)^2, \quad \pi^{(2)} = \frac{1}{6}\sum_{i>j}(P_{ii}-P_{jj})^2, \quad \pi^{(3)} = \frac{2}{3}\sum_{i>j}P_{ij}^2 \qquad (2)$$

By suitable choice of $\underline{q}$ and $\underline{h}$ one can determine the parameters $\pi^{(1)}$, $\pi^{(2)}$ and $\pi^{(3)}$ separately[1]. As $\pi^{(1)}$ is proportional to the square of the "strength", $\Delta V/\Omega$, of the defects the intensity is very sensitive to interstitial clustering. If interstitials of concentration c_i have condensed into c_i/n clusters each containing n interstitials the scattering cross section is enhanced (linear supperposition model):

$$S_{\mathrm{cluster}} = n\, S_{\mathrm{single\ int.}} \qquad (3)$$

From the measured scattering intensities the quantities $c\,\pi^{(1)}$ and $c\,\pi^{(3)}$ have been extracted. Fig. 1 shows their dependence on the initial defect density measured by the resistivity $\Delta\rho_o$ of a separate sample mounted directly beside the other sample during irradiation. Because there may arise errors (as indicated in fig. 1) the resistivity of the 185 nΩcm sample was measured directly at the single cry-

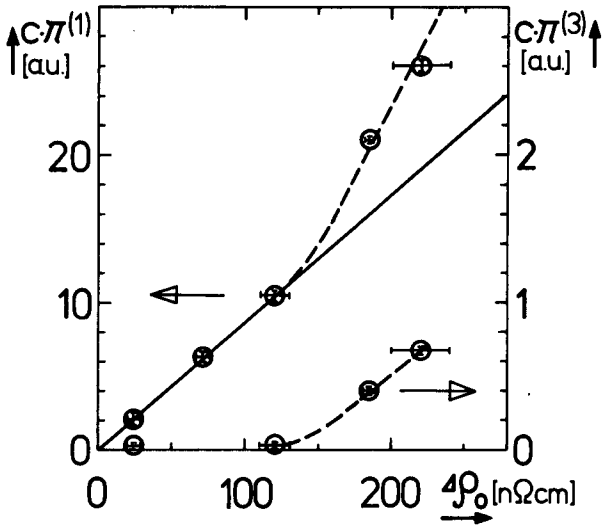


Fig. 1. Dependence of the defect strength parameter $c\,\pi^{(1)}$ and the symmetry parameter $c\,\pi^{(3)}$ on the defect density measured by $\Delta\rho_o$.

stal sample. In the range from 25 nΩcm to 120 nΩcm $c\,\pi^{(1)}$ increases proportional to $\Delta\rho_o$, indicating that the number n in formula (3) is constant over this range. Since at low doses primarily single interstitials (n = 1) are produced, we conclude that up to doses of $\sim 10^{19}$ e^-/cm^2 (corresponding to $\Delta\rho_o$ = 120 nΩcm) the damage pattern will consist still of single interstitials and clustering effects can be neglected. This conclusion is confirmed by the fact, that in the same range $c\,\pi^{(3)}$ is zero within the errors of the experiment. A vanishing $\pi^{(3)}$ is characteristic for single interstitials which have essentially tetragonal or cubic symmetry[1].

At high doses the deviations from linearity of $c\,\pi^{(1)}$ suggest the onset of interstitial clustering. A mean number of interstitials per cluster of $\bar{n} \simeq 1.4$ can be estimated according to formula (3) from the ratio of the observed intensity at $\Delta\rho_o$ = 220 nΩcm ($\phi t \simeq 2 \cdot 10^{19}$ e^-/cm^2) to the intensity extrapolated from low doses. The large increase of $\pi^{(3)}$ also indicates interstitial clustering at the indicated dose range. It shows that an essential fraction of the defects no longer have tetragonal or cubic symmetry. This observed beginning of interstitial clustering seems to be in good agreement with the observed larger clusters in the HVM at higher doses.

Irradiation induced interstitial clustering at high doses (the defect concentration being on the other hand considerably below the saturation

value corresponding to $\Delta\rho_o \simeq 760$ nΩcm[4]) may be explained by two mechanisms. First, the transfer of subthreshold energies from the irradiating electrons can induce jumps of the interstitials and thus force them to migrate during irradiation. Thus the migrating interstitials can come close enough to form more stable interstitial clusters. The rate at which di-interstitials are produced is essentially proportional to C_i^2. Alternatively interstitial clustering at higher doses may be viewed as a result of replacement collision chains which break off near interstitials leaving interstitial complexes. The number of such complexes will be strongly enhanced if at higher doses the mean distance between interstitials becomes smaller than the mean length over which collision chains can run. At the moment no decision can be made what would be the dominant process.

ANNEALING BEHAVIOUR OF COPPER

In Fig. 2 isochronal annealing curves are shown of the electric resistivity change and of the parameters $c\,\pi^{(1)}$ and $c\,\pi^{(3)}$ for the samples with 25, 120 and 185 nΩcm. The 120 nΩcm sample shows a small decrease of $c\,\pi^{(1)}$ at 28 K that can be understood by recombination of close Frenkel pairs and a very rapid increase at the end of stage I (40 K). This is due to the formation of interstitial clusters containing 5 - 10 interstitials (for details see ref. 1). Here only the most important differences to this behaviour which is observed at samples having different dose shall be discussed. For the 185 nΩcm sample the intensity at 28 K increases in both directions of q. This behaviour may be explained by the growth and rearrangement of clusters. After irradiation at high doses there exists a certain fraction of single interstitials which lie near other interstitials but which have not done the last few steps to clustering. At 28 K the thermal energy is sufficient for such interstitials to do these steps in the strong interaction fields of their neighbours thus building up additional and/or larger clusters. Towards the end of stage I the intensity is too high to

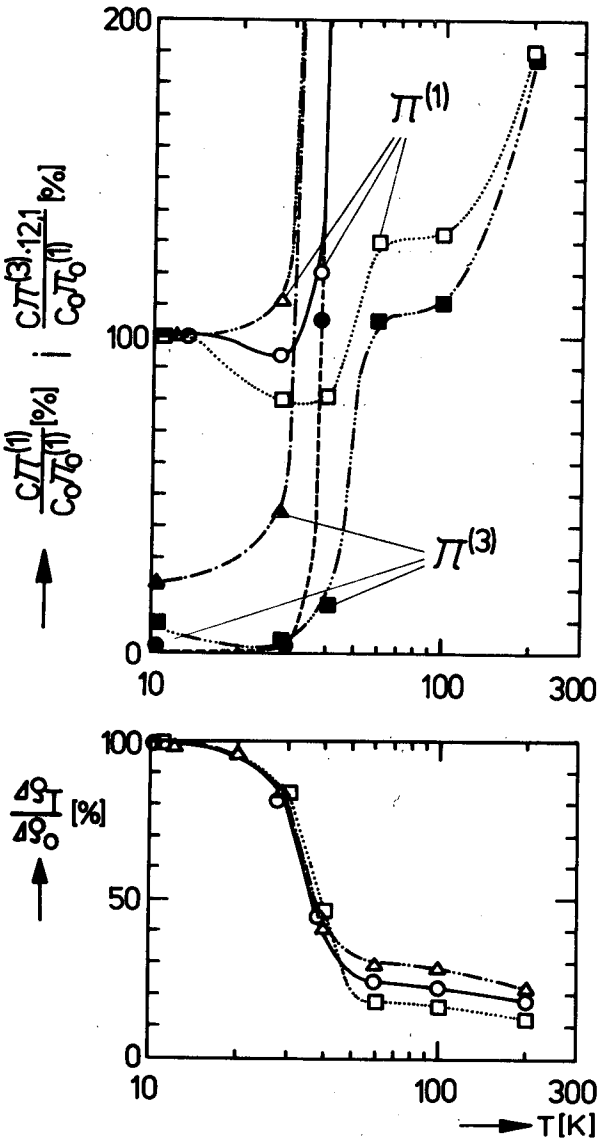


Fig. 2 Annealing behaviour of the parameters $c\,\pi^{(1)}$ (open symbols) and $c\,\pi^{(3)}$ (full symbols) and of the electrical resistivity (lower part)

□, ■ : $\Delta\rho_0$ = 25 nΩcm
○, ● : $\Delta\rho_0$ = 120 nΩcm
△, ▲ : $\Delta\rho_0$ = 185 nΩcm

be shown in fig. 2; it yields a cluster size of n ≈ 25 (at 40 K). For the 25 nΩcm sample we observe a larger fractional recovery at 28 K corresponding to the annihilation of a relatively larger number of close pairs. Between 28 and 40 K $c\,\pi^{(1)}$ does not change much, while the resistivity drops down to 50 %. This indicates again interstitial clustering. The mean number n of interstitials per cluster is n ∿ 1.6 at 40 K. The end of stage I is above 40 K for this lower defect density. At the next annealing step at 60 K we observe a mean number of n ≈ 7 interstitials per cluster. Between 60 and 100 K the cluster size remains almost constant. This is in contrast to the higher dose samples where large clusters grow in this temperature range. It could indicate, that at the large separation in which they are present in the low dose sample, clusters with n ≈ 7 interstitials are relatively stable. Above 100 K we observe, similar to the other samples, a further growth of the clusters. For a detailed discussion of the cluster nucleation and growth it should be noted that the cluster concentration after stage I (and at higher temperatures) is of the order of the impurity

concentration or below it for all samples.

After annealing the samples at temperatures of 200 and 300 K Huang scattering is restricted to such a small region near the Bragg peak that with our present instrumental resolution no detailed study is possible. At larger q-values the scattering can be measured and is described rather well by the Stokes-Wilson approximation that predicts a q^{-4} decrease in the intensity. For simple defect models (isotropic defect in isotropic matrix) Trinkaus[5] showed that in certain directions of q oscillations can be superimposed to the q^{-4}-intensity which yield further information upon clusters. This was established by model calculations for dislocation loops in Al by Larson[6]. The oscillatory structure is very prominent at the large angle side of (222)-reflections. Fig. 3 shows the intensities $I^+ \cdot q^4$ for positive and $I^- \cdot q^4$ for negative q-values at a (222)-reflection after 200 K annealing at the high dose samples.

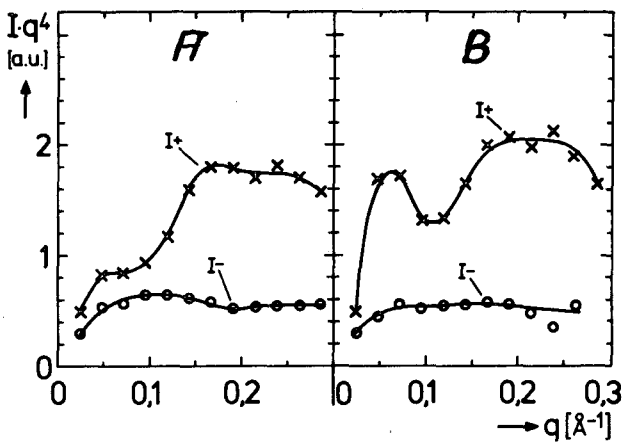


Fig. 3 Oscillations in the Stokes-Wilson scattering intensity after annealing at 200 K. I^+ at positive and I^- at negative values of q close to the (222) reflection.

A: $\Delta\rho_o$ = 185 nΩcm
B: $\Delta\rho_o$ = 220 nΩcm

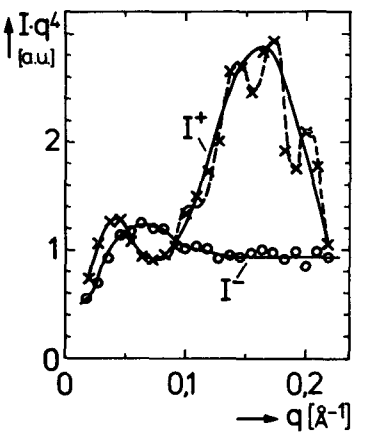


Fig. 4 Stokes-Wilson scattering after annealing at 600 K of a preirradiated sample; I^+ at positive and I^- at negative values of q close to a 400-reflection.

Although there may be a change of scale for Copper the curves $I^{(+)} \cdot q^4$ and $I^{(-)} \cdot q^4$ at 200 K agree in their general shape with the calculations by Larson for Aluminum. The theoretical $I^+ \cdot q^4$-curve has a sharp maximum at $q_{max} \sim 2.8/R$ (R = loop radius) which allows to estimate R from the experimental value of q_{max}. The broad maximum in the measured curve

suggests a distribution of loop radii. However taking $q_{max} \sim 0.2$ Å^{-1} one obtains a mean radius $\bar{R} \sim 14$ Å corresponding to a mean number $N \sim 100$ interstitials per loop. This value is in agreement with the estimated value from the absolute intensity.

The oscillatory structure may become more distinct for larger clusters and sharper size distributions. This is demonstrated in fig. 4 for a sample that contained trapping centers for the interstitials (introduced by a pre-irradiation with neutrons before the electron irradiation to $\Delta\rho$ = 220 nΩcm). Measurements were done after annealing at 600 K.

REFERENCES

1. P. Ehrhart and U. Schlagheck, J. Phys. F 4, 1575 and 1589 (1974)
2. W. Jäger and K. Urban, Proc. 4th Int. Conf. HVEM Toulouse 1975
3. P. H. Dederichs, J. Phys. F 3, 471 (1973)
4. G. Duesing, W. Sassin, W. Schilling and H. Hemmerich, Cryst. Lattice Def. 1, 55 (1969)
5. H. Trinkaus, Z. angew. Physik 31, 229 (1971)
6. B. Larson, this Conference

MEASUREMENTS OF CONDUCTION ELECTRON SCATTERING IN NEUTRON-IRRADIATED COPPER BY THE DE HAAS-VAN ALPHEN EFFECT*

Y. K. Chang, A. J. Arko, G. W. Crabtree, J. B. Ketterson
and L. R. Windmiller
Argonne National Laboratory, Argonne, Illinois 60439

R. J. Higgins
University of Oregon, Eugene, Oregon 97403

F. W. Young, Jr.
Oak Ridge National Laboratory, Oak Ridge, Tennessee 37830

ABSTRACT

The anisotropy of conduction electron scattering in copper single crystal due to dislocation loops produced by irradiation with a neutron dose of 10^{18} n/cm^2, has been studied by measuring the de Haas-van Alphen (dHvA) Dingle temperatures, X, for a number of orbits; these quantities measure the total scattering cross sections and are related to the electron relaxation times τ through $X = \hbar/2\pi k_B\tau$. Very large scattering anisotropy was found with the strongest scattering arising from the neck region. Results also showed that the dHvA (total) scattering rate due to dislocation loops is three orders of magnitude smaller than that due to edge dislocations, where the long-range (1/r) strain field dominates. This is consistent with the absence of a long-range strain field in the loop geometry. We have also found that the dHvA scattering rate due to dislocation loops is several times larger than the corresponding resistivity scattering rate.

INTRODUCTION

With the availability of accurate information on the Fermi surface (FS) of the noble metals, the study of the effect of various defect systems on the electronic transport properties becomes a fruitful area of research. A microscopic tool such as the de Haas-van Alphen (dHvA) effect

*Based on work performed under the auspices of the U. S. Energy Research and Development Administration and the National Science Foundation.

can be used to extract detailed information on conduction electron scattering from defects, which is averaged out in bulk transport measurements. The dHvA effect, which has been the most accurate tool for investigating the FS of metals, is capable of measuring the relaxation time τ_k over a restricted section of the FS, thus offering the possibility of comparing different regions of the FS which may have different relaxation times. The method was initially used to investigate the scattering mechanisms arising from (substitutional) impurities in the noble metals.[1] There it was found that the large-angle scattering from the localized impurity potential is largely responsible for the observed τ_k. The strain field associated with the impurity is relatively small and its contribution to τ_k may be ignored.[2]

Recently the dHvA effect has also been used to study the structural defects in the noble metals. So far only edge dislocations in copper[3-5] and vacancies in gold[6-7] have been reported. The results of the measurements on the edge dislocations indicate that the dHvA effect is very sensitive to small-angle scattering from the long-range strain field associated with the structural defect. The dHvA effect measures the <u>total</u> scattering cross section, in contrast to the resistivity, where scattering is weighted by the factor $(1-\cos\theta)$ which emphasizes large-angle scattering. In the case of edge dislocations, the long-range (1/r) strain field dominates the scattering with a negligible contribution arising from the core. However, in a loop geometry we expect the long-range strain field to cancel (for distances large compared with the loop radius). Preliminary measurements on a copper single crystal irradiated with a neutron dose of 10^{17} n/cm^2 supported this conclusion.[8] In that work a sample having a dislocation line density several hundred times higher than that used in the edge dislocation studies was used, yet the scattering rates were too small to be observable. No scattering anisotropy associated with loops was observed because the scattering rates were dominated by the impurity background in that sample. Thus measurement on samples having higher radiation doses as well as higher purity are required.

EXPERIMENTAL TECHNIQUE AND RESULTS

The copper single crystal used in this work was grown in a BN crucible using a modified Bridgmann method.[9] The as-grown crystal had a dislocation density of 3×10^4 cm^{-2} with a large region ($\sim$ 1 cm) being free of sub-boundaries. Its RRR was 15,000. Irradiation was done at Oak Ridge with a neutron dose of 10^{18} n/cm^2. The irradiated crystal had a RRR of 360, corresponding to a resistivity change, $\Delta\rho$, of 4.64×10^{-9} Ω-cm.

Precautions were taken while preparing the dHvA sample to avoid any possible strain damage to the sample. The field-modulation technique was used in the dHvA measurements. Dingle scattering temperatures, X, which are related to the electron relaxation time τ through the relation $X = \hbar/2\pi k_B\tau$, were measured and are shown in Fig. 1. The scattering rate is largest near the [111] neck region and smallest near the two belly regions. This is related to the fact that the neck region is on or near the Brillouin zone boundary and both the dog-bone and rosette are in partial contact with the zone boundary.

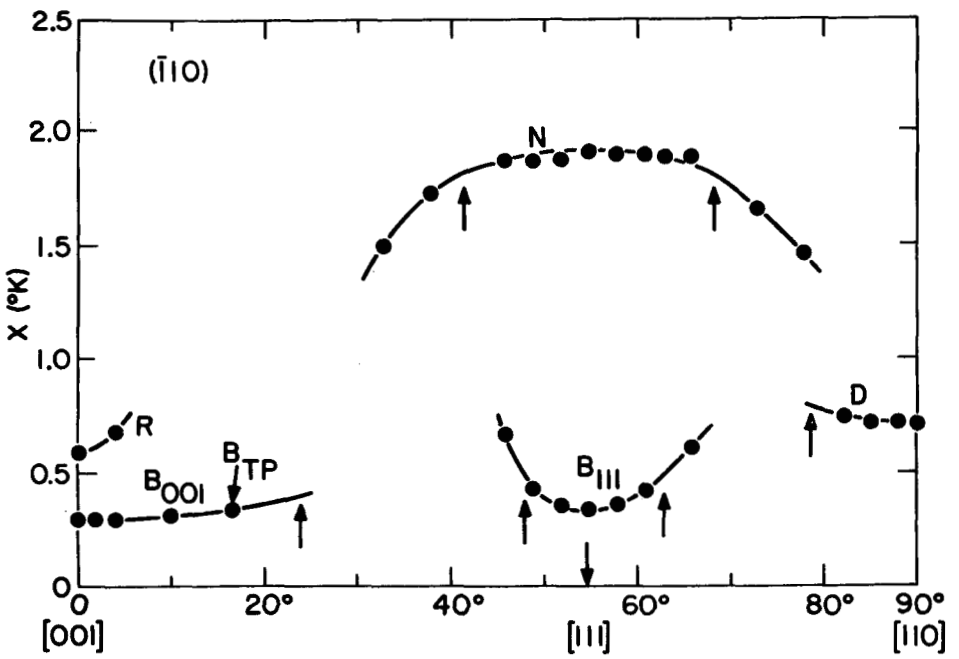


Figure 1. Experimental Dingle scattering temperatures. Arrows indicate the locations of spin-splitting zeros observed from rotation curves.

These orbits suffer larger fractional changes in the presence of a strain field.[5,10] The scattering rate of the neck orbit decreases as the magnetic field tilts away from the [111] direction. This is consistent with the fact that the scattering rate from other parts of the FS is weaker.

The scattering rate ratio of the neck to the belly (X_N/X_B) at [111] is about 5.5. Such a large ratio is comparable to that arising from edge dislocations.[3,5] The locations of spin-splitting zeros (arrows in Fig. 1) agree with those of Joseph et al.,[11] indicating no g factor changes. The rotation curves indicated no mosaic structure which can cause complications in the X measurements.[5,12]

DISCUSSION

The ratios of the scattering rates measured from the dHvA effect and the resistivity for several defect systems in copper (vacancy data were taken in gold) are listed in Table 1. These results are consistent with the strength and range of the strain field surrounding the defects. The long-range (1/r) strain field produced by the edge dislocation has a dominating effect on the scattering rate over that of the core.[5] The strain field surrounding a dislocation loop is mostly cancelled and has only a short-range ($1/r^2$) dependence. Results of vacancies in gold[6] indicated that an appreciable contribution comes from the vacancy strain field.

Table 1. Ratios of the dHvA scattering rate to the resistivity scattering rate of several defect systems in copper.

Defect System	$(\frac{1}{\tau})_{dHvA}/(\frac{1}{\tau})_{\rho}$
impurity	~ 1
vacancy (in Au)*	1 - 2
dislocation loop	3 - 7
edge dislocation	10^3 - 10^4

*Discrepancies are found between Refs. 6 and 7.

The scattering rate ratios of the neck to the belly at [111] for several defect systems are summaried in Table 2. This ratio has generally been known to be affected by the wavefunction character of the conduction electrons at the neck and the belly; a larger scattering rate results if the scatterer has similar wavefunction character as the scattering electrons.[13] For point defects the potential scattering is most important and this ratio is generally near or less than 1. However, for defect clusters, like dislocation loops and edge dislocations, the strain field

surrounding the cluster is large and this ratio increases to about 5.

Table 2. Scattering ratios of the [111] neck to the [111] belly of several defect systems in copper.

Defect System	X_N/X_B
magnetic impurity	$\sim 1/3$
nonmagnetic impurity	~ 1
vacancy (in Au)	~ 1
dislocation loop	5 - 6
edge dislocation	4 - 5

Our results indicate that the dHvA effect may become a useful and independent tool for investigating defect problems. Further understanding concerning the capability of the dHvA effect to tackle defect problems is necessary. Calculations based on the phase smearing approach[5,14] including the size distribution and displacement field together with measurements to determine the sign of the strain field surrounding the defects or defect clusters are being considered.

REFERENCES

1. M. Springford, Adv. Phys. 20, 493 (1971).
2. P. T. Coleridge, Phil. Mag. 26, 573 (1972); Phil. Mag. 27, 1495 (1973).
3. D. W. Terwilliger and R. J. Higgins, Phys. Letters A31, 316 (1970); Phys. Rev. B7, 667 (1973).
4. P. T. Coleridge and B. R. Watts, Phil. Mag. 24, 1163 (1971).
5. Y. K. Chang and R. J. Higgins, Phys. Rev. (in press).
6. Y. K. Chang, G. W. Crabtree, J. B. Ketterson and L. R. Windmiller, Bull. Amer. Phys. Soc. 20, 353 (1975).
7. B. Lengeler and W. Uelhoff, Phys. Letters A53, 139 (1975).
8. Y. K. Chang and R. J. Higgins, Phys. Cond. Matter (in press).
9. Y. K. Chang, Ph.D. Thesis (University of Oregon, 1974) (unpublished).
10. D. Shoenberg and B. R. Watts, Phil. Mag. 15, 1275 (1967).
11. A. S. Joseph, A. C. Thorsen, E. Gertner, and L. E. Valby, Phys. Rev. 148, 569 (1966).

12. S. Hornfeldt, J. B. Ketterson and L. R. Windmiller, J. Phys. E. 6, 265 (1973).

13. J. M. Ziman, Phys. Rev. 121, 1320 (1961).

14. B. R. Watts, J. Phys. F 4, 1371 (1974).

VOIDS, DISLOCATION LOOPS AND GRAIN BOUNDARIES AS SINKS FOR POINT DEFECTS

R. W. Balluffi
Department of Materials Science and Engineering
Cornell University, Ithaca, New York 14853

ABSTRACT

A review is given of our present knowledge of the manner in which voids, dislocation loops and grain boundaries act as sinks for point defects. A discussion is first given of idealized atomistic models for the sink action. The overall problem of the kinetics of defect annealing to sinks is then considered. Next, a discussion is given of additional complications which include the effects of sink stresses on the defect diffusion to sinks and the enrichment, or depletion, of solute atoms at sinks by the defect currents. Lastly, an abbreviated review is given of experimental observations, and an attempt is made to summarize briefly the state of the field.

INTRODUCTION

In the present paper we consider the manner with which already existing voids, dislocation loops and grain boundaries act as sinks for point defects. These sinks are often important sites for the destruction of the point defects produced by quenching or irradiation, and the effectiveness with which they operate is therefore of interest.

The destruction of defects at sinks is inherently complex since it involves the diffusion of the defects to the sinks and their ultimate destruction at the sinks which, in turn, may involve a sequence of mechanisms. Many aspects of the process are therefore presently obscure or unknown. We attempt to make the best of this situation by describing critically the current state of the field and emphasizing areas where our knowledge is inadequate. Earlier discussions by the writer of voids[1], loops[2,3] and grain boundaries[4] as sinks may be found elsewhere.

Two limiting types of sink action may be identified despite the complexity of the process. Under certain conditions the sink may destroy defects rapidly enough to maintain the excess concentration in the vicinity of the "surface" of the sink essentially at zero. In such cases the defects are destroyed at the maximum possible rate corresponding to the rate at which they are able to diffuse to the sinks; i.e., the rate is diffusion-limited. Under other conditions the destruction process may be sufficiently slow so that the defect concentration remains uniform everywhere, and the rate becomes limited by the rate of destruction at the sink; i.e., it becomes sink reaction-limited.

As a simple example, consider the annealing of an initially uniform distribution of vacancies (v's) to a distribution of well spaced voids. Each void will tend to set up a spherical diffusion field around itself, and the quasi-steady state current into each void is then[5]

$$\phi = 4\pi D r_o(\bar{c}-c_s), \tag{1}$$

where D = diffusivity, r_o = "effective radius" of sink (void radius), $\bar{c}$ = v concentration midway between adjacent voids and c_s = concentration maintained at void surface. Assuming that the rate of destruction on the surface is proportional to the impingment rate of v's, i.e., proportional to c_s, and that the rate of creation is equal to the rate which would exist at equilibrium, the net rate of destruction is $\kappa \cdot 4\pi r_o^2(c_s-c^o)$, where κ = rate constant, and c^o = equilibrium v concentration. Setting this rate equal to ϕ and solving for c_s, we obtain

$$\phi = 4\pi D r_o(\bar{c}-c^o)\eta; \qquad \eta = \frac{1}{1+D/r_o\kappa}. \tag{2a,b}$$

When $r_o\kappa \gg D$, $\eta = 1$, $\phi = 4\pi D r_o(\bar{c}-c^o)$, and the rate is diffusion-limited. On the other hand, when $r_o\kappa \ll D$, $\eta = r_o\kappa/D$, $\phi = \kappa \cdot 4\pi r_o^2(\bar{c}-c^o)$, and the rate is sink reaction-limited. This simple example suggests the use of η as a "sink efficiency" defined as

$$\eta \equiv \frac{\text{actual rate of destruction}}{\text{hypothetical rate of destruction if diffusion-limited}}. \tag{3}$$

A "perfect sink" therefore operates with an efficiency of unity. In much of our discussion we shall be concerned with the factors which determine η.

In the following we first review simple idealized models for the atomistic processes which are probably involved at the sinks. We then go on to discuss the overall problem of the kinetics of defect annealing to sinks. Next, a discussion is given of additional complications due to factors not considered in the simple models. These include the effects of sink stresses on the diffusion of the defects to the sinks, and the enrichment or depletion of solute atoms (impurities) at the sinks by the defect currents. Finally, an abbreviated review is given of experimental observations, and an attempt is made to summarize briefly the state of the field.

SIMPLE IDEALIZED MODELS FOR DEFECT DESTRUCTION AT SINKS

Voids

The destruction of point defects at a void surface should be similar in many respects to the corresponding process at a free surface. Void sinks are generally polyhedral[1], and the facets should therefore consist of singular or vicinal surfaces (Fig. 1a). By analogy with the kinetics

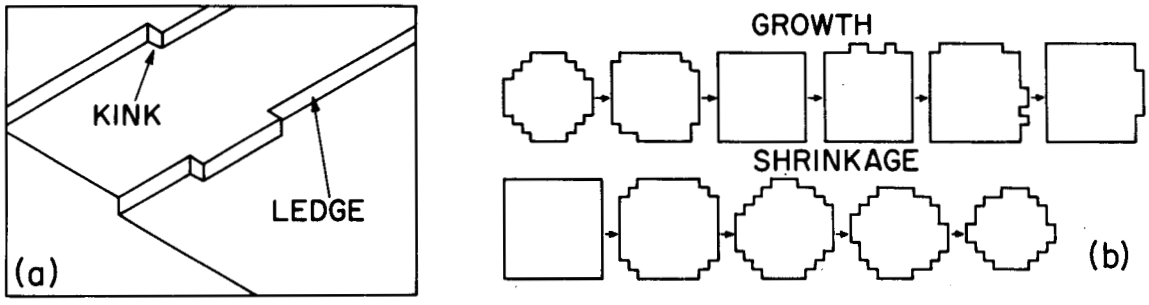


Fig. 1. (a) Local void surface structure: (b) Progressive sequences of ledge configurations on void surface during growth or shrinkage or, alternatively, jog configurations on dislocation loop.

of crystal growth[6] we would then expect the following steps to be involved in the destruction of a typical v or interstitial (i): (a) lattice diffusion to void; (b) adsorption on surface facet; (c) rapid surface diffusion to ledge; and (d) final destruction at kink in ledge. In this process the

relatively rapid surface diffusion tends to cause the surface to act as a "short circuit". The continued destruction of v's at a void, causing void growth, requires the continuous formation of kinks and ledges, since they tend to be eliminated during growth (e.g., Fig. 1b, above). New ledges must then be nucleated in the form of platelets of adsorbed v's on the facets (Fig. 1b, above), and new kink pairs must be nucleated by v condensation along the ledges (platelet edges), since corners and edges are not preferred sites for nucleation. On the other hand, if the void acts as a sink for i's (or source for v's) the corners and edges should act as preferential nucleation sites (e.g., Fig. 1b, below). The actual void shape maintained during growth or shrinkage therefore depends upon the relative rates of ledge formation and migration. If the migration rate is rapid, and the formation rate is slow, the ledge concentration will be small, and the void will remain polyhedral. This condition seems particularly possible during growth by v destruction (Fig. 1b, above), since the rate of nucleation of ledges may then be relatively slow. On the other hand, if the rate of ledge formation is particularly rapid at the corners (edges) the void may tend to be spherical as it shrinks by either i destruction or v creation (Fig. 1b, below).

In general, we expect the ledge and kink concentrations (and sink efficiency) to increase as the defect chemical potential, μ, increases. In the case of v destruction (Fig. 1b, above) the free energy of formation of a ledge nucleus (square platelet of v's of edge-length L and height h) is $\Delta G = 4LE - L^2h\mu_v/\Omega$ where E = ledge energy per unit length and Ω = atomic volume. The rate of nucleation is then proportional to $\exp [-\Delta G^*/kT] = \exp [-4E^2\Omega/kTh\mu_v]$, where ΔG^* = free energy of formation of a critical nucleus. A very rapid increase of the nucleation rate with μ_v is therefore predicted.

The overall sink efficiency is determined by the probability that an excess defect impinging on the void surface from the lattice reaches a kink and is destroyed there before it jumps back into the lattice. The kinetics of this problem are discussed below.

Dislocation Loops

The sink model for a simple loop is conceptually similar to that of the void. When the defects diffuse relatively rapidly in the dislocation the steps involved in point defect destruction are: (a) adsorption on dislocation; (b) rapid "pipe diffusion" to jog; and (c) final destruction at jog. If the defects diffuse relatively slowly in the dislocation the short-circuiting feature is, of course, absent. It appears[7] that v's diffuse relatively rapidly in dislocations, whereas there is some reason to believe[7] that i's may diffuse relatively slowly.

The continued destruction of defects at a loop requires the continued formation of jogs. For example, the destruction of v's at a v loop tends to grow off existing jogs, and the loop will therefore tend to become polygonal. New jog pairs must then be nucleated by v aggregation along the line (Fig. 1b, above), since the corners are not preferential nucleation sites. Conversely, during shrinkage the corners should act as preferential sources for jogs (Fig. 1b, below). The actual loop shape maintained during growth, or shrinkage, then depends upon the relative rates of jog formation and jog migration.

As in the case of ledges on surfaces, the concentration of jogs should increase with the point defect chemical potential. Application[3] of simple nucleation theory to jog nucleation by v aggregation on straight sections such as on the upper right of Fig. 1b shows that the loop should become increasingly "joggy" as μ_v increases.

The situation becomes more complicated in low stacking fault energy metals where the loops tend to dissociate. In FCC metals, for example, the loops tend to dissociate on {111} planes into patches of stacking fault bounded by partial dislocations (Fig. 2)[8,9,10]. When Frank loops become sufficiently large they often convert to prismatic loops. These dissociations tend to reduce the sink efficiency, since the jogs are then more complex, possess higher energies, and are more difficult to nucleate[3,11]. Balluffi[3] has discussed a number of aspects of the nucleation of such jogs and their ability to destroy further point defects.

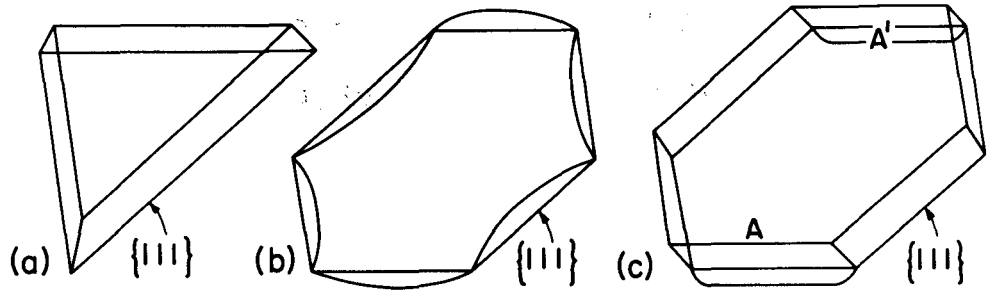


Fig. 2. Dissociated dislocation loops in FCC structure: (a) triangular Frank loop[8]; (b) hexagonal Frank loop[9]; (c) prismatic ½<110> loop[10].

In a manner analogous to the void sink, the efficiency of the loop sink is determined by the probability that an excess defect which diffuses to the loop reaches a jog and is destroyed there before it leaves the loop (see discussion of kinetics below).

Grain Boundaries

Low angle boundaries consist of planar networks of discrete lattice dislocations[12] and therefore act as sinks by means of the climb of the individual dislocations. The climb should occur by the usual jog migration mechanism as described above for the case of loops and elsewhere[3] for straight dislocations.

High angle boundaries consist of continuous slab-like regions of atomic disorder which vary considerably in structure depending upon the boundary type[13]. Because of this variation in structure, the detailed manner in which all high angle boundaries act as sinks is not entirely clear. It is quite certain, however, that many boundaries are capable of possessing well-defined grain boundary dislocations (GBD's) which can absorb point defects by climbing in the boundary and cause it to be an effective sink (Fig. 3a). A "well-defined" GBD is taken to be a discrete GBD

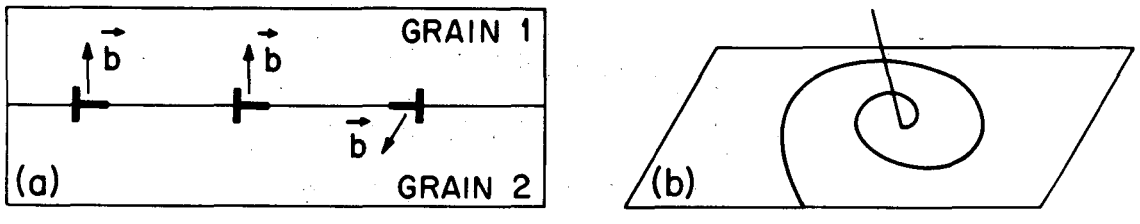


Fig. 3. (a) Climb GBD's in grain boundary sink; (b) GBD climb spiral in boundary due to impinging lattice dislocation.

which possesses a Burgers vector, $\vec{b}$, which is large enough to be "physically significant" (see below). The destruction of defects undoubtedly occurs at jogs in the same manner as at climbing lattice dislocations. The jog is therefore again a localized site where defects are permanently destroyed. This process is actually a form of internal crystal growth (dissolution) in which atoms are added to (subtracted from) either grain (Fig. 3a) at the boundary as the GBD's climb and is therefore analogous to crystal growth (evaporation) at a surface by ledge migration.

Apparently, well-defined GBD's exist only in boundaries for which at least one base vector of Bollmann's[14] DSC-Lattice is of appreciable magnitude. This condition is satisfied if at least one base vector of the Coincidence Lattice[14] is relatively small*. Such boundaries include so-called "plane-matching" boundaries[12]**. Suitable GBD's should usually be present as a result of the impingment of lattice dislocations (Fig. 3b). The GBD's will generally branch out at the point of impingment, and the sum of their Burgers vectors will equal the Burgers vector of the lattice dislocation. The GBD can then climb into a spiral of unlimited length (Fig. 3b). Such spirals are analogous to the ledge spirals which develop on crystal surfaces intersected by lattice dislocations during growth. It is also possible, of course, that GBD loops could be produced by the nucleation and subsequent collapse of point defect aggregates.

For these boundaries the steps involved in the destruction of a defect which diffuses rapidly in the boundary are: (a) adsorption on boundary, (b) rapid boundary diffusion to GBD, and (c) final destruction at jog on the GBD. The boundary diffusion step will, of course, be absent for a defect which diffuses relatively slowly in the boundary. By analogy with dislocation cores it is likely[7] that v's diffuse rapidly in boundaries. Also, there is some reason to believe[7] that i's may diffuse relatively slowly.

---

* The Coincidence Lattice is a convenient means of describing the degree of coincidence between the two lattices adjoining the boundary. As the degree of coincidence decreases, the Coincidence Lattice expands, and the DSC-Lattice generally shrinks.

** So-called "near-coincidence" boundaries may conceivably be an additional class of boundaries capable of supporting well-defined GBD's. However, no line structure has yet been detected in such boundaries[15].

The sink efficiency then depends on the probability that an excess defect which reaches the boundary by diffusion is destroyed at a jog before leaving the boundary (see discussion of kinetics below).

The situation is expected to be rather different when none of the primitive DSC-Lattice vectors have appreciable magnitudes normal to the boundary. This might occur if: (1) the Coincidence Lattice cell is large in all dimensions or (2) the boundary plane possesses a special orientation in the DSC-Lattice. The Burgers vector of any potential climbing GBD is then small, i.e., only a small fraction of a lattice Burgers vector*, and it is also possible that the core may be very relaxed[16]. The absorption of a point defect would then have to occur over a relatively large region and would be highly delocalized. Under such conditions the GBD would tend to lose its effectiveness as an easy site for the destruction of excess defects and therefore its physical significance as a sink. The mechanism of point defect destruction in such boundaries is not clear at present. It seems conceivable that defects might be destroyed by cooperative collapse processes in the boundary under more homogeneous conditions. Unfortunately, relatively little is known about such processes.

It is difficult to estimate the fraction of boundaries in a given situation which should be able to form suitable GBD's. Warrington and Boon[12] have recently attempted to estimate the fraction of random boundaries having sufficient coincidence to possess GBD's with at least one Burgers vector of significant magnitude. They concluded that a majority of boundaries could well be of this type. Ralph and co-workers[17] observed boundaries in a commercial steel and found that a majority showed line structure (i.e., GBD's with appreciable Burgers vectors). Essentially all polycrystals possess some texture, and it is therefore impossible to draw general conclusions about the climb GBD's which might form. However, it seems likely that under many conditions a large fraction of boundaries should be able to form suitable GBD's.

---

* Large Burgers vectors are always conceivable since any vector of the DSC-Lattice, which contains an infinite number of vectors which increase in magnitude without limit, is geometrically possible. However, we would expect GBD's with relatively large vectors to decompose into GBD's with smaller vectors in order to decrease their energy.

ON THE KINETICS OF DEFECT ANNEALING TO SINKS

The kinetics of defect annealing to existing sinks has been treated extensively in the literature with widely varying rigor. We confine our attention below to a few points of major present interest.

Annealing of Single Defect Type

Presumably, the annealing of a single defect type to a sink could be calculated by solving the appropriate diffusion equation in the lattice subject to realistic boundary conditions at the sink "surface"[5]. However, difficulties arise immediately because of the complications at the sinks which have been described above. The general solution at a void would involve the difficult determination of the ledge and kink configurations and the diffusion fluxes of defects in the surface region. These problems are obviously coupled. A qualitative description of the surface configuration problem has been given above. The diffusion problem may be simplified by employing the usual approximation of replacing the surface with a homogeneous slab of effective thickness $2w_s$ and a diffusivity D_s and the ledge with a homogeneous cylinder of effective diameter $2r_\ell$ and diffusivity D_ℓ. Both w_s and r_ℓ can be taken to be of the order of an interatomic distance. The traffic flow pattern of incoming defects which diffuse rapidly in the surface (boundary) would then be as illustrated by the arrows in Fig. 4a.

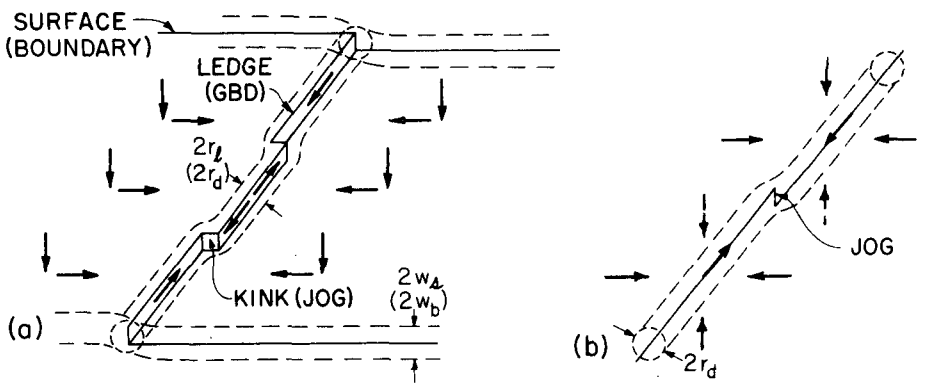


Fig. 4. Model for diffusion: (a) at void surface, or, alternatively, at grain boundary (parentheses); (b) at dislocation loop segment.

The general solution of this problem would involve determining the fluxes in the lattice, surface and ledge from solutions of the coupled diffusion equations in each region and finally obtaining the total current entering

the kinks. The efficiency would therefore depend upon at least the following: (1) binding energy of point defect to void surface, (2) diffusivity of point defect along void surface, (3) concentrations of ledges and kinks, (4) binding energy of point defect to ledge, (5) diffusivity of point defect along ledge, and (6) defect capture probability at kink. No general solutions have been reported for this formidable kinetic problem even with the simplifications introduced above.

The sink efficiency can vary considerably depending upon the relative magnitudes of the above parameters. For example, if the defects are destroyed readily along ledges and they act as efficient line sinks and if there is a large number of ledges present, a high efficiency is obtained. Alternatively, a high efficiency is obtained with a smaller number of ledges if defects adsorbed on the void surface are able to diffuse over possibly long distances to a ledge before jumping back into the lattice. A generally low efficiency is obtained when ledge nucleation is very slow and the average ledge concentration correspondingly small.

In the case of evaporation/condensation it is believed[6] that local defect equilibrium is maintained along each ledge*. With this simplification the present diffusion problem is reduced to finding the diffusion currents into the ledges. Again, no solutions of this simpler, but still formidable, problem have appeared. Finally, a major simplification occurs when the ledges are capable of maintaining defect equilibrium over the entire void surface so that the problem becomes "diffusion-limited". The solution for the lattice diffusion under this simple boundary condition, when any stress due to the void is ignored, is relatively straightforward. For example, a series solution[5] shows that an initially uniform distribution of defects anneals to well separated voids in a quasi-steady state mode which is well represented by the lowest order term given by Eq. (1) with $c_s = c^o$.

---

* The basic steps in crystal growth involve: (a) adsorption of atoms on surface, (b) diffusion of atoms on surface to ledges, and (c) incorporation of atoms at kinks on ledges. Detailed solutions for these kinetics are described in ref. 6.

The general solution for a dislocation loop presents similar difficulties, since it involves the determination of the jog configuration and the diffusion fluxes in the vicinity of the dislocation core. Again, these problems are coupled. The jog configuration has been discussed qualitatively above. The diffusion problem may be simplified as shown in Fig. 4b where the core has been replaced with a homogeneous cylinder of effective diameter $2r_d$ and diffusivity D_d. For a dislocation the magnitude of r_d is uncertain, and only reasonable guesses have been made. The anticipated traffic flow for defects which diffuse rapidly in the core is again indicated. In this case the efficiency would be determined by at least the following: (1) binding energy of point defect to dislocation, (2) diffusivity of point defect along dislocation, (3) concentration of jogs, and (4) defect capture probability at jog. Approximate solutions for the quasi-steady state diffusion of defects to a long straight edge dislocation using a similar model under the assumption that the jogs maintain local equilibrium have been obtained[3]. Wide variations in the efficiency are predicted, as expected, depending upon the probability of a defect in the core reaching a jog before jumping back into the lattice. So far, no such detailed calculations have been made for a loop although it is anticipated that the results would be generally similar.

Again, a major simplification occurs when the jogs maintain defect equilibrium everywhere along the core, and the kinetics become diffusion-limited. The solution for the diffusion to the sink under this boundary condition is again relatively straightforward when stress effects are neglected. For example, for an initially uniform distribution of defects diffusing to well spaced loops a series solution[5,18] again yields a current given by Eq. (1) with $c_s = c^o$. In this case, however, r_o is equal to the electrostatic capacitance of a conductor having the same geometry as the loop which is closely represented by a torus of major radius R_ℓ and minor radius r_d. Under many conditions $r_o \simeq R_\ell$[18].

The defect traffic problem at a grain boundary containing climbing GBD's is almost exactly analogous to the problem on a void surface when the defects diffuse rapidly in the boundary. (See Fig. 4a where the entities of interest are now enclosed in parentheses.) The discussion of the efficiency then follows along the same lines.

Annealing of Interacting Defects

When more than one type of point defect is present, and when interactions between the point defects occur, the diffusion problem becomes even more difficult both in the lattice and at the sink.

The so-called "chemical reaction" scheme[19] has been most widely used as an approximation to cope with such a situation in the lattice. In this method the rates of creation and destruction of the different defects in the lattice are approximated by simple terms which involve products of the defect concentrations (and their powers) and rate constants much as in the classical theory of chemical reaction rates. This approach is often incapable of taking into account the presence of concentration gradients in the material and the fact that the interacting defects in the lattice are not randomly distributed but are actually spatially correlated. A more general treatment is then required and work along these lines has appeared in a number of places[20].

No efforts have been made to analyze the complicated diffusion and destruction processes at the sinks in the presence of more than one type of defect. However, we remark on one effect which is easily recognized in the important case where mobile v's and i's are present together during irradiation at elevated temperatures and therefore engage in mutual annihilation. Under these conditions $D_i c_i \simeq D_v c_v$, and the lattice impingment rates of i's and v's are almost the same. As we have seen, continuous sink operation requires the continuous nucleation of defect aggregates, i.e., ledge platelets, kink pairs, jog pairs, etc. Mutual annihilation causes the buildup of critical nuclei of one defect type to be more difficult than would ordinarily be the case and therefore the sink efficiency would be reduced in this special situation. Analyses[21] of nucleation rates in the presence of mutual annihilation support this conclusion.

FURTHER COMPLICATING FACTORS

Effects of Stresses due to the Sinks

So far, the effects of stress fields due to the sinks have not been taken into account. In general, each sink produces a stress field which

falls off with distance from the sink, and a complete analysis of the defect diffusion must take this into account. Voids and small dislocation loops produce stress fields which can be derived approximately from the stress fields of spherical inclusions[22] whereas the stresses around a grain boundary are mainly due to the GBD's.

The magnitude of the effect is dependent upon the distance that the average defect reaching the sink migrates. Since the stress field is most intense near the sinks, the effects are largest when the defects migrate only short distances. Under many conditions the defects migrate over relatively long distances from locations well beyond the region of high stress. The so-called "biasing" effect of the stress on the quasi-steady state current to the sink is then relatively small, i.e., of the order of $\sim$10%, or less. In many situations the effect can therefore be neglected. Recently, however, there has been strong interest in the details of the effect of stress on the diffusion of v's and i's to voids and dislocations, since it is believed that relatively minor differential biasing may be responsible for void growth during reactor irradiation[1]. We therefore restrict ourselves to a few brief remarks about the status of this currently important problem.

The effect of stress on diffusion enters in two ways[23]. Firstly, the interaction between the stress and the defect in its lattice position produces a "drift force" on the defect. Secondly, the interaction between the stress and the defect in its saddle point for migration influences the jump frequency, i.e., diffusivity. Most recent work[22,24] has been concerned with solving one form or the other of the following diffusion equation subject to various boundary conditions:

$$\frac{\partial c}{\partial t} = \nabla\cdot(D\nabla c + \frac{Dc}{kT}\nabla U_f) + \dot{\theta} \quad . \tag{4}$$

Here, U_f is the interaction energy between the defect in its lattice position and the stress field, $D = D(0)\exp(-U_m/kT)$, where $D(0)$ = diffusivity in absence of stress, U_m = interaction energy between the defect in its saddle point and the stress field, and $\dot{\theta}$ = net rate of defect gain in lattice due to irradiation, recombination, etc. The above equation is based on a number of approximations. Firstly, it is assumed that D is

isotropic even though all defects, including those with the same symmetry as the unstressed lattice, will diffuse anisotropically in the presence of the non-hydrostatic stress produced by the sinks[25]. Secondly, no account is taken of the fact that the migrating defects may have a lower symmetry than the lattice[26] (e.g., [001] i's in a FCC lattice). Thirdly, Eq. (4) is a linearized relationship which breaks down when $|(a_o/\sqrt{2})\nabla U_f| > kT$[23,24] ($a_o$ = lattice constant). The energies U_f and U_m are difficult to determine and have usually been crudely estimated on the basis of the first order size interaction and the second order inhomogeneity interaction. A measure of the interaction strength has been L which is the distance from the sink at which the interaction energy becomes equal to kT. It then follows that the condition $|(a_o/\sqrt{2})\nabla U_f| < kT$ is satisfied only at distances $\gtrsim [L_f(a_o/\sqrt{2})]^{\frac{1}{2}}$. Estimates of L_f[24] for i's near dislocations range between 0.05 and 77Å. Therefore, in certain cases Eq. (4) may not be valid at distances as far out from the core as ~15Å.

Additional difficulties arise in choosing appropriate boundary conditions. The usual procedure for dislocations has been to assign a cutoff radius to the core where it is assumed that the defects are maintained at either equilibrium or at zero concentration[24]. The choice of the cutoff radius is rather arbitrary, and in many calculations the radius may have been outside the region of applicability of Eq. (4). Also, as emphasized above, there is no guarantee that equilibrium (or zero) boundary conditions apply near the core.

Solutions of Eq. (4) have been obtained[22,24] under different conditions including one, or more, of the following: (1) $U_m = 0$, $\dot{\theta} = 0$, neglect of angular dependence of U_f for edge dislocations, etc. Lack of space precludes a detailed description of this work. We conclude by noting that it is difficult to estimate the errors which may have accumulated due to the various approximations. Clearly, the present treatments are relatively crude, and they can only serve as general indicators of the magnitude of the effects which may exist. This is particularly true, in attempts to treat the relatively delicate problem of the relative bias factors for v's and i's in the void growth problem[1]. More reliable estimates of the interactions between the defects and the stress fields must be developed, and a

more general diffusion formalism should be employed. It would also be an improvement to use a discrete lattice calculation near the core.

Enrichment or Depletion of Solute Atoms (Impurities) at Sinks by Defect Currents

It is now well established that defect currents entering sinks can either enrich or deplete solute atom concentrations at the sinks depending upon the detailed nature of the interactions between the incoming defect "wind" and the solute atoms. Increases or decreases in the concentrations of solute atoms at the sinks can undoubtedly influence the sink action, and this phenomenon must therefore be considered.

Anthony[27] has described the enrichment or depletion at sinks due to vacancy currents and has also discussed models for the effect. Okamoto and Wiedersich[28] have investigated the effect of a combined current of v's and i's during high temperature irradiation. Large defect fluxes were obtained, and major solute atom effects at sinks such as voids were observed which included misfit coherency strains and the formation of new non-equilibrium phases on the void surface. These authors have also described simple models for the observed effects which are based on differing interactions of the migrating v's and i's with the solute atoms.

A number of sink properties may be affected by these phenomena. Firstly, the coherency stresses may produce diffusional biasing in the lattice and thereby influence defect diffusion to voids[29] or dislocations[30]. Secondly, if the solute atoms remain in solution a number of phenomena may occur directly at the sinks which could influence the kinetics. There is evidence[31] that solute atoms can cause the reconstruction of free surfaces and produce large changes in the surface diffusivity. Such phenomena might therefore influence the sink efficiency of voids. Similar effects presumably could occur in dislocation cores and grain boundaries. There is also evidence[32] that impurities segregate to kinks and ledges on surfaces during crystal growth causing blockage of their migration. These effects could therefore influence void sink action. Similar segregation effects might affect the migration rate of dislocation jogs. Also, the segregation of impurities to the embryos involved in ledge or kink nucleation[32] on voids or jog nucleation on dislocation loops

or GBD's would alter the energy of the critical nucleus and hence the rate of nucleation. Finally, if new phases form at the sinks, entirely new situations arise which could obviously have major effects on the sink action.

REVIEW OF EXPERIMENTAL OBSERVATIONS

We now briefly review available experimental observations with emphasis on the question of the sink efficiency, η, and the magnitude of the defect chemical potential, μ, driving the sink action.

Voids

Voids generally grow as polyhedra under quenching or irradiation conditions and shrink in more spherical form during annealing in accordance with Fig. 1b[1].

No relatively direct and satisfactory measurements of η for void growth have been made to the writer's[1] knowledge. However, in a number of annealing experiments[1] voids shrink with $\eta \simeq 1$.

There is evidence[33] that the conservative migration of an isolated void (bubble), which occurs by localized source and sink action at its surface, is sink reaction-limited rather than diffusion-limited when the driving force is sufficiently low.

Voids are observed to grow on grain boundaries subjected to normal stresses, σ, by receiving stress induced diffusion fluxes of v's from the boundaries. Calculated kinetics and experimental observations[34] are consistent with a relatively high η when $\mu_v \simeq \sigma\Omega \simeq 1.5\text{x}10^{-3}$ eV. The available results do not allow a more quantitative determination of η.

The growth of larger voids at the expense of smaller voids by vacancy diffusion (Ostwald ripening) appears[35] to occur with a relatively high η when $\mu_v = 2\gamma\Omega/R$ is in the range $\sim 5\text{x}10^{-5}$ to $3\text{x}10^{-2}$ eV (γ = surface energy, R = void radius). However, the data are insufficient to yield reliable η's.

Voids grow in Kirkendall diffusion zones at vacancy supersaturations of the order of a few percent, or less[36]; i.e., $\mu_v = kT\ell n\, c_v/c_v^o \lesssim 3\text{x}10^{-3}$ eV. In many cases a substantial fraction of the excess v's are destroyed at voids indicating a relatively high η.

Voids are observed to grow during high temperature irradiation by destroying a slightly larger number of mobile v's than i's[1]. Complicated models for void growth based on assumed diffusion-limited[37] and sink reaction-limited growth[38] have been developed. However, they do not allow a clear-cut conclusion regarding the magnitude of η. Norris[39] and Mansur, et al.[38] have measured the growth rate of individual voids under such conditions and find some support for the growth law $R \alpha t$ which suggests sink reaction-limited kinetics[1]. However, widely varying results are obtained for different voids in the same specimen, and the results depend upon the positions of the voids relative to other v and i sinks. Therefore, no definitive conclusion can be reached about η in these experiments.

Dislocation Loops

Widely varying loop shapes have been observed during growth including polygonal[7], smoothly rounded[37] and irregular "amoeba"[40] configurations. The configuration undoubtedly depends upon the driving force, the possible dissociation (Fig. 2), the presence of solute atoms[41], the mobilities of the defects involved, and probably other factors.

In the case of the high stacking fault energy metal Al, initially polygonal loops shrink uniformly in a circular shape[7] in accordance with Fig. 1b. However, in lower stacking fault energy metals such as Au, such shrinking loops (Fig. 2) remain polygonal, and they also shrink irregularly[7]. These results indicate that jog nucleation and loop shrinkage are more difficult for dissociated loops and that growth is probably also more difficult. In this respect Washburn[7] has observed that growing hexagonal Frank loops (Fig. 2b) which suddenly convert to prismatic loops (Fig. 2c) in Al assume a rhombus shape during further growth by the rapid climb of the A, A' segments in Fig. 2c. These results indicate that the A, A' segments may be relatively less dissociated than those drawn in Fig. 2c and that different loop segments can evidently climb at different rates even in this high stacking fault energy metal.

Relatively direct measurements[42] of η for stacking fault tetrahedra, which may be regarded as completely dissociated loops of the type in Fig. 2a, have been made for v's in quenched Au. Values of η in the range

0.5 to 0.9 were found near 60°C with $\mu_v \simeq 0.6$ eV. Also, η exhibited an activation energy of $\sim$0.07 eV and apparently decreased with a decrease in μ_v.

The growth of large loops at the expense of smaller loops by vacancy diffusion has been observed in Al[43] and Al + 6×10^{-3} at. % In[44]. The measured rate in the alloy was found[44] to be consistent with diffusion-limited kinetics implying $\eta \simeq 1$ for $\mu_v \simeq 0.04$ eV.

The growth of loops in Al + 3 at. % Mg due to a constant vacancy supersaturation induced in thin foils by surface oxidation is consistent with diffusion-limited kinetics implying $\eta \simeq 1$ for $\mu_v \simeq 0.015$ eV[45].

Measurements have been made of loop growth during high temperature irradiation under conditions where the loops destroy a slightly larger number of i's than v's. Growth laws of the type $R_\ell \alpha t^{1/3}$ in Co[46], $R_\ell \alpha t$ in Ni[47] and $R_\ell \alpha t^n$ where $0.3 < n < 1.3$ in Ti[48] were found. No simple conclusions may be drawn from these disparate results.

Grain Boundaries

Komem, et al.[4] have observed directly the climb of GBD's in high coincidence boundaries as they acted as sinks for excess i's. The operation of GBD spirals has been observed by Gleiter[49] in the related phenomenon of boundary migration.

The frequently observed[37,39,50,51] denudation of defect precipitation in the vicinity of boundaries provides direct qualitative evidence for boundary sink action. Under quenching or irradiation the excess defect concentrations are reduced near the boundary, and the formation of precipitates is therefore reduced. However, these observations, by themselves, are not adequate for determining η's. Chang and Siegel[52] have measured vacancy precipitate denudation at a variety of general boundaries in quenched Au and found little variation in the denudation. This suggests a high η for all such boundaries at the large driving force present ($\mu_v \simeq 0.6$ eV). However, the situation may be different at special boundaries. Makin[51] found loop denudation at general boundaries but not at coherent twin boundaries in Cu during high temperature irradiation. Norris[39] found void denudation at general boundaries and void enhancement at coherent twins in Ni during high temperature irradiation. Segall[53] found denudation

of vacancy precipitates at coherent twins in quenched Au, while Siegel[52] found some denudation at coherent twins but greater denudation at general boundaries. These results suggest that coherent twins, which should have low boundary diffusivities and GBD's with large Burgers vectors, may act under certain circumstances as only moderately good defect sinks but at the same time might have a preference for i's as a result of a diffusional bias due to the GBD's.

The shrinkage of voids during sintering occurs by the transport of v's from the voids to grain boundaries operating as vacancy sinks[54]. This process appears to proceed in copper with $\eta \simeq 1$ when μ_v is as low as $\mu = \gamma\Omega/R \simeq 10^{-5}$ eV[54].

Nabarro-Herring creep occurs by the transport of stress-motivated vacancy currents between grain boundaries and surfaces[55]. Tests with wires and foils show[55] that boundaries operate as efficient sources in this process with $\eta \simeq 1$ when $\mu_v = \Omega\sigma \simeq 3\times10^{-5}$ eV. Similar results should hold for cases where the boundaries act as sinks. Jones[55] has analyzed data for polycrystalline aggregates in which the boundaries act as both sources and sinks and has obtained results which indicate that η, averaged over the source and sink action, is within an order of magnitude of unity. However, it has been pointed out[56] that at sufficiently low stresses, i.e., low μ_v, the process may become sink (source) reaction-limited with a low η. This may be due, for example, to the fact that GBD spirals can then no longer operate effectively.

SUMMARIZING REMARKS

(1) The experimental observations reviewed above are fragmentary, and in only a few cases were sink η's determined with any reliability.

(2) Some care must be taken in interpreting the void experiments. For isolated voids it appeared that η becomes very small when the driving force is sufficiently reduced in accordance with the ledge nucleation and migration model. In several experiments high η's for v's were found with μ_v in the range 3×10^{-3} to 5×10^{-5}. In some of these experiments, the voids were either on grain boundaries or else were large enough to be

intersected by dislocations. Under these conditions ledge formation was probably easy, and high η's even at low μ_v's near 5×10^{-5} eV were achieved. Unfortunately, in the important case of high temperature irradiation it was not possible to establish η's for the i's and v's.

(3) Loop η's are undoubtedly influenced by the degree of dissociation. Loops in Al appeared to grow (and shrink) with a high η for v's with μ_v in the range 0.015 - 0.04 eV. Dissociated loops (tetrahedra) in Au operated with a high η for v's with large μ_v's near $\sim$0.6 eV but exhibited lower η's at lower μ_v's. Again, η's for i's and v's could not be established in the case of high temperature irradiation.

(4) The majority of grain boundaries appeared to operate with high η's even with μ's as low as $\sim 10^{-5}$ eV. Many of these boundaries undoubtedly contained already existing GBD's making the sink action easy. However, evidence exists that η eventually becomes small when μ is reduced sufficiently. It is interesting that no evidence was found for $\eta < 1$ at the higher μ's for any boundaries except the special coherent twins.

(5) The nature of the sink processes for voids, loops and boundaries seems reasonably well established on a qualitative basis except for the case of low coincidence boundaries. However, it is noteworthy that no quantitative treatments of the overall kinetics of defect destruction at any of these sinks have been attempted even though analogous processes have been treated for free surfaces and straight dislocations.

(6) The present analyses of stress biasing effects at sinks are approximate and are probably inadequate for the quantitative treatment of the delicate problem of void growth during high temperature irradiation. It is interesting to speculate that the void growth may actually be at least partially due to different η's for the v's and i's.

(7) Relatively little is known about the possibly important effects on η of the enrichment (depletion) of solute atoms which is induced by the defect currents.

(8) In general, there is a present need for quantitative experimental investigations of sink η's and for more ambitious modeling studies of the complex phenomena which are involved.

REFERENCES

1. R. W. Balluffi and D. N. Seidman, Radiation-Induced Voids in Metals, J. W. Corbett and L. C. Ianniello (ed.), p. 563, Nat. Tech. Info. Serv., U. S. Dept. of Commerce, Springfield, VA, 1972.
2. D. N. Seidman and R. W. Balluffi, in Lattice Defects and their Interactions, R. R. Hasiguti (ed.), p. 911, Gordon and Breach, NY, 1967.
3. R. W. Balluffi, Phys. Stat. Sol. 31, 443 (1969).
4. Y. Komem, P. Pétroff and R. W. Balluffi, Phil. Mag. 26, 239 (1972): R. W. Balluffi, Y. Komem and T. Schober, Surf. Sci. 31, 68 (1972).
5. F. S. Ham, J. Phys. Chem. Sol. 6, 335 (1958): C. P. Flynn, Phys. Rev. 133, A587 (1964).
6. J. P. Hirth and G. M. Pound, Condensation and Evaporation, p. 77 et seq., Macmillan, NY, 1963.
7. R. W. Balluffi and A. V. Granato, in Dislocation Theory - A Collective Treatise, F. R. N. Nabarro (ed.), Marcel Dekker, NY, to be published.
8. J. Washburn, in Radiation-Induced Voids in Metals, J. W. Corbett and L. C. Ianniello (ed.), p. 647, Nat. Tech. Info. Serv., U. S. Dept. of Commerce, Springfield, VA, 1972.
9. J. Silcox and P. B. Hirsch, Phil. Mag. 4, 72 (1959).
10. H. Kimura and R. R. Hasiguti, J. Phys. Soc. Japan 17, 1724 (1962).
11. R. M. Thomson and R. W. Balluffi, J. Appl. Phys. 33, 803 (1962).
12. D. H. Warrington and M. Boon, Acta Met. 23, 599 (1975).
13. H. Gleiter and B. Chalmers, High Angle Grain Boundaries, Pergamon Press, Oxford, 1972.
14. W. Bollmann, Crystal Defects and Crystalline Interfaces, p. 143 et seq., Springer-Verlag, NY, 1970.
15. R. W. Balluffi, P. J. Goodhew, T. Y. Tan and W. R. Wagner, to be published, J. de Physique.
16. P. H. Pumphrey, to be published, J. de Physique.
17. B. Ralph, private communciation (1975).
18. D. N. Seidman and R. W. Balluffi, Phil. Mag. 13, 649 (1966).
19. See, for example, A. C. Damask and G. J. Dienes, Point Defects in Metals, Gordon and Breach, NY, 1963.
20. See, for example: T. R. Waite, Phys. Rev. 107, 463 (1957): H. Mehrer, Z. für Naturforsch. 24a, 367 (1969): D. Peak, P. Brosious, Y. H. Lee, M. St. Peters, H. L. Frisch and J. W. Corbett, Rad. Effects 15, 61 (1972): M. Koiwa, Cryst. Latt. Defects 4, 65 (1973).
21. K. C. Russell, Acta Met. 19, 753 (1971): J. L. Katz and H. Wiedersich, J. Chem. Phys. 55, 1414 (1971).
22. W. G. Wolfer and M. Ashkin, J. Appl. Phys. 46, 547 (1975).

23. H. Johnson, Scripta Met. 4, 771 (1970).

24. H. K. Birnbaum, B. L. Eyre and W. Drotning, Phil. Mag. 23, 847 (1971): A. J. E. Foreman, Preferential Trapping of i Atoms at Dislocations as a Mechanism for Void Growth during Irradiation Damage, AERE-R-7629 (May 1974): P. T. Heald, Phil. Mag. 31, 551 (1975): W. G. Wolfer and M. Ashkin, Diffusion of v's and i's to Edge Dislocations, submitted for publ. (1975): M. H. Yoo and W. H. Butler, Steady State Diffusion of Point Defects in the Interaction Force Field, submitted for publ. (1975).

25. J. S. Koehler, Phys. Rev. 181, 1015 (1969).

26. H. Kronmüller, W. Frank and W. Hornung, Phys. Stat. Sol. (b)46, 165 (1971).

27. T. R. Anthony, in Diffusion in Solids, A. S. Nowick and J. J. Burton (ed.), p. 353, Academic Press, NY, 1975.

28. P. R. Okamoto and H. Wiedersich, J. Nucl. Mats. 53, 336 (1974).

29. F. V. Nolfi, Jr., Scripta Met. 7, 1181 (1973).

30. D. I. R. Norris, in The Physics of Irradiation Produced Voids, R. S. Nelson (ed.), AERE-R-7934, p. 134 (Jan. 1975).

31. G. Neumann and G. M. Neumann, in Diffusion Monograph Series, F. H. Wöhlbier (ed.), Diffusion Information Center, Bay Village, OH, 1972.

32. Ref. 6, p. 102, et seq.

33. W. Beeré and G. L. Reynolds, Acta Met. 20, 845 (1972).

34. D. Hull and D. E. Rimner, Phil. Mag. 4, 673 (1959): M. V. Speight and J. E. Harris, Met. Sci. J. 1, 83 (1967): R. Raj and M. F. Ashby, Acta Met. 23, 653 (1975).

35. F. N. Rhines, C. E. Birchenall and L. A. Hughes, Trans. A.I.M.E. 188, 378 (1950): J. L. Brimhall and B. Mastel, J. Nucl. Mats. 33, 186 (1969): J. T. Houston and K. Farrell, J. Nucl. Mats. 40, 225 (1971)

36. R. W. Balluffi, Acta Met. 2, 194 (1954): R. S. Barnes and D. J. Mazey, Acta Met. 6, 1 (1958).

37. See papers in the book cited in ref. 1.

38. L. K. Mansur, P. R. Okamoto, A. Taylor and C. Y. Li, Nucl. Metall. 18, 509 (1973).

39. D. I. R. Norris, Phil. Mag. 23, 135 (1971).

40. P. R. Okamoto, private communication.

41. T. Leffers and P. Barlow, Phil. Mag. 32, 491 (1975).

42. K. C. Jain and R. W. Siegel, Phil. Mag. 25, 105 (1972).

43. J. Silcox and M. J. Whelan, Phil. Mag. 5, 1 (1960).

44. J. Powell and J. Burke, Phil. Mag. 31, 943 (1975).

45. P. S. Dobson, S. Kritzinger and R. E. Smallman, Phil. Mag. 17, 769 (1968).

46. L. M. Howe, Phil. Mag. 22, 965 (1970).
47. D. I. R. Norris, Phil. Mag. 22, 1273 (1970).
48. A. Wolfenden and M. H. Yoo, Rad. Effects 22, 67 (1974).
49. H. Gleiter, Acta Met. 17, 565 (1969).
50. P. B. Hirsch and J. Silcox, Phil. Mag. 3, 897 (1958).
51. M. J. Makin, Phil. Mag. 18, 637 (1968).
52. R. W. Siegel, private communication.
53. R. L. Segall, Acta Met. 12, 117 (1964).
54. B. H. Alexander and R. W. Balluffi, Acta Met. 5, 666 (1957).
55. H. Jones, Mat. Sci. and Eng. 4, 106 (1969).
56. M. F. Ashby, Scripta Met. 3, 837 (1969): B. Burton, Mat. Sci. and Eng. 10, 9 (1972): B. Burton and G. L. Reynolds, Acta Met. 21, 1073 (1973).

ACKNOWLEDGEMENT

This work was supported by the Energy Research and Development Administration under Contract E(11-1)-2679. Additional support was received from the National Science Foundation through the Materials Science Center at Cornell University. Informative discussions with Drs. B. Ralph, P. R. Okamoto and R. W. Siegel are gratefully acknowledged.

POINT DEFECT ANNEALING NEAR VOIDS

R. A. Johnson and J. H. Fikus
Department of Materials Science
University of Virginia
Charlottesville, Virginia 22901

ABSTRACT

Kinetic calculations have been carried out for the annealing of vacancies and interstitials at voids under irradiation conditions. The case in which there is a small energy barrier between a defect and a void (such as might arise from strain effects or solute segregation at void surfaces) has been investigated in detail. With irradiation conditions which yield void swelling, it is found that a small barrier produces a significant bias parameter for preferential annealing. The bias parameter is relatively insensitive to temperature and irradiation rate, but varies with void radius, decreasing as the void size increases.

INTRODUCTION

The concentrations of vacancies and interstitials in metals being irradiated vary with time in a complex way. Within an appropriate time scale related to the temperature of the metal, individual vacancies and interstitials migrate and eventually disappear through mutual annihilation or by arrival at appropriate sinks. The sinks may be pre-existing, such as surfaces and dislocations, or may be created by annealing of defects themselves, such as voids and dislocation loops. The environment near a sink; void, dislocation, or surface, will be somewhat different than in the bulk (e.g. due to strains or solute segregation). Thus, there should be local variations in the diffusion parameters for a migrating defect near a sink. If the formation or migration energies are decreased as a migrating defect approaches a sink, the defect is effectively trapped at the sink and the surface of the sink can be approximated by an effective capture distance from the actual sink location. However, the case in which there is an energy barrier between the bulk and the

sink is considerably more complex. The present calculations were undertaken to investigate this effect, i.e., the case in which there is a small energy barrier between a migrating defect and a sink.

By grouping all the sink properties into boundary conditions, the time rate of change of vacancy and interstitial concentrations, C_v and C_i respectively, can be written

$$\frac{dC_v}{dt} = D_v \nabla^2 C_v + K_o - \alpha C_v C_i \tag{1}$$

$$\frac{dC_i}{dt} = D_i \nabla^2 C_i + K_o - \alpha C_v C_i, \tag{2}$$

where K_o is the production rate of separated Frenkel pairs due to irradiation and is assumed to be independent of time and position, $\alpha C_v C_i$ is the mutual annihilation rate, and $D_v \nabla^2 C_v$ and $D_i \nabla^2 C_i$ are diffusion terms. For this particular form of the diffusion terms, it has been assumed that the defect formation energies are independent of position and that the diffusion constants are independent of position and direction. Steady-state solutions to these equations for voids are reported in the present paper under boundary conditions for the effects outlined above. Metals are not in steady state under actual irradiation conditions, but the boundary conditions change sufficiently slowly with time for the steady-state approximation to be meaningful at any instant of time (after a transient at the onset of irradiation).

There has been considerable work in the past using equations similar to those to be investigated in the present study, especially in reference to the void-swelling problem in reactor materials. In the models investigated by Harkness and Li[1,2] and Wiedersich[3] the basic equations are the same as Eqs. (1) and (2) except that, instead of a diffusional term and exterior boundary conditions to account for the sinks, they use terms linear in the concentrations of the defects arriving at the sinks. Thus, their equations contain no concentration variation with position and sinks are assumed to be randomly dispersed throughout the material. Differing sink biases for vacancies and interstitials are assumed for the various kinds of sinks.

The basic equations used by Bullough, et al.[4-6] are similar to those of Harkness and Li and Wiedersich in that they contain the sink-bias parameter for dislocation sinks with the rate terms linear in the defect concentrations. Bullough and Perrin[4] include a diffusional term for migration of the defects to voids. Brailsford and Bullough[5,6] do not include the diffusional term and discuss different types of sinks and sink emission of vacancies in considerable detail. Their model is similar to that of Wiedersich except for the treatment of the emission of vacancies by certain sinks. In all these models, the essential point is that steady-state concentrations of vacancies and interstitials are found with a sink-bias parameter in a rate-theory model, and then void-swelling is deduced from these concentrations. Bullough and Perrin treat this latter step through a diffusional scheme, whereas it is handled through rate theory in the other cases.

In studies by Urban, et al.,[7] Foreman,[8] and Rothman, et al.[9] for foils, it has been assumed that the surface is an ideal sink. All three use equations essentially equivalent to Eqs. (1) and (2) except that Urban, et al. include a correctional term in D_v to account for the contribution of divacancies to the total vacancy migration, and Foreman and Rothman, et al. include cases in which there is a uniform sink concentration throughout the foil. Rothman, et al. have investigated the time dependent problem covering the initial transient period in addition to the steady-state problem.

CALCULATIONS

For a migrating defect approaching a sink, it is assumed that the formation energy is unchanged but that the activation barrier for the last jump to the sink is increased to a value $Q = E^m + E^b$ with E^m the bulk migration energy and E^b the additional barrier energy. Detailed consideration of the defect current at the surface from an atomistic viewpoint and its relation to continuum theory for an internal spherical sink lead to the approximation

$$E^b \approx kT \ln\left[1 + \frac{C^s - C^e}{b\left.\frac{dC}{dr}\right|_s}\right] \tag{3}$$

with C^s and $\left.\frac{dC}{dr}\right|_s$ the defect concentration and slope evaluated at the surface, C^e the equilibrium defect concentration, and b the atomic jump distance. For spherical geometry under steady state conditions, Eqs. (1) and (2) are

$$D_v\left[\frac{d^2C_v}{dt^2} + \frac{2}{r}\frac{dC_v}{dt}\right] + K_o - \alpha C_v C_i = 0 \tag{4}$$

$$D_i\left[\frac{d^2C_i}{dt^2} + \frac{2}{r}\frac{dC_i}{dr}\right] + K_o - \alpha C_v C_i = 0 \tag{5}$$

These equations are solved in a spherical region around a void out to a distance such that increasing this distance does not affect the results near the void. This essentially is equivalent to solving for a thick spherical shell for which zero barrier boundary conditions are used at the outer surface. The solutions are obtained by an iterative procedure using fifth-order Taylor expansions. The bias parameter Z is taken as the ratio of the flux of interstitials to the flux of vacancies into the void. Thus, for each choice of temperature T, irradiation rate K_o, barrier energies E_i^b and E_v^b, and void radius R, a bias parameter Z and the void growth rate $\frac{dR}{dt}$ are determined. Thus Z essentially is an intrinsic property of the void and irradiation conditions in that perturbations to the vacancy and interstitial fluxes arising from the existance of other sinks with possible bias parameters are neglected. The diffusion and recombination parameters are those given by Bullough and Perrin as being applicable to stainless steel and are listed in Table 1.

Table 1. Kinetic parameters, $D_v = D_v^\circ \exp(-E_v^m/kT)$, $D_i = D_i^\circ \exp(-E_i^m/kT)$ $\alpha/D_i = 10^{17}$, and $C_v^e = \exp(-E_v^f/kT)$.

D_v°(cm^2/sec)	D_i°(cm^2/sec)	E_v^f(eV)	E_v^m(eV)	E_i^m(eV)
0.58	10^{-3}	1.60	1.40	0.20

The results for T = 550°C, a high irradiation rate of $K_o = 10^{-3}$ dpa/sec (such as might be found in ion-bombardment or electron-microscope experiments), and a vacancy barrier but no interstitial barrier are shown in Fig. 1. The primary result of these calculations is that small barriers yield significant bias parameters.

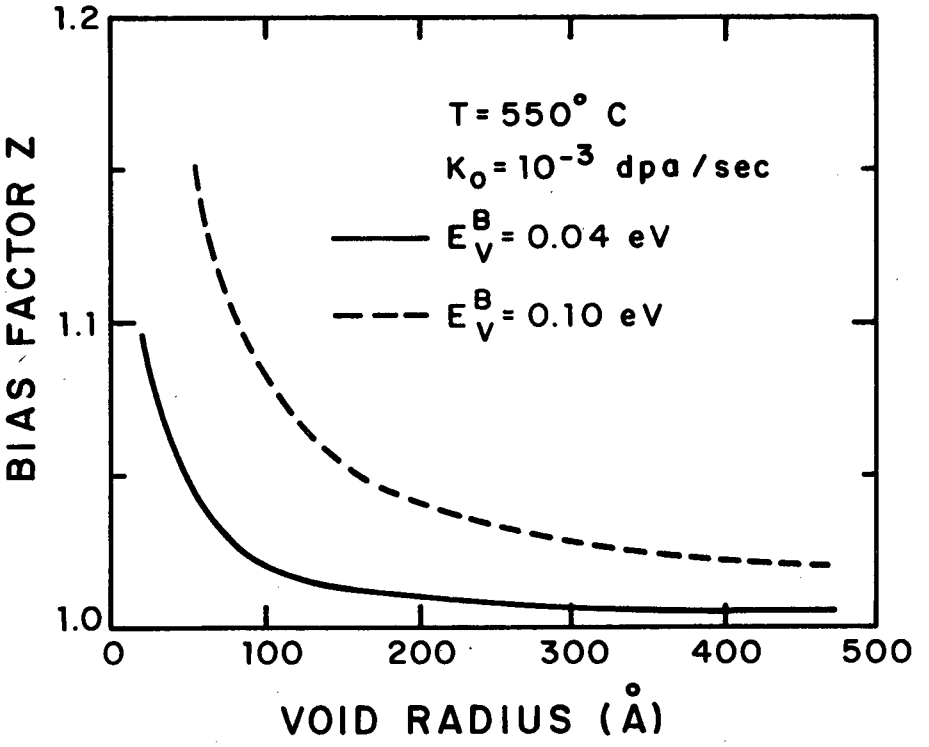


Figure 1. Variation of bias parameter Z with void radius R, with temperature T = 550°C, irradiation rate $K_o = 10^{-3}$ dpa/sec, vacancy barrier E_v^b = 0.04 eV and 0.10 eV, and interstitial barrier E_i^b = 0 eV.

Also, the bias parameter is a function of the void size, decreasing as the radius increases. An interstitial barrier essentially gives the reciprocal Z as a vacancy barrier of the same magnitude.

The calculated bias parameter is quite insensitive to parameter variations, as illustrated in Table 2. The vacancy and interstitial

fluxes change by orders of magnitudes as the temperature is varied from T = 400°C to T = 700°C and the irradiation rate is changed to $K_o = 10^{-6}$ dpa/sec (reactor irradiation rate), but Z, the ratio of the fluxes, only changes slightly.

Table 2. Effect on the bias parameter Z of varying temperature T(°C) and irradiation rate K_o (dpa/sec). Other parameters are: void radius R = 100 A, vacancy barrier $E_v^b = 0.04$ eV, and interstitial barrier $E_i^b = 0$ eV.

K_o T	400	550	700
10^{-3}	1.028	1.020	1.016
10^{-6}	1.026	1.019	1.015

DISCUSSION

The primary conclusion of the present study is that small barriers to defect annealing at void surfaces yield significant bias parameters. The same result is anticipated for cylindrical and planar geometry.

The approximation that the extra barrier exists only for the final jump to a sink should not be critical: the total barrier height should be the rate controlling factor. From the present results, it is difficult to assess the effect for a void with a varying barrier over its surface, as might well occur under conditions of solute segregation.

Certainly the detailed perturbation of kinetic parameters for defects near sinks is more complex than the simple model presented here. Effects of stress will vary with void size, solute segregation at sink surfaces is a complex phenomenon in its own right, and the effects of such segregation on kinetic parameters is hard to estimate. There is increasing evidence that surface contaminations play a decisive role in the kinetics of void growth in the bulk as well as in microscope foils.

In summary, it is found that variations in kinetic parameters for defects near sinks of the order of magnitude that is to be expected can be critical relative to the annealing of irradiation-produced defects. It is felt that a clear understanding of these interactions is required before realistic predictive models for this annealing can be developed.

REFERENCES

1. S. D. Harkness and C. Y. Li, Met. Trans. 2, 1457 (1971).
2. S. D. Harkness and C. Y. Li, Radiation Induced Voids in Metals, edited by J. W. Corbett and L. C. Ianniello (U.S.A.E.C., 1972, Conf-710601).
3. H. Wiedersich, Rad. Effects 12, 111 (1972).
4. R. Bullough and R. C. Perrin, Radiation Induced Voids in Metals, edited by J. W. Corbett and L. C. Ianniello (U.S.A.E.C., 1972, Conf-710601).
5. A. D. Brailsford and R. Bullough, J. Nucl. Materials 44, 121 (1972).
6. A. D. Brailsford and R. Bullough, ref. 2, p. 493.
7. K. Urban, M. Wilkens, and A. Seeger, ref. 1, p. 550.
8. A. J. E. Foreman, Rad. Effects 14, 175 (1972).
9. S. J. Rothman, N. Q. Lam, R. Sizmann, and H. Bisswanger, Rad. Effects 20, 223 (1973).

INTERACTIONS BETWEEN DISLOCATIONS AND POINT DEFECTS

N. Sumida, H. Fujita, K. Takemoto and A. Sawada
Department of Materials Science and Engineering
Faculty of Engineering, Osaka University
Suita, Osaka, 565, Japan

ABSTRACT

Copper and copper-aluminum alloys were irradiated using a 3MV EM, and the interactions between straight dislocations and point defects have been studied.

Edge-dislocations climb up during irradiation and the interstitial-type loops are not formed around them. On the other hand, screw-dislocations turn into the helical ones by absorbing interstitials induced by irradiation. During irradiation, the number of helical turns do not change but the radius of helix increases. At the same time, the interstitial-type dislocation loops are formed close by the helical dislocations. The growth rate of these loops is the same as that of the radius of helical dislocations.

From these facts, the sink efficiency of dislocations for point defects can be determined.

Furthermore, when the fresh screw-dislocations are introduced by in-situ deformation during irradiation, the interstitial-type loops are preferentially formed on the active slip planes. The enhanced nucleation of the loops is closely related to the point defects formed by the motion of dislocation-jogs.

INTRODUCTION

Behaviors of point defects induced by electron irradiation have been studied on various metals using an ultra-high voltage electron microscope as a function of the reflecting condition,[1,2] the crystal orientation,[1] and the accelerating voltage.[3] Existence of dislocations plays an important role[4,5] in these experiments because of their strong interaction with the point defects. The interaction is very sensitive to the character and shape of dislocations.

Moreover, the formation of dislocation loops induced by electron

irradiation may also be affected by the motion of dislocations, because the point defects are formed by the motion of their jogs.[6]

Present works are mainly concerned with some results of the sink efficiency of straight dislocations for point defects and preferential formation of dislocation loops on the active slip planes in Cu and Cu-Al alloys.

EXPERIMENTAL PROCEDURES

The specimens used were 99.99% purity copper and Cu-3at.%Al single crystals grown by a modified Bridgman technique. Perfect straight edge- and screw-dislocations were introduced into bulk specimens by bending and stretching, respectively. After that, the specimens were finished for electron microscope observation by electropolishing and then electron irradiation were carried out at various temperatures using a high voltage electron microscope of Hitachi HU-2000 type operated at 2 MV. On the other hand, the specimens were stretched directly inside the microscope using a stretching device[7] under observation at 2 MV, and the irradiation of 2 MeV electrons was made at room temperature.

Irradiation intensity for each experiment was measured with a Faraday cage located at a position between the projection lens and floresence screen. The specimen temperature was measured with a thermo-couple fixed at the tip of specimen holder. Stereoscopic observation was utilized to determine the three dimensional distribution of dislocation loops.

EXPERIMENTAL RESULTS AND DISCUSSIONS

Formation of Secondary Defects around Dislocations

It is well known that the interstitial-type dislocation loops are generally formed in copper by irradiation with energetic electrons. The formation of these loops, however, is suppressed around dislocation lines as well as the surface by absorption of interstitials nearby.[4,5] In these denuded zones of interstitial-type loops, small vacancy clusters are frequently formed at the later stage of irradiation,[5,8] as shown in

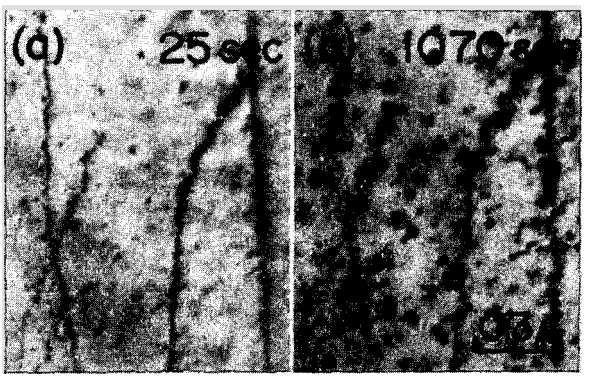


Fig. 1. Formation of vacancy-type secondary defects induced by the irradiation around dislocation lines in copper. Electron intensity is $1.4 \times 10^{19} e/cm^2 sec$ at 2 MV. Irradiation time is shown in each micrograph.



Fig. 2. Formation of vacancy clusters inside interstitial-type Frank loops in copper. Frank loops in (a) were formed by irradiation at 250°C for 185 sec, and the specimen was further irradiated at room temperature. $2 \times 10^{18} e/cm^2 sec$, 2 MV.

Fig. 1, because of accumulation of vacancies during irradiation. These phenomena are very sensitive to not only the irradiation temperature and the content of solute atoms but also the nature of dislocations. For example, small vacancy clusters are preferentially formed around two dislocations at the left hand side, but a part of dislocation at the right hand side changes to a helical one. Figure 2 is another example showing the same phenomenon near the interstitial type loops,[9,10] in which the density of vacancy clusters is different from each other along the dislocation lines. This is a reason why, the straight perfect edge- and screw-dislocations have been used for determination of the sink efficiency of dislocations for the interstitials in the following sections.

Interaction between Dislocations and Point Defects

Interaction between Edge-dislocations and Point Defects

The edge-dislocations strongly interact with point defects and make climb motion by absorption of interstitials. Figure 3 shows successive stages of climb motion of straight edge-dislocations in Cu-3at.%Al alloy irradiated at 200°C with an intensity of $2 \times 10^{19} e/cm^2 sec$. A black and a white arrow in Fig. 3 show the Burgers vector of the dislocations and a maker showing a fixed position, respectively. After irradiation for

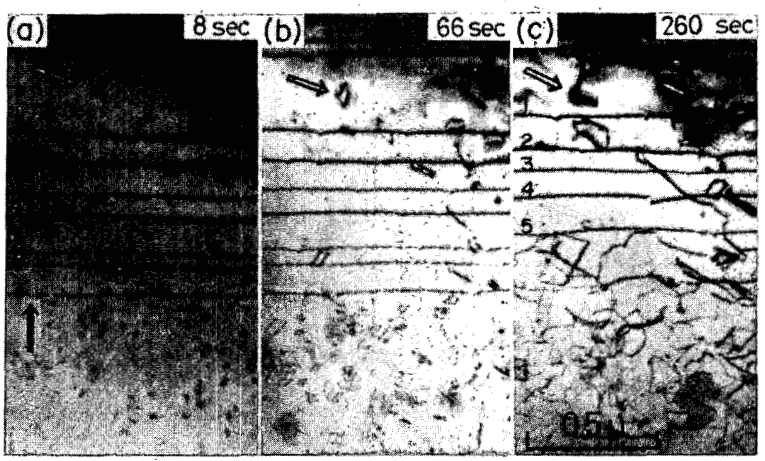


Fig. 3. Climb motion of edge-dislocations in Cu-3at.%Al irradiated at 200°C. $2x10^{19}e/cm^2sec$, 2 MV. The corresponding dislocations in (a) and (c) are shown with the same marks.

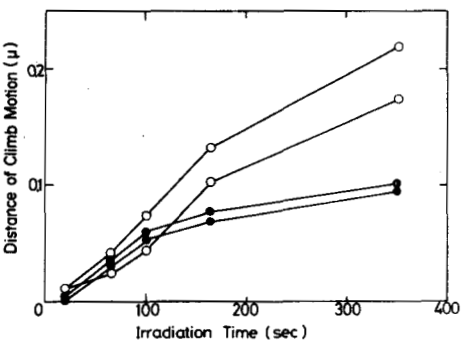


Fig. 4. The amount of climb motion of each dislocation against the irradiation time.

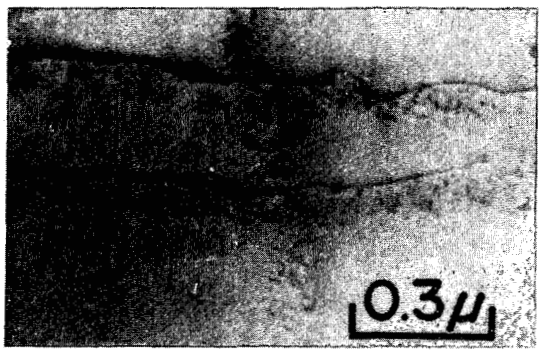


Fig. 5. Formation of vacancy clusters only on the compression side of edge-dislocations in copper. Irradiation was done at 100°C for 13.5 min. $1.8x10^{19}e/cm^2sec$, 2 MV.

8 sec, small interstitial-type dislocation loops appear in regions far from the dislocation lines. But these loops scarcely appear near the dislocation lines. These loop sizes increase with increasing irradiation time, but no loops are newly formed in the denuded zones around dislocations.

At the same time, all dislocations make climb motion due to the absorption of interstitials, as may be understood from the comparison with the position of each individual dislocation line in Fig. 3. The amount of climb motion of each dislocation in Fig. 3 is measured against the irradiation time, as shown in Fig. 4. Existence of different speeds of climb motion suggests that they are very sensitive to the position of dislocations in the specimen. Therefore, the sink efficiency of edge-dislocations

can be determined from both measurement of the radius of denuded zone and of the speed of climb motion.

When the irradiation temperature is considerably low, the vacancy clusters are formed in the denuded zone of interstitial-type loops.[11,12] Figure 5 is an example of this phenomenon in copper irradiated for 13.5 min at 100°C with an intensity of 1.8×10^{19} e/cm^{2}sec. Here, it is noted that the vacancy clusters are formed only in the compression side of edge-dislocations in which the interstitials contribute to the climb motion of dislocation.

Interaction between Screw-dislocations and Point Defects

When Cu and Cu-Al alloy specimens with straight screw-dislocations are irradiated, these dislocations turn into the helical ones by absorbing interstitials, as seen in Fig. 6. The number of their helical turns does not change but the radius of helix increases with increasing irradiation time. Growth speed of these helical dislocations along the radial-direction is the same as that of the interstitial-type loops induced by the irradiation, as shown in Fig. 6. Moreover, small vacancy clusters are also formed inside the helix at the later stage of irradiation as shown in an enlarged micrograph in Fig. 6(c). This phenomenon is the same as in the case of interstitial-type dislocation loops, as seen in Fig. 2. These results show that the interaction between screw-dislocations and point defects in the growth process is mainly due to the hydrostatic stress field around dislocations.

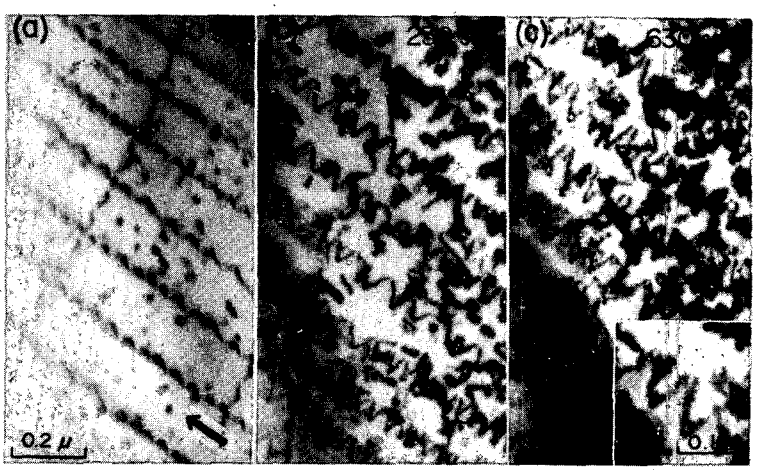


Fig. 6. Growth of helical dislocation in copper irradiated at room temperature. 2.5×10^{18} e/cm^{2}sec, 2 MV. Micrograph on down side of right hand side in (c) is an enlargement of a part of (c).

Enhanced Nucleation of the Dislocation Loops on the Active Slip Planes in Copper[6]

When electron irradiation is made immediately after screw-dislocations are moved on slip planes in copper, the interstitial-type loops are preferentially formed on these slip planes. Figure 7 is an example showing such phenomenon. Each broad band in Fig. 7(c) corresponds to an active slip plane of screw-dislocations. Figure 8 shows a stereo-pair of micrographs taken after the irradiation for 20 min. Distribution of the loops in Fig. 8 is shown schematically in Fig. 9. Here, it is noted that majority of the large loops are formed around the each active slip plane, and the denuded zone is formed near the slip plane. These facts mean that the nucleation of loops preferentially occurs on the active slip planes, and that the long range migration of interstitals induced by irradiation

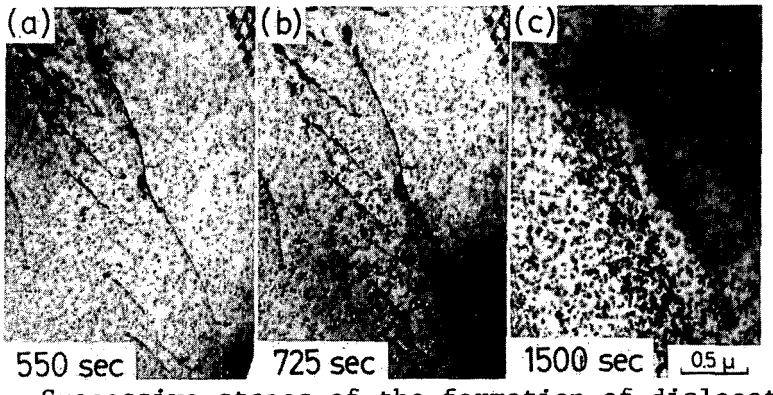


Fig. 7. Successive stages of the formation of dislocation loops irradiated at room temperature immediately after in-situ deformation in copper. $5 \times 10^{18} e/cm^2 sec$, 2 MV.

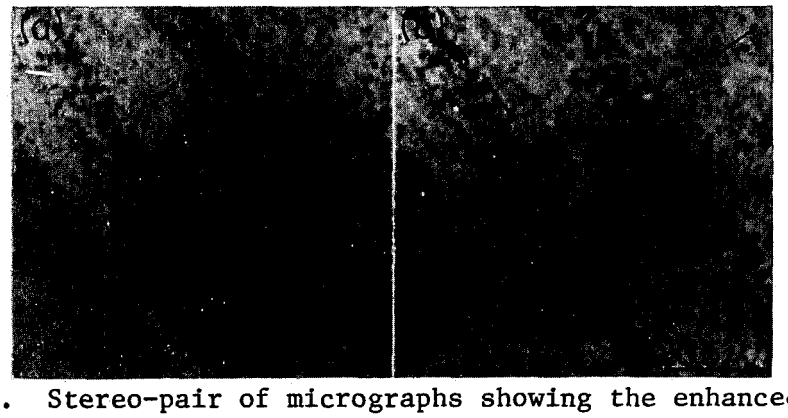


Fig. 8. Stereo-pair of micrographs showing the enhanced nucleation of loops on the active slip planes. These micrographs were taken after the irradiation for 20 min.

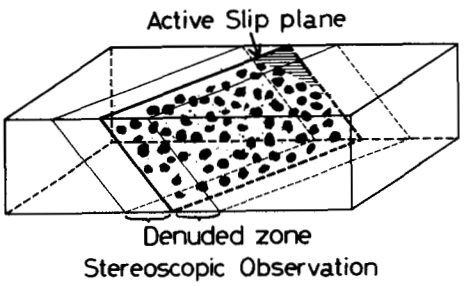


Fig. 9. Schematic illustration of distribution of dislocation loops around each active slip plane in Fig. 8.

is enhanced onto the active slip planes.

Similar phenomenon has been observed in other metals such as Cu-3at.%Al and Mo. Since the dislocation density on the slip planes is not so large under irradiation, it seems that the enhanced nucleation is not correlated with the interaction between point defects and individual dislocations. And thus, this phenomenon is probably related to the motion of dislocation-jogs.

The authors greatly appreciate to Messrs. K. Yoshida, M. Komatsu and T. Sakata for their help in operating microscope.

REFERENCES

1. H. Fujita, T. Tabata, K. Yoshida, N. Sumida and S. Katagiri, Japan. J. appl. Phys. 11, 1522 (1972).
2. N. Sumida and H. Fujita, to be published in J. Phys. Soc. Japan.
3. H. Fujita and N. Sumida, J. Phys. Soc. Japan 34, 838 (1973).
4. M. J. Makin, Phil. Mag. 18, 637 (1968).
5. M. Kiritani and N. Yoshida, Crystal Lattice Defects, p. 83, vol. 3, Gordon and Breach, Science Publishers Ltd., U.K., 1973.
6. N. Sumida, K. Takemoto, H. Mori and H. Fujita, Japan. J. appl. Phys. 14, 295 (1975).
7. T. Tabata, H. Mori, H. Fujita and I. Ishikawa, to be published in Japan. J. appl. Phys.
8. N. Yoshida and M. Kiritani, J. Phys. Soc. Japan 35, 1418 (1973).
9. K. Urban, Phys. Status solidi (a) 4, 761 (1971).
10. M. Meshii and K. Shiraishi, Electron Microscopy and Structure of Materials, p. 952, Univ. Calif. Press, Berkeley, 1972.
11. W. M. Stobbs, Phil. Mag. 27, 257 (1973).
12. N. Yoshida and M. Kiritani, J. Phys. Soc. Japan 38, 1220 (1975).

LONG-RANGE INTERACTION BETWEEN RADIATION-INDUCED POINT DEFECTS AND DISLOCATIONS

M. Kiritani, H. Takata, N. Yoshida*, and Y. Maehara**
Department of Material Physics
Faculty of Engineering Science, Osaka University
Toyonaka, Osaka, Japan

ABSTRACT

The growth and sharinkage of dislocation loops during high energy electron irradiation in a high voltage electron microscope were observed in detail, and the existence of the directional flow of interstitial atoms along the dilatation strain field gradient was confirmed.

Corners of interstitial type hexagonal dislocation loops in fcc metals grow faster, and the loops develop into six cornered stars. A similar shape of loops is observed during the shrinkage of quenched-in vacancy type hexagonal loops as the result of the retardation of the corners. Interstitial type loops in bcc metals often show many-petaled shape with steeply sticked out parts.

The dilatation strain field gradient towards a curved part of edge dislocation segment is large and small on the convex and concave side, respectively. Interstitial atoms feel the combination of large attraction and small repulsion or that of small attraction and large repulsion depending on which side of the curved dislocation has extra half plane of atoms. The directional flow under these strain field and the difference in the available volume to dislocation segment divided along the flow direction explain all the above experimental observations.

INTRODUCTION

A review of a systematic study of the development of damage structures and point defect properties with high voltage electron microscopy has been presented in another paper by the present author in this conference. In this short paper, utilizing the primitive advantage of

*Presently at Max-Planck-Institute, Stüttgart.
**Presently at Central Res. Lab., Sumitomo Metal Ind. Ltd., Amagasaki.

the electron microscopy, which enables the very local difference in the progress of phenomena, the local flow of radiation induced point defects under strain field will be concluded.

Pre-existing or radiation induced dislocation loops grow or shrink by the further electron irradiation. The shape of the loops exhibit directly the local difference of the absorption of point defects, and consequently from the analysis of the loop shape, the flow of the point defects around the dislocation will be infered. To the last of this paper, how the existence of these interactions has parts in the development of radiation induced structures in general will shortly be discussed.

EXPERIMENTAL TECHNIQUES

A high voltage electron microscope HU-2000 was used for the introduction of defects and simultaneous observations. Acceleration voltage of electrons was 1000 to 2000 kV, and the irradiation intensity was from 10^{17} up to 10^{19} electrons/cm^2·sec. A heating stage with universal tilting device was used. The temperature of a specimen was measured with a fine thermaocouple which was spot-welded to a small metal plate which tightly held a specimen in the heating stage.

Materials used were 99.9994% aluminum (Sumitomo Chemical), zone-refined aluminum (Kino's Lab., Hiroshima Univ.), 99.999% gold (Johnson Mathey Chemicals), 99.999% copper (JMC), 99.999% iron (JMC) and super-pure molybdenum (Kimura's Lab., Tohoku Univ.). All the microscope specimens were prepared by electrolytic polishing.

OBSERVATIONS

Interstitial Type Dislocation Loops in FCC Metals

The density of the loops nucleated by a strong electron irradiation ($>10^{19}$ electrons/cm^2·sec) in less pure aluminum is fairly high, and the loops do not grow large before they react with the neighboring loops. The shape of loops was recognized to be round at room temperature.

When super-pure aluminum is irradiated with week intensity ($\sim10^{18}$

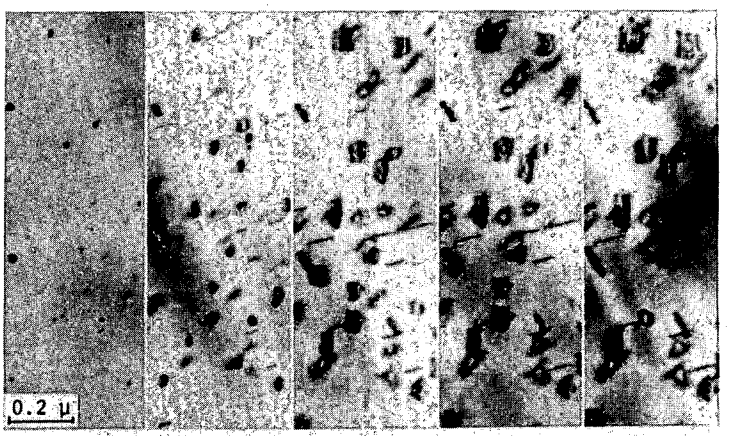


Fig. 1 Interstitial type dislocation loops formed in super-pure aluminum. 2000 keV, 6×10^{18} e./cm^2·sec, at room temperature.

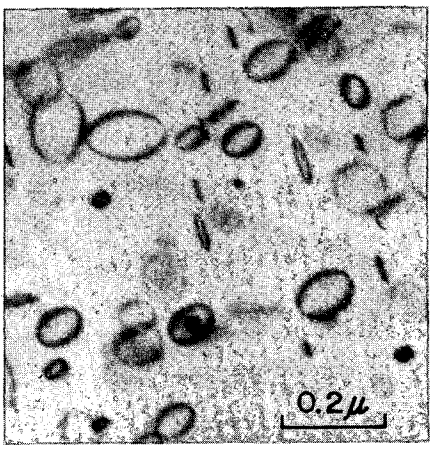


Fig. 2 Interstitial loops formed at 120°C in super-pure aluminum.

e./cm^2·sec), the number of loops becomes fairly small, and they grow into such a large size that the detailed shape can be observed as in Fig. 1. The basic shape of the loops is hexagonal bounded by [110] directions, and some exhibit triangle and octagon. A noticed characteristic of the shape common to all the loops is their sharp sticked out corners.

Even when super-pure aluminum is irradiated with a week irradiation intensity, the interstitial loops grow into perfect roundish shape when the specimen temperature is elevated as in Fig. 2.

Hexagonal faulted interstitial loops were observed to grow in gold at elevated temperatures. At slightly lower temperatures the loops exhibit a similar tendency in their shape as that observed in aluminum, though not pronounced. As shown in Fig. 3, the corner parts of hexagonal loops tends to grow faster than the straight part.

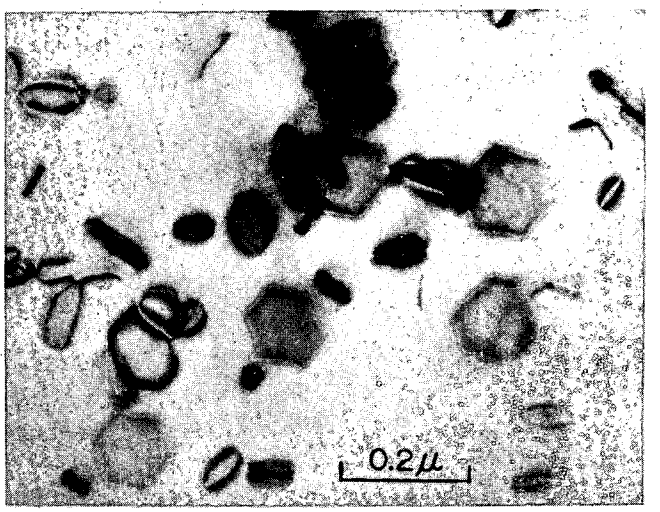


Fig. 3 Interstitial type dislocation loops in gold. 2000 keV, 1×10^{19} e./cm^2·sec, at 150°C for 250 sec.

Interstitial Type Dislocation Loops in BCC Metals

At low temperatures, the density of defect clusters formed in iron is so high that they proceeds into tangled dislocations before exhibiting their shape in detail. At high temperatures, the interstitial loops have clear rectangular shape on (100) planes with the sides along [100].

At intermediate temperatures, the interstitial type dislocation loops in iron are also on (100) planes, and they exhibit interesting characteristic shape as shown in Fig. 4. The image of loops lying parallel to the specimen foil is faint owing to the g·b=0 condition of (100) reflection, but it rather shows the detailed shape of the loops. The loops has a complicated shape with many sharply sticking out parts, exhibiting the shape as a flower with many petals. Elongated loops in the same figure are lying on other (100) planes almost parallel to the electron beam. The fine structure of their image which shows at first glance the shape analogous to helecal dislocations, is understood as the images from the loops whose shape is similar to those lying parallel to the foil plane. Dislocations on each opposite side of a petal has different sign and their image positions deviate alternatively from their real positions.

The loops formed at medium temperatures in molybdenum were found to lie on (111) planes differently from those in iron. The loops show the same characteristic petalous shape as in iron as shown in Fig. 5.



Fig. 4 Petalous dislocation loops formed in iron at 120°C. 2000keV, 1.6×10^{19} e./cm^2·sec for 570 sec.

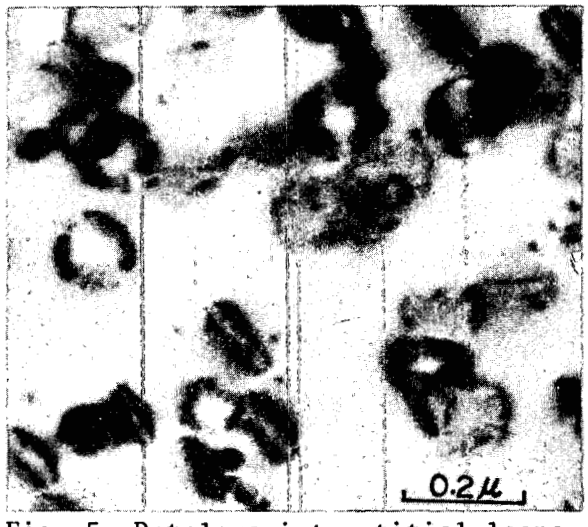


Fig. 5 Petalous interstitial loops formed in moblybdenum at room temp. 2000keV, 1.9×10^{19} e./cm^2·sec, 125sec.

Vacancy Type Dislocation Loops

Quench-induced vacancy type dislocation loops in aluminum suppress the interstitial cluster formation by electron irradiation. In the area with high density of vacancy loops, interstitial atoms have to make shrink and destroy the vacancy loops before they form their own clusters.

When an aluminum specimen with dispersed few numbers of large quench-induced vacancy type loops are irradiated, an interesting characteristic is observed during the shrinkage of the vacancy loops. In Fig. 6 originally hexagonal loops (a) diminish their area only from the straight parts, and finally become star like shape of six sticking out corners as in (d). Usually vacancy type large loops exhibit complicated shape by the combined effect of the easy nucleation of interstitial loops on the loop plane.

FLOW OF INTERSTITIAL ATOMS ALONG THE DILATATION FIELD GRADIENT

Interstitial atoms are believed to make their average flow around a dislocation line from the volume of compression to that of expansion along the gradient of the dilatation, and will finally be absorbed to the dislocation. The dilatation field around a corner of a hexagonal loop, representatively on the plane of the loop, was mapped in Fig. 7. If we suppose the loop to be interstitial type, the strain field outside the

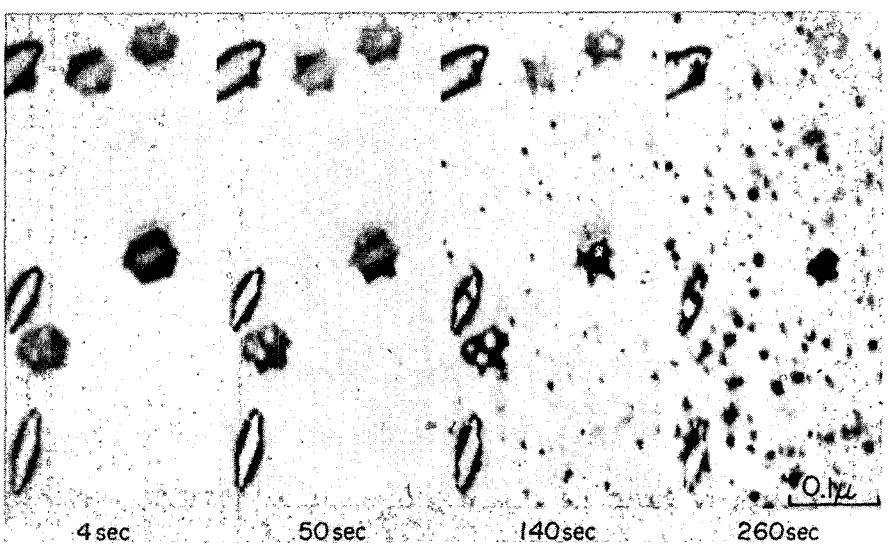


Fig. 6 Shrinkage of hexagonal vacancy type loops in quenched Al by electron irraditaion. 1500keV, 2×10^{19} e./cm^2·sec, at room temperature.

loop is expansion and the field gradient is extremely large at around the corner compared with that around the straight part. This means the interstitial atoms around the corner part are exposed to a large directional force towards the dislocation line. On the other hand, the field inside the corner part is that of compression and the gradient is smaller around the corner, and this means the less repulsion to interstitial atoms.

The direction of the gradient along which interstitials should make their flow is indicated by dotted lines in the same figure. The area of the strong attraction to interstitial atoms at around the corner is much larger than that for the same length of the dislocation of straight part.

It can be easily understood, imagining the three dimentional situations, that more arrival of interstitial atoms at the corners compared with that at the straight part, owing to the synergetic effect of the difference in the force on interstitials and the difference in the available volume. Accelerated arrival of interstitials results the shape of loops whose corner parts are sticking out.

For the vacancy type loops, all the signs in the above discussion are reversed, and consequently the corner parts do not absorb as much interstitials as that absorbed by the straight part. This results the star like shape of quenched-in loops.

When a growing interstitial loop happen to have a irregular shape, the concave part is accelerated by the same reason explained above and sticks out more and more. The tendency of the retardation of the convex part becomes more and more pronounced, like the final shape of the corner part in quenched-in loops in aluminum. This is the qualitative explanation for the flower like shape in iron and molybdenum.

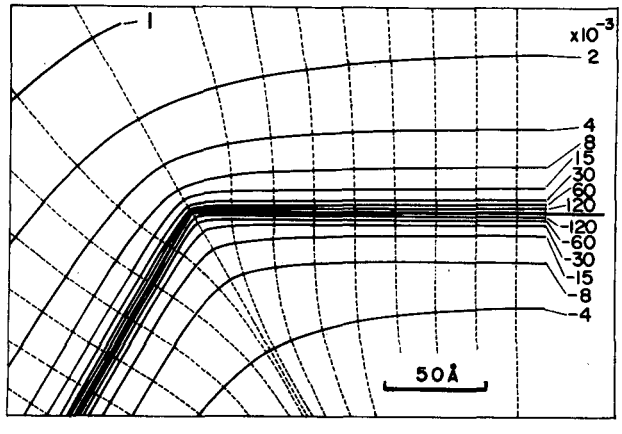


Fig. 7 Dilatation strain field around a corner of a hexagonal Frank loop.

When the irradiation temperature is high enough to enable the atomic size of steps or jogs to move around a dislocation loop, the loop does not show the shape resulted by the above interaction and become roundish. And when the loop density is high, the random cancellation of the strain field prevents the pronounced flow of interstitials and again results the roundish loops.

DISCUSSION

The existence of the long range migration of interstitial atoms along the dilatation strain field gradient should be regarded to exist generally in all metals. The effect of this interaction should be included in the overall understanding of the development of damage structures. A typical example is the growth of interstitial loops at vacancy mobile elevated temperatures. When vacancies are mobile, as discussed in another paper in the present conference, the product of the mobility and concentration of interstitial atoms becomes to maintain a complete balance with the same quantity of vacancies. Even under this balance conditions, interstitial loops can grow linearly with the irradiation time owing to the excess arrival rate of interstitial atoms by the long range interaction.

ACKNOWLEDGEMENT

The authors is grateful to Professors H. Fujita and F. E. Fujita for their continuous encouragements. They are also grateful to Messrs. K. Yoshida, M. Komatsu and T. Sakata for their help in operating the microscope.

REFERENCES

1) M. Kiritani and N. Yoshida: J. Phys. Soc. Japan 35, 306 (1973).
2) M. Kiritani, N. Yoshida and H. Takata: J. Phys. Soc. Japan 36,720(1974).
3) M. Kiritani, N. Yoshida, H. Takata and Y. Maehara: J. Phys. Soc. Japan 38, 1677 (1975).
4) N. Yoshida, M. Kiritani and F. E. Fujita: J. Phys. Soc. Japan 39, 170 (1975).

Some Considerations in the Splitting of Interstitial Frank Loops Formed by Irradiation

K. Seshan J. Grilhé* J. Washburn
IMRD, Lawerence Berkeley Laboratory
Univ. of California, Berkeley CA 94720

ABSTRACT

The splitting of interstitial loops formed by irradiation is considered in detail. It is shown that they may split to form obtuse - angled single shear faults on the intersecting {111} planes. A detailed description of the splitting is given in which the interstitial Frank loop is viewed as being made up of perfect dislocation loop and two shears.

The detailed description is then considered in the context of the formation of complex loops as are observed in quenching and irradiation studies. Experimentally observed geometries are explained viz, triangular loops within hexagonal ones etc.

The nucleation of a DC' loop in complex interstitial loop formation is shown to be feasible. DC' has the magnitude of a perfect dislocation loop and encloses an intrinsic shear.

* Laboratoire de Métallurgie Physique, Poitiers, France.

Splitting of Interstitial Frank Loops

Interstitial Frank loops are produced by radiation damage to metals (Eyre [1]) and ion damage to semiconductors (Seshan et al [2]). Depending on their size and stacking fault energy of the material they may be triangular, hexagonal etc. (Gaboriaud and Grilhé [3]). These geometries result from the disassociation of the Frank dislocation bounding the loop into a Shockley partial and a stair rod dislocation as first proposed by (Silcox and Hirsch [4]).

The splitting of an hexagonal vacancy Frank loop (a, b) is compared to that of an interstitial one (c,d) in Fig.1. In Fig. 1a, the faults are BOTH intrinsic and make an acute angle between them. The vacancy Frank loop could split to form an EXTRINSIC fault on the intersecting {111} plane as in Fig. 1b. The reason that this does not form, or is not expected to is that the extrinsic fault, requiring two shears, is difficult to nucleate and may have a higher energy.

However when the splitting of the interstitial loop is considered (Fig. 1c,d) the possibility of it splitting to form obtuse-angled INTRINSIC faults on the intersecting {111} plane is the more attractive one Fig.1d.

A detailed description of the splitting of the interstitial Frank loop $D\delta$ is shown in Fig.2. The loop $D\delta$ is viewed as being made up of a perfect dislocation DC and two shears δB and δA.

$$D\delta = DC + \delta B + \delta A$$

$$\frac{1}{3}[111] = \frac{1}{2}[110] + \frac{1}{6}[\bar{2}11] + \frac{1}{6}[1\bar{2}1]$$

Then the splitting of the loop $D\delta$ is simply equivalent to the disassociation of the loop DC.

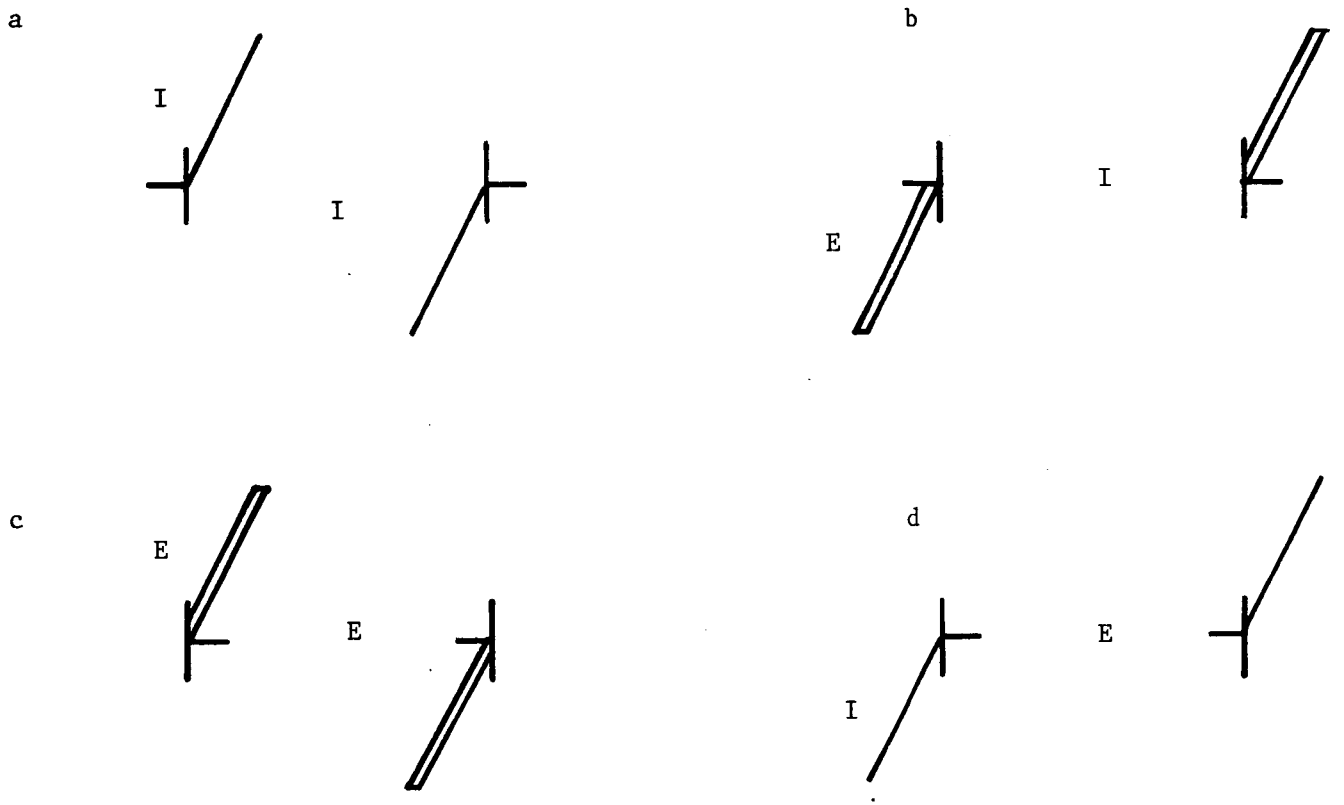


Fig. 1. a,b, *Splitting of a vacancy Frank loop* I : *Intrinsic fault*
c,d, *Splitting of an interstitial Frank loop* E : *Extrinsic fault.*

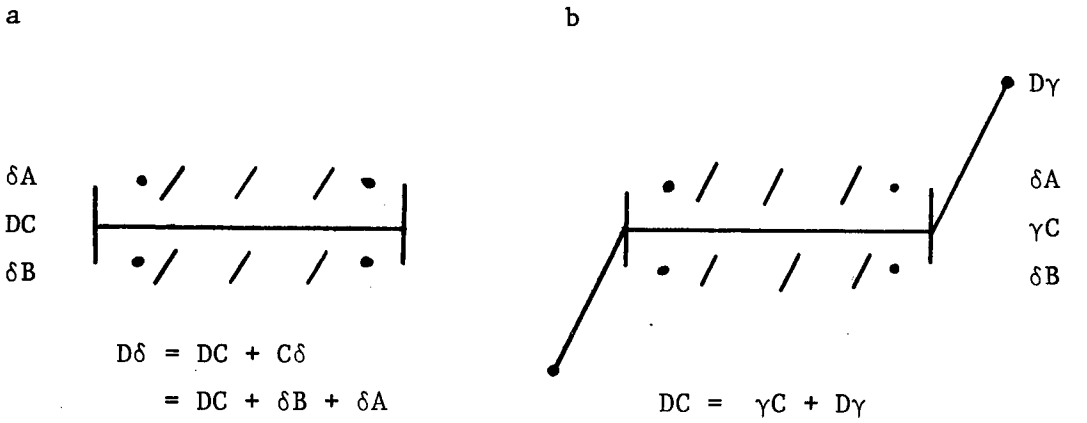


Fig. 2. *Detailed description on an interstitial Frank loop before (a) and after (b) splitting.*

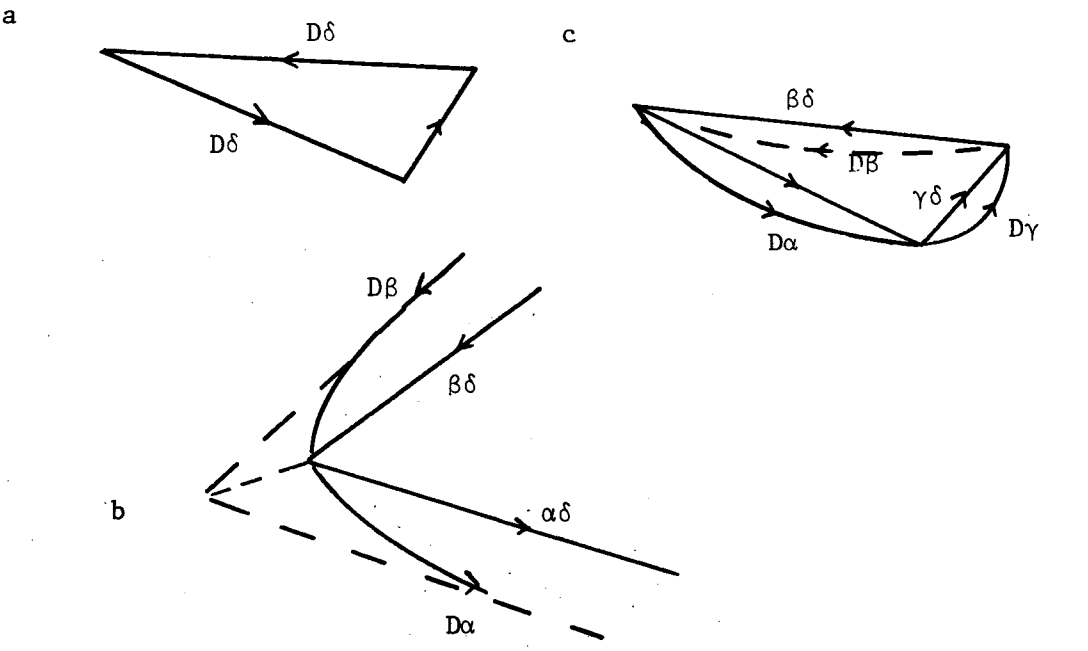


Fig. 3. *Splitting of a triangular interstitial Frank loop.*

$$DC \rightarrow \gamma C + D\gamma$$

Fig. 2b

$$\frac{1}{2}[110] \rightarrow \frac{1}{3}[111] + \frac{1}{6}[112]$$

On the basis of splitting it is possible to explain the relative absence of triangular interstitial loops and interstitial tetrahedra. In Fig.3 the splitting of a triangular interstitial Frank loop is shown. Since obtuse angled faults are formed the defect, after splitting, does not develop further Fig.3b,c.

Complex Loop Formation

The straight foreward application of splitting to complex loops predicts that triangular loops should form within hexagonal ones as shown in Fig.4. If the second loop B is also hexagonal one of its Shockleys would run into the stacking fault of the first loop A. Triangular loops within hexagonal ones have been reported by Edington and Smallman [5] and by Yoshida and Shimomura[6].

The case of the complex interstitial loop is seen in Fig.4. The nucleation of $D\delta$ on $D\delta$ leads to an intrinsic loop within an extrinsic one. However the direct nucleation of DC' (Fig.5b) i.e. DC and δA, leads to a perfect loop within a hexagonal loop, a configuration reported by Chadderton and Eisen[7]. $DC' = \frac{1}{6}\langle 114\rangle$ and is a perfect dislocation loop enclosing an intrinsic shear.

$$DC' = DC + \delta A$$

$$\frac{1}{6}[411] \quad \frac{1}{2}[110] + \frac{1}{6}[1\bar{2}1]$$

If the extrinsic fault energy is higher than the intrinsic, the nucleation of DC' would be attractive in vacancy complex loops.

Further properties of DC' are in print elsewhere[8].

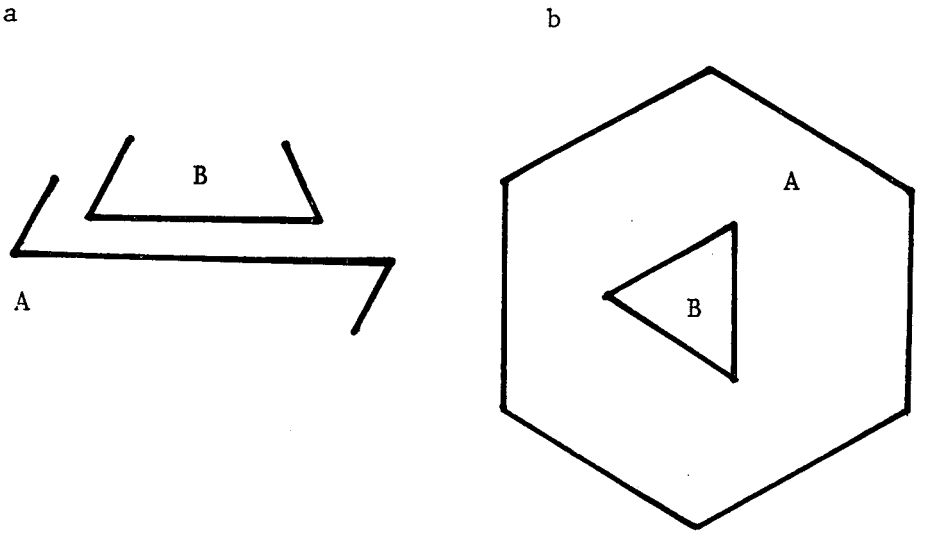


Fig. 4. *Explanation on the basis of splitting for triangular loops within hexagonal ones.*

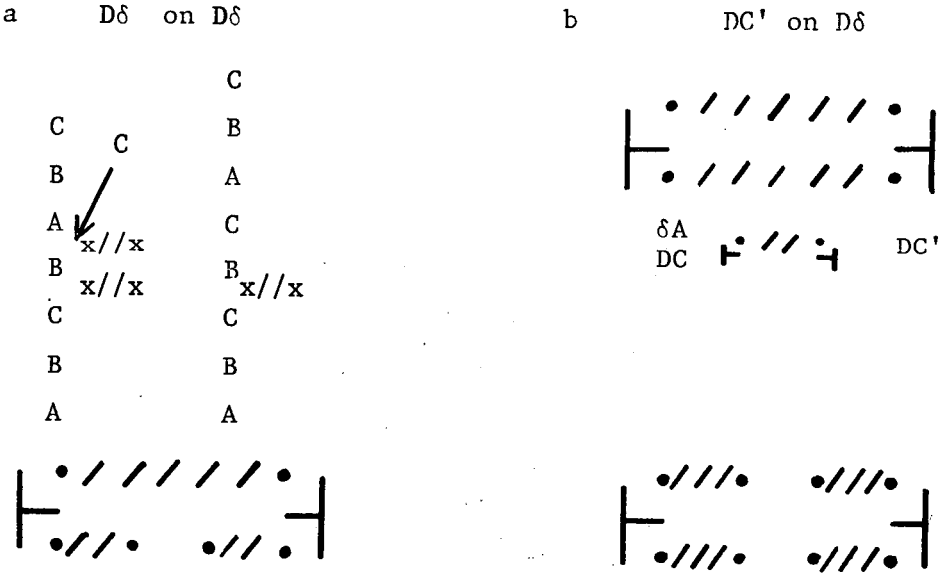


Fig. 5. *Nucleation of (a) Dδ on Dδ (b) DC' on Dδ in the formation complex intersitial loops.*

REFERENCES

1. B. L. Eyre, J. Physics F. 3, 422 (1973).
2. K. Seshan and J. Washburn, Phys. Stat. Sol.(a), 26, 345 (1974).
3. R. J. Gaboriaud and J. Grilhé, Phys. Stat. Sol.(b), 51, 579 (1972).
4. J. Silcox and P. B. Hirsch, Phil. Mag. 4, 72 (1959).
5. J. W. Edington and R. E. Smallman, Phil. Mag. 11, 1109 (1965).
6. S. Yoshida and Y. Shimomura, J. Phys. Soc. Japan, 18, 1950 (1963).
7. L. T. Chadderton and F. H. Eisen Rad. Eff 7, 129 (1971).
8. J. Grilhé, K. Seshan and J. Washburn, Rad. Eff. in print.

ACKNOWLEDGEMENTS

ERDA and IMRD, Lawerence Berkeley Laboratory are acknowledged for financial support. One of us (JG) would like to acknowledge NATO for a fellowship and the other (KS) the Lawerence Berkeley Lab. for a scholarship to work in France, at the laboratoire de Métallurgie Physique, Faculté des Sciences, Université de Poitiers.

CLIMB OF PRISMATIC LOOPS IN Cu-Al ALLOYS DURING IRRADIATION IN THE HVEM*

T. Kosel and J. Washburn
Inorganic Materials Research Division, Lawrence Berkeley Laboratory, &
Department of Materials Science & Engineering, College of Engineering,
University of California, Berkeley, California 94720

ABSTRACT

Nucleation and growth of prismatic interstitial loops was observed during irradiation in the HVEM at different temperatures and damage rates. The loops remained rhombus shaped throughout growth, with sides lying on {111} planes, suggesting low jog densities. Weak-beam electron micrographs showed that the loops were dissociated on the {111} planes containing the loop sides. A minimum damage rate, Φ_{min}, was found to be necessary to induce growth at measurable rates. This, together with the low jog densities observed, was taken to indicate that the climb rate was affected by the rate of jog nucleation, rather than controlled entirely by the rate of diffusion of point defects to the dislocations. Φ_{min} was found to be smaller for alloys of higher stacking fault energies, probably due to the influence of stacking fault energy on the energy of jog formation on an extended dislocation. The growth rate was found to be constant for individual loops observed over a large size range, suggesting that jog nucleation occurred preferentially at loop corners.

INTRODUCTION

It is generally accepted that the growth of voids in metals during irradiation requires the presence of dislocations, which absorb more interstitials than vacancies due to the stronger interaction of the larger strain fields of interstitials with dislocation strain fields. The dislocations climb at a rate determined by the difference between

*Supported by the U.S. Energy Research and Development Administration; partial support also provided by General Electric Foundation.

the absorption rates of interstitials and vacancies. If an energy barrier exists for the absorption of point defects at the dislocation core, the climb rate may be affected by the rate at which absorption occurs, rather than controlled only by the rate of diffusion of point defects to the dislocation.

The absorption or emission of point defects by a climbing dislocation requires the presence or nucleation of jogs, whose formation is more difficult in FCC metals of low stacking fault energy (γ) because of the splitting of perfect dislocations into a pair of Shockley partials separated by a ribbon of stacking fault. The formation of jogs on extended dislocations has been considered by several authors.[1,2,3] Calculations of the energy of completely extended jog pairs in Cu-7.5 wt.% Al (γ = 5 ergs per cm^2)[4] yield values of about 58 eV, depending on the estimate used for the energy of the closely spaced stair rod dipoles.[5] The energy of a double constriction on such a dislocation should be 107 eV. Thus, the formation of jogs on widely split dislocations is a difficult process; the exact mechanism is still unknown.

Theories of void formation[6] and of dislocation loop growth[7] in metals during irradiation generally assume diffusion controlled climb. In the present work evidence is presented which suggests that in FCC metals of very low stacking fault energy, climb may sometimes be affected by the rate of jog nucleation.

EXPERIMENTAL

Thin foils of Cu-Al alloys with 1.0, 3.5, and 7.5 wt.% Al were irradiated at 300°C and 450°C in an Hitachi Hu650 high voltage electron microscope operated at 650kV. The damage rate was varied by changing the excitation of the second condenser lens, and the beam current densities thus obtained were measured with a Faraday cup situated below the screen. Series of micrographs were taken during irradiation, and the loop growth rates were obtained from measurements of the loop sizes on contact prints.

OBSERVATIONS

Nucleation and growth of interstitial dislocation loops were observed over a range of temperatures. Although the maximum damage rate obtainable (about 1.5×10^{-4} dpa/sec with the beam focussed) was such that loops could not be nucleated above about 400°C, it was observed that loops nucleated at lower temperatures would still grow at 450°C at rather low damage rates, indicating that loop growth requires a lower supersaturation of point defects than does loop nucleation.

The loops observed were always rhombus-shaped prismatic loops with sides lying on {111} planes. Fig. 1 shows a typical set of loops grown at 300°C in a 110 foil of the 3.5 wt.% Al material. The correctly oriented Thompson tetrahedron is shown with the projected shapes of rhombus-shaped pure edge prismatic loops of all six a/2 <110> Burgers vectors. Type A, B, and C loops are out of contrast, since $\vec{g} \cdot \vec{b} = 0$. Type D and type E

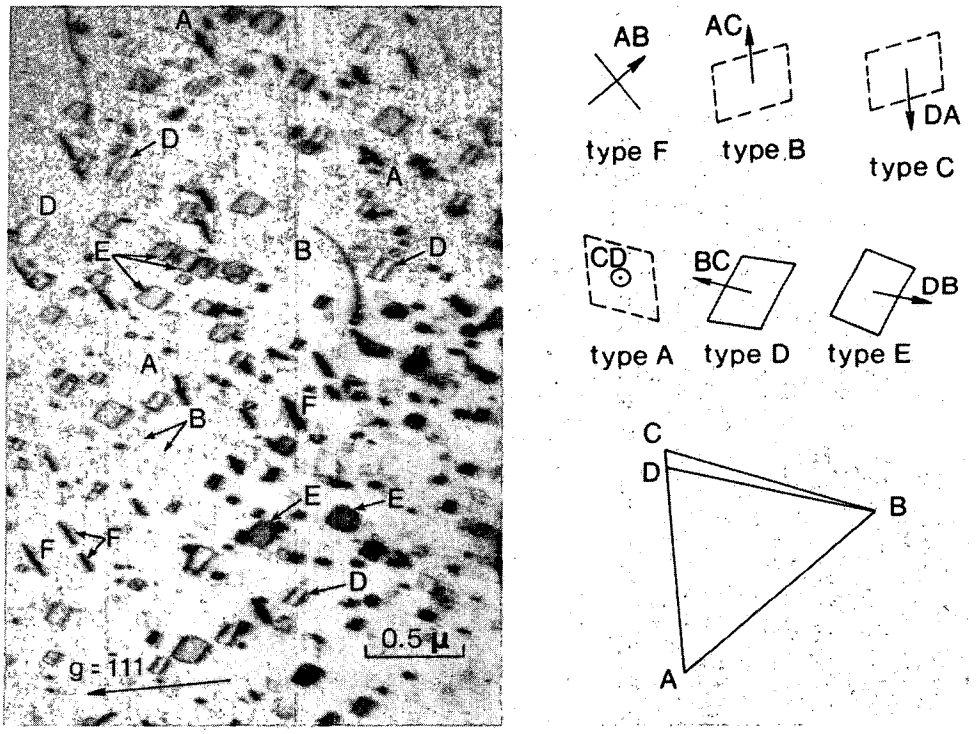


Fig. 1. Loops grown in Cu-3.5 wt.% Al at 300°C. The oriented Thompson tetrahedron and projected shapes of pure edge rhombus loops are shown.

loops each have a pair of sides, lying in the BCD {111} plane, which appear straight. Because the BCD plane is seen nearly edge on, this indicates that the dislocations have low jog densities, or at least equal densities of opposite-sign jogs. The curvature that appears on other sides is due to glide bowing of the side on the {111} plane.

A typical growth series, obtained using 0.081 amps/cm^2 (1.26 x 10^{-5} dpa/sec), is shown in Fig. 2. Notice that the loop sides which lie on inclined {111} planes are curved. Careful comparison of observed loop shapes with the projected shapes for pure edge loops indicates that the loops are generally rotated somewhat from the pure edge orientation, and that the curvature of the sides increases with increasing deviation from edge character. That the curvature of the sides is due to their being bowed out in their glide planes rather than to being heavily jogged is demonstrated in Fig. 3, which shows a loop with bowed sides which has slipped to the foil surface between micrographs. A slip trace is left which shows the intersection of the glide prism with the foil surface to be straight sided.

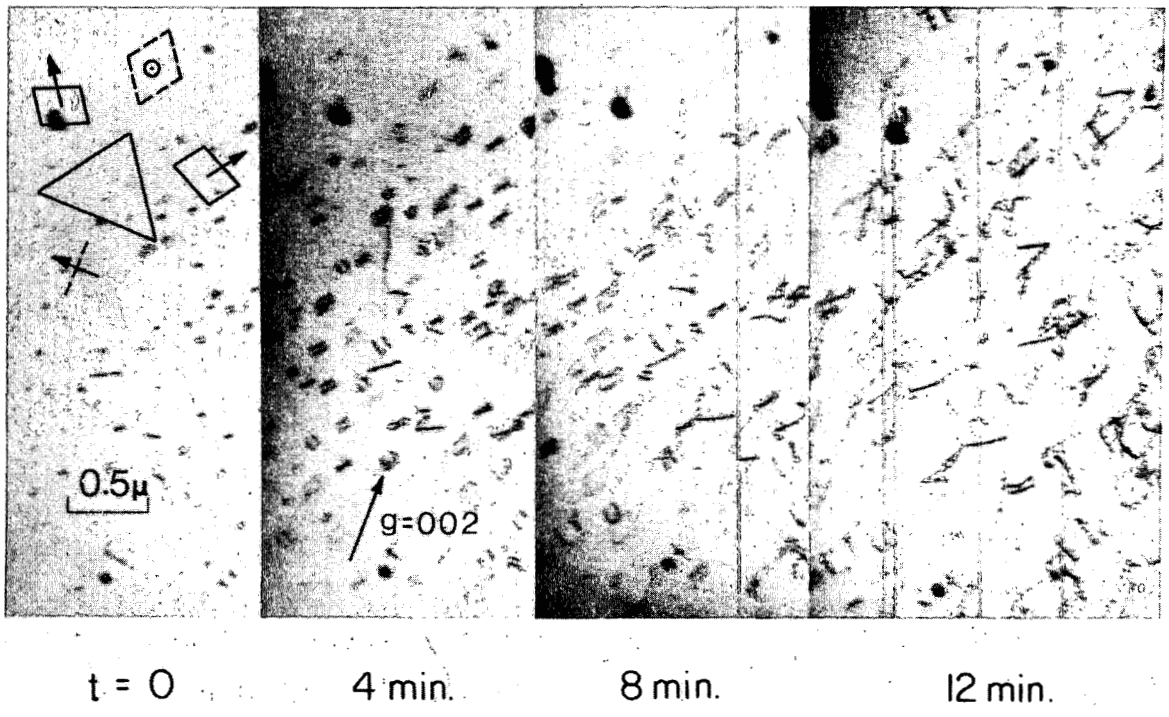


Fig. 2. Loops grown in Cu-3.5 wt.% Al at 300°C, 1.26 x 10^{-5} dpa/sec.

Loops were observed to grow at a constant rate. Fig. 4 shows the results of a preliminary determination of the dependence of the loop growth rate Γ on the beam current density Φ. It should be emphasized that the growth rates observed at the points at which the curves intersect the axis were negligibly small.

Fig. 5 shows a 650kV weak-beam image of a loop with both Shockley partials in contrast on the two sides lying in the inclined (111) planes. The splitting should not be visible on the other two sides since they lie in the nearly edge-on $(\bar{1}11)$ planes. This is a 110 foil of Cu-7.0 wt.% Al; $\vec{g} = 1\bar{1}3$; $\vec{b} = a/2\ [01\bar{1}] \rightarrow a/6\ [\bar{1}2\bar{1}] + a/6\ [11\bar{2}]$. A partially constricted superjog, about 46 Å high, is seen on one side, and it is also seen that the corners are at least partially constricted.

Isolated dislocations initially present in the foil were often observed to climb into helices with straight sides also lying in {111} planes, as in Fig. 2. The helices increased their diameters at about the same rate as the loops.

DISCUSSION

The observation (Fig. 4) that loop growth ceases below a certain beam current density indicates that there is an activation barrier for the absorption of interstitials by the loops. The supersaturation of interstitials was calculated using the model of Foreman,[8] and the partial molar free energy was found to be about 2 eV per interstitial even at 450°C and 0.01 amps/cm^2. Since this is much less than the energies calculated for extended jogs or for constrictions, jog nucleation must proceed via some intermediate configuration with an energy not much larger than 2 eV. Since weak-beam observations of the loops show that they do remain widely split while climbing, it is to be expected that the activation energy required will depend on the stacking fault energy through its effect on the width of splitting. The observation that lower supersaturations of interstitials are required to induce growth at 450°C of the less widely split loops in the lower Al content alloys implies that the activation barrier for growth is smaller in alloys of larger stacking

fault energy, as expected. Since the jog nucleation rate should depend on the number of nucleation sites on a loop, the observations of constant growth rate and very low jog density suggest that jogs may be preferentially nucleated at loop corners rather than along the loop sides. This might be expected if the corners are constricted, as they appear to be (Fig. 5).

The rotation of the loops was attributed to the presence of shear stresses in the foil. These stresses were estimated by measuring the radius of curvature of the loop sides. Calculations of the rotations to be expected due to such stresses, based on Bullough and Foreman's[9] expression for the total energy of a loop, predicted consistently larger rotations than those observed. However, in weak-beam micrographs the partial on the convex side was usually more curved than the other. When the partials are not resolved, this could lead to an overestimate of the curvature, and therefore of the stress acting on the loop.

REFERENCES

1. J. P. Hirth and J. Lothe, Theory of Dislocations, p. 531, McGraw-Hill Book Co., New York, 1968.
2. J. Friedel, Dislocations, chapter 6, Pergamon Press, Oxford, 1964.
3. R. M. Thomson and R. W. Balluffi, J. Appl. Phys. 33, 803 (1962).
4. D. J. H. Cockayne (Electron Microscope Unit, The University of Sydney, Sydney, Australia), private communication (February 1975).
5. T. Kosel, Irradiation Induced Dislocation Climb in Cu-Al Alloys of Different Stacking Fault Energies (Ph.D. Thesis, University of California, Berkeley), LBL-3590 (June 1975).
6. S. D. Harkness and Che-Yu Li, Met. Trans. 2, 1457 (1971).
7. M. Kiritani, N. Yoshida, H. Takata, and Y. Maehara, J. Phys. Soc. Japan 38, 1677 (1975).
8. A. J. E. Foreman, Rad. Effects 14, 175 (1972).
9. R. Bullough and A. J. E. Foreman, Phil. Mag. 9, 314 (1964).

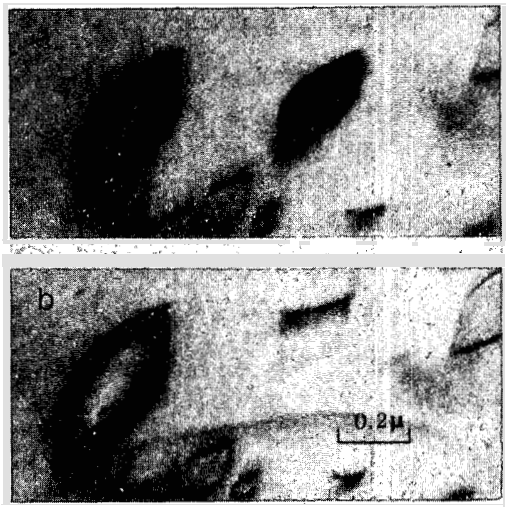


Fig. 3. A loop which slips to the foil surface leaving a straight-sided slip trace.

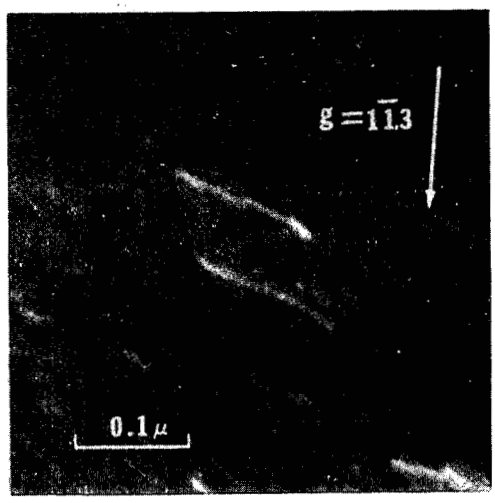


Fig. 5. 650kV weak-beam image of a loop with a partially constricted superjog.

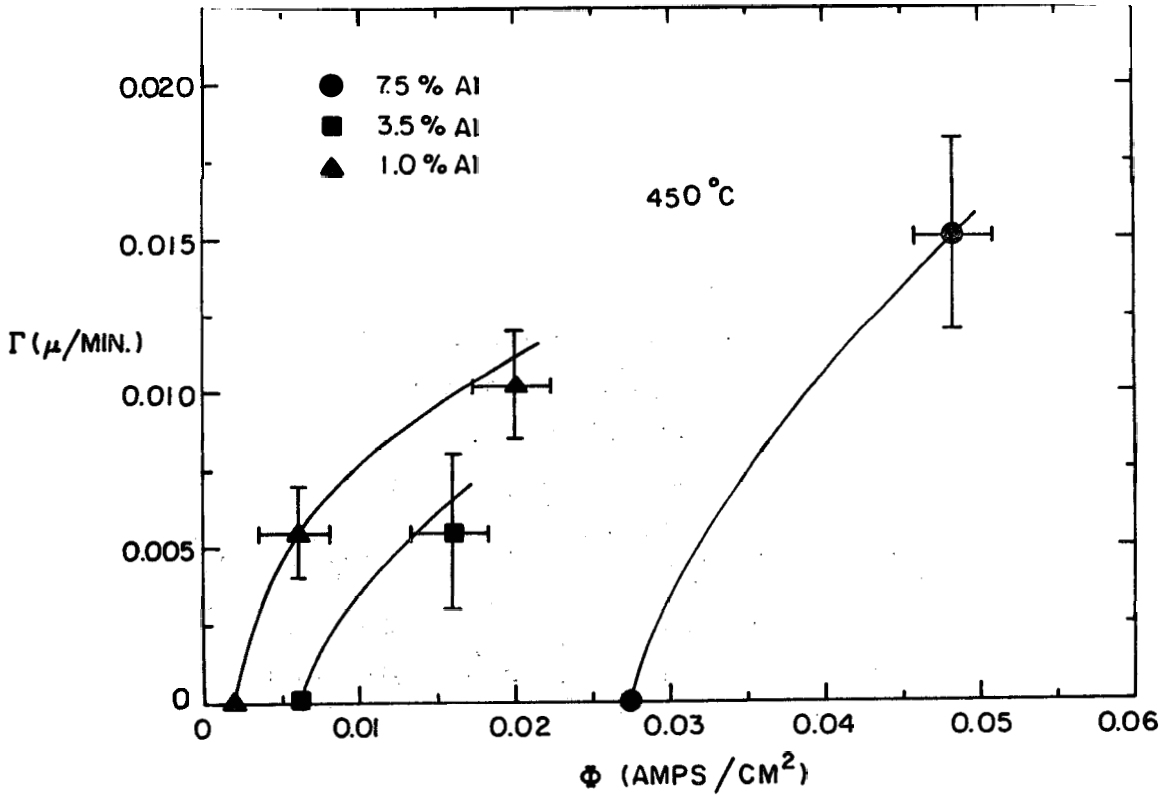


Fig. 4. Loop growth rate (Γ) versus beam current density (Φ) at 450°C.

THE BEHAVIOUR OF COLLISION CASCADES AT ELEVATED TEMPERATURES IN COPPER AND MOLYBDENUM CRYSTALS

C.A. English, B.L. Eyre, *J. Summers and H.Wadley
A.E.R.E., Harwell, Didcot, Oxfordshire, England.
*School of Maths. and Physical Sciences, Univ. of Sussex, Brighton, England.

ABSTRACT

Self-ion irradiation has been used to study the collapse of displacement cascades in pure copper, and molybdenum in the temperature range 20°C - 500°C. In 30 KeV self-ion irradiation of copper the number of vacancy loops formed from the cascades was observed to remain constant at temperatures below 300°C but to decrease sharply at temperatures above this. In 60 KeV self-ion irradiation of molybdenum a gradual decrease in the number of vacancy loops was observed above 200°C, an order of magnitude decrease occurring by 500°C. The variation in numbers is compared with the predictions of a model which considers only thermal vacancy emission from the loops. This was found to give very good agreement for the copper results but not for the molybdenum results. Preliminary results are also reported on the effect of temperature on the Burgers vectors of the vacancy loops and on 60 KeV self-ion irradiation of nickel.

INTRODUCTION

Void swelling in fast reactor core materials had demonstrated the importance of understanding damage structures generated in metals during elevated temperature irradiation. A particularly important question concerns the extent to which displacement cascades collapse to form vacancy loops at elevated temperatures and how they affect the formation and growth of voids. A convenient method of studying this aspect is to irradiate metals with self-ions having energies in the range for primary recoils produced during neutron irradiation, i.e. 1 - 200 KeV[1]. This approach has been adopted in the present work in which the effect of irradiation temperature on vacancy loop survival has been studied in two fcc metals, Cu and Ni and a bcc metal, Mo.

EXPERIMENTAL PROCEDURE

The experiments were carried out on specimens cut from single crystals, the specimen normals being <110> and <123> for copper, <110> for molybdenum and close to <110> for nickel. The techniques used in preparing the copper and molybdenum crystals and their purity has been discussed elsewhere[1]. The nickel crystal, obtained from Metals Research Ltd. was 4N pure. Thinned foils of each material were irradiated in either the Harwell Heavy Ion Accelerator or in the Harwell Lintott Separator. In the former the error limits on quoted temperatures were $\pm$ 25°C and in the latter $\pm$ 5°C.

Following irradiation at room temperature, specimens of all three materials contained a uniform distribution of vacancy defects and the principal objective of the electron microscope studies was to determine the influence of irradiation temperature on defect geometry, number density, N_d and size distribution. Two methods were used in determining the Burgers vectors of loops. The first was the so-called $\underline{l}$ analysis involving measurements of the directions of black-white streaking of dynamical images from small loops[2]. This method is known to be valid for Frank loops in copper but breaks down when applied to perfect loops particularly in more isotropic cubic crystals such as molybdenum. The second and more positive method, which we used in particular for molybdenum, was to compare the symmetry of dynamical black-white images obtained under well-defined two beam diffracting conditions with theoretically simulated images from known loops in an isotropic cubic crystal[3].

RESULTS

Considering first the results from copper irradiated with 30 KeV self-ions to a dose of 1×10^{12} ions cm^{-2}. Fig. 1 shows how N_d varies with irradiation temperature in <123> foils in the range 20-425°C. The defect counts were carried out on micrographs obtained with $\underline{g} = (200)$, $w_g = 0$ at a foil normal $\underline{Z} = [023]$. It can be seen that N_d remains constant up to 300°C and then decreases by about an order of magnitude between 300 and

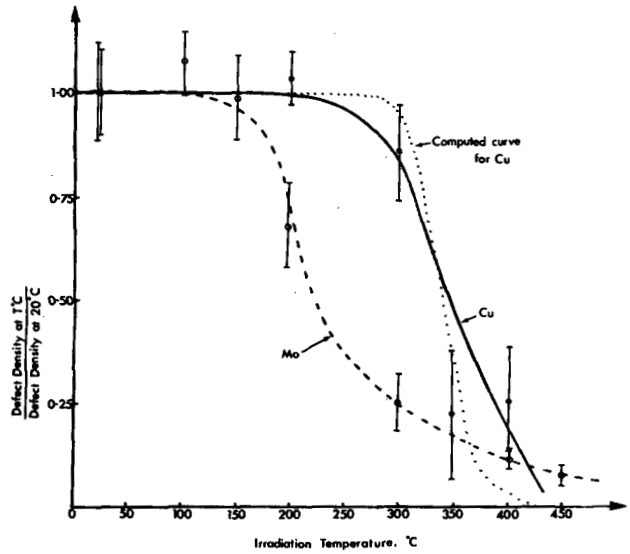


Fig. 1. Graph of the change in loop number density, versus irradiation temperature for self ion irradiation of Cu and Mo.

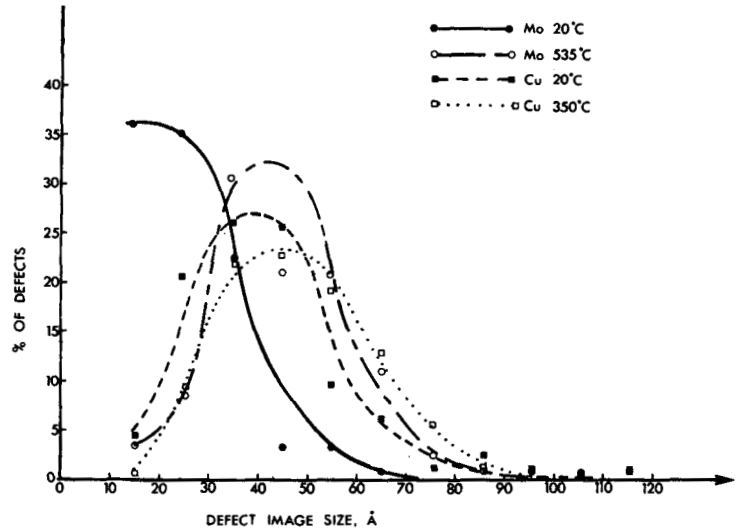


Fig.2. Defect image size for self-ion irradiation of Cu and Mo at elevated temperatures.

425°C. The image diameters were measured on large micrographs obtained with $g = (1\bar{1}1)$, $w_g < 1$, and $\underline{Z} = \langle 134 \rangle$. Fig. 2 shows the image size distributions based on measurements of 300 defects for specimens irradiated at room temperature and 350°C. A shift in the distribution towards larger image sizes occurs in the 350°C foils. This is reflected in the average image diameter which increases from 46 Å at 20°C to 55 Å at 350°C.

A preliminary assessment of the defect geometry in <123> foils was carried out by applying the $\underline{l}$ analysis to dynamical black-white images on micrographs obtained with $\underline{g} = (1\bar{1}1)$ and $\underline{g} = (220)$. The results showed that in the specimens irradiated at room temperature $\underline{l}$ for 97% of the loops lies along one of the <111> directions but as the irradiation temperature increased an increasing fraction of the images had $\underline{l}$ along <110> or some direction between <111> and <110>. Because of uncertainties in the interpretation of results from a simple l analysis, more detailed studies are being made of defects in <110> and <123> foils by combining measurements of $\underline{l}$ using different

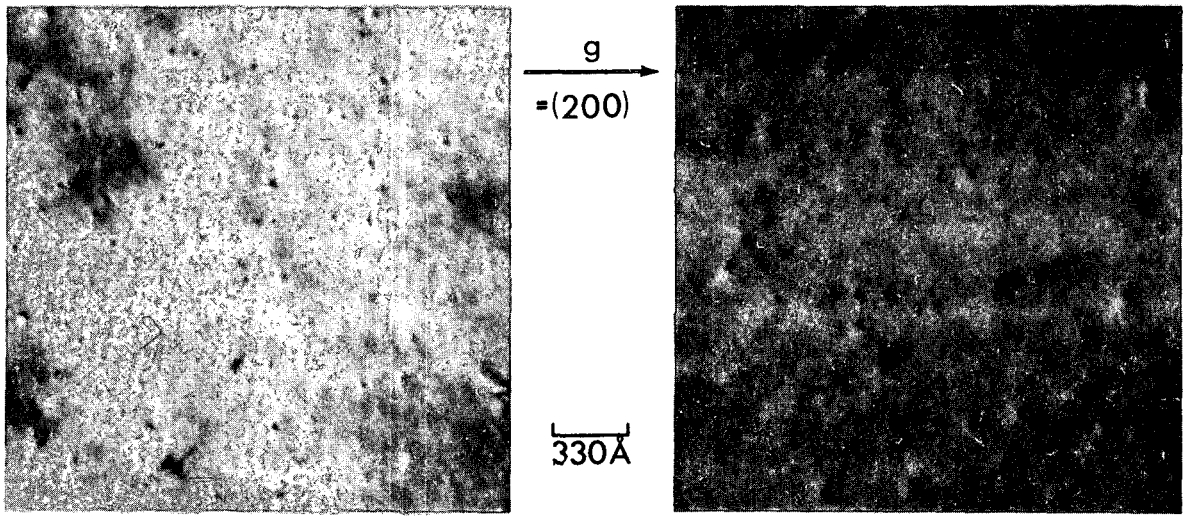


Fig. 3. Micrographs of foils irradiated at 350°C with 6×10^{11} 30 KeV Cu^+ ions/cm^2, (a) <011>, (b) <123>.

diffraction conditions as defined by $\underline{g}$ and $\underline{Z}$ with an examination of image symmetry. The results of such an analysis on <110> and <123> foils irradiated at 350°C have led to conclusions which differ in two respects to the indications from the preliminary survey. Firstly, as shown in Fig. 3, stacking fault tetrahedra and dissociated Frank loops can be identified in foils of both orientations. Secondly, the more comprehensive analysis did not show any evidence for perfect loops being present in foils irradiated at 350°C.

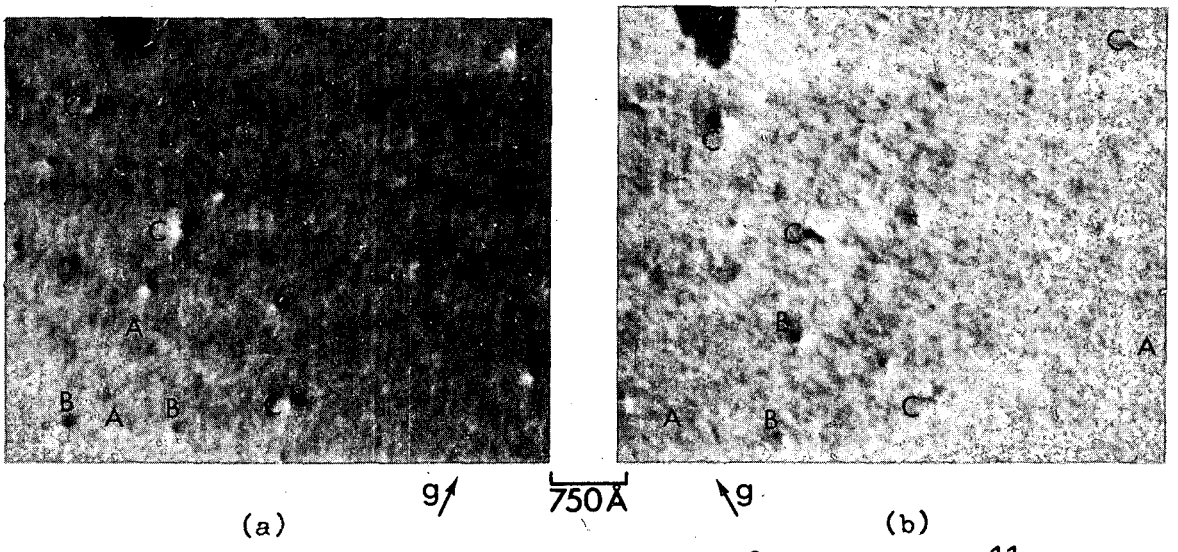


Fig. 4. Micrographs of foils irradiated at 350° with 7.4×10^{11} 60 KeV Mo^+ ions/cm^2, (a) $g = (2\bar{1}1)$, (b) $g = (21\bar{1})$.

Turning now to the results from the irradiation of molybdenum with 60 KeV Mo^+ ions to a dose of 7.4×10^{11} ions cm^{-2} in the temperature region 20°C - 535°C. The variation in N_d with irradiation temperature is included in Fig. 1 and it can be seen that in contrast to copper, N_d starts to fall between 150 and 200°C and has decreased by about an order of magnitude at 450°C. The Burgers vectors of loops were analysed using micrographs obtained with $\underline{g} = \pm (2\bar{1}1)$ or $\underline{g} = \pm (21\bar{1})$ at Z close to <011> and matching the symmetry of black-white images with that of theoretically computed images from known edge loops[3]. In the foils irradiated at high temperatures, >400°C, a good correspondence was obtained between a large proportion of the observed images and computed images for the two sets of perfect edge loops having $\underline{b}$ lying in the foil plane, i.e. $\underline{b} = \pm \frac{a}{2}[\bar{1}1\bar{1}]$ or $\underline{b} = \pm \frac{a}{2}[11\bar{1}]$. In these cases $|\underline{g}.\underline{b}| = 0$ or 2 for the two $\underline{g}$'s used and the images are easily identified as shown by the examples labelled A and B in Fig. 4. However, a number of the images are distorted from these ideal configurations(examples are labelled C in Fig. 4). Applying the results from calculation by Haussermann et al[4], we deduce that these distorted images are from non-edge perfect loops. Examination of the occurrence of such distorted images as a function if irradiation temperature has led to the general conclusion that the loops from initially on $\{110\}$ but shear to a perfect configuration at an early stage. However, they can only rotate to a pure edge configuration during irradiation at elevated temperatures. It is emphasised that we have obtained no evidence for loops having $\underline{b}$ other than $\frac{a}{2}$<111>.

The image size distribution for specimens irradiated at room temperature and 535°C is shown in Fig. 2 and this was obtained from measurements of 200 defects imaged with $\underline{g} = (01\bar{1})$, $w_g \leq 1$ at a foil normal of <155>. The average diameter increases from 27.7 Å at 20°C to 41.5 Å at 535°C.

Lastly, preliminary measurements have been made of the defect density in nickel irradiated with 60 KeV Ni^+ to a dose of 6×10^{11} ions cm^{-2} at temperatures between 20°C and 475°C. The results show that there is no significant decrease in N_d below 300°C but defects were not observed in specimens irradiated at 475°C. It is also interesting to note that some dissociation of the Frank loops towards stacking fault tetrahedra was

observed in foils irradiated at 200°C.

DISCUSSION

The results have exposed two important aspects of how temperature influences cascade collapse in fcc and bcc metals. The first is the fundamental difference that exists between copper and molybdenum regarding the temperature dependence of vacancy loop survival. The second is the effect irradiation temperature has on defect geometry.

Considering first the decrease in N_d with increasing irradiation temperature, the copper results can be accounted for by a simple thermal emission model. In this model it is assumed that cascade collapse to form loops is athermal and thus we can define a loop generation rate K_L which is simply the product of dose rate and defect yield, i.e. the number of loops formed per incident ion. The defect yield in self-ion irradiated copper at room temperature is 0.3[5]. This generation rate is then balanced against the loss rate of loops due to shrinkage by thermal vacancy emission. The rate equation for this latter process is -

$$\frac{dr_L}{dt} = \frac{-2}{b} D_s \exp \frac{(\gamma + F_{el})}{kT} B^2 \qquad (1)$$

where D_s is the self diffusion coefficient, γ is the stacking fault energy of faulted loops, F_{el} is the elastic self energy of the loop and B^2 is the cross sectional area of a vacancy. The experimentally measured values of N_d represents the number of visible loops, i.e. those having a radius greater than the minimum visible radius, r_{min} = 10 - 15 Å. Thus, we can calculate the time t_L, taken for the loops to shrink from an initial mean radius r_o (determined from the room temperature irradiated specimens) to r_{min} by integrating Eq. (1), i.e.

$$t_L = \frac{-b}{2 D_s} \int_{r_o}^{r_{min}} \exp - \frac{(\gamma + F_{el}) B^2}{kT} dr \qquad (2)$$

Then the calculated loop numbers at any temperature T is given by $(N_d)_T = K_L (t_L)_T$. We show in Fig. 1 the calculated variation in N_D with

irradiation temperature for copper and the striking feature is the close agreement with the experimental results. Although the N_D versus temperature data from nickel is incomplete, it would appear again that they can be accounted for by a thermal emission model.

With regard to the results from molybdenum, it is clear that the decrease in N_d at temperatures as low as 200°C cannot be accounted for by a thermal emission model. It is emphasised that the form of the N_d versus temperature curve is similar to that obtained by Bentley[6] from neutron irradiated molybdenum. We can therefore rule out any explanation that involves the close proximity of a free surface. A particularly important feature of Bentley's results is that the vacancy loop population is replaced by a fine distribution of voids. Moreover, in the present experiments we observed that the mean loop radius increases with increasing irradiation temperatures. Thus, we conclude that the reduction in N_d is not due to increased recombination of interstitial with vacancies in the cascade. Rather, we believe that the observed behaviour is a consequence of a temperature dependence in the cascade collapse process itself in bcc metals. An important factor in this may be the extremely high stacking fault energy characteristic of molybdenum and other bcc metals, so that when the vacancy migration temperature has been achieved the cascades break up rather than collapse, thus releasing the vacancies for void formation. Clearly this fundamentally different behaviour in bcc metals is of considerable importance and needs to be explored more thoroughly.

The question of the effect of irradiation temperature on the loop geometry is obviously quite complicated. However, a fundamental difference has been seen between the behaviour of loops in copper and molybdenum. In the bcc molybdenum the loops unfault at room temperature and the effect of increasing the irradiation temperature is to cause the loops to rotate to the pure edge configuration. In copper the loops remain faulted and at elevated temperature the dissociation of the Frank loops can result in complete stacking fault tetrahedra, in agreement with the work of Schindler[7]. The results of the irradiation at 350°C suggest that the surface influences the dissociation of the Frank loops in copper. In molybdenum the complete analysis, to be reported elsewhere, suggest that the surface influences

which particular perfect loop the $\{110\}$ loops unfault to.

REFERENCES

1. C.A. English, B.L. Eyre, H. Wadley, A.Y. Stathopoulos, The Effect of Solute Atoms on Collision Cascades in Copper and Molybdenum Irradiated with Self Ions, Proc. of this Conference.
2. M. Rühle, Phys. Stat. Sol., 19, 263 (1967); ibid, 19, 279 (1967).
3. B.L. Eyre, D.M. Maher and R.C. Perrin, Proc. 8th International Congress on Electron Microscopy, Canberra, 1, 436 (1974).
4. F. Haussermann, M. Rühle and M. Wilkens, Phys. Stat. Sol., 50, 445 (1972).
5. C.A. English, B.L. Eyre and J. Summers, Influence of Irradiation Temperature on Self Ion Damage in Copper, AERE R 7960 (1975).
6. J. Bentley, D. Phil. Thesis, Univ. of Birmingham (1974).
7. R. Schindler and M. Wilkens, unpublished work.

THE EFFECT OF SOLUTE ATOMS ON COLLISION CASCADES IN COPPER AND MOLYBDENUM IRRADIATED WITH SELF-IONS

C.A. English, B.L. Eyre, H. Wadley and *A.Y. Stathopoulos
A.E.R.E., Harwell, Didcot, Oxfordshire, England.
*Department of Metallurgy, University of Oxford, Oxon, England

ABSTRACT

This paper reports an examination of the effect material purity has on the numbers and sizes of the vacancy loops formed in collision cascades produced by self-ion irradiation of copper and molybdenum. It is shown that substitutional and interstitial impurities both markedly reduce the damage generated in molybdenum by 60 KeV Mo^+ ions but little effect is seen in copper irradiated by 30 KeV Cu^+ ions. These results are compared with recent observations of vacancy defects in type 316 stainless steel following irradiation with 40-200 KeV Cr^+.[1] The comparison highlights the much lower vacancy concentration retained in visible clusters in the complex alloy.

INTRODUCTION

Damage calculations[2,3] show that 95% of the point defects produced in a metal of intermediate mass, i.e. atomic weight 50-100, during neutron irradiation in a typical reactor spectrum are generated by primary recoils having energies in the range 5-200 KeV. A convenient method of simulating the collision cascades produced by such recoils is to irradiate specimens in an accelerator with self ions in the relevant energy range. This approach has been widely used together with electron or field-ion microscopy to study the vacancy rich centres of cascades and their collapse to form vacancy loops in a number of bcc and fcc metals (for a recent review see Eyre[4]). However, the influence of metallurgical parameters, such as purity, on vacancy survival in the cascades and the collapse process has received little attention. In this paper we report some preliminary results from a series of experiments aimed at determining the effect of interstitial and substitutional solutes on vacancy survival and loop formation in cascades. The experiments were carried out on single crystals of copper and molybdenum both in the pure and alloyed states.

EXPERIMENTAL PROCEDURE

The experiments were carried out on specimens cut from single crystals. The crystal orientation was generally close to <011> for both materials. The high purity copper was grown from the melt using the Bridgeman technique and was shown by activation analysis to contain <2 ppm oxygen and <1 ppm of carbon. A crystal of copper was doped with oxygen by introducing a low partial pressure of spec. pure gas into the furnace during growth of the crystal. The copper aluminium crystal was grown from a homogenised melt by the Bridgeman technique. The high purity molybdenum was purified by successive zone refining and then decarburised by holding it for 11 hours at a temperature of 1860°C in a partial pressure of 6×10^{-5} torr of oxygen followed by a vacuum ($<10^{-7}$ torr) anneal at 1800°C. The final resistivity ratio (293°K/4.2°K) was 10,300 ± 1000. Crystals of differing purity were prepared by either varying the number of zone passes which increases the level of substitutional impurities or by doping high purity crystals with carbon and nitrogen[5].

Discs 3 mm diameter and 0.5 mm thick were spark cut and then prepared for electron microscopy by first jet polishing and then electropolishing until perforation occurred. The thinned foils were irradiated in either the Harwell Heavy ion accelerator or in the Harwell-Lintott separator. The copper specimens were stored in high vacuum ($\sim 10^{-6}$ torr) until they were observed in the electron microscope.

The electron microscopy studies of the irradiated specimens aimed primarily at determining the influence of purity on the number and sizes of the collapsed vacancy clusters. Particular emphasis was placed on obtaining micrographs from each material under standard imaging conditions, so as to eliminate as far as possible, the way in which the microscopy was carried out as a variable. The defects were imaged using two beam conditions with various diffraction vectors both at the Bragg condition, i.e. $w_g = 0$, and at a positive deviation, i.e. w_g 0.5 - 1.0. At the Bragg condition defects lying within 1.6 ξ_g of the surface exhibit dynamical black-white images easily distinguished against background and which are therefore suitable for defect counting. With $w_g > 0.5$ the diffracting

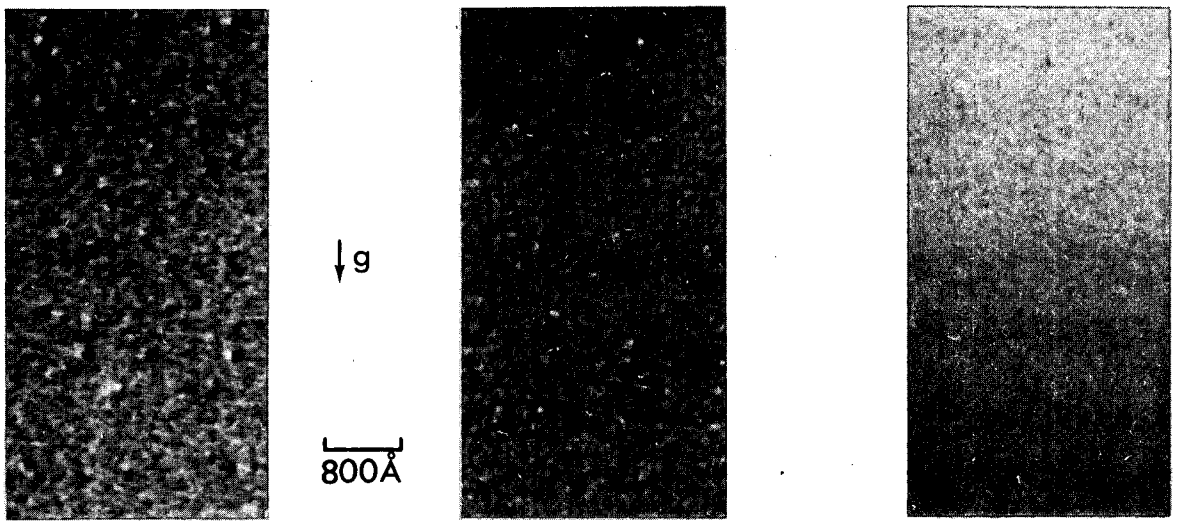


Fig. 1. Damage generated in molybdenum by 7.4×10^{11} 60 KeV Mo^+ ions cm^{-2}, (a) 4 PZR, (b) 1 PZR, (c) 4 PZR + 17 ppm N_2.

conditions are psuedo kinematical and the defects appear as black dots which are particularly suitable for measuring size distributions.

RESULTS

We present first the observations of damage in molybdenum of three purities following irradiation with 60 KeV Mo^+ ions to a dose of 7.4×10^{11} ions cm^{-2}. The experiments were carried out on four pass zone refined (4 PZR) molybdenum both before and after doping with nitrogen to a level of 17 atom ppm (4 PZR + 17 ppm N_2) which was retained in interstitial solid solution by quenching and on 1 PZR molybdenum which has a significantly higher substitutional solute level[5]. The defect number densities, N_d and size distribution in all three materials were measured on micrographs obtained with $\underline{g} = (0\bar{1}1)$ and $w_g \sim 0$ or ~ 1.0. The results were used to calculate mean defect sizes the defect yield, defined as the number of visible defects per incident ion, and cascade efficiency defined as the fraction of vacancies surviving to form a loop in each cascade. In calculating the latter parameter the mean number of vacancies generated in the cascades was calculated using the damage model proposed by Norgett et al[6].

Micrographs showing qualitatively the change in defect population with

TABLE 1. Results from 60 KeV Mo^+ irradiation of molybdenum.

Purity	Mean Defect size	Defect yield / Defect yield for 4 PZR Mo	Cascade Efficiency
High Purity (4 PZR)	27.7 Å	1.00	70%
Low Purity (1 PZR)	26.9 Å	0.32	64%
Nitrogen Doped (4 PZR + 17 ppm nitrogen)	19.2 Å	0.20	35%

purity are presented in Fig.1. The image size distribution are presented in Fig. 2 while the quantitative parameters are summarised in Table 1. It can be seen that there is a considerable decrease in both defect yield and cascade efficiency with decreasing purity.

Most recently experiments using the same irradiation conditions have been carried out in molybdenum doped with carbon again retained in interstitial solution. The micrographs presented in Figs. 3a and b show examples

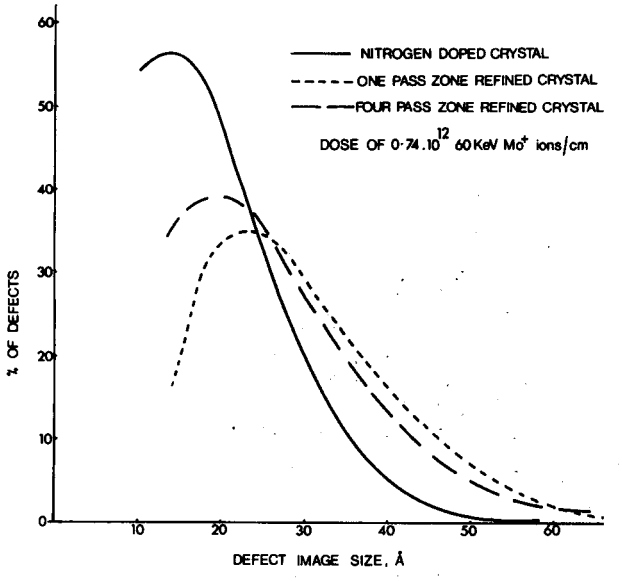


Fig. 2. Image size distribution for three purities of molybdenum irradiated with 7.4×10^{11} 60 KeV Mo^+ ions cm^{-2}.

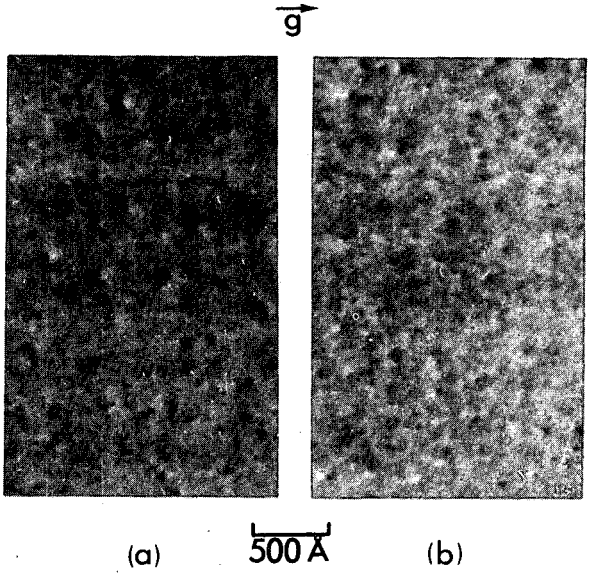
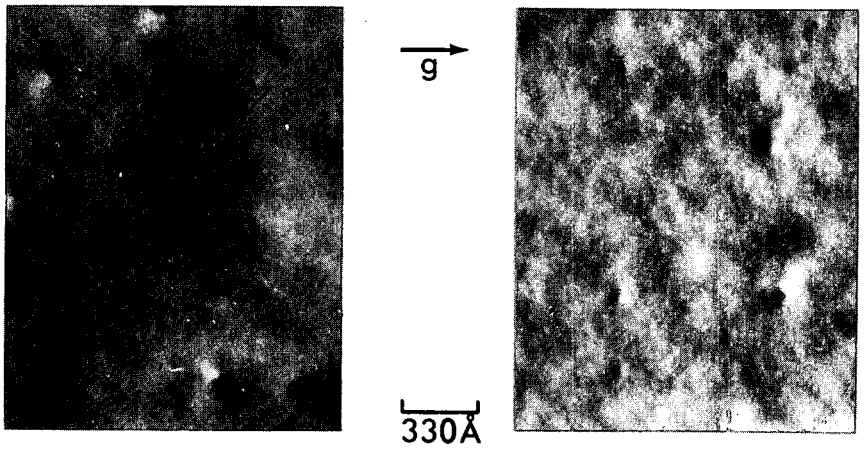


Fig. 3. Damage generated by irradiation with 5×10^{12} 60 KeV Mo^+ ions cm^{-2} in high purity molybdenum doped with carbon, (a) 65 atom ppm, (b) 270 atom ppm.

of the damage structure in two molybdenum specimens doped with 65 atom ppm (3a) and 270 atom ppm carbon (3b). Comparison with Fig. 1 shows that the effect of doping with carbon is qualitatively the same as for doping with nitrogen, the defect numbers and sizes decreasing with increasing solute content. However, quantitative analysis has shown that carbon has a smaller effect than nitrogen reducing the defect yield by a factor of 2 and the mean defect size by 30% in the higher carbon material.

The experiments on copper were carried out on pure material, copper doped with 600 atom ppm oxygen and a series of copper-aluminium alloys containing up to 10% aluminium. The irradiations were carried out with 30 KeV self ions to a dose of 2×10^{11} 30 KeV Cu^{+} ions cm^{-2}. In contrast to molybdenum the addition of these impurities to copper was found to have no significant affect on the quantitative defect parameters. This is illustrated qualitatively by the micrographs present in Fig. 4a and b which are of pure copper and copper-10% aluminium. The observations of the irradiated copper aluminium alloys has shown that the reduction in the stacking fault energy has resulted in an increased tendency for the Frank loops to undergo further dissociation towards stacking fault tetrahedra.



(a) (b)

Fig. 4. Comparison of the damage generated by irradiation with 2×10^{11} 30 KeV Cu^{+} ions cm^{-2} in (a) High purity Cu, (b) Cu-10% Al.

DISCUSSION

The results reported in the preceding section have clearly shown two contrasting features concerning the damage generated in molybdenum and copper crystals of given orientations during self-ion irradiation. On the one hand, in molybdenum the number and sizes of the vacancy loops are sensitive to the presence of low levels of both interstitial and substitutional impurities. In complete contrast the vacancy damage in copper is relatively insensitive to the presence of the two impurities.

A comparison of the damage structure in the series of copper specimens with that in type 316 stainless steel following irradiation with 40-200 KeV Cr^+ indicates that the lack of sensitivity in the damage structure to impurity content in the former is not simply a consequence of crystal structure. This is illustrated by Fig. 5 which shows the damage structure in copper irradiated with 30 KeV Cu^+ and in 316 steel irradiated with 40 KeV Cr^+. It is immediately obvious that both the number and sizes of the visible defects are appreciably higher in copper even though the incident ion energy and total dose are appreciably lower than in the steel. In the latter, obviously both the alloy and impurity elements have a strong influence on the number of vacancies surviving in loop form. This is confirmed by the fact that ageing solution treated material at 750° to remove the carbon from solution by precipitation increases the sizes of the defects produced by a given irradiation. More specifically the reduction in the

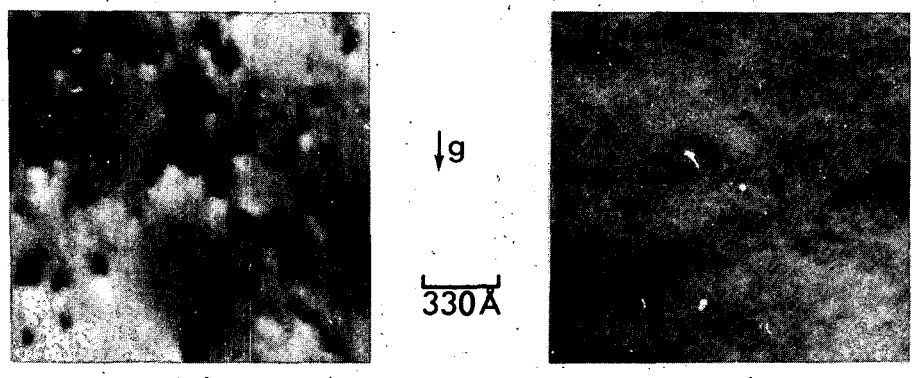


Fig. 5. Damage created in (a) copper irradiated with 1.0×10^{12} 30 KeV Cu^+ ions cm^{-2} and (b) Type 316 stainless steel irradiated with 5.0×10^{12} 40 KeV Cr^+ ions cm^{-2}.

level of carbon was estimated to be from 2,800 atom ppm in the unaged material to 230 atoms ppm in the aged. The mean defect size increased by 30% in the aged material although the defect yield did not appreciably change.

The explanation for these results may lie in the influence exerted by impurities on the distances over which interstitials are transported away from the cascades by focussed collision sequences. More specifically, we can argue that the strain fields associated with some atoms are responsible for defocussing focussed collision sequences and thus increasing the probability of recombination with the vacancies. This is consistent with interstitial solutes such as carbon and nitrogen, which have comparatively large misfit strains, having a significant effect. However, the present observations cannot rule out that the impurities may be influencing the number of vacancies participating in the collapse to loops in the cascade. We envisage that collapse could be inhibited if the vacancies in the cascade were trapped by impurities cascade.

It is hoped that by varying the size and mass of the alloying element in the copper some insight will be gained into the parameters controlling the effect of substitutional solutes. Similarly by varying the concentration of the interstitial solutes in molybdenum it is hoped to gain further information on their effect on the vacancy loops formed from the cascade.

REFERENCES

1. C.A. English, B.L. Eyre, K. Shoaib and T.M. Williams, J. Nucl. Matl. in press.
2. A.D. Marwick, The Primary Recoil Spectrum in the Simulation of Fast Neutron Radiation Damage by Charged-Particle Bombardment, AERE-R 7745 (May 1974).
3. C.M. Logan, J.D. Anderson, Z.A. Munir, Nucl. Tech. 22, 36 (1974).
4. B.L. Eyre, J. Phys. F., 3, 422 (1973).
5. D.J. Capp, D.Phil. Thesis, Univ. of Oxford, (1975).
6. M.J. Norgett, M.T. Robinson and I.M. Torrens, A Proposed Method for Estimating the Number of Atomic Displacement in Irradiated Metals, T.P. 494, (Sept. 1972).

HIGH TEMPERATURE NEUTRON IRRADIATION DAMAGE IN MOLYBDENUM

J. Bentley*
Department of Physical Metallurgy, University of Birmingham, England

B. L. Eyre
Metallurgy Division, A.E.R.E., Harwell, Oxfordshire, England

M. H. Loretto
Department of Physical Metallurgy, University of Birmingham, England

ABSTRACT

Molybdenum of 2 purities and a molybdenum alloy (TZM) have been irradiated at temperatures in the range 330°C to 850°C to fluences of 1 and 3 x 10^{20} fission n . cm^{-2}. A detailed transmission electron microscopy (TEM) study has been made of the damage structures. The dislocation substructures coarsen from one of rafts plus small vacancy loops to mainly network dislocations as the irradiation temperature increases, being distributed most coarsely in the purest material. Voids are observed at all irradiation temperatures coarsening in the usual way with increasing irradiation temperature, but shrinking with increased fluence. Several important effects are highlighted including those of material purity and irradiation temperature upon the raft distributions, the effect of irradiation temperature upon the vacancy loop population and the effect of irradiation temperature and fluence upon the void distributions.

INTRODUCTION

The behaviour of the damage structure in molybdenum neutron irradiated at 77 and 473°K was shown in a detailed and systematic series of experiments to depend sensitively on material purity and irradiation conditions[1-5]. A study of the recovery of these structures on post-irradiation annealing again revealed a strong dependence on these parameters as well as annealing conditions. From this series of experiments a clear picture of the behaviour of the interstitial component emerged. The experiments have been extended to higher irradiation temperatures[6-8] in order to gain a better understanding of the development of the vacancy component of the damage.

*Present address: Metals and Ceramics Division, Oak Ridge National Laboratory, Oak Ridge, Tennessee 37830 USA.

EXPERIMENTAL

The starting material for this investigation was "Climelt" arc-cast molybdenum rod and TZM alloy rod supplied by the Climax Molybdenum Company. From the molybdenum rod 4 pass zone refined high-purity single crystals (4PZR Mo) were grown and, together with the as-received (AR Mo) material, were annealed in high purity oxygen to reduce the carbon content to <0.1ppm and finally annealed at 1800°C for 3 hours at 10^{-8} torr. The TZM specimens were given a recrystallization anneal of one hour at 1600°C. The materials were fully characterized by electron microscopy, spark source mass spectrometry, and gamma activation techniques. Disc specimens of all 3 materials were irradiated at 330, 475, 575, 650, 750 and 850°C to integrated fluences ~1 and ~3 x 10^{20} fission neutrons cm^{-2} in the PLUTO reactor at AERE Harwell. Specimens were packed in molybdenum tubes and these, together with iron flux monitors, were sealed under one atmosphere of helium in stainless steel containers. The containers were mounted in fully instrumented irradiation rigs which were equipped with heaters and loaded into hollow fuel elements. The temperatures of the containers were monitored continually by thermocouples and were constant to within ± 5°C. Disc specimens were thinned for examination by TEM using a standard 2-stage electropolishing technique[9].

RESULTS

In the 4PZR Mo specimens there is a general coarsening of the damage structure with increasing irradiation temperature. The dislocation substructure (see Fig. 1) rapidly develops from one consisting of "rafts"[10] plus a fine distribution of small loops (>80% of which are vacancy in nature as determined by the depth dependence of the sense of the Black/White contrast) to one of network dislocations (with segments having $\underline{b}$ = <100> as well as $\underline{b}$ = 1/2 <111>) plus some large resolvable loops which have been analysed using the treatment of Maher and Eyre[1] to be of interstitial type. The dislocation substructures in the AR Mo and TZM are generally similar with the structures becoming finer as the material purity decreases. An exception does occur however in the TZM at the higher

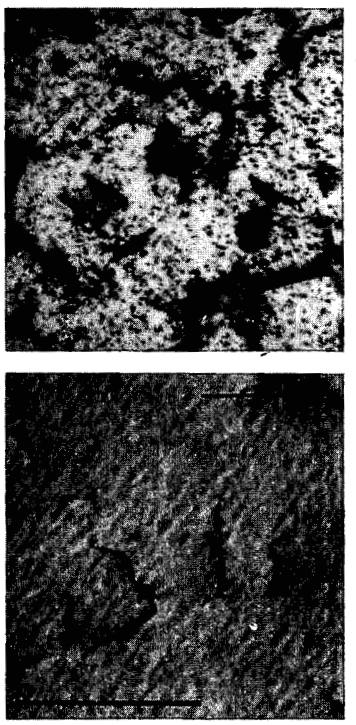


Fig. 1. Micrographs showing dislocation structures in 4PZR Mo irradiated to 3 x 10^{20} n.cm^{-2} a) T_{irr} = 330°C b) T_{irr} = 475°C. $\underline{z}$ = [023], $\underline{g}$ = [200], w_g ~1, t = 1600Å. Scale marker = 0.5μm.

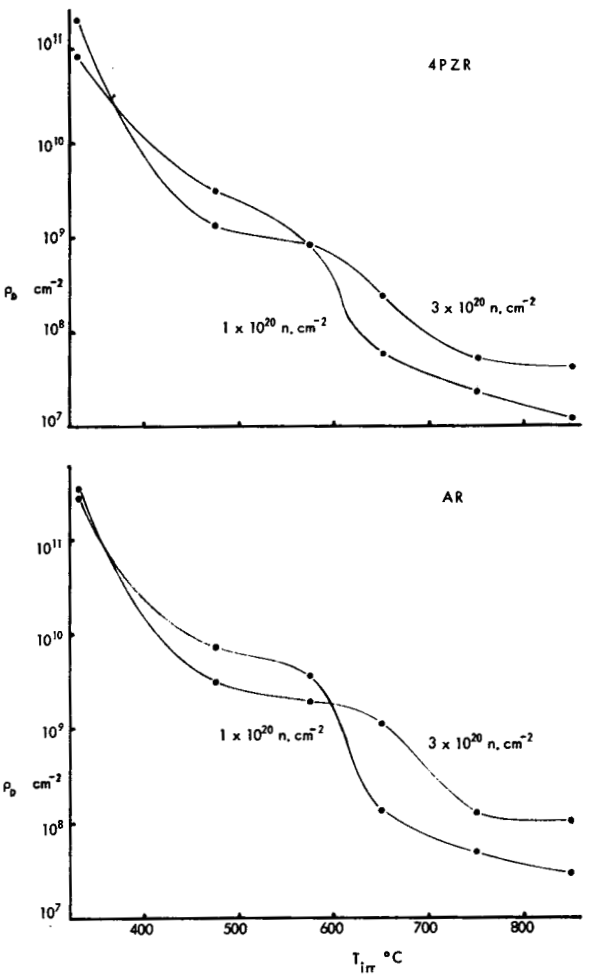


Fig. 2. Total dislocation densities ρ_b of irradiated structures.

irradiation temperatures where a high concentration of impurity stabilized vacancy loops form (see Bentley et al[8] for more details). The measured total dislocation densities ρ_b are shown in Fig. 2.

Voids are observed at all irradiation temperatures, the concentration decreasing and the size increasing with increasing irradiation temperature (see Fig. 3). In the AR Mo the voids are larger and occur on a coarser scale than in the 4PZR Mo and in the TZM significant void formation is limited to the intermediate irradiation temperatures. Significantly though for T_{irr}>575°C the voids shrink with increasing fluence although the void concentration does increase markedly. These features are shown in Figs. 4 and 5 which show the total void concentration N_v and the mean void radius $\bar{r}_3$ (radius of void of mean volume) as a function of irradiation temperature.



Fig. 3. Micrographs showing void structures in 4PZR Mo irradiated to 3×10^{20} n.cm^{-2} a) $T_{irr} = 330°C$ b) $T_{irr} = 475°C$ c). $T_{irr} = 850°C$. $\underline{z} = [155]$, $\underline{g} = [0\bar{3}3]$, $w_g > 0$, slightly overfocused, $t = 700$Å. Scale marker = 500Å.

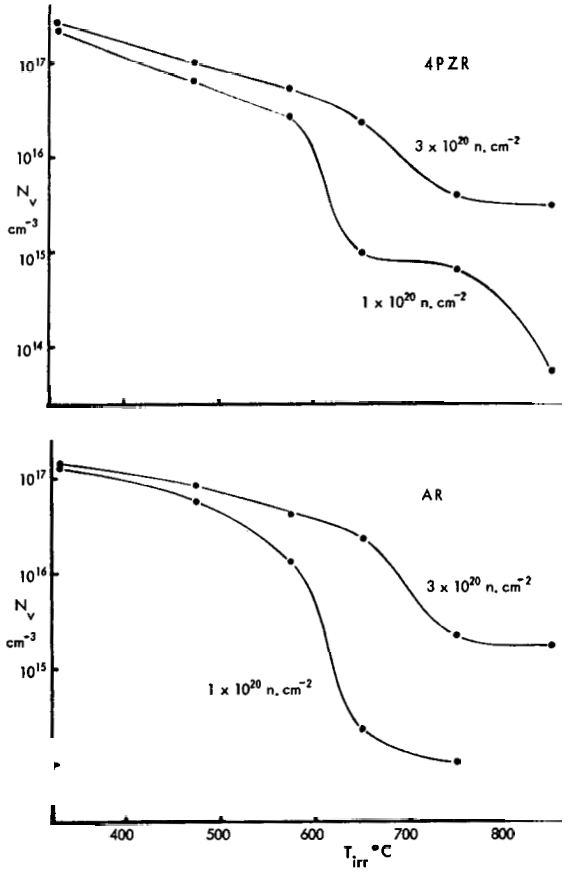


Fig. 4. Total void concentration N_V as a function of irradiation temperature.

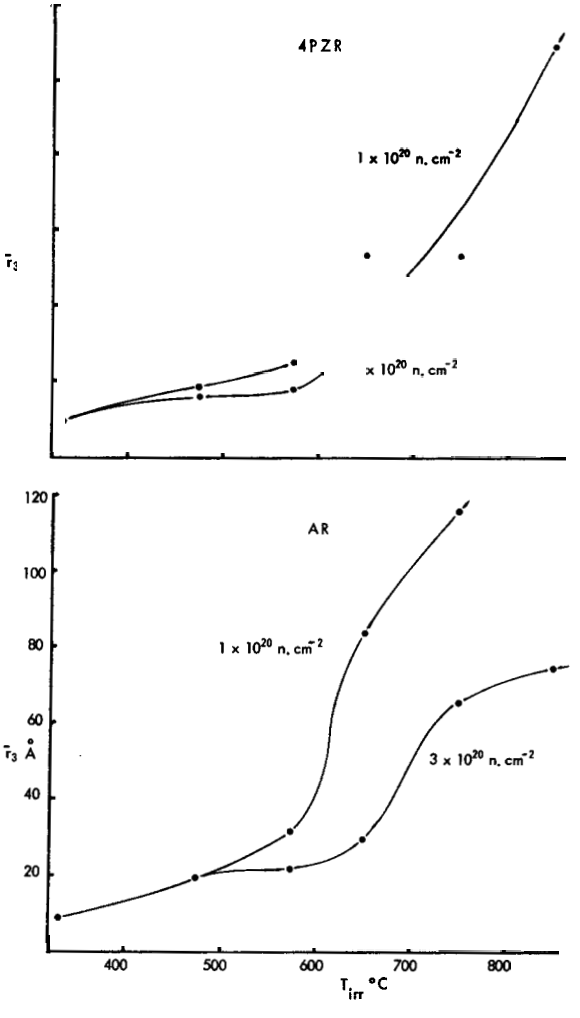


Fig. 5. Mean void radius $\bar{r}_3$ as a function of irradiation temperature.

DISCUSSION

It is possible to understand the strong influence of material purity and irradiation temperature upon the raft distributions from a consideration of their structure and formation[5,10]. Rafts form by loops having identical Burgers vectors gliding together as a result of the elastic interaction between the loops, but being prevented from complete coalescence by the limiting process of self climb. In the more impure material higher numbers of loops will be nucleated and R_{crit}^{glide} (the interaction distance for coalescence by glide[5]) will be decreased since $R_{crit}^{glide} \propto (\sigma_g)^{-1/4}$, where σ_g is the loop glide stress[5], thus leading to smaller rafts which are distributed on a finer scale, as observed (the raft radii are 1000, 400 and 250Å, and raft concentrations are 0.16, 2.0, and 3.3×10^{15} cm^{-3} for 4PZR Mo, AR Mo and TZM respectively, irradiated at 330°C to 3×10^{20} $n.cm^{-2}$). Calculations of self climb rates using the treatment of Eyre and Maher[5] show that at 330°C loop coalescence does not occur in times less than the irradiation time, but at 475°C coalescence occurs in times $<10^{-3}$ x irradiation time and thus rafts are no longer stable in agreement with the observations. An important practical consequence of loops coalescing by glide and climb is that they coarsen into a network at much lower homolagous temperatures and fluences than if the loops are sessile as in the fcc metals.

An interesting feature of the vacancy loops formed at the lower irradiation temperatures* is the rapid decrease in the vacancy loop concentration with increasing irradiation temperature as shown in Fig. 6. This behaviour cannot be explained by a simple vacancy emission model or by bias driven shrinkage but does however agree with self-ion damage results.[11] The model proposed is one in which cascade collapse to vacancy loops is difficult, possibly because of the very high stacking fault energy, the vacancies then being able to diffuse away and so reduce the driving force for loop

*The vacancy loops form as a result of in situ collapse of cascades but do not grow a) because of the bias term which causes more interstitials than vacancies to be attracted and b) because the loop spacing is too large for coalescence by glide to occur. Each loop has a limited lifetime as a result of the bias driven shrinkage.

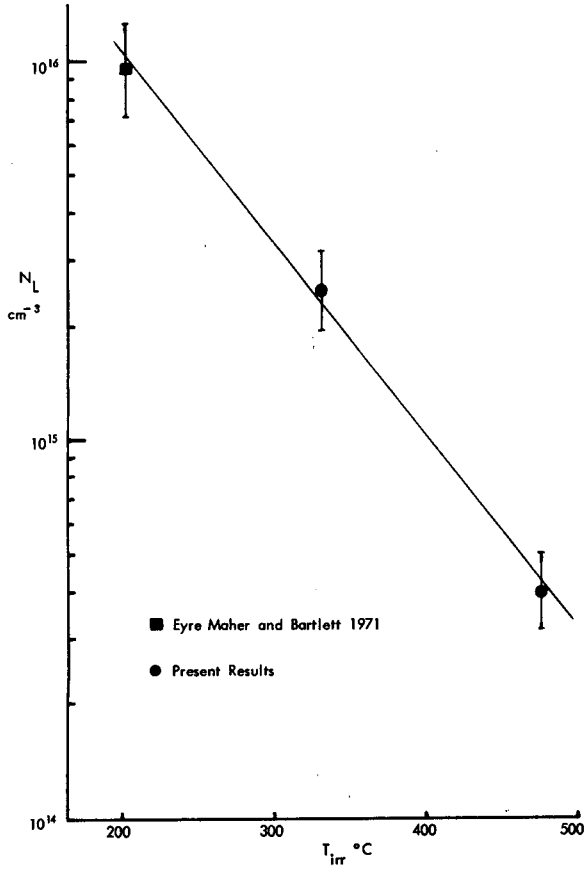


Fig. 6. Vacancy loop concentration N_L as a function of irradiation temperature.

nucleation. This behaviour should be contrasted with that in fcc metals[11] where the results can be fitted to a thermal emission model, since it has important consequences for void formation.[12]

As the vacancy loop concentrations decrease they are replaced by a high concentration of voids and therefore the vacancies are not lost by recombination or annihilation at dislocations or grain boundaries. Several important points emerge. First there is a low threshold temperature 330°C ($0.21T_m$) for voids to appear and also a low threshold dose (<0.05dpa). In fact the void concentration is more or less saturated at lower irradiated temperatures but comparison with high dose results[13] shows that nucleation is not complete at higher temperatures. From the observed behaviour that the void concentration does not increase proportionately with dose and also shows a temperature dependence consistent with a thermally activated nucleation mechanism, we conclude that voids do not nucleate in cascades but that the vacancies diffuse away from the cascades (collapse to loops is difficult) to the void nucleation sites (gas atoms which serve to stabilise the 3-D geometry), so that the situation is similar to that existing during electron irradiation and results in a low threshold temperature and dose for void formation[14].

The observation of void shrinkage with increasing dose at the higher irradiation temperatures (accompanied by an increase in the void concentration) cannot be explained by rate theory. In the present work the voids are distributed at random but after high doses they form a void

lattice. It is thus tempting to relate the void shrinkage to the first stages in the formation of a void lattice. As the void concentration in-increases the elastic interaction between voids[15] becomes important and the voids are too large and therefore redissolve, possibly due to a decrease in the effective vacancy formation energy by the inclusion of the extra energy term from the void-void interaction.

ACKNOWLEDGMENTS

The authors wish to thank A. F. Bartlett and E. A. Terry for their assistance in this work and one of us (JB) wishes to acknowledge the UKAEA, AERE, Harwell, for financial assistance during the course of this work in the form of a research studentship.

REFERENCES

1. D. M. Maher and B. L. Eyre, Phil. Mag. 23, 409 (1971).
2. B. L. Eyre, D. M. Maher and A. F. Bartlett, Phil. Mag. 23, 439 (1971).
3. D. M. Maher, M. H. Loretto and A. F. Bartlett, Phil. Mag. 24, 181 (1971).
4. D. M. Maher, B. L. Eyre and A. F. Bartlett, Phil. Mag. 24, 745 (1971).
5. B. L. Eyre and D. M. Maher, Phil. Mag. 24, 767 (1971).
6. J. Bentley, B. L. Eyre and M. H. Loretto, Eighth Intern. Congr. on Electron Microscopy, Vol. 1, Canberra, 1974, p. 612.
7. J. Bentley, Ph.D. Thesis, University of Birmingham, 1974.
8. J. Bentley, B. L. Eyre and M. H. Loretto, to be published in Proc. Intern. Conf. on Radiation Effects and Tritium Technology for Fusion Reactors, Gatlinburg, Tenn., October 1-3, 1975.
9. B. L. Eyre, D. M. Maher and A. F. Bartlett, AERE report R6298 (1970).
10. J. L. Brimhall and B. Mastel, Rad. Effects, 3, 203 (1970).
11. C. A. English, B. L. Eyre, J. Summers and H. Wadley. These proceedings.
12. B. L. Eyre. These proceedings.
13. V. K. Sikka and J. Moteff, J. Nucl. Mater., 54, 325, (1974).
14. R. Bullough, B. L. Eyre and K. Krishan, Proc. Roy. Soc. (in press).
15. V. K. Tewary and R. Bullough, J. Phys. F., 2, L69 (1972).

DISLOCATION-DEFECT INTERACTIONS AND MECHANICAL PROPERTIES OF CRYSTALS

A. V. Granato
Department of Physics and Materials Research Laboratory
University of Illinois at Urbana-Champaign
Urbana, Illinois 61801, U.S.A.

ABSTRACT

The influence of dislocation-defect interactions on mechanical properties of crystals is reviewed. Interactions are separated into those producing pinning and those producing viscous drag. Deformation behavior is classified according to the strength of the drag. For small drag, inertial effects become important. For intermediate drag, traditional theories resting on rate theory treatments become applicable. For large drag, viscoelastic behavior is obtained. Measurements are examined for information concerning the basic nature of different sources of short and long range pinning and of drag.

I. INTRODUCTION

The mechanical behavior (response to applied forces, or strain produced by a given stress) of a crystal is determined by the motion of point defects and dislocations in the crystal. The dislocation motion in turn, is determined by its interaction with other defects. Dislocations interact with point defects, electrons, other dislocations and the crystal lattice (Peierls stress and the phonon radiation field). We are primarily concerned here with dislocation interactions with point defects, although the other interactions can be represented with the same formalism. These interactions can be characterized in terms of forces which depend on the dislocation displacement y (restoring forces -Ky) or the dislocation velocity v (viscous drag forces -Bv).

The overall behavior can be classified conveniently with the help of simple models. The response $\varepsilon_{e\ell}$ of a crystal containing no defects to an applied stress σ is given by elasticity theory $\varepsilon_{e\ell} = \sigma/G$. If the crystal

contains point defects, there is an additional strain ε_p, so that the total strain ε is given by

$$\varepsilon = \varepsilon_{e\ell} + \varepsilon_p \quad . \tag{1}$$

The point defect strain may be paraelastic (stress induced rotation between equivalent positions of permanent dipoles with the help of thermal fluctuations), or diaelastic (induced dipole, as with a point defect which produces an internal strain). The classic example of a paraelastic point defect strain is that of carbon in iron (Snoek effect). Paraelastic effects have been classified and systematized by Zener,[1] using simple mechanical models consisting of series and parallel arangements of springs and dashpots, such as are shown in Fig. 1. More detailed descriptions have been given by Nowick and Berry, and by DeBatiste.[2]

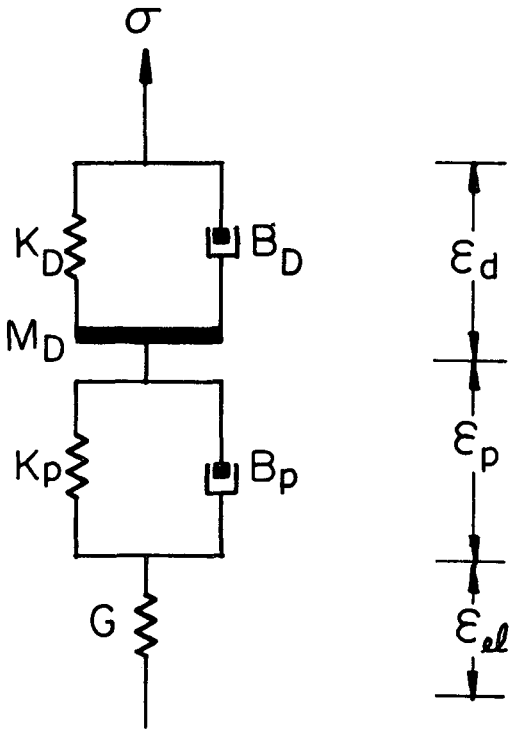


Fig. 1. Schematic representation of strain in a specimen containing point defects and dislocations.

This model is readily extended to include dislocation strains ε_d by using additional elements. The total strain ε is now given by $\varepsilon = \varepsilon_{e\ell} + \varepsilon_p + \varepsilon_d$. The dislocation strain is a diaelastic effect and requires a mass term in the general case.

Non-linear values for K_D and B_D may be required for finite σ, although linear values obtain for $\sigma \to 0$. The dislocation parameters, K_D and B_D, are related to those of the point defects K_p and B_p. In Section II, we first discuss the behavior of a crystal containing point defects but no dislocations. In Section III, we discuss the behavior of crystals containing both point defects and dislocations, at finite stress levels, emphasizing relations between these and relations between plastic flow

and amplitude dependent internal friction measurements. In Section IV, the theory of low amplitude diaelastic dislocation internal friction is outlined. In Section V, a brief survey of short range pinning effects found in radiation damage is made. Experiments providing evidence for long range locking effects are discussed in Section VI and for point defect drag effects in Section VII.

II. POINT DEFECT EFFECTS

For crystals containing no dislocations, or in practice for crystals for which the dislocations are completely immobilized, $\varepsilon = \varepsilon_{el} + \varepsilon_{p}$. However there are several possible contributions to ε_{p} which are additive, and can be represented by springs in series.

An early theoretical calculation by Dienes[3] indicated that irradiation with energetic particles would produce a bulk effect due to the alteration in number and strength of interatomic bonds which would increase all the ordinary elastic constants of copper by about 5 - 10% per at.% interstitials, but decrease them by approximately 1% per at.% of vacancies.

This prediction stimulated experimental studies of the effect of radiation on elastic constants. The early studies showed that there was a much larger indirect effect, dislocation pinning,[4,5,6] which overshadowed the direct effect. A sizable literature on the pinning effects developed and only recently has attention been returned to the direct effect. To determine accurately the magnitude of the direct effects of point defects on the elastic constants, it is imperative to eliminate dislocation effects.

Measurements by Rehn, et al., of the three independent elastic constants of a low dislocation density copper crystal at 4 K showed that the elastic-constant changes during irradiation are - 2%, - 15.8%, and - 18.1% per atomic percent of defects for the bulk modulus C_{44} and C', respectively. The percentage elastic-constant changes measured at 3.6 K after pulse annealing to different temperatures were different for different elastic constants in the same annealing range, and for different annealing regions for the same elastic constant. Also, the elastic-constant changes were strongly temperature dependent. This shows that there are several

different types of effects occurring, each of which depends upon the type of defect involved (close pairs or isolated defects).

Three different kinds of effects were found. The indirect dislocation-pinning effect was eliminated in these measurements. (i) The bulk-modulus change was small ($d\ln B/d\gamma \sim 1$), both with irradiation below 4 K and an annealing through state I_D, showing that the bulk effect first considered by Dienes, is small. (ii) The shear modulus changes during irradiation were large and cannot be a bulk effect. (iii) The relaxation effect discovered earlier by Nielson and Townsend[8] (NT) was confirmed.

These effects can be represented as in Fig. 2. The bulk effect $\varepsilon_p^{(B)}$ is small. The NT peak is a paraelastic effect $\varepsilon_p^{(p)}$ which anneals out with substage I_B in copper. (It was originally associated with I_C by Holder, et al.,[7] but a correction in temperature calibration of the NT measurements[9] subsequently identifies the peak with I_B.) A model for this peak consistent with its symmetry and annealing behavior was given by Holder, et al.,[7] in which the interstitial member of the close pair is at the fifth-neighbor distance from its vacancy. No peaks have been found associated with the other close pairs of copper. However similar relaxation peaks have also been observed in other metals.[10]

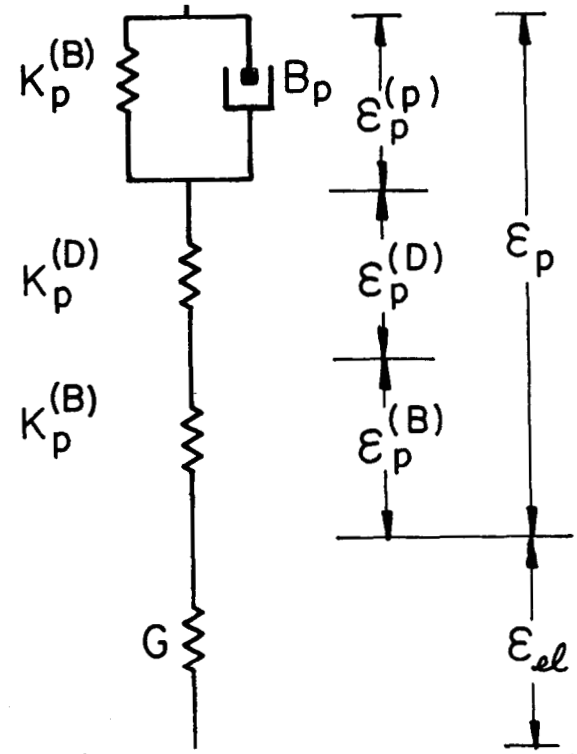


Fig. 2. Schematic representation of bulk paraelastic and diaelastic response of a crystal containing point defects.

The sign, magnitude and anisotropy of the change in the shear elastic constants in I_D found by Holder, et al.,[7] in Cu is that expected for a ⟨100⟩ split interstitial.[11] Strictly speaking a mass term should be included in Fig. 2 for the diaelastic effect, but this is so small that the resonance would not be directly detected by a mechanical measurement.

Thermal excitations or neutron scattering[12] would be required for these frequencies. However the effect is indirectly detected in mechanical measurements through its effect on the temperature dependence of the elastic constants. By analysis of this temperature dependence, the resonant frequency of this defect was found to be about 0.8×10^{12} Hz in close agreement with a calculated value by Dedericks, Lehmann, and Scholz. Subsequently, similar effects have been found in aluminum by Robrock and Schilling,[13] and the theory for the ⟨100⟩ split interstitial has been greatly elaborated.[14]

III. RELATIONS BETWEEN MACROSCOPIC PLASTIC FLOW AND INTERNAL FRICTION

Theories for plastic flow and internal friction have developed independently to a large degree, each emphasizing different aspects of dislocation behavior. But there exist close relationships between the effects.

The basic notions used in describing plastic flow can be illustrated with Fig. 3. The plastic strain ε_d produced by dislocations moving through a crystal is given by

$$\varepsilon_d = \Lambda b y \qquad (2)$$

where Λ is the dislocation density, b is the Burgers vector and y is the average dislocation displacement.

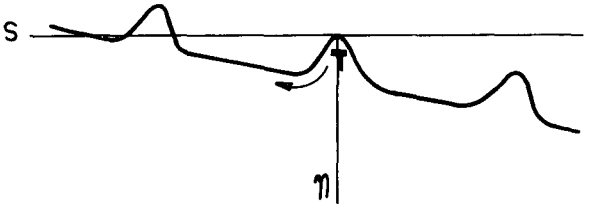


Fig. 3. Schematic representation of dislocation motion under stress through a crystal containing obstacles.

The average displacement y is given by the dislocation equation of motion

$$A\ddot{y} + B\dot{y} + Ky = b\sigma \qquad (3)$$

where $A \simeq \rho b^2$ is the mass per unit length of dislocation line, B is the dislocation viscosity and K is the restoring force constant for the dislocation. This form of equation of motion has been used by Weertman[15] and by Lenz and Lücke.[16] Comparing Eqs. 2 and 3, one obtains the model values M_d, B_d, and K_d from A, B and K by dividing the latter values by Λb^2. The coefficients B and K in Eq. 3 are phenomenological, and can arise from many sources. For finite σ, B and K may be non-linear functions of stress. The motion is impeded by obstacles, such as point defects, which can be represented either as positive or negative (repulsive or attractive) potential

wells. The effect of an external stress is represented by a tilting of the figure by an amount proportional to the applied shear stress σ.

In the traditional theories of plasticity,[17] it is supposed that the rate-limiting step is provided by the overcoming of the obstacles by thermal fluctuations. There are two implicit assumptions made: (1) that the process is a quasistatic one in which the dislocations do not overshoot the barriers by reason of their inertia, and (2) that the viscous drag provided by the medium is not so large that the time required to travel between the barriers is greater than that to overcome them. The former case should occur if the viscous drag provided by phonons, electrons, and other point defects is very small, and the latter if it is very large. We will call the conventional theory a "medium drag" case.

The "Medium Drag" (Quasistatic)Case.--The dislocation strain rate $\dot{e}$ is given by[18]

$$\dot{e}_d = \Lambda b v \tag{4}$$

where Λ is the mobile dislocation density and v is the average velocity. The velocity v is then given by rate theory as

$$v = d\nu \exp[-U(\tau)/kT] \tag{5}$$

where d is the distance between obstacles, ν is the effective attack frequency, $U(\tau)$ is the activation energy required to overcome the obstacle and kT has its usual meaning. τ is given by $\sigma - \sigma_G$, where σ_G is the background stress.

In the model of Fig. 1, there is no restoring force for large scale plastic flow, and the dashpot can be replaced by two non-linear dashpots. The first provides a "sliding friction" type of drag giving a limited stress σ_G so that the effective stress acting on the second dashpot is $\sigma - \sigma_G$ with the non-linear velocity dependence on σ of Eq. 5. The total strain rate $\dot{e}$ is then given by $\dot{e} = \dot{e}_{e\ell} + \dot{e}_d$ where $\dot{e}_{e\ell}$ is given by $\dot{\sigma}/G$ and $\dot{e}_d$ by Eq. 4. With Eq. 5 in Eq. 4, one obtains the formulation of Seeger.[17] If a power law is used in place of Eq. 5, one obtains the dislocation dynamics of Johnston and Gilman.[19] These relations may be used to relate[20] different types of plastic behavior.

If it is assumed that the dislocation interacts with a single point defect and the effects of dislocation line tension and back-jumping are

neglected, $U(\tau)$ can be calculated when the pinning interaction energy versus distance (or its gradient, the force-distance curve) is known. However, this cannot be calculated accurately at present since the maximum pinning force is expected to take place for distances between the dislocation center and the pinning point which are of the order of atomic dimensions where elasticity theory is not valid. It is therefore important to try to measure this force law.

The form of the expected force-distance $F(s)$ law for simple interactions (relaxation of the dislocation stress field for oversized or undersized point defects) is shown in Fig. 4. If it is assumed that $F(s)$ is a smooth function near its maximum, then $U(\tau)$ can be calculated as the area enclosed by $F(s)$ and the external force F. This yields the result

$$U(\tau) = U_o(1-\tau/\tau_M)^{3/2} \qquad (6)$$

where U_o is determined by the barrier height and τ_M is the stress required to overcome the barrier in the absence of thermal fluctuations. Using Eqs. 6 and 5 in 4, one then obtains[21,22]

$$\tau = \tau_M - AT^{2/3} \qquad (7)$$

as the expected temperature dependence of the strength or flow stress on this model, where A is a constant for constant strain-rate tests.

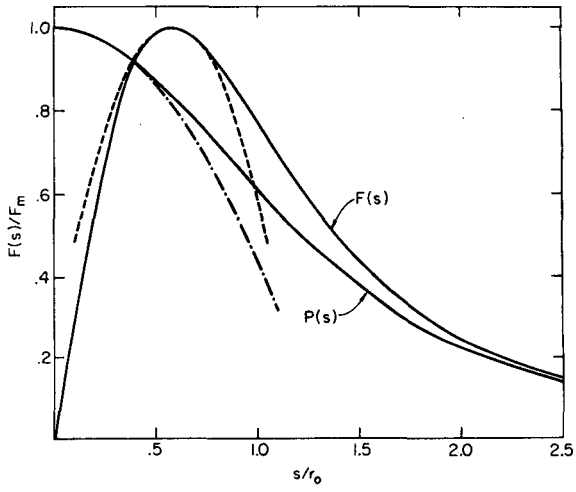


Fig. 4. Force-distance curve $F(s)$ for a dislocation interacting with a point defect. The dashed curve is a parabolic fit to $F(s)$ near its maximum.[22]

Many measurements have been analyzed with this and with predictions from other models, but it is difficult to verify this relation. It is first of all difficult to see from the derivation what the range of validity of Eq. 7 is. Other proposed laws have different exponents and the measurements are not accurate enough to determine the exponent. Also macroscopic plastic flow measurements are destructive and one cannot return to the same state of the specimen to repeat the measurement.

In contrast, the same interaction affects ultrasonic measurements under much more controlled conditions, both theoretically and experimentally. Ultrasonic measurements are usually analyzed with the help of the "string model,"[23,24] illustrated in Fig. 5. It is assumed in the model that there exist two kinds of pinning points, weak and strong. When a stress is applied, the dislocation segments bow out. If the stress amplitude is increased slowly, the dislocations may be pulled away from the weak pinning points. A large increase in strain for no increase in stress then occurs, and for a cyclic stress, the area in the stress strain curve represents the energy loss per half cycle. This loss is amplitude dependent. It is zero until the stress amplitude equals the mechanical breakaway stress $\tau_M = U_o/b^2L$ where L is the distance between weak pinning points. Beyond this, the decrement, which by definition is the loss per half cycle divided by the maximum stored elastic energy $\sigma_o^2/2G$, decreases as $1/\sigma_o^2$ and is as shown in Fig. 5c. In a real crystal, however, there is a distribution of dislocation segments L, which changes the shape of the decrement vs amplitude from that shown in Fig. 5c to that in Fig. 5d.

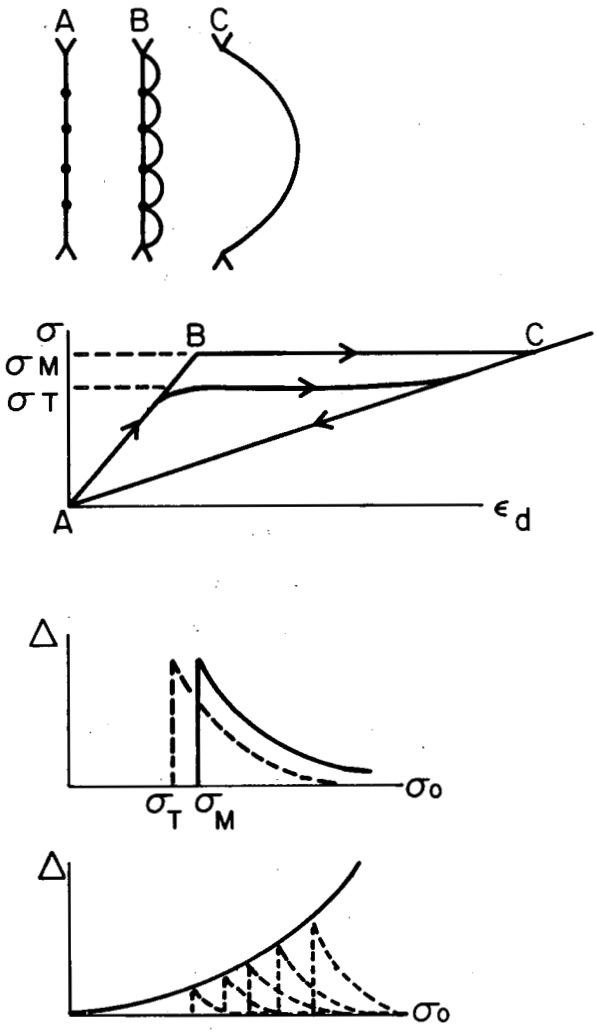


Fig. 5. (a) Dislocation displacement as a function of increasing stress for a dislocation segment with weak interior and strong exterior pinning points. (b) Stress-dislocation strain curve corresponding to (a) above for a cyclic stress. Breakaway occurs at a lower stress σ_T at finite temperatures than the mechanical breakaway stress σ_M. (c) Decrement versus stress amplitude for segments of same length. (d) Decrement versus stress amplitude for a distribution of weak pinning points.

This may be represented in a model by replacing B_d in Fig. 1 by a second spring. The first spring would have a limited strength and correspond to the tension forces arising from the weak pinners with spacing L_c, while the second spring would correspond to the strong pinners of spacing L_n. The restoring force K is given in good approximation by

$$K = \pi^2 C/L^2 \tag{8}$$

where $C \simeq Gb^2/2$ is the dislocation line tension. This is seen by comparing Eq. 3 with the string equation

$$A\ddot{y} + B\dot{y} - Cy_{xx} = b\sigma \tag{9}$$

with a solution of the form $y = y_o \sin \pi x/L$. A discussion of this approximation is given by Lenz and Lücke.[16]

It might be anticipated that the effect of thermal fluctuations would be to change the breakaway stress from σ_M at T = 0 to a lower value σ_T at finite T as indicated in Fig. 5. This is, in fact, the case, but a detailed analysis[21,25] shows that the $T^{2/3}$ law of Eq. 7 is to be expected only under very restricted conditions (mainly very low temperatures and relatively high purity specimens). An observation of the $T^{2/3}$ law of Eq. 7 is of especial significance since this form is required theoretically on very general grounds and measurements which purport to measure the force-distance profile between a dislocation and a single point defect should meet this requirement as a necessary and crucial test.

Internal friction measurements were made by Schwarz and Granato[22] between 1.7 and 20 K in undeformed single crystals of Al and Cu, having a total impurity content of approximately 40 ppm. The results for Cu are similar to those for Al, which are shown in Fig. 6, which shows the strain amplitude measurements for constant values of the decrement vs $T^{2/3}$ between 1.7 K and 7.2 K. This exponent gives the best linear computer fit to the data.

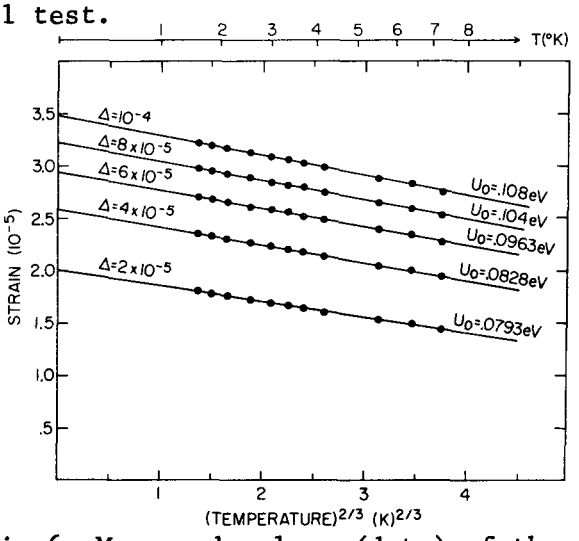


Fig.6. Measured values (dots) of the strain amplitude as a function of (temperature)$^{2/3}$ required to produce a constant value of the decrement Δ for different decrement levels in Al.[22]

Measurements in three samples gave almost identical results. This technique has not yet been applied to radiation damage studies.

The "Small Drag" (Inertial) Case.--Recently, a quite unexpected loss of strength in superconducting materials entering the superconducting state has been found. Since the initial reports by Kojima and Suzuki[26] and Pustovalov, et al.,[27] many studies have been made, which have recently been reviewed by Kostorz.[28] The results of Kojima and Suzuki for the stress-strain curve of a lead specimen changing between the normal and superconducting state are shown in Fig. 7.

There are currently two theories in contention to explain the effect. One by Natsik[29] can be thought of as an attempt to save the conventional rate theory approach. Natsik supposes that the frequency factor ν in Eq. 5 decreases in the normal state. In a second theory (the inertial model)[30,34] this approach is abandoned and it is supposed that the drag constant B at low temperatures is small enough so that dislocations can overshoot the obstacles inertially.

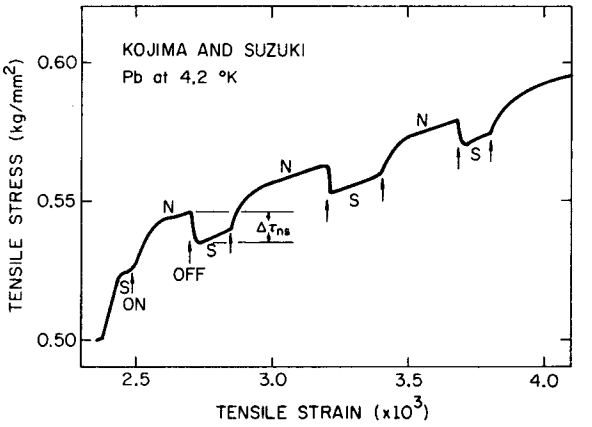


Fig. 7. Stress strain curve in lead as specimen is switched between the normal and superconducting state.[26]

The damping constant B is made up of contributions from phonon damping B_{ph}, electron damping B_e, radiation damping B_r, and point defect drag B_p:[31] $B = B_{ph} + B_e + B_r + B_p$. The phonon damping can be neglected at low temperatures. At T = 0 in the superconducting state, only the radiation damping remains. This is such that all dislocations, independent of their lengths or material, are expected to be underdamped at T = 0. This result explains the fact that these effects are found in all superconductors.[30]

In order to obtain the observed temperature dependence of the stress change, it is necessary to assume in the inertial model that the dislocations are also underdamped in the normal state, although by a lesser amount than in the superconducting state. This fact distinguishes the

inertial model from the changed frequency factor model, for which it is supposed that the dislocations are overdamped in the normal state.

Ultrasonic measurements by Read and Granato[32] establish the fact that dislocations can be underdamped in the normal state in Pb. The peak they find in decrement vs. frequency for lead in the superconducting state is too narrow to be an overdamped resonance. In the normal state, the peak is only very little broader than that found in the superconducting state, but still has a much stronger frequency dependence than is found at higher temperatures. Another example of ultrasonic data providing results which are similar to those obtained with macroscopic stress strain data, are those by Isaac, Schwarz and Granato.[33] The curves they obtain of breakaway stress vs. temperature are nearly parallel at low temperatures, a result which is again in conflict with the Natsik theory.

If the dislocations are still underdamped in the normal state, then it should be expected that they may become overdamped at higher temperatures where the phonon density increases. If so, one would expect to see an anomaly in the yield stress versus temperature curve.[30] Recent measurements in dilute Cu alloys by Kamada and Yoshizawa[34] shown in Fig. 8 provide evidence for this. Ultrasonic data by Schwarz[46] on copper with 1000 ppm of aluminum in Fig. 9 show results for the temperature dependence of

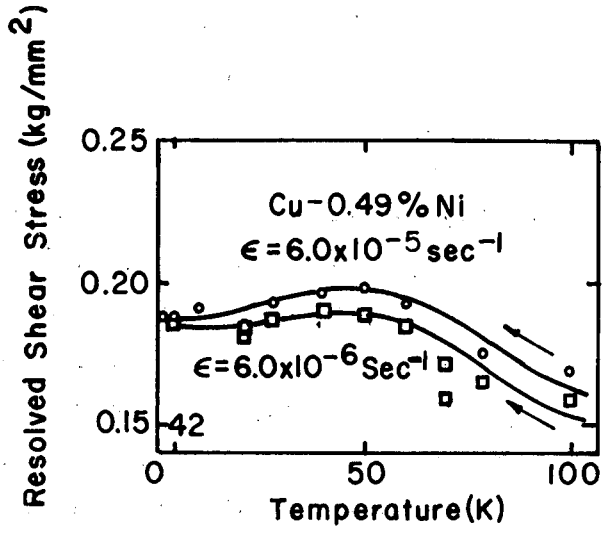


Fig. 8. Temperature dependence of the yield stress of a Cu-0.49% Ni alloy for two strain rates.[34]

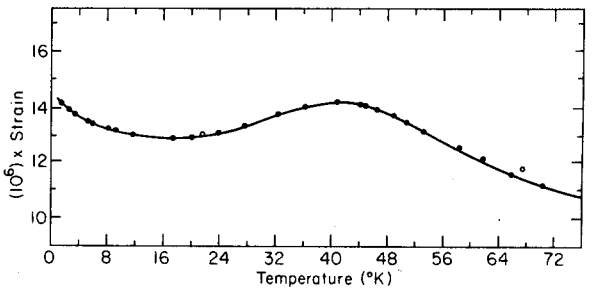


Fig. 9. Ultrasonic breakaway stress vs. temperature for a Cu-0.1% Al alloy.[35]

the ultrasonic breakaway stress. Again, the results are strikingly similar, but the ultrasonic measurements have the advantage of being more precise and reproducible. There are many physical implications of these and other more detailed results which, however, will not be discussed further here.

The "Large Drag" (Viscoelastic) Case.--Any mechanism which damps ultrasonic shear waves viscoelastically will also provide a viscous drag on dislocations since a moving dislocation generates a shear strain rate in the crystal. Eshelby[36] has given a simple relation relating the dislocation drag constant to the maximum decrement Δ_m and time constant τ_o for the internal friction peak for $\mathcal{E}_p$. This may be expressed as[36,37]

$$B = G \Delta_m \tau_o / (4\pi^2) \quad . \tag{10}$$

It is therefore not even necessary in such cases to know the mechanism of the damping to calculate the drag constant. This fact could have important applications in radiation damage studies. Weertman[37] has interpreted the creep of ice in terms of proton motion using Eshelby's relation. Data for ice by Schiller[38] are available from which the peak height and relaxation time at -10°C may be obtained. When a drag constant B is calculated from these data, a value about 7 orders of magnitude larger than typical room temperature phonon drag constants in metals is obtained. This drag, while linear in velocity, is so enormous that the travel time between obstacles indicated in Fig. 3 is much longer than the time to overcome obstacles, so that obstacle effects can be neglected. In place of Eq. 5 one has now simply

$$v = b\sigma/B \tag{11}$$

so that the deformation should be described as that of a simple linear viscoelastic solid[39] of the type first described by Maxwell (1868),[40] who used as a model of a solid a simple spring and viscous dashpot in series. In fact the observed deformation behavior of pre-deformed ice single crystals is described to a good degree of approximation by such a model as shown by Joncich, Holder, and Granato in Fig. 10. The upper curve shows two step-function stress pulses applied to the specimen, while the lower curve gives the strain response. This response is found to be approximately linear even for deformations as high as 10%. The response is

viscoelastic and not anelastic since there is a non-recoverable plastic strain.

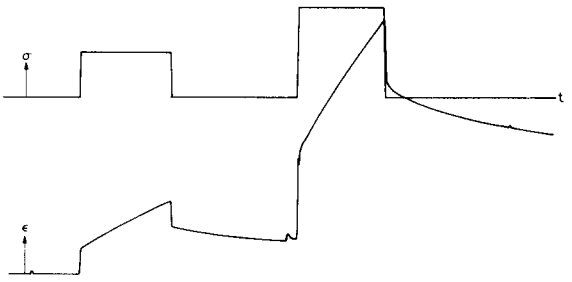


Fig. 10. Stress and strain as a function of time in ice single crystal at -10 °C.[39]

IV. INTERNAL FRICTION AT LOW STRESS AMPLITUDES

Much data has been obtained using low stress amplitude internal friction techniques. We here outline the basic theory required in the interpretation of such data. From Eqs. 2 and 3 the real (y_R) and imaginary(y_I) part of the average dislocation displacement y can be found and give the modulus defect ϕ and decrement Δ, respectively.

$$\phi = \Delta G/G = Gb\Lambda y_R/\sigma_o \quad \text{and} \quad Q^{-1} = \Delta/\pi = Gb\Lambda y_I/\sigma_o \quad . \tag{12}$$

The resulting decrement is of resonance type,[24] as indicated in Fig. 11. The resonance at $\omega_o^2 = K/A$ is limited by radiation damping.[41] Normally, phonon damping at room temperature is strong enough to overdamp the resonance, so that the maximum is broadened and appears at lower frequencies. The shape of the curves is then closely approximated by the standard Debye relaxation forms. There are small differences,[16] which seem to be beyond the limits of experimental accuracy to detect. Although the shapes of the resulting curves for the overdamped case are given in good approximation as relaxation curves, it seems useful to maintain a difference in nomenclature since the dislocation resonance effects are diaelastic effects, whereas relaxation is a term which has mostly been associated with paraelastic effects.

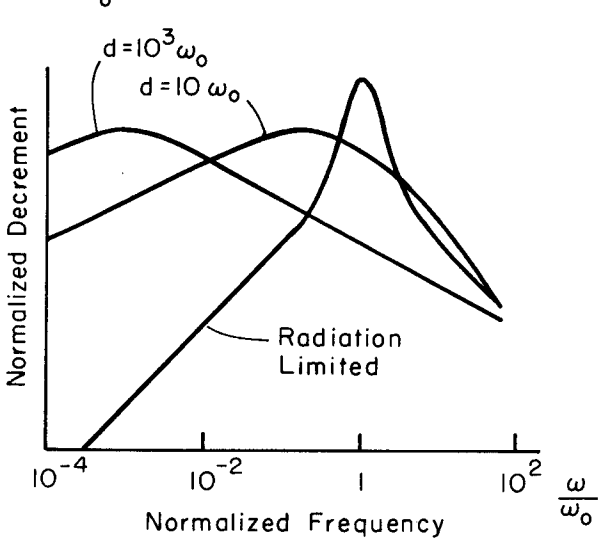


Fig. 11. Normalized decrement vs. normalized frequency for dislocation resonance.

For the overdamped dislocation resonance one then obtains

$$\phi = \Delta_R/[1+(\omega\tau)^2] \text{ and } Q^{-1} = \Delta_R\omega\tau/[1+(\omega\tau)^2] \tag{13}$$

where the relaxation strength Δ_R and the relaxation time are given by

$$\Delta_R = \Lambda Gb^2/K \quad \text{and} \quad \tau = B/K \quad . \tag{14}$$

For $\omega\tau \ll 1$, one then obtains

$$Q^{-1} = \Delta/\pi = \Lambda Gb^2\omega B/K^2 \quad \text{and} \quad \phi = \Delta G/G = \Lambda Gb^2/K \quad . \tag{15}$$

There are only two quantities in the theory which can be extracted from the data, K/Λ and B/Λ

$$\frac{K}{\Lambda Gb^2} = \frac{\phi}{\phi^2+(Q^{-1})^2} \quad \text{and} \quad \frac{B\omega}{\Lambda Gb^2} = \frac{Q^{-1}}{\phi^2+(Q^{-1})^2} \quad . \tag{16}$$

For $\omega\tau \ll 1$, these simplify to

$$\frac{K}{\Lambda Gb^2} = \frac{1}{\phi} \quad \text{and} \quad \frac{B\omega}{\Lambda Gb^2} = \frac{Q^{-1}}{\phi^2} \quad . \tag{17}$$

If K is determined by short range pinning, then with Eq. 8 one has the familiar L^4, L^2 pinning laws from Eq. 15. The curves themselves, however, do not reveal whether K and B arise from long range or short range interactions. This must be determined separately, for example by inspection of the magnitude of these quantities in relation to the defect concentrations, or their dependence on radiation flux, etc.

Measurements of Δ or ϕ as a function of $\omega\tau$, or of both quantities at a fixed $\omega\tau$ can be used to obtain K/Λ and B/Λ. Because many measurements belong to the latter category, it is most important to determine $\omega\tau$ which is simply given as the ratio ν of the measured loss to the relative modulus change ϕ

$$\nu = Q^{-1}/\phi = \omega\tau = \omega B/K \quad . \tag{18}$$

The various "peaks" observed in crystals containing dislocations (Koester cold-work[42] peak, Simpson-Sosin peak,[43] Hasiguti[44] peak, and even[16] the Bordoni peak[45]) can be described formally within the framework of dislocation resonance theory, with different values for the constants B and K.

Most of the interactions producing viscous drag B are long range interactions (phonon drag, electron drag, Snoek drag). One which is not is that which should occur when point defects on the dislocation are dragged along with the dislocation. This process was first suggested by Weertman,[15] and later reconsidered by Kamel, Schoeck, Blistanov and Shaskol'skaya,[46] Lücke and Schlipf,[47] and Simpson and Sosin.[43] Schoeck gave the first quantitative theory and applied the results to a discussion

of the cold-work peak in BCC metals. The theory is formally the dislocation resonance theory with B given by

$$B_p = nkT/DL_N \qquad (19)$$

where $n = L_N/L_c$ and D is the diffusion coefficient of the dragable point defects. Lücke and Schlipf showed that Eq. 19 gives a good approximation even for the case of a single dragging point.

The forces acting on a pinning point are indicated in Fig. 12a. There is a large AC component to drag the pinning point along with the dislocation and a small DC component tending to push pinning points to the side, making large segments grow larger at the expense of neighboring smaller segments. Observation and analysis of such effects could give information about point defect mobilities in dislocation cores. Fig. 12b shows schematically the shape of a dislocation segment which is dragging pinning points. The effects may be represented with the model of Fig. 1 with two components in series by splitting the dislocation displacement y into two parts y_1 and y_2, where y_1 is the displacement of the pinning points, opposed by the pinning point drag $B = B_p + B_{ph}$, with $L = L_N$, and y_2 is the displacement between the pinning points opposed by the drag $B = B_{ph}$ with $L = L_c$. For each y_1 and y_2 there is a decrement and modulus effect as indicated in Fig. 13. The dashed curves indicate how the curves would shift as more pinning points, which are dragged at low frequencies but not at high frequencies, are added.

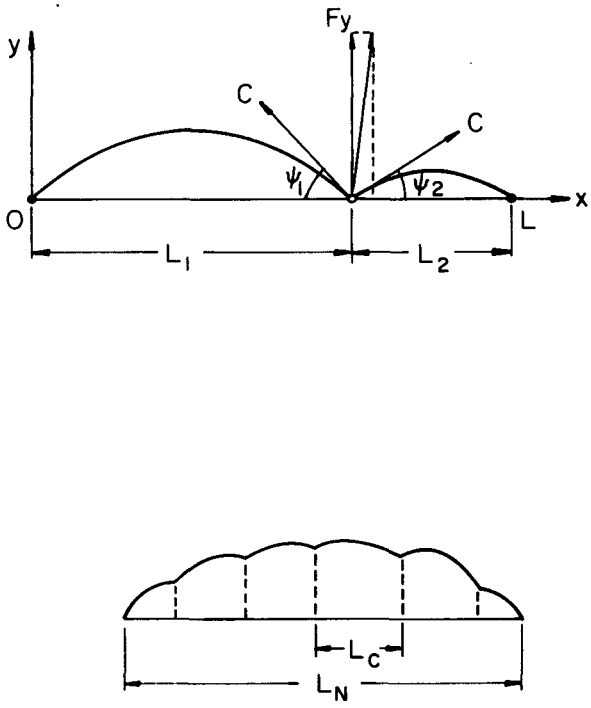


Fig. 12. Schematic diagram of forces and shape of a dislocation dragging point defects.

Long range Snoek - type locking and drag effects were first treated quantitatively by Schoeck and Seeger[48] and have since been discussed further by Eshelby[36] and Nabarro.[49] Nabarro has given a simple argument

for the maximum force σ_m required to pull a dislocation away from its Snoek atmosphere. The form of the interaction energy is indicated in Fig. 14. If the strain produced by ordering an atomic fraction c of atoms is βc, the energy gained by ordering a single atom at distance r from a dislocation is $\beta G b^3/4\pi r$ and complete ordering occurs out to a distance R_T at which this is greater than kT. One thus obtains

$$R_T = \beta G b^3/4\pi kT \quad . \tag{20}$$

The interaction energy in unit volume is $\beta cGb/2\pi r$, and the energy with which unit length of dislocation is bound in its atmosphere is $U = \beta cGbR_T = \beta^2 cb^5 G^2/4\pi kT$. The maximum force per unit length $F = U/R_T$ which is provided by a stress σ_m

$$\sigma_m = \beta Gc \quad . \tag{21}$$

For small displacements y compared to R_T, the locking stress is then easily found to be $\sigma = \sigma_m y/R_T$, so that the long range restoring force constant $(K_{\ell r})$

$$K_{\ell r} = \sigma_m/R_T = 4\pi kTc/b^3 \quad . \tag{22}$$

With the typical value of $b = 2.5 \times 10^{-8}$ cm, one then obtains $K_{\ell r} = 3.3 \times 10^{10}\, c(T/300)$. The total restoring force constant K is the sum of the short range (K_{sr}) and long range $(K_{\ell r})$ force constants[50]

$$K = K_{sr} + K_{\ell r} \quad , \tag{23}$$

where K_{sr} and $K_{\ell r}$ are given by Eqs. 8 and 22. The result for $K_{\ell r}$ in Eq. 22 differs from that used by Lenz and Lücke.[16]

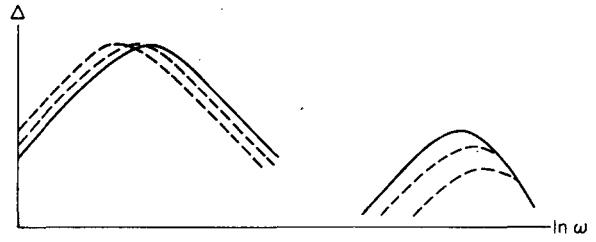


Fig. 13. Schematic diagram for damp-peaks vs. frequency as dragable pinning points are added.

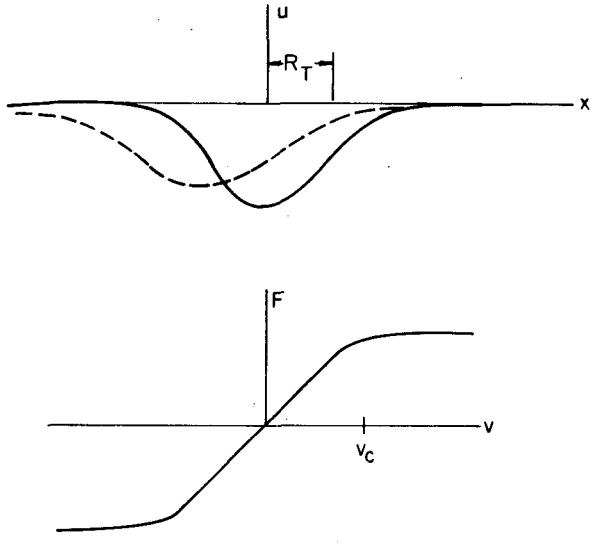


Fig. 14. Schematic diagram for interaction energy vs. dislocation position and force vs. velocity for a dislocation interacting with a Snoeck atmosphere.[48]

When the dislocation moves slowly, the atmosphere lags behind the dislocation as indicated in Fig. 14, and the viscous drag of Eq. 10 is

produced. The resulting force is as indicated in Fig. 14b. For small velocities there is a viscous drag force. At higher speeds, the atmosphere cannot keep up with the dislocation and the restoring force $K_{\ell r}$ is obtained for displacements $y \ll R_T$.

V. BRIEF SURVEY OF SHORT RANGE PINNING EFFECTS

Radiation damage measurements provide one of the best methods of determining changes in the parameters B and K, since it is reasonable to suppose that Λ stays constant during an irradiation. According to Eqs. 8, 15 and 23, if B is constant, $K_{\ell r} = 0$, and $\nu = Q^{-1}/\phi \ll 1$, one should expect Q^{-1} and ϕ to be proportional to L^4 and L^2, giving the familiar short range pinning laws for low frequency. If the number of pinning points (n) is proportional to the flux Φ, then, with

$$n = \Lambda/L = \Lambda/L_o + \beta\Phi, \text{ or } L = L_o/(1+\gamma\Phi) \tag{24}$$

so that

$$K_{sr} = (\pi^2 c/L_o^2)[1+\gamma\Phi]^2 \tag{25}$$

where $\gamma = \beta L_o/\Lambda$. This suggests inspection of the values of $Z = \Delta'$ and $Y = \phi'$, where Δ' and ϕ' are normalized to the starting values. Such results for copper irradiated by Thompson and Pare[51] at room temperature in the range $\nu = \omega\tau \ll 1$ demonstrate two things. First $Z \propto Y^2$, which is expected if B is constant and K_{sr} changes. Secondly, the linear dependence of $Z^{-1/4}$ and $Y^{-1/2}$ on flux are evidence of short-range pinning, for which $K = K_{sr} \propto L^{-2}$.

The significance of these and earlier results by Thompson and Holmes[6] can hardly be overstated. They supported strongly the string model and demonstrated that regular laws governed the behavior of the internal friction effects, but that one needed both decrement and modulus measurements and a means (sufficient radiation to completely immobilize the dislocations) to separate the dislocation component from other sources of internal friction.

The correspondence of $Z^{-1/4}$ and $Y^{-1/2}$ is not always found. Measurements of Y on copper using γ irradiation at several temperatures in the 300-400 K range by Thompson, et al.,[52] (TBBH) show that $Z^{-1/4} = Y^{-1/2}$, but n is not always linear in Φ. They find that n is linear in flux at the

higher temperatures, but increases less than linearly at the lower temperatures. A theory by TBBH was fitted to these data which describes the results in terms of diffusion between three reservoirs: the lattice, the dislocations, and nodes. A similar theory has been given by Simpson, Sosin and Johnson[43] and one by Shindlmayr, John, et al.,[53] includes the processes of point defect trapping and pinning point clustering on the dislocation lines. Evidence for trapping by impurities was given by Winterhager and Lücke[54] at MHz frequencies for isochronal annealing. They found that the pinning rate is lower at the lower temperatures in the 300-400 K range, but defects produced at lower temperatures become effective as pinning points at higher temperatures. Further evidence for impurity trapping is found by A. Förster, et al.,[55] who find that pinning stages occur at different temperatures in specimens with different low level concentrations of impurities.

Evidence of clustering is given by TBBH, who show that the number of pinning points is not linear in the flux, except at low doses. When the number of pinning points per segment length becomes ~ 1, a reduction in pinning point density occurs. Additional evidence is obtained from amplitude dependent measurements[51] which show that as radiation proceeds the strength of the pinning point increases.

Internal friction measurements can be used to survey for pinning stages. The measurements on Cu irradiated at low temperatures by Keefer, et al.,[56] and then heated isochronally reveal at least four pinning stages. When higher defect concentrations are used, only the first stage is observable.

Measurements demonstrating the possibility of measuring core diffusivities parallel to the dislocation line were made on Cu containing .006% Ge at 302°C by Oren and Bauer.[57] The decrement increases to a saturation value during application of an excitation stress and decays to its value prior to excitation when the stress is removed. A preliminary theory for this effect was given by Yamafuji and Bauer.[57] Here the number of defects is constant but the distribution changes. The matter is complicated, depending on the entropy associated with the distribution, and is amplitude dependent, and theories for the effect are still under development.[47]

In summary, it is found that internal friction measurements can be used to count the number and strength of pinning points, and information about defect migration in the lattice and on the dislocation is obtainable. The defect densities are normally very low ($c \sim 10^{-10}$), so that impurity interactions are very important while radiation-induced defect interactions are not, and dislocations are the ultimate sinks for the point defects.

VI. LONG RANGE PINNING

To find evidence of long-range pinning, it is useful to look for changes in internal friction in a region where long range migration of defects is known not to occur. Such is the case below stage I_E in copper. Measurements as a function of fast neutron dose made at 25 K by Thompson, Blewitt and Holmes[5] (TBH) are shown in Fig. 15. These results are well suited for analysis since (1) both Δ and ϕ were measured, so that ν and the location of the damping peak can be determined, (2) a long irradiation and annealing produced final values for Δ and ϕ, (3) the flux dependence of Δ and ϕ are measured, (4) the concentration of radiation-induced point defects is known.

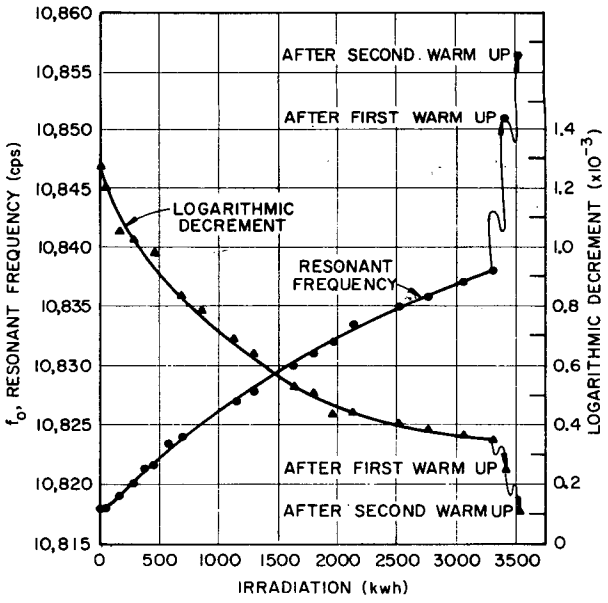


Fig. 15. Decrement and frequency of fast neutron irradiated copper at 25 K.[5]

Fig. 15 appears to be a typical type of pinning effect and would normally be interpreted as a short range pinning effect. The concentration of defects introduced can be calculated to be 1.3×10^{-7} from the data given by TBH. However, no defects are known to be mobile at 25 K.

The data may be analyzed with Eqs. 16-18 to obtain K, B, and ν. The value of ν ranges from .053 to .023 over the irradiation period, showing that the maximum in $\Delta(\omega)$ occurs at higher frequencies than the measured values so that the approximation of Eq. 17 applies. The resulting values of B and K are shown in Fig. 16. It may be seen that B does not change,

but that the restoring force K increases linearly with flux to about twice its original value. The linear dependence of K on Φ found rules out short range pinning forces resulting from dynamic lattice effects (replacement collisions, focussons, channeling), according to Eq. 25.

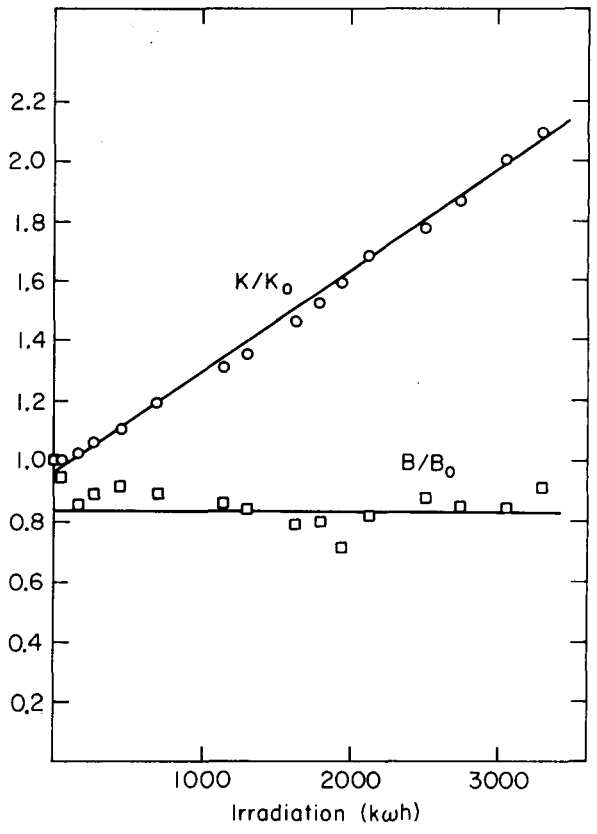


Fig. 16. Restoring force K and viscous force B constants vs. flux for Fig. 16.

From the values given by Nielsen and Townsend,[8] the relaxation strength and relaxation time per concentration c of I_B defects can be calculated. At 25 K, long range pinning from I_B does not occur, but a value of B of the order of 10^{-5} can be expected from Eq. 10. This is just about the order of magnitude of B expected as the starting value B_o from electron and phonon drag.[31] However, no effect is found and we conclude that I_B defects do not affect the results. No other substage anelastic peaks have been detected in copper. However, $\langle 100 \rangle$ split interstitials should become mobile at $\sim$ 45 K. These cannot produce any B effect at 25 K, but will produce a K effect if they are oriented in the dislocation stress field. If it is assumed that the free interstitials are randomly oriented on creation, and that the reorientation energy equals the migration energy, then one can calculate that the dislocations will not become Snoek - locked in the time available at 25°K. However, if one assumes that the free interstitials have energy enough on creation to fall into their lowest available states, then the resulting restoring force constant K can be calculated with Eqs. 8 and 22 in Eq. 23. Taking $c = 10^{-7}$, one then obtains $K_{\ell r}(25\ K) \sim 3 \times 10^2$. This is to be compared with the initial value of $K_{sr} = \pi^2 C/L_o^2$. The added restoring force then would double the starting value as observed

if the starting segment length $L_o \simeq 1.7 \times 10^{-3}$ cm. This is slightly larger than usual estimates, but is reasonable. Alternatively one can say that L_o must be at least this large, as there is no other means of producing the pinning. The resulting interpretation of Fig. 16 is then that free interstitials in concentrations $\sim 10^{-7}$ produce long range locking of the dislocations at 25 K. The dislocations thus magnify the point defect effects. This interpretation could be checked by doing similar measurements at a lower temperature or the same measurements followed by cooling to lower temperatures. It should then be expected that K will remain the same but that B will increase exponentially with decreasing temperature.

VII. SHORT RANGE DRAG EFFECTS

Simpson and Sosin[43] have interpreted the peaks they observe as a short-range drag effect. They suppose, in effect, that K stays constant and B increases. If the measurement frequency is originally on the low frequency side of a peak, then as n increases in Eq. 19, a peak in the measured damping should occur. There are difficulties with this interpretation.[58] It is found in those cases where sufficient data is available to form the quantity ν of Eq. 18, that the measurement frequency is usually much lower than that for which the maximum is expected. On the other hand, there is no need to assume that K is constant, and one should derive K, B and ν from the data. Some curves by Simpson, Sosin and Johnson[43] (SSJ) showing the peaking effect in Cu are shown in Fig. 17. When the data for specimen E-2 are analyzed according to Eq. 16, the results shown in Fig. 18 are obtained. One finds that both K and B increase linearly with Φ, while $\nu \ll 1$ through the whole process. Since the relaxation time τ is given by B/K, one has that

$$\tau = \frac{B}{K} = \frac{B_o}{K_o} \frac{[1 + b\Phi]}{[1 + k\Phi]} \quad . \tag{26}$$

Thus, if the relative change of B is much greater than that for K, one expects the ratio ν to first increase and finally become constant, as observed. This will lead to a peaking effect as indicated in Fig. 19 even when $\nu << 1$.

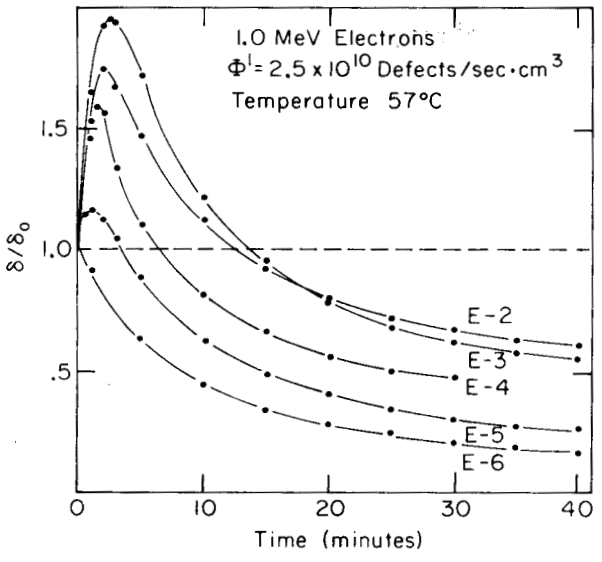


Fig. 17. Decrement vs. irradiation time in copper.[43]

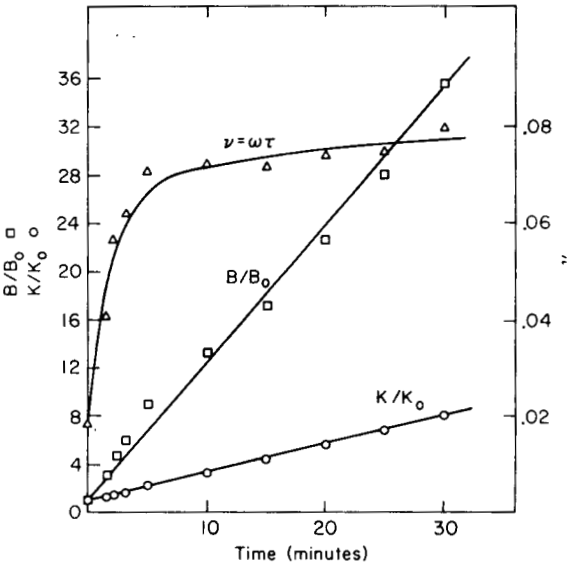


Fig. 18. B, K and ν for Fig. 17.

By using the concentration of defects (excluding close pairs) given by SSJ and Eq. 22, one sees that even if all defects were immobile at the radiation temperature, there are insufficient point defects to produce long range pinning. Long range Snoek drag can also be excluded since any such effect would also have appeared in the higher frequency measurements of TBBH[52] and Winterhager and Lücke.[54] It is therefore reasonable to suppose that this is a short range drag effect. The change in K may be supposed to result from non-dragable pinning points created by clustered point defects on the dislocation line. It was found by Simpson and Kirchoff[59] that when a specimen annealing at 41°C after quenching was irradiated, that a peaking effect appeared. A similar analysis of that data shows again that both K and B change during both annealing and irradiation, but that K increases more rapidly than B during the annealing and B more rapidly than K during the irradiation, producing a peak when irradiation begins as indicated in Fig. 19.

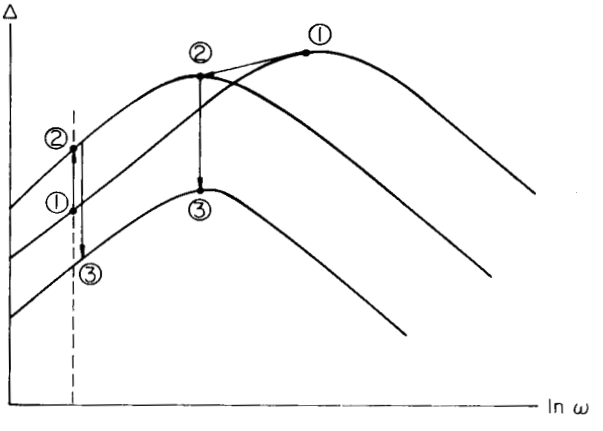


Fig. 19. Schematic representation of damping peak shifts with irradiation for Fig. 17.

ACKNOWLEDGEMENTS

I wish to thank my colleagues, J. S. Koehler, J. Holder, R. Schwarz, D. T. Read, R. Isaac and D. Joncich for many stimulating discussions, and D. Lenz and K. Lücke for a preprint[16] of their work. This research was supported by the Energy Research and Development Agency under Grant E(11-1)-1198 and by the National Science Foundation under Grant DMR 75-14726.

REFERENCES

1. C. Zener, in Elasticity and Anelasticity of Metals (University of Chicago Press, Chicago, 1948).
2. A. S. Nowick and B. S. Berry, in Anelastic Relaxation in Crystalline Solids (Academic Press, Inc., New York, 1972); R. DeBatiste, in Internal Friction of Structural Defects in Crystalline Solids (North Holland Publishing Co., Amsterdam, 1972).
3. G. J. Dienes, Phys. Rev. 86, 228 (1952); G. J. Dienes, ibid., 87, 666 (1952).
4. H. Dieckamp and A. Sosin, J. Appl. Phys. 27, 1416 (1956).
5. D. O. Thompson, T. H. Blewitt and D. K. Holmes, J. Appl. Phys. 28, 742 (1957).
6. D. O. Thompson and D. K. Holmes, J. Appl. Phys. 27, 713 (1956).
7. L. E. Rehn, J. Holder, A. V. Granato, R. R. Coltman and F. W. Young, Jr., Phys. Rev. B 10, 349 (1974); J. Holder, A. V. Granato and L. E. Rehn, Phys. Rev. Lett. 32, 1054 (1974); Phys. Rev. B 10, 363 (1974).
8. R. L. Nielsen and J. R. Townsend, Phys. Rev. Lett. 21, 1749 (1968).
9. J. R. Townsend, private communication.
10. J. A. DiCarlo, C. L. Snead, Jr., and A. N. Goland, Phys. Rev. 178, 1059 (1969)(W); S. Okuda and H. Mizubayashi, Phys. Rev. Lett. 34, 815 (1975) (W and Mo); V. Hivert, R. Pichon, H. Bilger, P. Bichon, J. Verdone, D. Dautreppe and P. Moser, J. Phys. Chem. Solids 31, 1843 (1970)(Fe).
11. P. H. Dederichs, C. Lehmann and Z. Scholz, Phys. Rev. Lett. 31, 1130 (1973).
12. R. F. Wood and M. Mostoller, Phys. Rev. Lett. 35, 45 (1975); H. R. Schober, V. K. Tewary and P. H. Dederichs, Z. Physik B 21, 255 (1975).
13. K. H. Robrock and W. Schilling, to be published; see also, papers at this conference by K. H. Robrock, V. Spiric, and L. E. Rehn.
14. See numerous papers at this conference.
15. J. Weertman, J. Appl. Phys. 28, 193 (1957).
16. D. Lenz and K. Lücke, to be published in Internal Friction and Ultrasonic attenuation in Crystalline Solids, D. Lenz and K. Lücke, eds., Vol. II, Springer-Berlin-Heidelberg-New York. While the present paper was in preparation, a preprint of a review by Lenz and Lücke (LL) was received. It has some similarities and some differences with the present account. The LL review is much longer and more restricted in range, so that many points are discussed more fully there. They restrict themselves to amplitude independent overdamped dislocation resonance effects, but they also emphasize the fact that only B and K can be determined from such measurements.

17. A. Seeger, in Dislocations and Mechanical Properties of Crystals (John Wiley and Sons., Inc., New York, 1957), p. 243.
18. F. Seitz and T. A. Read, J. Appl. Phys. 12, 470 (1941).
19. W. G. Johnston and J. J. Gilman, J. Appl. Phys. 30, 129 (1959).
20. R. Schwarz and A. V. Granato, to be published.
21. A. V. Granato and K. Lücke, to be published.
22. R. Schwarz and A. V. Granato, Phys. Rev. Lett. 34, 1174 (1975).
23. J. Koehler, in Imperfections in Nearly Perfect Crystals (Wiley, New York, 1952), p. 197.
24. A. V. Granato and K. Lücke, J. Appl. Phys. 27, 583 (1956).
25. L. J. Teutonico, A. V. Granato and K. Lücke, J. Appl. Phys. 35, 220 (1964); L. J. Teutonico, K. Lücke, F. W. Heuser, and A. V. Granato, J. Acoust. Soc. Amer. 45, 1402 (1969); K. Lücke, A. V. Granato, and L. J. Teutonico, J. Appl. Phys. 39, 5181 (1968); F. W. Heuser and K. Lücke, to be published; D. G. Blair, T. S. Hutchison and D. H. Rogers, Can. J. Phys. 48, 2943, 2955 (1970); ibid.,49, 633 (1971).
26. H. Kojima and T. Suzuki, Phys. Rev. Lett. 21, 896 (1968).
27. V. V. Pustavalov, V. I. Startsev, D. A. Didenko and V. S. Fomenko, Fiz. Metal. i Metalloved. 23, 312 (1967).
28. G. Kostorz, Phys. Status Solidi (b) 58, 9 (1973).
29. V. S. Natsik, Soviet Physics JETP 34, 1359 (1972).
30. A. V. Granato, Phys. Rev. Lett. 27, 660 (1971); A. V. Granato, Phys. Rev. B 4, 2196 (1971); M. Suenaga and J. M. Galligan, Scripta Met. 5, 63 (1971); U. F. Kochs, A. S. Argon and M. F. Ashby, in Thermodynamics and Kinetics of Slip, Progress in Materials Science, Vol. 19 (Pergamon Press, 1975).
31. A. V. Granato, to be published in Internal Friction and Ultrasonic Attenuation in Crystalline Solids, loc. cit.
32. D. T. Read, Ph.D. Thesis, University of Illinois, 1975; D. T. Read and A. V. Granato, to be published.
33. R. Isaac, R. B. Schwarz and A. V. Granato, to be published.
34. K. Kamada and I. Yoshizawa, J. Phys. Soc. Japan 31, 1056 (1971).
35. R. B. Schwarz, to be published.
36. J. D. Eshelby, Philos. Mag. 6, 953 (1961).
37. J. Weertman, in Physics and Chemistry of Ice, ed. by E. Whalley, S. J. Jones and L. W. Gold (Royal Society of Canada, Ottawa, 1973).
38. P. Schiller, Z. Physik 153, 1 (1958).
39. D. Joncich, J. Holder and A. V. Granato, to be published.
40. J. C. Maxwell, Philos. Mag. (IV) 35, 135 (1868).
41. J. A. Garber and A. V. Granato, J. Phys. Chem. Solids 31, 1863 (1970).
42. W. Köster, L. Bangert and R. Hahn, Arch. Eisenhütteniv. 25, 569 (1954).
43. H. M. Simpson and A. Sosin, Phys. Rev. B 5, 1382 (1972); H. M. Simpson, A. Sosin and D. F. Johnson, Phys. Rev. B 5, 1391 (1972).
44. R. R. Hasiguti, N. Igata, G. Kamoshita, Acta Met. 10, 442 (1962).
45. P. G. Bordoni, Ric. Sci. 19, 851 (1949).
46. R. Kamel, Acta Met. 9, 65 (1961); G. Schoeck, Acta Met. 6, 617 (1963); A. A. Blistanov and M. P. Shaskol'skaya, Fizika Tverdogo Tela 6, 735 (1964) [English translation in Soviet Phys.-Solid State 6, 573 (1964)]
47. K. Lücke and J. Schlipf, in The Interactions between Dislocations and Point Defects, B. L. Eyre, ed., Vol. 1, AERE-Rep.-5944 (Harwell, 1968), p. 118.

48. G. Schoeck and A. Seeger, Acta Met. 7, 469 (1959).
49. F. R. N. Nabarro, in Theory of Crystal Dislocations (Oxford Press, London, 1967), p. 420.
50. G. Sokolowski and K. Lücke, to be published; G. Sokolowski, Thesis, TH Aachen, 1973.
51. D. O. Thompson and V. K. Pare, J. Appl. Phys. 31, 528 (1960).
52. D. O. Thompson, O. Buck, R. S. Barnes and H. B. Huntington, J. Appl. Phys. 38, 3051, 3057, 3068 (1967).
53. R. Schindlmayr and K. Lücke, to be published in Internal Friction and Ultrasonic Attenuation in Crystalline Solids, loc. cit.; R. John, D. Lent and K. Lücke, to be published.
54. P. Winterhager and K. Lücke, in The Interactions between Dislocations and Point Defects, loc. cit., p. 214.
55. U. Förster, H. F. R. Kaufmann, D. Lenz, V. Naundorf and K. Lücke, to be published.
56. D. Keefer, J. C. Robinson and A. Sosin, Acta Met. 13, 1135 (1965).
57. K. Yamafuji and C. L. Bauer, J. Appl. Phys. 36, 3288 (1965); E. G. Oren and C. L. Bauer, Acta Met. 15, 773 (1967).
58. K. Lücke and A. V. Granato, to be published.
59. H. M. Simpson and S. J. Kerchoff, Phys. Rev. Lett. 33, 155 (1974).

EFFECT OF IRRADIATION POINT DEFECTS ON THE INTERNAL FRICTION PEAKS OF COLD WORKED COPPER

P. Moser, C. Minier, J. Lauzier

Departement de Recherche Fondamentale, Section de Physique du Solide
CEN-Grenoble, BP 85 Centre de Tri, 38041 GRENOBLE CEDEX (France)

ABSTRACT

In cold worked copper the internal friction is decreased by electron irradiation between 20-140 K and increased between 140-280 K. In a copper specimen containing a convenient dislocation network, it is possible to develop Hasiguti type peaks.

INTRODUCTION

Below room temperature, the internal friction spectrum of cold worked copper presents five peaks. Two of them are "lattice-dislocation interaction" peaks (Bordoni B_1 and B_2) explained in terms of double kink generation on dislocation loops of special orientations[1,2]. Three of them are "cold work point defect-dislocation interaction" peaks (Hasiguti P_1, P_2 and P_3)[3].

By using successively cold work and irradiation on copper samples, we compare the nature and the pinning effect of both cold work defects and irradiation defects.

MATERIAL AND METHODS

High purity copper (99,999 %) was annealed for 5 hours at 800°C under a 10^{-6} Torr vacuum, then defects were introduced by 300 K cold work followed by 20-30 K electron irradiation. Two apparatus, in line with a Van de Graaf accelerator were used, both allowing "in situ" cold work, irradiation and internal friction measurements, the first one for S_1 referred samples (1 % torsional cold work at 300 K ; 20 K, 3 MeV, irradiation of 0.3 - 25 x 10^{18} el.cm^{-2} ; torsional oscillations of f = 2 Hz creating a maximum sample strain of $\varepsilon = 10^{-5}$)(Fig. 1, 4, 5, 6)[4], the second one for S_2 referred samples (smaller 300 K cold work : < 0,1 % ; smaller irradiation doses :

28 K, 2 MeV, 4×10^{15} el.cm^{-2} ; higher frequency : 630 Hz and higher sensitivity $\varepsilon = 10^{-7}$ in bending mode) (Fig. 2, 3)[5].

EXPERIMENTAL RESULTS

Cold work

Fig. 1 shows the internal friction of the 300 K cold worked sample S_1 during successive warming-up. We observe Bordoni B_2, Hasiguti P_1 and P_3 peaks[6]. During annealing the Hasiguti peak P_1 increases and then decreases.

The dotted curve on Fig. 2 corresponds to the sample S_2, having a smaller amount of cold work, just enough for giving a nice B_2 peak but no P_1 peak. Fig. 3a, obtained in comparable conditions shows the amplitude

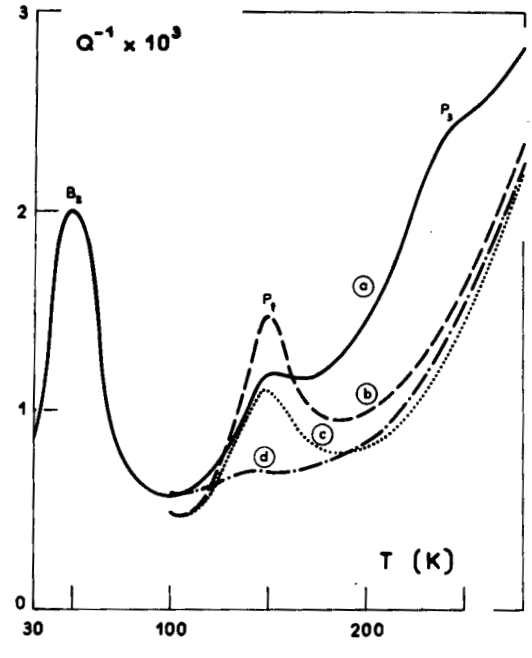


Fig. 1 : Internal friction during warming-up of the 1 % cold worked copper sample S_1 (a : after 300 K cold work. b,c and d : after warming-up to 340 K, 380 K and 420 K respectively). Measurement frequency f = 2 Hz.

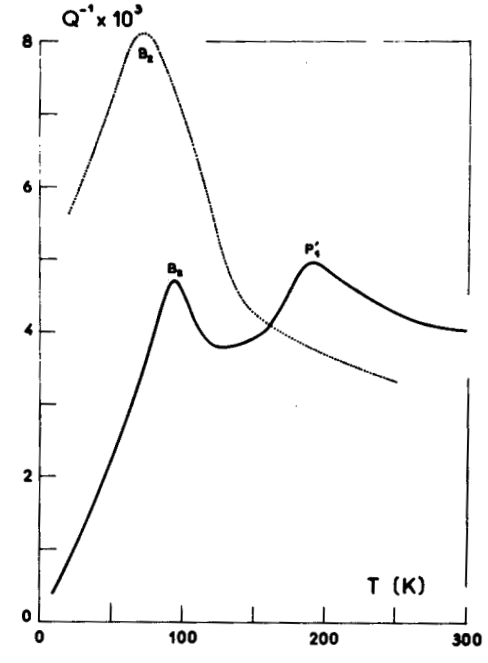
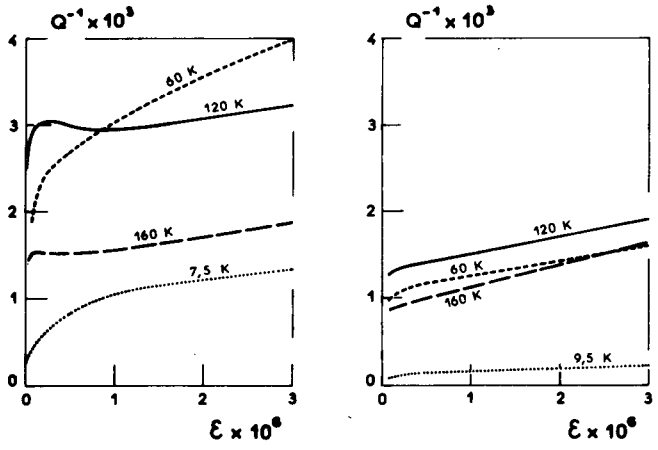


Fig. 2 : Internal friction of a lightly cold worked sample S_2 before (...) and after (___) electron irradiation (28 K, 2 MeV, 4×10^{15} el.cm^{-2} and 300 K annealing, f = 630 Hz).



a b

Fig. 3 : Amplitude dependence of internal friction at different measurement temperatures before and after 28 K irradiation followed by 300 K annealing for the sample S_2 (f = 630 Hz).

dependence of the internal friction. A rapid variation is observed at low strains ($\varepsilon < 10^{-6}$) and low temperature which was attributed to thermally activated motion of preexisting geometrical kinks[7].

Cold work followed by irradiation

For observing the interaction of irradiation defects with preexisting dislocations, the samples S_1 (Fig. 1a) and S_2 (Fig. 2 dotted curve) are of particular interest : the B_2 peak is well developped indicating the presence of a dislocation network made of long dislocation loops free from interacting defects[2]. The absence of Hasiguti peaks shows the absence of an appreciable concentration of cold work point defects in a form which can interact with dislocations.

After a 27 K irradiation (2 MeV, 4×10^{15} el.cm^{-2}) followed by 300 K annealing the sample S_2 shows a small B_2 peak and a new P_1' peak (Fig. 2 full line curve). This peak P_1' presents the same characteristics as those of the P_1 Hasiguti peak appearing after cold work. The amplitude dependence mentioned above is practically suppressed by the irradiation (Fig. 3b).

Fig. 4 shows the results obtained with a sample S_1. Before irradiation, a small Hasiguti peak P_1 is present (curve 1). During the warming-up, immediately after a heavy 20 K irradiation (3 MeV, 1.2×10^{18} el.cm^{-2}) the internal friction is drastically reduced by a pinning stage occuring at 50 K [8] and observed on the modulus curve simultaneously obtained (curve 4). On the contrary, between 150 and 275 K, the internal friction is

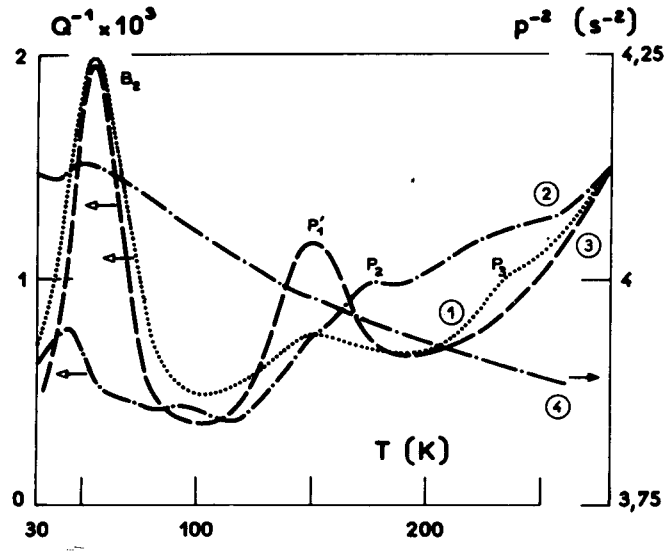


Fig. 4 : Internal friction spectra of a S_1 sample after 1 % cold work at 300 K (curve 1), an irradiation at 20 K with a dose of 1.2x 10^{18} el.cm^{-2} (curve 2) and an annealing at 300 K (curve 3). Curve 4 shows the frequency measurement corresponding to curve 2.

increased with broad maxima at 180 and 240 K (curve 2). After 300 K annealing, the peak B_2 is partly restored and a new peak P_1' appears as in Fig.2. The temperature shift due to the difference in measurement frequencies gives, for P_1', an activation energy of 0.3 eV.

Fig. 5 presents the irradiation dose effect on internal friction spectrum of sample S_1 after 300 K annealing. With increasing doses, the background decreases. The Bordoni B_2 peak decreases in size and width. As shown on Fig. 6 the peak P_1' increases first, then goes to a maximum for 1.2 x 10^{18} el.cm^{-2} and finally decreases. The slope of the decay of the B_2 peak, and the dose giving the highest P_1' peak depend strongly on the amount of the initial cold work. In aluminium and gold, a similar beha-

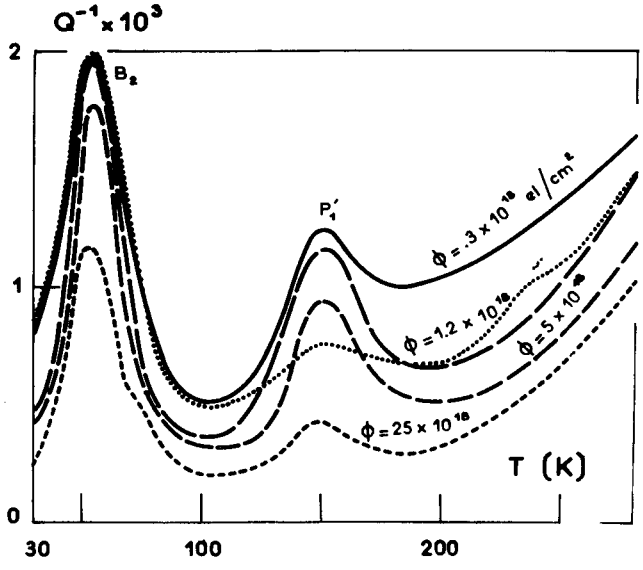


Fig. 5 : Internal friction of S_1 samples, after 1 % cold work and 20 K irradiation to different doses irradiation to different doses followed by 300 K annealing (f = 2 Hz). Before irradiation (...).

viour was observed[9, 10].

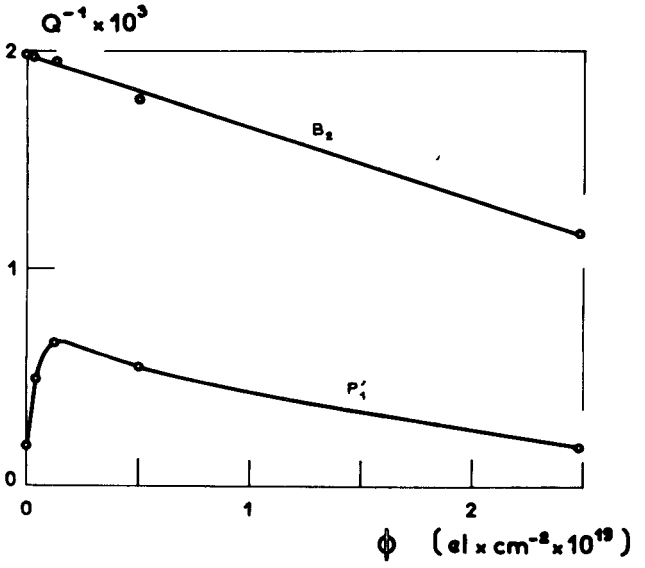


Fig. 6 : Irradiation dose dependence of the Bordoni B_2 peak and Hasiguti type P'_1 peak.

DISCUSSION

The significant reduction of the internal friction, and the disappearance of the amplitude dependence observed at low temperatures and low strains on Fig. 3 mean that even a low concentration of irradiation point defects ($< 10^{-7}$) is sufficient to hinder the motion of the preexisting geometrical kinks.

The 80 % decrease of the Bordoni peak B_2 and its asymetrical shape (Fig. 4 curve 2) result from the length reduction of the dislocation loops by pinning attributed to the long range interstitial migration[8]. The incomplete restoration of the B_2 peak after room temperature annealing means that the immobile pinning interstitials are annihilated by combination with migrating vacancy type defects, allowing the dislocation loops to return to their approximate original lengths.

The complete analogy between the P'_1 irradiation peak and the P_1 cold work peak shows that the same mechanism, involving the same point defect, occurs for both peaks. The conditions for the appearance of these peaks suggest that the most probable mechanism is the thermomechanical interaction of dislocations from vacancy type defects[11]. Nevertheless we cannot exclude an interpretation in which the point defects are impurity atoms[12], but dragged to dislocations by a vacancy mechanism. The variation of the P'_1 peak amplitude with the dose is correctly interpreted by Mercier's model[13].

The small maxima observed at 180 K and 240 K (fig. 4 curve 2) anneal

out similarly to the well known Hasiguti peaks P_2 and P_3 created by cold work and situated at the same temperature[6]. This behaviour suggests that the 150-275 K internal friction is a continuum of Hasiguti peaks resulting from the interaction between preexisting dislocations and more and more complex irradiation defects.

CONCLUSION

The internal friction spectrum of cold worked copper is strongly changed by introducing point defects :

- The stage I_E defect (free migrating interstitial) decreases the internal friction in the range of Bordoni peak B_2 through a pinning mechanism.
- Stage II defect (interstitial agglomerates) increases the internal friction in the range of P_2 and P_3 peaks through a Hasiguti mechanism.
- The stage III defect (vacancy or divacancy) annihilates the previous effects and develop a Hasiguti type peak P'_1 observable when the sample contains a convenient dislocation network.

REFERENCES

1. A. Seeger, J. de Phys. 32 C2, 193 (1971).
2. W. Benoit, G. Fantozzi, Second European Conference on Internal Friction and Ultrasonic Attenuation in Solids (Rome, 1975).
3. J. Perez, P. Peguin, G. Fantozzi, P. Gobin, Ann. Phys. 5, 303 (1970).
4. R. Pichon, F. Vanoni, P. Bichon, G. de Keating-Hart, P. Moser, Rev. Phys. Appl. 5, 427 (1970).
5. J.C. Soulié, J.P. Jodeau, Y. Depierre, C. Minier, Rad. Eff. 11, 221 (1971).
6. J. Lauzier, M. Ory, G. Fantozzi, C. Minier, P. Moser, Phys. Stat. Sol. to be published.
7. M. Ory, J. Lauzier, C. Minier, G. Fantozzi, P. Moser, Second European Conference on Int. Frict. and Ultras. Atten. in Solids (Rome, 1975).
8. D. Keefer, J.C. Robinson, A. Sosin, Acta Met. 13, 1135 (1965).
9. G. Fantozzi, J. Perez, W. Benoit, P. Moser, Z. Kabsch, Rad. Eff. 11, 277 (1973).
10. O. Mercier, W. Benoit, P. Moser, G. Fantozzi, P. Perez, P. Gobin, V. Internal Conference on IFUA, Aachen (1973).
11. B. Bays, W. Benoit, P.A. Grandchamp, J. de Phys. 32 C2, 153 (1971).
12. G. Sokolowski, K. Lücke, V. Int. Conf. on IFUA, Aachen (1973).
13. O. Mercier, W. Benoit, Rad. Eff., to be published.

POINT DEFECT DISLOCATION PINNING IN IRRADIATED COPPER

C. Minier, J. Lauzier and S.L. Seiffert
Section de Physique du Solide, Département de Recherche Fondamentale, Centre d'Etudes Nucléaires de Grenoble
BP 85, Centre de Tri, 38041 Grenoble Cedex France

ABSTRACT

We investigate the problems of the quantitative analysis of dislocation pinning at very low temperatures and stress the importance of strain amplitude, measurement temperature, and eventual depinning. The variation in pinning rates between 9 K and 140 K are compared with theories and the influence of electron energy is discussed.

INTRODUCTION

The proposal by Koehler[1] and Granato-Lücke[2] (K-GL) that dislocation motion may be impeded by discrete pinning defects has provoked considerable analysis and discussion. Despite the successes of this vibrating string model, application in the Hz to kHz frequency range remains problematical and open questions have arisen experimentally[3,4], Lücke et al[5] have especially expressed the importance of the influence of measurement strain amplitude. We have performed detailed internal friction and modulus measurements at low frequency ($\sim$ 700 Hz) on well-annealed copper samples during electron irradiation to further clarify existing problems.

STRAIN AMPLITUDE STUDIES

In an attempt to verify to very low irradiation temperatures the squared-functional dependence predicted between the modulus defect and the dislocation damping in the (K-GL) model, we have confirmed for our experiments the importance of applied strain amplitude[6]. As seen in Fig.1 the slopes of a log-log plot of the normalized modulus defect and normalized damping changes in a low temperature irradiated sample, exhibit a decrease in value toward an expected theoretical value of 1/2 with decreasing strain amplitude.

We have also established that during electron irradiation a peak in

the damping can occur while the modulus defect decreases continuously, the presence of which is dependent on strain amplitude and temperature. Fig. 2 summarizes these results. The peak is largest at high strain amplitudes, diminishes and disappears at the lowest applied strain amplitudes. These effects are in contrast to the experimental and theoretical results of Simpson and Sosin et al (SS)[7,8] of a peaking effect during irradiation which they attribute to point defect dragging by moving dislocations and report as essentually strain amplitude-independent.

No peaking effect is observed for irradiation temperatures below 60 K, even at large applied strain amplitudes. Although the defect dragging model of (SS) does not explicitly include a temperature dependence treatment, it suggests a peaking effect in the damping at all irradiation temperatures. Seeger[9,10] and Hornung[10] have presented further analysis in which they attribute the "peaking effect" in irradiated metals and its strong temperature dependence to a "dislocation-enhanced Snoek effect".

PINNING-RATE MEASUREMENTS AT LOW TEMPERATURES

Many questions have been raised in trying to understand and verify the various (one-interstitial and separate conversion-two-interstitial) models. Important among attempts to resolve these questions are the experimental results of Thompson and Buck[11] in irradiated copper, who show that the pinning-rate measured above 77 K goes through a minimum near 160 K. The minimum is taken as evidence of a thermal conversion mechanism in the two-interstitial model. The ratio of pinning rates in their study obtained between 80 K and the minimum n_{80}/n_{160} is $\simeq$15. Our pinning-rate measurements at very low temperatures, have shown that the effect of measurement temperature is important when interpreting pinning-rate results [12]. From Fig. 3, the pinning-rate measured at 4 K exhibits a maximum near 70 K where the ratio n_{70}/n_4 is $\simeq$ 5. Then it decreases to a minimum near 150 K and subsequently increases. The ratio of pinning-rates at the minimum ($n_{70}/n_{140} \simeq 1.5$) is about ten times smaller than the Thompson-Buck result. In Fig. 4 we show the ratio of numbers of pinners $n_{y4,z4}/n_{yT,zT}$, deduced from modulus and damping measurements respectively, by measuring at 4 K and at T K following an irradiation at T K. The ratio is not too different from one up to about 70 K, after which it increases abruptly.

Thus the quantitative analysis of pinning-rate data taken at various measurement temperatures is questionable, and further suggests the existence of two classes of dislocations, of which, one form becomes dominant during measurement above 80 K (the Bordoni peak range) and along which perhaps line diffusion may take place.

Separate quantitative analyses of the pinning-rate minimum have been proposed based on the conversion-two-interstitial model, differing directly in restrictions on migration. An analysis presented by Simpson and Sosin[13] assumes that Stages I and III defect forms migrate three-dimensionally. This model fits the Thompson-Buck pinning-rate minimum results quite well above 80 K by accounting for impurity effects. We have extended this calculation to lower temperatures using their parameters and find agreement through the maximum in pinning-rate near 70 K down to 40 K, below which the values determined theoretically become several orders too small. This difference below 40 K indicates the importance of other processes, namely, the direct creation of point defects at dislocations which we will discuss later.

Concurrently, Frank and Seeger[14] have proposed a conversion-two-interstitial model based on the presence of Stage I defect configurations which migrate one-dimensionally. Two types of crowdion defects are postulated, the "on-line", migrating in the direction of its self-vacancy and having a small chance of pinning dislocations, if it is not converted ; and the "off-line", which has a greater possibility of intercepting dislocations before converting. The threshold energy for the creation of on-line crowdions is given as about 9 eV and for off-line crowdions as about 19 eV. This energy difference has received support experimentally by Roth and co-workers[15], but does not appear in experiments performed as a function of variable incident electron energy, which we discuss next.

INFLUENCE OF ELECTRON ENERGY

The defect production and annihilation mechanisms for different values of the incident electron energy were studied at 20 K, followed by isochronal measurements up to room temperature. The electron doses were chosen such that the magnitude of pinning during irradiation at each energy studied would be approximately the same. The sample was well annealed before each change in electron energy. Fig. 5 summarizes these results where the number of pinners n, per dislocation length, as deduced

by the Granato-Lücke models from damping measured at 9 K, is plotted as a function of anneal temperature. Two pinning regions appear. Stage I near 40-70 K, and Stage III in the range of 140-200 K. Depinning is evident above 200 K, particularly in the results obtained following irradiation at 0,7 MeV and above.

We may then distinguish three numbers experimentally : those defects created on dislocations by irradiation at 20 K, n_c ; arriving during Stage I, n_I ; and n_{III} during Stage III. In Fig. 6 the corresponding effective cross-sections n/Φ are plotted as a function of maximum transfer energy. The values of threshold energies for Stage I and III appear not very different. **Additional experimental studies at lower energies are in progress to clarify this crucial point. These additional experiments are hoped also to elucidate the small evidence of lower threshold energy for creation occurring at dislocations exhibited in curve n_c.**

STABILITY OF DEFECTS ON DISLOCATIONS

The possibility of defects diffusing along dislocations has always been neglected in the interpretation of pinning-rates. In the earlier pinning studies of Keefer et al[16] a reduction in pinning takes place during isochronal anneal between 90 to 170 K, particularly in samples containing very small defect concentrations. We show that depinning in this temperature range is more or less accentuated depending on the sample measured, with depinning more apparent from modulus measurements than from damping measurements. Fig. 7 shows this clearly for a sample exhibiting the largest amount of depinning. The damping exhibits pinning in Stages I and III. Small depinning occurs above 70 K with a larger amount after 200 K. By contrast, the modulus results show strong depinning between 120 and 170 K. Such a discrepancy between derived pinning point numbers may be explainable by a two-dislocation model incorporating different line tensions for the separate dislocation types. Thus the internal friction being measured may well correspond to dislocations with apparently the weakest line tension since the modulus defect is probably influenced by a superposition of the contributions of both dislocation types as discussed by Thompson and Buck[11]. Defect mobility along one dislocation

type would then be fixed or restricted, while along the other, defects would be allowed to migrate.

CONCLUSIONS

We have demonstrated that numerous experimental precautions must be realized before the usual interpretation of dislocation pinning experiments can be done quantitatively.

Measurements of the pinning-rate at very low temperatures show that it goes through a maximum at 70 K, **and since depinning in the range between 100-160 K is not always verifiable, the results favor a model of two interstitials with conversion.**

REFERENCES

1. J.S. Koehler, in Imperfections in Nearly Perfect Crystals, W. Schockley (ef.), p. 197, Wiley, New York, 1952.
2. A. Granato and K. Lücke, J. Appl. Phys. 27, 583 (1956).
3. C.R. Heiple and H.K. Birnbaum, J. Appl. Phys. 38, 3294 (1967).
4. V.K. Paré and H.D. Guberman, J. Appl. Phys. 44, 32 (1973).
5. K. Lücke, G. Roth and G. Sokolowski, Acta Met. 21, 237 (1973).
6. J. Lauzier, C. Minier and S.L. Seiffert, Phil. Mag. 31, 893 (1975).
7. H.M. Simpson, A. Sosin, G.R. Edwards and S.L. Seiffert, Phys. Rev. Lett. 26, 897 (1971).
8. H.M. Simpson and A. Sosin, Phys. Rev. (B) 5, 1382 (1972).
9. A. Seeger, Proc. 5th Internl. Conf. Internal Friction and Ultrasonic Attenuation in Crystalline Solids, Aachen 1973, to be published.
10. A. Seeger and W. Hornung, Proc. 5th Internl. Conf. Internal Friction and Ultrasonic Attenuation in Crystalline Solids, Aachen 1973, to be published.
11. D.O. Thompson and O. Buck, Phys. Stat. Sol. 37, 53 (1970).
12. J. Lauzier and C. Minier, Rad. Eff. 22, 191 (1974).
13. H.M. Simpson and A. Sosin, Rad. Eff. 2, 299 (1970).
14. W. Frank and A. Seeger, Cryst. Latt. Defects 5, 141 (1974).
15. G. Roth, H. Wollenberger, Ch. Zechau, and K. Lücke, Proc. 5th Internl.

Conf. Internal Friction and Ultrasonic Attenuation in Crystalline Solids. Aachen 1973, to be published.

16. D.W. Keefer, J.C. Robinson and A. Sosin, Acta, Met. 13, 1135 (1965).

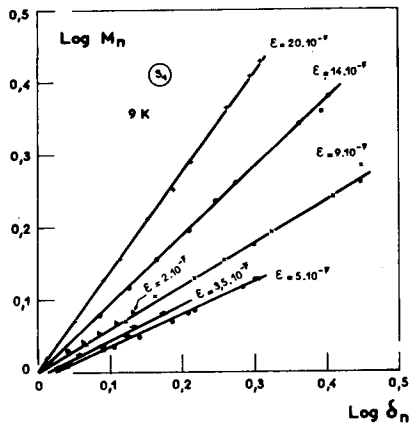


Fig.1 - Log-Log plot of the inverse normalized modulus defect M_n as a function of the inverse normalized damping at 9 K.

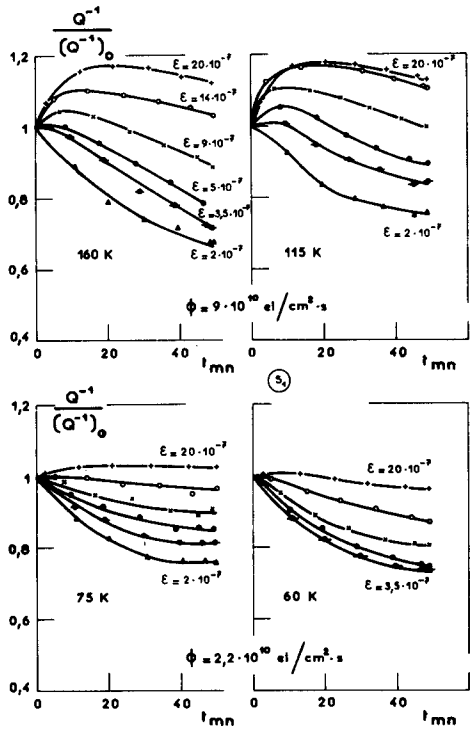


Fig.2 - Normalized damping change associated with several strain amplitudes plotted as a function of irradiation time.

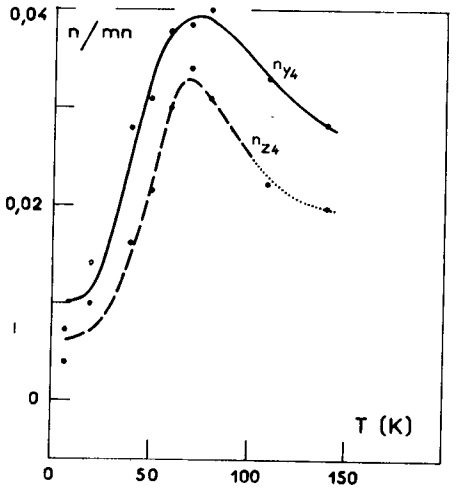


Fig.3 - Pinning rate measured at 4 K plotted as a function of irradiation temperature.

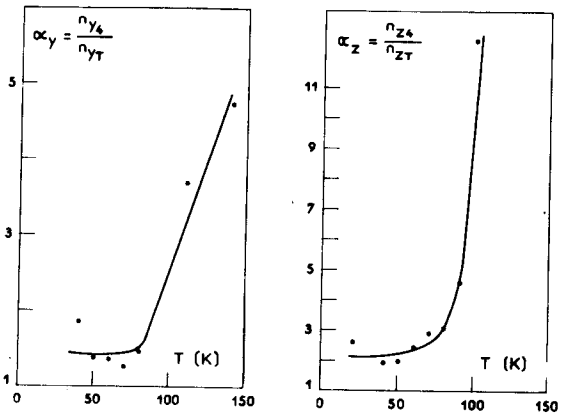


Fig.4 - The ratios $n_{y4,z4}/n_{yT,zT}$ of the pinning rates deduced from modulus and damping measurements versus irradiation temperature T K.

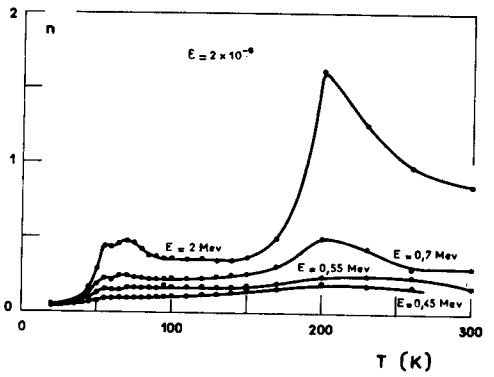


Fig.5 - The number of dislocation pinners n as a function of isochronal anneal temperature.

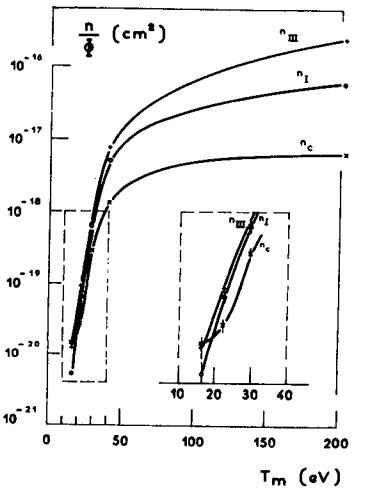


Fig. 6 - Effective cross sections n/ϕ versus maximum transfer energy T_m.

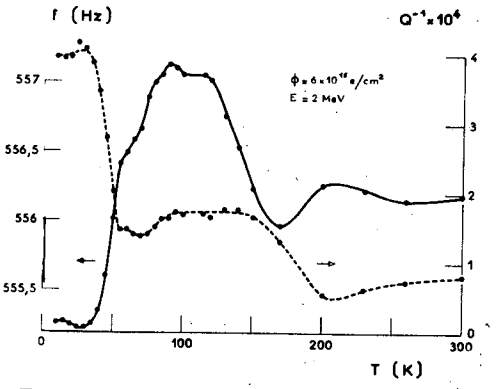


Fig.7 - Comparison plot of isochronal anneal on the resonant frequency and damping change, measured at 9 K, as a function of anneal temperatures.

STAGE III DISLOCATION PINNING IN SILVER RESULTING FROM GAMMA IRRADIATION

R. A. Van Konynenburg and M. W. Guinan
Lawrence Livermore Laboratory
Livermore, California 94550

ABSTRACT

The objectives of this work were fourfold: (1) to test the validity of the vibrating string dislocation model in silver, (2) to determine in which annealing stage long-range migration first occurs, (3) to measure the migration energy and identify the defect responsible for observed annealing, and (4) to investigate the possibility of dislocation pipe diffusion. Apparatus is described which is capable of continuously measuring changes in the elastic modulus and internal friction during gamma irradiation over the temperature range from <4 K to well above room temperature. A novel hollow-cylinder sample geometry permits use of a source strength of only 1 Ci. Survey experiments over a wide temperature range and isothermal irradiations above room temperature are discussed. The results are explained in terms of the Koehler-Granato-Lücke vibrating string dislocation model and the Thompson-Buck-Huntington-Barnes defect-dislocation interaction model.

GENERAL DESCRIPTION

We have performed experiments[1] on silver of the type pioneered by Thompson et al.[2-4] with copper. The approach was briefly as follows: Point defects were created in high purity silver by gamma irradiations; their behavior was studied by continuously monitoring the internal friction and the elastic modulus of a specimen that was driven in mechanical vibration; the temperature was controlled in order to study the kinetics of the observed behavior; and the damage was annealed out in situ after each experiment so as not to disturb the dislocation structure.

APPARATUS AND SAMPLE

The apparatus design was similar to that of Thompson and Glass[5], and is described in detail elsewhere[1]. Key parameters involving the apparatus and sample are as follows:

Sample form - Hollow cylindrical, <111> oriented single crystal

Impurities - <1 ppm starting, 50 ppm final, primarily Si

Dislocation density and structure - unknown, stabilized with 500°C anneals.

Mounting - Four sliding pins at midplane

Background apparatus damping - $< 1.4 \times 10^{-5}$

Source - 1 Curie ^{60}Co rod, inside sample

Flux - 3.6×10^{9} gamma/(cm^2-sec)

Damage rate uniformity - ±25% over 90% of sample volume

Temperature uncertainty - ±0.25K during single run; ±0.5 K between runs.

Drive and detection - Electrostatic drive, FM detection, automatic phase control

Frequency - 24-27 kHz, measured to precision of 0.1 Hz.

Max. strain amplitude - 10^{-8}

Damping measurement - Free decay, resonance curve width, and drive voltage at constant amplitude. Precision - 1%.

EXPERIMENTS

We first performed survey experiments to observe the background damping and to find out in what temperature range pinning effects could be detected. We observed a broad Bordoni peak in the annealed sample prior to irradiation. It was centered at 81 K, with half maximum values at 25 K and 190 K. The decrement was 5×10^{-3} at the maximum.

After irradiation at 4 K for 24 hours with a 20-Curie source, we performed a continuous warmup. In the temperature range between 65 K and 90 K, we observed an increase in frequency of 0.06% compared to the annealed condition. This change appeared to be significant in comparison to the scatter in the data. There was no significant change in damping compared to the annealed condition in this temperature range, however. When

the sample was warmed up to room temperature and above, major changes in damping and frequency were observed, so we decided to conduct isothermal irradiations in that region. When the sample was subsequently recooled to 4 K and again warmed up, the changes were observed to persist over the whole temperature range. In particular, the damping was about 15% lower at 4 K, and about 48% lower at room temperature. The observed peak was decreased about 32% in height and shifted down in temperature to 70 K.

We also observed in other experiments that it was possible to saturate the damping change in a reasonable time, but the frequency continued to change even after long irradiation. For example, in a 75°C isothermal irradiation with a 96-Curie source, the damping stopped changing in 10 hours, while the frequency was still increasing after 23 days.

The mounting was improved to eliminate sample deformation prior to the isothermal runs. Four isothermal irradiations with the 1-Curie source were performed at the following temperatures: 24.8, 34.8, 44.0, and 53.0°C. Between irradiations the sample was annealed to return the damping and frequency to their initial values. The decrement data are shown in Fig. 1. (Note that the scales are not the same for each temperature.) At the end of the 24.8°C and 34.8°C runs, the 96-Curie source was inserted for about 150 hours. It was observed that the modulus defect change nearly doubled, with little or no concomitant change in the damping.

INTERPRETATION

The Bordoni peak[6] has been observed by several workers. Its presence after annealing may be accounted for by deformation near the mounting pins, which had not yet been treated to promote sliding when this observation was made.

We interpret the frequency change in the range between 65 and 90 K to be due to long range migration of a point defect in Stage I. The damping change which should have accompanied it was probably below the sensitivity of our measurement. The somewhat high Stage I temperature is due to the low defect concentration and the fact that it was a continuous warmup rather than an isochronal anneal. This interpretation agrees with

the results of Keefer and Robinson[7]. The fact that damping and modulus changes which occurred near room temperature were seen to persist down to 4 K indicates that the samples were sensitive to pinning over the entire temperature range.

Since the frequency continued to change long after the damping change had saturated, the results cannot be explained by the Koehler-Granato-Lücke (KGL) vibrating string model[8,9] if only one dislocation component is assumed. We have therefore assumed, as have others in the past[10-14], that there are two groups. Furthermore, we have assumed that one group has a much higher average loop length than the other, so that both groups may contribute to the modulus defect, but only the group with the greater average length is responsible for the observed pinnable damping. This model was proposed but rejected by Paré and Guberman[15]. The irradiations with the large source at the end of the 24.8°C and 34.8°C runs suggest that the (assumed) shorter group did not contribute significantly to the damping changes observed earlier in the experiments. This enables us to interpret the damping data using the KGL model. We are not able to interpret the frequency data quantitatively because it never saturated.

In interpreting the damping data, we decided to use the Thompson-Buck-Huntington-Barnes (TBHB) defect-dislocation interaction model[3] because of the similarity between our results and theirs[2]. We did not attempt to fit the data to the Simpson and Sosin defect dragging model[16] because we did not observe an initial increase in the damping, and because the vibration frequency was above the range where the dragging effect appears to dominate the pinning effect.

We did a simultaneous fit of the TBHB model to all the damping data from the four isothermal runs, using a CDC 7600 computer. It was necessary to use three transient terms in the expansion given by the TBHB model, since the higher order terms were not found to be negligible as in their work on copper. The final fit is shown by the curves in Fig. 1. The standard deviation is 1.4%, which is comparable to the precision of measurement.

The values of the parameters arrived at with this fit appear to be

reasonable. In particular, we obtained a lattice migration energy for the defect responsible for the pinning of 0.48 eV, a dislocation spacing of 10^{-3} cm, a pipe diffusion energy of 0.30 eV, and a defect-node binding energy of 0.43 eV. The value of the pre-exponential term in the lattice diffusion relaxation time and a calculation of the diffusion length from the Einstein relation indicate that the lattice diffusion is free (untrapped). The value of the pre-exponential term in the pipe diffusion relaxation time and the value of the binding energy for the nodes, indicates wide splitting of the extended dislocations, which is consistent with the low stacking fault energy of silver.

Because of the rather low value of the lattice migration energy and the fact that divacancies or di-interstitials are extremely unlikely at the low defect concentrations used, we believe some form of the single interstitial atom is responsible for the observed pinning.

CONCLUSIONS

We conclude that the results can be explained by the KGL vibrating string model if two dislocation components are assumed, one of which has a much higher average loop length than the other. The survey experiments are consistent with long-range migration in Stage I in silver. E_m is about 0.48 eV for the defect which pins dislocations in Stage III in silver, using gamma irradiation and low defect concentrations. This defect is most likely the single interstitial atom. Pipe diffusion is necessary to explain the results. The migration of point defects and their interaction with dislocations can be explained by the model of Thompson, Buck, Huntington, and Barnes.

ACKNOWLEDGMENTS

This work was performed under the auspices of the U. S. Atomic Energy Commission (now the U. S. Energy Research and Development Administration). The work reported was part of a PhD thesis submitted to the University of California-Davis. Financial support for one of us (R.V.K.) was provided

by the Fannie and John Hertz Engineering Scholarship Foundation.

REFERENCES

1. R. A. Van Konynenburg, Stage III Dislocation Pinning in Silver Resulting from Gamma Irradiation, UCRL-51486 (Nov. 14, 1973) and PhD Thesis, University of California-Davis (1973).
2. D. O. Thompson, O. Buck, R. S. Barnes, and H. B. Huntington, J. Appl. Phys. 38, 3051 (1967).
3. D. O. Thompson, O. Buck, H. B. Huntington, and R. S. Barnes, J. Appl. Phys. 38, 3057 (1967).
4. D. O. Thompson and O. Buck, J. Appl. Phys. 38, 3068 (1967).
5. D. O. Thompson and F. M. Glass, Rev. Sci. Instr. 29, 1034 (1958).
6. P. G. Bordoni, Ricerca Sci. 19, 851 (1949).
7. D. W. Keefer and J. C. Robinson, Annual Technical Progress Report, AEC Unclassified Programs, GFY 1969, AI-AEC 12860, 61 (1969).
8. J. S. Koehler, Imperfections in Nearly Perfect Crystals, p. 197, Wiley, New York, 1952.
9. A. Granato and K. Lücke, J. Appl. Phys. 27, 583, 789 (1956); 28, 635 (1957).
10. D. O. Thompson and V. K. Paré, J. Appl. Phys. 31, 528 (1960).
11. D. Keefer, J. C. Robinson, and A. Sosin, Acta Met. 13, 1135 (1965); and 14, 1409 (1966).
12. G. A. Alers and D. O. Thompson, J. Appl. Phys. 32, 283 (1961).
13. R. Stern and A. Granato, Acta Met. 10, 92, 358 (1962); J. Appl. Phys. 33, 458 (1962).
14. P. L. Gruzin and Yu. D. Zharov, Dokl. Akad. Nauk. SSSR 164, 1280 (1965).
15. V. K. Paré and H. D. Guberman, J. Appl. Phys. 44, 32 (1973).
16. H. M. Simpson and A. Sosin, Phys. Rev. B5, 1382 (1972).

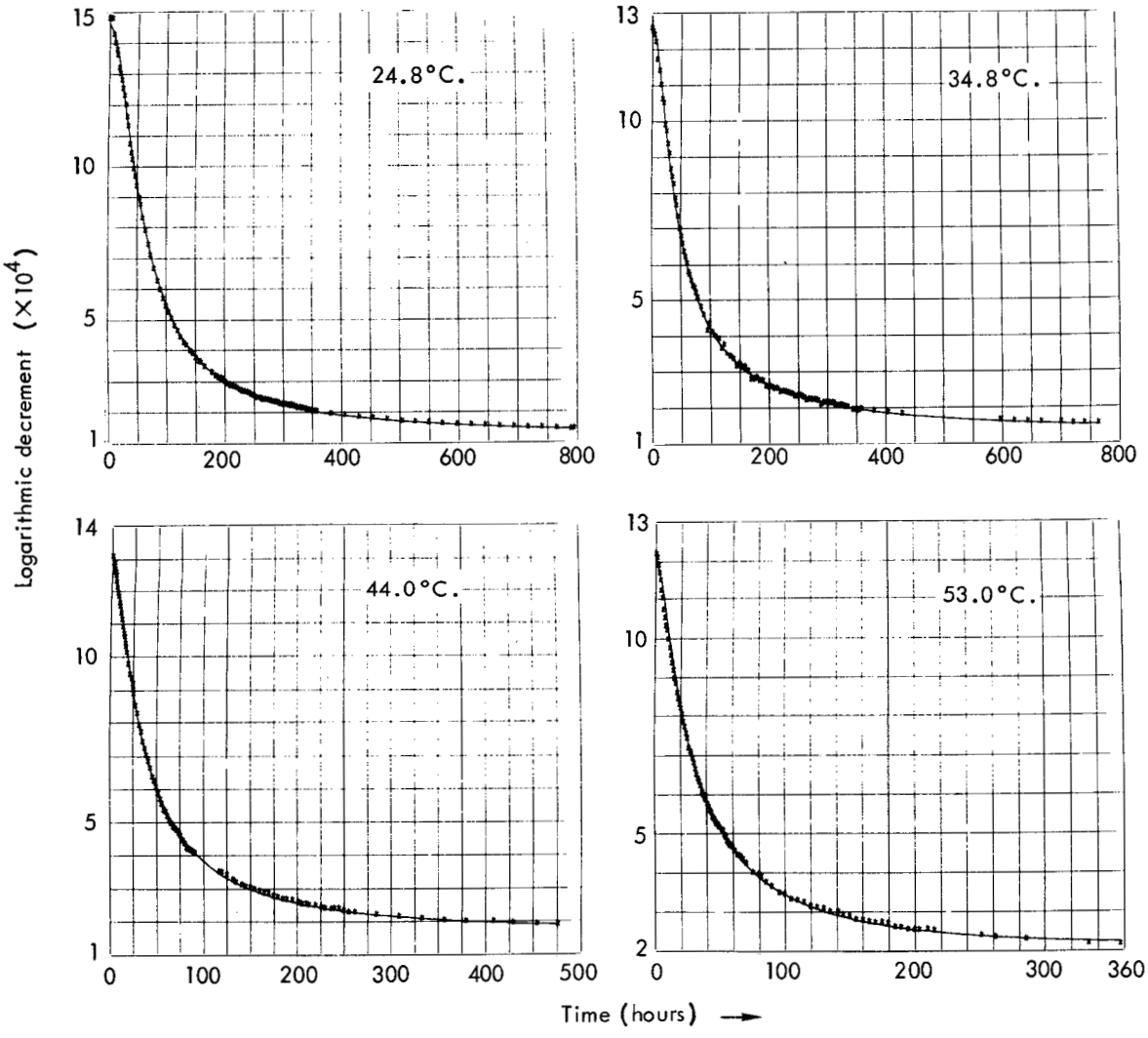


Fig. 1 Damping Data

EFFECTS OF LOW TEMPERATURE NEUTRON IRRADIATION ON THE MECHANICAL PROPERTIES OF IRON SINGLE CRYSTALS

K. Kitajima, H. Abe, S. Takamura* and S. Okuda*
Research Institute for Applied Mechanics,
Kyushu University, Hakozaki, Fukuoka 812
* Japan Atomic Energy Research Institute
Tokai-mura, Ibaraki 319-11, Japan

ABSTRACT

Measurements were made on tensile properties and their recovery characteristics of single crystals of pure iron and iron containing carbon of 4~60 ppm irradiated in reactor to the dose of 3×10^{16}~ 3×10^{17}nvt (>0.1 MeV) at ~5 °K. The yield stress showed large softening at $\leq$ 90 °K saturating to a value nearly independent of orientations for $\geq 1\times10^{17}$ nvt. The softening recovered and hardening set in at several temperature stages. The activation energies of the recovery and the activation parameters of plastic deformations at various annealing stages were determined. Carbon suppressed the softening and it's recovery but much enhanced the hardening at the stage of 300 ~ 400 °K.

INTRODUCTION

Fundamental mechanisms of the irradiation hardening in iron are still in a stage of controversy. The problems to be solved may be, (1) what is the species of lattice defects responsible for irradiation hardening, (2) what is the mechanism of the formation of the lattice defects, and (3) how is explained the mechanism of hardening based on interactions of the defects with dislocations.

Sato and Meshii[1,2,3] showed that the interactions of self-interstitials with dislocations result in the softening of yield stress on the iron single crystals irradiated by electron at very low temperatures. Similar softening was also found in iron irradiated by neutron at low temperature by Groh et al.[4] on polycrystals and Kitajima et al.[5,6] on single crystals. Their works include the effects of annealings after irradiation.

On the other hand, large effects of impurity elements, particularly of interstitial impurities, on irradiation hardening of BCC metals have been emphasized.[7~11] In these works lattice defects responsible for the hardening are surmised to be some complex defects, i.e. irradiation defects combined with interstitial impurity atoms, which are formed at temperatures higher than room temperature.

This paper intends to provide some fundamental informations connecting the two aspects of studies.

PROCEDURE AND RESULTS OF EXPERIMENTS

Material used is Johnson Matthey's pure iron (total metallic impurities of ~ 10 ppm, spectroscopic analysis) zone-refined by 5 ~ 15 passes in the atomosphere of wet and dry hydrogen. Single crystals of 1 mm in diameter and 200 mm in length were produced by the strain anneal method, then decarburized to reduce residual interstitial impurities to < 0.1 ppm.[10] Controlled amount of carbon was doped into some of the specimens. The single crystals were then cut into 5 ~ 6 pieces with the length of 25 mm or 30 mm. The specimens were irradiated in the Liquid Helium Temperature Loop of JRR-3 in Japan Atomic Energy Research Institute at 5 °K for 10 ~ 90 hr to the dose of 3×10^{16} ~ 3×10^{17}nvt (>0.1MeV).

Tensile tests were carried out on as-irradiated specimen at temperatures of 64 °K, 77 °K and 90 °K, and the effects of various post irradiation annealings, isochronal and isothermal annealings at temperatures between 100 °K and 373 °K, were pursued on stress-strain

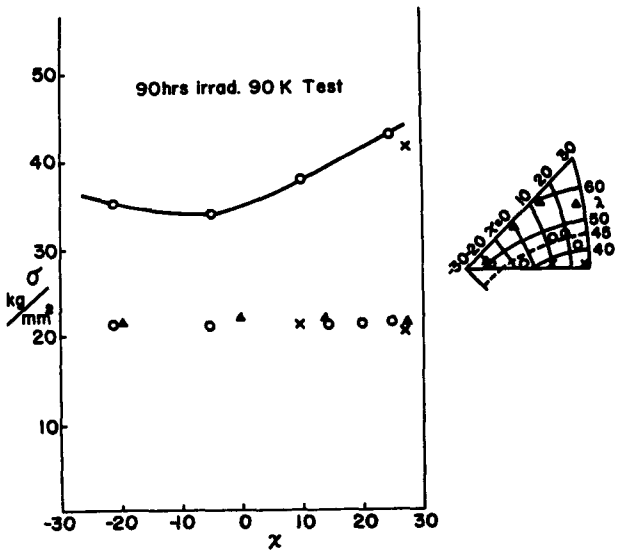


Fig.1 Orientation dependence of yield stress of as-irradiated (lower), JRR-3 90 hr, and unirradiated specimen (upper curve). χ; the angle between the plane of maximum shear stress and (101), λ; the angle between the tensile axis and [11$\bar{1}$].

curves at various testing temperatures. The strain rate was about 10^{-4} sec^{-1}, and reduced sometimes to the one tenth of it.

Fig.1 shows the orientation dependence of yield stress of as-irradiated specimen tested at 90 °K. Compared with the unirradiated ones, irradiated specimens showed large softening in all orientations and had the nearly equal yield stress independent of orientations. Fig.2 illustrates the effects of isochronal annealings on the stress-strain curves tested at 90 °K of the specimens with the same orientation. The orientation and the dose dependence of the isochronal annealing curves of 90 °K yield stress are shown in Fig.3 and Fig.4 respectively. The amount of softening saturates at the dose of ~ 1×10^{17}nvt as seen in Fig.4. The recovery of softening becomes appreciable near 100 °K, and continuously slows down up to ~ 200 °K. From the isothermal annealing curves of the initial stage of the recovery 100 ~120°K, the activation energy of the recovery was calculated as ~ 0.26 eV.[6] The activation energy was increased to ~0.33 eV for the range of 130 ~ 140 °K and ~ 0.5 eV

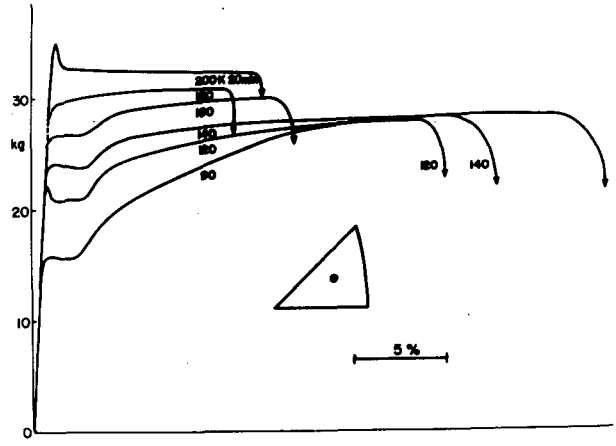


Fig.2 Effects of isochronal annealings (20 min) on stress-strain curve of irradiated specimen tested at 90 °K. JRR-3 65 hr.

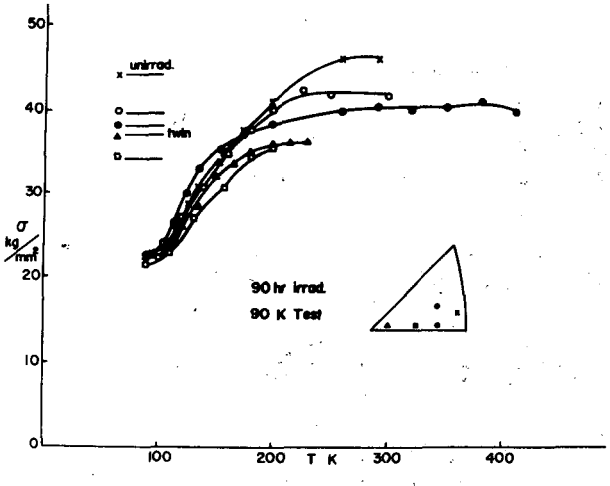


Fig.3 Orientation dependence of isochronal annealing curves (20 min) on 90 °K yield stress of irradiated specimen. JRR-3 90 hr.

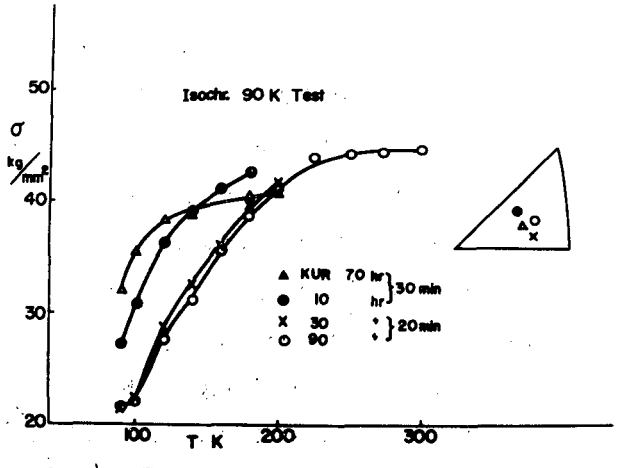


Fig.4 Isochronal annealing curves (20 min and 30 min) on 90 °K yield stress of irradiated pure iron. JRR-3 10, 30, 90 hr and KUR 70 hr.

for the range of 190 ~ 210 °K. Fig.5 shows the isochronal annealing curves of the yield stress tested at 200 °K. It can be seen the recovery of softening takes place near 200°K, and slow hardening in the range of 300 ~ 400 °K with the activation energy of ~ 0.9 eV. The temperature dependences of yield stresses of the specimens annealed for 20 min at temperatures 150 °K, 200 °K and 273 °K are shown in Fig. 6, the activation volumes calculated from the strain rate sensitivities in Fig.7, and in Fig. 8 the activation energies obtained by using the Figs.6 and 7. It is noted that the softening of as-irradiated specimen increases as the increase of

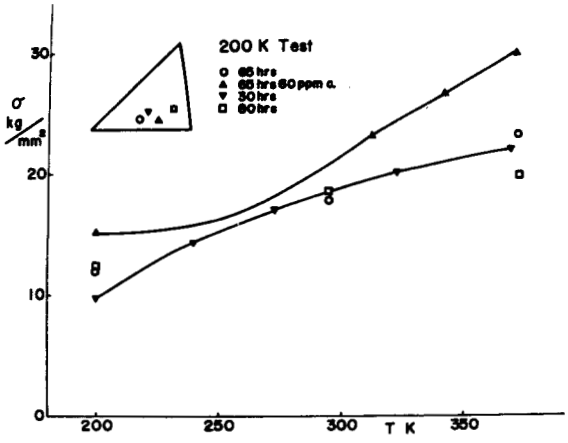


Fig.5 Isochronal annealing curves (20 min) on 200 °K yield stress of irradiated pure iron, JRR-3 30 hr, and 60 ppm C iron, JRR-3 65 hr.

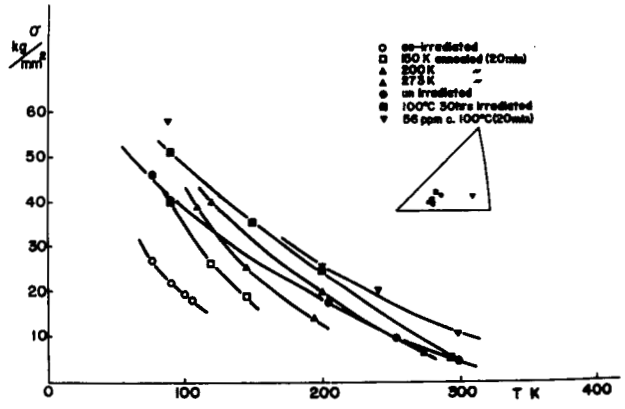


Fig.6 Temperature dependence of yield stress of as-irradiated and annealed (20 min at 150, 200, 273°K) pure iron, annealed 60 ppm C iron (20 min 373 °K), JRR-3 80 hr, and ambient temperature irradiated pure iron, JRR-3 30 hr.

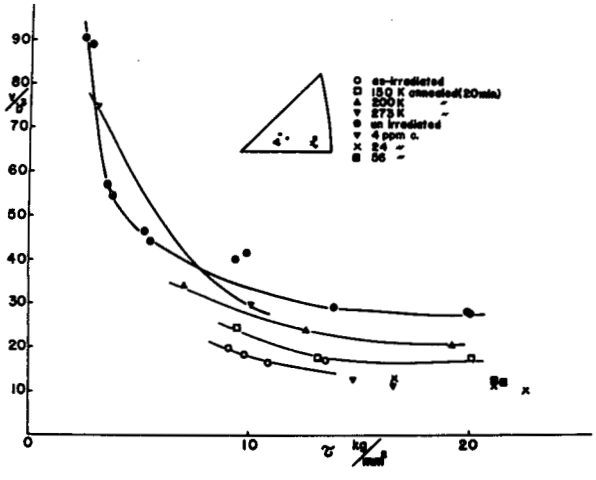


Fig.7 Activation volumes of the specimens in Fig.6 and as-irradiated 4, 24, 56 ppm C iron, JRR-3 30 hr.

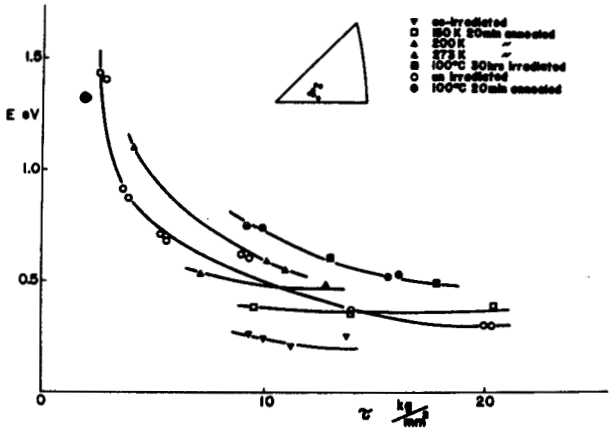


Fig.8 Activation energies of the specimens in Fig.6.

test temperature, and the specimens annealed at 150 °K and 200 °K show hardening at ~ 90 °K but still softening at ~ 150 °K. Activation volume decreases by irradiation but increases again by annealings.

The effects of carbon contents on the softening and recovery characteristics of irradiated specimen are shown in the Figs.5, 6, 7 and 8. Carbon generally suppresses the softening of as-irradiated specimen, but the activation volume is nearly equal to that of as-irradiated pure iron Fig.7. By annealings carbon suppresses the second stage recovery, but enhances appreciably the 350 ~ 400 °C hardening, Fig.5, with the activation energy of ~ 0.9 eV, which is nealy equal to that of diffusion of carbon.

DISCUSSIONS

Low temperature neutron irradiation causes qualitatively similar characteristics of softening as in the case of electron irradiation,[3,4] but quantitatively very different, e.g. Sato and Meshii's results[3] on the orientation dependence of the yield stress show much less softening in $\chi \sim 0°$ but larger one in $\chi \sim 30°$ than the present results in Fig.1. The difference might be attributed to the different nature of lattice defects, or to the different shape and size of specimen.

The theory of softening in BCC metals was proposed by some authors.[2,12] The elastic interactions between screw dislocations and homogeneously dispersed point defects envisaged in the theory of Sato and Meshii,[2] however, could not be applied without modifications for the present case of high density interstitials localized around the depleted zone characteristic to neutron irradiation. One might have to take into account the dislocation core interstitial interaction.[6]

Neutron irradiated specimen shows several stages of recovery of softening, and hardening, corresponding to the stages observed by other methods of measuring such as electrical resistivity, internal friction and magnetic after effects.[13] The rapid recovery of softening near 100 ~ 120 °K with the activation energy of ~ 0.26 eV, Figs.2 ~ 4, may correspond to annihilation of interstitials by migration to vacancies or other sinks in the stage I_E[13]. In this stage many stable di-interstitials[14] are considered to be formed around the depleted zone besides some impurity-inter-

stitial pairs or impurity-di-interstitial combinations, since the density of interstitial is much larger than that of impurities there. Then, the characteristics of the yield stress of 150 °K or 200 °K annealed specimen shown in Figs.6 ~ 8 may be attributed to the interaction between the di-interstitials and dislocations. On the other hand, by annealings in the stage II at 150 ~ 250 °K and the stages III and IV at 300 ~ 400 °K, the clusters of interstitial may increase their sizes absorbing successively interstitials, which might be produced by the dissociation of impurity-interstitial pairs or migration of di-interstitials, though the detailed kinetics of them are not yet determined.[13] The specimens annealed at > 273 °K or irradiated at ambient temperature show the temperature dependent hardening as seen in Fig.6. This was attributed to rather small clusters of interstitials such as I_3 or I_4,[10] since they can be overcomed by thermal activation and might become unstable in close interaction with dislocation as suggested by dislocation channelling. By annealings at higher temperatures the clusters of interstitial may overgrow or be annihilated by absorbing vacancies, which may start to migrate at $\gtrsim$ 300 °C with the activation energy > 1 eV.[15,16] Thus hardening recovers after passing through maximum value.[10,4]

Carbon atoms may provide the site of sink for interstitials in the stage I_E recovery and form carbon-interstitial pair, which might be stable up to the dissociation temperature of 260 °K,[17] thus the stage II recovery is suppressed as seen in Fig.5. At the temperature higher than 260°K, the dissociated carbon and free carbon may migrate to interstitial cluster and form a firm barrier against the movement of dislocations, which may be the cause of large and temperature independent[5,6] hardening of iron containing carbon shown in Fig.6 and also the radiation anneal hardening reported by Wechsler.[9]

The authors would like to present their sincere thanks to the menbers of LHTL group and JRR-3, Japan Atomic Energy Research Institute, and to Dr. N. Tsukuda, and Messrs. Y. Miyamoto and Y. Fujiwara, the Research Institute for applied Mechanics Kyushu University, for their invaluable helps in the experimental works.

REFERENCES

1. A. Sato, T. Mifune, M. Meshii, Proc. 2nd Int. Conf. Strength of Metals and Alloys. II, ASM, 747 (1970).
2. A. Sato, M. Meshii, Acta Met. 21 753 (1973).
3. A. Sato, M. Meshii, Scripta Met. 8 851 (1974).
4. G. Groh, F. Vanoni, P. Moser, Defects and Defect Clusters in BCC Metals and Their Alloys, Ed. Arsenault, 19 (1973).
5. K. Kitajima, H. Abe, Bull. Res. Inst. Appl. Mech., Kyushu Univ. No.40 (1973) (in Japanese).
6. K. Kitajima, H. Abe, N. Tsukuda, Rep. Res. Inst. Appl. Mech. Kyushu Univ., XXII, No.70, 209 (1975).
7. J. G. Y. Chow and S. B. McRickard, Flow and Fracture of Metals and Alloys in Nuclear Environments, ASTM STP 380, 120 (1964).
8. S. B. McRickard and J. G. Y. Chow, Acta Met. 14 1195 (1966).
9. S. M. Ohr, L. E. Hinkle, M. S. Wechsler and C. W. Chen, Proc. 2nd Intern. Conf. Strength of Metals and Alloys, ASM, 742 (1971), M. S. Wechsler, D. G. Alexander, R. Bajaj and O. N. Carlson, Defects and Defect Clusters in BCC Metals and Their Alloys, Ed. R. J. Arsenault, 127 (1973).
10. K. Kitajima, Proc. Intern. Conf. Strength of Metals and Alloys, Supplement Trans. Japan Inst. Metals, 9 182 (1968).
11. J. S. Bryner, Acta Met. 14 323 (1966), J. S. Bryner and J. G. Y. Chow, Acta Met. 18 191 (1970).
12. R. J. Arsenault and T. Cadman, Defects and Defect Clusters in BCC Metals and Their Alloys, Ed. R. J. Arsenault, 19 (1973).
13. H. Bilger, H. Hivert, J. Verdone, J. L. Leveque and J. C. Soulie, Proc. Intern. Conf. Vacancies and Interstitials in Metals. II, Julich, 751 (1968), D. Dautreppe, Studies in Radiation Effects in Solids Vol.3, Ed. G. J. Dienes, 1 (1969).
14. N. Yoshida, M. Kiritani, F. E. Fujita, J. Phys. Soc. Japan, 39 170 (1975).
15. Y. Ikeda, T. Gotoh, K. Abiko and H. Kimura, Crystal Lattice Defects, 5 163 (1974).
16. M.Kiritani, N. Yoshida, H. Takata, Y. Maehara, J. Phys. Soc. Japan 38 1677 (1975).
17. A. Sato, M. Meshii, Phys. Stat. Sol. a)22 253 (1974).

MECHANICAL EFFECTS OF ELECTRON IRRADIATION IN IRON SINGLE CRYSTALS*

M. Meshii and A. Sato**
Department of Materials Science and Engineering
Northwestern University
Evanston, Illinois 60201
U. S. A.

ABSTRACT

Electron irradiation (2 MeV, up to 6 x 10^{18} e/cm^2) decreased the yield stress of iron single crystals in the temperature range from 4.2° to 80° K. The softening effect was highly dependent on the tensile axis orientation. The temperature and strain rate dependency of the yield stress was increased by the irradiation. The annealing of the softening took place between 90° and 150° K. The observation is consistent with an intrinsic solid solution softening mechanism based on the enhancement of screw dislocation motion due to dispersed interstitials.

INTRODUCTION

Low temperature electron irradiation produces a softening effect in iron.[1,2] As the self interstitials are known to interact strongly with dislocations,[6] this softening phenomenon aroused curiosity about the possible mechanisms. It has been reported that low temperature neutron irradiation also causes the softening effect.[2,4]

In this manuscript, the nature of the electron irradiation softening is further investigated by examining the effects of tensile axis orientation, the temperature and strain rate dependence of the yield stress and the effect of post-irradiation annealing. As the deformation

* This research was supported by the U. S. Energy Research and Development Administration (formerly AEC).

** Present address: Department of Metallurgy, Tokyo Institute of Technology, Ookayama, Meguro-ku, Tokyo, Japan.

structures of the irradiated and unirradiated iron specimens were nearly identical,[5] the enhancement of dislocation motion by electron irradiation appears to be primarily responsible for the observed softening. The misfit strain associated with dispersed interstitials exerts a couple force on screw dislocations, enhancing the double kink formation,[6] and can be the cause of the softening. The orientation dependence suggests that the core structure of a screw dislocation and/or the potential variation for the screw dislocation gliding on the different slip planes may also be sensitively altered by the presence of the interstitials.

EXPERIMENTAL RESULTS

The experimental procedures are detailed in our earlier reports.[1,7] The essential points are: (1) The Battelle-AISI iron containing less than 5 wt. ppm of non-metallic impurities and 30 wt. ppm of metallic impurities was used as the starting material; (2) The single crystal growth and the subsequent annealing were performed in the ZrH_2 purified hydrogen atmosphere; (3) The 2 MeV electron irradiation was carried out below 60° with dosages up to 6.2×10^{18} e/cm^2 (estimated interstitial concentration $\sim$ 100 ppm).

Orientation Dependence

The dependence of the yield stress of bcc metals on the crystallographic orientation of the tensile axis is well known.[8] However, the correlation of this orientation dependence with the effects of solutes, or point defects, has not been investigated except in a few cases.[7] In this investigation two directional parameters, λ and χ, were varied to study the relation of the orientation with the irradiation effect. λ represents the angle between the tensile axis and [110], and was $\sim 10°$ when χ was varied. χ represents the angle between [101] and the normal to the maximum resolved shear stress plane containing the primary Burgers vector, $a/2[11\bar{1}]$. Therefore the maximum resolved shear stress plane coincides with the (211), (101) and (112) planes for $\chi = -30°$, 0° and 30° respectively. The variation of the irradiation softening with χ was striking (Fig. 1). At $\chi \cong 30°$ a large softening effect was observed.

With the dosage of 1.5×10^{18} e/cm^2, the yield stress was reduced by 60%. The resulting yield stress was $\sim$ 25 kg/mm^2 (expressed by the tensile stress) at 60° K, the lowest yield stress ever reported in iron at this temperature range. The irradiation softening effect for $\chi = 0$ was mild, a reduction of yield stress by 10% with similar irradiation. Consequently, the post-irradiation yield stress decreases spontaneously with χ from -30° to 30°.

The effect of λ was examined at $\chi = 30°$ (Fig. 2). The softening effect remained large as λ was increased from 10° to 20°. On the other hand, when λ was reduced slightly from 10°, the magnitude of the softening decreased rapidly and was less than 20% at $\lambda \cong 4°$.

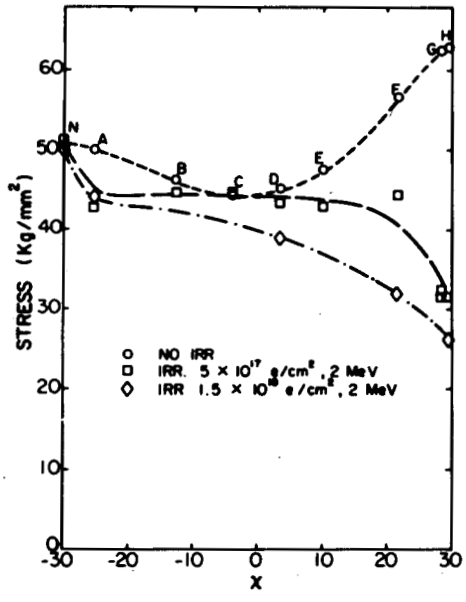


Fig. 1: Yield stress vs. χ relation.

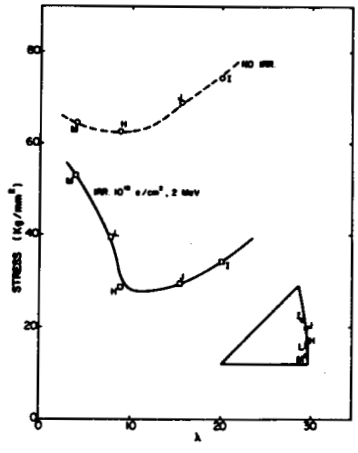


Fig. 2: Yield stress vs. λ relation.

Temperature and Strain Rate Dependence of Yield Stress

The temperature dependence of the yield stress, $\partial\sigma/\sigma T$, was increased by the irradiation in spite of the fact that the magnitude of the yield stress decreased. Therefore the fraction of softening was large between 40° and 80° K (Fig. 3).

Since electron irradiation improved the ductility of the iron, the strain rate dependence could be more reliably determined over the temperature range from 4.2° to 80° K in the irradiated iron (Fig. 4). The irradiation increased the strain rate dependence. The strain rate dependence also increased with the temperature and reached the maximum between 40° and 60° K. It appeared to decrease with a further increase in temperature.

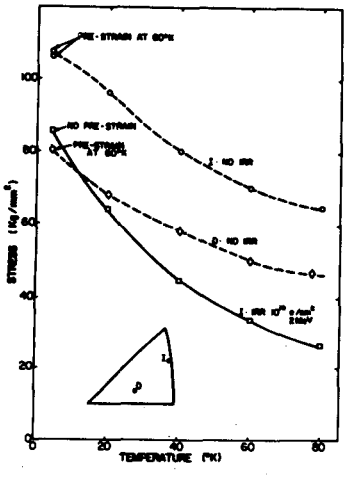


Fig. 3: Yield stress vs. temperature relation. The solid line represents the yield stress of irradiated specimens. The yield stress of unirradiated specimens at 4.2° K was determined after prestrain at 60° K.

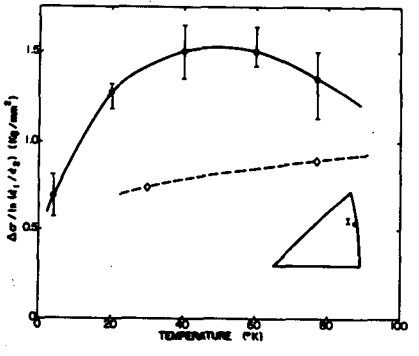


Fig. 4: Strain rate dependence of yield stress vs. temperature dependence. The solid line represents irradiated specimens. The data for unirradiated specimens (open diamond) are not as reliable as those of irradiated specimens, as the specimens failed before a number of strain rate changes could be carried out.

Recovery of Irradiation Softening

When the irradiated iron specimens were annealed at a temperature above 90° K, the softening effect was reduced (Fig. 5). This recovery peak of the irradiation softening centered around 105° K and the recovery effect appeared to saturate near 150° K.

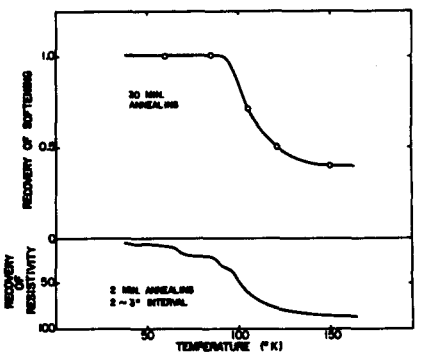


Fig. 5: Isochronal recovery of electron irradiation softening and irradiation induced resistivity.

DISCUSSION

The resistivity recovery of electron irradiated iron indicates that no free migration of interstitials takes place below 100° K.[9] The dislocation-interstitial interaction is considerably larger than the dislocation-vacancy interaction.[10] As the interactions can be regarded as primarily elastic in nature, a similar situation should exist in bcc metals. Therefore the softening effect is caused by the interstitials of nearly random distribution. According to an electron microscopic investigation[5] of the dislocation structure in irradiated and unirradiated iron single crystals after deformation at 60° K, there was little difference in structure between the two types of specimens. In both cases, screw dislocations were uniformly distributed throughout the specimens. This structural observation supports a softening mechanism due to an increase in dislocation mobility. A theory has been proposed[6] to explain an increase in dislocation mobility by point defects. The formation of double kink is promoted by a local misfit strain, since its stress field exerts a couple force on a screw dislocation. The apparent activation volumes and energies can be calculated from the temperature and strain rate dependence of the yield stress. These

quantities were clearly reduced by electron irradiation, supporting the contention that the dislocation motion is aided by the interstitials.

The mechanism of the electron irradiation softening strongly supports the intrinsic mechanism for the low temperature strength of iron and suggests a mechanism for the solid solution softening phenomenon. On the other hand, an extrinsic mechanism such as gettering of carbon and nitrogen atoms in iron by titanium (scavenging mechanism) has been reasonably well established.[11] It has also been proposed in a series of recent investigations in niobium and tantalum base alloys that the solid solution softening effect occurs exclusively in ternary systems and that the softening effect is attributed to the effect of the solute-solute interaction on dislocation motion.[12,13] Therefore the possibility of the extrinsic mechanism for the observed irradiation softening must be examined carefully.

The interstitial impurity content of the specimens used in this study does not favor the extrinsic possibility. The softening effect also decreased with increasing impurity content. The disappearance of the softening effect at the temperature range where the free migration of interstitials occurs also discourages the extrinsic possibility. Another experiment supports this conclusion. The electron irradiation increased the microyield stress (determined as 10^{-4} plastic strain) although the macroyield stress was reduced. If the irradiation is to reduce the resistance of the impurities to dislocation motion, it is difficult to explain the hardening effect on the microyielding. However, the intrinsic mechanism proposed in this report provides a logical explanation for this seemingly contradictory observation.[14] The orientation dependence of the electron irradiation softening effect also supports the intrinsic mechanism. The orientation dependence of the yield stress of pure bcc metals can be understood by the asymmetric core structure of screw dislocations or by the asymmetric distribution of the potential for the dislocation motion to different directions. The core configuration or the potential distribution is expected to be extremely sensitive to the local atomic disturbance (or the local strain field). The presence of interstitial atoms would change the atomic arrangement

significantly and may cause the observed orientation dependence of the softening effect.

REFERENCES

1. A. Sato, T. Mifune and M. Meshii, Proc. Second Int. Conf. on Strength of Metals and Alloys, p. 747 (1970) A.S.M., Metals Park, Ohio; A. Sato and M. Meshii, phys. stat. sol. 18A, 699 (1973).
2. P. Groh, F. Vanoni and P. Moser, Proc. Int. Conf. Defects and Defect Clusters in BCC Metals and Their Alloys, Gaithersburg, Md., Nuclear Metallurgy, vol. 18, AIME, New York, p. 19 (1973).
3. M. Meshii, T. Mifune and K. Ono, Proc. Int. Conf. on Strength of Metals and Alloys, Supplement to Transactions of the Japan Institute of Metals 9, 193 (1968).
4. K. Kitajima, H. Abe and N. Tsukuda, Reports of Research Institute for Applied Mechanics, Kushu University 22, 209 (1975); also a report in this proceeding.
5. J. Nagakawa, A. Sato and M. Meshii, Phil. Mag., in press.
6. A. Sato and M. Meshii, Acta Met. 21, 753 (1973).
7. A. Sato and M. Meshii, Scripta Met. 8, 851 (1974).
8. For a review, J. W. Christian, Proc. 2nd Int. Conf. on Strength of Metals and Alloys, p. 31 (1970) A.S.M., Metals Park, Ohio.
9. A. Sato and M. Meshii, phys. stat. sol. 22A, 253 (1974).
10. M. S. Bapna and M. Meshii, phys. stat. sol. 40, 725 (1970); 51, 437 (1972).
11. W. C. Leslie, Met. Trans. 3, 1 (1972).
12. M. G. Ulitchny, A. A. Sagues and R. Gibala, Proc. Int. Disc. Mtg. on Defects in Refractory Metals, p. 245 (1972) S.C.K./C.E.N. Mol, Belgium (1972).
13. M. G. Ulitchny, A. K. Vasudevan and R. Gibala, Proc. Third Int. Conf. on Strength of Metals and Alloys, p. 505 (1973) Cambridge, England.
14. A. Sato and M. Meshii, phys. stat. sol. 28A, 561 (1975).

RADIATION EMBRITTLEMENT OF METALS AND ALLOYS*

M. S. Wechsler
Ames Laboratory ERDA
and Department of Materials Science and Engineering
Iowa State University
Ames, Iowa 50010

ABSTRACT

Radiation embrittlement refers to enhanced fracture susceptibility and reduction in load-carrying capacity exhibited by irradiated metals. Three types of radiation embrittlement are identified: (1) radiation embrittlement in nominally ductile metals, (2) radiation embrittlement in metals that undergo a ductile-brittle transition, and (3) high-temperature grain boundary embrittlement. This paper deals with type (1) and, more briefly, type (2) radiation embrittlement.

Radiation embrittlement in nominally ductile metals is characterized by the premature onset of plastic instability, which causes a sharp decrease in the macroscopic plastic strain that the material can sustain before necking (uniform strain) and breaking (fracture strain). Dislocation channeling seems to be largely responsible and experimental results are reviewed. The origin of dislocation channeling is discussed.

Irradiated metals that exhibit a ductile-brittle transition show an increase in the transition temperature but the nature of the transition (shear to cleavage fracture) does not appear to be greatly altered. A key factor is the temperature dependence of yielding and how it is affected upon irradiation. Impurities exert an influence on the stability of radiation-produced defect clusters and thus can alter the amount of radiation embrittlement experienced upon irradiation at somewhat elevated temperatures.

In general, radiation embrittlement appears to stem mostly from changes in plastic properties (particularly in the trend toward more dynamic and inhomogeneous plastic deformation) rather than from changes in the inherent fracture process.

*Work performed at Ames Laboratory, Iowa State University, under contract with the Energy Research and Development Administration.

INTRODUCTION

The primary issues in mechanical metallurgy are, of course, strength and ductility. It is now a fairly well accepted proposition that most factors or treatments that strengthen metals also cause a decrease in ductility, although the effect of grain size is an important exception. It comes as no surprise, therefore, that radiation hardening is almost always accompanied by a decrease in ductility.

For a number of reasons, radiation embrittlement is a more difficult subject to treat than radiation hardening. As has been pointed out in earlier reviews[1,2], radiation embrittlement may take several forms, depending particularly on the nature of the metal and on the test temperature. Also, several measures of ductility can be used, which are indicators of different fundamental aspects of mechanical behavior and may be derived from different types of tests. In what follows, we refer mainly to uniform elongation and reduction in area from tensile tests, ductile-brittle transition temperature from notched bar impact tests, and fracture toughness from tests on double cantilever beam samples. Uniform elongation is a measure of how much strain the metal can tolerate before work hardening no longer compensates for the stress increase due to local reductions in area, thus causing plastic instability. As such, uniform elongation is perhaps a reflection of the metal's plasticity rather than its fracture behavior. Nevertheless, the onset of plastic instability signals the inevitable and autocatalytic rupture of material. In the present context, therefore, the tendency of irradiated metals to exhibit reductions in uniform elongation is considered to be a type of radiation embrittlement.

The above discussion illustrates another reason for the complexity of radiation embrittlement in that the fracture process is always preceded by some amount of prior plastic deformation. Therefore, the phenomenon of radiation embrittlement is inextricably connected with that of radiation hardening.

Particularly from the point of view of fundamental aspects, it is convenient to separate the subject into: (1) radiation embrittlement in nominally ductile metals, (2) radiation embrittlement in metals that undergo a ductile-brittle transition, and (3) high-temperature grain boundary embrittlement. This paper deals principally with radiation effects on yield and fracture behavior at lower temperatures (below $0.5T_m$; T_m = melting temperatures in °K) where the fracture path is transcrystalline and creep rupture is not an important consideration.

RADIATION EMBRITTLEMENT IN NOMINALLY DUCTILE METALS

The earliest observations of radiation effects on the yielding behavior of metals were made on high-purity copper, notably by Blewitt et al.[3], Diehl et al.[4,5], and Makin et al.[6,7]. The essential features of these effects, illustrated in Fig. 1 (Makin[8]), are: (1) increase in yield stress; (2) increase in the ultimate tensile stress, but to a smaller extent than the increase in yield stress; (3) decrease in the rate of work hardening; and (4) decrease in uniform elongation or strain. Items (2)-(4) are alternative manifestations of the same essential result, i.e., that the load-carrying capacity of the irradiated metal is sharply curtailed by the onset of premature plastic instability. Furthermore, these alterations in the shape of the tensile stress-strain curve for copper appear to be broadly representative of ductile metals of all three crystal structures and of pure metals and complex alloys alike. Fig. 2 shows, for example, the load-extension curves for unirradiated and irradiated ferritic steel (Wechsler et al.[9]) for several test temperatures. Ferritic steel exhibits a ductile-brittle transition, but we refer here to the decrease in uniform strain in the ductile domain. As seen in Fig. 3, the uniform strain is strongly decreased upon irradiation as measured over a range of temperatures above, say, 100°K where the fracture occurs by shear, not cleavage.

The origin of the decrease in uniform strain upon irradiation is elucidated by observations of slip lines on polished surfaces of deformed samples. Some of the first observations of this type were

again performed on neutron-irradiated copper. Blewitt et al.[3] pointed out that plastic deformation becomes inhomogeneous in irradiated copper with coarse deep slip steps appearing on the surface separated by regions essentially undeformed. By contrast, slip in unirradiated copper is quite homogeneous. The same is true for irradiated BCC metals and for samples deformed in tension and in compression. Fig. 4 illustrates the case for unirradiated and neutron-irradiated single crystal niobium strained 10% in tension.[10] Whereas homogeneous slip is apparent for the unirradiated sample, the irradiated sample exhibits deep coarse slip bands separating regions that are not deformed at all. Fig. 5 shows similar results for vanadium deformed in compression.[11] The fact that irradiated metals exhibit inhomogeneous coarse slip means that local regions of the sample become heavily deformed although the strain averaged over the entire gage length may be quite low. As a result, the heavily strained regions reach the point of plastic instability, which is manifested in a decrease in uniform strain.

The coarsening of slip upon irradiation is probably a consequence of dislocation channeling, in which radiation-produced defect clusters are removed upon post-irradiation plastic deformation. As is pointed out in a recent review[12], dislocation channeling is widely exhibited in irradiated or quenched FCC, BCC, or HCP metals. The correspondence between surface slip steps and dislocation channels seems firmly established since the plane of the channels are consistent with the slip plane in the given metal. Furthermore, the correspondence was directly demonstrated by Sharp[13] by preserving the contours of the deformed surface of irradiated copper, as is seen in Fig. 6. The concentration of slip in localized bands in irradiated metals is thus associated with the formation of dislocation channels. The radiation-produced defect clusters are apparently removed when slip dislocations are set in motion along the slip plane in the earliest stages of deformation. The slip process then continues by the motion of subsequent slip dislocations along the same incipient channel in preference to the nucleation of a new band in an adjacent region of the crystal. As a result, the deformation becomes considerably more localized than is the case

for unirradiated metals.

The amount of strain concentrated in the dislocation channels can be estimated by the shear displacement or offset occurring in microstructural features through which the dislocation channels pass. Fig. 7 from the work of Tucker et al.[14] shows a high-magnification TEM photomicrograph of a dislocation channel (approximately vertical at C) in Nb irradiated at 50°C to 4.4 x 10^{18} neutrons/cm^2 and strained 6.6 percent in tension. As indicated, the trace of the dislocation channel at C is $[\bar{2}11]$ and the channel plane is probably $(0\bar{1}1)$. Two segments of a helical dislocation are seen at AA' and BB'. The helical dislocation with axis along $[01\bar{1}]$ was apparently sheared in two by the dislocation channel. Dislocations with Burgers vector (a/2) $[\bar{1}11]$ moving in the $(01\bar{1})$ plane are believed to have produced the dislocation channel and the observed offset. From measurement of the width of the channel (about 4500 Å) and the component along $[\bar{2}11]$ of the shear displacement (about 9500 Å), one calculated that the shear strain in the channel is about 220 percent.[12,14] This corresponds to an average of about 1.8 slip dislocations per $(0\bar{1}1)$ plane within the channel. Typically, 1-3 dislocations per plane were observed at various intersections of dislocation channels and microstructural features in Nb[14] and Cu[15]. The high strain that can reside within the channels is also apparent in Fig. 6.

Since dislocation channeling and the resultant coarsening of slip are so closely implicated in the radiation-produced decrease in uniform strain and premature ductile fracture, an important fundamental aspect of radiation embrittlement is the mechanism by which the defect clusters or dislocation loops are eliminated by the moving slip dislocations. Mechanisms have been proposed[16-18] whereby slip dislocations interact with the radiation-produced loops and cause them to be incorporated into the slip dislocation. Also, observations have been briefly described[19] involving in-situ straining in the electron microscope in which such dislocation interactions seem to occur. However, the mechanism of Saada and Washburn[16] requires that the loop and slip dislocation have the same or opposite Burgers vectors, and the other

mechanisms[17,18] appear to be unique to FCC metals. Noggle and Narayan[19] have mentioned a 4-step dislocation reaction mechanism that is applicable also to BCC metals, but a complete account has not yet been presented. They also indicated evidence for the prismatic slip of loops when interacted by a slip dislocation. Such prismatic slip can lead to contact between loops resulting in coalesence or mutual annihilation depending upon whether the vacancy or interstitial character of loops is the same or different, respectively. A point to be taken into consideration is that dislocation channeling has been observed by Sharp[13] in neutron-irradiated copper deformed at temperatures as low as 4 °K, indicating that long-range thermal activation is not a necessary factor.

Another suggestion for the mechanism of defect cluster elimination by moving slip dislocations leading to the formation of dislocation channeling is adiabatic heating[14]. High-speed cinephotography was employed by Makin and Sharp[20] to measure the speed of slip line formation in irradiated copper. Even at 3800 frames per second the initial slip line moved across the field of view within one frame, thus setting a lower limit of 300 cm/sec for the velocity of formation of slip bands or about 10^{-3} sec for the formation time. Furthermore, the shear strain in the dislocation channel was observed to be about 300 percent[15], thus corresponding to a shear strain rate of about 3×10^{3} sec^{-1}. By contrast, the applied tensile strain rate averaged over the entire gage length of the sample was 10^{-3} sec^{-1}. For unirradiated copper, Pond[21] employed an interferometric cinemicrographic technique with an applied tensile strain rate between 3×10^{-4} and 3×10^{-3} sec^{-1}. On a local scale, the slip bands were not distributed homogeneously throughout the deformed crystal, nor did the slip bands move with a uniform velocity. However, the maximum velocity appeared to be about 3×10^{-5} cm/sec. Similar maximum slip band formation velocities were observed by Pond[21] for aluminum. Earlier velocity measurements by Haasen and Siems[22] on aluminum gave values below 10^{-3} cm/sec, roughly in agreement with those of Pond[21].

The burden of the above discussion is to emphasize the intense and rapid slip band formation that occurs in irradiated metals as

compared to unirradiated ones. Marked temperature rises are known to take place in metals at high strain rates. An extreme case was described by Zener[23], in which a localized temperature increase of more than 900°C was demonstrated by the formation of thin layers of martensite in a ferritic steel after rapid deformation. Freudenthal and Weiner[24] and Eshelby and Pratt[25] have indicated that a large shear on many closely-packed planes can give an appreciable local increase in temperature given by Freudenthal and Wiener's Eq. (7), viz.

$$\Delta T \cong \frac{\tau\delta}{2\ell\rho c}$$

where τ is the shear stress on the slip plane, δ is the shear displacement, ρ is the density, c is the specific heat, and 2ℓ is the assumed distance between dislocations on nearby parallel slip planes whose simultaneous motion gives rise to the slip band (or dislocation channel). If n is the average number of dislocations per plane that sweep down the dislocation, b is the Burgers vector and d is the interplanar distance between slip planes, we may set $(\delta/2\ell) = (nb/d)$, whereby

$$\Delta T = \frac{\tau nb}{\rho cd} = \frac{\tau\gamma}{\rho c}$$

where γ is the shear strain in the dislocation channel. Letting n = 2 and substituting values appropriate to Cu[15], Nb[14], and V[11], we obtain ΔT = 14, 80, and 144°C. These temperature increases do not appear sufficient to cause the annealing of defect clusters within the channel. However, the calculation assumes that the energy of plastic deformation is distributed uniformly among all the atoms within the channel. If the energy were dissipated preferentially near the defect cluster barriers, the temperature increase could perhaps be greater. The dynamic interaction between moving dislocations and barriers is such that the kinetic energy of the interacting dislocation segment is delivered to the barrier, thus exciting local thermal vibrations. Such interactions are discussed by Suzuki[26], Takamura and Morimoto[27], and Ookawa and Yazu[28].

Ductile fractures, particularly in the absence of inclusions, are sometimes observed to occur in thin lamellar regions known as "shear disks" that lie parallel to the shear plane. Since the shear disk is a region of high shear strain, it resembles a dislocation channel. As discussed by Tegart[29], a stress concentration τ^* exists at the tip of a shear disk given by

$$\tau^* + \left(\frac{c'}{r}\right)^{1/2} \tau$$

where c'is the length of the shear disk, r is the radius of curvature at the tip of the disk, and τ is the applied shear stress. Also, high tensile stresses develop at the interface between the shear disk and the region ahead of it where the strain is lower. This tends to produce cracks (shear cracks). When the shear crack propagates rapidly across the sample, temperature increases occur and the fracture is called an adiabatic shear fracture. Rice and Levy[30] have calculated the local temperature elevations accompanying plastic deformation near the tips of running and stationary cracks, based on known solutions for the stress and strain near the crack tip. However, insufficient data are available for a quantitative test of the results.

Other commonly used ductility parameters, in addition to uniform strain are fracture strain and reduction in area (at the fracture surface). When the uniform strain is reached and necking begins, all of the subsequent deformation is concentrated in the region of the neck. This local extension depends on specimen dimensions (specifically, on the ratio of gage diameter to length) and is therefore not a material constant. Reduction in area, however, does not depend on specimen dimensions and is a valid measure of the amount of plastic deformation that can be sustained before fracture occurs.

Tensile tests on a number of metals, e.g., Cu[8], Fe[31], steel[9], Nb[10], and V[32], have indicated that the reduction in area at fracture is affected by irradiation to only a slight extent, if at all. This statement refers to test temperatures above the ductile-brittle transition temperature (for metals that exhibit such a transition) and below the

equicohesive temperature (i.e., for transgranular, not intergranular, fractures). Fig. 8 illustrates results for a ferritic steel. By comparison with Fig. 3, it is seen that above about 100°K the reduction in area is reduced upon irradiation to a much lesser extent than the uniform strain. Furthermore, the true fracture stress (load at fracture divided by area of the fracture surface) is not changed significantly upon irradiation[9,31,33] (see, for example, Fig. 4 of Ref. 9 or Fig. 6 of Ref. 33). Still further, there appears to be no significant change in the metallographic appearance of the fracture surface (Fig. 9, Ref. 9). On balance, then, it seems that the principal effect of irradiation on nominally ductile metals below the equicohesive temperature is to alter the nature of plastic flow through strain concentration, not by any change in the mechanism of the fracture process itself.

RADIATION EMBRITTLEMENT OF DUCTILE-BRITTLE METALS

A ductile to brittle transition upon decrease in temperature is displayed most prominently by BCC metals. These metals also exhibit an increase in yield stress with decrease in test temperature. The origin of the temperature dependence of yielding has not been definitely established (for review, see Ref. 54), but two general approaches are apparent: intrinsic mechanism based on the atomic arrangement of the BCC crystal lattice and extrinsic mechanism based on interstitial impurities. Thorium is an interesting metal in this connection since, despite the fact that it has the FCC structure below 1400°C, it nevertheless has a high solubility for interstitial impurities. The solubility of carbon, for example, in Th is reported[34] to be 3500 wt ppm at room temperature. Furthermore, Peterson and Skaggs[35] have shown that, while high-purity Th (4 wt ppm C) shows very little temperature dependence of yielding typical of an FCC metal, considerable temperature dependence is exhibited upon increasing the carbon concentration. Also, low-carbon Th does not display a ductile-brittle transition, but a transition is observed for Th containing 300, 1600, and 2100 wt ppm carbon (see Fig. 4.31, Ref. 36). For BCC metals also there is a distinct decrease in temperature depend-

ence of yielding with decreasing interstitial impurity concentration, as has been shown, for example, for C in Fe[37,38], O in Nb[39-41], N in Ta[42], O in V[43-45], and N in V[45,46].

Figure 8 indicates that the ductile-brittle transition temperature (DBTT) in unirradiated A212B steel, as revealed by reduction in area on smooth tensile samples tested at a low strain rate of 2.7×10^{-4} sec^{-1}, occurs at about $62^{o}K$. Upon irradiation at $60^{o}C$ to 1×10^{19} n/cm^2 (E>1 MeV) the DBTT increases by somewhat greater than $10^{o}K$. By contrast, when the tests are conducted with notched bars (Charpy samples) under impact loading (Fig. 9), the DBTT for unirradiated samples is at about $278^{o}K$, and the same irradiation increases the DBTT by about $103^{o}K$. In addition to the increase in DBTT, the irradiation also produces a decrease in fracture energy (absorbed energy for fracture) in the ductile domain by about 30%. This decrease in energy is the equivalent (under the high strain-rate triaxial stress conditions of the impact test) of the decrease in area under the stress-strain curves of Fig. 2 (which apply to smooth samples tested under uniaxial stress conditions). Thus, the decrease in fracture energy on the ductile shelf is apparently another manifestation of the coarsening of slip discussed in the previous section. Fig. 9 also shows plots of the percent of the fracture surface exhibiting fibrous fracture characteristic of fracture by a shear mechanism. The transition from fibrous to crystalline fracture surface appearance occurs over the same temperature range as the transition indicated by fracture energy for both unirradiated and irradiated samples.

The fact that the ductile-brittle transition is observed for metals that exhibit a strong temperature dependence of yielding gives credence to the Ludwik-Davidenkov criterion for the DBTT.[9,33,47] The criterion, illustrated in Fig. 10, assumes that the material will be ductile or brittle depending upon whether the yield stress σ_y or the cleavage fracture stress σ_c is reached first as the stress is increased at a given temperature. Thus, the point of intersection between the σ_y and σ_c curves defines the DBTT. The cleavage fracture stress is assumed to be relatively independent of temperature, strain rate and microstructural features such as the defect clusters introduced upon irradiation. The

yield stress, however, increases rapidly with decreasing test temperature and is increased upon irradiation. Thus, the DBTT is shifted upward on the temperature scale upon irradiation. The increase in the DBTT upon irradiation occurs chiefly, therefore, as a result of the radiation hardening. However, it is difficult to test the criterion quantitatively using notched bar impact tests to determine DBTT and smooth-sample tensile tests to determine σ_y since corrections to σ_y must be applied to provide for differences in strain rate and stress state (triaxiality correction or plastic constraint factor[47]) that apply to the two types of tests. Such a test of the criterion was attempted by Wechsler et al.[9] and led to the conclusion that radiation hardening is in itself adequate to explain the observed increase in DBTT upon irradiation based on the Ludwig-Davidenkov criterion, but exact agreement required a decrease in the triaxiality correction from 2.1 to 1.7 or an increase in σ_c upon irradiation. Better agreement was obtained by Wullaert et al.[33c] based on information from instrumented impact tests.

The temperature dependence of yielding in FCC metals is greatly increased upon irradiation, as has been known for some time.[3,5,8] In this regard, radiation-produced defect clusters have a similar effect as that of interstitial impurities in FCC thorium (see above). For BCC metals, where the temperature dependence is often quite large even for unirradiated samples, the dependence on test temperature of the increase in yield stress upon irradiation is not clear. In some cases, an increased temperature dependence upon irradiation was reported (e.g., W[48], Nb[49], Fe[50,51]), whereas other studies (e.g., Nb[10] and steel[9]) seemed to indicate very little change in the temperature dependence. For V, Arsenault and Pink[52] reported that the temperature dependence is increased, decreased, or not changed depending on whether the oxygen concentration is low (< 90 wt ppm), medium (100-300 wt ppm), or high (1800 wt ppm). A similar study by Wechsler et al.[43] seemed to indicate increased temperature dependence upon irradiation with increasing oxygen concentration for test temperatures above about 200°K, but the dependence on oxygen concentration was reversed at still lower temperatures where twinning may be a factor. In a recent study,[11,53]

oxygen was observed to increase the radiation-produced defect cluster density in vanadium and to increase the stability of the defect clusters against annealing. Furthermore, the trapping of oxygen appears to be associated with radiation-anneal hardening[54] observed in V[43,53,55-59] and Nb[60-62]. A decrease in the fracture strain upon annealing in the temperature range where radiation-anneal hardening takes place has been reported for Nb[60] and V[32,55]. Furthermore, the radiation embrittlement in the as-irradiated condition (irradiation temperature, $\sim$ 85°C) appears to increase with increasing oxygen concentration[32]. The critical role of impurities in radiation embrittlement is also illustrated by the increased radiation embrittlement of pressure vessel steels upon irradiation at 288°C (550°F) that accompanies the presence of trace impurities like Cu and P[63]. This effect may be associated with the increased stability of defect clusters with increasing impurity concentrations, similar to the effect of oxygen in vanadium[53], but further work needs to be done to establish the mechanism more definitely.

REFERENCES

1. M. S. Wechsler, p. 296 in Interaction of Radiation with Solids, J. Nihoul et al., Eds., North-Holland Publishing Co., Amsterdam, 1965.
2. J. O. Stiegler and J. R. Weir, Jr., p. 311 in Ductility, American Society for Metals, Metals Park, Ohio, 1968.
3. T. H. Blewitt, R. R. Coltman, R. E. Jamison, and J. K. Redman, J. Nucl. Mater. 2, 277 (1960).
4. J. Diehl, C. Leitz, and W. Schilling, Phys. Lett. 4, 236 (1963).
5. J. Diehl, p. 129 in Radiation Damage in Solids and Reactor Materials, International Atomic Energy Agency, Vienna, 1962.
6. M. J. Makin, A. D. Whapham, and F. J. Minter, Phil. Mag. 6, 465 (1961).
7. M. J. Makin and F. J. Minter, Acta Met. 8, 691 (1960).
8. M. J. Makin, p. 627 in Radiation Effects, W. F. Sheely, Ed., Gordon and Breach, New York, 1967.

9. M. S. Wechsler, R. G. Berggren, N. E. Hinkle, and W. J. Stelzman, p. 242 in Irradiation Effects in Structural Alloys for Thermal and Fast Reactors, STP 457, American Society for Testing and Materials, Philadelphia, 1969.
10. M. S. Wechsler, R. P. Tucker, and R. Bode, Acta Met. 17, 541 (1969).
11. R. Bajaj, Radiation Damage in Vanadium Doped with Oxygen, Ph.D. Thesis, Iowa State University, Ames, Iowa, 1975.
12. M. S. Wechsler, p. 19 in The Inhomogeneity of Plastic Deformation, American Society for Metals, Metals Park, Ohio, 1973.
13. J. V. Sharp, p. 417 in Proceedings, Fourth European Regional Conference on Electron Microscopy, Rome, 1968.
14. R. P. Tucker, M. S. Wechsler, and S. M. Ohr, J. Appl. Phys. 40, 400 (1949).
15. J. V. Sharp, Phil. Mag. 16, 77 (1967).
16. G. Saada and J. Washburn, J. Phys. Soc. Jap. (Suppl.) 18, 43 (1963).
17. J. L. Strudel and J. Washburn, Phil. Mag. 9, 491 (1964).
18. A. J. E. Foreman and S. V. Sharp, Phil. Mag. 19, 931 (1969).
19. J. Narayan and T. S. Noggle, in Solid State Division Annual Progress Report, ORNL-4952, May 1974, p. 43; ORNL-5028, May, 1975, p. 34.
20. M. J. Makin and J. V. Sharp, Phys. Stat. Sve. 9, 109 (1965).
21. R. B. Pond, p. 1 in The Inhomogeneity of Plastic Deformation, American Society for Metals, Metals Park, Ohio, 1973.
22. P. Haasen and R. Siems, Z. Metallk. 48, 315 (1957).
23. C. Zener, p. 3 in Fracturing of Metals, American Society for Metals, Metals Park, Ohio, 1948.
24. A. M. Freudenthal and J. H. Weiner, J. Appl. Phys. 27, 44 (1956).
25. J. D. Eshelby and P. L. Pratt, Acta Met. 4, 560 (1956).
26. T. Suzuki and T. Ishii, p. 159 in Physics of Strength and Plasticity, A. S. Argon, Ed., M. I. T. Press, Cambridge, Mass., 1969.
27. J. Takamura and T. Morimoto, J. Phys. Soc. Japan Suppl. 18, 28 (1963).
28. A. Ookawa and K. Yazu, J. Phys. Soc. Japan Suppl. 18, 36 (1963).
29. W. J. McGregor Tegart, Elements of Mechanical Metallurgy, Macmillan, New York, 1966, p. 200.

30. J. R. Rice and N. Levy, p. 277 in Physics of Strength and Plasticity, A. S. Argon, Ed., M. I. T. Press, Cambridge, Mass., 1969.

31. J. G. Y. Chow and S. B. McRickard, p. 120 in Flow and Fracture of Metals and Alloys in Nuclear Environments, STP 380, American Society for Testing and Materials, Philadelphia, 1965.

32. O. N. Carlson, D. G. Alexander, M. S. Wechsler, and R. Bajaj, unpublished work.

33. R. A. Wullaert, D. R. Ireland, and A. S. Tetelman, p. 20 in Irradiation Effects on Structural Alloys for Nuclear Reactor Applications, STP 484, American Society for Testing and Meterials, Philadelphia, 1970.

34. R. Mickelson and D. J. Peterson, Trans. ASM 50, 340 (1958).

35. D. T. Peterson and R. L. Skaggs, Trans. Met. Soc. AIME 242, 922 (1968).

36. J. F. Smith, O. H. Carlson, D. T. Peterson, and J. E. Scott, Thorium: Preparation and Properties, Iowa State University Press, Ames, 1975.

37. D. F. Stein and J. R. Low, Acta Met. 14, 1183 (1966).

38. D. F. Stein, J. R. Low, and A. E. Seybolt, Acta Met. 11, 1253 (1963).

39. K. V. Ravi and R. Gibala, Scripta Met. 3, 547 (1969).

40. K. V. Ravi and R. Gibala, Acta Met. 18, 623 (1970).

41. K. V. Ravi and R. Gibala, p. 83 in Second International Conference on the Strength of Metals and Alloys, Vol. I, American Society for Metals, Metals Park, Ohio, 1970.

42. R. Lachenmann and H. Schultz, Scripta Met. 4, 709 (1970).

43. M. S. Wechsler, D. G. Alexander, R. Bajaj, and O. N. Carlson, p. 127 in Defects and Defect Clusters in B.C.C. Metals and Their Alloys, Nuclear Metallurgy, Vol. 18, National Bureau of Standards, Gaithersburg, Md., 1973.

44. O. N. Carlson, D. G. Alexander, and G. Elssner, in preparation.

45. O. N. Carlson and D. G. Alexander, Rev. High-Temperature Mater. 11, 261 (1974).

46. R. W. Thompson and O. N. Carlson, J. Less-Common Metals 7, 321 (1964).

47. A. R. Rosenfield, E. Votava, and G. T. Hahn, p. 63 in Ductility, American Society for Metals, Metals Park, Ohio, 1968.

48. J. M. Galligan, p. 241 in Defects in Refractory Metals, CEN/SCK, Moc, Belgium, 1972.

49. S. M. Ohr, M. S. Wechsler, C. W. Chen, and N. E. Hinkle, p. 742 in Second International Conference on the Strength of Metals and Alloys, Vol. II, American Society for Metals, Metals Park, Ohio, 1970.

50. G. P. Seidel, Phys. Stat. Soc. 25, 175 (1968).

51. K. Kitajima, Trans. Jap. Inst. Met. Suppl. 9, 182 (1968).

52. R. J. Arsenault and E. Pink, Mater. Sci. Eng. 8, 134 (1971).

53. R. Bajaj and M. S. Wechsler, these proceedings.

54. M. S. Wechsler, p. 235 and p. 257 in Defects in Refractory Metals, CEN/SCK, Mol, Belgium, 1972.

55. G. R. Smolik and C. W. Chen, J. Nucl. Mater. 35, 94 (1970).

56. F. A. Smidt, Rad. Effects 10, 205 (1971).

57. K. Shiraishi, K. Fukaya, and Y. Katano, J. Nucl. Mater. 44, 228 (1972); 54, 275 (1974).

58. D. F. Hasson, p. 147 in Defects and Defect Clusters in B.C.C. Metals and Their Alloys, National Bureau of Standards, Gaithersburg, Md., 1973.

59. J. Venetch, A. A. Johnson, and K. Mukherjee, J. Nucl. Mater. 34, 343 (1970).

60. M. J. Makin and F. J. Minter, Acta Met. 7, 361 (1969).

61. S. M. Ohr, R. P. Tucker, and M. S. Wechsler, Phys. Stat. Soc. 2, 559 (1970).

62. R. P. Tucker, S. M. Ohr, and M. S. Wechsler, p.215 in Radiation Damage in Reactor Materials, I. A. E. A., Vienna, 1969.

63. J. R. Hawthorne, p. 96 in Irradiation Effects on Structural Alloys for Nuclear Reactor Applications, STP 484, American Society for Testing and Materials, Philadelphia, 1970.

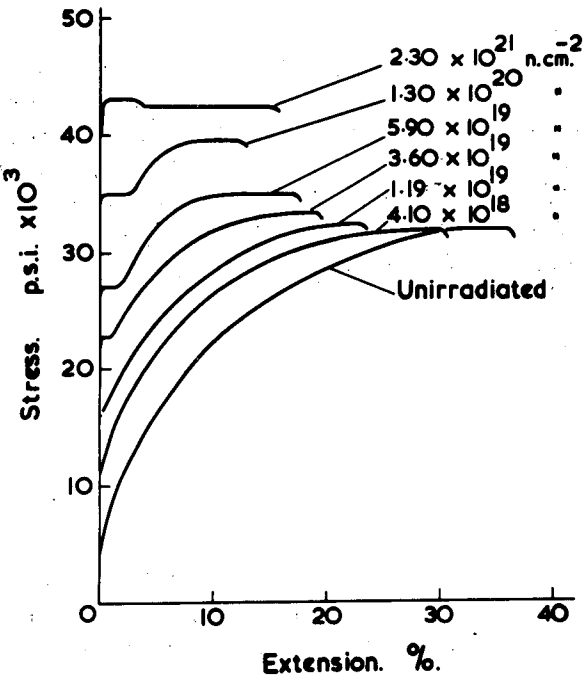


Fig. 1. Stress-strain curves for polycrystalline copper tested at 20°C after various epithermal neutron doses at 80°C. Fast neutron doses are approximately 10% of the indicated values. After Makin[8].

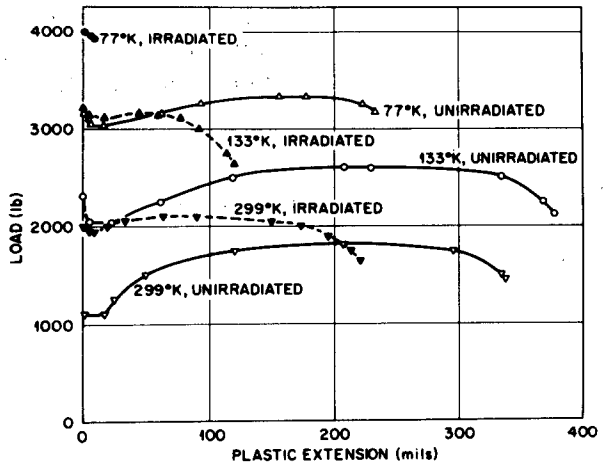


Fig. 2. Load-extension curves for unirradiated and irradiated A212B steel tested at indicated tempertures and strain rate of 2.7×10^{-4} sec^{-1}. Radiation dose and temperature, 1×10^{19} neutrons/cm^2 (E > 1 MeV) at 60°C. After Wechsler et al.[9].

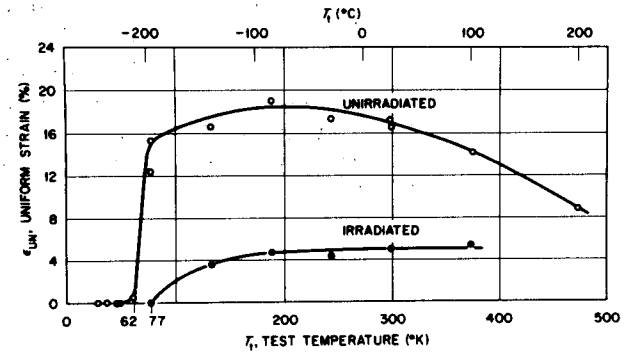


Fig. 3. Uniform strain versus test temperature for unirradiated and irradiated A212B steel tested at a strain rate of 2.7×10^{-4} sec^{-1}. Radiation dose and temperature, 1×10^{19} neutrons/cm^2 (E > 1 MeV) at 60°C. After Wechsler et al.[9].

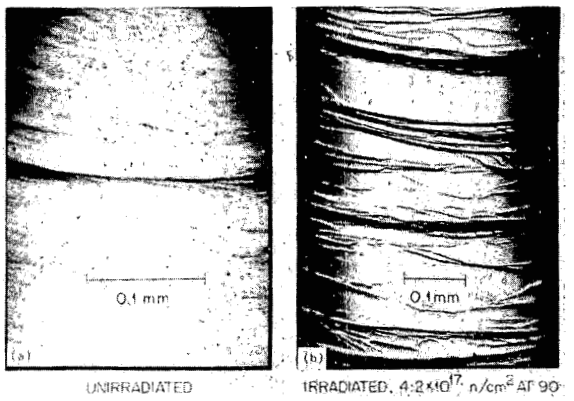


Fig. 4. Slip bands in single crystal niobium after 10% strain as viewed in direction perpendicular to axis (vertical) and to $[1\bar{2}1]$ direction (horizontal). After Wechsler et al.[10].

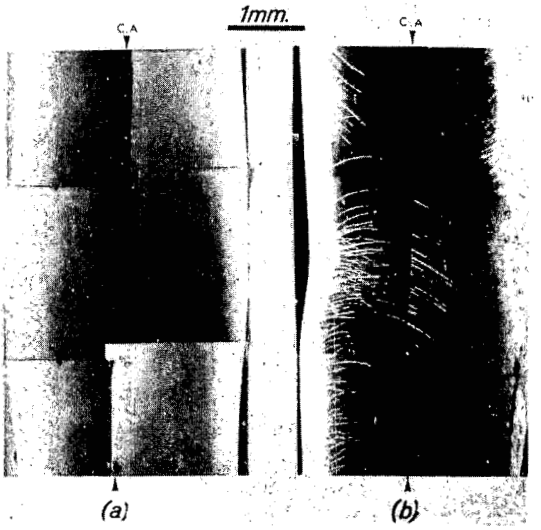


Fig. 5. Scanning electron micrographs of vanadium - 95 wt ppm oxygen single crystals deformed 12% in compression at room temperature: (a) unirradiated, (b) irradiated to 1.4 x 10^{19} neutrons/cm^2 (E > 1 MeV) at 95°C. After Bajaj[11].



Fig. 6. Correspondence between surface steps and dislocation channels in neutron-irradiated and deformed copper. Surface of sample (S) was electroplated (E) after deformation and before thinning and examination in the electron microscope. After Sharp[13].

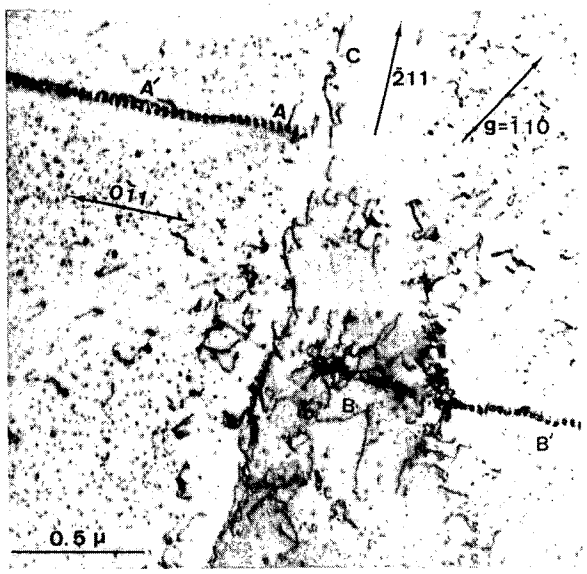


Fig. 7. TEM photomicrograph of niobium irradiated to 4.4×10^{18} neutrons/cm^2 (E > 1 MeV) at 50°C and strained 6.6% at room temperature. Dislocation channel (C) has sheared the dislocation helix into segments AA' and BB'. After Tucker et al.[14].

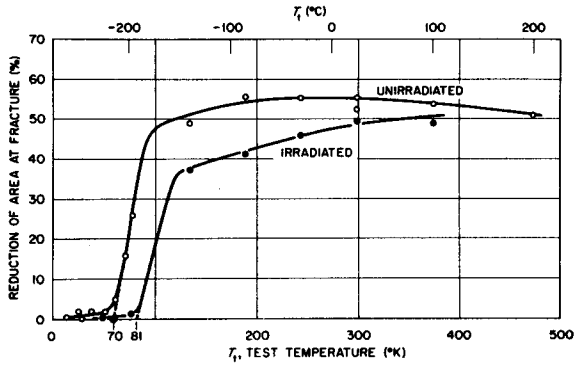


Fig. 8. Reduction in area at fracture versus test temperature for unirradiated and irradiated A212B steel tested at a strain rate of 2.7×10^{-4} sec^{-1}. Radiation dose and temperature, 1×10^{19} neutrons/cm^2 (E > 1 MeV) at 60°C. After Wechsler et al.[9].

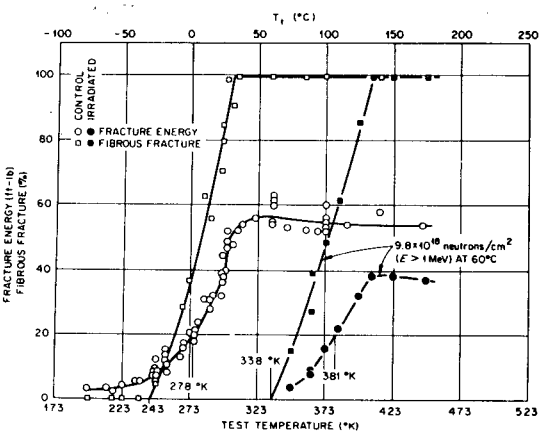


Fig. 9. Fracture energy and percent fibrous fracture appearance versus test temperature for unirradiated and irradiated A212B steel notch-impact tests. After Wechsler et al.[9].

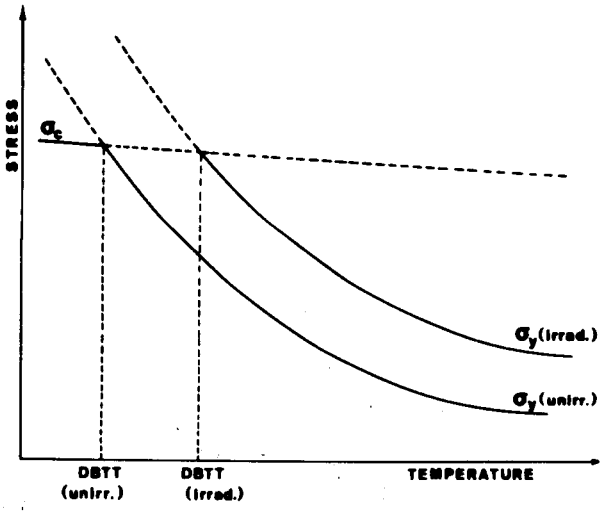


Fig. 10. Schematic illustration of the Ludwig-Davidenkov criterion for the ductile-brittle transition temperature (DBTT). σ_y is the yield stress and σ_c is the cleavage fracture stress.

THE INFLUENCE OF OXYGEN IMPURITY ATOMS ON DEFECT CLUSTERS AND RADIATION HARDENING IN NEUTRON-IRRADIATED VANADIUM*

R. Bajaj
Advanced Reactors Division
Westinghouse Electric Corporation
Madison, Pennsylvania 15663

and

M. S. Wechsler
Ames Laboratory ERDA and Department
of Materials Science and Engineering
Iowa State University
Ames, Iowa 50010

ABSTRACT

Single crystal TEM samples and polycrystalline tensile samples of vanadium containing 60-640 wt ppm oxygen were irradiated at about 100°C to about 1.3×10^{19} neutrons/cm^2 (E>1 MeV) and post-irradiation annealed up to 800°C. The defect cluster density increased and the average size decreased with increasing oxygen concentration. Higher oxygen concentrations caused the radiation hardening and radiation-anneal hardening to increase. The observations are consistent with the nucleation of defect clusters by small oxygen or oxygen-point defect complexes and the trapping of oxygen at defect clusters upon post-irradiation annealing.

INTRODUCTION

Several investigations have revealed a post-irradiation annealing resistivity stage in BCC metals at about $0.2T_m$ (T_m = melting temperature in °K); for reviews see[1-4]. The resistivity annealing stage has been observed in neutron-irradiated vanadium at about 175°C ($\simeq 0.2T_m$) by Perepezko *et al.*[5], Stanley *et al.*[6], and McIlwain *et al.*[7]. The origin of the $0.2T_m$ annealing stage has been debated in the literature: Johnson[8,9]

*Work performed at Ames Laboratory, Iowa State University, under contract to the U. S. Energy Research and Development Administration.

indicates an explanation in terms of the annealing of an intrinsic radiation-produced defect such as the vacancy, whereas Wechsler et al.[10] favor the trapping of interstitial impurity atoms at radiation-produced defect clusters. Internal friction measurements (Snoek damping) in neutron-irradiated vanadium have also been reported by Stanley et al.[6], Eto et al.[11,12], and McIlwain et al.[7]. The Snoek peak due to oxygen in solid solution is observed to decrease during annealing at temperatures between 100 and 200°C. The decrease in oxygen in solid solution during annealing deduced from resistivity measurements and from oxygen Snoek damping were observed to be in fairly good agreement[7].

Radiation-anneal hardening[13], an additional increase in yield stress upon post-irradiation annealing, is also observed at $0.2T_m$ in vanadium[14-20]. The present work indicates that radiation-anneal hardening may be due to the motion of interstitial impurities to radiation-produced defect clusters, which strengthens them as barriers to slip dislocations. The present work also shows that the increase in yield stress of vanadium as indicated by samples in the as-irradiated condition (irradiation temperature, about 100°C) also increases with increasing oxygen concentration, as was reported earlier by Hasson and Arsenault[21] and Arsenault and Pink[22]. These effects are correlated with the density and size distribution of defect clusters as revealed by transmission electron microscopy (TEM).

EXPERIMENTAL PROCEDURE AND RESULTS

Single crystal TEM samples and polycrystalline tensile samples were prepared with oxygen concentrations ranging from 60 to 640 wt ppm oxygen and irradiated at about 100°C to about 1.3×10^{19} neutrons/cm^2 (E>1 MeV). A portion of the samples were subjected to one-hour post-irradiation anneals at temperatures up to 800°C. The density and size distribution of defect clusters in the TEM samples were determined with a Zeiss particle size analyzer and the tensile samples were tested at room temperature at a strain rate of 1.67×10^{-4} sec^{-1}.

The defect cluster size distribution curves had a peaked shape. For samples in the as-irradiated condition, the average size was 138, 77, and

73 Å for samples with 95, 300, and 500 wt ppm oxygen, respectively, and upon post-irradiation annealing at 500°C, the average size increased to 310, 191, and 157 Å, respectively.

The total density of defect clusters of all sizes is shown in Fig. 1 as a function of the post-irradiation annealing temperature, with the values for as-irradiated samples plotted at the irradiation temperature. It appears that the density of defect clusters increases with increasing oxygen concentration. Furthermore, we note that the defect cluster density first starts to decrease at about 300°, 400°, and 500°C for 95, 300, and 500 wt ppm oxygen, respectively, which indicates that the defect clusters are more stable against annealing for vanadium with higher oxygen concentrations. For anneals above 600°C, the defect cluster density was too low to enable meaningful counts of defect clusters.

In order to attempt to correlate the density and size distributions with radiation hardening, we employ a dispersed barrier model, such as that applied to neutron-irradiated niobium by Tucker and Wechsler[23] and Loomis and Gerber[24]. The increase in yield stress due to the radiation-produced barriers (defect clusters) is given by

$$\Delta\sigma = \sigma_i - \sigma_u = 2\,\frac{K_1}{K_2}\,Gb\left(\sum_j n_j d_j\right)^{1/2} \tag{1}$$

where σ_i and σ_u are the yield stresses in the as-irradiated and post-irradiation-annealed material, respectively, G is the shear modulus, b is the Burgers vector of the slip dislocation, and n_j is density of defect clusters in the jth size interval centered at diameter d_j. The constant K_1 arises from setting the force F necessary to surmount the barriers equal to $F = K_1 Gb^2$. Also, K_2 arises from the possibility that

$$\ell = K_2 \bar{\ell} \tag{2}$$

where ℓ is the effective interbarrier distance, $\bar{\ell}$ is the average interbarrier distance

$$\ell = \left(\sum_j n_j d_j\right)^{-1/2} \tag{3}$$

and K_2 is a constant close to unity that incorporates geometrical considerations as discussed by Kocks[25]. We may calculate $\bar{\ell}$ from our measured size distributions and the results are shown in Fig. 2 as a function of oxygen concentration. We see that $\bar{\ell}$ decreases with increasing oxygen concentration.

Figure 3 consists of a plot of $\Delta\sigma = \sigma_i - \sigma_u$ for vanadium with 60, 205, and 640 wt ppm oxygen as a function of annealing temperature. We see that the increase in yield stress upon irradiation and the radiation-anneal hardening increase with increasing oxygen concentration. Furthermore, the general recovery toward the unirradiated yield stress starts at about 500°C and is completed at 700°C.

DISCUSSION

The correlation between the density and size distribution of the defect clusters as determined by transmission electron microscopy and the radiation hardening as determined by yield stress measurements was carried in accordance with Eqs. (1-3). Values of $\bar{\ell}$ and $\Delta\sigma$ were taken from Figs. 2 and 3, respectively, and G and b were taken equal to 6.77×10^3 kpsi and 2.63 Å, respectively. The resulting values of K_1/K_2 are plotted versus annealing temperature in Fig. 4. The increase in K_1/K_2 with increasing annealing temperature is interpreted as an indication that oxygen migrates to the defect clusters during post-irradiation annealing and strengthens the defect clusters as barriers to dislocation motion. Thus, we conclude that the radiation-anneal hardening is due chiefly to the influence of interstitial impurity trapping in strengthening the defect clusters and not to changes in the density and size distribution of the clusters. This conclusion agrees in general terms with those of Shiraishi et al.[17] and Smidt[20], although there are some differences in detail. The conclusion also agrees with the earlier work on neutron-irradiated niobium[23,26], but it differs somewhat with the interpretation of Loomis and Gerber[27] who correlated the radiation hardening with defect clusters of sizes only below 70 Å.

The increase in the defect cluster density with increasing oxygen

concentration (Fig. 1) upon irradiation at about 100°C is believed to be due to the formation during irradiation of small aggregates of oxygen atoms or oxygen-point defect complexes which serve as nucleation centers for the formation of the defect clusters. This is consistent with the results of Eto et al.[12], who observed a decrease in Snoek damping due to oxygen in vanadium upon irradiation at about 60°C to 2×10^{17} and 5×10^{19} neutrons/cm^2 (E>1 MeV). The increased stability against annealing with increasing oxygen concentration (Fig. 1) may be due to the trapping of oxygen at the defect clusters. As indicated in the Introduction, oxygen trapping may also be responsible for the $0.2T_m$ resistivity annealing stage and for the decrease in Snoek damping upon post-irradiation annealing. It also provides an explanation for the retardation of strain aging that has been observed in irradiated vanadium containing oxygen[27].

CONCLUSIONS

1. Upon increasing the oxygen concentration, the defect cluster density in neutron-irradiated vanadium increases, the average size decreases, and the stability against annealing increases.

2. Higher oxygen concentrations in vanadium also have the effect of increasing the radiation hardening and radiation-anneal hardening.

3. Based on a dispersed barrier model embracing defect clusters of all sizes, the radiation-anneal hardening is due principally to a strengthening of the defect clusters as barriers to slip dislocation motion, not to changes in the density and size distribution of the defect clusters.

4. The observations are consistent with the nucleation of defect clusters by small oxygen or oxygen-point defect complexes upon irradiation and the trapping of oxygen at defect clusters upon post-irradiation annealing.

REFERENCES

1. J. Nihoul, in Vacancies and Interstitials in Metals, edited by A. Seeger et al., North-Holland Publishing Company, Amsterdam, 1969, p. 839.

2. H. Schultz, Mater. Sci. and Eng. 6, 189 (1968).
3. J. Moteff, in Radiation Effects, edited by W. Sheely, Gordon and Breach, New York, 1967, p. 727.
4. R. de Batist, J. Nihoul, and L. Stals, editors, Defects in Refractory Metals, SCK/CEN, Mol, Belgium, 1972.
5. J. H. Perepezko, R. F. Murphy, and A. A. Johnson, Phil. Mag. 19, 1 (1969).
6. J. T. Stanley, J. M. Williams, W. E. Brundage, and M. S. Wechsler, Acta Met. 20, 191 (1972).
7. J. F. McIlwain, C. W. Chen, R. Bajaj, and M. S. Wechsler, in Effects of Radiation on Substructure and Mechanical Properties of Metals and Alloys, Special Technical Publication 529, American Society for Testing and Materials, Philadelphia, 1973, p. 529.
8. A. A. Johnson, Scripta Met. 7, 1 (1973).
9. A. A. Johnson, Scripta Met. 7, 15 (1973).
10. M. S. Wechsler, J. M. Williams, and J. T. Stanley, Scripta Met. 7, 7 (1973).
11. M. Eto, K. Fukaya, and K. Shiraishi, J. Nucl. Mater. 48, 365 (1973).
12. M. Eto, Y. Matsuo, S. Ishino, and Y. Mishima, J. Nucl. Mater. 52, 309 (1974).
13. M. S. Wechsler, in Defects in Refractory Metals, SCK/CEN, Mol, Belgium, 1972, p. 235 and p. 257.
14. J. Venetch, A. A. Johnson, and K. Mukherjee, J. Nucl. Mater. 34, 343 (1970).
15. G. R. Smolik and C. W. Chen, J. Nucl. Mater. 35, 94 (1970).
16. K. Shiraishi, K. Fukaya, and Y. Katano, J. Nucl. Mater. 44, 228 (1972).
17. K. Shiraishi, K. Fukaya, and Y. Katano, J. Nucl. Mater. 54, 275 (1974).
18. D. F. Hasson, in Defects and Defect Clusters in B.C.C. Metals and Their Alloys, Nuclear Metallurgy, Vol. 18, National Bureau of Standards, Gaithersburg, Md., 1973, p. 147.
19. M. S. Wechsler, D. G. Alexander, R. Bajaj, and O. N. Carlson, in Defects and Defect Clusters in B.C.C. Metals and Their Alloys, Nuclear Metallurgy, Vol. 18, National Bureau of Standards, Gaithersburg, Md., 1973, p. 127.
20. F. A. Smidt, Rad. Eff. 10, 205 (1971).

21. D. F. Hasson and R. J. Arsenault, Rad. Eff. 21, 203 (1974).
22. R. J. Arsenault and E. Pink, Mat. Sci. Eng. 8, 141 (1971).
23. R. P. Tucker and M. S. Wechsler, Rad. Eff. 3, 73 (1970).
24. B. A. Loomis and S. B. Gerber, Acta Met. 21, 165 (1973).
25. U. F. Kocks, Acta Met. 14, 1629 (1966).
26. S. M. Ohr, R. P. Tucker, and M. S. Wechsler, Phys. Stat. Sol. A2, 559 (1970).
27. M. S. Wechsler and R. Bajaj, Scripta Met. 8, 885 (1974).

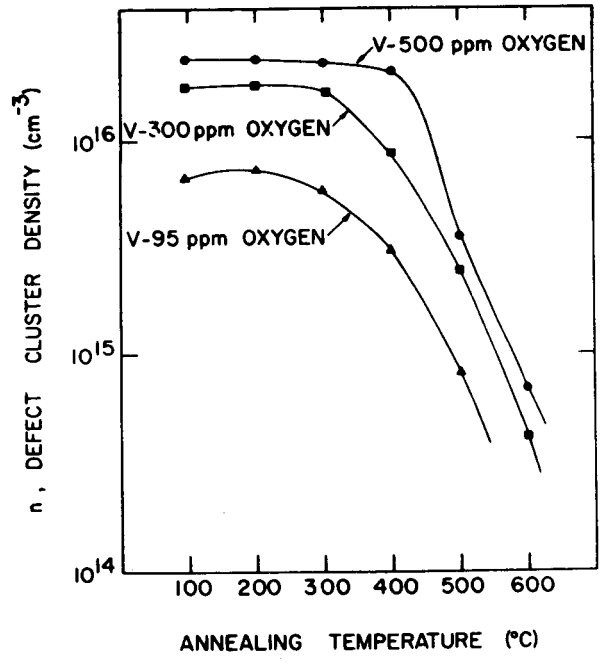


Fig. 1: Density of defect clusters versus post-irradiation annealing temperature. Irradiation dose and temperature, 1.4×10^{19} neutrons/cm^2 (E>1 MeV) at 95°C. One-hour anneals; as-irradiated plotted at 95°C.

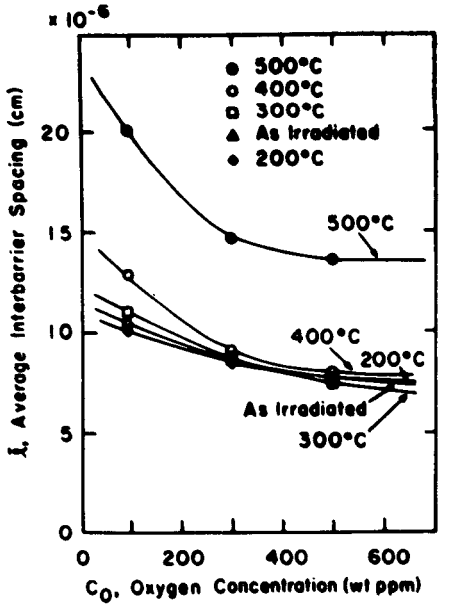


Fig. 2: Average interbarrier distance versus oxygen concentration for as-irradiated and post-irradiation-annealed vanadium.

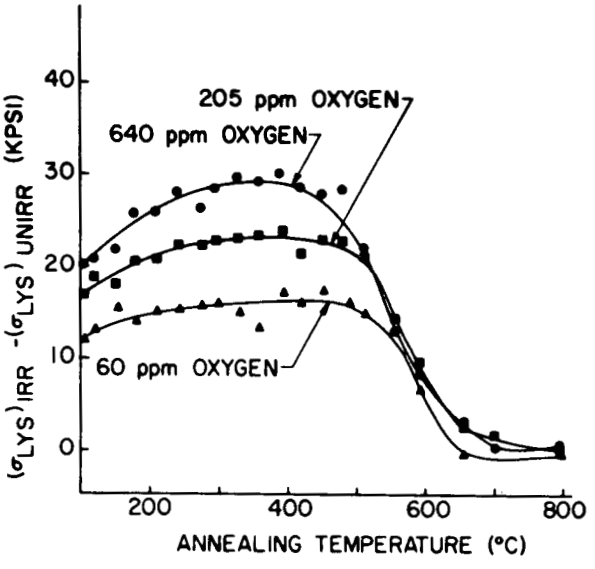


Fig. 3: Difference between lower yield stresses for irradiated and unirradiated vanadium containing 60, 205, and 640 wt ppm oxygen versus annealing temperature. Irradiation dose and temperature, 1.2×10^{19} neutrons/cm^2 (E>1 MeV) at 105°C. One-hour anneals. Room temperature tests.

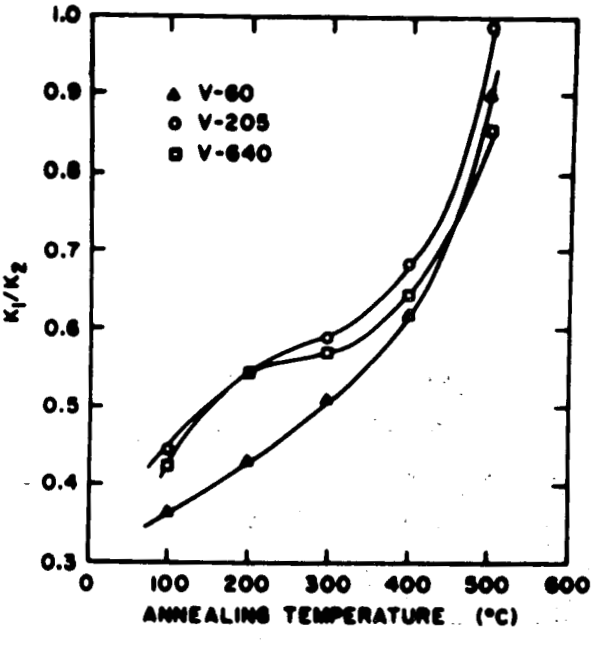


Fig. 4: K_1/K_2 versus post-irradiation annealing temperature for vanadium - 60, 205, and 640 wt ppm oxygen.

DEFORMATION CHARACTERISTICS OF HIGH PURITY NEUTRON IRRADIATED VANADIUM*

J. Bressers
Euratom Lab.
Petten (N.L.)
The Netherlands

R.J. Arsenault
Engineering Materials Group
University of Maryland
College Park, Maryland

ABSTRACT

An investigation of the effect of neutron damage on the low temperature deformation characteristics of high purity vanadium ($R_{300K}/R_{4.2K} \simeq 1100$) was undertaken to determine if reducing the impurity interstitial content to a low level would result in a large difference in the effective stress between irradiated and non-irradiated samples. The results do indicate that as the impurity interstitial content decreases the difference in effective stress increases.

INTRODUCTION

The changes in the yield stress at low temperatures produced by neutron irradiation appear to be a very sensitive function of the impurity interstitial content.[1,3] (In all cases, yield stress refers to the resolved yield stress.) The magnitude of the increase in the yield stress (τ_y) at low temperatures increases as the impurity interstitial content decreases. If the yield stress is considered to consist of two

*This research was supported in part by U.S. ERDA under Contract No. AT(40-1)3612.

components: the effective stress (τ^*) and a long range internal stress (τ_i), then it is possible to examine the effect of the neutron damage on both components of τ_y. The effective stress of yielding for the neutron irradiated samples will be defined as τ^*_{IRR} and the effective stress of yielding for the non-irradiated samples will be defined as τ^*. The difference of $\tau^*_{IRR} - \tau^*$ is defined as $\Delta\tau^*$. The reason for the decrease in $\Delta\tau^*$ as the interstitial content increases is not apparent. One possibility is that the neutron produced defect, which is the short range barrier (s.r.b.) to dislocation motion, producing the increase in τ^*, is a complex, e.g. a divacancy or di-interstitial. As the single defects migrate during and after irradiation to form these complexes, the single defect captures an impurity interstitial, and this type of complex has a low mobility [4]. This mechanism could be defined as a prevention mechanism. Another possibility is that the impurity interstitial migrates to the neutron produced s.r.b. and "cancels" out it's effect. For example, if the neutron produced defect were a di-vacancy, then the di-vacancy would interact with the moving dislocation through a "modulus effect".[5] If the O_2 atom diffuses into the defect then the modulus difference and the "modulus effect" are thereby reduced. This could be defined as a cancelation mechanism. The above two mechanisms are based on the assumption that τ^* of the non-irradiated b.c.c. metal is independent of impurities. If it is assumed that τ^* decreases upon decreasing the interstitial concentration, then there is another possible mechanism. In this case the yield stress of the irradiated samples at 77°K changes by a small amount due to changing the interstitial concentration, but the yield stress of the non-irradiated samples at 77°K changes by a large amount due to a small increase of the interstitial concentration.

The purpose of this investigation was to determine if reducing of the impurity interstitial content to lower levels results in a further increase in $\Delta\tau^*$ at low temperatures.

EXPERIMENTAL PROCEDURE

The single crystals used in this investigation had a RRR of ~1100. The details of production are described elsewhere[6]. The methods of temperature control and testing have been described before[7].

EXPERIMENTAL RESULTS

The stress-strain curves of the neutron irradiated samples tested at 300°K were serrated and very similar to those obtained from neutron irradiated Cu single crystal samples[8] (Fig. 1.) The extent of the serrated flow decreases as the temperature decreases, and at 240°K it has almost completely disappeared. In general a well defined yeild drop occured at all test temperatures provided the sample was not prestrained. A prestrain of 1 - 3% at 300°K was required to prevent twinning for test temperatures of 77°K and below. However, 20°K was the lowest test temperature below which prestraining did not prevent twinning. At 77°K it was possible to test several non-prostrained samples without noticeable twinning, and the lower yield stress was in agreement with the yield stress obtained from the pre-strained samples.

The slip lines were examined both optically and with a scanning electron microscope. It appears that the primary $(\bar{1}01)$ was the operative slip plane in all cases, along with some secondary slip on (101) [111] system.

Fig. 2 is a plot of τ_y vs temperature for both non-irradiated and irradiated samples. The discussion of the differences in yield stress between irradiated and non-irradiated samples will be confined to that where slip has occured primarily on the primary slip plane. It is evident that the difference in the τ_y between the irradiated and non-irradiated samples increases with decreasing test temperature. At 77°K the difference is about 12 kg/mm^2. If the two components of τ_y are taken into account it is then possible to consider the effect of neutron damage on each component. The increase of τ_i due to irradiation is about 1 kg/mm^2, the τ_i for non-irradiated samples is about 1 kg/mm^2. The $\Delta\tau^*$ due to irradiation is zero at 300°K and about 11 kg/mm^2 at 45°K.

DISCUSSION

As mentioned in the introduction, previous investigations[1-3] have indicated that if the impurity interstitial content decreases then neutron irradiation damage produces a large increase in the effective stress (τ^*) at low temperatures. The present results obtained from higher purity vanadium indicate that the difference ($\Delta\tau^*$) in effective stress between the irradiated and non-irradiated samples at low temperatures is greater than that previously observed (Fig. 3).

The decrease in $\Delta\tau^*$ at 77°K with increasing O_2 concentration is the result of the large change in τ^* of the non-irradiated samples due to a relatively small change in O_2 concentration. For example, τ^* increases from 13 kg/mm^2 for an O_2 content of about 10 wt-ppm to 19 kg/mm^2 for an O_2 content of about 15 wt-ppm, and finally 24 kg/mm^2 for an O_2 content of 61 wt-ppm. The neutron damage results in τ^*_{IRR} increasing from about 23 kg/mm^2 to 30 kg/mm^2 in the same O_2 range.

The large values τ^*_{IRR} obtained from the higher purity neutron irradiated samples indicate that neutron damage produces a change in the rate controlling mechanism of deformation at low temperatures. The differences in the values of ΔH_o (activation energy at $\tau^*=o$) between irradiated and non-irradiated samples, 0.6 eV and 0.4 eV, respectively, support the idea that neutron damage does produce a change in the rate controlling mechanism.

CONCLUSIONS

The present data indicates that the difference in effective stress between irradiated and non-irradiated samples increases with decreasing impurity interstitial content. The apparent reason for this increase is that the effective stress of non-irradiated samples decreases significantly upon reducing the impurity interstitial content to a low level. The present data reconfirms previous results which indicated that the increase in τ^*_{IRR} is probably due to a change in rate controlling mechinism and that the defect responsible is small, e.g. a di-vacancy.

REFERENCES

1. R. J. Arsenault and E. Pink, Material Sci. Eng., 8, 141 (1971).
2. R. J. Arsenault and T. Cadman, Defects and Defect Clusters in B.C.C. Metals and Their Alloys, Vol. 18, Nuclear Met. AIME, 1973, p 41.
3. C. Chen and R. J. Arsenault, To be published in Met. Trans.
4. R. A. Johnson, Acta Met. 12, 513 (1967).
5. R. Bullough and R. C. Newman, Phil. Mag., 7, 529 (1962).
6. J. Bressers, R. Creten, G. Van Holsbeke, J. Less-Common Metals 39, 7 (1975).
7. R. J. Arsenault, "Experimental Methods of Materials Research". H. Herman (ed.), Wiley, N.Y. 1967, p. 215.
8. T. Koppenaal and R. J. Arsenault, Metallurgical Reviews, 1971, p 175.

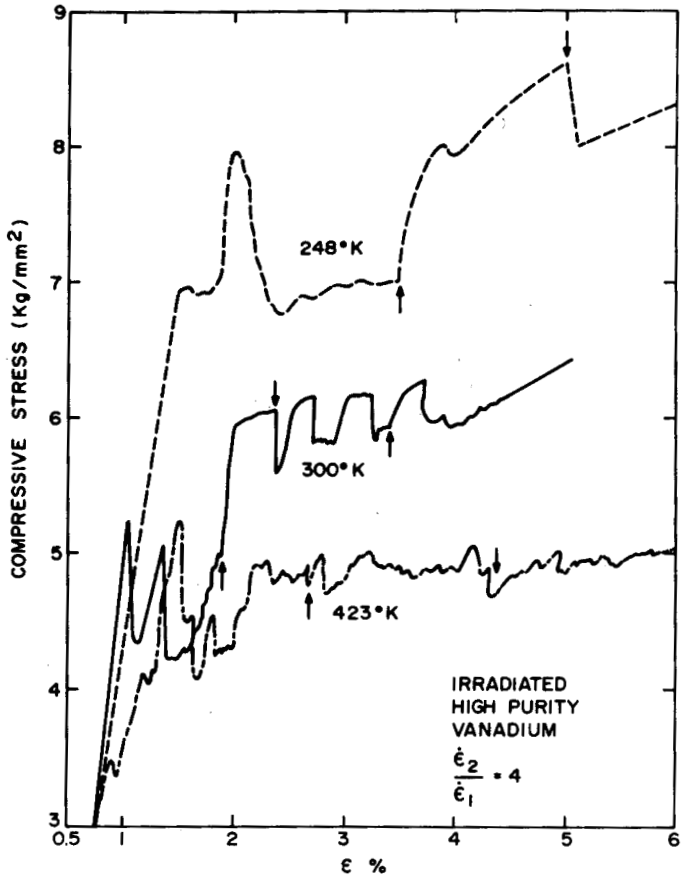


Fig. 1
Compressive stress vs total strain of neutron irradiated high purity vanadium at three different test temperatures.

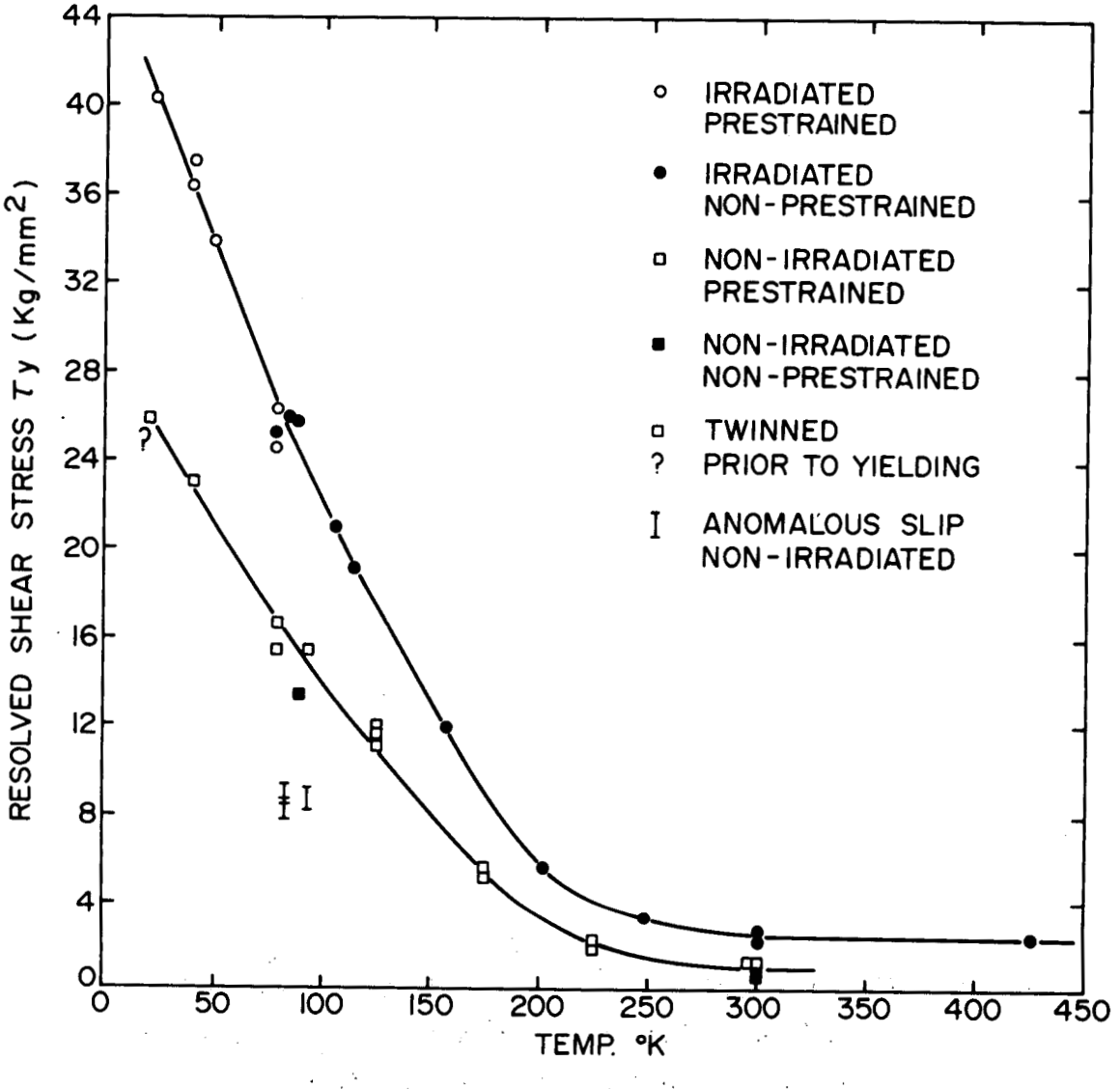


Fig. 2. Resolved shear stress of yielding vs temperature of irradiated and non-irradiated high purity vanadium.

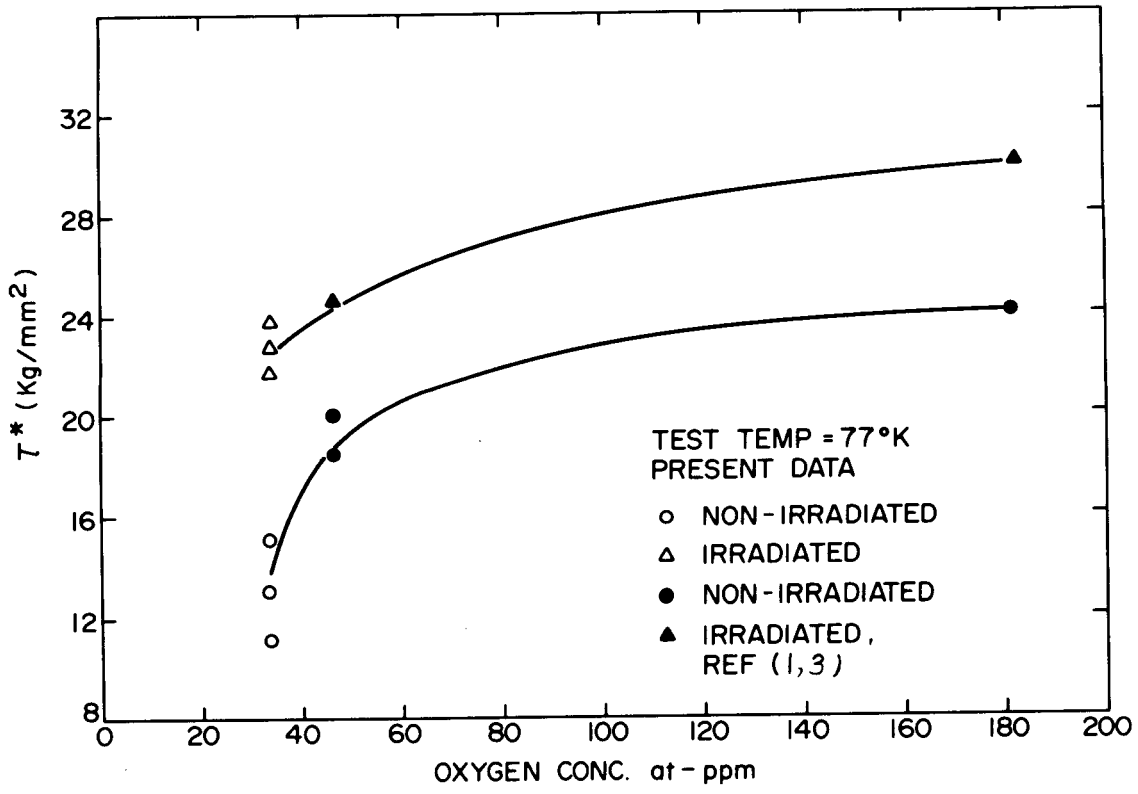


Fig. 3. The effective stress of yielding at 77°K of irradiated and non-irradiated vanadium as a function of oxygen concentration.

THEORY OF DIFFUSION AND TRAPPING OF HYDROGEN AND HELIUM IN METALS, A REVIEW*

W. D. Wilson
Sandia Laboratories
Livermore, California 94550

ABSTRACT

The theory of trapping and diffusion of helium and hydrogen in metals is reviewed. The fundamental aspects of the behavior of these particles is emphasized and hence ab initio methods of calculation of interatomic potentials are described. In particular, two-body free-electron and Hartree-Fock calculations for closed shell systems are described and compared for an example case, $He\text{-}Cu^{+}$. Helium defect aggregates studied using these potentials are reviewed and several previously unreported calculations of helium clustering in tungsten are given. A brief discussion of the quantum nature of the diffusion of light particles is also given.

INTRODUCTION

It is fortunate that several excellent and recent reviews of the behavior of hydrogen[1] and helium in metals[2-4] have been written. The literature is becoming so vast and the number of conferences so great[5] that a brief review such as this could not even serve as a proper bibliography. Research in this area of hydrogen (and its isotopes) and helium in metals is being driven by technologies such as the controlled-thermonuclear reactor, the hydrogen economy, and high energy (14 MeV) neutron generation. The extensive nature of the subject matter, therefore, requires that this review be severely limited. The nature of this conference also dictates that this review be restricted, in particular, to fundamental theoretical methods of interest to the physics of defects

*This work is supported by the United States Energy Research and Development Administration.

in solids. The local electronic and atomistic aspects of helium and hydrogen atoms in metals and hydrides as related to the diffusion and trapping of these particles will, therefore, be stressed. Where possible, the theories described will be compared with experiment.

Throughout this review, ab initio calculations will be considered of paramount importance. The quantum nature of these light particles will be discussed from the point of view of their electronic interaction with local metal atoms in a crystal and also from the point of view of their diffusion in a metal lattice. The helium particle, having a closed and tightly bound electronic shell is simpler to consider from an interaction standpoint than the open-shell hydrogen atom. The first method of approach in either case, however, is to consider the gas-metal interactions to be comprised of two-body potentials. Such two-body interatomic potentials and the methods developed to obtain them will be presented in the section entitled "Two-Body Interatomic Potentials." In the section entitled "Application of the Two-Body Potentials," the results of the application of these interatomic potentials to the study of the diffusion and trapping of multiple helium atoms in metals will be reviewed. A study of hydrogen self-diffusion in titanium hydride using two-body potentials will also be described. A discussion of methods of furthering our understanding of the behavior of helium and hydrogen in metals is given in the section entitled "Discussion." In particular, the small-polaron formalism of Flynn and Stoneham[6,7] will be briefly discussed.

TWO-BODY INTERATOMIC POTENTIALS

The simplest and, hence, most common assumption made in the treatment of defects in solids is that the particles interact via two-body forces. A functional form for the interaction might be chosen containing parameters which are fitted to independent (of the defect) experimental information such as cohesive energy, interatomic separation, compressibility, elastic constants, phonon dispersion curves, etc. A recent review of such empirical potentials has been provided by Johnson.[8] One

of the limitations of this approach is that at all interatomic separations except near equilibrium where the experimental data is fitted, the potential is extrapolated. The difficulty with this technique when applied to helium or hydrogen in metals, clearly, is that data concerning the interaction of the defect with the lattice does not exist. A more fundamental calculation must, therefore, be performed.

Several theoretical methods have been applied to the study of such two-body interactions.[9-12] A model employed by Wedepohl[11] assumes the atomic charge distributions to interact classically with a correction made in the overlap region for the increase in kinetic and exchange (X) energies. This correction is made in the free-electron approximation or some multiple, α, thereof. Wilson and Bisson[12] have used this method to determine the interaction of both homonuclear and heteronuclear pairs of rare gas atoms and found that the choice of Slater exchange ($\alpha = 1$), by overestimating this effect, agreed best with experiment in every case. Gordon and Kim[13] included correlation in their calculation using a similar model and showed that the correlation energy varied with separation the same as the exchange energy, indicating that overestimating the exchange is somewhat equivalent to including a degree of correlation.

Improving these effective two-body interactions is far from straightforward. Clearly, the free-electron approximation can be done away with by writing the radial part of the wave functions as linear combinations of Slater or Gaussian orbitals and directly calculating the Coulomb and exchange integrals. This is enormously computer-time consuming; the time required to calculate these quantities grows as N^4, where N is the number of basis functions. Interactions between high Z elements in even a small cluster would, therefore, be out of the question. Besides, it has been shown[14] that some fraction, α ($\sim 2/3$), of the full free-electron exchange (X) gives quite close agreement with the exact result. This makes it at least possible to vary α to study the effect of this exchange approximation on the final result of the (defect) calculation.

But such an "exact" treatment of the integrals involved allows a next step in the improvement process to be more easily achieved. Up

to now in our discussion, correlation of the electronic motions due to the fact that, aside from the Pauli Principle, electrons repel each other by Coulomb forces alone have been neglected. This correlation is explicitly excluded when we assumed (Hartree-Fock) that each electron experiences the spherically averaged potential due to the other electrons. By writing the total wave function of the two-body system as a linear combination of determinental functions, each determinant representing a particular electronic "configuration," these correlation effects can be included. Such configuration-interaction calculations have been found to be essential in describing even simple systems such as F_2. This should not be viewed as a higher-order correction term as the F_2 molecule is not even bound in the absence of this configurational mixing!

Even if the two-body system were "exactly" calculated as Kolos and Wolniewicz[15] did for H_2, we would still have a "free" interaction. Lattice effects such as those that serve to bind an $O^=$ in the MgO[16] lattice would still play an undetermined role. In order to include such polyatomic effects, we can go back to the free-electron exchange approximation and develop a cluster model. Gordon and Kim[13] did this in the "non-distortable" atom approximation described earlier, but Slater[17] and Johnson and Smith[18] developed a completely self-consistent solution known as the "multiple scattering wave" $X\alpha$ method.

An alternative, more exact, method of handling polyatomic systems makes no such free-electron approximation. Instead, the core electron functions for an isolated atom are calculated exactly and used to construct a suitable "pseudopotential" which is then used when interactions between these atoms are calculated.[19-21] In this way, the exact Hartree-Fock matrix elements are reproduced for the atom, correlation effects can be included by the usual configuration interaction technique, and the number of integrals required is reduced tremendously (e.g., copper (Z = 29) becomes a four-electron atom).

By way of an example of these methods, Fig. 1 shows the $He\text{-}Cu^+$ interaction calculated by several radically different methods. The first method is due to Rimmer and Cottrell[22] and is essentially an empirical

potential. The method involves averaging a He-He potential[23] and a Cu-Cu potential[24] (fitted to crystal data on Cu) in such a way that the resulting potential is the minimum obtained upon variation of the copper and helium "radii." The actual He-He and Cu-Cu potentials used by Rimmer and Cottrell were employed for comparison purposes rather than more modern versions. Method two is that employed by Wilson and Bisson[12] using Slater exchange ($\alpha = 1$) and labelled "free-electron" in the figure. A "frozen-core" Hartree-Fock calculation was also performed which allows no 4s or 4p mixing. A fourth calculation was performed in the Hartree-Fock approximation[25] using the N = 5 basis set of Huzinaga[26] for He and the copper functions of Basch, Hornbach and Moskowitz.[27] A fifth $He\text{-}Cu^+$ interaction due to Melius[28] is shown and was calculated using a pseudopotential approach with an extended basis set. The $He\text{-}Cu^\circ$ potential calculated by Melius is also plotted for comparison.

It is interesting to note that the simplest of these ab initio approaches, the free-electron calculation, is in excellent agreement with the Rimmer and Cottrell (RC) empirical potential (except at small separations where the RC potential does not apply). This is because neither approach allows distortion of the Cu^+ and He, a good approximation to closed shell rare-gas pairs. It is also interesting to note that the "frozen-core" Hartree-Fock approximation, which essentially is a non-distortable atom potential like the free-electron calculation, agrees well with the free-electron calculation despite the fact that the integrals are explicitly calculated. When excited state mixing is allowed, as in the full Hartree-Fock and pseudopotential calculations in Fig. 1, the electrons are free to rearrange, even to the extent of promoting a d orbital into an s state, lowering the total energy.

APPLICATION OF THE TWO-BODY POTENTIALS

Because of the approximations involved in two-body calculations, Wilson and Bisson[12] made several variations of these potentials in their calculations involving helium in copper. It was found that the activation energy for helium interstitial motion was relatively insensitive (0.45 eV -

0.71 eV) to the choice of potentials. The "core" or small separation region of the metal-metal potentials was taken from the free-electron calculations as well as the entire potential involving the rare gas atom.

The Wilson and Bisson calculations of rare gases in copper were not the first. An early work by Rimmer and Cottrell[22] used an empirical potential for the lattice atoms due to Huntington.[24] For the gas-metal interaction, an average of a gas-gas theoretical potential[23] and the metal-metal Huntington potential was devised as described above and plotted in Fig. 1. The strain energy for a helium interstitial was 1.7 eV which compares at least qualitatively with the (1.74 eV to 3.22 eV) calculations of Wilson and Bisson. Rimmer and Cottrell found the helium atom to go into an existing vacancy with zero strain energy, while Wilson and Bisson[29] obtain only 0.13 eV, again rather encouraging agreement. Unfortunately, Rimmer and Cottrell did not calculate activation energies. Although other face-centered-cubic (f.c.c.) metals were studied, the results differ markedly from Cu. They were not subjected to the same wide variation of potentials that Cu was subjected to, however, and are excluded from the summary Table 1.

Having established for the simple case of a helium interstitial in copper that the activation energy for diffusion is relatively insensitive to the choice of two-body potential, these methods were then applied to the helium interstitial in body-centered-cubic (b.c.c.) metals.[30] It was generally found that interstitial activation energies in V, Fe, Mo, Ta and W were in the $\leq$ 0.25 eV range, approximately half that obtained in Cu (see Table 1). It should be noted from Table 1 that there are significant differences between the b.c.c. metals and Cu. Several variations of the Fe potential were made with little change in the results, but mainly, for the purposes of this discussion, the b.c.c. metals will be compared as a group with Cu. It is first of all seen from Table 1 that helium interstitial formation energies in b.c.c.'s are approximately a factor of two greater than in Cu, but such formation energies lead to such low solubilities that this difference may not be experimentally verifiable. The strain energy required to place a He atom in an existing vacancy in b.b.c. is an order of magnitude greater than for Cu. The rate-limiting step for

substitutional motion of He was found to be the initial jumping of the helium atom to an adjacent interstitial position.[29] From Table 1 it is clear that such substitutional motion of the helium requires high activation barriers to be overcome and hence occurs at high temperatures ($\sim$ 400°K/eV to first-order) only. The volume changes calculated by Johnson, Bisson and Wilson[31] for the b.c.c.'s are also given in the table for completeness.

These simple calculations formed the basis for the calculations of the properties of several complex defect configurations in W[32] and Cu.[33] Tungsten was chosen from among the b.c.c.'s because of the experiments of Kornelsen[34] who implanted W with He at energies below the threshold for damage production and then heated the samples to remove the helium. Pre-irradiation with other rare-gases created the defect sites into which the helium could migrate. The activation energies associated with the peaks of these experimental thermal helium release spectra are given in Column 3 of Table 2. The notation used in the table is the following:

HeV → He substitutional ≡ He in a vacancy

He_nV → n He atoms in a single vacancy

nHe → n isolated He interstitials

V_i^j → subscript refers to the number of vacancies, superscript refers to the neighbors involved; e.g., V_2^I is a first-neighbor divacancy.

$He(VKr)^{II}$ → He atom in a second-neighbor divacancy containing a Kr atom

An important point to be emphasized in noting the agreement between theory and experiment in Table 2 is that the interatomic potentials employed were determined from first principles; no attempt was made to fit the Kornelsen data.

In Table 3 are given the binding energies of small helium clusters in W and Cu calculated by the author and C. L. Bisson. The calculations were done in the absence of a vacancy in order to determine if interstitial

helium clustering can occur and also in the presence of a vacancy. It is seen that such interstitial clustering in the absence of a vacancy is more likely (greater binding) in W than in Cu due to the larger strains induced by the rare gas in the b.c.c. In either case, however, the presence of a vacancy dramatically increases the binding energy of each He atom. An important feature of the He_nV clusters in Cu is that the binding energy of the sixth helium atom is significantly higher than for five or seven atoms. This is due to symmetry and is responsible for the large growth of these clusters during irradiation. This may also account for the percolative formation of bubbles in irradiated metals.

Up to now we have discussed complex defects only in W, but Wilson, Bisson and Baskes[33] have calculated the binding energies of up to ten helium atoms in up to four vacancies in Cu. Table 4 contains a summary of their results. An interesting observation can be made about these complex defects: the binding energy required to dissociate (remove one helium atom from) a He_NV_N cluster (number of helium atoms = number of vacancies) is relatively constant; that is, nearly independent of N, for these small clusters. A narrow distribution or band of binding energies might therefore be expected for this particular species of defect cluster. This was also pointed out in the W calculations reported above.[32] If a single binding energy for the helium in each defect complex, rather than a distribution of binding energies, is assigned and the Kornelsen data least-squares fit using a first-order release model, the dashed curve in Fig. 2 is obtained.[35] That is, the data are indicative of a more continuous distribution that can be modelled with about ten single activated thermal release spikes. Baskes and Jones[35] allowed a Gaussian distribution of activation energies in a similar fit of the actual Kornelsen data and were able to fit the data quite exactly as also seen in Fig. 2. Some experimental difficulties may account for some of the shape of these curves[36] as discovered later by Edwards and Kornelsen[37] in Ni.

Other calculations involving helium in metals should be mentioned. Wilson and Bisson[38] found that the activation energy ($\sim$ 0.47 eV) for divacancy motion was effectively increased to 0.74 eV by the presence of a helium atom in that divacancy. Calculations of helium behavior in

h.c.p. Ti are being performed by Johnson, et. al.[39] Dynamic calculations of Frenkel pair recombination in tungsten, using the identical potentials reported above, are underway at Lawrence Livermore Laboratory by Stewart and Guinan.[40] They have found that a single helium does not prevent such recombination, but that several helium atoms can introduce a barrier to the process. Oxygen and nitrogen interstitials in b.c.c.'s have been treated by Tewary.[41]

Turning our attention now to hydrogen defects in metals, we find less has been done from a diffusion and trapping point of view than for helium. Several fundamental theoretical calculations[42] have been reported, but these have had a different and more highly theoretical objective.

This absence of theoretical activity may in part be due to the difficulties encountered in an open shell calculation as discussed earlier. However, it has been found in the case of interactions involving hydrogen atoms that the unrestricted Hartree-Fock (UHF) method (different orbitals for different spins) gives quite good results without the difficulties of an open shell procedure (double Hamiltonian, etc.). The UHF method[25] was applied to the Ti-H interaction in TiH_2. Using the resulting interatomic potential for the $^4\Sigma^-$ state of Ti-H and the free-electron approximation for the other required interactions, the self-diffusion of hydrogen in TiH_2 was studied.[43] Fig. 3 is a plot of the potential seen by a hydrogen atom in its motion along a <111> direction from its normal tetrahedral (T_d) site to an adjacent octahedral (O_h) hole and then into a first-neighbor vacant site. The anharmonic oscillator potentials fitted by Korn and Zamir[44] to inelastic neutron scattering data are also given in Fig. 3. The calculated energy levels by Wilson and Bisson[43] are shown in the figure to agree within the experimental error. Again, it is to be emphasized that these calculations are based upon ab initio potentials and were not fitted to the experimental data.

Wiedersich, Burton and Katz[45] have extended classical nucleation theory to include the effects of helium on void nucleation. Barnes[46] has presented a theory of swelling of reactor materials involving inert-gas bubble migration. Wilson, Bisson and Baskes[33] have developed a solution to a coupled set of rate-equations employing the binding and

activation energies they calculated atomistically. Baskes[47] has included diffusion terms in this coupled system of equations as well. These calculations extend into "continuum-like" approaches and, in the spirit of the restriction of this work described in the introduction, will not be treated further.

DISCUSSION

The defect calculations on helium in metals discussed above are performed in the infinite mass limit; that is, the lattice is allowed to relax to its minimum energy configuration for each point along the path of migration of the defect. For the hydrogen self-diffusion calculations shown in Fig. 3, the lattice is frozen at all points along its path. These approximations each violate the assumptions made by Flynn and Stoneham[6] in their treatment of light-particle diffusion as the analog of the motion of a small polaron.[48]

In this study, the light particle (helium or hydrogen) in an interstitial position is assumed to be vibrating about its normal site with a local mode frequency "well above" the highest lattice frequency. The hydrogen or helium atom can jump, therefore, without the lattice following its motion in much the same way that electrons in a molecule move without the nuclei following (the Born-Oppenheimer approximation). This is completely opposite to the usual assumptions about diffusion; (e.g., self-diffusion in metals) where the lattice follows the motion of the diffusing particle at every point in its path. When the light particle is sitting in its interstitial site, before a jump, it exerts forces on the surrounding lattice; the lattice atoms must then relax to achieve equilibrium. The relaxation of the lattice atoms lowers the potential energy of the light interstitial serving to trap the particle. This is analogous to a point charge in an insulating medium polarizing the surrounding atoms whose dipoles then interact with the charge to trap it. This charge plus its associated local dipoles is known as a "polaron." It is not surprising, then, that the Flynn and Stoneham[6] theory has great similarity to the treatment of the small polaron by Holstein.

Although Norgett and Stoneham[7] were able to apply the small-polaron theory to their treatment of the hopping of V_k clusters in fluorides, they did so by calculating the "activation energy" from the lattice relaxation energy. What has not yet been done is the fundamental step: the calculation of the diffusion coefficient or even the matrix elements of the transition from detailed knowledge of the Hamiltonian. Only such a calculation can answer the fundamental question of the importance of treating light particles using small-polaron theory. An excellent review of these considerations has been provided by Sussman.[49]

ACKNOWLEDGMENTS

The author is deeply indebted to M. I. Baskes, C. L. Bisson, C. F. Coll, H. D. Jones, S. C. Keeton and C. F. Melius, of this Laboratory. These individuals not only acted in a tutorial manner but were willing to transmit their results and ideas prior to publication.

REFERENCES

1. R. B. McLellan and C. G. Harkins, Mat. Sci. and Eng. 18, 5 (1975).
2. G. M. McCracken, Rep. Prog. Phys. 38, 241 (1975); also Japan J. Appl. Phys. Suppl. 2, 269 (1974).
3. P. Shewmon, to be published.
4. R. Blackburn, Met. Rev. 11, 159 (1966).
5. "Effect of Hydrogen on Behavior of Materials," Jackson Lake Lodge, Moran, Wyoming, September 7-11, 1975; "The Hydrogen Economy Miami Energy (THEME) Conference," Miami Beach, Florida, March 18-20, 1974; "Report on the APS Summer Study on Physics Problems Relating to Energy Technologies: Radiation Effects on Materials," Brookhaven National Laboratory, Upton, New York (Rev. Mod. Phys. Suppl. 3 (1975). June 17-24, 1974; "Conference on Surface Effects in Controlled Thermonuclear Fusion Devices and Reactors," Argonne, Illinois, January 10-21, 1974; First Topical Meeting on the Technology of Controlled Nuclear Fusion," American Nuclear Society, San Diego, California, April 16-18, 1974; "International Conference on Applications of Ion Beams to

Metals," Sandia Laboratories, Albuquerque, New Mexico, October 2-4, 1973; "International Conference on the Applications of Ion Beams to Materials," University of Warwick, ENGLAND, September 8-12, 1975, "International Conference on Ion Beam Surface Layer Analysis," Nuclear Research Center, Karlsruhe, GERMANY, September 15-19, 1975; "American Nuclear Society 1975 National Meeting," San Francisco Hilton, San Francisco, California, November 16-21, 1975.

6. C. P. Flynn and A. M. Stoneham, Phys. Rev. B1, 3966 (1970); A. M. Stoneham and C. P. Flynn, J. Phys. F3, 505 (1973).
7. M. J. Norgett and A. M. Stoneham, J. Phys. C6, 238 (1973).
8. R. A. Johnson, J. Phys. F3, 295 (1973).
9. P. Gombas, Handbuch de Physik, Vol. 36, ed. by S. F. Flügge (Springer-Verlag, Berlin, 1956).
10. A. A. Adolphson, Phys. Rev. 133, A990 (1964); 178, 76 (1969).
11. P. T. Wedepohl, Proc. Phys. Soc. (London) 92, 79 (1967).
12. W. D. Wilson and C. L. Bisson, Phys. Rev. B3, 3984 (1971).
13. R. G. Gordon and Y. S. Kim, J. Chem. Phys. 56, 3122 (1972). In particular, see their Fig. 6 for Ar-Ar where the correlation and exchange energies are given as a function of interatomic separation.
14. R. D. Cowan, A. C. Larson, D. Liberman, J. B. Mann, and J. Wahler, Phys. Rev. 144, 5 (1966).
15. W. Kolos and L. Wolniewicz, J. Chem. Phys. 51, 1417 (1969).
16. R. E. Watson, Phys. Rev. 111, 1108 (1958).
17. J. C. Slater, J. Chem. Phys. 43, S228 (1965).
18. K. H. Johnson and F. C. Smith, Jr., Phys. Rev. B5, 831 (1972).
19. J. C. Phillips and L. Kleinman, Phys. Rev. 116, 287 (1959).
20. C. F. Melius and W. A. Goddard III, Phys. Rev. A10, 1528 (1974).
21. C. F. Melius, B. D. Olafson and W. A. Goddard III, Chem. Phys. Lett. 28, 457 (1974).
22. D. E. Rimmer and A. H. Cottrell, Phil. Mag. 2, 1345 (1957).
23. J. C. Slater and J. G. Kirkwood, Phys. Rev. 37, 682 (1931).
24. H. B. Huntington, Phys. Rev. 91, 1092 (1953).
25. The ATMOL programs developed at Atlas Computer Laboratory in Chilton, Berkshire by V. Saunders were employed.
26. S. Huzinaga, J. Chem. Phys. 42, 1293 (1965).

27. H. Basch, C. J. Hornback and J. W. Moskowitz, J. Chem. Phys. 51, 1311 (1969).
28. C. F. Melius, private communication.
29. W. D. Wilson and C. L. Bisson, Rad. Effects 19, 53 (1973).
30. W. D. Wilson and R. A. Johnson, "Interatomic Potentials and Simulation of Lattice Defects," ed. by Pierre C. Gehler, J. R. Beeler, Jr., and R. I. Jaffee, p. 375, Plenum Press, 1972.
31. R. A. Johnson, C. L. Bisson and W. D. Wilson, Rad. Effects, 25, 155 (1975).
32. W. D. Wilson and C. L. Bisson, Rad. Effects 22, 63 (1974).
33. W. D. Wilson, C. L. Bisson and M. I. Baskes, submitted to Phys. Rev.
34. E. V. Kornelsen, Rad. Effects 13, 227 (1972).
35. M. I. Baskes and H. D. Jones, private communication.
36. E. V. Kornelsen, private communication.
37. D. Edwards, Jr. and E. V. Kornelsen, Surface Sci. 44, 1 (1974).
38. W. D. Wilson and C. L. Bisson, to be published in Rad. Effects.
39. R. A. Johnson, C. L. Bisson and W. D. Wilson, submitted to International Conference on Computer Simulation for Materials Applications, April 1976.
40. R. Stewart and M. Guinan, ANS Trans. 21, 164 (1975); also private communication.
41. V. K. Tewary, J. Phys. F3, 1515 (1973).
42. For example, D. Hilton, N. H. March and A. R. Curtis, Proc. Roy. Soc. (London) 300, 391 (1967); I. Isenberg, Phys. Rev. 79, 736 (1950).
43. W. D. Wilson and C. L. Bisson, Proc. of the International Conference on the Effects of Hydrogen on the Behavior of Materials, Jackson, Wyoming, September 7-11, 1975.
44. C. Korn and D. Zamir, J. Phys. Chem. Solids 31, 489 (1970).
45. H. Wiedersich, J. J. Burton and J. L. Katz, J. Nucl. Mat. 51, 287 (1974).
46. R. S. Barnes, J. Nucl. Mat. 11, 135 (1964).
47. M. I. Baskes, private communication.
48. T. Holstein, Ann. Phys. 8, 325 (1959); Ann. Phys. 8, 343 (1959).
49. J. A. Sussmann, Ann. Phys. (Paris) 6, 135 (1971).

Table 1: Summary of formation and activation energies for helium in copper and b.c.c. metals. In parentheses are given the volume changes, calculated by Johnson, et. al.[a], in units of atomic volume.

	Formation Energy in Interstitial Site	Energy Required to Place He in Existing Vacancy	Interstitial Activation Energy	Activation Energy for He in a Vacancy[c]
I	1.99		0.62	
Cu[b] II	2.10		0.71	
III	1.97	0.13	0.45	2.15
IV	3.22		0.54	
V	1.74		0.49	
VI	2.03	0.15	0.57	1.88[d]
V	4.61 (0.39)	1.65 (-0.18)	0.13	3.20
Fe	5.36 (0.93)	1.61 (0.21)	0.17	3.98
Mo	4.91 (0.46)	1.04 (-0.07)	0.23	4.19
Ta	4.23 (0.44)	0.93 (-0.26)	∿0.	3.44
W	5.47 (0.56)	1.05 (-0.05)	0.24	4.75

a Ref. 31

b Models I-V are from Ref. 12, Model VI from Ref. 30 includes non-central forces.

c Mutual diffusion, see text and Ref. 29.

d This is the relative energy of helium in a vacancy and an isolated interstitial position; the path was not mapped as for Model III.

Table 2: Theoretical dissociation energies for each of the configurations suggested by Kornelsen.[a] The notation is given in the text; energies are in eV and are relative to the perfect lattice.

Calculated Energies Relative to the Perfect Lattice	Theoretical Binding Energy, eV	Experiment (Kornelsen)
He V→He + V	4.39	4.05
4.40→5.44 + 3.35		
$He_2V_2^{I} \rightarrow He\ V_2^{II}$ + He	4.42	4.37
8.38→7.36 + 5.44		
$He(VKr)^{I} \rightarrow He + (VKr)^{1}$	4.40	3.84
13.72→5.44 + 12.68		
$He_2V \rightarrow He$ + He V	2.89	3.14
6.59→5.44 + 4.40		
$He_3V \rightarrow He + He_2V$	2.52	2.88
9.87→5.44 + 6.95		
$He_4V \rightarrow He\ He_3V$	2.50	2.41
12.81→5.44 + 9.87		

[a] Ref. 34

Table 3: Binding energy of $(N + 1)^{st}$ helium atom to a cluster of N atoms in Cu and W both in the presence and absence of a single vacancy. A negative sign indicates anti-binding.

	Interstitial Clustering (no vacancy)		Substitutional Clustering (one vacancy)	
N	Cu	W	Cu	W
0	-	-	1.84	4.40
1	0.09	0.33[a]	0.79	2.89
2	0.18	0.81	0.57	2.52
3	0.09	0.58	0.66	2.51
4	0.18	0.40[a]	0.60	2.31
5	-0.02	0.91[a]	0.86	2.52
6			0.25	1.03[a]
7			0.24	

[a]These are only estimates; the energy had not fully converged to its minimum value.

Table 4: Binding energies, in eV, of the $j^{\underline{th}}$ helium atom in a cluster, (i,j), where i is the number of vacancies in Cu. The energies were calculated for "end points" only, the path of migration was not determined in each case.

Number of Vacancies	Number of Helium Atoms in the Cluster									
	1	2	3	4	5	6	7	8	9	10
0	-	.08	.18	.08	.18	-.02	-	-	-	-
1	1.84	.79	.57	.66	.60	.86	.25	.24	.20	.20
2	1.84	1.84	1.09	.66	.85	.90	.75	.85	.67	.85
3	1.84	1.84	1.84	1.25	.89	.99	.69	.78	.98	.70
4	1.97	1.84	1.73	1.93	1.25	1.13	1.12	1.10	.65	.82

FIGURE CAPTIONS

Fig. 1: The He-Cu^+ interatomic potential calculated by a) the Rimmer and Cottrell[22] empirical method, b) the free-electron method and Slater exchange[12] ($\alpha = 1$), c) the Hartree-Fock method[25] and d) a pseudopotential method due to Melius.[28] The He-Cu° potential due to Melius[28] is also shown for comparison.

Fig. 2: Helium release rate versus temperature for a tungsten crystal pre-irradiated with krypton (+) by Kornelsen. The dashed curve is a least squares fit to the data due to Baskes and Jones using an attempt frequency of 10^{13} sec^{-1} for single activated processes and the peak values of Kornelsen. Note the narrowness of the individual peaks. The solid curve is a least squares fit due to Baskes and Jones using the same model but allowing a distribution of activation energies for each peak.

Fig. 3: Comparison of our ab initio potential (solid line) with the empirical fits of Korn and Zamir[44] in two approximations: ⊡ the best least squares fit and ⧋ the best fit consistent with the empirical activation energy. The calculated energy levels of our (periodic) potential for the atom in the T_d site are shown as well as the experimental value.

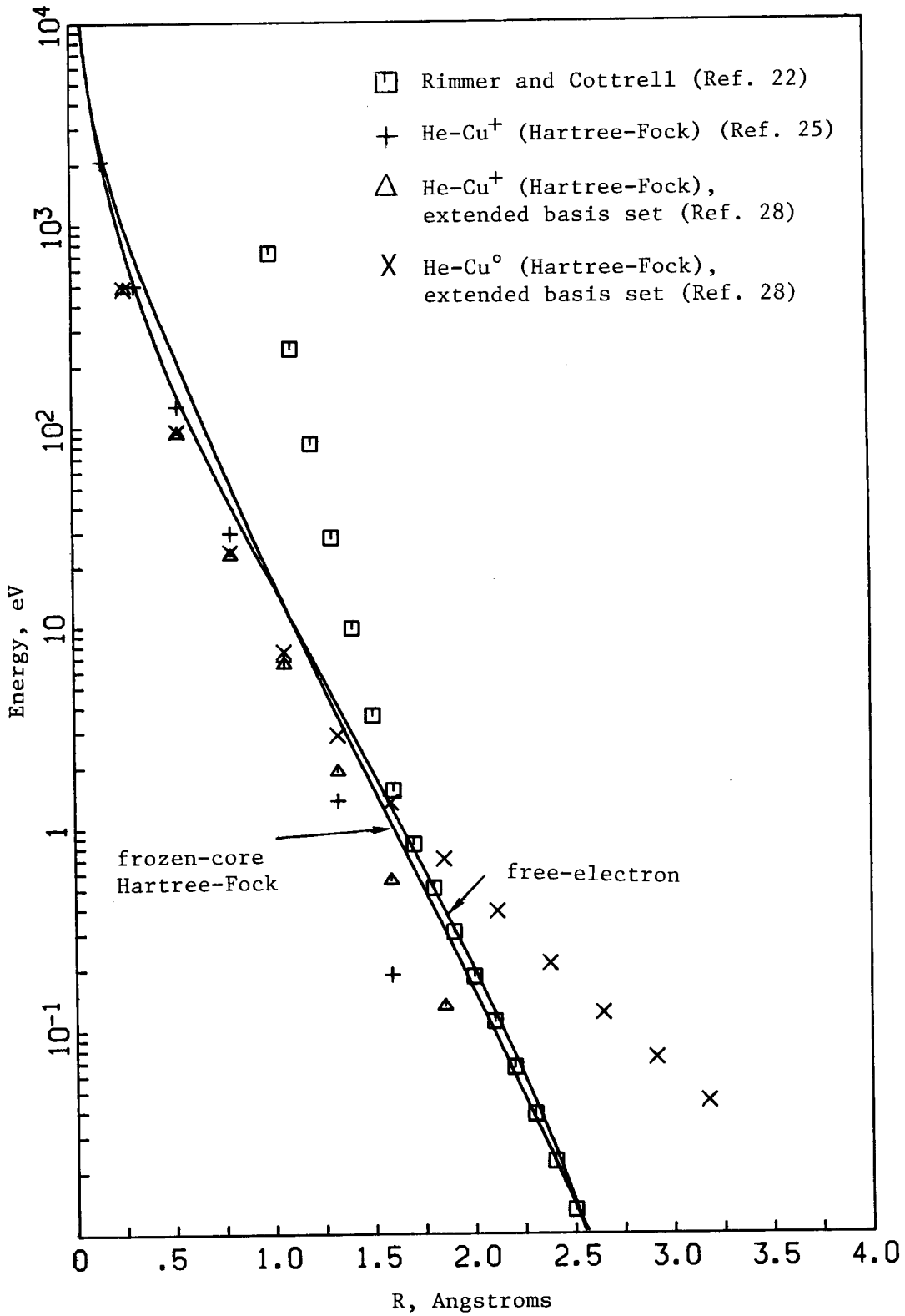

Rimmer and Cottrell (Ref. 22)
He-Cu+ (Hartree-Fock) (Ref. 25)
He-Cu+ (Hartree-Fock), extended basis set (Ref. 28)
He-Cu° (Hartree-Fock), extended basis set (Ref. 28)
frozen-core Hartree-Fock
free-electron
Energy, eV
R, Angstroms
10^4
10^3
10^2
10
1
10^-1
0
.5
1.0
1.5
2.0
2.5
3.0
3.5
4.0

Fig. 1

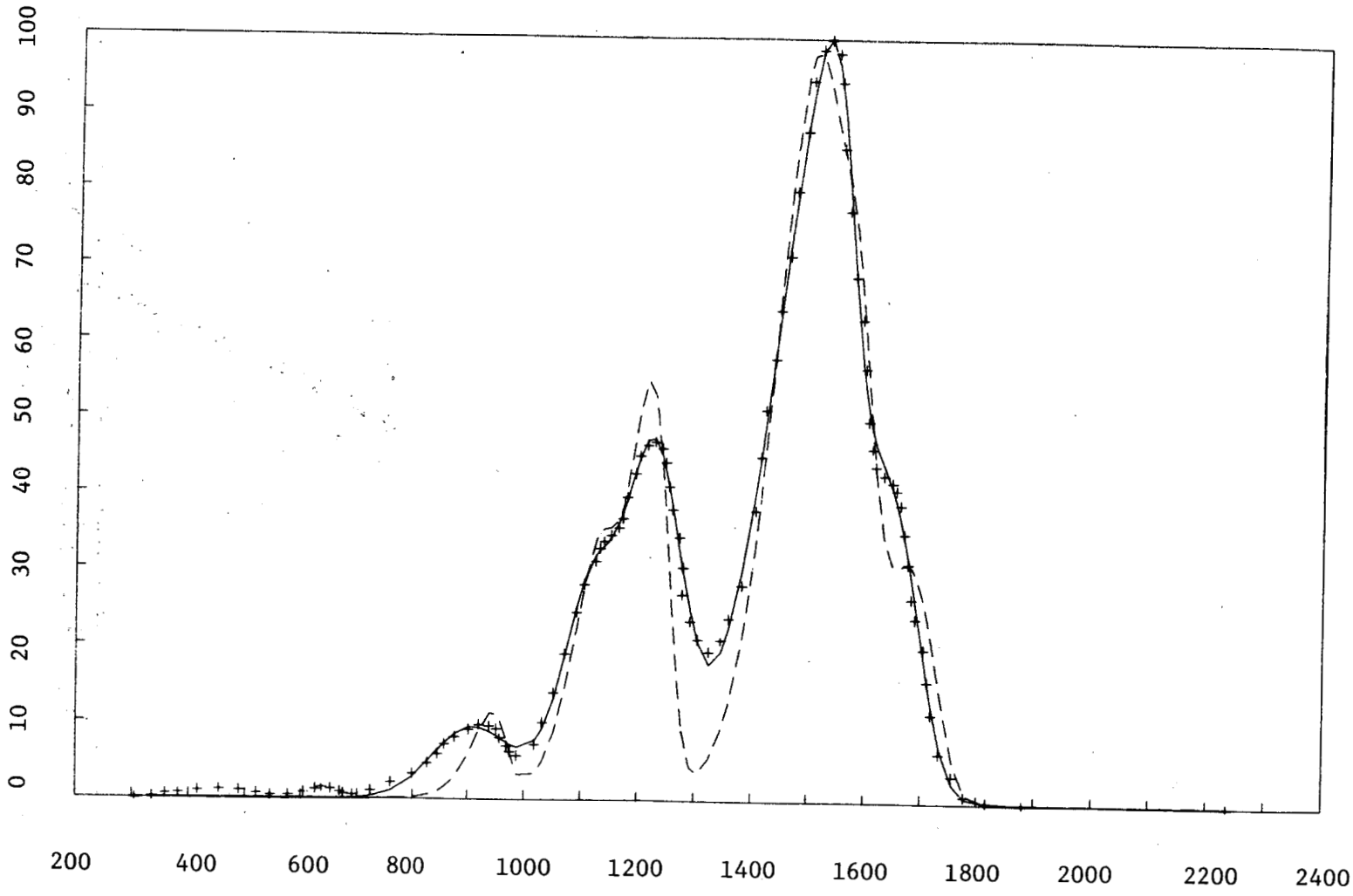

0
10
20
30
40
50
60
70
80
90
100
200
400
600
800
1000
1200
1400
1600
1800
2000
2200
2400
Temperature (°K)

Fig. 2

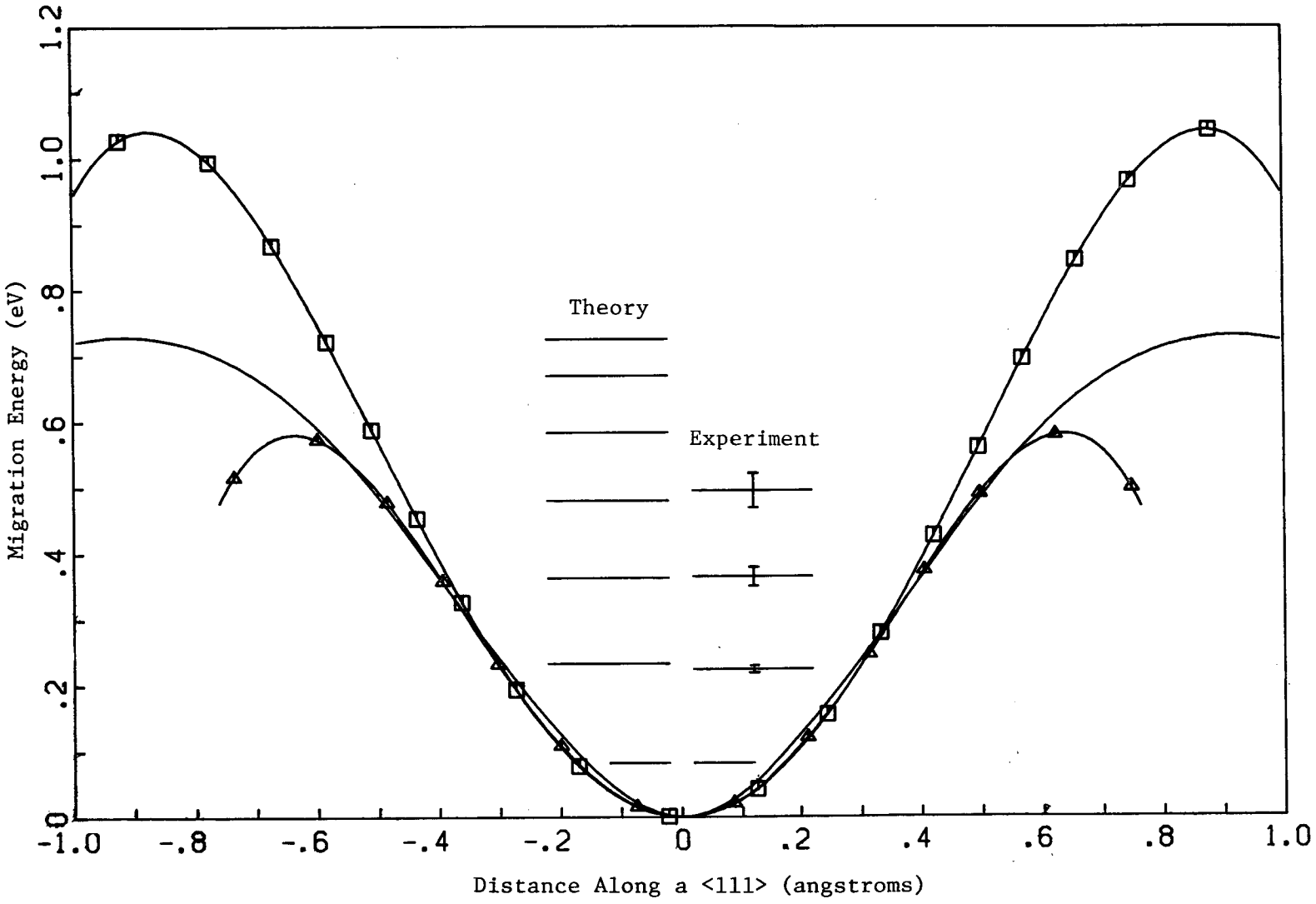

Migration Energy (eV)
1.2
1.0
.8
.6
.4
.2
0
-1.0
-.8
-.6
-.4
-.2
0
.2
.4
.6
.8
1.0
Theory
Experiment
Distance Along a <111> (angstroms)

Fig. 3

RADIATION ENHANCED DIFFUSION AND THE EFFECTIVENESS OF 14-MeV NEUTRONS*

G. J. Dienes
Brookhaven National Laboratory
Upton, New York 11973

Radiation enhanced diffusion is the phenomenon of increased atomic interchange brought about by the production of mobile defects. This effect can be investigated with high sensitivity by various solid state reactions in alloys, particularly in short-range ordering systems. This sensitivity is of great advantage for comparing the effectiveness of 14-MeV neutrons with fission reactor neutrons because of the low flux - low exposure limitation of currently available 14-MeV neutron sources. The effectiveness comparison obtained in such an experiment is limited to a comparison of the rates of production of mobile defects. Neutron damage is, of course, far more complex, involving the production of defect clusters, spikes, focusing collisions, transmutations, etc. In the long run, systematic studies of each of these effects are required since the scaling factor between 14-MeV and reactor neutrons can hardly be expected to be the same for the different radiation effects. The radiation enhanced diffusion experiments summarized here are to be regarded as the first step in such a program.

The first radiation enhanced diffusion experiment with 14-MeV neutrons was carried out on solute clustering in an Au-Fe (17% Fe) alloy using the Mössbauer effect for measuring the magnetic ordering temperature, T_o.[1] Neutron irradiation at room temperature produces clustering by means of radiation-enhanced diffusion, while annealing at high temperatures is required to produce clustering thermally. The change in T_o, which increases upon clustering, was assumed to be proportional to the change in local order. The radiations were carried out at Livermore at the rotating target neutron source (RTNS) with 14.8-MeV neutrons and in the LPTR (a light-water reactor) with reactor neutrons. For interpreting the data in terms of radiation enhanced diffusion the simple linear theory (i.e. radiation enhanced diffusion

coefficient proportional to flux at low flux) was assumed valid.[2] The results showed that in this solute clustering alloy the 14-MeV neutrons are more effective by about a factor of 10 than the reactor neutrons (energy greater than 0.1 MeV) in producing mobile lattice defects. This result is qualitatively significant but the scaling factor obtained cannot be considered as truly quantitative since several assumptions had to be used to derive it. This is because the detailed kinetics of the clustering reaction in this alloy has not been determined.

Far better quantitative results were obtained in a series of experiments on α-brass, an alloy in which short-range ordering kinetics and radiation enhanced diffusion have been investigated in detail.[3,4] The radiations were again carried out at Livermore at the RTNS and in the LPTR with careful monitoring of the fluence. The increase in short-range order was measured by the decrease in resistivity at liquid nitrogen temperature. The exposure range covered was from a fluence of about 10^{14} n/cm^2 to about 2×10^{17} n/cm^2 (E>0.1 MeV for LPTR exposures). The most reliable comparison for mobile defect production is at low fluence where complicating effects (e.g. disordering by spikes and damage accumulation) are minimal. The results show that at low fluence the 14.8-MeV neutrons produce a 10 ± 2 times greater number of mobile defects than the reactor neutrons.[5] At high fluence increase in resistivity, presumably caused by damage accumulation, was observed in α-brass and the rate of increase was accelerated by exposure to 14-MeV neutrons relative to reactor neutrons, but only by about a factor of 2. This last observation must remain qualitative at the present time since the kinetics of this process has not been studied quantitatively.

It should be re-emphasized that the experiments discussed here indicate the relative number of mobile defects produced by the knock-ons, not the total number of defects. This is because only part of the extra energy deposited in the lattice by a 14.8-MeV neutron is going into the creation of mobile defects. As already indicated, a variety of experiments will be required to characterize the difference between 14.8-MeV and reactor neutrons.

REFERENCES

* Research supported by the Energy Research and Development Administration.

1. R. J. Borg and G. J. Dienes, J. Appl. Phys. 46, 99 (1975).
2. G. J. Dienes and A. C. Damask, J. Appl. Phys. 29, 1713 (1958).
3. A. C. Damask, J. Phys. Chem. Solids 4, 177 (1958).
4. R. E. Larsen, G. J. Dienes, and A. C. Damask, Acta Metall. 12, 1141 (1964).
5. A. C. Damask, R. van Konynenburg, R. J. Borg, and G. J. Dienes, Radiation Effects (submitted).

RADIATION ANNEALING IN Ag AND Au DUE TO ENERGETIC DISPLACEMENT CASCADES*

R. S. Averback and K. L. Merkle
Materials Science Division
Argonne National Laboratory
Argonne, Illinois 60439
USA

ABSTRACT

Radiation annealing due to energetic displacement cascades has been studied in Ag and Au. Thin film specimens, 2500 Å, were doped to various concentrations of Frenkel pair defects by irradiating with 150 keV protons at temperatures below 10 K. Subsequently, the specimens were irradiated below 10 K with energetic, ∿540 keV, self-ions. Electrical resistivity measurements were used to monitor the concentration of defects as a function of dose. In Au, approximately 5% of the doped in Frenkel pairs, annealed during the 540 keV Au irradiation. The annealing volume associated with individual cascades was found to be 2.1×10^{-16} cm^3. In Ag approximately 5% of the doped in defects annealed during a 500 keV Ag irradiation and the annealing volume of the cascade was found to be 5×10^{-16} cm^3. In addition, the effects of doping concentration and specimen temperature during doping was investigated.

INTRODUCTION

Measurements of the production rate of point defects, $d\Delta\rho/d\phi$, where $\Delta\rho$ is proportional to the concentration of defects and ϕ is the ion dose (cm^{-2}), as a function of the concentration of irradiation induced defects, provide a means to determine the volume of energetic displacement cascades and the density of defects within the cascades.[1] A reduction in $d\Delta\rho/d\phi$ with increasing concentration of defects, or radiation annealing, can be effected by two mechanisms. The first mechanism requires the displacement of additional atoms by the test irradiation. The newly produced vacancies and interstitials can be deposited within the spontaneous recombination volume, (S.R.V.) of their respective anti-defect, leading to annihilation of the pair. In this process, the amount of annealing is proportional to the total S.R.V. of the current defect population. The second mechanism is the annihilation of close Frenkel pairs induced by subthreshold events. This process is different that the first in that the defect population is

*Work supported by the U.S. Energy Research and Development Administration.

reduced during irradiation, whereas for the first, only $d\Delta\rho/d\phi$ is reduced. Subthreshold annealing events should be proportional to the close pair concentration.

This study concentrates on subthreshold annealing events due to cascades, a process not previously studied. This mechanism for radiation annealing is of interest because it provides information about the distribution of energy around a displacement cascade, whereas saturation effects due to overlapping of cascades gives information about the volume of the crystal directly damaged during a displacement cascade. To observe subthreshold annealing events due to a cascade, it is necessary to increase the concentration of close Frenkel pairs over that which would be produced by a cascade. In this way, the subthreshold annealing is increased without much affecting the annealing involving displacements. In this experiment, Ag and Au thin film specimens were doped with Frenkel pairs using a 150 keV proton irradiation at low temperature $\sim$10 K. This type of irradiation produces predominantly Frenkel pair type defects with few defect clusters. Subsequently, the specimens were irradiated with $\geq$ 500 keV self-ions. By comparing the production rates of doped and undoped specimens, the contribution of subthreshold annealing can be obtained. Doping irradiations at 45 K (above Stage I in Ag) were also performed to verify that the observed annealing effect was in fact caused by the recombination of close Frenkel pairs.

EXPERIMENTAL

The details of the experimental procedure will be published elsewhere; however, two comments are appropriate here. The specimen thicknesses ranged between 1800 and 3500 Å and therefore, 1) a size effect was introduced in the electrical resistivity and 2) the damage was not distributed homogeneously.[2] One of us (KLM) has shown previously that the size effect can lead to an increased initial $d\Delta\rho/d\phi$, but at defect concentrations as high as our lowest doping concentrations, the size effect is negligible.[3] The effect of an inhomogeneous defect distribution on $d\Delta\rho/d\phi$ curves is not as clear. We find experimentally, however, that 1) the initial production rate is not much affected by specimen thickness; 2) production rate curves

fall lower for thicker specimens; 3) extrapolation of the production rate curves to the saturation resistivity yield approximately the same value independent of thickness for not too thick specimens.

RESULTS

Figure 1 clearly illustrates the subthreshold annealing effect; it is a plot of the defect resistivity versus dose for an Ag specimen which has been irradiated below 10 K with 150 keV protons and subsequently irradiated with 500 keV Ag^{++}. The proton damage approaches saturation approximately exponentially; upon irradiating with Ag^{++}, the defect resistivity initially decreases with dose, reaches a minimum, and finally increases, tending to saturate near the value obtained for the undoped specimen. Representative production rate curves for Ag specimens doped to different defect concentrations, are shown in Fig. 2. In these curves, the proton irradiation induced defect resistivity is included in the total defect resistivity.

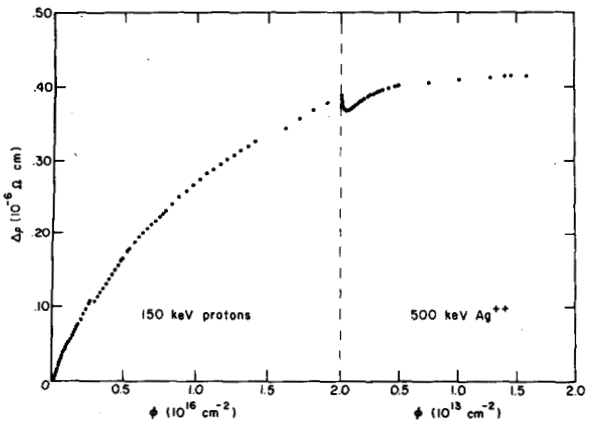


Fig. 1. The radiation induced defect resistivity versus dose for an Ag specimen irradiated at 10 K with 150 keV protons and 500 keV self-ions.

Curves 1 and 1a are the production rates for the undoped specimen showing the raw and size corrected data, respectively. These two curves illustrate the magnitude of the size correction and the portion of the curve where it is significant. The production rates for all but one of the doped specimens increase with dose initially, reach a maximum and decrease thereafter. The initial production rates are most suppressed from that of the undoped specimen for the most heavily doped specimens; for a sufficient concentration of proton induced defects (i.e., close pairs) the initial production rate is in fact negative. The one curve (4900) which does not show a suppressed $d\Delta\rho/d\phi$, but rather an enhanced production rate, represents the specimen that was doped at 45 K. All of the curves, regardless of doping conditions, saturate at approximately the same resistivity,

$\sim$0.41$\mu\Omega$-cm, the saturation resistivity obtained from fast neutron[4] deuteron[5] and the present proton irradiations.

The production rate curves for Au are plotted in Fig. 4. The same general features are observed in Au as in Ag. 1) The curve (3) for the specimen doped by a proton irradiation below 10 K shows an initially negative $d\Delta\rho/d\phi$, which increases with dose, reaches a maximum and decreases thereafter. 2) The curve (2) for the specimen doped at 45 K decreases with dose over the entire range, and the initial production rate is greater than the corresponding $d\Delta\rho/d\phi$ for the undoped specimen. There are, however, significant differences between the Au and Ag results. 1) The saturation resistivity for the low temperature doped specimen appears $\sim$20% higher than the undoped specimen; 2) $d\Delta\rho/d\phi$ for the low temperature doped specimen reaches a maximum significantly above the corresponding $d\Delta\rho/d\phi$ for the undoped specimen.

ANALYSIS

The production rate for energetic heavy ions incident on a thin film doped with Frenkel pairs is given by

$$\frac{d\Delta\rho}{d\phi} = -\frac{\rho_f}{N_o a}\,(C_P - C_A)\,V_a\,\left(1 - \frac{V_A}{V_o}\right) + A\,\left(1 - \frac{2\alpha_r\,\Delta\rho}{\rho_f}\right) \qquad (1)$$

ρ_f is the Frenkel pair resistivity; N_o the concentration of atoms; a the specimen thickness; C_P and C_A the defect concentrations in the doped and annealed states, respectively; V_a the volume around a cascade in which close pairs annihilate, V_A the total annealed volume; V_o the specimen volume, α_r[6] the spontaneous recombination volume for vacancies and interstitials, and A a function of the displacement cross section. At zero dose Eqn. (1) yields

$$V_a = \frac{N_o a\,\left(-\frac{d\Delta\rho}{d\phi} + A\right)}{\Delta\rho_a} \qquad (2)$$

where $\Delta\rho_a$ is the total resistivity increment annealed by the cascade and is given by

$$\Delta\rho_a = \frac{C_P - C_A}{N_o}\,\rho_f \qquad (3)$$

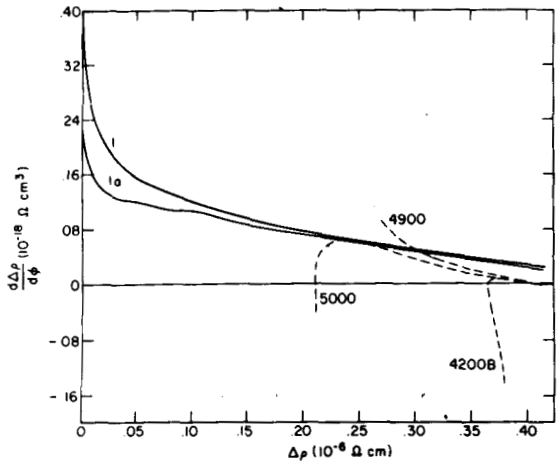


Fig. 2. Representative production rate curves for self-ion irradiated Ag. 1 and 1a, undoped; 4900 doped at 45 K; 4200 B and 5000, doped at 10 K.

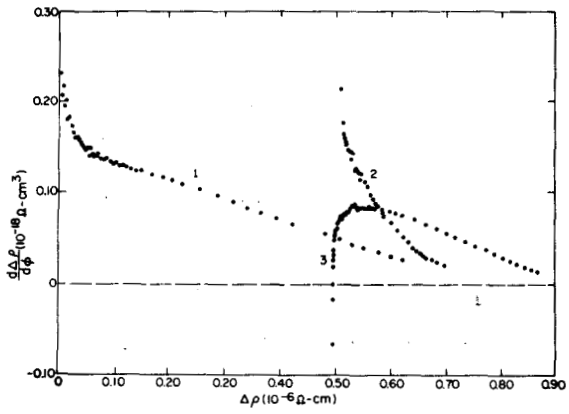


Fig. 3. Production rate curves for self-ion irradiated Au; (1) undoped (2) doped at 45 K; (3) doped at 10 K.

From Fig. 1 it is observed that the subthreshold annealing effect is complete after low dose. The production rate curve at high dose is, therefore, determined by the second term is Eqn. (1) and A and α can be deduced from the production rate curves. V_a and $\Delta\rho_a$ are then obtained from the low dose measurements assuming A and α_r to be independent of $\Delta\rho$.

Table I. The subthreshold annealing and spontaneous recombination volumes in Au and Ag. $\Delta\rho_d$ is the proton induced resistivity increment, E the self-ion energy, and $\Delta\rho_A$ the resistivity increment annealed by subthreshold events.

Spec #	$\Delta\rho_d$ (Ω-cm)	a(cm)	(at. vols.)	V_a (cm³)	E (keV)	$\Delta\rho_A$	$\frac{\Delta\rho_A}{\Delta\rho_d}$
Ag 4800	8.3×10^{-8}	3.48×10^{-5}	300	6.2×10^{-16}	500	1.68×10^{-9}	.020
Ag 4200 A	1.6×10^{-7}	3.48×10^{-5}	300	6.0×10^{-16}	500	3.3×10^{-9}	.021
Ag 5000	2.14×10^{-7}	2.39×10^{-5}	300	5.1×10^{-16}	500	1.0×10^{-8}	.047
Ag 4200 B	3.87×10^{-7}	3.48×10^{-5}	300	3.9×10^{-16}	500	2.8×10^{-8}	.072
Ag 1	0	2.33×10^{-5}	280	-	540	-	-
Au 6000 A	4.94×10^{-7}	2.35×10^{-5}	138	2.1×10^{-16}	540	2.6×10^{-8}	.052
Au 6000 B	0	2.35×10^{-5}	170	-	540	-	-

Table I lists the annealing volumes with other relevant data for cascades in both Au and Ag. The above analysis is based on the assumption that α_r and A can be extrapolated to low $\Delta\rho$. This implies that the S.R.V.s of defects are not sensitive to their detailed configuration. In view of the initial production rate curves for the 45 K proton irradiation doped Ag and Au and for the undoped specimen, this assumption seems questionable but should not greatly effect our results.

CONCLUSIONS

The results show that the radii of the annealing volumes of cascades in Ag and Au are 4.9×10^{-6} cm and 3.7×10^{-6} cm respectively. If splitting into subcascades is taken into account,[7] these distances are reduced about a factor of two. The distances should be considered minima since in the analysis of the data, the efficiency to anneal a close pair within the annealing volume, was taken to be 1. This excludes the possibility that a close pair within V_a survives, but is later induced to recombine by another cascade. It was also assumed that the annealing volume is spherical.

A second aspect of this paper is that the radiation annealing effect in Au is similar to that in Ag. For Ag, Stage I is well understood; interstitial migration occurs between 13 and 35 K. It was, therefore, not surprising that the radiation annealing of close Frenkel pairs in Ag was observed for the 10 K doping irradiation, and not for the 45 K irradiation. For Au, however, recovery of electron irradiated Au has been observed below 1.0 K.[8] This experiment would indicate, if interpreted in the same model used for Ag, that despite interstitial motion below 10 K, close pairs can survive at 10 K. Similar results from subthreshold electron irradiations of Au have also been reported.[9] A second explanation for this effect is that subthreshold events release interstitials from traps, and since mobile at 10 K, they can annihilate at vacancies.

We observe that the initial $d\Delta\rho/d\phi$ for both Au and Ag doped at 45 K with proton induced damage is significantly higher than the $d\Delta\rho/d\phi$ for a corresponding resistivity increment induced by self-ions. This indicates that for a self-ion irradiation, the ratio of the S.R.V. to resistivity, per defect, is considerably higher in cascade damage than in a homogeneously distributed vacancy rich (manyinterstitials are lost to the surface at 45 K) defect distribution.

Finally we find that the saturation resistivity in Ag is the same for self-ion damage and proton damage. Although this is the same value that was obtained before using neutron and deuteron irradiations, we have 1) gone to higher defect concentrations, 2) have used different segments of the same film for the two types of irradiations, and 3) even used one

specimen and irradiated it first with protons and then with self-ions. This is interesting in view of the differences in the saturation resistivity obtained by electron versus neutron irradiations in Cu, and Pt.[4,11]

ACKNOWLEDGMENTS

The authors are grateful to L. Singer for growing the thin film specimens and to L. J. Thompson for assistance in running the accelerator facility.

REFERENCES

1. W. Kesternich and K. L. Merkle, Application of Ion Beams to Metals, ed. S. T. Picraux, E. P. EerNisse and F. L. Vook, Plenum Press, New York, (1974) p.495.
2. K. B. Winterbon, P. Sigmund and J. B. Sanders, Mat. Fys. Med. Dan. Vid. Selsk, 37, No. 14 (1970).
3. K. L. Merkle, Physics of Ionized Gases ed. V. Vujnovic, Rovinj, Yugoslavia p.526 (1974).
4. G. Burger, H. Meissner, W. Schilling, phys. stat. sol. 4, 281 (1964).
5. H. G. Cooper, J. S. Koehler, J. W. Marx, Phys. Rev. 97, 599 (1956).
6. G. Lücke and R. Sizmann, phys. stat. sol. 5, 683 (1964).
7. K. L. Merkle and R. S. Averback, this conference.
8. R. C. Birtcher, W. Hertz, G. Fritsch, and J. Watson, this conference.
9. F. Dworschak, Ch. Lehmann, H. Schuster, H. Wollenberger and J. Wurm in Proc. of the Intern. Conf. on Solid State Physics Research with Accelerators, 1967, BNL-50083 (C-52) p.327.
10. J. A. Horak and T. H. Blewitt, phys. stat. sol. 9, 721 (1972).
11. G. Duesing, W. Sassin, W. Schilling, H. Hemmerich, Crystal Lattice Defects, 1, 55 (1969).

ENHANCED ATOMIC MOBILITY DUE TO LOW DOSE NEUTRON IRRADIATION AS MEASURED IN A Ag-30 at % Zn ALLOY BY ZENER RELAXATION METHODS

M. Halbwachs, J. Hillairet, H. Gonzalez* and J. Cost**
Centre d'Etudes Nucleaires de Grenoble
38041 Grenoble, France

ABSTRACT

Mean atomic jump rates have been measured during and after short-time neutron irradiations of a fcc Ag-30 at % Zn alloy by monitoring the rate of the Zener relaxation. Measurements made at 40°C immediately after rapid suppression of the flux showed significant enhancement of the atomic mobility for a flux of $\sim 10^{11}$ fast n/cm^2·sec and an irradiation time of only 30 sec. The subsequent decrease of the atomic mobility to the thermal equilibrium value was studied and found to follow simple exponential decay. The results are discussed in terms of the nature and concentration of mobile defects created by cascades, the mechanism for defect annihilation and the concentration of sinks.

INTRODUCTION

Zener relaxation methods have proved to be a powerful tool for determination of atomic mobility in various alloys under conditions of equilibrium[1] and under non-equilibrium conditions in which mobile defect concentrations are enhanced by quenching[2-4] and plastic deformation.[5] The reason for the success of these methods is inherent; they provide a measure of the mean atomic jump rate and thus a quantity which is proportional to the defect concentration, assuming a single mobile defect. The application of this technique to radiation studies has obvious advantages since it provides the capability for *in situ* monitoring of the

*On leave from Commission Nacional de Energia Atomica, Buenois-Aires, Argentina.

**On leave from School of Materials Engineering, Purdue University, West Lafayette, Indiana 47907, USA.

mobile defect concentration introduced by irradiation.

Preliminary experiments describing Zener relaxation studies of radiation-enhanced atomic mobility under steady fast neutron flux have recently been reported for a Ag-30 at % Zn alloy.[6,7] These results have shown enhancement factors of from 3 to 10^4 over the temperature range from 160°C to 40°C for a steady flux of 9 x 10^{11} fast n/cm^2·sec. It is the purpose of this paper to report preliminary results of an investigation of the build-up and decay of enhanced atomic mobility due to short, low flux irradiations by fast neutrons.

METHOD

The experimental method and the sample used in this study are the same as previously described.[6,7] The method is essentially one of elastically loading or unloading the sample at appropriate times in the irradiation schedule and measuring the resulting anelastic strain. The anelastic strain rate is then analyzed by methods described in the literature[1,3,4] to determine the time-dependence of the relaxation rate.

The relaxation rate for the Zener relaxation is given by

$$\tau^{-1} = Ac_v\nu_v + Bc_i\nu_i \qquad (1)$$

where the subscripts v and i refer to vacancies and interstitials and c and ν are the concentrations and jump frequencies of these two species. The constants A and B depend respectively upon the efficiencies with which vacancy and interstitial jumps modify the short range order to produce the Zener relaxation. The value of A is known to be near unity,[1] while that of B is unknown, but may be considered to be near unity until determined otherwise. By monitoring the value of τ^{-1} at a fixed temperature so that ν_v and ν_i are constant, information about the instantaneous concentration of mobile defects responsible for the relaxation can be obtained. In this study τ^{-1} was monitored before, during and after short irradiations (range of 30 sec to 600 sec) at the relatively low flux of 9 x 10^{10}n/cm^2·sec (E>1 MeV). With such small dose irradiations, the experiment becomes one of rapidly injecting defects and then measuring the enhancement and the subsequent decay of the atomic jump rate and thus the defect concentration.

The anelastic strain was measured either after the application or the removal of the load, since it was determined that the displacement curves were equivalent. Also, checks were made which demonstrated that the Zener relaxation was the only mechanism contributing to the displacements. All measurements were performed at 40°C. Between runs the sample was annealed at 250°C for several hours, a treatment found to eliminate radiation-produced sinks.[7]

RESULTS

Figs. 1 and 2 show for 40°C the flux, anelastic response curves, and the resulting time-dependent mean atomic jump rate (obtained by the method of local slope analysis[3,4]) for the shortest and longest injections made at a flux of 9×10^{10} n/cm^2·sec. These findings are consistant with the measurements on the same sample for long irradiations ($> 10^3$ sec) at higher flux.[6,7] The fluence shown in Fig. 1 is the smallest possible at this flux, since the reactor was started as rapidly as permissible, and immediately upon reaching the maximum flux, the control rods were dropped. It may be noted that although the load change has been applied well before the start of the irradiation (typically several hundred seconds), there is a negligible anelastic response until the flux is applied. This is in agreement with the long relaxation time ($\sim 4 \times 10^7$ sec) at thermal equilibrium at 40°C in this alloy.[4] With the start of the irradiation, the defect concentration, as evidenced by τ^{-1}, increases. It does not reach a steady value for the short injection in Fig. 1 as it does for the injection of 600 seconds at maximum flux shown in Fig. 2. Here the mean atomic jump rate is found to reach a constant value of 3.2×10^{-4} sec^{-1} after about 200 seconds of irradiation. In both figures it may be observed that when the flux is cut, the defect concentration starts to drop, requiring several hundred seconds to decay to a value which can not be detected. An analysis of the kinetics of this decay for the various injection experiments indicated it to be simple exponential, as shown in Fig. 1*. The values of the exponential time constant θ for defect decay for the various runs are reported in Table 1 and show reasonable agreement

* Run 160 was an exception to this (see Fig. 2).

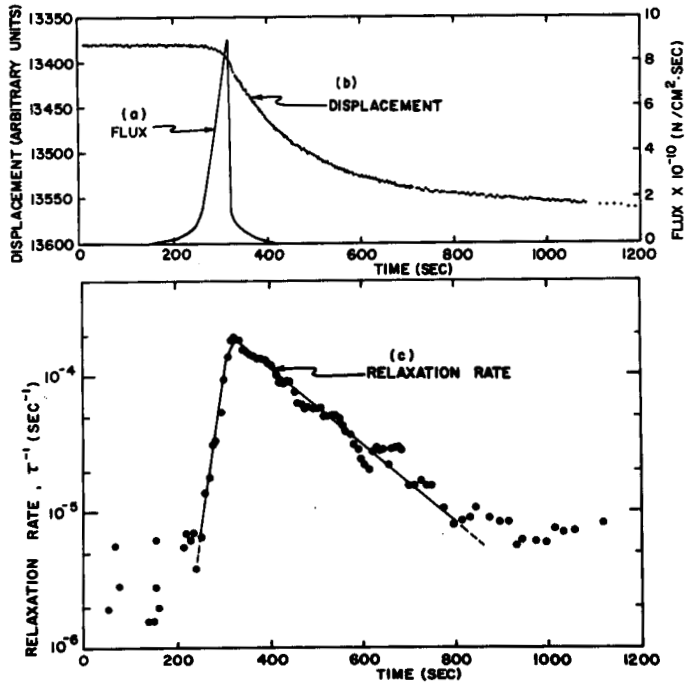


Fig. 1. (a) Neutron flux, (b) anelastic displacement curve and (c) mean relaxation rate versus time for the lowest fast neutron dose.

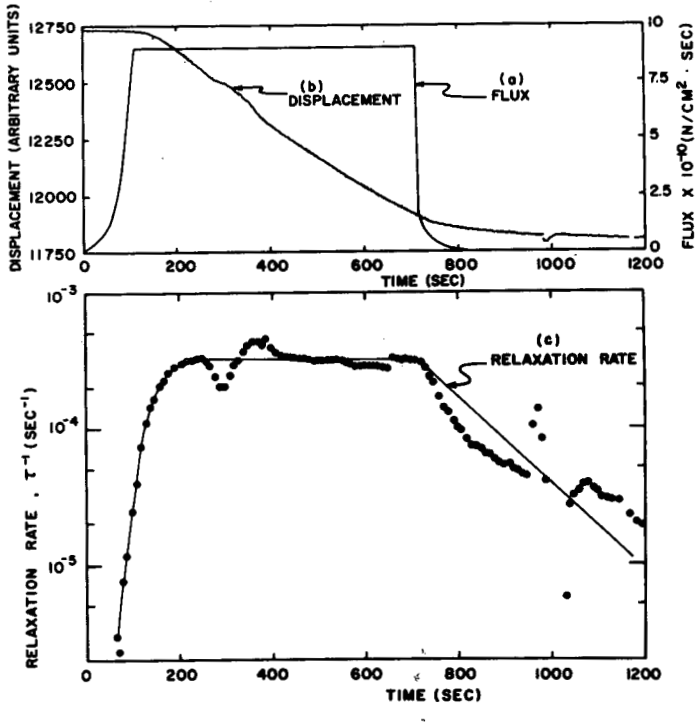


Fig. 2. (a) Neutron flux, (b) anelastic displacement curve and (c) mean relaxation rate versus time for the largest fast neutron dose studied, 600 sec at a flux of 9×10^{10} n/cm^2·sec.

between runs. Also shown in Table 1 are $\tau^{-1}(0)$, the value of the relaxation rate at the start of decay, and ψ_{decay}, the fraction of the total anelastic response which takes place after the irradiation is stopped. It may be noted in Table 1 that ψ_{decay} is typically less than 0.05 of the total anelastic response. This is because the rate of defect annihilation for this sample is appreciably greater than the maximum rate of the Zener relaxation, $\theta^{-1} >> \tau^{-1}(0)$.

Table 1. Values Obtained from Neutron Injection Experiments Using Two Methods of Analysis.

Run	Fluence (n/cm^2)	ψ_{decay}	Slope analysis		Direct analysis, Eq.(4)			
			$\tau^{-1}(0)$ (sec^{-1})	θ (sec)	$\tau^{-1}(0)$ (sec^{-1})	θ (sec)	$\frac{\tau(0)}{\theta}$ calc.	$\frac{\tau(0)}{\theta}$ Eq.(5)
153	0.3×10^{13}	0.038	3.3×10^{-4}	150	2.7×10^{-4}	141	26	26
157	0.3×10^{13}	0.027	1.8×10^{-4}	103	2.0×10^{-4}	123	41	37
158	0.3×10^{13}	0.017	1.4×10^{-4}	83	1.1×10^{-4}	145	63	58
158a	0.3×10^{13}	0.045	1.8×10^{-4}	152	3.1×10^{-4}	144	22	22
158b	0.3×10^{13}	0.016	1.5×10^{-4}	98	1.5×10^{-4}	110	61	62
159	1.4×10^{13}	0.026	3.2×10^{-4}	60	5.1×10^{-4}	53	37	40
159a	1.4×10^{13}	0.057	4.8×10^{-4}	109	6.5×10^{-4}	90	17	17
160	5.7×10^{13}	0.030	3.2×10^{-4}	138	1.9×10^{-4}	191	28	33

In the slope analysis method to obtain $\tau^{-1}(t)$, 10 or more data points were least squares fit to obtain the slope. The derivative curve is extremely sensitive to minor experimental fluctuations in the anelastic response curve, e.g., the deviations in $\tau^{-1}(t)$ which appear in the middle of the irradiation and during the decay in Fig. 2 are of experimental origin.

DISCUSSION

The experimental result of simple exponential decay of the defect concentration indicates that a single defect is annihilating by diffusing to fixed sinks. Since it is reasonable to assume that the interstitial mobility differs from that of the vacancy, the alternative interpretation, that two defects with the same mobility are annihilating, is unlikely.

We can express the simple exponential decay as

$$dc_d/dt = c_d \nu_d c_s \tag{2}$$

where the effective concentration of sinks c_s gives the probability per defect jump that the defect annihilates, the subscript d refers to either the vacancy or the interstitial, and $\theta^{-1} = \nu_d c_s$. Also shown in Table 1 are experimental values for the ratio $\tau(0)/\theta$, which for all injections is significantly greater than unity. Since $\tau(0)/\theta = c_s/c_d$, then we have the result that $c_s >> c_d$. This is in accord with the previously discussed finding that annihilation occurs at fixed sinks rather than by pair recombination. Also, as discussed by Berry and Orehotsky,[4] when the concentration of sinks is greater than the concentration of defects, gradients in the defect concentration do not develop during the annealing and the defect concentration decays homogeneously. This is an important finding since the method of slope analysis used to obtain the time dependence of the atomic jump rate is only valid if annealing is homogeneous.[4]

It is possible to make an independent determination of the values of $\tau^{-1}(0)$ and θ that were obtained by the slope analysis method. This is done by a direct analysis of the anelastic response curve. For a single, but time-dependent, relaxation rate, the anelastic response curve is given by

$$\ell n(1 - \psi) = - \int_o^t \tau^{-1}(t)\, dt \tag{3}$$

where ψ is the fraction of the total anelastic strain. Integration of Eq. (2) to obtain the time dependence of $\tau^{-1}(t)$ and then substituting into Eq. (3) and rearranging gives a function relating ψ to the time of decay,

$$h(t) = - \ell n \left[1 + \frac{\tau(0)}{\theta} \ell n(1 - \psi)\right] = t/\theta \tag{4}$$

A plot of this function versus time should give a straight line with a slope of $1/\theta$. The value of the parameter $\tau(0)/\theta$ in Eq. (4) may be obtained from ψ_{decay}, the maximum experimental value of the anelastic response function obtained at $t/\theta >> 1$,

$$\tau(0)/\theta = [- \ell n(1 - \psi_{decay})]^{-1} \tag{5}$$

In Fig. 3 a plot of h(t) is shown for the anelastic response curve of the injection experiment in Fig. 1 (Run 158a). A good linear fit of the data is found for the first 0.9 of the decay. The slope of the straight line portion gives θ = 144 sec in good agreement with the value for θ found by

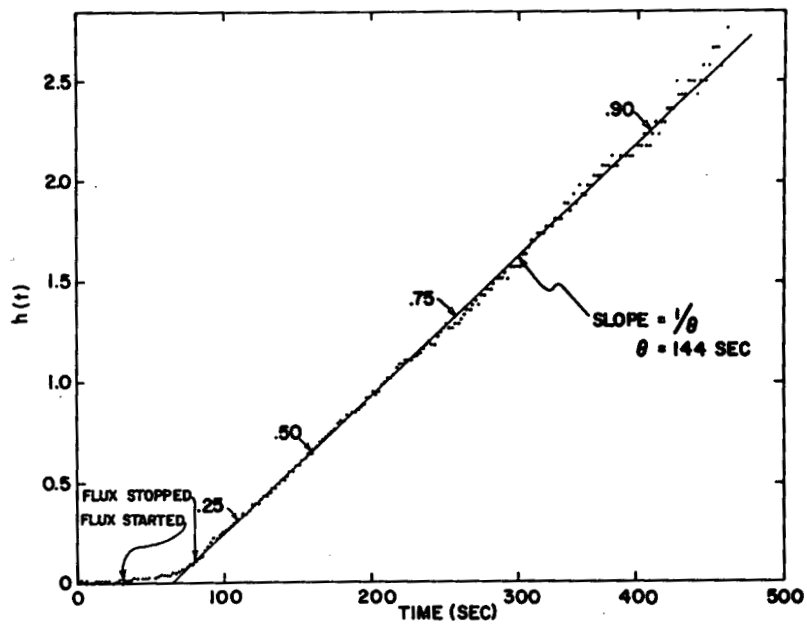


Fig. 3. Anelastic displacement for same run as in Fig. 1, but plotted according to Eq. (4) which predicts h(t) to be linear with time if the annealing is simple exponential. The numbers along the straight line portion indicate the fractional decay.

the local slope analysis method. Similar good agreement is found for the θ and $\tau^{-1}(0)$ values reported in Table 1 for the other injection experiments. This agreement between the two methods of analysis tends to confirm the values obtained and to validate the method of slope analysis. The related hypothesis that annealing is occuring homogeneously is also strengthened, since it can be shown that with inhomogeneous annealing, the function h(t) is not proportional to the time. It should be pointed out that the method of direct analysis of the anelastic response curve, as we have presented it here, does not take into consideration the fact that the Zener relaxation involves a spectrum of relaxation times rather than a single time. Since the characteristics of the spectrum of relaxation times are well known for Ag-Zn alloys,[1] this correction can be made in future analyses where space limitations are not restrictive.

If we assume vacancies to be the dominant defect, it is possible to calculate several important concentrations since the vacancy mobility for this alloy at 40°C is known with good accuracy (roughly a factor of three) to be $\nu_v = 6\times10^{5}$ sec^{-1}.[4] Using average values for the five runs at the fluence of 0.3×10^{13} n/cm^2·sec gives the following: the vacancy concentration at the start of decay, $c_v(0) = \tau^{-1}(0)/\nu_v \simeq 3\times10^{-10}$; the concentration of sinks, $c_s = (\theta\nu_v)^{-1} \simeq 10^{-8}$; the concentration of cascades, c_c = fluence·$\sigma \simeq 9\times10^{-12}$ (where σ = 3 barns); and the number of vacancies created per cascade, $c_v(0)/c_c \simeq 35$. If interstitial defects are assumed, the above values are less by a factor ν_i/ν_v.* The values reported above should be considered as tentative since there are possible experimental difficulties which may be inherent in the use of the Zener relaxation for irradiation studies. One such difficulty is that irradiation events might somehow locally change the alloy composition and thus modify the mobility of defects or even the nature of the relaxation. Such an effect could, for instance, occur if focusing occurred differently for different elements in the alloy. Further studies are being made to determine if such effects as this are important.

*The concentration of cascades would be unchanged.

REFERENCES

1. A. S. Nowick and B. S. Berry, Anelastic Relaxation in Crystalline Solids, p. 248, Acad. Press, New York, 1972.
2. A. S. Nowick, Phys. Rev. 82, 551 (1951).
3. J. R. Cost, Acta Met. 11, 1313 (1963).
4. B. S. Berry and J. L. Orehotsky, Acta Met. 16, 683, 697, (1968).
5. C. H. Neuman, D. Lazarus and D. B. Fitchen, J. Phys. Chem. Solids, 20, 170 (1961).
6. M. Halbwachs, H. Gonzalez and J. Hillairet, Scripta Met. 9, 575 (1975).
7. M. Halbwachs, J. Hillairet, H. Gonzalez and J. Cost, submitted for publication to Rad. Effects.

ENHANCED DIFFUSION OF Zn IN Al UNDER Ne IRRADIATION

S. M. Myers
Sandia Laboratories, Albuquerque, New Mexico 87115

ABSTRACT

The diffusion rate of Zn in Al has been enhanced by factors $\sim 10^2$ - 10^4 under 80 keV Ne irradiation at 130°C. Diffusion couples were formed by ion implantation of Zn, and the concentration profiles were determined by ion backscattering. The data are analyzed by numerically solving the coupled diffusion equations for vacancies, interstitials and atoms, and by scaling the profiles of vacancy and interstitial production rates from the theoretical profile of Ne energy into atomic processes. The enhanced diffusion rate is linear in flux, indicating that the mobile point defects annihilate predominantly at fixed sinks. The average distance to annihilation is $\simeq$ 700 Å, except for the first $\simeq$ 500 Å of the solid where it is much less. Free vacancies and interstitials are found to be created by the Ne at a rate about forty times smaller than the atomic displacement rate, suggesting a high annihilation probability within the parent damage cascade.

Atomic diffusion rates in solids may be enhanced by orders of magnitude under ion irradiation.[1] This effect usually results from the creation of vacancies and interstitials, which increases the atomic migration rates by the vacancy and interstitial mechanisms. Because it senses directly the concentrations of mobile point defects, enhanced diffusion provides a useful tool for the study of radiation damage; in particular, it may be used to determine both the rates of free vacancy and interstitial production and the mechanisms and rates of their annihilation.

In this paper we report measurements of Zn diffusion in Al under Ne irradiation. The relatively high Z of the irradiating ion and the high damage rates, up to $\sim$ 1 dpa/sec, complement the large body of previous work with light ions, neutrons, and electrons at much lower damage rates.[1] The objective is to achieve an understanding of enhanced diffusion in this system, especially with regard to the creation and

annihilation of free vacancies and interstitials. From the flux dependence of the enhanced diffusion coefficient we establish that vacancies and interstitials annihilate predominately at fixed sinks. It is further shown that by analyzing the shape of the diffused Zn profiles over the entire Ne range and beyond, the production and annihilation rates of the mobile point defects may be estimated independently. This then determines all of the important parameters in the theoretical model.

The diffusion couples were formed by ion implanting 50 keV Zn into single-crystal Al at room temperature, to a fluence of either 0.8 or 3×10^{16} at/cm^2. This method avoids interfacial effects which may arise with deposited films, and it permits the starting Zn concentration to be everywhere less than the solid solubility. An isothermal series of 80 keV Ne irradiations followed, at fluxes of $1.4 - 70 \times 10^{13}$ at/cm^2-sec and a temperature of 130°C. The irradiations were interspersed with 2.0 MeV He backscattering measurements[2] to determine the Zn concentration-versus-depth profile. The resolution ($\simeq$ 300 Å full width at half maximum) and range (0 - $\simeq$ 20,000 Å) of this measurement are well suited to the diffusion distances of interest ($\sim$ 3000 Å). Representative concentration profiles from one isothermal series are shown in Fig. 1.

Several qualitative features in Fig. 1 are noteworthy. Most striking of these is that the starting Zn profile does not broaden uniformly; instead, a lower amplitude tail emerges from the main peak. The intersection of this tail with the peak occurs at approximately the same concentration throughout. The phenomenon is unrelated to the solid solubility since the latter is $\simeq$ 2 at.% at 130°C,[3] and also since the effect scales approximately in concentration when the amount of implanted Zn is increased by a factor of 4. A second important feature is the change in the shape of the tail as the irradiation proceeds: concaved upward at first, the tail later develops a negative second derivative in the vicinity of 3000 Å.

The equations governing the diffusion of vacancies v, interstitials i, and Zn atoms are[4]

$$\frac{\partial C_v}{\partial t} = D_v \frac{\partial^2 C_v}{\partial x^2} + P_v - \frac{D_v}{\ell^2} C_v - K_{iv} C_i C_v \qquad (1)$$

$$\frac{\partial C_i}{\partial t} = D_i \frac{\partial^2 C_i}{\partial x^2} + P_i - \frac{D_i}{\ell^2} C_i - K_{iv} C_i C_v \qquad (2)$$

$$\frac{\partial C_{Zn}}{\partial t} = \frac{\partial}{\partial x}\left(D'_{Zn} \frac{\partial C_{Zn}}{\partial x} \right) \qquad (3)$$

with boundary conditions

$$C_v(x = 0,t) = C_i(x = 0,t) = 0, \quad D'_{Zn} \left.\frac{\partial C_{Zn}}{\partial x}\right|_{x=0} = 0 \qquad (4)$$

where

$$D'_{Zn} = F_v C_v D_v + F_i D_i C_i + D_{Zn} \quad . \qquad (5)$$

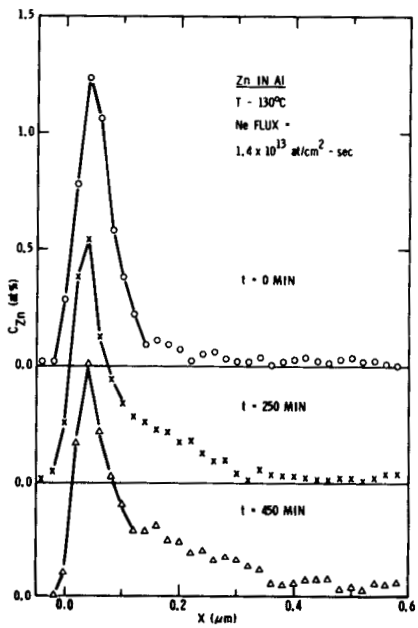


Fig. 1. Experimental Zn concentration profile in Al under Ne irradiation. The Zn fluence is 0.8×10^{16} at/cm^2.

The terms following the derivative on the right side of Eqs. (1) and (2) correspond, in order, to the production of vacancies and interstitials, to their annihilation at fixed sinks, and to their annihilation by mutual recombination. The parameter ℓ is the average distance traveled by a point defect before it annihilates at a fixed sink, and D_{Zn} is the Zn diffusivity in the absence of irradiation.

We have numerically solved Eqs. (1) - (3) for the present case by using the method of lines and the stiff integrator of Hindmarsh.[5,6] In this calculation the production rates P_v and P_i are assumed to be equal to each other, and to vary with depth in proportion to the energy into atomic processes as calculated by Brice.[7] The peak amplitude P_m in the depth profile of $P_v = P_i = P$ was set to a representative value of 10^{-3} at^{-1} sec^{-1}. The vacancy-interstitial recombination coefficient is set to zero since, as will be seen below, the vacancies and interstitials

annihilate predominantly at fixed sinks. To give the degree of near-surface peaking of the diffused atomic profile seen in Fig. 1, it is necessary to have the annihilation rates D_v/ℓ^2 and D_i/ℓ^2 vary with depth. This variation might arise from sinks being introduced by the Zn and/or Ne beams. As a first approximation we let

$$\ell^2 = \frac{(700\ \text{Å})^2}{1+500\ \exp[-x^2/(500\ \text{Å})^2]} \tag{6}$$

so that the annihilation rate is much more rapid in the first $\simeq 500$ Å. Finally, since the unenhanced diffusion coefficient D_{Zn} for Zn in Al is nearly identical to that for Al self diffusion,[8] it is a fairly good approximation to take $F_i = F_v = 1$. The resulting theoretical Zn profile is shown in Fig. 2 as a function of time together with the profile of P for comparison.

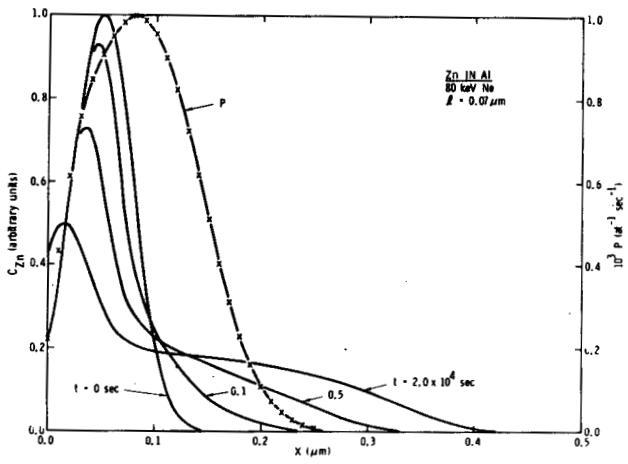


Fig. 2. Theoretical Zn profile in Al under Ne irradiation.

The theoretical profiles in Fig. 2 are in good semiquantitative agreement with the experimental data in Fig. 1, although the time scales differ because of the somewhat arbitrary selection of P_m. In particular, features such as the near-surface peaking, the approximately constant

concentration level where the tail intersects the peak, and the emergence of a negative second derivative at about 3000 Å are all reproduced. The last feature is sensitive to the asymptotic value ℓ = 700 Å in Eq. (6), and we believe this value to be correct within a factor of 1.5. The detailed behavior of ℓ in the first $\simeq$ 500 Å is less certain, although Eq. (6) is probably qualitatively correct.

The enhanced diffusion coefficient D'_{Zn} varies greatly over the depth range of interest, and consequently it is convenient to define an "effective" diffusivity D^*_{Zn} which is a measure of the average diffusion rate. This is accomplished by plotting as a function of irradiation time the square of the parameter W, where W is defined to be the distance from the half amplitude fall-off of the peak to the half amplitude point on the diffused tail. This is done for the theoretical system of Fig. 2 in Fig. 3A, where the slope is seen to be well defined for values of W up to $\sim$ 2000 Å. The parameter D^*_{Zn} is then defined as though the diffused tail were a complimentary error function in a region of uniform diffusivity i.e.,

$$D^*_{Zn} = (1.1)\,\frac{W^2}{t} \quad . \tag{7}$$

A similar plot is shown in Fig. 3B for the experimental data of Fig. 1. Again the slope is well defined, so that the determination of D^*_{Zn} is unambiguous.

The Ne flux dependence of the experimentally-determined parameter D^*_{Zn} is shown in Fig. 4, where it is seen to be linear rather than square root. This is consistent with the annihilation of vacancies and interstitials predominantly at fixed sinks, but inconsistent with the dominance of vacancy-interstitial recombination.[9] Hence we conclude that the fixed-sink mechanism dominates.

Within the above model, the only remaining unknown is the constant of proportionality between the Ne flux ϕ and the peak value P_m in the mobile defect production profile $P = P_v = P_i$. To obtain this constant we first note that when the fixed-sink annihilation mechanism dominates, D^*_{Zn} is proportional to P_m. The ratio $P_m/D^*_{Zn} = 2.2 \times 10^{10}$ cm^{-2} is then taken from the theoretical model of Figs. 2 and 3A, permitting P_m to be

calculated from the experimental data. The result is $P_m/\phi = 1.6 \times 10^{-17}$ cm^2.

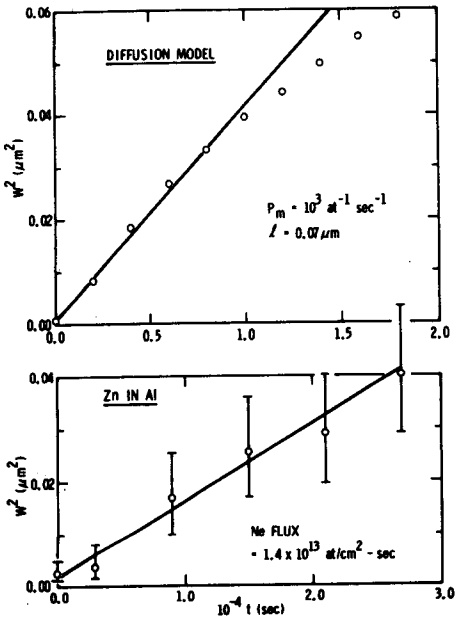


Fig. 3. Theoretical (A) and experimental (B) penetration plots for Zn in Al under Ne irradiation.

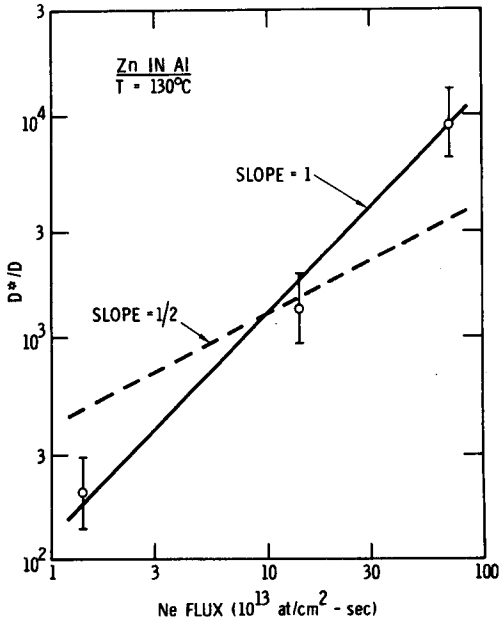


Fig. 4. Enhancement factor as a function of Ne flux. The unenhanced diffusion coefficient is $D = 0.54 \times 10^{-16}$ cm^2/sec.

The above peak rate for free vacancy and interstitial formation may be compared with the maximum atomic displacement rate P'_m. The latter is calculated from the peak rate of energy deposition into atomic processes, $\phi \times 24.2$ eV/Å,[7] using the Kinchin-Pease model.[10] The result, $P'_m/\phi = 6.3 \times 10^{-16}$ cm^2, is greater than P_m/ϕ by a factor of 40. We interpret this to mean that, of the vacancies and interstitials created in the Ne damage cascade, all but about one in forty are annihilated before they can migrate away from the cascade. A similarly high annihilation fraction within a heavy ion cascade has been reported by Blewitt and coworkers,[11] who concluded that one vacancy in $\simeq 10^2$ escaped the secondary ion cascade during neutron irradiation of Cu_3Au.

The authors are indebted to D. K. Brice for his calculation of the energy into atomic processes and for several helpful discussions. Valuable technical assistance was provided by C. T. Fuller.

REFERENCES

1. A review and extensive bibliography of enhanced diffusion has recently been given by Y. Adda, M. Beyeler, and G. Brebec, Thin Solid Films 25, 107 (1975).
2. For a discussion of this technique, see W. K. Chu, J. W. Mayer, M.-A. Nicolet, T. M. Buck, G. Amsel, and F. Eisen, Thin Solid Films 17, 1 (1973).
3. M. Hansen, Constitution of Binary Alloys (McGraw-Hill, New York, 1958), p. 148.
4. See for example N. Q. Lam, S. J. Rothman, and R. Sizmann, Rad. Eff. 23, 53 (1974).
5. G. D. Byrne and A. C. Hindmarsh, ACM Trans. on Math. Software 1, 71 (1975).
6. The details of the numerical method will be described elsewhere by S. M. Myers, D. E. Amos, and D. K. Brice, to be published.
7. D. K. Brice, J. Appl. Phys. 46, 3385 (1975), and private communication.
8. N. L. Peterson and S. J. Rothman, Phys. Rev. B1, 3264 (1970).
9. G. J. Dienes and A. C. Damask, J. Appl. Phys. 29, 1713 (1958).
10. G. H. Kinchin and R. S. Pease, Rep. Prog. Phys. 18, 1 (1955).
11. T. H. Blewitt, A. C. Klank, T. Scott, and W. Weber in Radiation-Induced Voids in Metals, ed. by J. W. Corbett and L. C. Ianniello (Nat. Tech. Info. Service, Springfield, Virginia, 1972) p. 757.

KINETICS OF INTERSTITIALCY DIFFUSION IN ELECTRON IRRADIATED CU-NI ALLOYS

R. Poerschke and H. Wollenberger
Hahn-Meitner-Institut für Kernforschung[+)]
D 1 Berlin 39 , Glienickerstr. 100

ABSTRACT

Cu-Ni alloys around the 5o:5o composition show decomposition effects in the temperature range in which interdiffusion is caused by migrating vacancies. In the present work it is shown that this atomic decomposition occurs during electron irradiation also at low temperatures starting at 12o K upwards. The decomposition is followed by measurements of the residual resistivity. The decomposition kinetics is studied by isothermal irradiation and isochronal annealing experiments in the temperature range 12o K - 62o K. For the temperature range 12o K - 37o K the data are consistently interpreted by interstitialcy diffusion and a diffusion path of the interstitials which is terminated by trapping and recombination. By fitting the model calculations to the data the reaction parameters for trapping and recombination are determined.

By isothermal irradiations the equilibrium decomposition state could be attained down to 4oo K which is 27o K below the lower temperature limit investigated formerly by thermal treatments. The residual resistivity of the equilibrium state is found to depend linearly on temperature between 4oo K and 77o K.

INTRODUCTION

Almost all previous work on radiation enhanced diffusion in alloys has been done above room temperature[1-3]. The results have been explained by stage III interstitial or vacancy (V) effects An unique answer to the question whether the interstitial atom

---

[+)] This work has been performed while the authors worked at the Van de Graaff-Labor, Aachen, der Kernforschungsanlage Jülich

(IA) migrating in stage I can cause interdiffusion (ID) has not been given up to now . It is to be expected that mass transport via interstitialcy migration can occur in a binary alloy only if the two constituent atoms are of similar size[4]. Otherwise the required exchangeability of the two constituents in the IA position will be limited. A suitable candidate with respect to atomic size should be the Cu-Ni system. Moreover, investigations of the interaction of the Cu IA with the Ni impurity have shown that Ni atoms do not act as traps for migrating Cu IA, i.e. no immobile Cu-Ni complexes are produced as it is the case for many other impurities in Cu[5-7]. Finally, in Cu-Ni ID can easily be followed by large resistivity changes due to short range decomposition[8,9].

RESULTS

In the present paper the most important results obtained for an alloy containing about 59 at% Ni are given. For more results and detailed discussion see Ref. 10. Prior to irradiation the samples were annealed for 4 h at 87o K and slowly cooled down to 29o K. The irradiations were performed with 3 MeV electrons. The samples were mounted to a continuous flow helium cryostat. The electrical resistivity was determined by standard equipment at 4 K. In Fig.1 the resistivity change of an alloy containing 59 at% Ni is shown versus dose for isothermal irradiation at different irradiation temperatures. At all temperatures starting with 12o K negative resistivity changes are observed, for equal doses these changes increase with increasing temperature.

DISCUSSION

A quantitative comparison of the resistivity changes at 12o K irradiation to those during thermal annealing in the temperature range 62o K up to 800 K yields the average number of jumps per radiation induced defect to be at least about 60

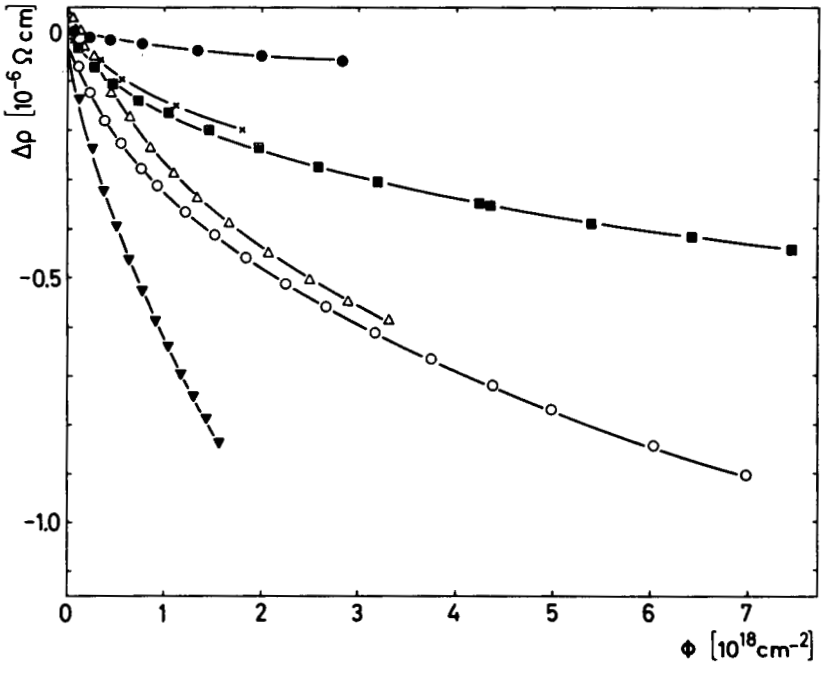


Fig. 1. Radiation induced resistivity decrease vs. fluence at ● -120 K, x - 150 K, ■ - 180 K, △-232 K, o - 304 K and ▼-353 K.

at 120 K[10]. Obviously, V cannot provide this mass transport. Close pair annealing cannot contribute significantly to the ID because of the large number of jumps per defect required for a qualitative explanation of the results. Obviously, the freely migrating IA is responsible for the observed effects. The IA diffusion kinetics has already been studied in dilute alloys for irradiation temperatures in stage III[5-7]. The respective experiments could be explained quantitatively by assuming the IA diffusion path to be terminated by trapping reactions and recombination. According to this model, the jump rate (JR) of atoms due to IA jumps is given by[3,10]

$$C_i \cdot D_i = \frac{\sigma \cdot \varphi}{4\pi \cdot r_t \cdot C_t \sqrt{1 + \frac{2 \cdot r_v \cdot \sigma}{r_t \cdot C_t} \cdot \phi}} \qquad (1)$$

σ is the cross section for freely migrating IA, φ the dose rate, $r_t c_t$ is the trapping term, r_v, r_t are the capture radii of the vacancies and traps, respectively, and Ø is the irradiation dose. According to Eq.(1), the JR and, therefore, the ID

coefficient decreases with increasing electron dose. Physically, this dependence arises from the fact that each trapped IA leaves an immobile vacancy in the lattice. Hence, the vacancy concentration increases with increasing dose and, therefore, the average path length of the IA decreases.

The relation between the ID coefficient and the resistivity data has been studied at high temperatures where equilibrium vacancies exclusively are responsible for diffusion. As a result the following Eq. has been obtained[10]:

$$-d\varrho/dt = \frac{(\varrho - \varrho_\infty)^{1.75}}{3.75 \times R^{0.75}} \times C_v \times D_v \qquad (2)$$

$d\varrho/dt$ is the rate of resistivity change, ϱ the residual resistivity measured at 4 K at time t, ϱ_∞ the equilibrium resistivity corresponding to the annealing temperature. R is the maximum resistivity change to be observed when going from a statis-

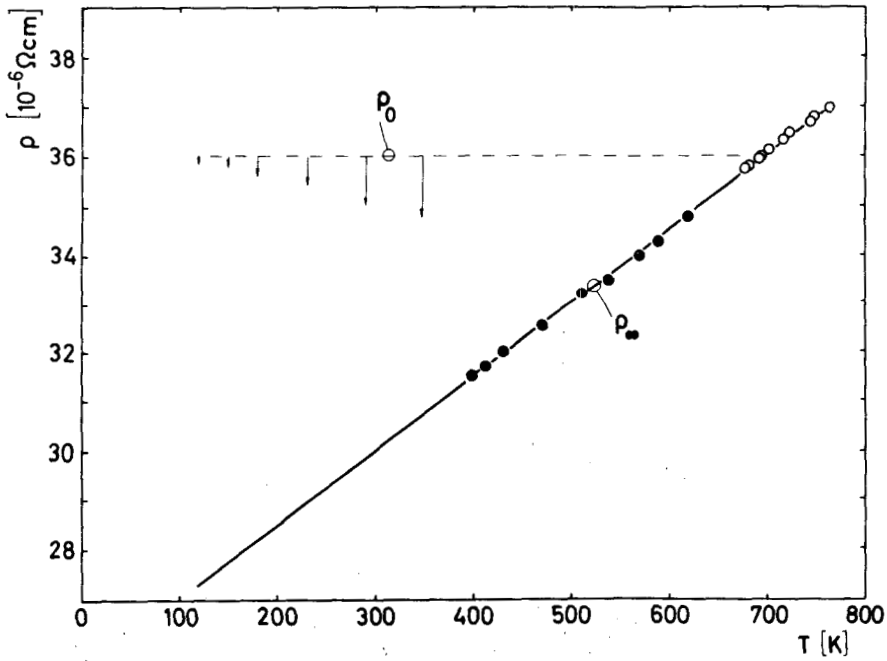


Fig. 2. Temperature dependence of the equilibrium resistivity, equilibrium has been attained by thermal treatment (O) and irradiation (●). The preirradiation resistivity $\varrho_0 = 36 \times 10^{-6}\ \Omega$cm has been established by 6 h annealing at 870 K and 24 h cooling to 290 K. The arrows show the total resistivity changes at different irradiation temperatures.

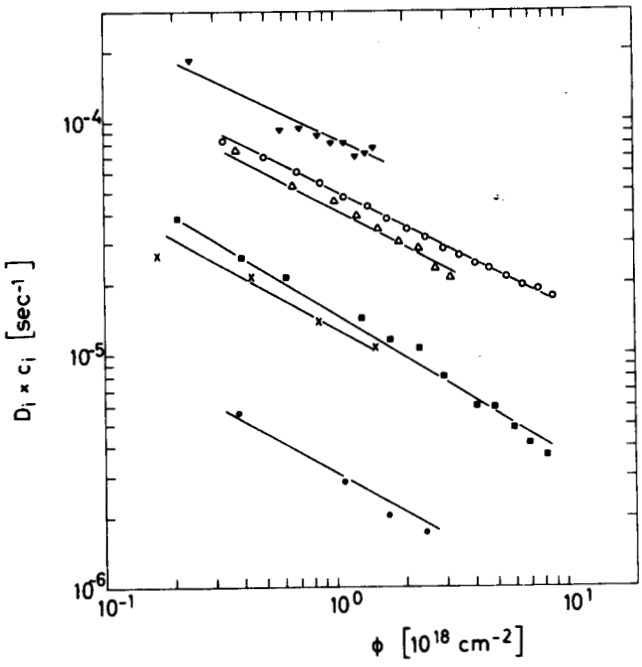


Fig. 3. Double logarithmic plot of the interstitialcy jump rate vs. fluence, symbols correspond to Fig. 1 .

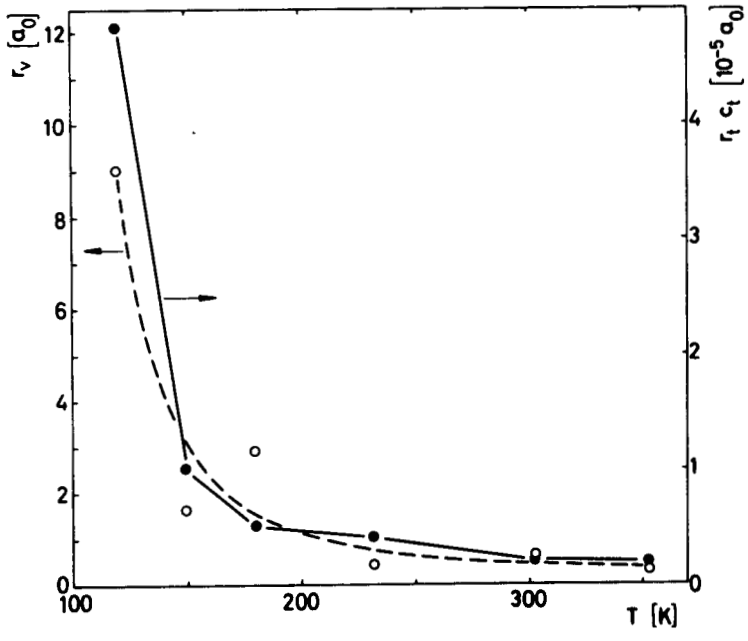


Fig. 4. Temperature dependence of $r_t c_t$(●) and r_v(o)

tical distribution of atoms to a perfectly clustered distribution.

The equilibrium resistivity ρ_∞ has been determined by annealing and radiation experiments in the temperature range 386 K up to 770 K. The results are shown in Fig. 2. ρ_∞ depends linearly on the temperature. Extrapolation of ρ_∞ to the melting temperature and to T = 0 yields R = 20 $\mu\Omega$cm. Assuming the linear extrapolation of the equilibrium resistivity to be valid for the temperature range of our irradiation experiments, we can evaluate the JR of the defects causing ID from our resistivity data.

Fig. 3 shows a double logarithmic plot of the JR versus dose at temperatures from 120 K up to 350 K. The JR is obviously proportional inversely to the square root of the electron dose ϕ. Fitting Eq.(1) to our data yields r_v and $r_t c_t$, as shown in Fig. 4. Both quantities decrease with decreasing temperature. The temperature dependence of $r_t c_t$ might be due to a temperature dependence of both r_t and c_t. In dilute copper alloys such a temperature dependence has been explained by that of r_t because of the significant role of the IA trapping by solute atoms being present in the fixed concentration c_t and the negligible concentration of residual impurities[7]. In our case it cannot be excluded that different impurities or impurity clusters act as traps (TableI[1]) of different depths (i.e. with different capture radii). Then also c_t would have to be considered as temperature dependent. Preliminary annealing results indicating a stepwise isochronal annealing seem to confirm such an interpretation[10].

The absolute values obtained for r_v are in the same order of magnitude as found in pure copper at 50 K. The temperature dependence, however, is much stronger than the $T^{-1/3}$ dependence found in pure copper[11]. This dependence could be explained by drift diffusion of the interstitial in the elastic potential of the vacancy. The temperature dependence found here would indicate an interaction energy being proportional to 1/r

(r-distance of IA and V)compared to $1/r^3$ for the elastic interaction .One could speculate that in this Cu-Ni alloy at least below 160 K (ferromagnetic Curie temperature) the point defects interact magnetically.

REFERENCES

1.(a) References are collected in: Y. Adda, M. Beyeler and G. Brebec, Thin Solid Films, 25, 107 (1975)

2. R. Poerschke and H. Wollenberger, Radiation Effects 24, 217 (1975)

3. R. Poerschke, Berichte der KFA Jülich, Jül-1100-FF (1974)

4. M. J. Koczak, H. Herman and A. C. Damask, Acta Met. 19, 303, (1971)

5. F. Dworschak, H. Schuster, H. Wollenberger, and J. Wurm, Phys. stat. sol. 29, 75 (1968)

6. A. Kraut, F. Dworschak, and H. Wollenberger, Phys. stat. sol. (b) 44, 805 (1971)

7. F. Dworschak, R. Lennartz, and H. Wollenberger, J. Phys. F 5,400 (1975)

8. W. Schüle and H. P. Kehrer, Z. Metallk. 52,168 (1961)

9. E. W. v. Royen, G. Brandsma, A. L. Mulder, and S. Radelaar, Scripta Met. 7, 1125 (1973)

10. R. Poerschke and H. Wollenberger, to be published in Journ. of Phys. F

11. D. E. Becker, F. Dworschak, and H. Wollenberger, Phys. stat. sol. (b) 54, 455 (1972)

SELF-DIFFUSION IN SILVER UNDER ELECTRON IRRADIATION*

S. J. Rothman, Nghi Q. Lam, L. J. Nowicki, and C. A. Beck**
Materials Science Division
Argonne National Laboratory
Argonne, Illinois 60439

ABSTRACT

Self-diffusion in silver single crystals under irradiation by $\sim 10^{15}$ 2-MeV e/cm^2-s has been studied from room temperature to 420°C. At T >288°C, no enhancement is observed above the value of thermal diffusion (7.3×10^{-18} cm^2/s at 288°C). At lower temperatures, diffusion is obscured by an artifact of the sectioning technique.

INTRODUCTION

The tracer-sectioning technique[1] has been so successful[2] in precise diffusion measurements that we have tried to apply it to radiation-enhanced diffusion. In this method, a thin layer of radiotracer is deposited on the surface of the sample, diffusion is allowed to take place for a time t, and the distribution of radioisotope is determined by sectioning the sample accurately perpendicular to the diffusion direction and radioassaying the sections. The diffusion coefficient D is determined from the variation of specific activity C as a function of distance x from the surface.

Two major difficulties are encountered in applying this technique to radiation-enhanced diffusion. First, the radiation-enhanced D, D_{rad}, is calculated[3] to be so small that sections 10 to 20-Å thick must be taken; this difficulty can, in principle, be overcome by the use of electrochemical sectioning techniques.[4] Second, the surface on which the radiotracer is deposited acts as a sink for the radiation-induced mobile point defects, which are responsible for the enhancement.

* Work performed under the auspices of the USERDA.

**Now at Nuclear Engineering Department, Stanford University, Calif.

Thus, the value of D_{rad} near the surface is even lower than in the bulk. Furthermore, at steady state D_{rad} depends on x as[5]

$$D_{rad}(x) = D^{\circ}_{rad}\{1 - \exp[-1.15 (J K_{iv}/D_i D_v)^{1/4} x]\}, \quad (1)$$

where D°_{rad} is the value of $D_{rad}(x)$ in the bulk (independent of x), J is the defect production rate, K_{iv} is the rate constant for mutual recombination of vacancies and interstitials, and D_i and D_v are the diffusion coefficients of interstitials and vacancies, respectively. Near the surface $x(JK_{iv}/D_i D_v)^{1/4} \ll 1$ and

$$D_{rad}(x) = D_x x \quad . \quad (2)$$

For a steady-state defect distribution D°_{rad} is related to D_x by[6]

$$D^{\circ}_{rad} \simeq D_x^2/2J. \quad (3)$$

With the thin-layer initial condition, Eq. (2) gives the penetration plot of the radioisotope[7] as

$$C = \left(M/D_x t\right) \exp\left(-\frac{x}{D_x t}\right) , \quad (4)$$

where M is the amount of isotope deposited. At large x but still within the defect production range, $x(JK_{iv}/D_i D_v)^{1/4} \gg 1$, D_{rad} becomes independent of x, and the penetration plot is the usual Gaussian[8]

$$C = \left(M/\sqrt{\pi D_{rad} t}\right) \exp\left(-x^2/4D_{rad} t\right) . \quad (5)$$

We had to work in the first of these regions for reasons that will become apparent later. As a system, we chose the diffusers' standard, self-diffusion in silver.[9-12]

Our first experiments[13] measured self-diffusion under a flux of 270-keV protons. Penetration plots described by Eq. (4) were obtained, with values of D_{rad} somewhat larger than predicted from the simple theory,[3] a somewhat different temperature dependence, and the $(J)^{1/2}$-dependence predicted for dominant mutual recombination.[3,14] The interpretation of these results was complicated by uncertainty as to

the attainment of a steady-state defect distribution* and the effect of collision cascades. To attain steady state, we attempted to study self-diffusion under bombardment of α-particles from a long-lived ^{210}Po source,[6] but this only led to tarnishing of the silver. To avoid the cascade problem, diffusion anneals were carried out under bombardment by 2 MeV electrons. These are described below.

EXPERIMENTAL

Sample Preparation

One end of the cylindrical single crystals of 5N silver was ground, polished, and chemically polished.[4] After a preanneal at 955°C, the polished face was chemically repolished, anodized, stripped, and plated or evaporated with a thin layer (<10 Å) of ^{110m}Ag.

Irradiation

The sample was held in a large copper block with ∿1 cm protruding toward the beam. The heat introduced by the electron beam was removed by flowing hot oil, chilled water, or liquid nitrogen through a pipe brazed to the block; surface temperatures between room temperature and 420°C were obtained. The surface temperature was extrapolated, with an uncertainty of ± 10°C, from readings on thermocouples which were placed into holes spark cut into the crystal in a row parallel to the axis, spaced a few millimeters from each other and from the bombarded surface. The thermocouple voltages were measured with a high-impedance millivoltmeter. The sample was bombarded in a vacuum of 5×10^{-7} Torr by ∿190 $\mu a/cm^2$ of 2-MeV electrons in a Van de Graaff. The defocused electron beam was swept at a frequency of 1200 Hz. A Faraday cage cooled with chilled water or liquid N_2 was used to prevent false current readings due to the emission of secondary electrons.

Diffusion Analysis

After irradiation, the samples were sectioned by the anodizing-stripping technique,[4] and the sections were radioassayed for ^{110m}Ag.[12]

*Because of the nearness of the surface, steady state is attained more rapidly than in the experiments on bulk samples.

Two blank samples, in which the sample was sectioned directly after deposition of the radioisotope without any intervening treatment, were also run.

RESULTS

High-temperature Runs

Excellent penetration plots that followed Eq. (5) from x = 0 were obtained for irradiation at 421, 358, and 354°C, and the values of D obtained fall on the line for diffusion without irradiation, Fig. 1.

Anneals at 288-306°C produced penetration plots with two Gaussians. Three of five such plots are shown in Fig. 2. It is tempting to interpret the Gaussians nearer x = 0 as representing diffusion due to equilibrium vacancies and the second Gaussians as due to radiation-enhanced diffusion. The D's from the first Gaussian do fall on the "without irradiation" line of Fig. 1, indicating that the concentration of radiation-induced defects near the surface is small compared to the equilibrium vacancy concentration. However, the second Gaussians, or tails, may not represent radiation-enhanced diffusion. Similar tails have been obtained without irradiation[12] and on a blank sample. The latter was associated with black spots on the autoradiograph, which probably indicated accumulation of radiotracer in a surface blemish. Also, values of D_{rad} obtained from the tails are scattered over a factor of 10, which suggests that an artifact is being measured. Thus, we cannot conclude that enhancement is observed at T > 288°C under a defect production rate of $\sim 6 \times 10^{-8}$/s. Also, it is the possibly artifact nature of the tails that makes us reluctant to measure D_{rad} deep inside the sample.

Low-temperature Runs

Irradiation at 178, 206, and 227°C gives penetration plots linear in log C vs x (Eq. 4) near the surface (Fig. 3). This radical change in the type of penetration plot suggests that enhanced diffusion is being observed. Values of D_{rad} calculated from these plots via Eq. (3),

plotted in Fig. 1, are higher ($\sim 10^{-15}$ cm^2/s) than the values of $D_{thermal}$ obtained under electron irradiation at 354 and 358°C. This difference is possible only if the defect concentrations in the lower temperature samples have not reached steady state early in the bombardment, which is highly unlikely in view of the relatively high temperature. Also, these D_{rad}'s are an order of magnitude higher than those obtained under proton irradiation,[13] even though J for the proton irradiation was an order of magnitude higher than for electron irradiation. Although at least part of this difference may be explained by the sinks introduced by proton bombardment, these three values of D_{rad} are questionable. The D_{rad} calculated from the simple theory is $\sim 5 \times 10^{-18}$ cm^2/s at 178°C.

To resolve why these values are so high, several blank samples were run, and typical "penetration plots", Fig. 3, resemble the linear log C vs x curves obtained above. Thus, the penetration observed in the irradiated samples could be, in part, an artifact, and must be corrected to take account of this effect. (Similar "blank" plots have also been observed on gold[15] and on a silver sample sectioned by rf sputtering).

CONCLUSION

The present results indicate that extreme care must be taken in tracer measurements of radiation enhanced diffusion in the near surface region, as such measurements can be falsified by artifacts.

ACKNOWLEDGMENTS

We thank R. Lowers and A. Youngs for operating the Van de Graaff, R. Siegel and R. Sizmann for discussions, and D. Gupta of IBM for sectioning a sample on his rf-sputtering apparatus.

REFERENCES

1. T. S. Lundy, in Techniques of Metals Research, vol. IV, pt. 2, p. 379ff, Ed. R. A. Rapp, Wiley, New York, 1970.
2. N. L. Peterson, in Solid State Physics, vol. 22, p. 409ff, F. Seitz and D. Turnbull, eds. Academic Press, New York, 1968.
3. W. M. Lomer, Diffusion Coefficients in Copper Under Fast Neutron Irradiation, AERE-TR-1540, 1954.
4. Nghi Q. Lam, S. J. Rothman, and L. J. Nowicki, J. Electrochem. Soc. 119, 715 (1972).
5. Nghi Q. Lam, S. J. Rothman, and R. Sizmann, Rad. Effects, 23 53 (1974).
6. U. Ermert, W. Rupp, and R. Sizmann, Int. Conf. on Vacancies and Interstitials in Metals, vol. 2, p. 30 KFA Jülich, Germany, 1968.
7. O. G. Sutton, Micrometeorology, p. 216 McGraw-Hill, New York, 1953.
8. J. Crank, The Mathematics of Diffusion, p. 10, Oxford University Press, Oxford, England, 1956.
9. R. E. Hoffman and D. Turnbull, J. Appl. Phys. 22, 74 (1951).
10. C. T. Tomizuka and E. Sonder, Phys. Rev. 103, 1182 (1956).
11. S. J. Rothman, N. L. Peterson, and J. T. Robinson, phys. stat. sol. 39, 635 (1970).
12. Nghi Q. Lam, S. J. Rothman, H. Mehrer, and L. J. Nowicki, phys. stat. sol.(b) 57, 225 (1973).
13. Nghi Q. Lam, S. J. Rothman, K. L. Merkle, L. J. Nowicki, and D. J. Dever, Thin Solid Films 25, 157 (1975).
14. J. V. Sharp, Radiation Enhanced Diffusion, AERE-R-6267, 1969.
15. W. Rupp, U. Ermert, and R. Sizmann, phys. stat. sol. 33, 509 (1969).

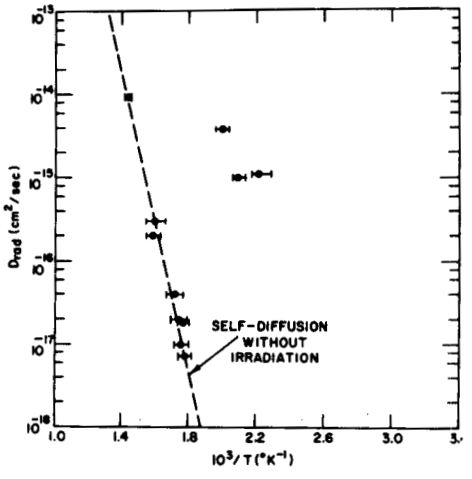


Fig. 1. Plot of log D_{rad} vs 1/T.

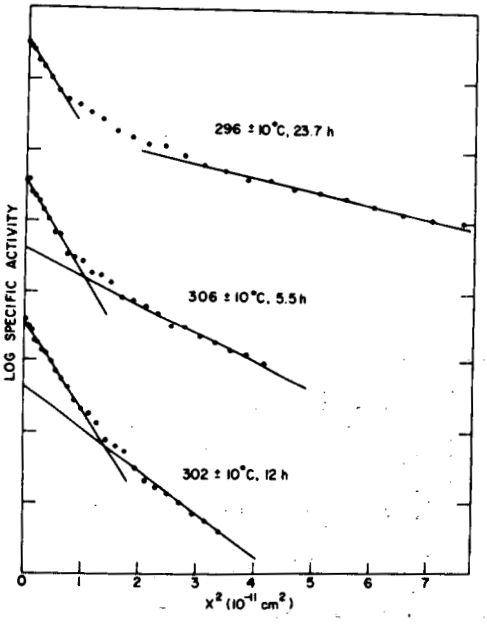


Fig. 2. Plots of log C vs x^2 for self-diffusion in silver under electron irradiation at temperatures near 300°C. Each division on the ordinate is a factor of 10.

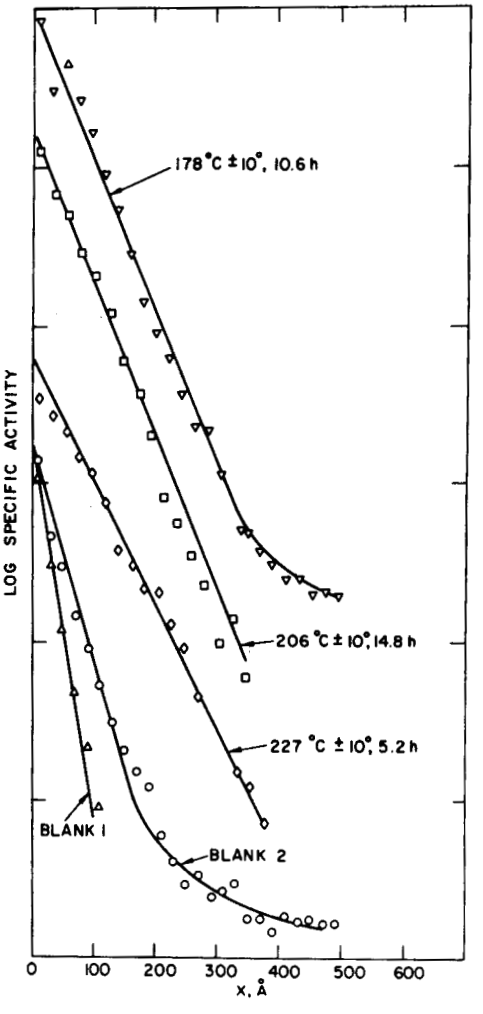


Fig. 3. Plots of log C vs x for self-diffusion in silver under electron irradiation at temperatures near 200°C and for no diffusion treatment. Each division on the ordinate is a factor of 10.

PHASE INSTABILITY IN CRYSTALS UNDER IRRADIATION

G. Martin
DT. SRMP, CEN Saclay
BP n° 2,91190 - Gif/Yvette FRANCE

ABSTRACT

A diffusion term is introduced in the standard chemical rate model of the defect population in crystals under irradiation.

For point defect generation rates larger than a critical value (g^{**}), the uniform point defect population is shown to be unstable with respect to spatial fluctuations of the point defect concentration. g^{**} is temperature dependant.

Several effects including the *nucleation* of *arrays* of point defects clusters, or *radiation induced precipitation* may occur above the instability threshold.

Defect-defect interaction potentials play a crucial role in the numerical value of this threshold.

INTRODUCTION

One fascinating aspect of radiation damage studies is that irradiation offers an almost unique way of maintaining solids in far from equilibrium quasi steady states.

Indeed most of the radiation damage studies provide ample evidence for the reorganisation of solids during irradiation (e.g. amorphisation, second phase precipitation or re-solution, order-disorder transformation, point defects clustering, etc...). This reorganisation is of course linked to the behavior of the radiation generated point defects in the solid. However the fact that the point defects (PD) generation rate (g) may play the role of an intensive variable entering the description of the possible states of a solid under irradiation has been

suggested only recently [1].

Once g is recognized to be a measure of the strength with which the solid is drawn away from its equilibrium state, one simple question arises : is it possible to bring the crystal in a state sufficiently far from equilibrium to be unstable. The study of non equilibrium induced structures has undergone recent developments [2], and it is worth trying to apply the techniques developped in this field to the problem of crystals under irradiation.

The quasi steady state reached by the solid under irradiation is usually described by a homogeneous chemical rate model [3] : the PD are uniformaly injected into the system at a rate g, and are annihilated according to homogeneous chemical reactions. The mean PD steady state concentrations are provided by such models.

The purpose of this paper is to show that provided that the PD generation rate is larger than a critical value g^{**}, the uniform PD population may become unstable with respect to spatial PD concentration fluctuations. For a given crystal, g^{**} is shown to be temperature (T) dependant, i.e. an instability limit of the crystal under irradiation will be drawn in a g vs T plot. Above this limit ($g > g^{**}(T)$), certain harmonics of the PD concentration fluctuations will grow in amplitude, leading to a spatially periodic PD clustering. Other consequences of the model will be discussed in the last section.

EXISTENCE OF AN INSTABILITY THRESHOLD

Equations of the Problem

For the sake of simplicity, we restrict ourselves here to single defects : vacancy (v) and interstitial (i). The same formalism may be extended to higher order defects [4]. The concentration at the point $\vec{r}$ and time t of each type of defect (v or i) is governed by :

$$\frac{\partial C(\vec{r},t)}{\partial t} = \left.\frac{\partial C}{\partial t}\right|_{chem} + \left.\frac{\partial C}{\partial t}\right|_{diff} \qquad (1)$$

The first term in the RHS of Eq. (1) describes the contribution of chemical reactions to the local balance of PD, and the second one is the diffusion term. According to the standard chemical rate theory [3]:

$$\left.\frac{\partial C_v}{\partial t}\right|_{chem} = g - K_{iv} C_i C_v - K_v (C_v - C_v^\circ)$$
$$\left.\frac{\partial C_i}{\partial t}\right|_{chem} = g - K_{iv} C_i C_v - K_i C_i \qquad (2)$$

where C_v° is the thermal vacancy concentration and K_{iv}, K_v, K_i respectively the rate constants for i-v recombination, v or i capture on the PD sinks.

In its most general form, the contribution of diffusion contains two terms [5],

$$\left.\frac{\partial C_v}{\partial t}\right|_{diff} = D_v \left[\nabla^2 C_v - \vec{\nabla} \frac{\vec{F}_v C_v}{\Omega k_B T}\right] \qquad (3)$$

where D_v is the vacancy diffusion coefficient, Ω the atomic volume and k_B and T have their usual meaning; $\vec{F}_v$ is the dirft force on the vacancies which derives from the v-v, v-i interaction potentials : $V_{vv}(\vec{r}' - \vec{r})$ and $V_{iv}(\vec{r}' - \vec{r})$:

$$\vec{F}_v(\vec{r},t) = - \vec{\nabla} \int [C_v(\vec{r}',t)\, V_{vv}(\vec{r}' - \vec{r}) + C_i(\vec{r}',t)\, V_{iv}(\vec{r}' - \vec{r})]\, d\vec{r}' \qquad (4)$$

The integration in Eq. (4) is taken over the total volume of the sample. Expressions similar to Eq. (3) and (4) hold for the interstitials.

If we now assume that K_{iv}, K_i, K_v in Eq. (2) are independent of $\vec{r}$, Eq. (1) has a uniform steady state solution $\bar{C}_v$, $\bar{C}_i$, (i.e. independent of $\vec{r}$).

Let us now discuss the stability of this solution with respect to spatial PD concentration fluctuations.

Linear Stability Analysis

Let us study the response of the system governed by Eq. (1) to a small amplitude oscillation of the PD concentration around the uniform steady state value; e.g. for vacancies :

$$\varepsilon_{kv}(\vec{r},t) = C_v(\vec{r},t) - \bar{C}_v = \varepsilon_{kv}^0 \exp(i\vec{k}\cdot\vec{r} + \omega_k t) \qquad (5)$$

The sign of the real part of ω dictates the stability of the steady state. If it is negative, the concentration wave described by Eq. (5) will be damped. If it is positive, the concentration wave amplitude grows with time, and the spatial symmetry of the PD population breaks down.

Since the ε_k^0 are assumed to be small, Eq. (2-4) may be linearized [5] and Eq. (1) gives :

$$\omega_k \vec{\varepsilon}_k = (\bar{\bar{R}} - k^2 \bar{\bar{D}}) \vec{\varepsilon}_k \tag{6}$$

where $\vec{\varepsilon}_k$ is a vector of components ε_{kv} and ε_{ki} (Eq. (5)), and $(\bar{\bar{R}} - k^2 \bar{\bar{D}})$ is the following matrix :

$$\begin{matrix} - K_{iv}\bar{C}_i - K_v - k^2 D_v (1 + \alpha_{vvv}) & - K_{iv}\bar{C}_v - k^2 D_v \alpha_{viv} \\ - K_{iv}\bar{C}_i - k^2 D_i \alpha_{iiv} & - K_{iv}\bar{C}_v - k^2 D_i (1 + \alpha_{iii}) \end{matrix} \tag{7}$$

whith $\alpha_{lmn} = \bar{C}_l V_{mn} (\vec{k}) / \Omega k_B T$.

The ω_k are the eigen values of the matrix. A simple inspection of the matrix elements shows that ω_k is always negative if $k = 0$ (infinite wave length) or if all the interaction potentials are set equal to zero.

Thus, the steady state is stable with respect to chemical reactions plus random diffusion. A similar conclusion was reached numerically by de Fontaine [6] in a model including divacancies and by Fiche [7] in a model including higher order multi-defects. This results from the fact that the chemical reactions in Eq. (1) do not contain self catalytic stages which are the source of chemical instabilities [8]. A non zero defect-defect interaction potential is a necessary condition for the appearence of instabilities.

DOMAIN OF INSTABILITY

Border of the Domain

In studying the sign of the eigen values ω of $\bar{\bar{R}} - k^2 \bar{\bar{D}}$, as a function of $\vec{k}$, one is faced with two different types of parameters : those which caracterise the crystal (crystalline structure, lattice

parameter, dislocation density, PD formation, migration and interaction parameters), and those which caracterise the environment of the crystal, namely the temperature T and the PD generation rate g. These two parameters are the *intensive variables* which determine the properties of the steady state of the crystal.

For a given crystal it is then possible to calculate numericaly the dispersion curve $\omega(\vec{k})$ for each value of the intensive variables g, T. Fig. 1 shows an example of such curves calculated for a model nickel crystal ⁎.

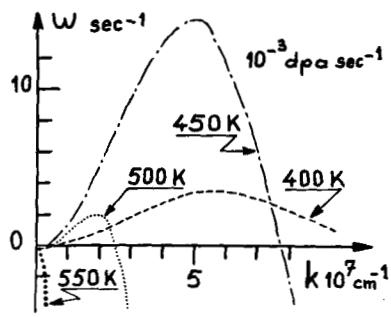


Fig. 1 : Dispersion curves at various temperature for "nickel" under 10^{-3} dpa sec^{-1}.

The following observations can be made : for g = 10^{-3} dpa/sec : at T = 550°K all PD concentration waves are damped; at T < 500°K however some concentration waves will be amplified. This proves the existence of a critical temperature T_c below which, the PD steady state concentration becomes unstable.

Below this temperature, PD concentration waves with very short wave length are still damped, due to the diffuse interface energy term, well known in the theory of spinodal decomposition [9]. On the other hand PD concentration waves with very large wave length are also damped, due to the chemical part $\bar{\bar{R}}$ in the matrix $\bar{\bar{R}} - k^2 \bar{\bar{D}}_k$. This effect does not appear in the theory of spinodal decomposition. Concentration waves with intermediate wavelength however will be amplified with a relaxation time $1/\omega(k)$. At some intermediate wavelength, $2\pi/k_M$, ω goes through a maximum $\omega(k_M)$.

Fig. 1 also shows that for a given value of g, $\omega(k_M)$ varies with temperature. At the critical temperature T_c, $\omega(k_M)$ is

---

⁎ The details of the parameters which were chosen for this calculation and the sensitivity of the result to these parameters is given in [4].

obviously zero; at a very low temperature, $\omega(k_M)$ tends toward zero, since PD migration rates become infinitely small. At some intermediate temperature T_M, $\omega(k_M)$ has its maximum maximorum value which depends on g : $\omega(k_M, T_M, g)$.

Performing the same type of calculation for several values of g, gives the critical temperature T_c as a function of g or equivalently the critical point defect generation rate g^* as a function of T, an example of which is shown on Fig. 2.

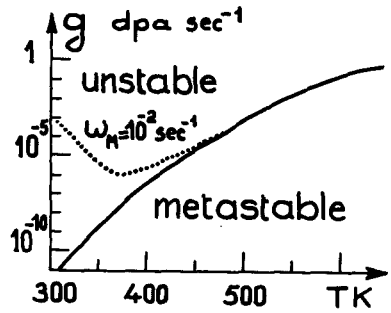


Fig. 2 : The domain of instability for "nickel" under irradiation (full line). See Ref. [4]. Along the dashed line, $\omega(k_M) = 10^{-2}$ sec^{-1}.

The solid line represents the limit above which the PD uniform population is unstable with respect to spatial fluctuations.

Behavior of the Crystal in the Domain of Instability

Inside the domain of instability, the uniform steady state PD population will collapse into PD clusters distributed in a spatially periodical arrangement, with an inter-cluster distance of the order of $2\pi/k_M$.

However for a given value of g, this collapse will proceed with a relaxation time larger or equal to $1/\omega(k_M, T_M, g)$. As an example, the dashed line in Fig. 2 represents the locus of the points where $\omega(k_M) = 10^{-2}$ sec^{-1}. An important question is to know if this relaxation time is smaller than the incubation time for the nucleation of PD clusters by the classical nucleation mechanism [10]. In other words, irradiating inside the domain of instability does not guarantee the generation of a spatially periodical PD clustering. The standard nucleation and growth mechanism which operates as soon as $g \neq 0$ may be more rapid than the homogeneous transformation which we have just modeled.

Since the model relies on a linear stability analysis, it is unable to predict the form which the PD clusters will assume at longer times. In the particular case where the clusters form voids, we have demonstrated elsewhere [11] that the void lattice generated by such a mechanism is stabilized during the growth of the voids by the overlapping of the PD diffusion fields around each cavity. This guarantees that the periodical clustering which may appear in the domain of instability is not a transient state, but should persist at longer times. There is another interesting consequence of the model in the case of dilute solid solutions. Provided that the solute enters chemical like reactions with the PD, it will undergo the homogeneous transformation just described : this gives a possible mechanism for radiation *induced* precipitation in thermodynamically stable solid solutions [12].

Finaly this model points to the crucial importance of the PD generation rate (or of the irradiation flux) in the understanding of morphological changes under irradiation. As an example, in a pulsed regime, although the average PD generation rate may be rather low, the crystal may be brought in the domain of instability during the irradiation pulses and developp quite unexpected morphologies. This may be of importance for the design of the first wall of fusion reactors.

This crucial importance of the irradiation flux also suggests the type of experimental work to be undertaken in order to check the validity of this model.

As a summary, high flux irradiation may trigger a periodical nucleation of PD clusters in crystals. The position and shape of the instability limit in the g vs T plot may be simply calculated. Crucial parameters of the calculation are the defect-defect interaction potentials.

Acknowledgements : Stimulating discussions with D^r Y. Adda are warmly acknowledged.

REFERENCES

1 Y. Adda, M. Beyeler and G. Brebec, Thin Solid Films, 25, 107 (1975).

2 I. Prigogine and R. Lefever, Adv. Chem. Phys., 29, 1 (1975).

3 M. Gomolinski and G. brebec, J. Nucl. Mater., 43, 59 (1972).

4 G. Martin, Phil. Mag. (in press).

5 P. Flynn, Point Defects and Diffusion, p. 467, Oxford (1972).

6 D. de Fontaine, Fourier-Space computer simulation of crystalline imperfections, III, UCLA-ENG 7475 (Oct. 1974).

7 C. Fiche, private communication.

8 P. Glansdorff and I. Prigogine, Thermodynamic Theory of Structure, Stability and Fluctuations, Wiley Interscience, New York, 1971.

9 e.g. J.E. Hilliard, Phase transformations, p. 497, ASM 1970.

10 M. Lott and C. Fiche, Les phénomènes de précipitation et leurs consequences sur les propriétés de quelques familles d'alliages industriels, p. 25. Collective vol. INSTN - Saclay, France 1973.

11 P. Benoist and G. Martin, this issue

12 A. Barbu and A.J. Ardell, Scr. Metall. (in press).

EFFECTS OF HEAVY-ION IRRADIATION ON THE MORPHOLOGY OF γ/γ' ALLOYS*

D. I. Potter and H. A. Hoff
Materials Science Division
Argonne National Laboratory
Argonne, Illinois 60439

ABSTRACT

Nickel-ion irradiation of a two-phase γ/γ' Ni-Al alloy is shown to accelerate coarsening at low doses and to cause changes in γ' size, shape, and distribution at higher doses. The former results from irradiation-enhanced diffusion, whereas the other three changes are shown to originate from the interaction of γ' with the dislocations that develop during irradiation. At 550°C and a damage rate of 2.7×10^{-3} dpa/s, the γ' approaches a stable or steady-state mean diameter of $\sim$85 Å. This, in contrast to previous work, is shown to result from the balance between irradiation-enhanced coarsening and particle fragmentation due to dislocation cutting. Dislocation loops that develop early in the irradiation cause and are centered at regions devoid of γ'. Microstructural features produced by different irradiation conditions can be understood in terms of these mechanisms.

The stability of precipitates during irradiation has recently been considered from a fundamental viewpoint and is of considerable importance in reactor applications. One of the better understood systems, i.e., binary alloys of nickel and aluminum, has been modeled by Nelson et al.,[1] and the results have been extended to describe the behavior of PE-16, an alloy of commercial importance. The Nelson model is based on balancing two opposing processes governing precipitate stability: thermal growth, possibly accelerated by irradiation-enhanced diffusion, and irradiation-enhanced dissolution, in which the incident radiation removes the outer layers of precipitates by recoil and/or disordering processes. Figure 1, taken from Nelson et al.,[1] shows that a steady-state γ' particle size of

*Work supported by the U.S. Energy Research and Development Administration.

∿150 Å in diameter is reached early in the irradiation process at 550°C. Our observations suggested that the mechanisms of recoil and disordering dissolution were not sufficient to describe γ' morphologies developed during irradiation; therefore, we determined alternate mechanisms, which are presented here.

Twenty 3-mm disks per run of Ni-6.35 wt % Al in the solution-annealed, water-quenched condition were sequentially irradiated using 3.2-MV-$^{58}Ni^{+}$ ions. The samples, sectioned to a depth of ∿5000 Å, were examined by electron microscopy using high-resolution, dark-field imaging. Damage rates in the examined regions were ∿2.7 x 10^{-3} dpa/s. Particle-size distributions were obtained from measuring 1200-2000 particles per sample on a Zeiss sizer, and from these both the mean and most frequently observed sizes were obtained.

Figure 2 presents the particle sizes that were observed as a function of dose at 550°C. As in Nelson's model, the mean particle size appears to approach a steady state. However, the steady-state diameter of ∿85 Å is significantly smaller than that predicted, ∿150 Å. Also, the dose required to reach steady state is more than an order of magnitude greater than that predicted. Most importantly, the size vs dose curve exhibits a maximum, which is not suggested by the Nelson model. Apparently, a mechanistic change occurs between ∿6 and 20 dpa, which is confirmed by the micrographs shown here.

Figure 3 shows the morphological development of γ' with dose. The zero dpa sample was shielded from the beam during irradiation and was at temperature for ∿4.5 h. The greatly increased γ' size in the 5.6-dpa sample demonstrates irradiation-enhanced coarsening. During conventional thermal coarsening, the time to reach this size would be ∿120 h. This is large compared with the irradiation time of ∿0.5 h. Another feature evident from a comparison of Fig. 3a and b is the alteration of γ' distribution. For particle sizes ≳100 Å, conventional thermal coarsening maintains a uniform γ' distribution, such as that of Fig. 3a. This uniform distribution is altered by irradiation even at doses as low as ∿1 dpa, and extended regions devoid of γ' become apparent as in Fig. 3b. Also,

note in Fig. 3 that, with increasing dose, the shape of the γ' particles changes from spherical (0, 1.7 dpa) to cuboidal (5.6 dpa) and then to fragmented ($\gtrsim$19.4 dpa). The first change also occurs in conventional thermal coarsening, but the change to fragmented is characteristic of the irradiation environment. The simple mechanisms of recoil and disordering dissolution are not sufficient to describe these morphological developments.

All above-mentioned features can be interpreted in terms of the dislocation structure that develops during the irradiation and the interaction of γ' with these dislocations. Figure 4 shows the γ' network structure early in its development. Spherical regions, devoid of γ', project as $\sim$370-Å circles in the micrograph. The corresponding bright-field micrograph, Fig. 4b, shows dislocation loops (seen by residual contrast, not all loops are in contrast) and voids. The spatial relationship between γ' and the loops and voids is made visible by superimposing a negative of the dark-field image, Fig. 4c, on the bright-field image, see Fig. 4d. The superimposing shows clearly that regions devoid of γ' surround dislocation loops and are favored sites for void nucleation. A detailed loop analysis showed the loops were predominantly Frank faulted, all of which were extrinsic, i.e., interstitial loops. In the alloy investigated, γ' has a positive misfit, and its presence in the compressive field of the loop is energetically unfavorable.

The development of the γ' morphology during different irradiation conditions, Fig. 5, can now be understood by associating γ'-devoid regions with the interior of the dislocation loops. At lower temperatures, Fig. 5a, the defect density is relatively high and the mobilities low, causing high loop densities and slower growth rates. This results in a tight γ' network. At a higher temperature, Fig. 5b, irradiation to the same dose results in lower loop density and larger loops, thus the γ' denuded regions are farther apart and larger in extent. The trend continues to higher temperatures, Fig. 5c.

With increasing dose, the γ' particles that are evident between the loops are eventually pushed from several sides by the expanding loops. Continued loop growth can then occur only if the dislocations Orowan loop

the γ', as they do in PE-16,[2] or cut through the γ'. Both theoretical considerations of the loop stress, compared with the cutting stress, as well as experiments on aged-deformed-reaged materials in the absence of irradiation[3] suggest that the dislocations cut the γ' and this causes the fragmentation observed, for example in Fig. 5d.

CONCLUSIONS

1. At temperatures between 300 and 700°C, γ' coarsening was accelerated by irradiation to low doses.

2. The γ' morphology is related to the dislocation structure that develops during irradiation. This structure is made up primarily of interstitial Frank faulted loops. The interiors of these loops are devoid of γ', cause circles of no γ' contrast at low doses, and lead to network structures of γ' at higher doses.

3. Particle coarsening reaches an apparent steady-state mean size of $\sim$85 Å at 550°C, 2.7×10^{-3} dpa/s for Ni-6.35 wt % Al. We suggest that this results from a balance between radiation-enhanced coarsening and fragmentation by dislocation cutting.

4. The simple recoil and disordering mechanisms proposed by Nelson et al.,[1] to describe the development of the γ' morphology under irradiation conditions are not sufficient to account for the more complex structural developments reported here.

REFERENCES

1. R. S. Nelson, J. A. Hudson, and D. J. Mazey, J. Nucl. Mater. 44, 318 (1972).

2. K. R. Williams and S. B. Fisher, Rad. Effects 15, 243 (1972).

3. D. I. Potter and H. A. Hoff, to be published.

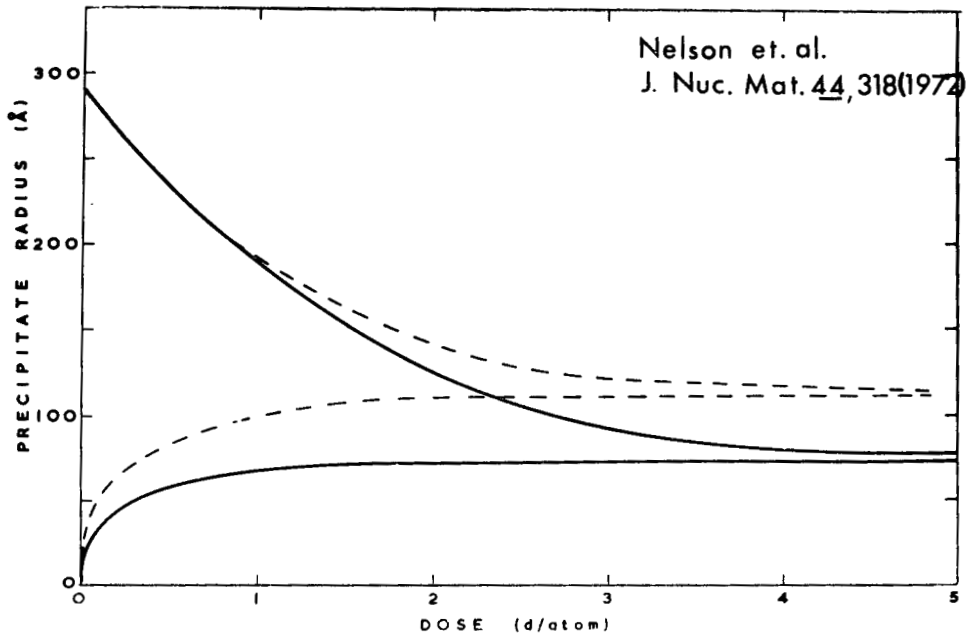


Fig. 1. Change in precipitate radius with dose. The continuous curves are for a damage rate of 10^{-2} dpa/s, and the dashed curves are for 10^{-6} dpa/s. The curves are calculated for Ni-6.7 wt % Al, T = 550°C, and $\sim 10^{16}$ particles of γ'/cm^3.

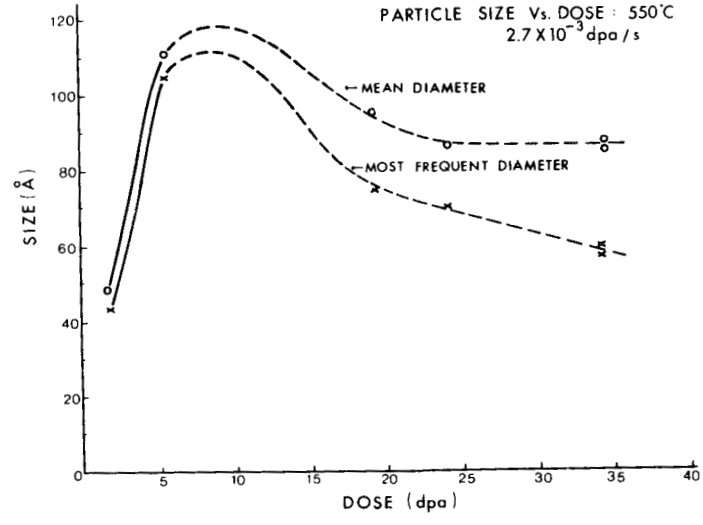
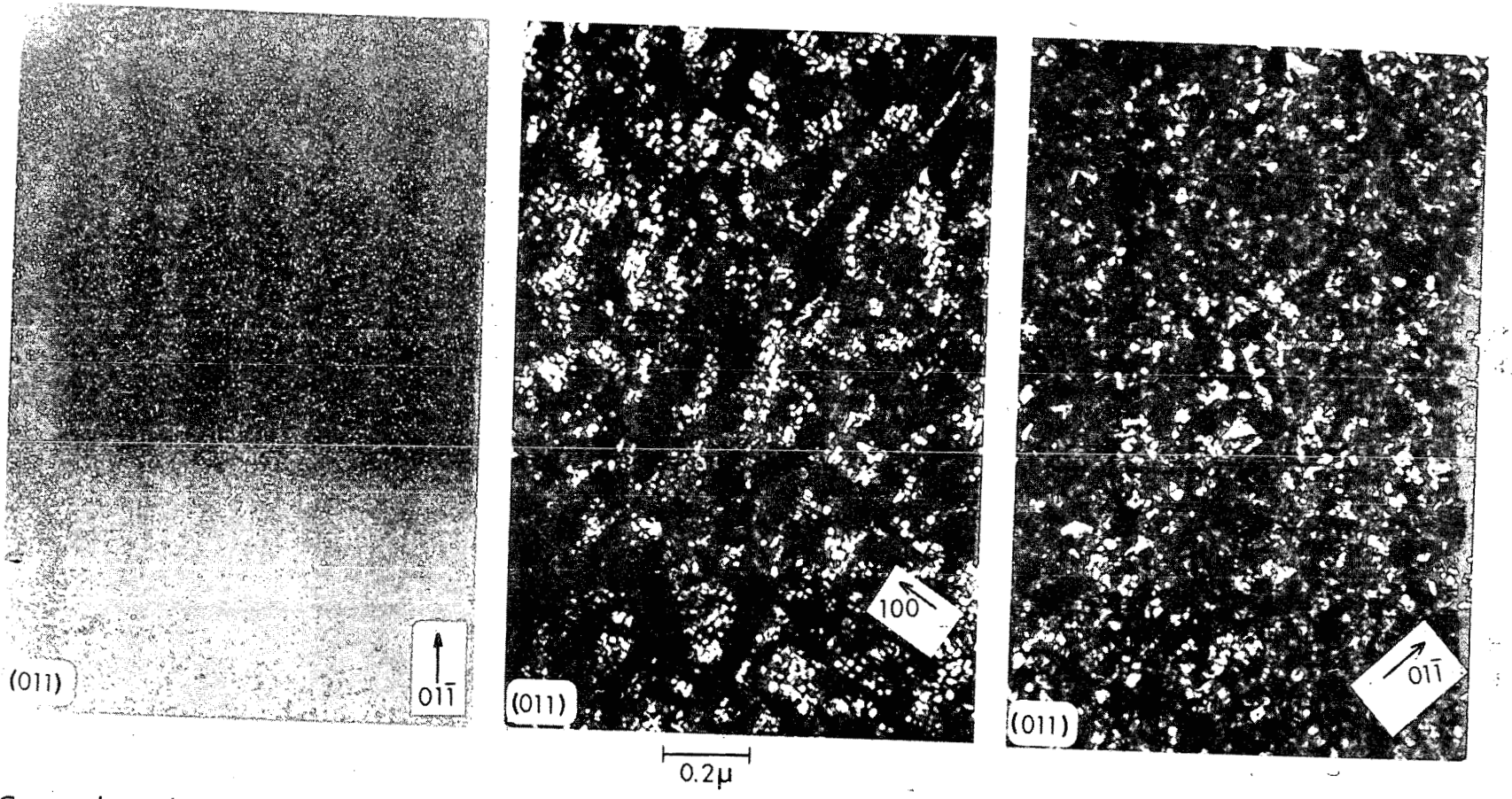


Fig. 2. Mean and most frequently observed γ' diameter plotted vs irradiation dose under conditions noted.



Control : 0 dpa, 550 °C
Spherical γ'

(a)

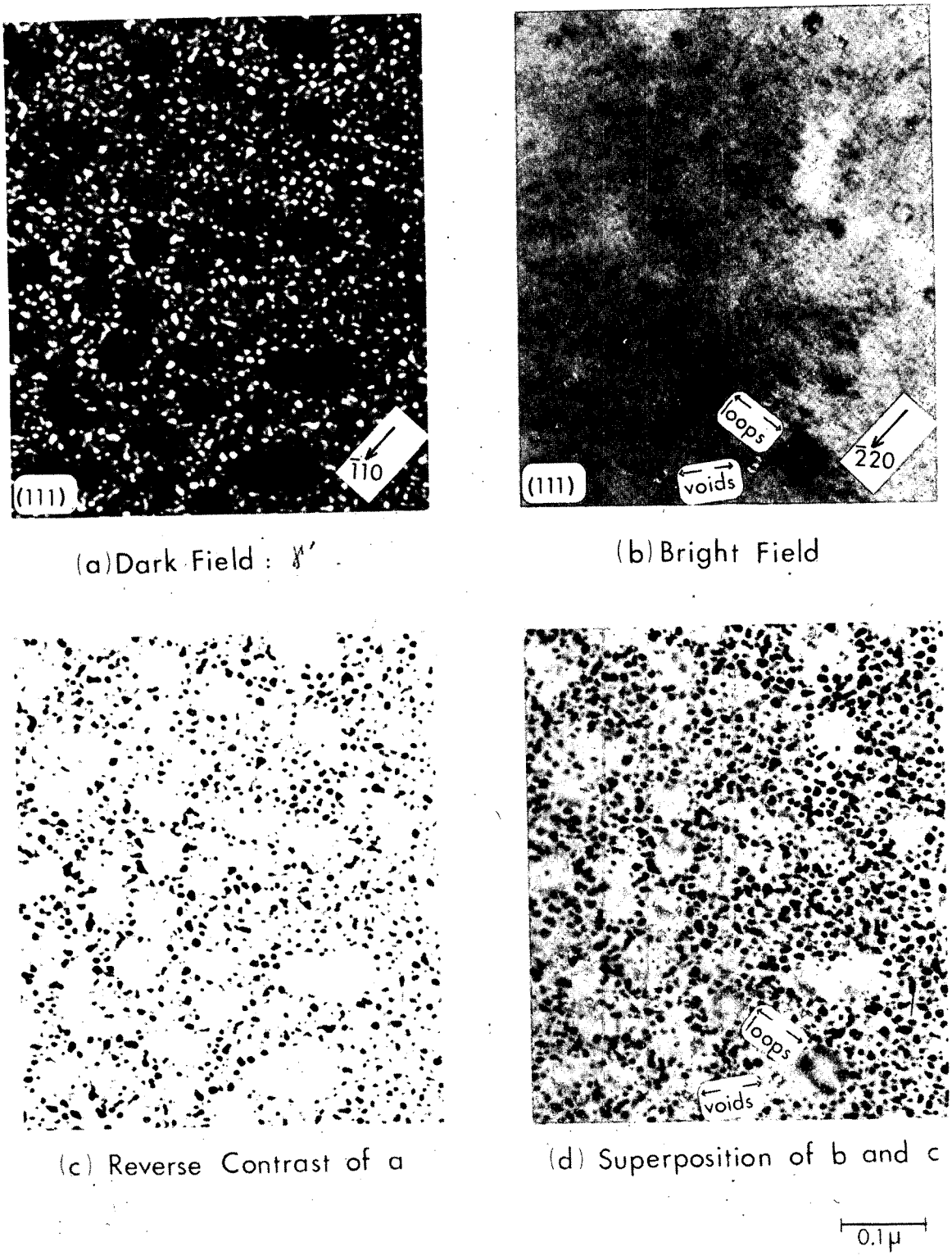
5.6 dpa/550 °C
Cuboidal γ'

(b)

19.4 dpa/550 °C
Fragmented γ'

(c)

Fig. 3. The γ' morphology that results from various damage doses at 550°C and 2.7×10^{-3} dpa/s.



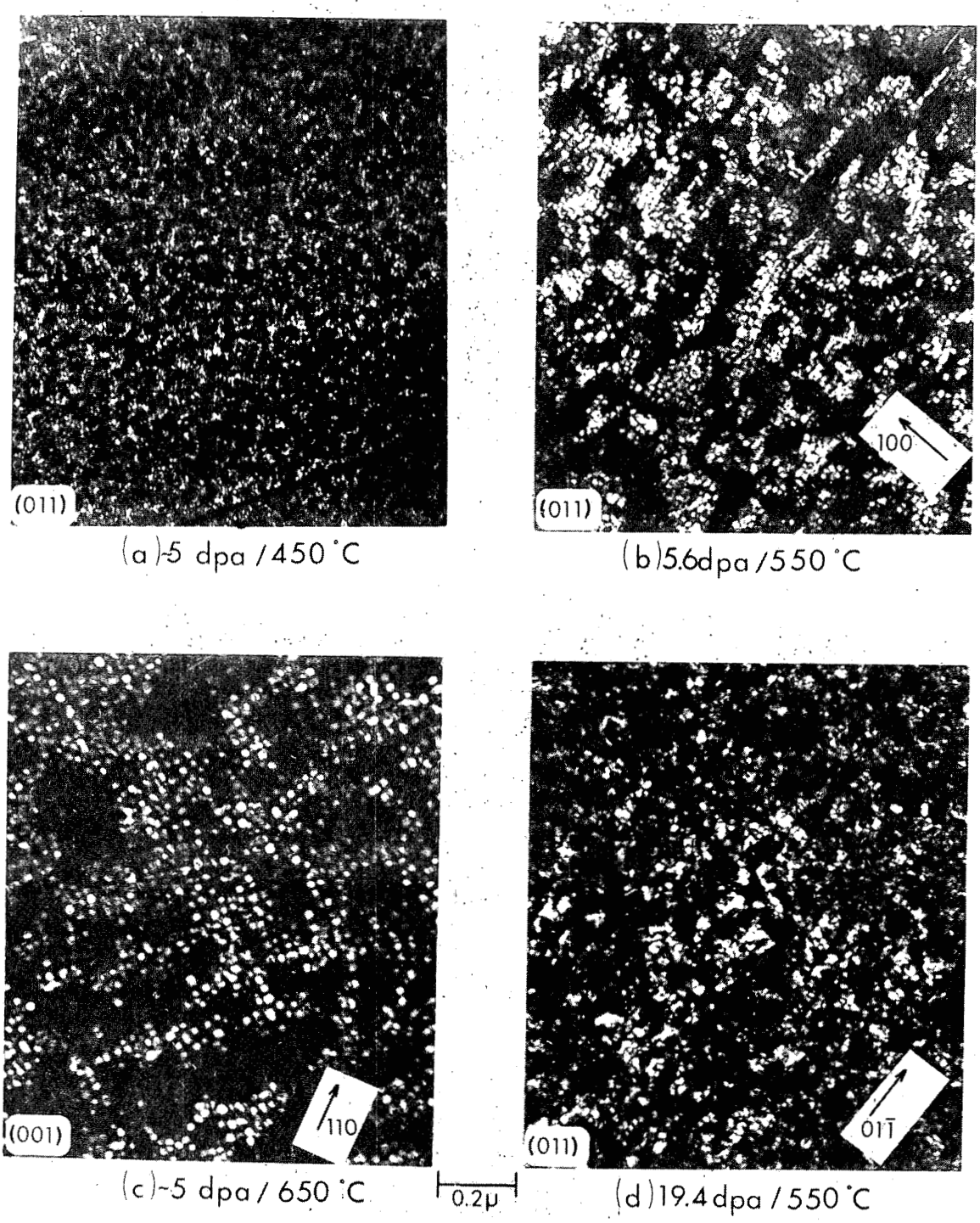
(a) Dark Field : γ'

(b) Bright Field

(c) Reverse Contrast of a

(d) Superposition of b and c

Fig. 4. The γ' morphology that results from 1.7 dpa at 550°C and 2.7×10^{-3} dpa/s.



(a)-5 dpa / 450 °C (b)5.6dpa / 550 °C

(c)-5 dpa / 650 °C (d)19.4 dpa / 550 °C

Fig. 5. The γ' morphology that results during different irradiation conditions but at a fixed dose rate of $\sim 2.7 \times 10^{-3}$ dpa/s.

EFFECT OF ELECTRON IRRADIATION ON PRECIPITATION OF CARBON & NITROGEN IN ALPHA IRON

T. Takeyama and H. Takahashi
Metals Research Institute, Faculty of Engineering, Hokkaido University,
Sapporo 060 Japan

ABSTRACT

Vacancies and interstitials were introduced in solution quenched Fe-0.025 wt%C and Fe-0.03 wt%N alloys by the aid of electron irradiation in a 650 kV HVEM, and the interaction between the point defects and the solute atoms was studied from the results of aging behavior revealed by the precipitation phenomena. The sequence of precipitation of quench-aging is ε-carbide and cementite for Fe-C alloy and α''-nitride and γ'-nitride for Fe-N alloy. In the irradiated area, however, no visible precipitates appeared on both the aged specimens. As it was certain that mainly a large number of vacancies must remain in the irradiated area, supersaturated carbon or nitrogen atoms are considered to migrate and be trapped by the single vacancies to form C-V pairs or N-V pairs. (C:carbon, N:nitrogen, V:vacancy) Therefore, the precipitation phenomena were prevented by the trapping effect. The dissociation of the C-V pair or N-V pair was observed by the existence of the precipitation in the irradiated area at higher aging temperature. The detrap temperature of the C-V pair and N-V pair was 240 and 200°C, respectively. Above the temperatures unusually large particles of cementite and smaller particles of α''-nitride than the precipitates in the un-irradiated area were observed.

INTRODUCTION

The behavior of point defect is expected to serve as a site for the nucleation to accelerate the precipitation and/or a trap for the solute atom to retard it. Point defects can be introduced by neutron irradiation, and the interaction between the point defects and solute atoms in alpha-iron has been studied by several workers.[1,2] However, the defects introduced by neutron irradiation is too complicated to investigate the behavior of solute atoms. It has been shown that in the electron microscope the

intense electron beam for imaging can produce a point defect when the accelerating voltage exceeds a threshold value.[3] This investigation was carried out to study the interaction between the interstitial solute atoms in iron and point defects produced by the irradiation of high energy electrons in a high voltage electron microscope (HVEM) through the aid of quench-aging behavior.[4,5]

MATERIALS AND EXPERIMENTAL PROCEDURE

The iron used in the present experiment is re-electrolytic pure iron produced by Showadenko Co. Ltd. Fe-0.025 wt%C and Fe-0.03 wt%N alloys were prepared. Fe-C alloy was homogenized in an evacuated quartz capsule for one hour at 730°C and Fe-N alloy was heat-treated at 600°C, then quenched into iced water by crushing the capsule. Thin foil for transmission electron microscopy was prepared from the disk specimen of 3mm in diameter by the jet-polishing technique. The foil was irradiated by electrons at the accelerating voltage of the 650 kV HVEM in a fluence of $1.7 \times 10^{21} e/cm^2$ for the Fe-C alloy and $1.8 \times 10^{21} e/cm^2$ for the Fe-N alloy at room temperature. The area of irradiation was 10μm diameter spot. Under the irradiation condition, defects due to displacement damage could occur in the foil specimen but noticeable defect clusters were not produced on the viewing screen. After irradiation, the foil specimen was transferred to an evacuated glass tube and heat treated at temperatures from 60 to 400°C. The observation was carried out at the accelerating voltage of 350 kV which was below the threshold value of iron.

RESULTS AND DISCUSSION

Fe-C alloy

The sequence of precipitation on quench-aging is ε-carbide and cementite. The irradiated structure before aging showed no distinction between the irradiated area and its surrounding un-irradiated area, namely no visible defect clusters were observed except dislocations which might be introduced by quenching. The aged structures under the temperature of 200°C showed many ε-carbide in the un-irradiated area but no visible

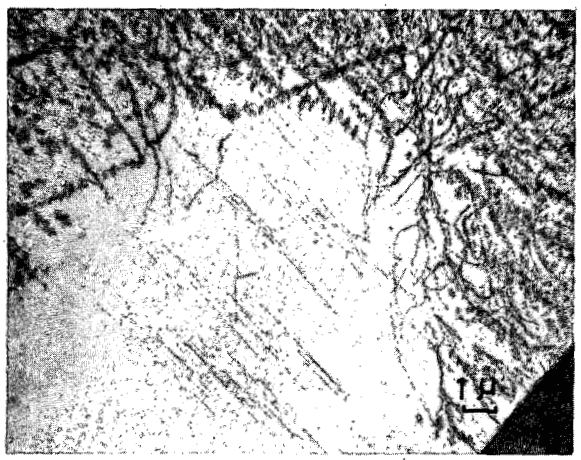


Fig. 1. Aged 20 min at 200°C after irradiation in a fluence of 1.7 x 10^{21} e/cm^2 at room temperature.

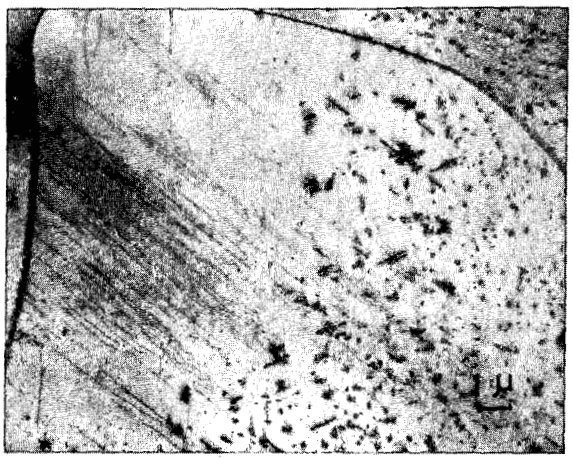


Fig. 2. Aged 20 min at 234°C after irradiation in a fluence of 1.7 x 10^{21} e/cm^2 at room temperature.

precipitates appeared in the area of irradiation. Fig. 1 showed an example aged 20 min at 200°C after irradiation. The ε-carbide was observed on {100} habit plane in the matrix especially on dislocations in the surrounding un-irradiated area, but precipitates were not observed in the irradiated area even on dislocations. In the irradiated area, the dislocation did not act as a preferential precipitation site. Fig. 2 showed the structure aged 20 minutes at 234°C after irradiation. No visible precipitates appeared in the area of irradiation, although the cementite precipitated on the un-irradiated matrix.

The Frenkel pair or the interstitial-vacancy pair must be produced in the irradiated area. As the migration energy of self-interstitial in iron is about 0.33eV, the mobility of it is probably very high. The interstitial which acts as preferential sinks will rapidly migrate and annihilates with vacancy, sinks at surfaces or grain boundaries. It also aggregates to produce interstitial clusters which may be too small to observe. On the contrary, the motion energy of vacancy is 0.68-1.3 eV, so the vacancy must be immobile at room temperature.[6] Therefore, a large number of vacancies probably exist in the lattice as an isolated vacance. The supersaturated C atom will migrate to and be trapped by the single vacancy, and the following reaction will take place in this irradiated area.

C + V--------C-V pair

The binding energy of C atom to the vacancy is reported to be 0.41 eV. which is greater than that of the ε-carbide of 0.27 eV. Consequently, as suggested by Fujita and Damask,[7] Fig. 1 will indicate that the formation of the metastable ε-carbide is prevented by the trapping of C atom at the vacancy. The binding energy of the cementite is supposed to be 0.42-0.89 eV. which is higher than the binding energy of C atom to the vacancy. The formation temperature of cementite was considered to be higher than the temperature of dissociation of C-V pair. However, as is showen in Fig. 2, although the cementite precipitated in the un-irradiated area at the aging of 234°C, precipitate of cementite or the dissociation phenomenon of C-V pair was not observed in the area of irradiation. Due to the high binding energy between C atom and vacancy the C-V pair is highly stable even at the precipitation temperature for the cementite. It was clearly observed that there was no relation between the precipitation temperature of the cementite and the dissociation temperature of the C-V pair.

The dissociation of C-V pair occurred at a temperature above 240°C, namely the cementite was observed in the irradiated area. Fig. 3 showed an unusual growth of cementites in the irradiated area after aging one hour at 246°C. At this temperature, C atom can freely move in the lattice and nucleate the cementite and/or aggregate to the cementite. Usually, in the case of the rapid growth of the cementite, coherent strain may be increased at the particle-matrix interface which will act as an agent to inhibit further growth and punch out dislocations. However, unusual growth of cementite surrounded with no dislocations was observed at the central part of the irradiated area which is considered to be the high density area of the C-V pair and excess vacancies. It is very probable that the single vacancy may become mobile at this temperature, and is absorbed on to the cementite-matrix interface and will act to relieve the coherent strain developed during

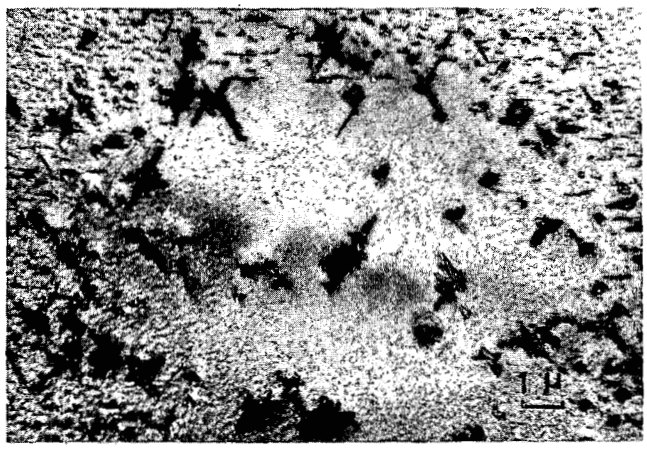


Fig. 3. Aged one hour at 246°C after irradiation in a fluence of 1.6 x 10^{21} e/cm^2 at room temperature.

the growth of the precipitate. 240°C is supposed to be the lowest temperature limit where the trapped C atom is released from the vacancy.

Fe-N alloy

The sequence of precipitation on quench-aging is α"-nitride and γ'-nitride. The Fe-N alloy also showed the same trapping effect for the solute atoms by defects produced by irradiation but different precipitation behavior from the Fe-C alloy. Fig. 4 (a), (b) and (c) showed the same area of the specimen but different structures after various aging steps. Fig. 5 (a) showed the structure aged 30 min at 130°C after irradiation. The surrounding unirradiated area showed a large amount of metastable α"-nitride ($Fe_{16}N_2$). On the other hand, in the central part of the irradiated area no such precipitation is observed. As the results of no precipitation in the irradiated area, it is considered that the most of N atom has been trapped by point defect. Presumably, N atom is bound mainly in the form of V-N pair and/or I-N cluster. The former may be composed of one N atom trapped in each vacancy and the latter N atoms and self-interstitials of iron. The up-quenching heat treatment was applied to find the dissociation phenomenon of V-N pair which is supposed to occur at a lower temperature than the dissociation temperature of I-N cluster. Fig. 4 (b) showed the structure up-quenched 15 min at 220°C after the heat-treatment described above. The un-irradiated area showed the precipitate particles which are much larger than the ones shown in Fig. 4 (a), but the irradiated area still showed no evidence of precipitation. Fig. 4 (c) showed the structure re-aged 30 min at 130°C. The precipitates in the un-irradiated area have no significant changes from those of the structure shown in Fig. 4 (b). On the contrary, a large number of small precipitate particles appeared in the irradiated area. It is considered that the dissociation of the V-N pair occurred already at this heat-treatment of 220°C. Therefore, free N atom released from the vacancy precipitated in the form of many small particles of α"-nitride. Presumably, the I-N cluster in the lattice may act as a site for the nucleation of the precipitation. Fig. 5 showed the structure up-quenched 15 min at 200°C after aging 30 min at 130°C, and then re-aged 18 hours at 130°C. The lowest temperature of the dissociation of the V-N pair was determined at 200°C as a result of the combined heat-treatments of various up-quenching

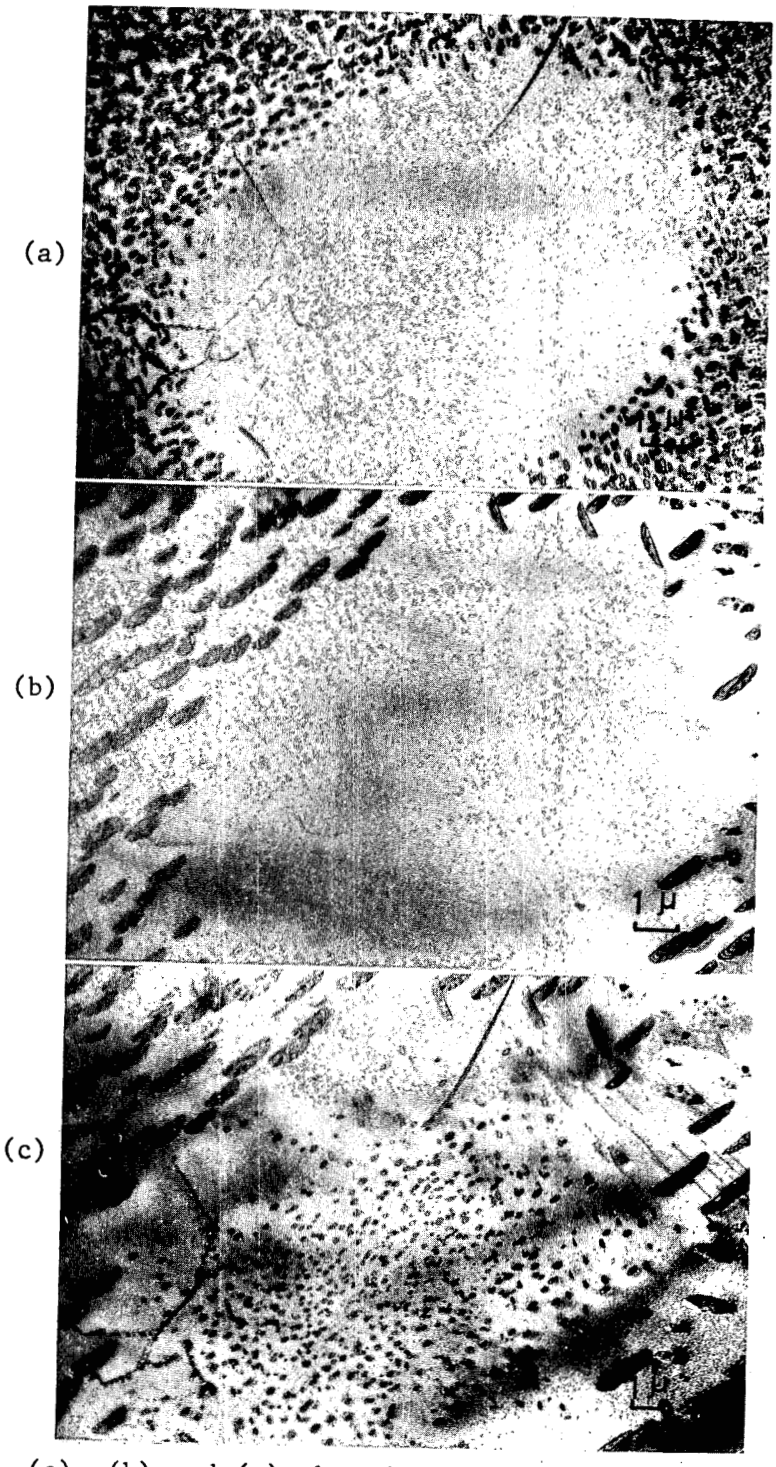


Fig. 4. (a), (b) and (c) showed the same area of the specimen but different structures in a variety of heat-treatments after irradiation in a fluence of 1.8×10^{21} e/cm^2 at room temperature.
(a) aged 30 min at 130°C,
(b) further aged 15 min at 220°C,
(c) re-aged 30 min at 130°C.



Fig. 5. Up-quenched 15 min at 200°C after aging 30 min at 130°C, and then re-aged 18 hours at 130°C.

temperatures and then re-aging at 130°C.

CONCLUSION

The interaction between the interstitial solute atoms in iron and point defects produced by the irradiation of high energy electrons in a HVEM was studied by the aid of precipitation phenomena.

1) The precipitation of the ε-carbide and/or the cementite was prevented by the trapping of C atom in vacancy. The detrap of the C-V pair occurred at the temperature above 240°C.

2) The precipitation of the α"-nitride was prevented by the trapping of N atom in vacancy. The detrap of the N-V pair occurred at the temperature above 200°C.

REFERENCES

1. D.Hull and I.L.Mogford, Phil. Mag., 6, 535 (1961).
2. H.Wagenblast and A.C.Damask, J. Phys. Chem. Solid, 23, 221 (1962).
3. M.J.Makin, Phil. Mag., 18, 637 (1968).
4. T.Takeyama and H.Takahashi, J. Phys. Soc. Japan 35, 939 (1973).
5. T.Takeyama and H.Takahashi, J. Phys. Soc. Japan 38, 1783 (1975).
6. R.A.Johnson, Phys. Rav., 134, A. 1329 (1964).
7. F.E.Fujita and A.C.Damask, Acta Met., 12, 331 (1964).

POSITRON ANNIHILATION IN PERFECT AND IMPERFECT METALS: A BRIEF REVIEW*

Allen N. Goland
Brookhaven National Laboratory
Upton, New York 11973

ABSTRACT

The current renaissance of investigations of positron annihilation in solids has its origins in the observation that positrons interact strongly with certain crystal-lattice defects. Three properties of the annihilation process are being measured to gain information about the defects or about the local environment of the positron at the instant of its annihilation: positron lifetime, angular correlation of the two annihilation quanta, and Doppler broadening of the 511-keV annihilation line. Until the physics of positron behavior in solids is fully understood, the phenomenon will continue to be useful in a manner analogous to electrical resistivity recovery for identifying the recovery stages in irradiated metals. Ultimately, it is destined to provide detailed quantitative information such as the formation volume of vacancies, vacancy-impurity binding energies and electron momentum distributions and densities at defect sites.

INTRODUCTION

About ten years ago evidence began to accumulate suggesting that positrons can become trapped at imperfections in solids. This conclsion was based upon observations that the characteristics of the annihilation process could be influenced by changes in the concentration of defects in the solid in which the annihilations occurred. For example, the shape of the two-photon angular-correlation curve changed as a function of sample deformation or temperature[1,2] as did the mean lifetime of the positrons.[3] Similarly, a parameter describing the lineshape of the Doppler-broadened annihilation photopeak at 511 keV

also exhibited this property.[4] To explain these results, several groups[5,6] proposed a phenomenological trapping model which actually had been introduced earlier by Brandt.[7]

The central assumption of the simple trapping model is that positrons annihilate in a solid from a free or a trapped state. Escape from traps is neglected, and the rate of trapping κ is assumed to be proportional to the concentration of traps, c. Thus, $\kappa = \mu c$, where μ is a parameter characterizing a specific trap type in a given solid.

West[8] has shown that if any characteristic of the annihilation process R is a linear function of the positron state, then

$$\frac{R_f - \bar{R}}{\bar{R} - R_t} = \frac{\mu c}{\lambda_f} \quad , \tag{1}$$

where λ is the annihilation rate, and the subscripts f and t refer to free or trapped states, respectively.

In practice, R has been taken to be the positron lifetime, or a shape parameter derived from a two-photon angular-correlation curve or from a Doppler-broadened annihilation line spectrum. The fundamental assumptions in this simple model are that it is experimentally possible to determine R_f and R_t individually, and that only one defect species at a time acts as an effective trap during various portions of an experiment. Evidently, by analogy to electrical-resistivity measurements in radiation-damaged metals, positron experiments can be useful in studies of defect behavior even when the precise nature of the imperfections is not specifically known. However, were it not for the additional theoretical and experimental effort of recent years,[9-21] interest in the positron annihilation technique as a tool for studying defects might not have continued to grow so rapidly. Studies of positrons in perfect metals as well as in metals containing either equilibrium or nonequilibrium concentrations of defects are required in order to develop positron annihilation as a new technique for defect research.

POSITRON SOURCES

Out of the many beta emitters, only a handful are suitable as positron sources. Each satisfies some of the following criteria: reasonably long half-life, minimal gamma-ray background, ease of preparation, ability to withstand adverse environmental conditions, and moderate cost for a supply in the form of carrier-free radionuclide of adequate strength for experiments. In Table 1 are listed some useful or potentially useful sources. Others can be produced in targets bombarded by various particles from accelerators. However, except in special cases, the utility of such sources has been limited by other problems such as the high background from competing reactions or from nuclear decay.

Table 1. Possible Positron Sources

Source	Halflife	% β^+ Decay	Method of Preparation	End-point Energy (MeV)
*^{22}Na	2.58 y	89	^{27}Al(^{3}He,2α)	0.54
^{44}Ti/^{44}Sc	48 y	80	^{45}Sc(p,2n); ^{45}Sc(d,3n)	1.47
^{55}Co	18.2 h	60	^{58}Ni(p,α) ; ^{56}Fe(p,2n)	1.50
^{57}Ni	36.0 h	50	^{56}Fe(^{3}He,2n)	0.85
*^{58}Co	71.3 d	15	^{58}Ni(n,p) ; ^{55}Mn(α,n)	0.48
*^{64}Cu	12.9 h	19	^{63}Cu(n,γ)	0.65
*^{68}Ge/^{68}Ga	275 d	88	^{66}Zn(α,2n)	1.90
^{90}Nb	14.7 h	54	^{90}Zr(p,n) ; ^{90}Zr(d,2n)	1.50

* indicates commonly-used sources.

The positron ranges corresponding to the endpoint energies can be as much as 20% greater than those for electrons of the same energies. However, a beta emitter produces a continuous energy spectrum, and the mean range of the positrons from a given source is much shorter than the maximum. The flux at some depth x is given by

$$I = I_o \exp(-\alpha x) \qquad (2)$$

where the linear absorption coefficient, α, has been empirically determined.[22-23] Table 2 contains values of the depth α^{-1} in Al, Cu or Au at which the positron flux is e^{-1} (37%) of its value, I_o, at the surface for positrons from the four most commonly used sources. Also shown in parentheses are the ranges of positrons possessing the maximum energy.

Table 2. e-Folding Distance in Al, Cu and Au for Positrons from Four Common Sources

Source	Al	Cu	Au
^{58}Co	90.4 μm (7.86×10^{-2}cm)	27.4 μm (2.71×10^{-2}cm)	12.6 μm (1.6×10^{-2}cm)
^{22}Na	76.3 μm (9.23×10^{-2}cm)	23.1 μm (3.10×10^{-2}cm)	10.7 μm (1.86×10^{-2}cm)
^{64}Cu	118. μm (1.18×10^{-1}cm)	35.7 μm (4.05×10^{-2}cm)	16.4 μm (2.35×10^{-2}cm)
$^{68}Ge/^{68}Ga$	543. μm (4.25×10^{-1}cm)	165. μm (1.42×10^{-1}cm)	76.3 μm (7.68×10^{-2}cm)

It is evident from the values given in Table 2 that the majority of the positrons penetrate to a depth which is considerably smaller than the range of a positron with the maximum energy of the beta spectrum. Thus, the results of experiments in which nonuniform defect densities exist over depths comparable to α^{-1} have to be examined for evidence of this effect. For example, experiments involving quenching or irradiation plus quenching in particular must be analyzed with care for near-surface variations.

Positron experiments are usually performed with sources of μCi to mCi strength (1 μCi $\equiv 3.7 \times 10^4$ disintegrations/sec). The annihilation rate of positrons in metals is of the order of 5×10^9 sec^{-1}. A simple calculation reveals that there is never more than one positron at a time in a sample. Positron-positron interactions are absent, and

experiments consist of collecting data for a long series of independent events. In the later discussion of positron trapping by defects a set of rate equations will be introduced. In view of the foregoing, they should be regarded as statistical equations describing the probability that a positron is still present after spending a time, t, in a solid.

POSITRON SLOWING DOWN

Positrons enter a sample with relatively high velocities, and rapidly slow down to near thermal velocities in a metal. All theoretical treatments[24] arrive at the same conclusion that this slowing-down time is short relative to positron lifetimes provided the sample temperature is not too low. The positron loses energy via ionizing collisions, plasmon creation, a minor amount of bremsstrahlung emission, electron-hole excitation and phonon creation. Until rather recently, the positron-phonon mechanism had been ignored by theorists. However, Mikeska[10] and Perkins and Carbotte[9] independently investigated this interaction and found that at low temperatures it can be the most important process by which positrons lose energy. The latter authors showed that in Na at 190 K, for example, the positron-phonon interaction begins to dominate the approach of the positron to thermal equilibrium with the lattice, if the positron effective mass $m^* = m$, the bare mass. The minimum temperature attained by the positrons in Na before annihilation in a sample at absolute zero is about 20 K. Recently, Kubica and Stewart[25] using a high-resolution angular-correlation apparatus have measured a thermalization temperature of $10 \pm 10°K$ in a Mg crystal held at 4.2 K.

Upon entering the solid, the positron immediately becomes surrounded by its own polarization cloud which has the effect of screening it from the strong Coulomb interactions in the metal. The higher the electron density, the more strongly screened is the positron. In the final brief period before its annihilation, the positron slowly migrates through the lattice. The details of this diffusion process have been clarified in several recent theoretical publications,[26-29] stimulated largely by interest in positron-defect interactions.

POSITRON TRAPPING BY DEFECTS

In order to understand why positrons are trapped at certain types of defects it is only necessary to introduce a few basic ideas. First, it has been shown[30] that the probability per unit time for annihilation into two photons whose total momentum lies between p and p + dp is given by the expression,

$$\sum_{\text{occ. i}} \lambda_i^{2\gamma}(\underline{p})d\underline{p} = \sum_{\text{occ. i}} \frac{2\, r_o^2 c}{(2\pi)^3} \left| \int \psi_-^i(\underline{r})\psi_+(\underline{r})\exp(i\underline{p}\cdot\underline{r}) \right|^2 d\underline{p} \quad . \tag{3}$$

In Eq. (3) the sum is to be taken over all occupied electron states, i. $\psi_-^i(\underline{r})$ is the electron wavefunction for state i, $\psi_+(\underline{r})$ is the positron wavefunction, r_o is the classical electron radius and c, the velocity of light. The total annihilation rate $\lambda^{2\gamma}$ is then found by integrating Eq. (3) over all electron momenta, and applying Parseval's theorem to obtain,

$$\lambda^{2\gamma} = 2\pi r_o^2 c \sum_{\text{occ. i}} \int \left|\psi_-^i(\underline{r})\right|^2 \left|\psi_+(\underline{r})\right|^2 d\underline{r} \quad . \tag{4}$$

If the annihilation rates are calculated without inclusion of positron-electron correlations in an electron gas, the resulting values are an order of magnitude less than the measured ones. To account for this discrepancy, an enhancement factor is included in the expression for the annihilation rate when an independent-particle model is used. This factor reflects the large increase in local electron density in the vicinity of the positron.

From Eq. (4) it is clear that the annihilation rate in a solid depends upon the electron density at the positron. Thus, if a positron migrates to a site of low electron density relative to the average value, the probability per unit time that it will annihilate is reduced. In practice, this will manifest itself as an increase in the lifetime of the positron. As a matter of fact, a solid can contain many regions of lower than average electron density, the most obvious type being a

vacant lattice site. However, under appropriate conditions, clusters of vacancies, vacancy-impurity complexes, voids and dislocations may also be present.

The second point to be made is that it has been shown theoretically that vacancies are in fact favorable trapping sites. Hodges,[17] Arponen et al.,[31] Hodges and Stott,[18] Seeger,[32] Bergersen and Taylor,[33] and Brandt and Fahs[34] have all investigated the trapping of positrons at a vacancy. Hodges represented the vacancy by a potential well centered at r = 0 and a Wigner-Seitz sphere of radius R_a surrounding it. This positron potential exhibits strong Coulomb repulsion near ion centers and screening of the Coulomb interaction in the interstitial and vacancy regions. Positron-electron correlations were neglected by Hodges although his effective potential was calculated by treating the positron and its polarization cloud as a neutral pseudo-atom interacting with the lattice atoms through a pairwise potential. More recently, Brandt and Fahs[34] have considered the problem using a statistical theory of the electron distribution around a vacancy. The positron wavefunction and the redistribution of the electrons around a vacancy were initially calculated in a self-consistent manner. A new self-consistent potential for the system composed of a positron occupying a vacant site was then determined, and used to deduce new electron and positron distributions. Brandt and Fahs deduced values of the positron-vacancy binding energy from their theory for a number of metals. Their values are considerably larger than those obtained by Hodges, ranging from 4 to 8 eV. They point out that this arises because they took into consideration the electron redistribution around the positron in the vacancy, a process neglected by Hodges. In any case, it appears that positrons are trapped at vacancies in most metals with binding energies sufficient to make detrapping unlikely.

Hodges and Stott[18] extended their theory of the positron work function[35] to a discussion of positron behavior near voids or external surfaces of metals. Treating the void as an internal surface they concluded that for large voids the positron states of lowest energy are probably localized in a potential "trough" at the void-metal interface.

Unless the positron work function, ϕ_p, is greater than about 0.39 Ryd., these positron bound states, localized at the surface, can exist. The binding energy depends upon ϕ_p and ranges in value from about 0.03 Ryd. for Li to $\sim$ 0.25 Ryd. for Al. Within their approximate one-dimensional model Hodges and Stott reached the conclusion that positronium (Ps) formation in voids was less probable than the formation of bound surface states. If Ps does form, there will be states which extend over the entire void volume.

We conclude that in a metal containing nonequilibrium concentrations of defects several types of positron traps may be present. If vacancies and voids can act as trapping centers, then vacancy complexes can be expected to trap positrons, also. On the other hand, calculations by Stott and Kubica[36] indicate that single interstitial atoms of the host metal or of an impurity are repulsive centers for the positron.

The simple trapping model can be extended to allow for the simultaneous presence of several types of traps. Assuming that a positron in trap type j has an annihilation rate λ_j, we write the rate equations for $p_L(t)$, the probability that a positron is free in the metal at time t, and $p_j(t)$, the corresponding probability for a trapped positron in the form,

$$dp_L(t)/dt = - \lambda_L p_L(t) - \sum_{j=1}^{m} \kappa_j(T) p_L(t) \quad , \tag{5}$$

$$dp_j(t)/dt = - \lambda_j p_j(t) + \kappa_j(T) p_L(t) \quad . \tag{6}$$

The trapping rate for each type of trap is $\kappa_j(T)$. Equations (5) and (6) have been discussed by Seeger[32] and Hall et al.[37] They presuppose no escape from traps, and allow for the possibility that the trapping rate is temperature dependent. Frank and Seeger[11] have given a more extensive theoretical treatment of the trapping model on the basis of Waite's theory of diffusion-limited reactions. Their equations reduce to Eqs. (5) and (6) when escape from traps is neglected.

All of the theories mentioned treat in a cursory way annihilations with core electrons. They proceed from an electron gas model including electron-positron and electron-electron correlations as well as sophisticated screening models. They strive to match measured annihilation rates for the alkali metals and are generally in rather poor agreement, although a recent approach for perfect metals by Lowy and Jackson[16] seems to yield somewhat better results. Nevertheless, experimental results for metals in other columns of the periodic table suggest that the fraction of annihilations with electrons in higher momentum states is appreciable. While these events may not be attributable solely to core states, it is plausible to assume that a large percentage of them can be so identified. Collaborative experiments in progress at Brookhaven[38,39] and Bell Labs.[40] will shortly provide additional quantitative information about core electron-positron annihilations, and the positron wavefunction. The method of separating experimental data into core and valence electron contributions may then require revision. The significance of this statement will become evident as the methods of annihilation detection and data analysis are considered in the next section.

DETECTION AND ANALYSIS OF ANNIHILATION IN METALS

Those interested in the experimental details of annihilation detection and subsequent data analysis can refer to a large number of excellent summaries;[8,41] only the salient features and some critical comments will be offered here.

Statistics and the selection rules governing positron annihilation state that the most probable event is annihilation accompanied by the emission of two photons. The total energy of the photons equals the rest mass of the two particles ($2\ mc^2$) minus the binding energy of the electron. Momentum must be conserved also, and because the positron is assumed to be thermalized, the final momentum is taken to be that of the electron. Three-photon decay is less likely than two-photon decay by the factor 1/372, while decay from a bound Ps state in bulk metals has not been positively observed.

Three kinds of experiments have been devised to detect the two-photon annihilation process: the lifetime spectrum is measured, the angular correlation between the two nearly collinear gamma rays is determined or the width of the Doppler-broadened annihilation photopeak is measured. The latter two properties can yield information about the electron momentum distribution in a solid, whereas the lifetime is related to the local electron density as pointed out earlier.

From the previous discussions of positron trapping at defects, it is evident that phenomenological models using empirically-defined parameters can be used to study defects systematically. The parameters are different for each type of measurement.

Lifetime Method

The standard coincidence techniques are used to record a time spectrum which is the distribution of positron lifetimes in a sample. The usual parameter is the mean lifetime $\bar{\tau}$ which can be extracted as the centroid of the time spectrum. Electronic techniques have been devised for accurately detecting shifts in the centroid brought about by trapping of positrons in vacancies, for example, where the electron density is low. However, the centroid-shift measurement is a relative one, and does not furnish values for the lifetimes of free and trapped positrons, τ_f and τ_t, respectively. These must be deduced from analysis of the spectrum, taking care to accurately determine the time resolution of the system. It is not always obvious where trapping is involved that saturation of the effect has occurred, or that no trapping is taking place. The mean lifetime is then the weighted average of the two extreme values. In any case, the lifetimes in metals can be within a factor of two or so of the instrumental resolution, and a computer analysis of the data is necessary even if only one lifetime is important. Accurate lifetime values can only be deduced from accumulation of many counts. With a standard fast-slow coincidence system this can take several days during which drift and stability of the electronics must remain at a minimum. However, new developments in fast-fast coincidence systems such as that reported by Hardy and Lynn[42] can reduce data-collection times to minutes without a sacrifice of resolution.

Since lifetime measurements provide unique information regarding electron densities at defects it seems likely that they will be employed increasingly once these new techniques become generally known.

Angular-Correlation Method

Measurements of the angular correlation between the two annihilation quanta can, in principle, be performed as accurately as desired by increasing the distance between the source and the detectors. However, because the positrons are distributed nonuniformly throughout the sample (which is in effect the source), great care must be taken to calculate the optical resolution function of the instrument. As applied to radiation-induced defects there is an increasing tendency to use the ratio of peak counting rate to normalized total area as the parameter R defined in the Introduction. The basis for this is the assumption that core annihilations are less probable at a vacant site, and consequently valence electron annihilations are more probable. Thus, the angular distribution becomes narrower as trapping increases, and this is reflected in an increase in the peak counting rate at the expense of the counting rate in the tails of the distribution. Good statistics can be achieved by counting at only a few angular positions along the distribution.

Arbitrary decomposition of the angular distribution into "valence" and "core" components is often carried out. However, this procedure is not on completely solid ground. High momentum state valence electrons can be included as core states, for example. Moreover, surprisingly large core state fractions seem to be required to explain some experimental results.[43] That core states are involved is evident from several kinds of experiments and calculations. Kubica,[44] for example, has shown that the effects of lattice expansion on annihilation rates at low temperatures can be explained in terms of increased overlap of the positron wavefunction with core states.

While annihilation rates are increased by the enhanced local electron density, it has been shown that the positron is only weakly coupled to its surroundings by virtue of the screening that arises from

this enhancement. Therefore, it does not perturb the electron momentum distribution characteristic of the solid. However, if the screening changes, as it will at a defect, the momentum distribution may be influenced more strongly by the positron. These matters must be clarified through careful experiments on equilibrium concentrations of defects.

Doppler-Broadening Method

Owing to the poor energy resolution of scintillator-photomultiplier combinations, Doppler-broadening measurements were for a long time considered too insensitive to be gainfully employed in annihilation studies. The advent of the high efficiency, high resolution Ge(Li) detector has altered this picture.[45] Measurements of the annihilation photopeak require only one detector. Hence the counting rate can be high, and experiments performed relatively rapidly with good statistics. MacKenzie and his colleagues[46] have led the way in demonstrating that changes in the lineshape of the photopeak correspond to variations in the defect structure of metals. Using the ratio of counts in channels around the peak to total counts in two symmetrically-placed groups in the wings as a lineshape parameter, they have investigated equilibrium and nonequilibrium defect concentrations in numerous metals. In fact, more studies of defects in irradiated metals have been performed by this means than any other.

Doppler-broadening measurements are still not regarded seriously as a technique for determining electron momentum distributions. Nevertheless, it should be remarked that a broadening of 1.6 keV is associated with an electron of only 10 eV corresponding to an angle of 6.25 mrad in an angular-correlation experiment. As a good Ge(Li) detector will have a resolution of $\sim$ 1.2 - 1.3 keV at 514 keV, structure in the high-momentum components of the angular distribution can be detected. Recent modifications in the Doppler-broadening method have further enhanced the capabilities of this technique.[38-40]

CONCLUDING REMARKS

It seems clear now that after a somewhat prolonged nucleation period,[47-49] the growth of positron physics as applied to radiation-effects research has begun in earnest. Major new efforts are starting throughout the world, and several reports from established research groups are evident in these proceedings. Therefore, the purpose of this brief review has been to introduce the basic theoretical and experimental concepts currently in use by those in the field. Hopefully, this will have the beneficial effect of making the subsequent shorter and more specific positron papers understandable to the uninitiated.

ACKNOWLEDGEMENT

The author wishes to express his deep appreciation to K. G. Lynn for his many illuminating discussions and his critical reading of this manuscript.

REFERENCES

* Research supported by the Energy Research & Development Administration.

1. I. K. MacKenzie, G.F.O. Langstroth, B.T.A. McKee, and C. G. White, Can. J. Phys. 42, 1837 (1964).
2. S. Berko and J. C. Erskine, Phys. Rev. Lett. 19, 307 (1967).
3. I. K. MacKenzie, T. L. Khoo, A. B. McDonald, and B.T.A. McKee, Phys. Rev. Lett. 19, 946 (1967).
4. I. K. MacKenzie, Phys. Letters 30A, 115 (1969).
5. B. Bergersen and M. J. Stott, Sol. St. Commun. 7, 1203 (1969).
6. D. C. Connors and R. N. West, Phys. Letters 30A, 24 (1969).
7. W. Brandt, in Proc. International Conference on Positron Annihilation (A. T. Stewart and L. O. Roellig, eds.), Academic Press, New York, 1967, p. 80.
8. R. N. West, Adv. Phys. 22, 263 (1973).
9. A. Perkins and J. P. Carbotte, Phys. Rev. B1, 101 (1970).

10. H.-J. Mikeska, Z. Physik 232, 159 (1970); Phys. Lett. 24A, 402 (1967).
11. W. Frank and A. Seeger, Appl. Phys. 3, 61 (1974).
12. B.B.J. Hede and J. P. Carbotte, J. Phys. Chem. Solids 33, 727 (1972).
13. J. P. Carbotte and A. Salvadori, Phys. Rev. 162, 290 (1967).
14. A. Sjölander and M. J. Stott, Phys. Rev. 5B, 2109 (1972).
15. F. Bhattacharyya and K. S. Singwi, Phys. Rev. Lett. 29, 22 (1972).
16. D. N. Lowy and A. D. Jackson, Phys. Rev. (to be published).
17. C. H. Hodges, Phys. Rev. Lett. 28, 284 (1970).
18. C. H. Hodges and M. J. Stott, Sol. St. Commun. 12, 1154 (1973).
19. T. M. Hall, K. C. Jain, R. W. Siegel, and A. N. Goland, Bull. Am. Phys. Soc. 18, 54 (1973) and Phys. Rev. (to be published).
20. B.T.A. McKee, H. C. Jamieson, and A. T. Stewart, Phys. Rev. Lett. 31, 634 (1973).
21. I. K. MacKenzie, T. E. Jackman, C. G. White, C. W. Schulte, and P. C. Lichtenberger, Appl. Phys. 7, 141 (1975).
22. R. B. Evans, Atomic Physics, McGraw-Hill Co., 1955.
23. G. I. Gleason, I. D. Taylor and D. L. Tabern, Nucleonics 8, 12 (1951).
24. See for example, J. P. Carbotte and H. Arora, Can. J. Phys. 45, 387 (1967).
25. P. Kubica and A. T. Stewart, Phys. Rev. Lett. 34, 852 (1975).
26. W. Brandt, Appl. Phys. 5, 1 (1974).
27. B. Bergersen, E. Pajanne, P. Kubica, M. J. Stott, and C. H. Hodges, Sol. St. Commun. 15, 1377 (1974).
28. B. Bergersen and E. Pajanne, Appl. Phys. 4, 25 (1974).
29. A. Seeger, Appl. Phys. 7, 85 (1975).
30. S. de Benedetti, C. Cowan, W. Konneker and H. Primakoff, Phys. Rev. 77, 208 (1950).
31. J. Arponen, P. Hautojärvi, R. Nieminen and E. Pajanne, Sol. St. Commun. 12, 143 (1973).
32. A. Seeger, J. Phys. F. 3, 248 (1973).
33. B. Bergersen and D. W. Taylor, Can. J. Phys. 52, 1594 (1974).
34. W. Brandt and J. H. Fahs (to be published).

35. C. H. Hodges and M. J. Stott, Phys. Rev. B7, 73 (1973).

36. M. J. Stott and P. Kubica, Phys. Rev. B11, 1 (1975).

37. T. M. Hall, A. N. Goland, and C. L. Snead, Jr., Phys. Rev. B10, 3062 (1974).

38. F. Geisler, K. G. Lynn, and A. N. Goland, Bull. Am. Phys. Soc. 20, 580 (1974).

39. K. G. Lynn and A. N. Goland (to be published).

40. J. R. MacDonald, R. A. Boie, L. C. Feldman, and M. F. Robbins, Bull. Am. Phys. Soc. 20, 580 (1974).

41. See for example, J. A. Merrigan, J. H. Green and S-J Tao in Physical Methods of Chemistry (A. Weissberger and B. W. Rossiter, eds.) Wiley and Sons, New York, 1972, Vol. 1 Part IID, pp. 501-586.

42. W. H. Hardy, II and K. G. Lynn, IEEE Trans. Nucl. Sci. (to be published).

43. K. G. Lynn, private communication.

44. P. Kubica, Doctoral Thesis, Queen's University, Kingston, Canada 1975 (unpublished).

45. K. Rama Reddy, R. A. Carrigan, Jr., S. De Benedetti, and R. B. Sutton, Bull. Am. Phys. Soc. 12, 74 (1967); G. Murray, Phys. Lett. 24B, 268 (1967); F.H.H. Hsu and C. S. Wu, Phys. Rev. Lett. 18, 889 (1967); I. K. MacKenzie and B.T.A. McKee, Bull. Am. Phys. Soc. 12, 687 (1967).

46. I. K. MacKenzie, J. A. Eady, and R. R. Gingerich, Phys. Lett. 33A, 279 (1970), and ref. 8.

47. J. H. Kusmiss, C. D. Esseltine, C. L. Snead, Jr., and A. N. Goland, Phys. Lett. 32A, 175 (1970).

48. C. L. Snead, Jr., A. N. Goland, J. H. Kusmiss, H. C. Huang, and R. Meade, Phys. Rev. B3, 275 (1971).

49. C. L. Snead, Jr., A. N. Goland, T. M. Hall, and F. W. Wiffen, Bull. Am. Phys. Soc. 18, 394 (1973).

DIRECT EVIDENCE FOR VACANCY CLUSTERING IN ELECTRON IRRADIATED COPPER BY POSITRON ANNIHILATION

S. Mantl and W. Triftshäuser
Institut für Festkörperforschung der Kernforschungsanlage Jülich
517 Jülich, Germany

ABSTRACT

Doppler-broadening measurements have been performed on copper irradiated by electrons to different doses and on quenched gold. From the shape of the Doppler broadening curve a defect specific parameter R was determined. From the information deduced from the R-parameter and from the similar annealing behavior of electron irradiated copper and quenched gold, we conclude that in both metals in stage III vacancies become mobile and form small clusters.

INTRODUCTION

Positron studies on metals containing vacancies in thermal equilibrium[1-3] have demonstrated the high sensitivity of positrons to vacancies. Therefore it seemed interesting to investigate the effect of annealing on positron annihilation experiments. Using the two state trapping model[3] a defect specific parameter R was deduced, which allows the identification of the type of trap in the sample from the shape of the Doppler broadening curve.

EXPERIMENTAL DETAILS AND RESULTS

We performed measurements of the Doppler broadening[4,5] of the 511 keV annihilation radiation for copper samples, irradiated with electrons at helium temperature to different doses and on quenched gold specimens. At each dose three polycrystaline samples of dimensions 10 mm x 12 mm and 0.3 mm thick were irradiated simultaneously. Two of the specimens were used for positron annihilation measurements; while a third sample with the same thickness was used for resistivity measurements. The cop-

per samples were etched and annealed before irradiation and had residual resistivity ratios R (300 K)/R (4.2 K) between 1000 and 1500. After the irradiation, a 10-μCi ^{22}Na positron source was inserted between the two positron samples to achieve a sandwich arrangement while maintaining the specimens at a low temperature.

The Doppler broadening apparatus had an energy resolution of 1.12 keV at 514 keV which was achieved by using a coaxial Ge(Li) detector. The electronics were temperature stabilized to within a few tenths of a degree. The counting time for one spectrum was ten minutes and for each temperature point nine spectra were recorded. These spectra were shifted mathematically to a common centroid before being added together all by a PDP11/40 computer. This resulted in a total number of counts of 4×10^6. The stability of the centroids was within ± 0.1 channel. The full width at half-maximum of the 511 keV line was expanded to about 30 channels. The lineshape parameters I_v and I_c were calculated after subtracting a small linear background from the spectrum.

I_v is a small area in the center of the spectrum (corresponding to the peak height in angular correlation measurements with a geometrical resolution of 2 mrad) divided by the total area. I_c is the sum of two segments on either wing of the peak (corresponding to the regions from 10 to 16 mrad) divided also by the total area. Thus I_v is a measure of annihilations of positrons primarly with conduction electrons and I_c is associated with annihilations with core electrons.

Samples were irradiated to different doses, corresponding to residual resistivity changes of 126, 65 and 30 $\times 10^{-9}$ Ωcm. For the highest dose the isochronal annealing was started at 31 K. In the case of the highest and the lowest dose each temperature step was 10 % of the preceding temperature, whereas for the medium dose the temperature steps were 15 %. All positron-annihilation measurements were made at 10 K, while the resistivity measurements were performed at 4.2 K. The results are shown in Fig. 1, where the lineshape parameter difference ΔI_v is the difference between I_v and the characteristic value for the annealed specimen.

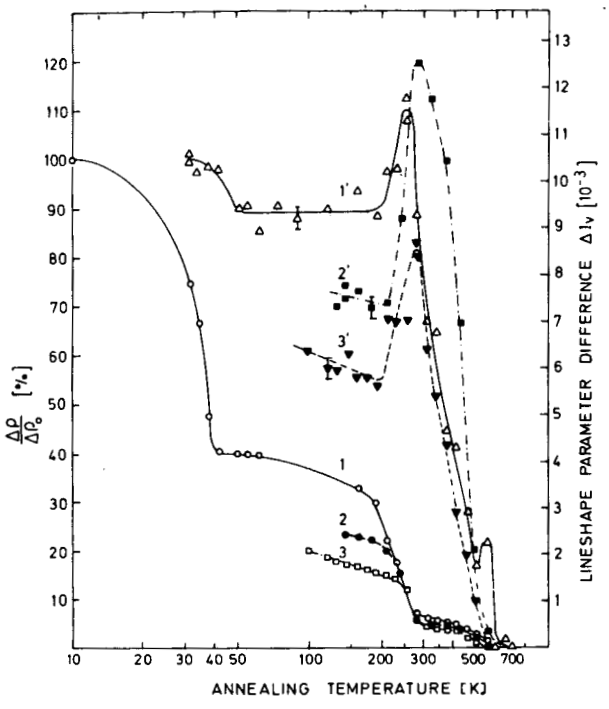


Fig. 1. Lineshape parameter difference ΔI_V and resistivity as a function of the annealing temperature for electron irradiated copper for different doses: 1 $\Delta\rho_o$ = 126 nΩcm
2 $\Delta\rho_o$ = 65 nΩcm
3 $\Delta\rho_o$ = 30 nΩcm

In recovery stage I the lineshape parameter I_V decreases due to the decrease in the number of vacancies in this stage. At lower doses a decrease in I_V is also observed in stage II. The most startling effect, however, is the increase of the lineshape parameter I_V in the annealing stage III, where the resistivity decreases sharply. If the positrons were being trapped by the same type of defect as in stage I and II, I_V should decrease too. The increase of I_V in stage III indicates that the type of the dominating trapping sites has changed. Further annealing results in a decrease of the lineshape parameter I_V as well as of the resistivity. The recovery process is completed at about 650 K.

The identification of the type of defect formed during isochronal annealing in stage III is made possible by determining a defect specific parameter R on the basis of the two state trapping model, from the shape of the Doppler broadened 511 keV line.

$$R = \left| \frac{I_V - I_V^f}{I_c - I_c^f} \right| \equiv \left| \frac{I_V^t - I_V^f}{I_c^t - I_c^f} \right| \quad , \qquad (1)$$

where I_V^f and I_c^f are the characteristic lineshape parameters in the free states and I_V^t and I_c^t are the concentration independent saturation values in the trapped states. The R-parameter is concentration independent, if only one type of trapping center in the sample predominates[5]. Fig. 2 shows the R-parameter as a function of the annealing temperature for the three different doses. During stage I and II the R-parameter has a

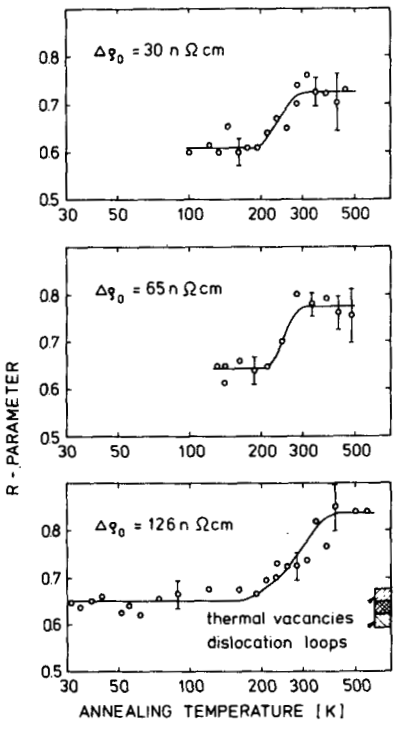


Fig. 2. R-parameter versus annealing temperature of electron-irradiated copper for different doses. Indicated are the values of R for vacancies in thermal equilibrium and for dislocation loops.

value between 0.61 and 0.65, which is identical to the value determined independently for thermal vacancies. This suggests, that the positrons are trapped by single vacancies in stage I and II. In stage III, R increases, which indicates that the nature of the dominating trapping center is changing. From electron microscopy[6] it is known that interstitials are present in the form of dislocation loops above stage III. However, dislocation loops cannot be the dominant traps because their R value, determined from copper single crystals containing dislocation loops, which were produced by neutron irradiation above room temperature[7], is even somewhat lower than for single vacancies. Therefore, we conclude that above stage III in copper positrons are still trapped by vacancy type defects, which no longer have the form of single vacancies. The increase of the R-value suggests that small, probably three dimensional vacancy cluster act as traps for the positrons. This implies that the vacancies have become mobile during the annealing stage III.

This interpretation is further supported by similar results on quenched gold. Gold samples, of 99,999 % purity, were rapidly quenched from 1220 K down to 210 K. In these samples, where only vacancies are formed in the quench, a similar recovery behavior was observed. Fig. 3 shows the lineshape parameter I_v and the R-parameter during the annealing.

The increase of the R-parameter in the temperature range of stage III in quenched gold supports the previous interpretation that the increase of the R-value for electron irradiated copper has to be attributed to a rearrangement of the vacancy type defects. Since stacking fault tetra-

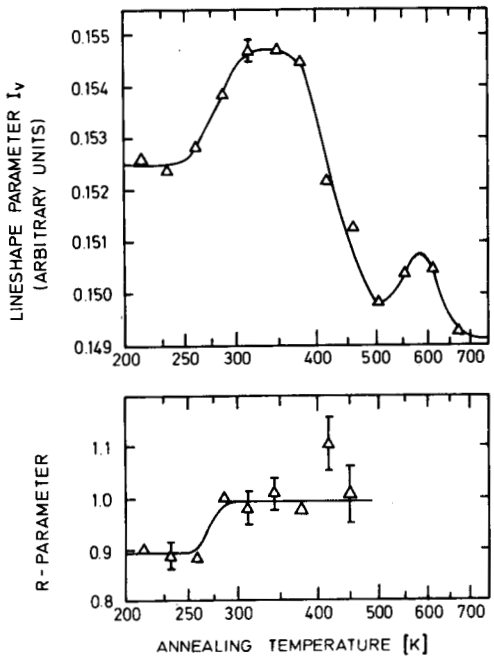


Fig. 3. Lineshape parameter I_V and R-parameter for quenched gold as a function of the annealing temperature.

hedra are expected to give a similar or smaller R-value as dislocation loops one has further to conclude that during the annealing of quenched gold the vacancies form first small three-dimensional clusters before aggregating into stacking fault tetrahedra observed in electron microscope[6].

REFERENCES

1. B. T. A. McKee, W. Triftshäuser and A. T. Stewart, Phys. Rev. Lett. 28, 358 (1972)
2. W. Triftshäuser and J. D. McGervey, Appl. Phys. 6, 177 (1975)
3. R. N. West, Positron Studies of Condensed Matter, Taylor and Francis Ltd., London, 1974
4. I. K. MacKenzie, Phys. Lett. 30A, 115 (1969)
5. S. Mantl and W. Triftshäuser, Phys. Rev. Lett. 34, 1552 (1975)
6. B. L. Eyre, J. Phys. F: Metal Phys. 3, 422 (1974)
7. M. Rühle, F. Häusermann and M. Rapp, phys. stat. sol. 39, 609 (1970)

VACANCY MIGRATION AND VOID FORMATION DURING THE ANNEALING OF ELECTRON IRRADIATED MOLYBDENUM

M. Eldrup and O.E. Mogensen
Chemistry Department, AEK Risö
4000 Roskilde, Denmark

and

J.H. Evans
Metallurgy Division, A.E.R.E. Harwell
Oxfordshire, U.K.

ABSTRACT

The positron annihilation technique (PAT) was used to study the annealing of 10 MeV electron irradiated molybdenum from room temperature up to 1000°C. In addition the recovery was monitored by resistivity measurements and transmission electron microscope observations. The combination of these techniques gave a consistent picture of the defect recovery during annealing. Of particular importance proved to be the sensitivity of PAT parameters to vacancy type defects. In the stage III annealing region (150°C-350°C) the resistivity recovery coincided with a sharp rise in the long positron lifetime from 200 psec (typical for a positron trapped in a mono-vacancy) to about 420 psec (typical for a void). In the same region a clear narrowing of the positron annihilation angular correlation curve was observed. Both facts are strong indications that vacancy cluster (void) formation, and hence vacancy migration, takes place in stage III. At higher temperatures the long positron lifetime increases further showing coarsening of the voids. The presence of voids was confirmed by transmission electron microscopy on material annealed to 900°C. The ability of PAT measurements to follow the development of voids, from mono-vacancies up to sizes resolvable by electron microscope, clearly shows the power of this new technique in examining defects in metals.

INTRODUCTION

The use of positron annihilation techniques (PAT) to study defects in metals is now becoming well-established. Among the applications of the method have been the determination of vacancy formation energies[1,2] and the study of voids[3,4,5] while, more recently PAT has been used to examine the defect behaviour during annealing of radiation induced damage[6,7]. Ref. 6 describes the annealing of molybdenum after neutron irradiation at $\sim$ 50°C, and changes in PAT parameters were correlated with mechanisms leading to the growth of voids. Voids formed by low temperature neutron irradiation followed by annealing was simultaneously discovered by electron microscopy[8]. The role of vacancy loops in the void formation process[6] has later been confirmed again by electron microscopy[9]. However, of considerable additional interest were the processes responsible for the PAT results in the so-called stage III recovery region (150°C-300°C). In molybdenum as in the few noble metals there has been some debate on the nature of the migrating species[10]. Many point defect experiments have indicated that the stage is a result of the annihilation of vacancies and interstitials, but none have convincingly demonstrated which of the species is the mobile one. In the PAT work on neutron irradiation damage recovery one of the conclusions was that vacancy clusters were created in stage III, therefore, implying the migration of a vacancy type defect.

However, neutron irradiation has the disadvantage that the damage created is not particularly well characterized. On the other hand, in electron irradiation the damage configuration is believed to be much simpler, most of the damage being formed as single vacancy-interstitial pairs. In the work described below we have, therefore, studied the recovery of electron irradiated molybdenum. In addition to the angular correlation and lifetime PAT results, data on the recovery were obtained by liquid helium resistivity measurements and transmission electron microscope examination. The combination of these techniques gave a very consistent picture of the recovery, in that the positron annihilation results clearly showed vacancy clustering taking

place during the stage III resistivity recovery, thereby strongly supporting the model stating mono-vacancy migration in this region. This conclusion was further strengthened by the evidence from PAT that some of the vacancy clusters were three dimensional, i.e. voids. Annealing above stage III resulted in coarsening of the voids and their presence was finally confirmed by electron microscopy.

In the following section the experimental details and the results will be described. The next section contains a discussion of the results obtained and a concluding section ends the paper. A more detailed discussion of many of the problems touched upon in this short conference contribution will appear in a forthcoming paper[11].

EXPERIMENTAL AND RESULTS

The material used in this work was produced by zone refining low-carbon arc-cast molybdenum obtained from the Climax Molybdenum Company. After four passes in the zone refiner the material was rolled to 0.25 mm, cut to size and then annealed for two hours at 2000°C in vacuum to remove residual gases. For the resistivity measurements the specimens were cut into the size of 5 cm x 0.5 cm, for the lifetime measurements into two pieces of 1 cm x 1 cm, and for the angular correlation measurements into one piece of 1 cm x 2 cm. The electron irradiation was made at 10 MeV with the Risø Linac Accelerator to a dose of 2×10^{18} electrons/cm^2, the average dose rate being 2×10^{13} electrons/cm^2/sec. The temperature of the specimens did not exceed 50°C during irradiation. After irradiation the specimens were subjected to a stepwise isochronal annealing treatment up to 1000°C with measurements being made after each annealing step. The overall isochronal heating rate was 1°C/minute. The PAT measurements were all done at room temperature.

The radiation induced resistivity changes and the subsequent recovery on annealing were measured by standard potentiometric methods with specimens immersed in liquid helium. The resistivity results are shown with open circles in Fig. 1.

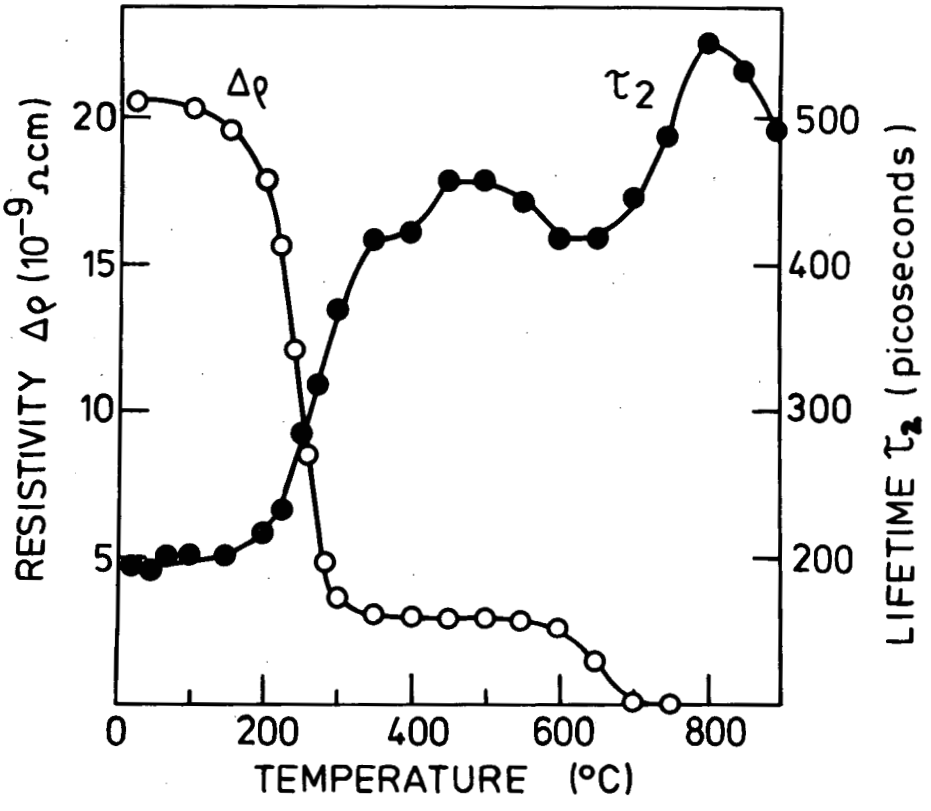


Fig. 1. The recovery of induced resistivity (open circles) and the behaviour of the long positron lifetime, τ_2 (filled circles) during the isochronal annealing of electron irradiated molybdenum. Heating rate was $1^{\circ}C\ min^{-1}$.

A positron's lifetime is measured by determining the time difference between the emission of two γ-quanta. The first γ is emitted from the positron source (often ^{22}Na) almost simultaneously with the positron, and the second γ is one of the two 0.51 MeV quanta emitted when the positron annihilates with an electron in the sample being investigated. The distribution of positron lifetimes in a given material is referred to as the lifetime spectrum. It has the shape of one - or a sum of several - decaying exponentials, each with a certain mean lifetime (the inverse of the slope). The finite time resolution of lifetime spectrometers results in some smearing of lifetime spectra[2]. We used a standard lifetime spectrometer[2] with a time resolution characterized by its full width at half maximum being about 400 psec.

For the positron source, 20μCi of ^{22}Na in the form of NaCl was sandwiched between two nickel foils of thickness 1 mg/cm^2. The molybdenum samples were put one on either side of the source and this sandwich then placed between the two γ-ray detectors. Analysis of the positron lifetime spectra obtained was carried out by use of the computer program Positronfit[12]. It deconvolutes the measured spectra and corrects them for the positrons annihilating in source nickel foils (ca 10% of the positrons), the resulting parameters of the analysis being the lifetimes of the decaying exponentials and their relative intensities (i.e. the areas of each component relative to the total area of the spectrum). The measured spectra for irradiated samples were resolved into two exponentials, a shortlived one (τ_1) from positrons in the bulk material and a longlived one (τ_2) from positrons trapped in defects[11]. The filled circles in Fig. 1 show the variation of τ_2 with temperature. Only one lifetime component with τ = 118±2 psec was present in the nonirradiated samples.

A positron annihilation angular correlation curve shows the distribution of angles between the two γ-quanta resulting from an electron-positron annihilation event. The annihilation quanta are emitted in almost opposite directions, a small deviation from 180° being proportional to the total momentum of the annihilating pair. Since the positron is thermalized before annihilation the momentum is almost exclusively due to the electron, and, roughly speaking, is an angular correlation curve, therefore, showing the momentum distribution of the electrons with which the positron annihilates[2]. We used a standard linear slit configuration[2], with each of the two detectors covering a solid angle, as seen from the specimen of 1.44 mrad x 178 mrad. A 30 mCi $^{22}NaCl$ external positron source was used for the measurements, giving around 1.8 x 10^5 counts in the peak of a curve in a 20 hours run. The angular correlation curves were analysed by the computer program Paacfit[13] which fits a measured curve by a sum of gaussians. In this way a useful mathematical description of curves or components of curves may be obtained[11]. It turned out that the nonirradiated specimens gave an angular correlation curve with a full width at half maximum (FWHM)

of 13.1 mrad ascribed to positrons annihilating in the bulk molybdenum. For the irradiated specimens at temperatures below 175°C an additional, narrower component (FWHM = 10.3 mrad) was present. In the range from 175°C to 400°C this component narrowed with increasing temperature and above 400°C the width was roughly constant with FWHM = 6.6 mrad. Hence in the final analysis a sum of these three characteristic curve components was fitted to each of the measured curves leaving the computer to determine their relative intensities (i.e. the area of each component divided by the total area)[11]. Fig. 2 shows the relative intensities of the 10.3 mrad and 6.6 mrad components (termed "Vacancies" and "Voids" respectively) as function of annealing temperature.

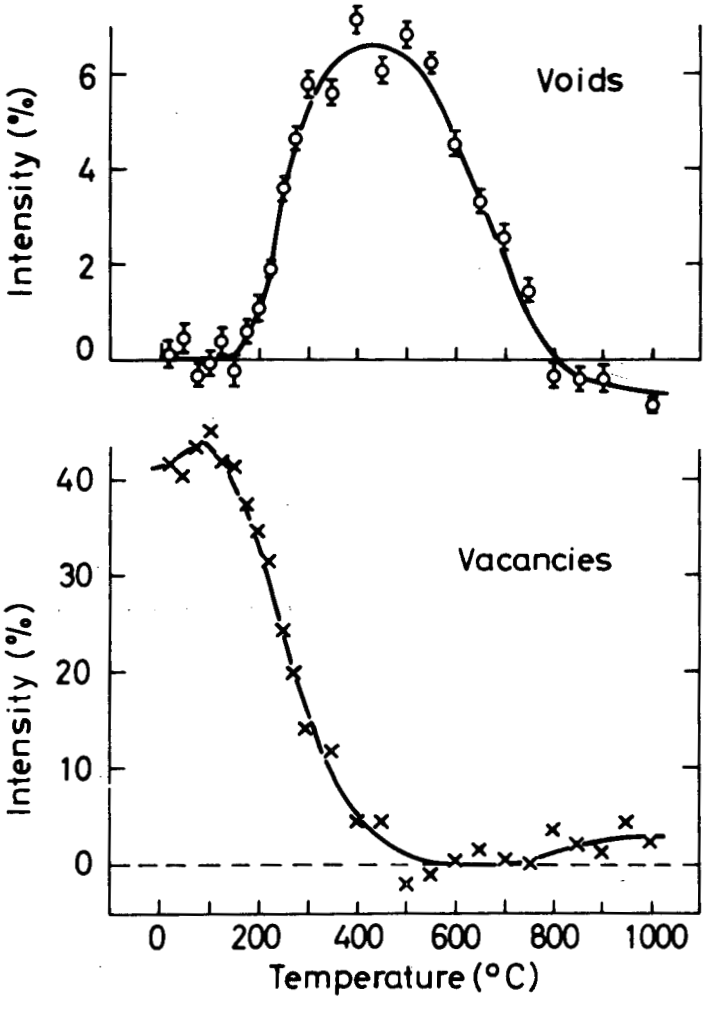


Fig. 2. Intensities of angular correlation curve components ascribed to positrons trapped in vacancies (FWHM = 10.3 mrad) and voids (FWHM=6.6 mrad) as function of annealing temperature.

Specimens as irradiated and annealed to 400°C and 900°C were examined by transmission electron microscopy. At 900°C voids of about 30 Å diameter and a concentration of 1-5 x 10^{13} cm^{-3} were observed. At 400°C one void was found (not considered statistically significant) and in the as irradiated sample none.

DISCUSSION

First let us shortly discuss the effects on PAT parameters which will result from the presence of defects in a material. It is well-established that in many metals positrons will get trapped in vacancies when the concentration is above ca 10^{-7} vacancies pr. atom. A trapped positron will experience a lower electron density in the vacancy than in the bulk material and hence its lifetime against annihilation with an electron will increase compared to the bulk value. If several vacancies cluster and form positron traps with more space than in a mono-vacancy the electron-positron overlap will decrease even further and the positron lifetime increase above the vacancy lifetime. A similar effect is observed on angular correlation curves. Trapped in a vacancy a positron will annihilate primarily with the outer electrons of the atoms. These electrons have lower momentum on the average than have the electrons with which the positron annihilates when being in the bulk. The resulting angular correlation curve will, therefore, be narrower than a curve for the bulk material, and the more space the positron gets in the trap the narrower becomes the angular correlation curve. These expectations are in good agreement with experimental findings.[11]

In the present work the first important result regards the stage III recovery region (150° - 350°C). As mentioned previously the defects created by the irradiation are believed to be mainly mono-vacancies and maybe some divacancies. The change in resistivity suggests that around 8.5 x 10^{-5} vacancies pr. atom are created by the irradiation. Hence a large fraction of positrons must be trapped before they annihilate, and the τ_2 = 200 psec (Fig. 1) as well as the 10.3

mrad component (Fig. 2)* can reliably be ascribed to positrons trapped mainly in mono-vacancies. The large drop in resistivity in stage III, mainly due to annihilation of vacancies and interstitials, is accompanied by a strong increase in τ_2 to over 400 psec (Fig. 1) and a strong decrease in intensity of the angular correlation vacancy component at the expense of an intensity increase of a much narrower component (Fig. 2). This must mean that positrons now get trapped in defects with appreciably more empty space than in a mono-vacancy. Dislocations and hence dislocation loops seem to give lifetimes between the bulk and vacancy lifetimes[14,15], and thus the only reasonable explanation of the results is that three dimensional vacancy clusters (voids) which trap positrons are formed in stage III. This further implies that vacancies are the mobile species in stage III, since it seems very difficult to imagine vacancy cluster growth as a result of interstitial migration.

The second important result regards the annealing stages above 600°C. The resistivity decrease around 650°C is a result of the disappearance of vacancy loops formed in stage III[6,9]. τ_2 changes only little in this region, emphasizing that vacancy loops influence PAT parameters only to a small extent. Above 650°C τ_2 rises to reach 550 psec at 800°C showing that coarsening of voids takes place at the expense of their concentration (indicated by the decrease of the void component intensity in Fig. 2). Above 800°C the voids start to anneal out and at 1000°C complete annealing is obtained. Final confirmation of the presence of voids was given by the 900°C electron microscopy result. The very low concentration of voids demonstrates the sensitivity of PAT to large defects.

CONCLUSION

In the present work the annealing of electron irradiated molybdenum was followed by positron annihilation lifetime and angular correlation measurements as well as by resistivity measurements and transmission electron microscope observation. A clear picture emerges of the processes taking place in the most pronounced annealing stages.

In stage III vacancies migrate, some to annihilate with interstitials, some to form vacancy loops, and some to form small voids. Around 650°C the loops anneal out and voids start to coarsen before they disappear close to 1000°C. The fact that it is possible by PAT to follow the development of voids from mono-vacancies up to sizes where they can be studied by electron microscopy indicates the potential of this new technique in defect studies.

REFERENCES

1. A. Seeger, J. Phys. F: Metal Phys. 3, 248 (1973).
2. R. N. West, Adv. Phys. 22, 263 (1973).
3. O. Mogensen, K. Petersen, R. M. J. Cotterill, and B. Hudson, Nature 239, 98 (1972).
4. R. M. J. Cotterill, I. K. MacKenzie, L. Smedskjaer, G. Trumpy, and J. H. O. L. Träff, Nature 239, 99 (1972).
5. W. Triftshäuser, J. D. McGervey, and R. W. Hendricks, Phys. Rev. B 9, 3321 (1974).
6. K. Petersen, N. Thrane, and R. M. J. Cotterill, Phil. Mag. 29, 9 (1974) and Phil. Mag. (in press).
7. S. Mantl and W. Triftshäuser, Phys. Rev. Letters 34, 1554 (1975).
8. J. H. Evans, S. Mahajan, and B. L. Eyre, Phil. Mag. 26, 813 (1972).
9. J. H. Evans, AERE Report 7966 (1975).
10. L. Stals, J. Nihoul, J. Cornelis, and P. DeMeester, Phys. Stat. Sol. (a) 18, 283 (1973).
11. M. Eldrup, O. E. Mogensen, and J. H. Evans, J. Phys. F: Metal Phys. (submitted).
12. P. Kirkegaard and M. Eldrup, Computer Phys. Commun. 3, 240 (1972); ibid 7, 401 (1974).
13. P. Kirkegaard and O. Mogensen, Risö-M Report 1615 (1973).
14. B. T. A. McKee, S. Saimoto, A. T. Stewart, and M. J. Scott, Can. J. Phys. 52, 759 (1974).
15. The positron lifetime in dislocations in Mo seems to be close to 150 psec. K. Petersen (private communication).

INVESTIGATIONS OF NEUTRON IRRADIATED IRON BY POSITRON ANNIHILATION AND INTERNAL FRICTION MEASUREMENTS

M. Weller[+], W. Triftshäuser[++], and J. Diehl[+],
MPI für Metallforschung, Institut für Werkstoffwissenschaften, Stuttgart (+)
and Institut für Festkörperforschung, KFA Jülich (++), Germany

ABSTRACT

In iron neutron irradiated at low temperatures reactions of interstitial solute atoms with vacancies take place. Products of these reactions could be identified more clearly.

Introduction. Radiation damage in iron as well as in other b.c.c. metals is strongly influenced by small amounts of interstitial impurities. Recovery of iron after low temperature neutron (or electron) irradiation is not completely understood, especially not at higher temperatures, where vacancy migration is expected. Possible temperatures for vacancy migration, stated by different authors, extend from about 200 up to 500 K [1, 2, 3]. Quenching experiments, failured because of the superposition of carbide precipitation [3, 4]. For a further study of these problems, a combination of measuring techniques, which are specially sensitive to distinct defects, were used in this investigation: positron annihilation and internal friction measurements.

From internal friction measurements, information on the behaviour of defects with symmetry lower than that of the lattice, mainly interstitial impurities or self interstitials, can be obtained, as earlier experiments on neutron irradiated iron showed [5, 6]. Positron annihilation experiments, which are appropriate for the selective investigation of vacancies, have up to now been applied mainly to f.c.c. metals with vacancies in thermal equilibrium [7]. Recent experiments on neutron irradiated iron, doped with nitrogen and carbon [8], showed greater effects on positron annihilation

angular correlation than it could be expected from earlier observations [9]. This indicates, that also in iron positron measurements are very sensitive to vacancies.

Experimental. Polycristalline iron wires of 1 mm in diameter, were purified in dry hydrogen (resistivity ratio $R(300\,K)/R(4{,}2\,K) \approx 1000$). A part of the samples was doped with 85 or 160 at. ppm carbon in CH_4-H_2. Residual hydrogen was removed by annealing in vacuum. The neutron irradiations were carried out in the Karlsruhe reactor FR 2 at $\approx 20\,K$ [10]. Afterwards all samples were transferred in liquid nitrogen into the measuring apparatus for positron annihilation and internal friction.

Results and Discussion. Fig. 1 shows positron annihilation angular correlation curves of carbon doped iron measured at 77 K after irradiation with 6.10^{16} and 3.10^{17} n/cm^2 ($E > 0{,}1$ MeV) and after annealing at 670 K. With increasing neutron dose the coincidence counts at small angle increase, combined with a decrease at greater angles. A similar behaviour is found in f.c.c. metals such as copper, silver, or gold with vacancies in thermal equilibrium, however the relative effect is greater in the present case. Identical curves as for the annealed sample are obtained for purified iron and iron doped with carbon or nitrogen in the unirradiated state as well as after annealing at $\approx 670\,K$ [8]. This indicates full annealing of positron trapping defects at 670 K.

The annealing behaviour was investigated in more detail by measuring the coincidence counting rate at the peak of the angular correlation curve during isochronal annealing between 77 and 670 K. The measuring temperature was always 77 K, the temperature time steps were 10 K/10 min, from 390 K upwards 20 K/20 min (same as for the internal friction measurements). The results are shown in Fig. 2. The curves are normalized in respect to each other in the fully annealed state between 580 and 670 K.

Considering at first the data at 77 K, immediately after irradiation, the

peak counting rate (PCR) is increased by the neutron irradiation (compare Fig. 1). However, this increase is more pronounced in iron with carbon than in pure iron. For the lower neutron dose, there is nearly no change as compared to the annealed state for purified iron, whereas for doped iron a rise of about 15 % is observed. For the higher dose the increase of the PCR of doped iron has about twice the height of pure iron. This indicates a relatively strong dependence of positron trapping sites, i. e. of defect production during irradiation, on interstitial solute contents. Such a dependence of defect production from impurity contents was also found with resistivity measurements on iron doped with nitrogen [11] and niobium with nitrogen [12]. A reduction of the spontaneous recombination of Frenkel defects by interstitial impurities metals is considered to cause this effect.

The annealing curves show at higher temperatures basically similar stages for pure and doped iron, but also interesting differences. Between 77 and about 200 K the curves raise up to a more or less pronounced maximum. This temperature range coincides with annealing stages I and II in neutron irradiated iron [5], in which the largest part of the resistivity increase anneals out. The origin of the increase in the PCR is not fully understood as yet. As the PCR is not only determined by the concentration, but also by the arrangement of the trapping defects [13] rearrangements of vacancies in defect cascades produced during neutron irradiation and/or clustering of interstitials into dislocation loops might contribute to this effect. Since it is less pronounced in doped iron, interstitial impurity atoms seem to suppress partly such rearrangements. Between about 200 and 260 K all samples exhibit a decrease being larger for the doped samples than for the purified ones. This stage coincides with a recovery stage in iron, which is observed after irradiation with neutrons or electrons as well as after cold work [1]. Annealing out of interstitials previously trapped at impurities is considered to be a possible interpretation

of this stage.

At temperatures above 300 K, the PCR decreases in all samples until it reaches the value before irradiation at ~ 670 K. This annealing occurs in the purified samples in a strong annealing stage, being composed of two substages around about 400 and 550 K. A reliable interpretation of this relatively broad annealing stage in pure iron cannot be given before the low temperature increase of the counting rate is understood. Annealing out of vacancies and/or vacancy clusters may be possible.

In case of doped iron, however, a close correspondence between the annealing curves above 300 K and the annealing behaviour revealed by the internal friction measurements can be established[14]. In Fig. 2 both carbon doped samples show two distinct stages at about 320 to 380 K (≈ 50-100 °C) and 500 to 580 K (≈ 230-310 °C). In Fig. 3 the high temperature part from the curve of the sample with 3.10^{17} n/cm^2 is compared with the internal friction measurements[14], which were obtained with an inverted torsion pendulum (≈ 1 Hz). Plotted are isochronals of the heights of the carbon Snoek peak (at 36 °C) and of an additional internal friction peak, appearing at 90 °C.

As can be seen from Fig. 3 the main annealing stage of the PCR at 50-100 °C corresponds to a strong decrease of the carbon Snoek peak, that is that carbon atoms disappear from solid solution. From the coincidence of the temperatures of these two stages, the suggestion first made by Damask[15] can be proved rather directly, that migrating carbon is trapped at single or multiple vacancies. The increase of the Snoek peak at higher temperatures (dotted curve; the increase is in reality superimposed by a decrease due to precipitation of carbide) correlates well with the second, smaller stage in the PCR. In the same temperature range the 90 °C relaxation peak anneals out. From an analysis of the internal friction data[6], this peak was assigned to the relaxation of carbon-vacancy complexes formed by carbon trapping. This fits very well to the Snoek peak and

positron data. The annealing of these complexes apparently results in a reduction of the PCR (and in re-solution of carbon). From this it can be deduced, that the complexes themselves are weak trapping centers for positrons and anneal by dissociation. In addition, the vacancy type reaction partners of carbon must disappear immediately after dissociation, otherwise the PCR should increase.

Further conclusions can be drawn as regards vacancy annealing in iron: Since carbon reacts with vacancies at 50...100 °C on the one hand, vacancies (or defects of vacancy type) must be present (not annealed) at least up to these temperatures. On the other hand the temperature range of complex annealing (230...310 °C) sets an upper limit for the annealing of vacancies in neutron irradiated iron. For a detailed analysis, whether single or multiple vacancies anneal out, further investigations are necessary, although there are indications that they are single vacancies.

REFERENCES

1. J. Nihoul, Vacancies and Interstitials in Metals (A. Seeger et al. eds.), North Holland (1969).
2. H. Schultz, Scripta Met. 8, 721 (1974).
3. W. Glaeser and M. Wever, phys. stat. sol. 35, 367 (1970).
4. F. Ichikawa, K. Yamakawa and F. E. Fujita, Scripta Met. 6, 929 (1972).
5. H. Bilger, V. Hivert, J. Verdone, J.L. Leveque and J.C. Soulie, Intern. Conf. Vacancies and Interstitials in Metals, Vol. II, 751 (1968).
6. M. Weller and J. Diehl, Proc. 5th Int. Conf. Int. Friction Ultrason. Atten., Vol. I, 352 (1975).
7. B.T.A. McKee, W. Triftshäuser and A.T. Stewart, Phys.Rev.Letters 28, 358 (1972).
8. M. Weller, J. Diehl and W. Triftshäuser, Solid State Communications, in press.
9. C.L. Snead, Jr., A.N. Goland, J.H. Kusmiss, H.C. Huang, R. Meade, Phys. Rev. B 3, 275 (1971).

10. W. Decker, J. Diehl, K. Hain, H. Katheder and Ch. Leitz, Kerntechnik 8, 257 (1966).

11. H. Wagenblast, F.C. Schwerer, J.A. Horak, Rad. Effects 14, 203 (1971).

12. D. Keil, W. Decker, J. Diehl, Rad. Effects, in press.

13. S. Mantl and W. Triftshäuser, Phys. Rev. Lett. 34, 1554 (1975).

14. M. Weller and J. Diehl, Scripta Met., to be publ.

15. H. Wagenblast, A.C. Damask, J. Phys. Chem. Solids 23, 221 (1962).

FIGURES

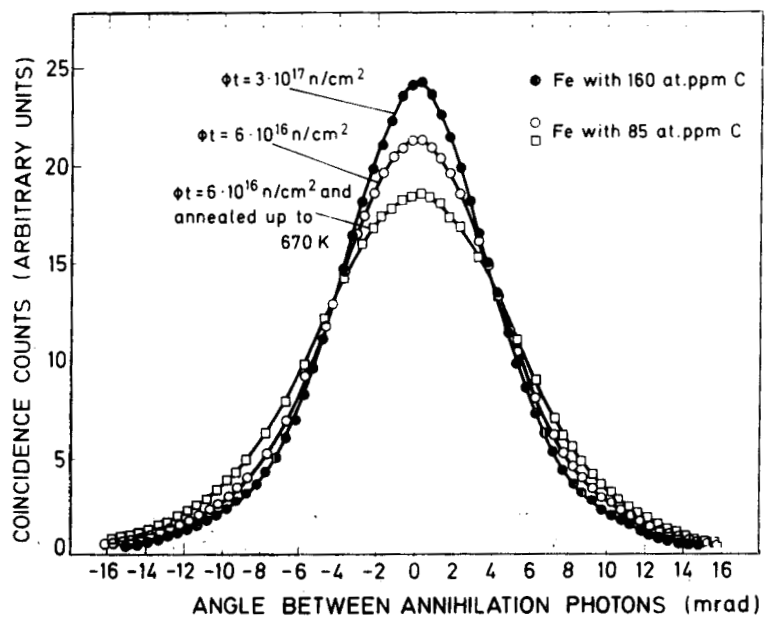


Fig. 1. Angular correlation curves for iron doped with carbon after neutron irradiation with 6.10^{16} and 3.10^{17} n/cm^2 and after annealing up to 670 K.

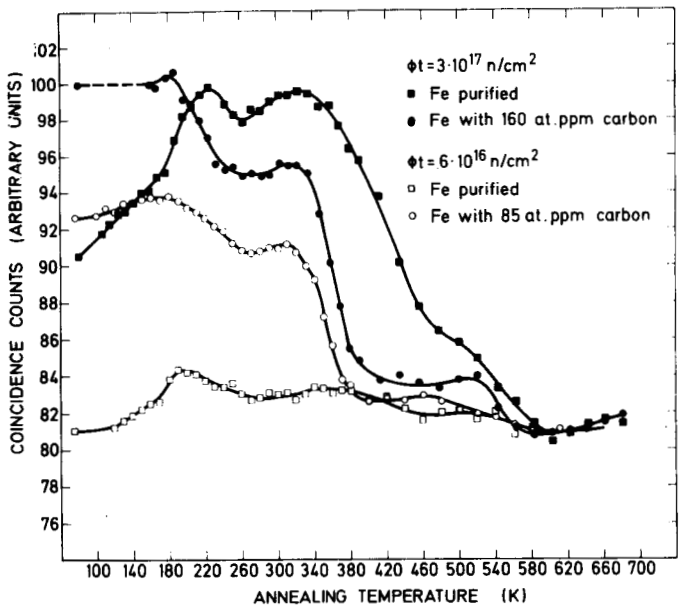


Fig. 2. Coincidence counts at the peak of the angular correlation curve at isochronal annealing for pure iron and iron doped with carbon ($\phi t = 6.10^{16}$ and 3.10^{17} n/cm^2).

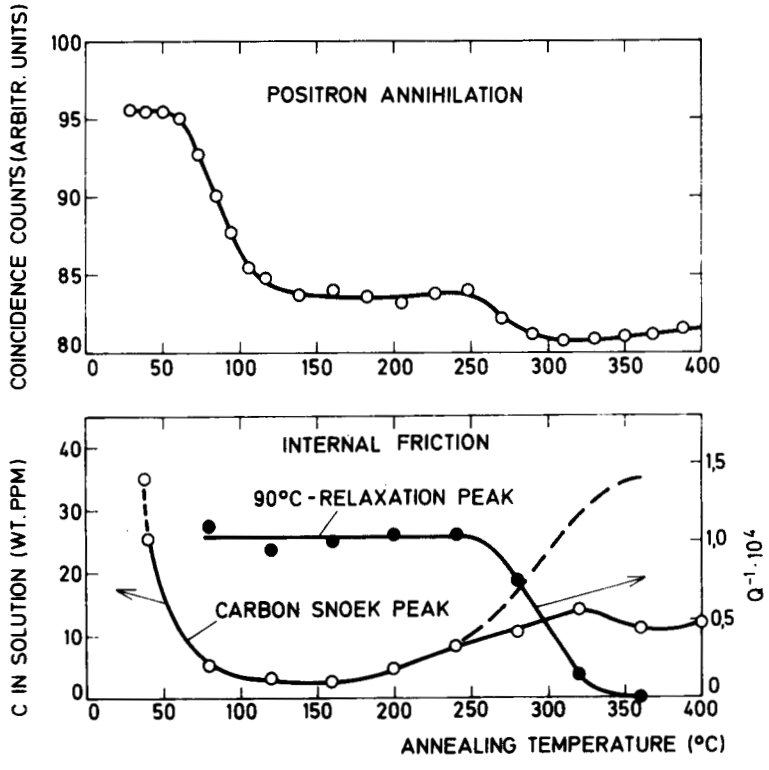


Fig. 3. Comparison of internal friction and positron angular correlation at isochronal annealing for irradiated iron ($\phi t = 3.10^{17}$ n/cm2) doped with 160 at. ppm carbon.

ANNEALING OF DISLOCATION LOOPS IN NEUTRON-IRRADIATED COPPER INVESTIGATED BY POSITRON ANNIHILATION

W. B. Gauster,* S. Mantl,
T. Schober and W. Triftshäuser
Institut für Festkörperforschung der Kernforschungsanlage Jülich
517 Jülich, Germany

ABSTRACT

Positron annihilation angular correlation measurements were carried out on neutron-irradiated copper as a function of annealing temperature. Two types of specimens were used - single crystals irradiated with fast neutrons, and ^{10}B-doped polycrystalline samples irradiated with thermal neutrons. All irradiations were at ~ 320 K. A structure in the annealing curve, not previously observed by other techniques, indicates that between 460 and 600 K the dislocation loops present after irradiation dissociate and more effective positron trapping sites are formed.

INTRODUCTION

Positron annihilation has become a defect-specific technique to study vacancies in thermal equilibrium as well as radiation-induced vacancies, vacancy aggregates and dislocation loops.[1] In such experiments it has been possible to follow vacancy migration and clustering during the annealing of electron-irradiated molybdenum[2] and copper[3] and to investigate void formation in neutron-irradiated molybdenum[4] and aluminum.[5]

Reported here are annealing studies on two sets of copper samples. In one case, single crystals were irradiated with fast neutrons; in the other, ^{10}B-doped copper polycrystalline specimens were exposed to thermal neutrons. Following both irradiations, done at ~ 320 K, positron annihilation angular correlation measurements were carried out after isochronal annealing steps.

*Visiting scientist, 1974-75. Permanent address: Sandia Laboratories, Albuquerque, New Mexico, 87115. Work supported by the United States Energy Research and Development Administration, ERDA.

SAMPLES AND IRRADIATIONS

Single Crystals

The neutron-irradiated crystals were furnished by F. W. Young, Jr., Oak Ridge National Laboratory. They were grown from 99.999 percent pure copper by a Bridgman technique and had uniform dislocation densities before irradiation of less than $10^6/cm^2$, as found from x-ray rocking curves. The samples were irradiated in the Oak Ridge Bulk Shielding Reactor to integrated neutron doses (energy > 0.6 MeV) of up to $10^{19} n/cm^2$. Previous positron annihilation angular correlation measurements on the same samples had shown an enhancement of peak counting rate as a function of neutron dose.[6]

Boron-doped Copper

For the second set of samples, nominally 99.999 percent pure copper was used as the starting material. Approximately 0.35 at.%, the room temperature solubility limit, of boron enriched in ^{10}B to a level of 92% was added to the copper. The boron isotope was obtained from Oak Ridge National Laboratory. The alloy was made by heating the copper-boron in an induction furnace at approximately 1400°C for 20 minutes in a reduced atmosphere of purified argon. After machining, the samples were annealed close to the melting point for about 5 hours. Three sets of the finished samples were irradiated in the Jülich MERLIN reactor to thermal neutron doses of approximately 3×10^{19}, 6×10^{19} and 10^{20} n/cm^2.

Damage was produced in the samples as a result of the reaction $^{10}B(n,\alpha)^7Li$, which takes place when a ^{10}B atom captures a thermal neutron. The α particle has an energy of 1.474 MeV, the ^7Li, 0.842 MeV.[7]. The ranges of the two particles are different, so that it is possible to distinguish concentric spherical damage shells around boron precipitates. Figure 1 shows these characteristic shells, which have been observed in similar studies.[8,9] The inner sphere is associated with damage by the lithium, the outer by helium. Both regions of damage consist principally of dislocation loops. The electron microscopy showed, however, that

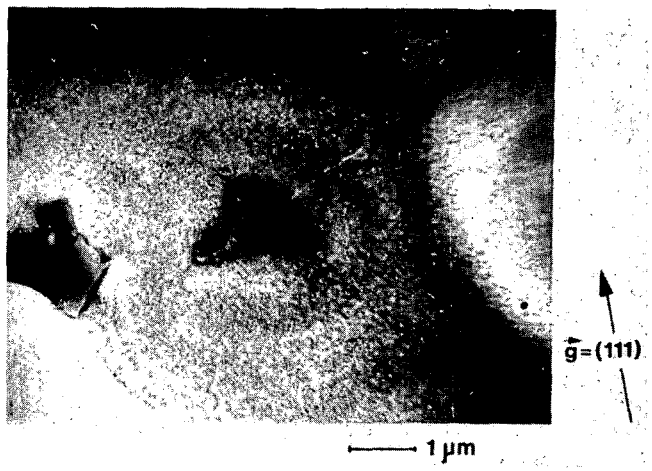


Fig. 1. TEM bright field image of spherical damage shells in Cu-B specimen, (110)-orientation.

there were very few such precipitates in the samples used for the present experiments, and that most of the boron had gone into solution. The damage was thus uniform throughout most of the sample material. Figure 2 shows electron micrographs of the two types of sample material: a) is the ^{10}B-doped copper irradiated with thermal neutrons; b) is the copper single crystal irradiated with fast neutrons. In both cases the "black spot" damage that is associated with dislocation loops predominates. This correspondence in the damage structure as seen by electron microscopy is supported by the overall similarity in the annealing behavior of the two types of samples as observed by positron annihilation, which is discussed next.

ANGULAR CORRELATION MEASUREMENTS

The sample and detector geometry was the same as one used previously for measurements on non-irradiated metal samples as a function of specimen temperature.[10] Thus the heating for the annealing steps was done without having to remove the sample from the measurement apparatus. After a preliminary run in which increments of 10% of the absolute temperature of the preceding steps were used, 5% increments with 20-minute holding times were followed in all annealing measurements.

The positron source was a thin disc of ^{64}Cu, with an initial activity of approximately 800 mCi. Each source was used for 24 hours. At several temperatures a complete angular correlation curve was mapped out; more usually coincident counts at the peak of the correlation curve only were

recorded, with a slit resolution of 2 mr and total counts per data point of the order of 3×10^5.

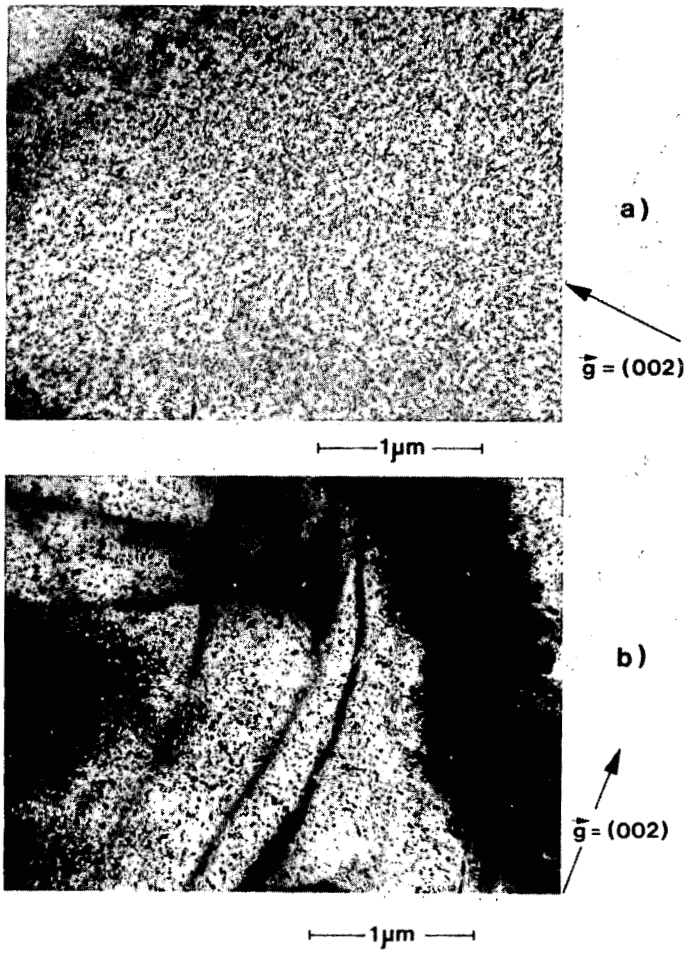


Fig. 2. Kinematical TEM bright field image, (110)-orientation. a): ^{10}B-doped Cu irradiated with thermal neutrons; b) Cu single crystal irradiated with fast neutrons.

ANNEALING CHARACTERISTICS

The peak angular correlation counts as a function of annealing temperature, corrected for source decay, for a neutron-irradiated copper crystal are shown in Fig. 3. For comparison, the results of integral diffuse x-ray scattering measurements[11] on similarly grown and irradiated copper crystals are shown on the same graph. As discussed in Ref. 11, electrical resistivity data follow the same curve, within measurement

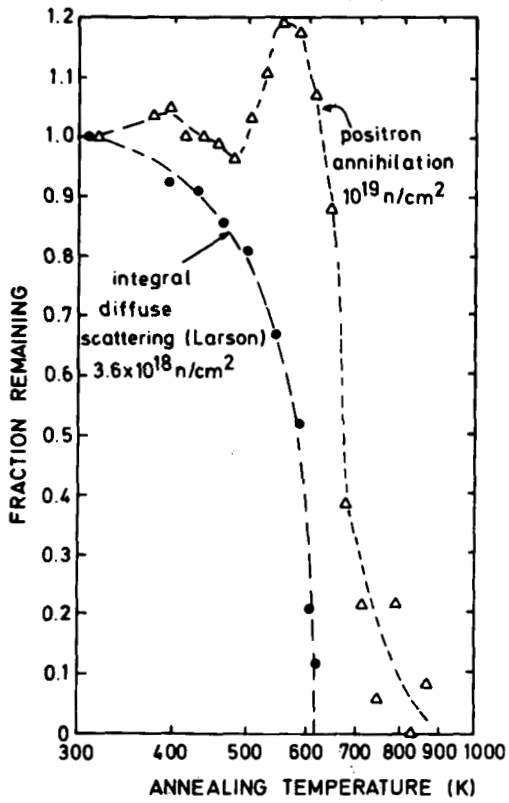


Fig. 3. Annealing characteristics of neutron-irradiated copper as measured by positron annihilation and by integral diffuse x-ray scattering

error, as the diffuse scattering points. The normalization in the plot is such that the value of the parameters for the irradiated samples is one, and the value before irradiation and after complete annealing is zero.

The most striking feature of the plot is the rise, peaking for an annealing temperature of about 560 K, in the positron annihilation peak counts. The diffuse scattering and resistivity values are sensitive primarily to the total number of defects, while positron annihilation characteristics have been shown to reflect the state of aggregation of "open volume" defects. Thus the measurements indicate that in the temperature interval of approximately 480 K - 600 K the originally dominant defect type may be replaced by more effective positron trapping sites.

Similar measurements on a sample irradiated to 10^{18} n/cm^2 showed the same behavior. The peak occurred at the same temperature as for the 10^{19} n/cm^2 sample, but it was less pronounced.

The results for the boron-doped copper, irradiated to 10^{20} n/cm^2 thermal are shown in Fig. 4. The peak is seen to occur at the same temperature as for the other samples, its height corresponding to that for the 10^{18} n/cm^2 fast-neutron-irradiated pure copper sample. An additional feature is noted: At about 800 K there is another increase in the count rate, and even after annealing at 1000 K it does not return to the pre-irradiation value. This small peak, which may have to do with aggregation of the helium present in the sample because of the decay of the boron, will be the subject of further investigation.

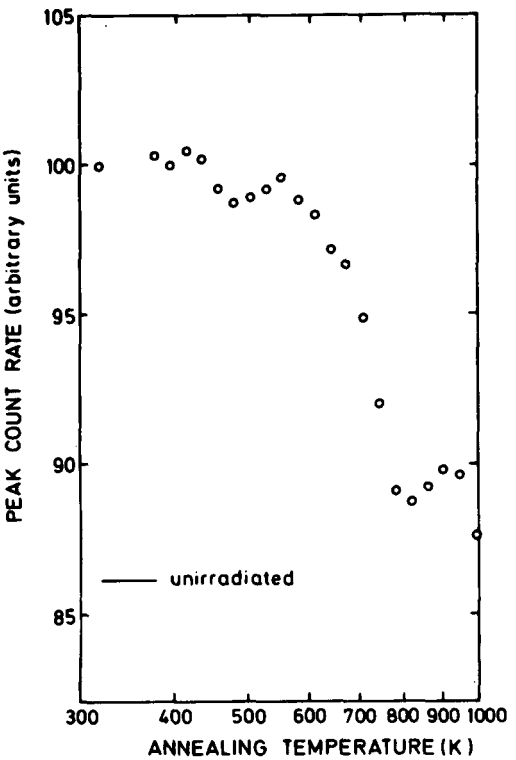


Fig. 4. Annealing characteristics of thermal-neutron-irradiated Cu-0.35 at.% ^{10}B as measured by positron annihilation.

The fact that the peak at 560 K in the annealing curve is seen for both sets of samples indicates that it is not associated with metallurgical features peculiar to either type of specimen. Two types of mechanisms suggest themselves to account for the effect. 1. The dislocation loops, at least the "vacancy-like" ones, could dissociate into single vacancies and small clusters. These aggregates could be stabilized sufficiently by the anisotropic strain fields about the interstitial-like loops to not find sinks during the annealing.[12] 2. A second model is that used to interpret annealing stage VI of neutron-irradiated molybdenum[4] in terms of the growth of voids at the expense of dislocation loops with a subsequent coarsening of the voids.

Because of the magnitude of the peak in the case of the 10^{19} n/cm^2 fast-neutron-irradiated sample, similar to the large effect seen due to voids in neutron-irradiated aluminum,[5] it is likely that void formation does play a role.

CONCLUSIONS

The annealing curves of copper neutron-irradiated above room temperature have been shown in positron annihilation measurements to have significant structure that has not been observed by other methods. The data indicate that in a narrow temperature interval the dislocation loops present after irradiation become unstable and that vacancy clusters or voids are formed before annealing is completed.

REFERENCES

1. A recent review of work on metals is W. Triftshäuser, Festkörperprobleme XV, 381 (1975).
2. J. H. Evans and M. Eldrup, Nature 254, 685 (1975).
3. S. Mantl and W. Triftshäuser, Phys. Rev. Letters 34, 1554 (1975).
4. K. Petersen, N. Thrane and R. M. J. Cotterill, Phil Mag. 29, 9 (1974).
5. W. Triftshäuser, J. D. McGervey and R. W. Hendricks, Phys. Rev. B 9, 3321 (1974).
6. W. B. Gauster and S. R. Dolce, Solid State Commun. 16, 867 (1975).
7. H. A. Bethe, Rev. Mod. Phys. 22, 213 (1950).
8. P. Vela, J. Hardy and B. Russell, J. Nucl. Mater. 26, 129 (1968).
9. A. Hishinuma, Y. Katano and K. Shiraishi, J. Nucl. Mater. 52, 103 (1974).
10. W. Triftshäuser and J. D. McGervey, Appl. Phys. 6, 177 (1975).
11. B. C. Larson, J. Appl. Cryst. 8, 150 (1975).
12. H. Trinkaus, private communication.

CRITICAL CURRENT CHANGES IN Nb_3Sn IRRADIATED WITH FAST NEUTRONS AT 6 K*

B. S. Brown, R. C. Birtcher, T. H. Blewitt, and D. G. Wozniak
Materials Science Division
Argonne National Laboratory
Argonne, Illinois 60439
USA

ABSTRACT

The critical current (J_c) was measured in Nb_3Sn as a function of neutron dose at 6 K up to 1.8×10^{18} n/cm^2 (E > 0.1 MeV). An increase in J_c of up to 33% at H = 32 kOe was observed after 1.2×10^{18} n/cm^2 in material with a high unirradiated J_c of 1.5×10^6 A/cm^2 at 4.2 K. Decreases were observed in J_c after higher doses and the size of the increase in J_c and dose of maximum J_c were a function of magnetic field. The dose and field dependence of the J_c changes are explained by a model that considers the changes in flux pinning and J_c due to changes with dose in critical temperature, upper critical field, and defect micorstructure. Observation of the change of the thermal transition to the normal state are understood by considering the radiation damage in the Cu-Sn stabilizing cladding.

Multifilament copper-clad Nb_3Sn wires** were irradiated in a fast neutron spectrum at 6 K up to 1.8×10^{18} n/cm^2 (E > 0.1 MeV).[1] The critical current (J_c) was measured without warm-up as a function of dose and applied magnetic field up to 32 kOe. Important considerations in the experiment were that the irradiation was performed at cryogenic temperatures and the unirradiated J_c (J_{co}) was high being 1.5×10^6 A/cm^2 at 32 kOe and 4.5 K. All previous studies of the effects of neutron irradiation on the superconducting properties of Nb_3Sn were either made with low J_{co} material or irradiated at ambient reactor temperatures (~100°C).

*Work supported by the U.S. Energy Research and Development Administration

**Wires were supplied by M. Suenaga of Brookhaven National Laboratory.

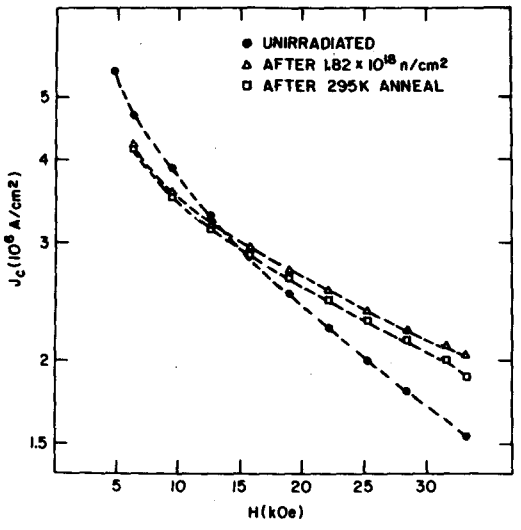


Fig. 1. Critical current of Nb_3Sn during irradiation and annealing.

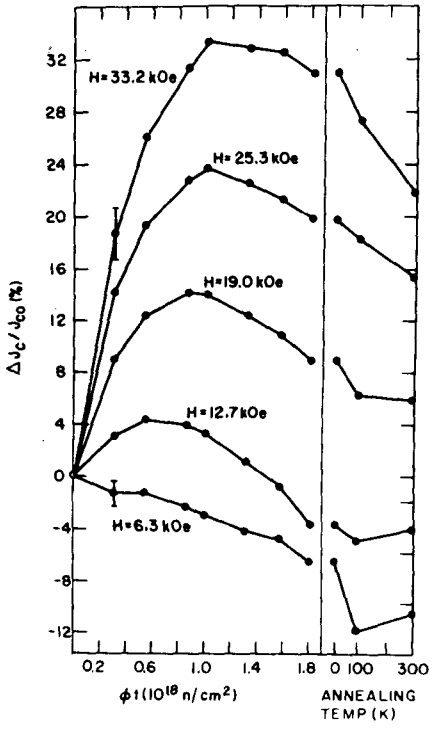


Fig. 2. Fractional change of critical current as a function of field, dose and annealing temperature.

The results of the irradiation are shown in Figures 1 and 2 with $\Delta J_c = J_c - J_{co}$. It is seen in Fig. 2 that even for material with a high J_{co}, J_c ($H > 6$ kOe) can be increased upon irradiating with fast neutrons at 6 K. The increase was largest at the highest field with decreases occurring at low fields. As the dose was increased, J_c increased to a saturation value and then decreased for higher doses with the saturation dose being largest for the highest field. No change in the critical temperatures T_c was measured (±1 K) and it was, therefore, estimated that T_c decreased $\leq$ 1 K at the highest dose (T_{co} = 17.5 K). Approximately 15% of the change in J_c recovered after an 83 K anneal and 25% by 295 K. These J_c changes are explained by a model that considers the change in J_c resulting from the neutron irradiation as due to three terms: changes in T_c (and, therefore, the thermodynamic critical field H_c), changes in H_{c2} resulting from the decrease of the

electronic mean free path, and changes in the defect microstructure. It is probable that the initial increase in J_c is due to the enhanced pinning from cascades. The saturation and eventual decrease in J_c at higher doses are due to a saturation in the cascade pinning that occurs after a dose at which the deleterious effects of T_c and H_{c2} changes become significant.

The field dependence of the saturation dose can be qualitatively explained on this basis, if one realizes that the most fundamental measure of the flux pinning in a type-II superconductor is the volume pinning-force density F_p ($=J_cB$) as a function of reduced magnetic field $h = H/H_{c2}$, where H_{c2} is the upper critical field.[2] It has been observed for many of the high-field superconductors that the pinning-force density obeys a scaling law of the form

$$F_p = H_c^m f(h,d) \tag{1}$$

where the exponent m is $\sim$2.5, and f(h,d) is a function of the reduced field h and the defect microstructure represented by d.[3] The variables d and h can be separated by expressing the field dependence as

$$f(h,d) = A(d)\ h^n(1-h)^2 \tag{2}$$

where n is a constant. The dose dependence of the three terms in F_p (T_c, H_{c2} and d) can be seen by calculating the differential change in F_p with dose:[1]

$$\frac{\Delta J_c}{J_{co}} = \frac{\Delta F_p}{F_p} = \left[C_1 \frac{\partial \ln T_c}{\partial(\phi t)} + C_2(h) \frac{\partial \ln H_{c2}}{\partial(\phi t)} + C_3 \frac{\partial \ln A(d)}{\partial(\phi t)} \right] \Delta(\phi t) \tag{3}$$

The first term in brackets is negative, since T_c decreases with dose. The third term is positive as the pinning from the defect cascades increases with dose. However, at high doses saturation occurs as in the case of Nb[4] due to overlap of the neutron damaged regions and this term becomes smaller as a function of dose. The first and third terms are not functions of applied field, whereas the coefficient of the second term is strongly dependent on H, i.e., negative at low fields and positive at high fields. The change in J_c by this term is due to an

increase in H_{c2} from the radiation induced defects increasing the normal state resistivity. The observed behavior of $\Delta J_c/J_{co}$ being negative at low H and positive at higher H can be accounted for by correctly chosing the magnitudes of C_1, C_3 and $C_2(h)$. Moreover, since the magnitude of the positive third term decreases with dose the field above which $\Delta J_c/J_{co}$ is positive should increase with dose as is observed. The cascade overlap is seen to be significant after low doses, since a peak is observed at 6×10^{17} n/cm^2 for H = 12.7 kOe, which is consistent with the observations in Nb[4] since this is only slightly lower than the saturation dose observed in Nb. This model could not be quantitatively tested since it was not possible to install a magnet capable of measuring H_{c2} (>130 kOe).

The thermal transition current I_T which corresponds to the complete transition to the normal state was also measured and is shown in Fig. 3. The peak in I_T versus dose occurs at a smaller dose for all applied fields than the peak in J_c. The transition from the superconducting to the normal state depends on the applied field, current density, and heat generated by the voltage drop across the sample. I_T depends on both thermal and fundamental superconducting properties. The Nb_3Sn layers are embedded in a Cu-Sn alloy, and the increase in normal-state resistivity with irradiation and the Wiedemann-Franz law indicate that the thermal conductivity of the cladding will decrease with dose. Therefore, I_T will depend on the F_p changes, as discussed above, and on the decrease in the thermal conductivity of the cladding as the dose increases.

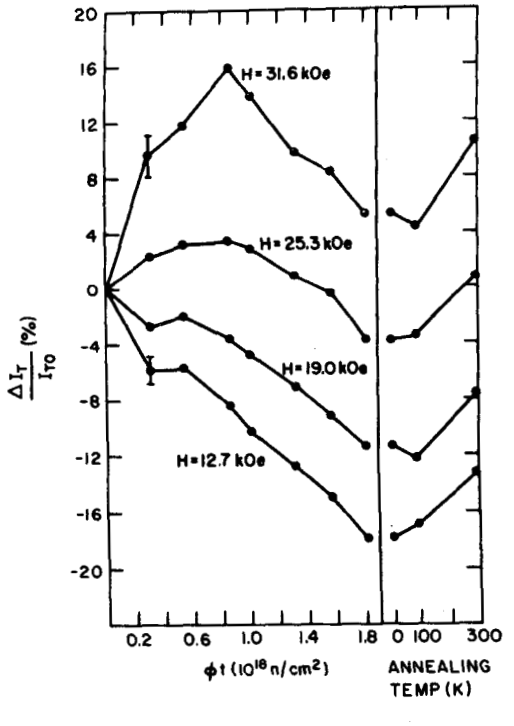


Fig. 3. Fractional change of thermal transition current.

As the capability of the cladding to conduct heat from the Nb_3Sn decreases with dose, it is expected that I_T should decrease with dose more rapidly than J_c as observed. The apparent inconsistent increase in I_T during annealing also can easily be understood when the cladding is considered. Figure 3 shows that only 25% of the J_c change recovers after a 295 K anneal. However, it is expected that more than 60% of the resistivity increase in the cladding recovers by 295 K. The thermal conductivity returns to within 40% of its unirradiated value, whereas 75% of the J_c enhancement remains, with the result that I_T increases.

ACKNOWLEDGMENTS

The authors gratefully acknowledge the experimental assistance of T. L. Scott and the many helpful discussions with E. J. Kramer.

REFERENCES

1. B. S. Brown, T. H. Blewitt, D. G. Wozniak and M. Suenaga, to be published in the Journal of Applied Physics, December 1975.
2. A. M. Campbell and J. E. Evetts, Adv. in Physics 21, 199 (1972).
3. E. J. Kramer, J. Appl. Phys. 44, 1360 (1973).
4. B. S. Brown, Proc. of International Discussion Meeting on Flux Pinning in Superconductors, St. Andreasburg, Germany (September 1974), Akademie der Wissenschaften, Göttingen 1975, p.200.

NEUTRON IRRADIATION DAMAGE ON THE SUPERCONDUCTING PROPERTIES IN VANADIUM AND Nb-Ti ALLOYS

H.Tsubakihara*, S.Katoh, M.Nishimoto, and T.Okada
Department of Nuclear Engineering, Osaka University
Yamadakami, Suita, Osaka, 565, Japan

ABSTRACT

A new model of radiation induced reduction in critical current density of superconductor has been proposed. The "breakup model" is based on the breakup of the precipitates acting as pinning centers due to incident neutrons. This model can explain not only the degradation of J_c but also the decrease in T_c occurring in α-precipitated Nb-Ti alloys. Responsible result has been obtained with X-ray diffraction intensity measurements.

INTRODUCTION

Neutron irradiation affects on superconductivity mainly in two ways; (i) radiation-induced defects act as pinning centers, resulting in the enhancement of critical current density J_c, and (ii) radiation-induced defects shorten the mean free path of conduction electrons leading to the reduction in critical temperature T_c and upper critical field H_{c2}. These effects are obvious in pure superconducting metals[1-6] and in at least qualitative agreement with theory.

A number of investigations on irradiated superconducting alloys[5,7-11] exist yielding valuable information about the change in J_c, which are important from the applicability of these alloys to magnets in fusion reactors and particle accelerators depending on the ease of fabricability, high H_{c2} and high J_c. The radiation induced change in superconducting properties of these alloys, however, did not always correspond even qualitatively to the theory, mainly because of their rather complicated

---

*Present address: Faculty of Science and Technology, Department of Electrical Engineering, Kinki University; Higashiosaka, Osaka, Japan.

metallurgical structure.

We have already reported a part of experimental study on the basic problem of interactions between flux lines and reactor irradiation induced defects[2]. In this paper we will discuss the mechanism of radiation-induced reduction in J_c of Nb-Ti alloys which may eventually become important component in fusion reactor magnets. We have made a systematic study covering two kinds of Nb-Ti alloys, with particular attention to finding the differences in the effect of radiation arising from differences in metallurgical structure of samples, which was varied by changing the duration of aging.

EXPERIMENTALS

Copper-clad wires of Nb-47.6at%Ti and Nb-59.8at%Ti(named #A and #B, respectively), 0.25mm in core and 0.35mm in outer diameter, were formed by cold working to an area reduction ratio of 99.998 and 99.87%, respectively, and aged at 380°C for $0 \sim 1 \times 10^4$min.

The standard four terminal method was used to obtain J_c and T_c. The value of J_c was measured in a transverse magnetic field H(up to 10T) at 4.2K. The value of T_c was defined as midpoint of the super-normal transition curves of the samples. The temperature of sample was controlled by precisely adjusting the position of it above the surface of liquid helium and measured using Ge sensor. The growth of the precipitates upon aging was examined by X-ray diffraction using goniometer attached to a Rigakudenki Rota-Flex, RU-200PL. A sample of 0.25mmϕ whose Cu cladding was removed, was mounted on the goniometer. Diffracted X-ray was filtered with graphite (0002) and monochromatic CuK_α radiation was counted by scintillator. The relative intensities of β-matrix phase and precipitate phase diffractions were studied using isochronal step scanning (step width; $0.01 \sim 0.02°$ and integration time/step; $40 \sim 80$sec).

All these measurements were made with sample both before and after irradiation. The irradiation to these samples was performed at reactor temperature, in the pneumatic tube or else in the hydraulic facility of the Kyoto University Research Reactor.

RESULTS AND DISCUSSIONS

Effect of Irradiation on Precipitates

All the X-ray diffraction angles observed in the unirradiated samples #B aged 10^4min coincide to the calculated values from pure Ti (hcp) and pure Nb (bcc). The phase of precipitates, therefore, has been identified as Ti-enriched α-phase (hcp).

The relative amount of α-phase in presence was ascertained from the measured intensity of the (110)α diffraction line. The peak height of the line was normalized for various samples with reference to the peak height of the (110)β line. Appreciable change of the fiber structures was not confirmed in back Laue photographs. The resulting ratios ($I_\alpha(110)/I_\beta(110)$) are, therefore, a qualitative description of the extent of α-phase precipitates. Relative intensity data showing precipitation behavior in the samples both #A and #B are presented in Fig.1 as I_α/I_β vs. aging time curves with various neutron fluences. It is apparent that small amounts of α-precipitates are formed by the aging longer than 5×10^3min (I_α/I_β=0.005 at 10^4 min) in sample #A. On the other hand, in the sample #B, the presence of

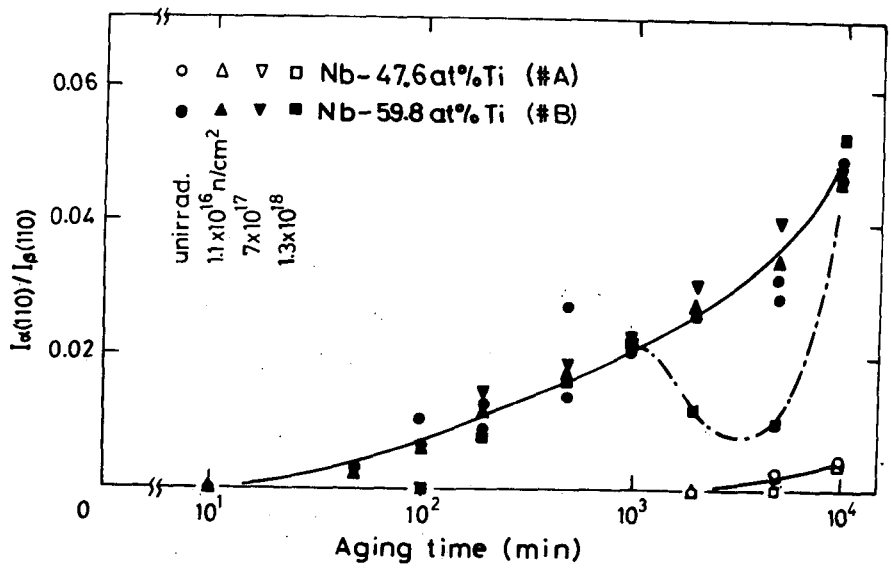


Fig.1 Extent of α-phase precipitation as a function of aging time at 380°C for Nb-47.6at%Ti and Nb-59.8at%Ti with various neutron fluence.

α-precipitates are confirmed after aging for 50min and the ratio of I_α/I_β is about 0.05 at $1x10^4$min. As can be seen from this figure, there is a rapid decrease of the relative intensity of #B aged between $1x10^3$ and $1x10^4$ min for the neutron fluence of $1.3x10^{18}$n/cm^2. This radiation-induced reduction gives an evidence to the breakup model of α-precipitates due to the irradiation.

Effect of Irradiation on Superconductivity

The value of J_c before and after neutron irradiation to the fluence up to $1.3x10^{18}$n/cm^2 is presented in Fig.2, measured under 5.05T. In the case of #A, the change is always in the positive direction. The direction of change is reversed in #B, except when aged for periods shorter than 50 min. As already pointed out, #B aged beyond 10min contain α-precipitates. Therefore, the present results indicate that the pinning effectiveness of α-precipitates in superconducting Nb-Ti alloys is reduced by the irradiation.

The effect on T_c brought by irradiation to a fluence up to $1.3x10^{18}$ n/cm^2 is presented in Fig.3. It is seen that the effect is almost nil for #A for all periods of aging, which is also the case with #B up to 100min aging. Beyond 100min, however, irradiation tends to reduce T_c, which indicate that the precipitates are disintegrated by the irradiation, and which serves to increase the Ti concentration in the matrix.

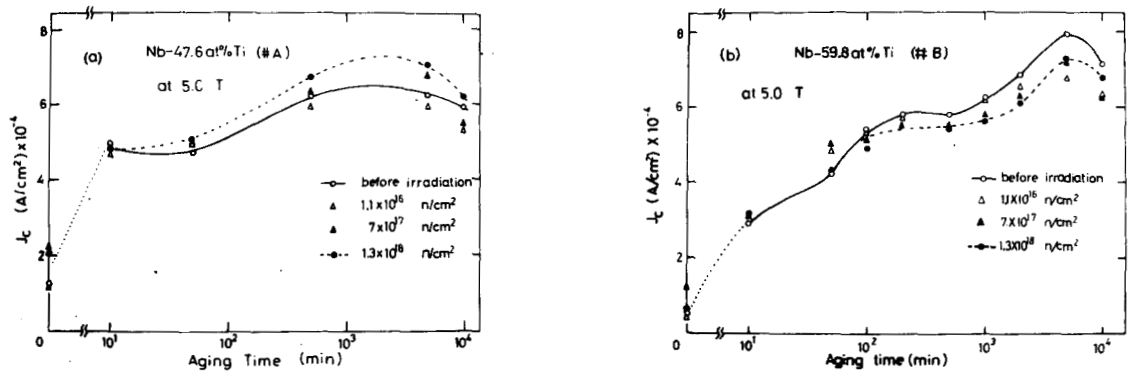


Fig.2 Effect of neutron fluence on J_c vs. aging time in sample #A (Nb-47.6at%Ti) and sample #B (Nb-59.8at%Ti).

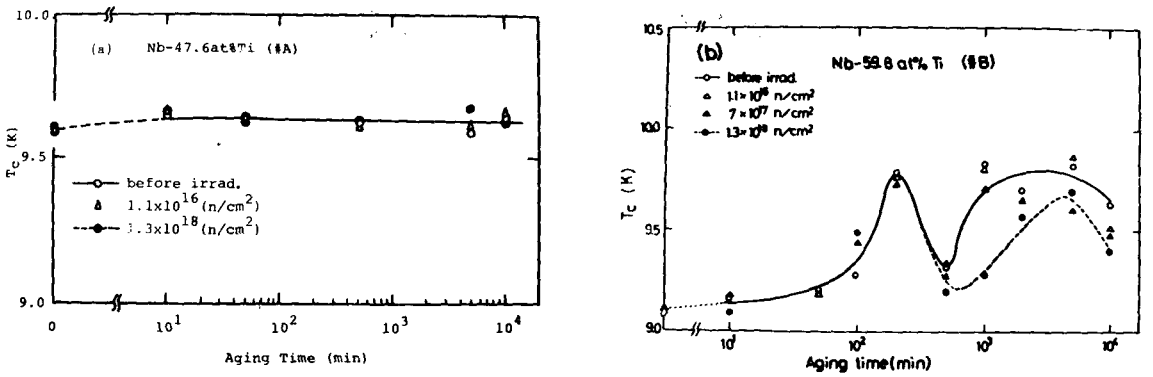


Fig.3 Effect of neutron fluence on T_c vs. aging time in sample #A (Nb-47.6at%Ti) and sample #B (Nb-59.8at%Ti).

CONCLUSIONS

Cullen and Novak[12] suggested a model as one possible explanation for the radiation-induced reduction on J_c, namely "shorting path model" as sketched in Fig.4. The defect site is a region where the free energy is lower than that of the matrix for flux lines. These region will act as pinning centers against flux line motion. If the incident neutrons produce in the barrier regions, low energy sites impinge upon one another and effective "shorting paths" will be formed for flux line motion. Thus the flux lines can be free to move along these paths, and J_c of this specimen is reduced by the irradiation. But we point out that even if the degradation of J_c is caused by shorting in the flux line motion paths due to defect overlap, this model does not seem to give us an apparent explanation for such decrease in T_c occuring in these heavily cold worked and precipitated Nb-Ti alloys. Similar suspicion was suggested by Pollock et al.[10] who observed the degradation in J_c, T_c and H_{c2} of Nb-Ti-V disordered alloys irradiated with neutrons.

A new model of radiation-induced reduction in J_c has been proposed, namely, "breakup model" which is based on the breakup of the precipitates acting as pinning centers due to insident neutrons. The breakup mechanism which can be anticipated on physical grounds is as follows.

(1) Mechanism due to displacement spike (shown in Fig.5 (a))

The solute atoms in the precipitated particles (Ti atoms in precipitates) are dissipated into matrix by energetic neutrons. Thus pinning effectiveness of the precipitates is weakened and the density of solute atoms (Ti atoms) in the matrix is enhanced by the irradiation.

(2) Mechanism due to thermal spike (shown in Fig.5 (b))

Struck atoms receiving energy up to displacement energy are not displaced but become "hot" relative to another lattice atoms at ambient temperature, and thus the thermal spike produces heated regions at a temperature above two-phase ($\alpha+\beta$) region. Precipitated particle is resolved into matrix by such a localized "solution treatment".

It is not clear which is dominant between these two mechanisms, but they can well explain the degradation of J_c in superconducting alloys.

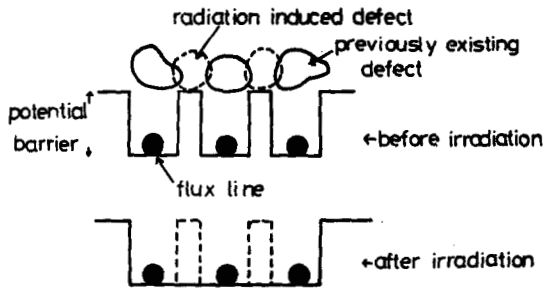


Fig.4 Schematic drawing of shorting path model (after Onishi[13]).

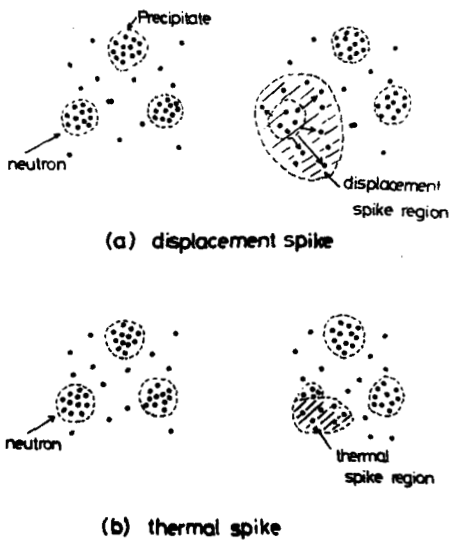


Fig.5 Schematic drawing of breakup mechanisms of precipitates due to neutron irradiation (after Liu et al.[14]).
Densities of black spots correspond to those of solute atoms.

The authors wish to thank T.Horiuchi, Y.Monju and S.Tsurutani of Asada Fundamental Research Laboratory, Kobe Steel Ltd., for their sample preparations and for valuable discussions. We are indebted to Dr. J.Yamamoto, Y.Tsuji, Y.Wakisaka and H.Makiyama of Low Temperature Center of Osaka University for their help in the experiments using liquid helium. Acknowledgement is also due to Dr. H.Yoshida of the Research Reactor Institute of Kyoto University for the several helpful discussions and help with the neutron irradiation.

REFERENCES

1. H.Tsubakihara, M.Nishimoto, T.Okada and T.Suita, Technol. Repts. Osaka Univ., 24, 37 (1974).
2. H.Tsubakihara, T.Okada and T.Suita, Mat. Sci. Eng., in press.
3. S.T.Sekula, J. Appl. Phys., 42, 16 (1971).
4. R.T.Kernohan and S.T.Sekula, J. Appl. Phys., 38, 4904 (1967).
5. P.S.Swartz, H.R.Hart, Jr. and R.L.Fleischer, Appl. Phys. Lett., 4, 71 (1964).
6. H. Berndt, N.Kartascheff and H.Wenzl, Z. angew. Phys., 24, 305 (1968).
7. M.Soell, 7th Sympo. on Fusion Technol., p311 (1972).
8. T.Sugisaki, T.Okada and T.Suita, Technol. Repts. Osaka Univ., 21, 385 (1971).
9. J.P.McEvoy, Jr. and R.F.Decell, Appl. Phys. Lett., 4, 43 (1964).
10. J.T.A.Pollock, V.Sadagopan and H.C.Gatos, Trans. Met. Soc. AIME, 245, 2350 (1969).
11. H.Tsubakihara, T.Okada, T.Suita, T.Horiuchi, K.Matsumoto and S.Tsurutani, J. Nucl. Sci. Technol., 11, 452 (1974).
12. G.W.Cullen and R.L.Novak, J. Appl. Phys., 37. 3348 (1966).
13. T.Onishi, Circulars of the Electrotechnical Lab. Rept., No.175 (1973).
14. K.S.Liu, O.Kawano, Y.Murakami, H.Yoshida, Radiation Effects, 15, 37 (1972).

THE EFFECTS OF REACTOR NEUTRON, 14-MeV NEUTRON AND ENERGETIC-CHARGED-PARTICLE IRRADIATIONS ON THE CRITICAL CURRENT IN Nb_3Sn*

Don M. Parkin
Los Alamos Scientific Laboratory
Los Alamos, New Mexico 87545

and

C. L. Snead, Jr.
Brookhaven National Laboratory
Upton, New York 11973

ABSTRACT

Multifilamentary Nb_3Sn wires have been irradiated at ambient temperature with HFBR neutrons, 14-MeV neutrons and 17-MeV protons. The fluence dependence of the critical current density (J_c) at 40 kG has been compared in these cases by calculating the corresponding damage energy/atom (dea). Results of this analysis show that the rapid reduction in the critical current in Nb_3Sn as described by Parkin and Schweitzer occurs at 0.2 ± 0.05 eV/atom for the HFBR and 17-MeV-proton irradiations, whereas no significant reduction in critical current has been observed after 0.29 eV/atom with 14-MeV neutrons. Extension of this analysis to published data on the effects of neutron and charged-particle irradiations both at ambient and low temperature on critical temperature (T_c) and J_c shows that the maximum value of J_c' occurs at $0.15 \pm .5$ eV/atom and that reductions in T_c are a function of eV/atom. A model based on site exchange disorder which accounts for these results is discussed.

INTRODUCTION

The effects of radiation on the critical current density (J_c) and critical temperature (T_c) of Nb_3Sn have been studied by a number of investigators[1-10] utilizing a variety of experimental techniques. A review of

*Work performed under the auspices of the United States Energy Research and Development Administration.

the published data shows that the majority of the investigators performed facility ambient temperature ($T > 50°C$) irradiations using energetic charged particles and reactor neutrons, with only a few experiments performed below 50K.[4,9,10] The general behavior of J_c under irradiation is that at low fluence J_c increases as a function of fluence, and if the experiment is performed long enough a maximum value in J_c, the magnitude of which is in part dependent on the initial value of J_c and the temperature and type of irradiation, is obtained. Upon further irradiations, J_c starts to decrease. Some experiments however have resulted in only increases[9] or only decreases[7] in J_c.

In this paper we present a model for the radiation-produced changes in J_c. This model is based upon two aspects of the radiation-produced defect cascade: defect agglomerates that act as flux pinning centers, and site exchange disorder in the A-15 lattice. This model is used to compare radiation-produced changes in J_c and the fluence dependence of reductions in T_c.

MODEL

The capability of both energetic-charged-particle and neutron irradiation produced defect cascades to produce defect structures that can act as flux pinning centers in superconductors with a resulting increase in J_c has been shown by a number of investigations.[1-6,8-10] Another established property of defect cascades is their ability to reduce the degree of order in ordered alloys. In particular, measurements of changes in the order parameter in neutron irradiated Nb_3Sn[11] and Nb_3Al[12] have shown a simple relationship between changes in T_c and the order parameter as calculated from a model by Aronin.[13]

The relationship between J_c and T_c in A-15 superconductors has been examined recently by Rassman and Muller.[14] They have shown that when J_c is plotted as a function of $\Delta T_c = (T_o - T_c)$, where T_o is the critical temperature of the ideal material and T_c is the measured critical temperature, J_c increases to a peak value at $\Delta T_c \approx 0.5 - 2$ K and then decreases as $J_c = A \exp[b(T_c - T]$. This behavior demonstrates that as T_c decreases,

there is an initial increase in J_c from defect pinning centers. At some critical amount of disorder in the A atom-chains the superconducting current in these chains is sharply reduced.

Based on the above results, we write the radiation-produced change in J_c as $\Delta J_c'$

$$\Delta J_c' = (J_c' - J_{c_o}) = g(T,p,\phi t) + h(d,\phi t) \quad (1)$$

where $g(T,p,\phi t)$ represents the effects of flux pinning on J_c and $h(d,\phi t)$ represents the effects of A-chain conductivity. The function $g(T,p,\phi t)$ has been shown to be a function of irradiation temperature T, irradiation type p, and irradiation fluence ϕt. We assume that $h(d,\phi t)$ is only a function of order (disorder) d, and fluence.

It is usually assumed that there is a minimum size for a radiation-induced defect cluster to be an effective pinning center. Wohlleben[5] has shown that for low-energy proton and deuteron irradiations of Nb_3Sn the magnitude of $\Delta J_c'$ (maximum) is related to the number of recoil cascades above $\approx$20 keV. This implies that for a given irradiation temperature, $g(t,p,\phi t)$ is proportional to the number of recoil cascades above some threshold energy. On the other hand, if we calculate the amount of radiation-produced disorder using the usual Kinchin and Pease type formulas for disorder based on replacement sequences and include electronic losses, we find that $h(d,\phi t)$ is a function of the damage energy cross section $E_D(E)$.[15] Let us assume we can express $h(d,\phi t)$ as

$$h(d,\phi t) = f(E_D\phi t) \quad (2)$$

$E_D\phi t$ is the damage energy per atom (dea) with units of eV/atom. This equation has two very important implications. First, radiation-produced changes in T_c should be a function of $E_D\phi t$ independent of experimental parameters such as temperature and irradiation type. Second, there is a value of $E_D\phi t$ where $h(d,\phi t) < 0$ and if $h(d,\phi t)$ decreases sharply enough then the maximum value of ΔJ_c should be a function of $E_D\phi t$.

RESULTS AND DISCUSSION

The appropriate damage energy cross section has been calculated for published data on radiation-produced changes in T_c and J_c (see Table I). As given in Table 1, the normalized spectrum-averaged damage energy cross section is defined as

$$\langle \bar{E}_D \rangle = \int_{E_1}^{E_2} E_D(E)\phi(E)\,dE \Big/ \int_{E_x}^{E_2} \phi(E)\,dE \qquad (3)$$

where E_1 and E_2 are the energy limits of the radiation spectrum, $E_D(E)$ is the energy-dependent damage energy cross section, $\phi(E)dE$ is the differential radiation spectrum and E_x is the low-energy cut off for which the radiation flux is given. With the corresponding values of $E_D(E)$ Equation 3 applies both to neutron and charged-particle irradiations.

For the neutron irradiation data the computer code DØN[15] was used to calculate $\langle \bar{E}_D \rangle$ and for the energetic-charged-particle data the Rutherford cross section was utilized in calculating $\langle \bar{E}_D \rangle$. The final value of $\langle \bar{E}_D \rangle$ given in Table 1 was obtained by separately calculating

Table 1. Comparison of the Effects of Irradiation on Nb_3Sn

Radiation Type	$\langle \bar{E}_D \rangle$ (b eV)	J_{cirr} (max) (particles/cm^2)	dea (eV/atom)	Material Type	Irradiation Temp	J_c (40 kG) (A/cm^2)	Ref.
HFBR	9.7×10^4	2×10^{18}	0.19	m.[4]	~60°C	$\sim 10^6$	7
CP-5	1.2×10^5	1.2×10^{18}	0.15	m.[4]	~6 K	$\sim 10^6$	10
PLUTO	9.7×10^4	9×10^{17}*	0.09	t.[5]	70°C	--	8
p^1-1 MeV	7.2×10^6	2.3×10^{16}	0.17	d.ℓ.[6]	~100°C	2×10^5	5
p^1-2 MeV	3.9×10^6	3×10^{16}	0.12	d.ℓ.[6]	~100°C	2×10^5	5
p^1-3 MeV	2.7×10^6	7×10^{16}	0.19	d.ℓ.[6]	~100°C	2×10^5	5
p^1-17 MeV	6×10^5	3×10^{17}	0.18	m.[4]	~60°C	$\sim 10^6$	this work
d^2-3 MeV	5.8×10^6	3.2×10^{16}	0.19	d.ℓ.[6]	~100°C	2×10^5	5
d^2-15 MeV	1.3×10^6	1×10^{17}*	0.13	v.d.[7]	~25 K	2.5×10^5	4
O^3-24 MeV	3.5×10^8	3×10^{14}	0.11	v.d.[7]	~110°C	4×10^5	6

[1] proton
[2] deuteron
[3] oxygen
[4] multifilimentary wire
[5] tape
[6] diffusion layer
[7] vapor deposited
* isolated fluence value

$\langle \bar{E}_D \rangle$ for Nb and Sn and obtaining an average value using a 3:1 Nb to Sn ratio. Relative to Nb this procedure increased $\langle \bar{E}_D \rangle$ by 4-10%. An exception to the above procedures was the 17-MeV-proton data, where only the results of Logan et al.[16] for Nb were used in obtaining $\langle \bar{E}_D \rangle$.

Table 1 summarizes a comparison of the maximum value of J_c' (40 kG) for a series of irradiation data in which sufficient fluence dependence was reported to establish J_c' (max). A good correlation is obtained by assuming J_c' (max) is a function only of $\langle \bar{E}_D \rangle \phi t$. Figure 1 gives the dependence of J_c' on $\langle \bar{E}_D \rangle$ for two types of data. Samples irradiated in

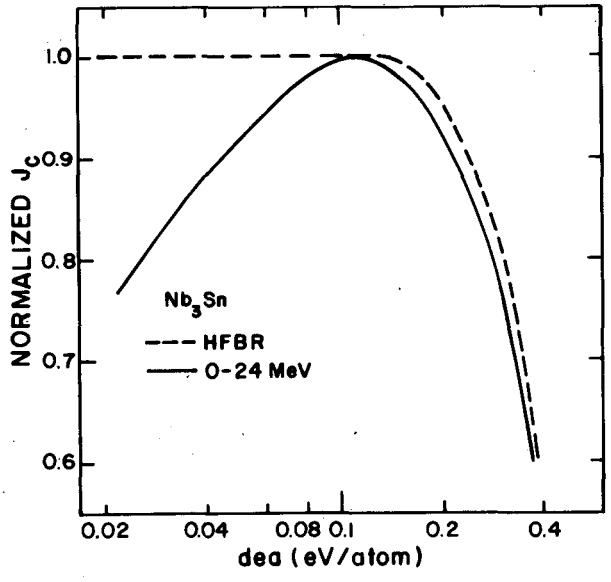


Fig. 1. Critical current, J_c, normalized to its maximum irradiated value as a function of damage energy per atom for neutron (HFBR ref. 7) irradiated and oxygen ion irradiated (ref. 6) Nb_3Sn.

the HFBR showed decreases in J_c' whereas the 0-24-MeV ion irradiations show an increase in J_c' followed by a decrease.

The data for Nb_3Sn samples irradiated with 14.9-MeV neutrons at the Lawrence Livermore Laboratory are not given in Table 1 since no significant reductions in J_c' (40 kG) have been seen. The samples have been.

irradiated to a fluence of 1 x 10^{18} n/cm^2. Using a value of $\langle \bar{E}_D \rangle$ = 2.9 x 10^5 beV gives a value of 0.29 eV/atom for the irradiation. This result suggests that for the damage effect described here the damage energy calculated for 14.9-MeV neutrons is an over-estimate relative to the other calculations.

Figure 2 compares the normalized critical temperature, $T_n = T_{co}/T_c'$, for three irradiations as a function of $\langle \bar{E}_D \rangle \phi t$. The neutron data (HFBR

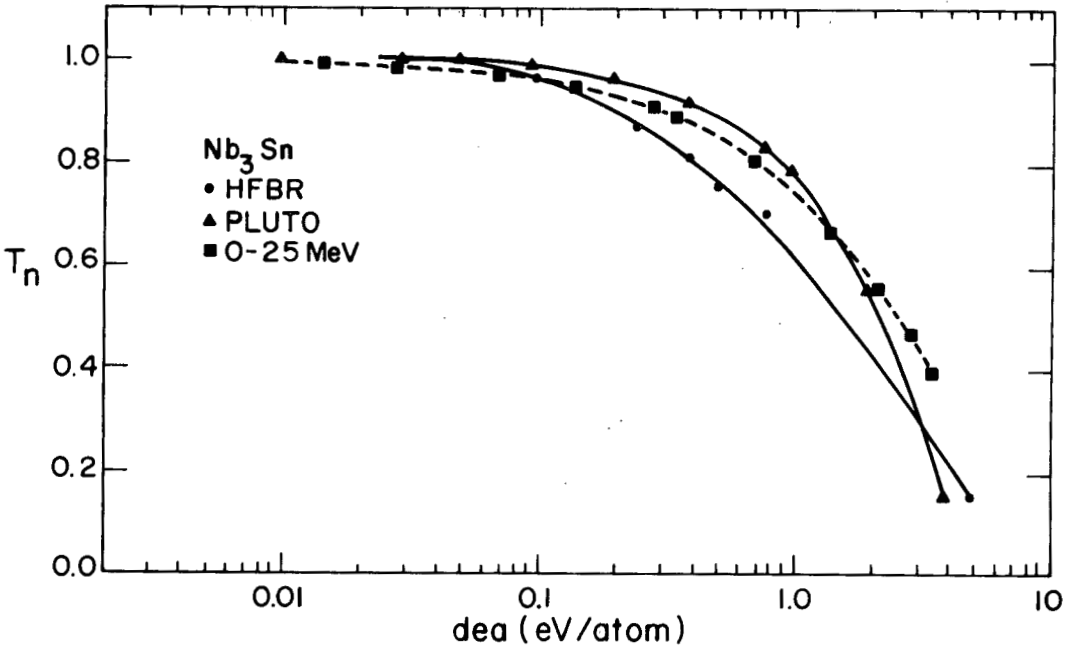


Fig. 2. Normalized critical temperature, $T_n = T_{co}/T_c'$ as a function of damage energy per atom for neutron (HFBR ref. 7., PLUTO ref. 8) irradiated and oxygen ion (ref. 17) irradiated Nb_3Sn.

and PLUTO) are ambient-temperature irradiations (see Table 1) whereas the 0-25-MeV[17] data are low temperature (<30 K). The data show good agreement. However, there is one important difference between the HFBR data and the other data. The HFBR data were obtained using an inductive technique which measures the volume-averaged T_c, whereas the other data were obtained using a resistive technique which measures the highest continuous T_c path. This difference in measurement technique could partly explain the relative increased sensitivity of the HFBR data to irradiation.

In summary it is concluded that the normalized spectrum-averaged damage energy cross section is an appropriate parameter to compare radiation-produced changes in T_c and the maximum value of J_c' in Nb_3Sn for energetic-charged-particle and reactor-neutron irradiations. In comparing 14-MeV-neutron irradiations, the calculated value of $\langle \bar{E}_D \rangle$ is an overestimate.

REFERENCES

1. G. W. Cullen, R. L. Novak, and J. P. McEvoy, Jr., RCA Rev. 25, 479 (1964).
2. P. S. Swartz, H. R. Hart, Jr., and R. L. Fleisher, Appl. Phys. Lett. 4, 71 (1966).
3. G. W. Cullen and R. L. Noval, J. Appl. Phys. 37, 3348 (1966).
4. H. T. Coffey, E. L. Keller, A. Patterson and S. H. Autler, Phys. Rev. 155 , 355 (1967).
5. K. Wohlleben, Z. Angew Phys. 27, 92 (1969).
6. G. Ischenko, H. Mayer, H. Voit, B. Besslein, and E. Handl, Z Physik 256, 176 (1972).
7. D. M. Parkin and A. R. Sweedler, IEEE Trans. Mag. 11, 166 (1975).
8. R. Bett, Cryogenics 14, 361 (1974).
9. M. Soell, H. Bauer, K. Boening and R. Bett, Phys. Lett. 51A, 83 (1975).
10. B. S. Brown, T. H. Blewitt, D. G. Wozniak, and M. Suenaga, J. Appl. Phys. (Dec. 1975).
11. A. R. Sweedler, D. G. Schweitzer, and G. W. Webb, Phys. Rev. Lett. 33, 168 (1974).
12. A. R. Sweedler and D. E. Cox, Phys. Rev. B 12, 147 (1975).
13. L. R. Aronin, J. Appl. Phys. 25, 344 (1954).
14. G. Rassmann and P. Muller, J. Less Common Met. 39, 335 (1975).
15. D. M. Parkin and A. N. Goland, Brookhaven National Laboratory Report, BNL-50434 (1974).
16. C. M. Logan, J. D. Anderson, and A. K. Mukherjee, J. Nucl. Mater. 48, 223 (1973).
17. B. Besslein, G. Ischenko, S. Klaumiinzes, P. Muller, H. Neumuller, K. Schmelz, and H. Adrian, Phys. Lett. 53A, 49 (1975).

STUDIES OF VOID FORMATION IN PURE METALS

J.M. Lanore, L. Glowinski*, A. Risbet**, P. Regnier, J.L. Flament,
V. Levy, Y. Adda.
Commissariat à l'Energie Atomique - Centre d'Etudes Nucléaires de Saclay - FRANCE

ABSTRACT

In this paper we will describe recent experiments on the effect of gases on the final configuration of vacancy clustering (void or loop), and on the local effects at dislocations.
The contribution of this data to our general knowledge of void formation will be discussed, and Monte Carlo calculations of swelling induced by irradiation with different particles presented.

INTRODUCTION

A great deal of theoretical and experimental studies on void formation have been published in the past several years, and are related in the proceedings of a few major conferences [1, 2, 3, 4, 5].

Despite the number of publications, the fundamental basis of void formation are still under discussion. Thereby, the usual steady state models of nucleation and growth fail to reproduce experimental results, especially if different types of irradiating particles are involved.

* Actually at Thomas J. Watson Research Center - Yorktown Heights N.Y. 10598

** Actually at Université des Sciences et Technologie de Lille
59 Villeneuve d'Asq. France.

The origin of this resides in the fact that if every one agrees that gases and dislocations are necessary to form voids, little is known on what happens in the vicinity of a dislocation or how gases influence the final configuration of vacancy clustering (void or loop).

In this paper we will first summarize the results already published[6] on local effects at dislocations. Then we will present experiments performed on well known materials irradiated by different types of particles, which will lead us to a model of void nucleation. The proposed mechanism will be tested by Monte Carlo simulation of void formation in copper irradiated by self-ions, electrons or neutrons in different experimental conditions.

EFFECT OF DISLOCATIONS

Two main informations have been taken out of our experiments.

1. Voids are seen to nucleate preferentially in the compression side of dislocations with an edge component. This fact seems to be general and has been observed for all types of irradiating particles and all the metals investigated. Examples of this are given of Fig. 1. Furthermore the presence of a certain number of dislocations

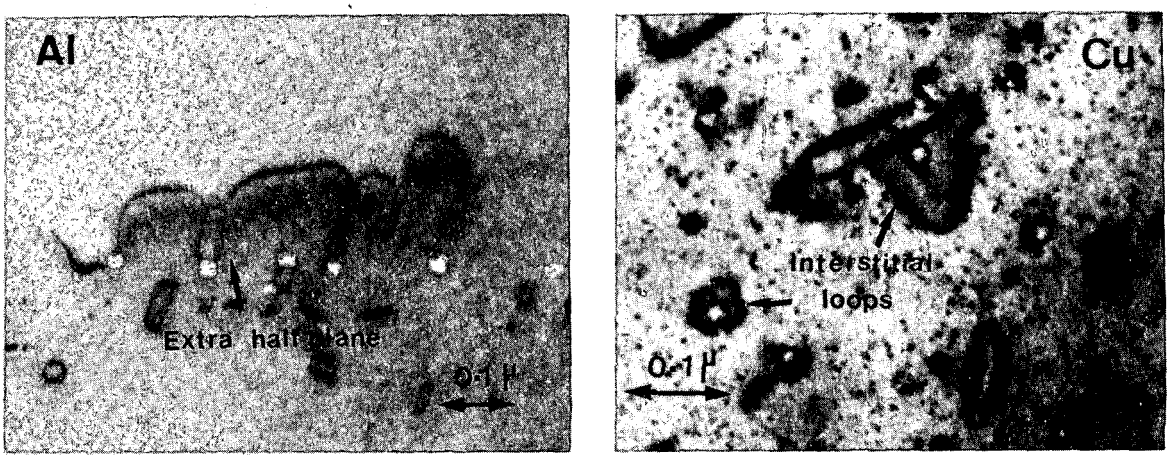


Fig. 1 - Nucleation of voids near dislocations

a) Neutron irradiated Al

b) Copper irradiated by 500 keV Cu^+ ions.

seem necessary although not sufficient for void nucleation. Thus in agreement with previous experiments[7, 8], it has been shown that to nucleate voids in Cu or Ni under electron irradiation in the H.V.E.M., one must at first put into the metal a high dislocation density by cold work or low temperature irradiation. These facts are also emphasized by the correlation existing between void number and dislocation density. Thus in ion bombarded copper and neutron irradiated magnesium (fig. 2) void number increases with dislocation density.

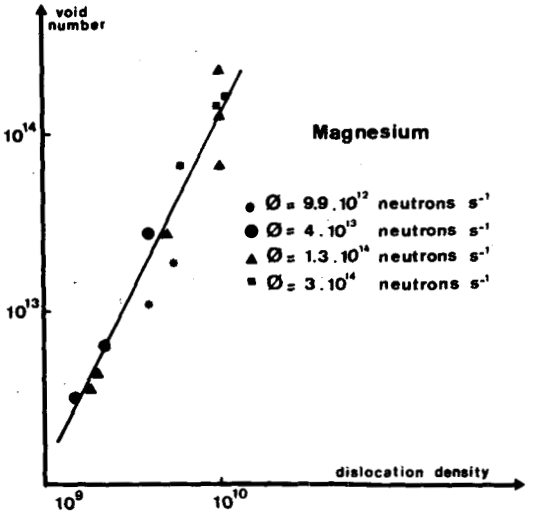


Fig. 2

2. Void growth is affected by the vicinity of a dislocation. As already stated by Norris[7], we have seen in electron irradiations that the growth rate of an individual void depends of its distance to a dislocation. Furthemore, the plots of mean void size versus dose for neutron irradiated Mg and Al and ion bombarded Cu (fig. 3) indicate that in the initial stages where all the voids are in the vicinity of dislocations (fig. 1), a much higher growth rate is observed.

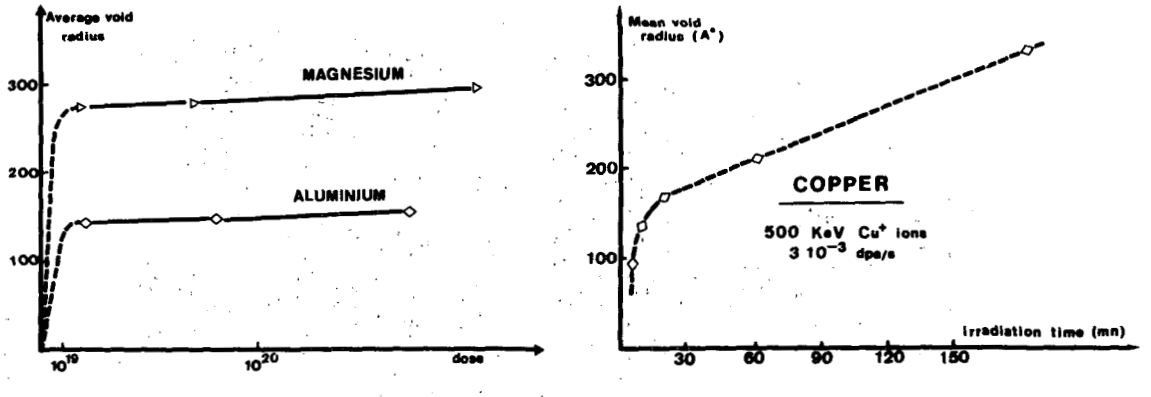


Fig. 3

The fact that voids appear on the compression side of edge dislocations, and the enhanced growth rate observed, are good evidence that dislocations do act as biased sinks absorbing intertitials preferentially to vacancies, and furthermore suggest the existence of a vacancy concentration peak in its vicinity which is not explained by the steady state models.

In fact Monte Carlo simulation of neutron radiation damage in the vicinity of an edge dislocation in aluminium[6, 9], reveals, during transient states, the presence of this peak at about 300 lattice parameters of the dislocation (fig. 4). This peak remains at steady state if the dislocation is considered as a non symmetric sink. Until steady state is reached only the embryos located at the vacancy concentration peak can grow.

The presence of this peak explains the enhanced growth rate of voids, which is observed in the early stages of irradiation. Fig. 5 compares the experimental results to those of the simulation of void growth in the presence of a climbing dislocation ; they are in good agreement.

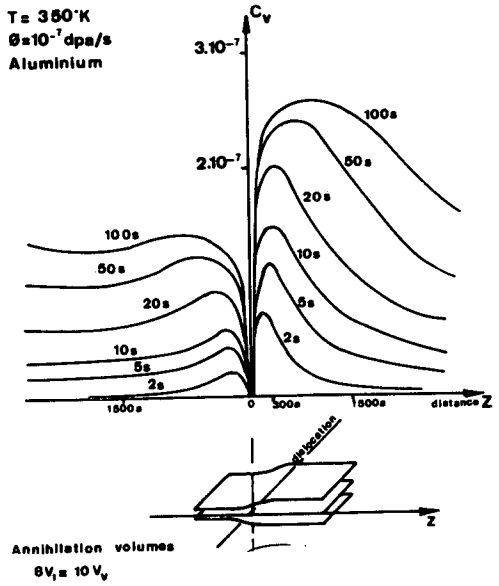


Fig. 4 - Vacancy concentration around an edge dislocation transient effects.

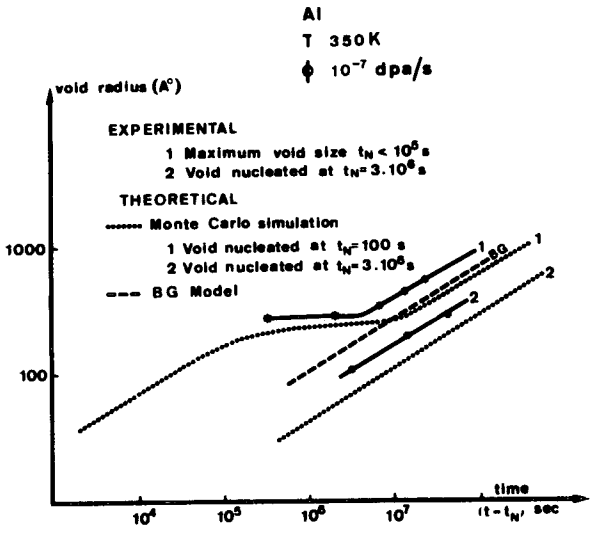


Fig. 5 - Void growth in Al.

FINAL CONFIGURATION OF VACANCY CLUSTERING

Three main factors seem to influence the final configuration of vacancy clustering, namely : gas content, dose rate and the nature of the irradiating particle. Let us summarize the experiments leading to major informations on the subject.

1. Self-ion bombarded thoroughly outgassed copper and nickel do not lead to void formation, whereas voids occur in the presence of originally occluded or implanted gases (fig. 6). This clearly shows that to form voids gas atoms are necessary in the early life of a vacancy cluster stabilizing it against collapse to a vacancy loop.

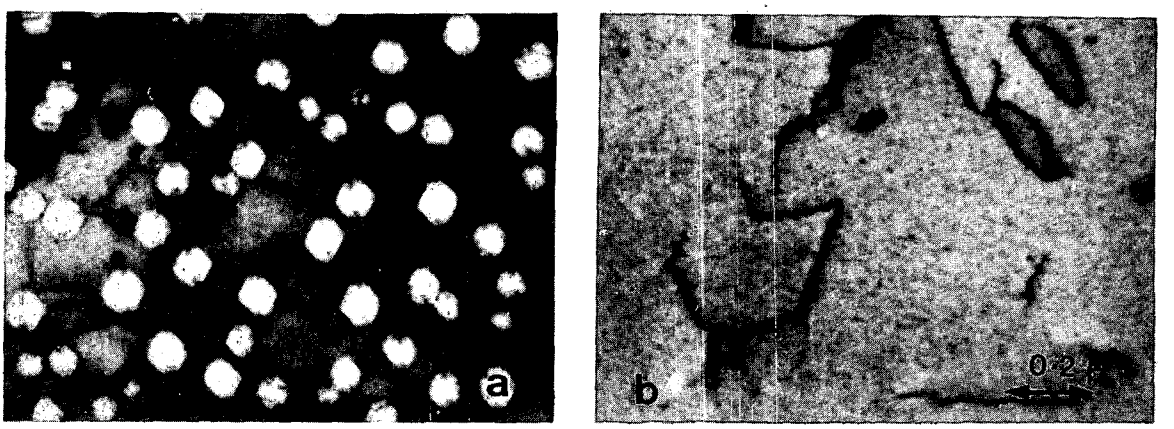


Fig. 6 - Effect of occluded gases on void nucleation
a - Annealed* copper b - Outgassed* copper

2. Both soluble and insoluble gases affect nucleation ; fig. 7 illustrates the effect of increasing amounts of oxygen or helium implanted before irradiation of thoroughly outgassed copper with 500 keV Cu^+ ions. One must note that the nucleation of both voids and interstitial loops are affected by gases ; moreover gas concentrations well below solubility limit affect void nucleation, and void number quickly saturates with gas content at low temperatures.

3. Gas effect is temperature dependent ; the temperature of maximum swelling,

* The mentions annealed and outgassed refer to metals treated at high temperature respectively at 10^{-5} torr and 10^{-8} torr.

and the extent of the swelling domain, depend extensively on gas content. Thus a shift of the swelling peak to high temperatures is observed when gas concentration increases. Fig. 8 giving the swelling versus temperature curves for annealed and outgassed Ni^+ bombarded nickel, and 1 MeV electron bombarded Cu illustrate this effect.

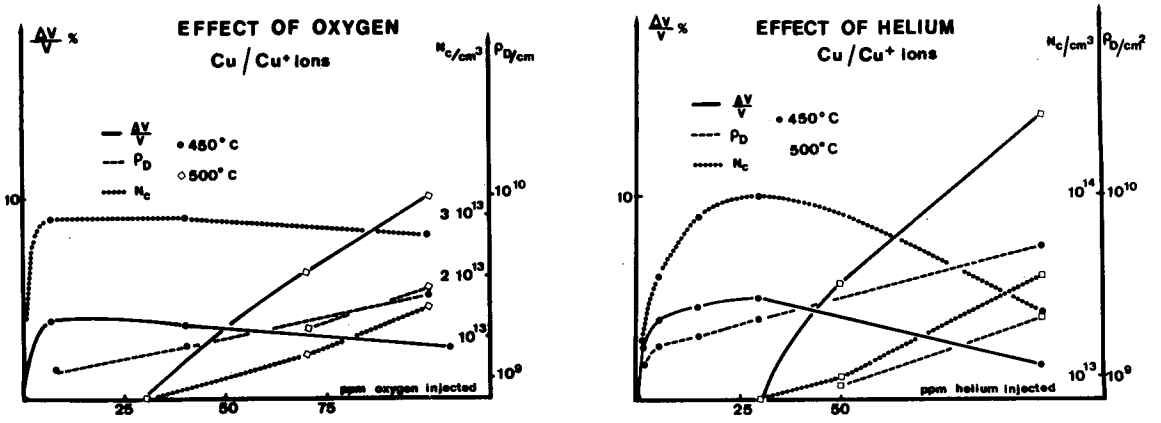


Fig. 7 - Effect of preinjected gases on void formation in self ion bombarded copper.

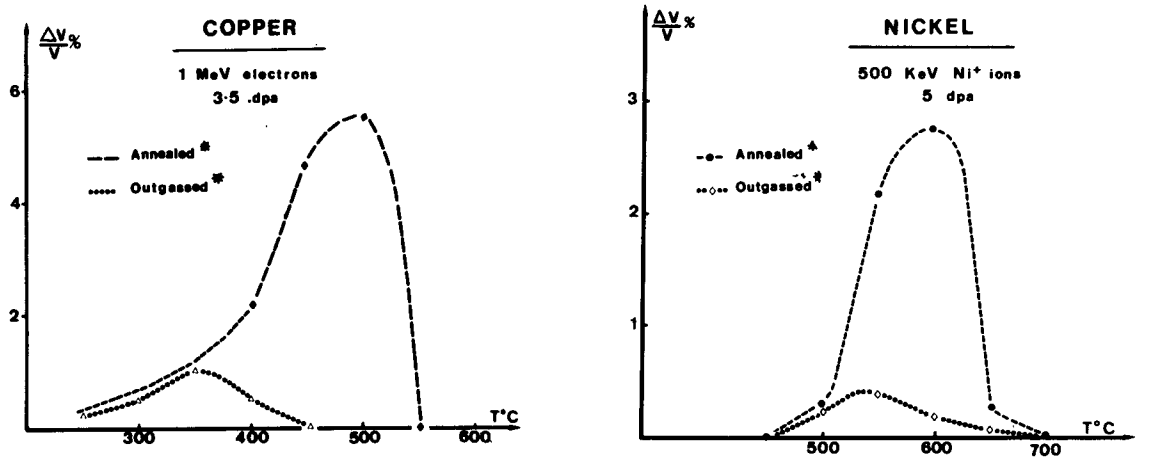
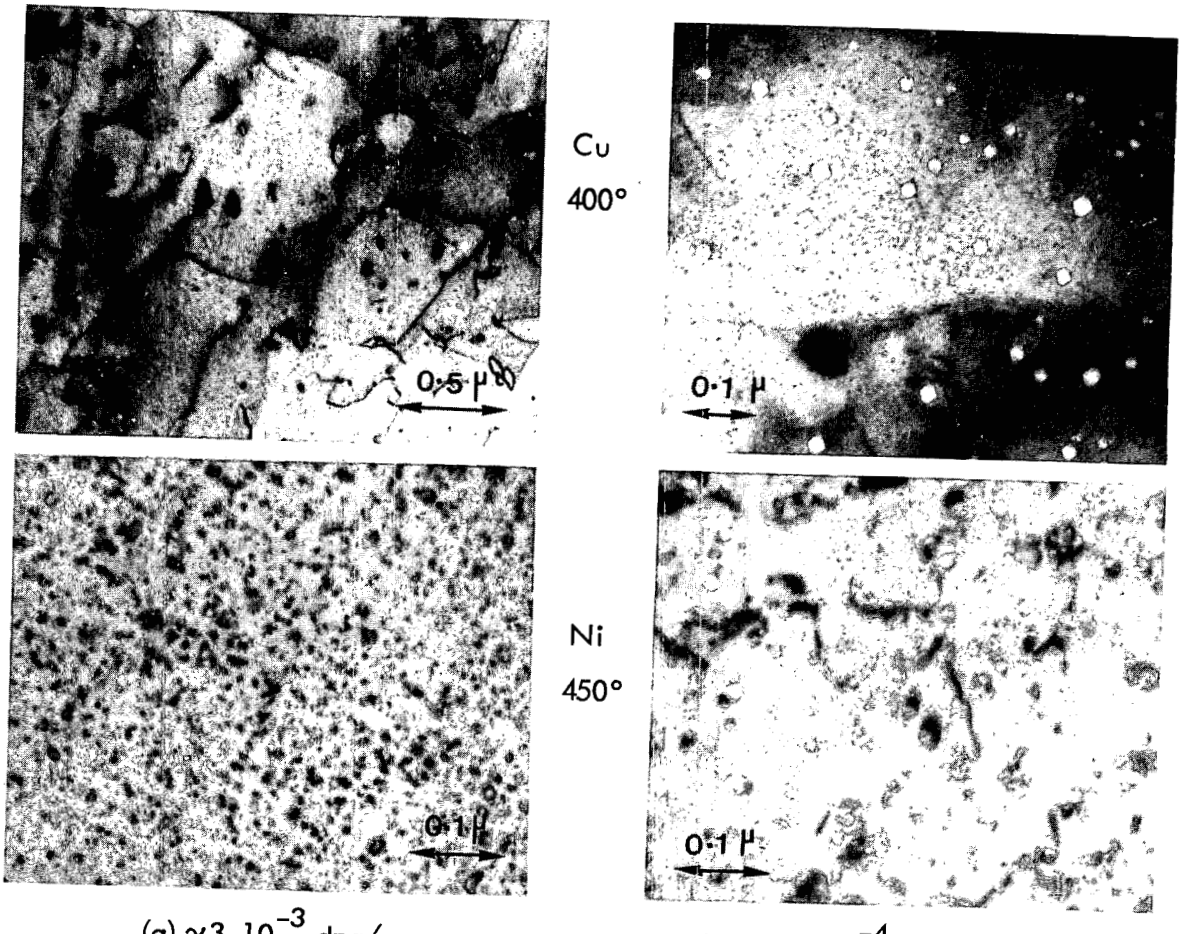


Fig. 8 - Effect of outgassing on the temperature range of swelling.

4. Experiments performed on self ion bombarded Cu and Ni show that at constant irradiation time the lower cut off temperature of swelling depends on dose rate.

Thus, at 400°C in Cu and 450°C in Ni only loops are seen after about 3 hours irradiation at $2\text{-}3.10^{-3}$ dpa/s (fig. 9a), whereas voids occur if the irradiation is carried out at $2\text{-}3.10^{-4}$ dpa/s although the dose is ten times smaller (fig. 9b).



(a) $\sim 3.10^{-3}$ dpa/s (b) $\sim 3.10.^{-4}$ dpa/s

Fig. 9 - Effect of flux on void formation

5. At low temperatures voids are formed on proton or electron irradiation and not with self ions. Furthermore the void domain extends to much higher temperatures with protons than with electrons or self-ions. This is illustrated on fig. 10 which givesthe swelling versus temperature curves for Ni and Cu irradiated at the same damage rate ($\sim 3.10^{-3}$ dpa/s) by different particles.

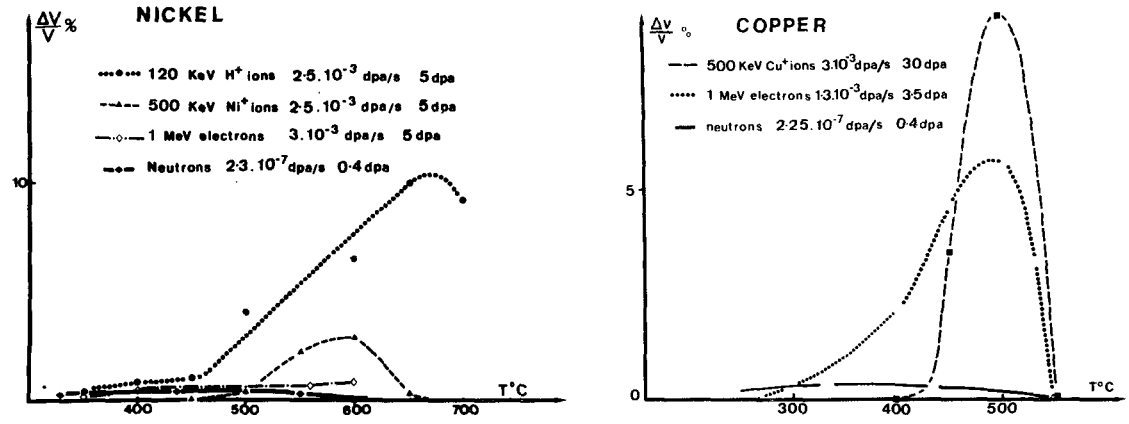


Fig. 10 - Effect of the irradiating particle on void formation.

These results rule out a certain number of assumptions on void formation published in the litterature.

Thus our experimental data clearly shows that void nucleation on submicroscopic gas bubbles is not the essential mechanism, since soluble gases at concentrations below solubility, lead to void formation in copper or nickel. On the other hand the effect of gases is not due as proposed by different authors[10, 11, 12], to a lowering of surface energy. In this case, one should expect different effects from oxygen and helium on void nucleation since only oxygen has an appreciable effect on the surface energy of copper[13,14].

Finally, experiments on dose rate and the effect of the irradiating particle clearly show that the shift in the temperature range of swelling is not simply due to an increase of recombinaisons with dose rate as generally assumed.

In fact all our experiments point out that the temperature range of swelling is nucleation limited and that gases play a major role. Most the results can be explained if one assumes that gas atoms stabilize a vacancy cluster against collapse to a vacancy loop or annihilation by vacancy emission. Thus, the final configuration of vacancy clustering, resulting as proposed by Adda[15], from a competition between vacancy clustering and the diffusion of gas atoms to the cluster, would

control the lower cut off temperature of swelling ; whereas at high temperature the main effect is probably to limit vacancy emission of the small cluster, because of the work required to compress the gas. This effect, is only sensitive if a certain amount of gas is present in a small cluster, that is why higher gas concentrations are necessary to affect void nucleation in the high temperature range.

MONTE CARLO CALCULATIONS OF VOID FORMATION IN COPPER

To test these assumptions we have performed a Monte Carlo simulation of void formation in copper irradiated by self-ions, electrons and neutrons[19]. These calculations take into account gases, dislocations as well as the spatial distribution of the defects created by the irradiating particle. The general method is published[16], the particular feactures of the computation are the following.

1. Treatment of vacancy clusters : A vacancy cluster is always defined by the number of vacancies (n) and the number of gas atoms (p) it contains. Furthermore depending of the value of n and p we distinguish 3 types of vacancy defects :
- if n is less than a critical value n^* no fundamental distinction is made between a void and a loop. The model used to treat the emission or capture of vacancies and gas atoms is very similar to the one described by Wiedersich and al[17].
- if n becomes larger than n^* we consider that if the cluster contains gas atoms ($p \neq 0$) it gives a void, whereas if it has no gas atoms ($p = 0$) it collapses into a dislocation loop. Furthermore the binding energy of a vacancy with a void or loop is assumed to be different[19].

2. Defect source - The defects are always introduced in the crystal at the experimental damage rate. For the simulation of electron irradiation the defects are Frenkel pairs ramdomly distributed in respect to space and time. In the case of self-ions or neutrons the defects are introduced in the simulated crystal in the form of cascades computed by the Marlowe program, but after the recombinations occuring during the first vacancy jump.

3. Choice of the simulated crystal cell. To reduce calculation time, and according to the results already obtained in the absence of gas atoms, we have considered the phenomena in a portion of crystal in the vicinity of a dislocation on the compression side . As a consequence of this choice, the computed swelling is too large, and only relative values are thus available.

4. Material parameters : A certain number of constants and more particularly the binding energies of vacancies to the different agregates and the constants relative to gas atoms are not known. They have been adjusted to a limited number of qualitative experimental results.

Results -

The comparaison of experiment to simulation are given on fig. 11. To make it easier, since only relative values of swelling are available, we have corrected all the computed values of swelling by a constant coefficient obtained by adjusting one experimental point.

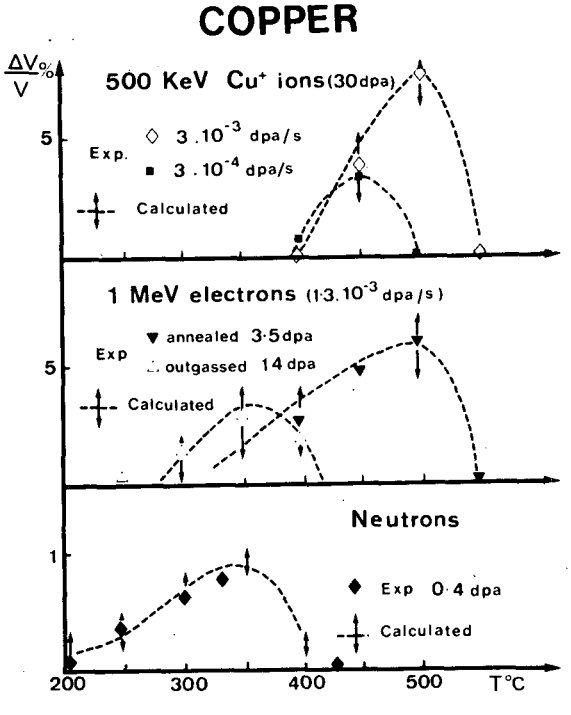


Fig. 11 - Comparison of Monte Carlo calculations with experiment.

We can see on these curves that this model is in good agreement with experiment. In particular it reproduces very well the temperature range of swelling, observed in low dose rate self ion experiments, and neutron irradiations ; these results being computed with the values of the parameters adjusted on other experiments.

Furthermore the simulation gives informations on the details of the nucleation mechanisms. Thus it emphasizes that vacancy loops are issued of the larger vacancy clusters in the cascade.

For voids the computations points out, that they result essentially of an homogeneous coprecipitation of mobile vacancy defects and gas atoms. The stabilisation of a sub-critical large vacancy cluster created in the cascade by gas atoms seems to operate only when the cascade contains the gas atoms ; this is the case if the cascade is generated by a proton or an α particle. This effect could explain why in some neutron irradiations, void number depends only of the total number of cascades and not at the rate which they are produced[9].

CONCLUSIONS

This work has emphasized that the final configuration of vacancy clustering : void or loop results from a competition between the clustering rate of vacancies and the diffusion of gas atoms to the cluster. Monte Carlo calculations based on this assumption reproduce reasonably well the experimental swelling versus temperature curves for all the different types of irradiating particles if dislocation densities are available. Thus, for this simulation to be completely previsional a model describing the evolution of dislocations must be elaborated.

AKNOWLEDGEMENTS

We wish to thank Dr Doan for helpfull discussions during the preparation of this manuscript.

REFERENCES

1. Radiation damage in reactor materials AIEA - Vienne 1969. Vol.2
2. Voids formed by irradiation of reactor materials - ed. S.F. Pugh, M.H. Loretto D.I.R. Norris - Proc. B.N.E.S. Conference Reading 1971
3. Radiation induced voids in metals - J.W. Corbett, L.C. Ianello, USAEC Symp. Series 26 Conference 710601 (1972)
4. D.I.R. Norris, Radiation effects 14 (1972) 1 et 15 (1972) 1

5. The physics of irradiation produced voids - Harwell 1974 - AERE 7934
6. A. Risbet, G. Brebec, J.M. Lanore, V. Levy, J. Nucl. Mat. 56 348 (1975)
7. D.I.R. Norris - Phil. Mag. 23 136 (1971)
8. M.J. Makin - Phil. Mag. 25 761 (1972)
9. V. Levy in (5)
10. L. Katz, M. Gruinan, R.J. Borg Phys. Rev. 4 330 (1971)
11. K.C. Russel, D. Hall in defects and defect clusters in B.C.C. metals and alloys. Nuclear Metallurgy vol. 18 Edited by R.J. Arsenault (1973)
12. L. Katz, H. Wiedersich. J. Chem. Phys. 55 1414 (1971)
13. E.D. Hondros, M. McLean - Colloque Int. CNRS 187 p. 219 (1970)
14. M.F. Felsen, P. Regnier, L.D. Glowinski (to be published)
15. Y. Adda in (3)
16. J.M. Lanore - Rad. Effects 22 153 (1974)
17. H. Wiedersich, J.J. Burton, J.L. Katz, J. Nucl. Mat. 51 287 (1974)
18. V. Levy, J.M. Lanore, J. Hillairet, Phil. Mag. 28 2 389 (1973)
19. L.D. Glowinski, J.M. Lanore, C. Fiche, Y. Adda (to be published).

EVALUATION OF TIME-DEPENDENT VOID NUCLEATION THEORY UNDER ION BOMBARDMENT CONDITIONS

J. A. Sprague,[a] K. C. Russell,[b] and Y. H. Choi[c]
[a] Naval Research Laboratory, Code 6395, Washington, D. C. 20375
[b] AERE, Harwell, Oxfordshire OX11, ORA, England*
[c] Dept. of Materials Science and Engineering, Massachusetts Institute of Technology, Cambridge, MA 02139

ABSTRACT

The applicability of a steady state and time-dependent homogeneous void nucleation theory to charged-particle irradiation experiments was investigated. The steady-state theory was found to be inappropriate, since significant changes in a metal's microstructure would likely occur before the void nucleation rate could reach steady state. Two types of time dependence were examined, that of the point defect concentrations at the beginning of an irradiation and the longer-term time dependence of void nucleation. It was found that vacancy and interstitial clustering significantly reduce the relaxation time for the point defect concentrations. An efficient form of time-dependent homogeneous nucleation theory was applied to ion bombardment conditions to predict void size distributions.

INTRODUCTION

Since the initial discovery of void formation in irradiated metals, there have been a number of investigations, both experimental and theoretical, aimed toward determining the fundamental mechanisms controlling this technologically important phenomenon. One subject that has been given a great deal of theoretical attention has been the nucleation of stable three-dimensional voids from irradiation-produced vacancies. The subject of void nucleation is necessarily complex, even for the simplest metal and irradiation conditions, and several mechanisms have been investigated theoretically.

*Permanent address: Dept. of Materials Science and Engineering, Massachusetts Institute of Technology, Cambridge, MA 02139

The simplest form of void nucleation theory that is applicable to irradiated metals deals with the homogeneous nucleation of voids in the presence of mobile vacancies and interstitials. The basic principle of this theory[1-2] is that a void embryo can grow by the capture of vacancies and can shrink by either the capture of interstitials or the emission of vacancies. The balance between growth and shrinkage processes determines a critical nucleus size, below which an embryo is more likely to shrink, and above which it is more likely to grow. At steady state, the growth and shrinkage kinetics determine the concentration of critical nuclei and thus the rate of nucleation.

This steady-state theory will not be valid, however, if changes in the metal's microstructure significantly alter the arrival rates of point defects during time periods the same order of magnitude as, or shorter than, the relaxation time required to establish the steady-state embryo distribution. This complication may be especially acute for the case of charged-particle irradiation experiments, which are done on a much shorter time scale than neutron irradiations. The aims of this paper are to examine the applicability of steady-state void nucleation theory to high-dose rate irradiations and to explore the use of a time-dependent theory to describe these experiments.

STEADY STATE THEORIES

The first step in a steady-state nucleation calculation is to determine the concentrations of vacancies and interstitials, which may be calculated by a pair of coupled rate equations,[3-4] which balance production of defects, their loss to fixed sinks, and their loss by mutual recombination. Using these quantities, steady-state homogeneous nucleation theory[1-2] then calculates the critical nucleus size, the equilibrium distribution of void embryos less than that size, the steady-state nucleation rate of critical-size embryos, and an incubation time required for the embryo distribution to reach steady state. To test the applicability of this theory to high-dose-rate irradiations, the equations were evaluated for parameters representative of nickel[7] and the

following conditions: displacement rate G = $1x10^{-2}$ displacements per atom per second (dpa/sec); T = 525°C; dislocation density $\rho_d = 2x10^{10}\,cm^{-2}$, and dislocation bias for interstitial capture[4] of 0.01. The results were a critical nucleus of 14 vacancies; a nucleation rate of $2.75x10^{16}$ nuclei per cm^3 per sec; and an incubation time of 116 sec. Thus a high homogeneous nucleation rate was predicted, but a significant amount of damage (1.16 dpa) would accumulate before the nucleation rate approached steady state. Also, the steady-state concentrations of void embryos smaller than the critical size represented a sink strength of $2.65x10^{11}\,cm^{-2}$, which would in itself perturb the system. It appeared, therefore, that the steady-state void nucleation theory would not always be appropriate for ion irradiation conditions.

TIME-DEPENDENT THEORIES

Point Defect Concentrations

At the start of an irradiation, the vacancies and interstitials will be at thermal equilibrium, and their concentrations will build to steady-state values as the irradiation progresses. If the microstructure does not change significantly during the build-up, the time required for the approach to steady state may be expressed as a relaxation time.[3] For nickel with a dislocation density of $1x10^{9}\,cm^{-2}$ this relaxation time is 160 sec, which implies that ~1.6 dpa would accumulate at $1x10^{-2}$ dpa/sec during the initial transient in the point defect concentrations. A major approximation in the above calculation is the assumption that no microstructural changes occur during the transient period, since a large amount of damage will accumulate at charged-particle damage rates. In the present study, the initial time dependence of the point defect concentrations was calculated while allowing for the clustering of vacancies into void embryos and interstitials into dislocation loops. The interstitial clustering was calculated with the model used by Hayns.[9] The vacancy clustering was described by homogeneous void nucleation equations.[1-2]

These considerations produced the following set of equations:

$$\frac{dC_v}{dt} = G+G_v^{th}-P_vD_vC_v-R\ C_IC_v+2\ \beta_v(1)\ \exp\frac{\delta G_1^o}{kT}\rho(2)-2\ \beta_v(1)\ C_v + \beta_I(2)\ \rho(2) \quad (1)$$

$$\frac{dC_I}{dt} = G-P_ID_IC_I - R\ C_IC_v - 2\gamma_I\ (1)\ C_I + \gamma_v(2)\ S\ (2) \quad (2)$$

$$\frac{dS(n)}{dt} = \gamma_I\ (n-1)\ S(n-1) - [\gamma_I(n) + \gamma_v(n)]S(n) + \gamma_v(n+1)S(n+1) \quad (3)$$

$$\frac{dR(n)}{dt} = \beta_v(n-1)\rho(n-1) - [\beta_I(n)+\beta_v(n)+\beta_v(n-1)\ \exp\frac{\delta G_{n-1}^o}{kT}]\ \rho(n) + [\beta_I(n+1) + \beta_v(n)\ \exp\frac{\delta G_n^o}{kT}]\ \rho(n+1) \quad (4)$$

where C_v and C_I are the concentrations of vacancies and interstitials, D_v and D_I are their diffusion coefficients, P_v and P_I are the total strengths of fixed sinks for vacancies and interstitials,[4] R is the recombination coefficient, $\beta_v(n)$ and $\beta_I(n)$ are the arrival rates of vacancies and interstitials at a void of n vacancies, $\rho(n)$ is the concentration of that size voids, and δG_n^o is the free energy change of the system on adding one vacancy to a void embryo of n vacancies.[1-2] The concentration of loops containing n interstitials is given by S(n), and $\gamma_v(n)$ and $\gamma_I(n)$ are the arrival rates of vacancies and interstitials at this size loop. For the initial transient calculations, the displacement rate was 1×10^{-2} dpa/sec, the initial dislocation density was 1×10^{8}, the dislocation bias was 0.1. Figure 1 shows the vacancy and interstitial concentration as a function of time for an irradiation temperature of 525°C. The vacancy sink strengths of the interstitial loops and voids[4] are shown in Fig. 2. These results indicated that vacancy and interstitial clustering greatly reduce the initial relaxation time for the point defect concentrations. The sink strength of the interstitial loops increased very rapidly during the initial stages of the irradiation, when the balance between the point defect concentrations favored interstitial arrival.

Homogeneous Void Nucleation

While Eq. (1) through (4) can be used to describe the nucleation and growth of voids and dislocation loops, the number of equations becomes prohibitive for calculations considering large defect cluster sizes.

Even if the dislocation density is assumed constant, over 6000 simultaneous differential equations would be required to consider voids up to 50Å diameter. The number of necessary equations can be reduced, as was done by Choi, et al.,[10] by recasting Eq. (4) in the form[6]

$$\frac{\partial}{\partial t}\left[\rho(n,t)\right] = \frac{\partial}{\partial n}\left[\beta_v(n)\,\rho'(n)\,\frac{\partial}{\partial n}\,\frac{\{\rho(n,t)\}}{\{\rho'(n)\}}\right], \qquad (5)$$

where $\rho'(n)$ is the pseudo-equilibrium value of $\rho(n,t)$, giving zero current between size classes.[1-2] This is essentially the diffusion equation for a variable diffusivity, which can be solved numerically by considering only selected values of n. In the present study, 40 equations were used to cover voids containing up to 3920 vacancies. The dislocation density was assumed to be constant. For a steady high-dose-rate irradiation, it was found that the vacancy and interstitial concentrations change slowly after the initial transients, so a steady state calculation was used for these quantities.

Two representative results of the nucleation calculation are shown in Figs. 3 and 4, which show the distributions of embryo sizes as functions of time for a displacement rate of 1×10^{-2} dpa/sec. The curves in Fig. 3 were calculated for T = 525°C, $\rho_d = 5\times10^{11}\,cm^{-2}$, a dislocation bias of 0.1, while those in Fig. 4 represent T = 625°C, $\rho_d = 7\times10^{10}\,cm^{-2}$, and a bias of 0.1. Little can be said about the absolute quantities shown here, pending a parametric study of the behavior of this theory. The general features of the results, however, are quite reasonable. As an irradiation proceeds the distribution of void embryos broadens to larger sizes until the voids have a sufficient sink strength to slow the nucleation, by reducing C_v and increasing β_I/β_v. This reduces the concentration of smaller voids, leaving a size distribution of growing voids. An increase in irradiation temperature produces a lower concentration of voids with a broader size distribution.

CONCLUSIONS

The applicability of steady-state and time-dependent homogeneous void nucleation theory to the description of charged-particle irradiation experiments has been investigated. The steady-state theory was judged to be inappropriate for these cases, since the high damage rates used in these experiments cancause large changes in the microstructure of a metal

before the void nucleation rate can approach steady state.

A study of the initial transient behavior of the vacancy and interstitial concentration indicated that vacancy and interstitial clustering will reduce the relaxation time for the point defect concentrations so that a small fraction of a displacement per atom will be produced during the approach to steady state.

By writing the equations of the time-dependent homogeneous void nucleation theory in the form of the diffusion equation, they may be practically applied to the conditions of charged-particle irradiation experiments. This theory may be used to directly predict void size distributions with general features that qualitatively correlate to experimental results. A later parametric study of this theory will examine its quantitative predictions and their relationship to experiments.

REFERENCES

1. K. C. Russell, Acta Met. 19, 753 (1971).
2. J. L. Katz and H. Wiedersich, J. Chem. Phys. 55, 1414 (1971).
3. H. Wiedersich, Rad. Effects 12, 111 (1972).
4. A. D. Brailsford and R. Bullough, J. Nucl. Mater. 44, 121 (1972).
5. R. W. Powell and K. C. Russell, Rad. Effects 12, 127 (1972).
6. J. Feder, K. C. Russell, J. Lothe, and G. M. Pound, Adv. Physics 15, 111 (1966).
7. J. A. Sprague, J. E. Westmoreland, F. A. Smidt, Jr., and P. R. Malmberg, J. Nucl. Mater. 54, 286 (1974).
8. T. D. Ryan and A. Taylor, Applications of Ion Beams to Metals, S. T. Picraux, E. P. Eernisse, and F. L. Vook, (eds.), p. 675, Plenum Press, New York (1974).
9. M. R. Hayns, J. Nucl. Mater. 56, 267 (1975).
10. Y. H. Choi, A. L. Bement, and K. C. Russell, "The Effect of Fusion Burn Cycle on First Wall Swelling," in proceedings of the International Conference on Radiation Effects and Tritium Technology for Fusion Reactors, Gatlinburg, Tennessee, 1-3 Oct 1975, to be published.

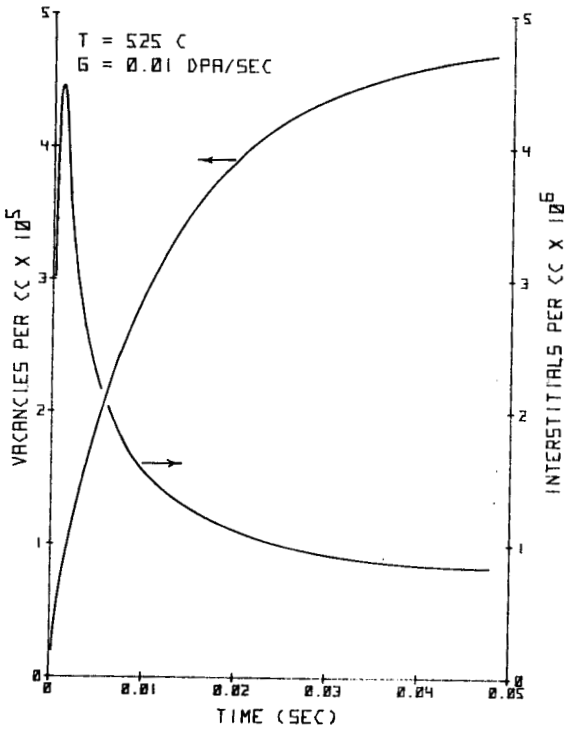


Fig. 1 - Initial time dependence of vacancy and interstitial concentrations. See text for conditions.

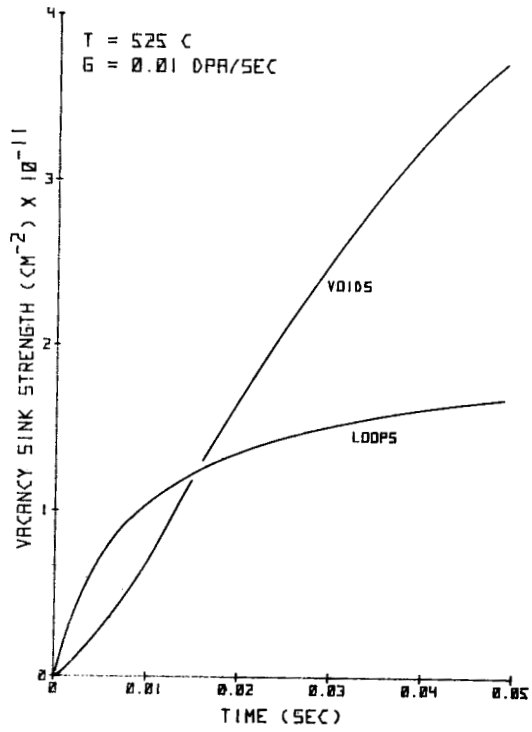


Fig. 2 - Initial time dependence of vacancy sink strength of voids and interstitial loops.

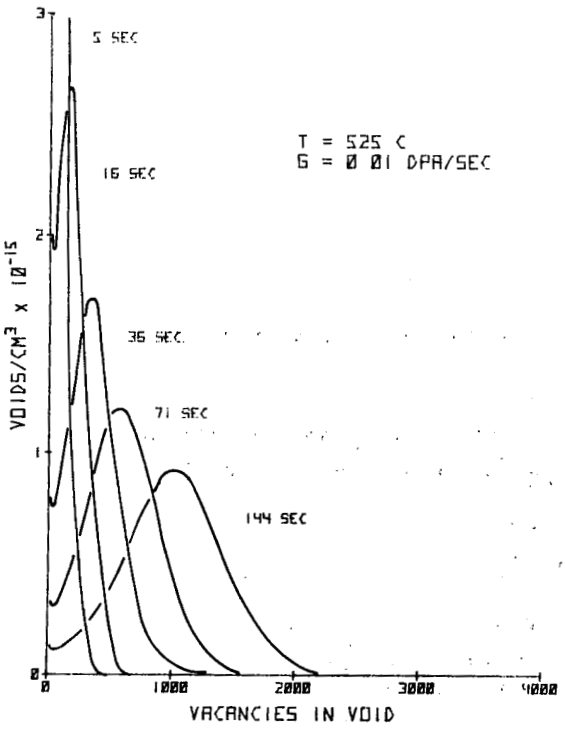


Fig. 3 - Void distributions calculated for T=525°C. See text for other conditions.

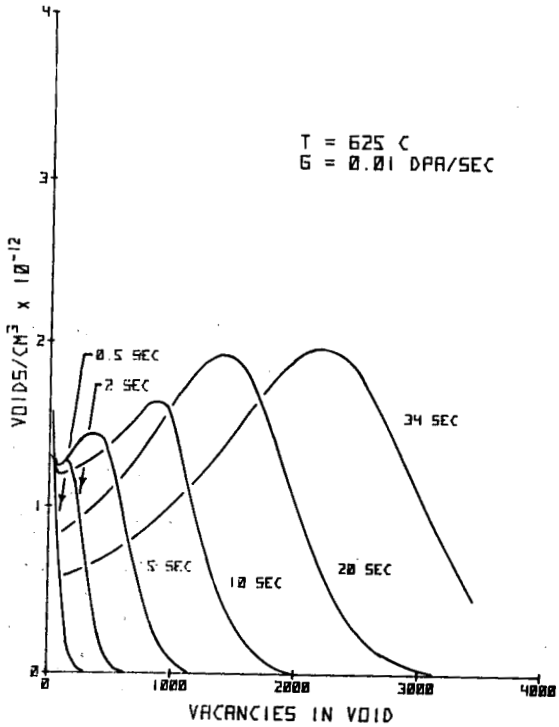


Fig. 4 - Void distributions calculated for T=625°C. See text for other conditions.

EFFECT OF Be DOPING ON VOID SWELLING IN NICKEL*

P. R. Okamoto, A. Taylor
H. Wiedersich
Materials Science Division
Argonne National Laboratory
Argonne, Illinois 60439

ABSTRACT

Ni-Be alloys containing 0.1, 0.3, and 0.7 at. % beryllium have been irradiated with 3.2-MeV $^{58}Ni^{+}$ ions at 425, 525, and 625°C. Dose levels between 1 and 30 dpa have been obtained at a calculated dose rate of $\sim 3 \times 10^{-3}$ dpa/sec. Preliminary transmission-electron microscopy examination of samples irradiated to ~17 dpa show that at 525 and 625°C the void volume fraction in the Ni-0.1 at. % Be alloy is quite similar to that in pure Ni. However, between 0.1 and 0.7 at. % Be, the void volume fraction decreases by a factor of ~40 at 525°C and ~3 at 625°C.

INTRODUCTION

It has been recognized for some time that the fraction of vacancies and interstitials mutually annihilated by recombination can be increased, if substitutional solute atoms strongly trap self-interstitial atoms. As originally suggested by Harkness and Li,[1] this would provide a means of limiting void swelling, since fewer excess interstitials and vacancies would exist for the formation of dislocation loops and voids. However, to be effective, the solute-interstitial binding energy must be comparable to or greater than the vacancy migration energy.[2] Consequently, Blewitt and co-workers[3] made a search for doping elements in Ni that would decrease stage I recovery and increase stage III recovery, since this implies a

*Work supported by the U.S. Energy Research and Development Administration.

solute-interstitial binding energy of the necessary magnitude. Both undersized and oversized solutes were investigated, and it was found that Be, which has the smallest atomic volume of all the metals, was the only dopant which caused a substantial decrease in stage I recovery and a corresponding increase in stage III recovery.

To demonstrate the swelling suppression predicted for Be-doped Ni, Ryan[4] irradiated pure Ni and Ni-1 at. % Be alloys at 520°C with $^{58}Ni^{+}$ ions at a dose rate of $\sim 4 \times 10^{-3}$ dpa/sec. Ryan found that at 45 dpa the void volume fraction in the Ni-1 at. % Be sample was ~50 times less than in pure Ni. However, a large number density of plate-shape precipitates was also observed, which introduced an ambiguity as to whether the swelling suppression was associated with the presence of the precipitates or to enhanced recombination due to the trapping of self-interstitials by the Be atoms in solution. The appearance of precipitates was unexpected, since 1 at. % Be is below the solubility limit of ~2.5 at. % Be at 520°C. A second series of experiments using lower Be concentrations was therefore initiated in an attempt to minimize the formation of precipitates.

PRELIMINARY RESULTS

Alloys doped with 0.1, 0.3, and 0.7 at. % Be were irradiated with 3.2-MeV $^{58}Ni^{+}$ ions at 425, 525, and 625°C. Dose levels between 1 and 30 dpa were obtained using a dose rate of $\sim 3 \times 10^{-3}$ dpa/sec. In these experiments, the specimens were covered with 200-mesh molybdenum grids to allow, during subsequent postirradiation examinations, a direct comparison of irradiated and unirradiated areas that have otherwise identical histories within the same electron microscope specimen.

Postirradiation examination of the bombarded specimens by transmission-electron microscopy are still in progress. To date, only those specimens irradiated to ~17 dpa have been analyzed. Nevertheless, several points of interest have emerged from these examinations. The first is that decomposition of these dilute and normally single-phase solid solutions could not be suppressed at any of the irradiation temperatures investigated. The second point is that in all cases decomposition occurs only in the

irradiated areas. An example illustrating this behavior is shown in Fig. 1 for the case of a Ni-0.1 at. % Be alloy irradiated at 525°C. The absence of precipitates in the unirradiated areas clearly indicates that decomposition of these alloys is a radiation-induced phenomenon and is not the result of the thermal history associated with the irradiation.

Figure 2 shows the void microstructures that develop after 17 dpa as a function of temperature and Be concentration. The corresponding swelling parameters are summarized in Table 1. For purposes of comparison, Ryan's 525 and 600°C data for pure Ni are also included.

Table 1. Comparison of Void Formation in Ni-Be Alloys Irradiated to 17 dpa at 525 and 625°C

	Ni*	0.1 Be	0.3 Be	0.7 Be
Mean Dia. (A)	310	442	210	220
Void Conc. (cm^{-3})	14×10^{14}	8×10^{14}	6×10^{14}	2×10^{14}
Vol. Frac. (%)	3	4	0.4	0.1
Mean Dia. (A)	575	587	457	519
Void Conc. (cm^{-3})	3×10^{14}	6×10^{14}	5×10^{14}	1×10^{14}
Vol. Frac. (%)	7	7	4	2

*Values interpolated from data at 525 and 600°C. Ryan[4]

The low-temperature form of the radiation-induced microstructure observed at 425°C was characterized by a high density of loop-like defects that are aligned along <100> directions. Selected area diffraction patterns exhibit weak precipitate reflections as well as streaking of the matrix reflections, which are characteristic of Frank loops. The

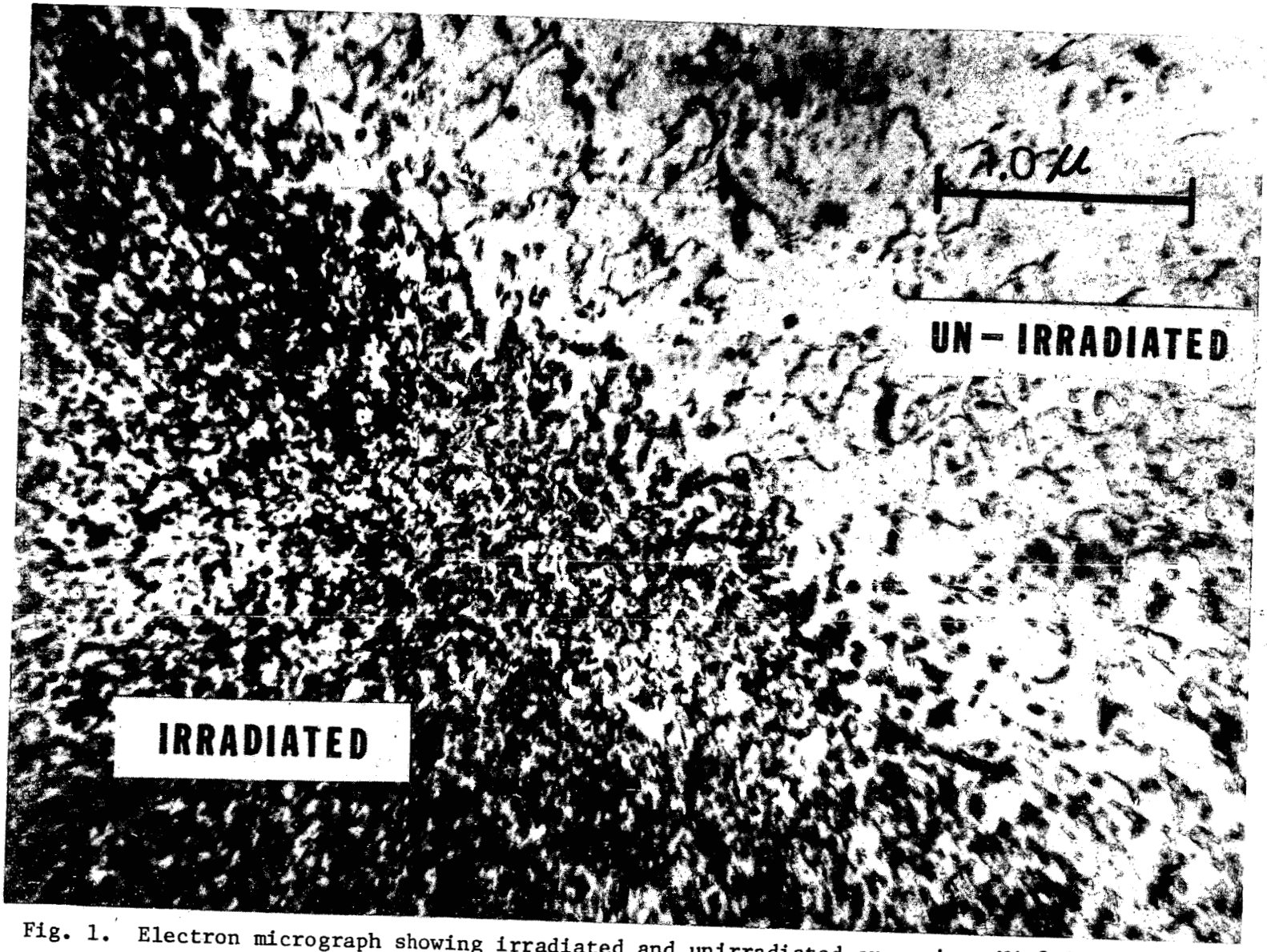


Fig. 1. Electron micrograph showing irradiated and unirradiated areas in a Ni-0.1 at. % Be alloy irradiated with 3.2-MeV $^{58}Ni^{+}$ ions at 525°C to ∿17 dpa.

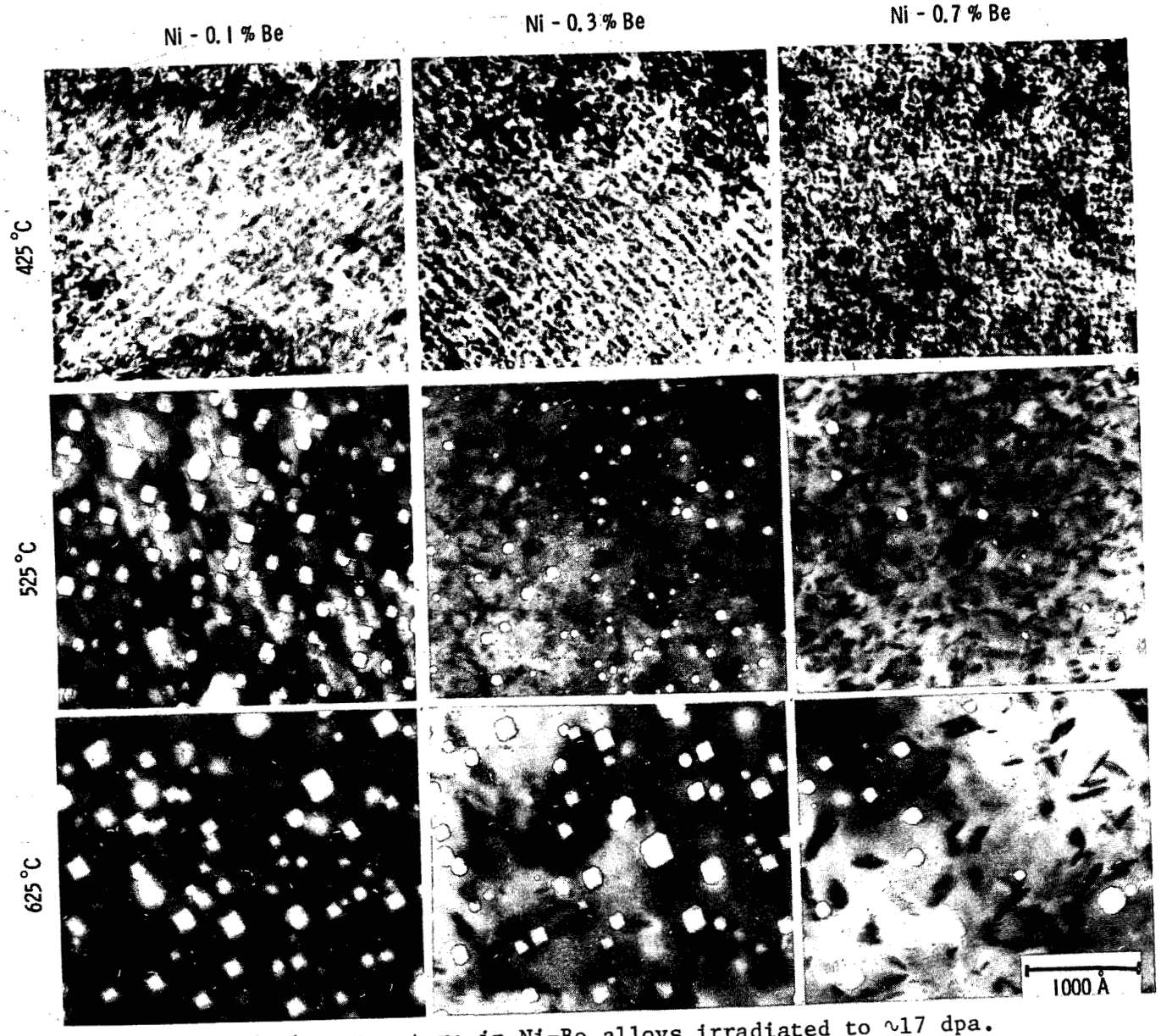


Fig. 2. Void microstructure in Ni-Be alloys irradiated to ∿17 dpa.

aligned defect structure may therefore be composed of loops as well as precipitates. However, more extensive selective dark-field imaging will be required before firm conclusions can be reached. Also, no voids were observed in any of the alloys irradiated at 425°C.

At the higher temperatures, the precipitates do not show any tendency toward alignment and appear to be randomly distributed. The precipitate distribution occurs on a much coarser scale at 625°C than at 525°C, but at both temperatures the density of the precipitates and their average size increases and decreases, respectively, on going from 0.1 to 0.7 at. % Be.

Taking into account the slightly different temperatures and dose levels used by Ryan, Table 1 shows that at 525 and 625°C the void volume fraction in the Ni-0.1 at. % Be alloy is quite similar to that in pure Ni. This indicates that Be additions >0.1 at. % Be are required to obtain significant reduction in swelling.

The last point of interest is that at 525°C the void volume fraction decreases by a factor of ∿40 on going from 0.1 to 0.7 at. % Be but only by a factor of ∿3 at 625°C. Consequently, Be doping appears to be much more effective at 525°C than at 625°C in suppressing void formation in Ni. However, since the final precipitate distribution is sensitive to both temperature and Be concentration, the question arises as to whether the suppression is the result of enhanced recombination induced by solute-interstitial trapping effects or to variations in the precipitate distribution.

DISCUSSION

Although the limited amount of data analyzed to date prevents an unambiguous interpretation of the role played by the precipitates in the suppression of swelling, it has raised an equally important question as to why phase decomposition occurs at all in these dilute solid solution

alloys. Since the Be levels investigated are well below the solubility limits at the irradiation temperatures used in this study (∿2, 2.5, and 4 at. % Be at 425, 525, and 625°C, respectively), the formation of precipitates cannot be solely due to radiation-enhanced diffusion.

We would like to speculate that precipitation is induced by the interstitial-solute drag mechanism recently proposed by Okamoto and Wiedersich.[5] They noted that, in a number of irradiated metals and alloys, undersized and oversized solutes tend to be enriched and depleted, respectively, around point-defect sinks. To account for this correlation, they suggested that undersized solutes interact preferentially with self-interstitial atoms and undergo long-range migration due to the formation of <100> mixed dumbbells. Consequently, undersized solutes tend to be dragged toward defect sinks by the interstitial flux, whereas oversized solutes tend to be depleted around defect sinks by the vacancy flux. This mechanism is believed to play an important role in the formation of precipitates on sinks such as voids and Frank loops in irradiated austenitic stainless steels doped with silicon.[5]

Frank loops are frequently observed to form ordered arrays, particularly at lower temperatures. The segregation of Be to Frank loops would therefore be consistent with the aligned precipitate structure observed at 425°C in the Ni-Be alloys. The decrease in precipitate density and increase in precipitate size with an increase in temperature is also consistent with the behavior expected of Frank loops. Furthermore, the recent Johnson-Lam[6] time-dependent, rate formulation of the solute drag mechanism predicts quite large segregation effects when the solute-interstitial binding energy is large, as is the case with Be in Ni. Moreover, for dose rates comparable to those used in this study, i.e., $\sim 10^{-3}$ dpa/sec, the theory predicts significant segregation to sinks between 0.2 T_m and 0.6 T_m, with maximum segregation occurring at $\sim 0.45\ T_m$. For Ni, this would correspond to 525°C where Be doping was observed to be most effective in suppressing void formation. Since the temperature dependence of the impurity-trapping effect is reflected in the segregation phenomenon, the

optimum temperature at which the vacancy-interstitial recombination due to trapping of self-interstitials is maximized should coincide with the "peak" segregation temperature.[7] Therefore, our results suggest that trapping of self-interstitials by Be atoms in the matrix contributes, at least in part, to the reduction in void swelling.

ACKNOWLEDGMENTS

The authors gratefully acknowledge the assistance of B. J. Kestel, P. M. Baldo, and C. Steves whose support made this work possible. The authors also thank Dr. N. Q. Lam for many fruitful discussions.

REFERENCES

1. S. D. Harkness and Che-Yu Li, Radiation-Induced Voids in Metals and Alloys, USAEC Symposium Series, CONF-7010601 (1972), p. 798.
2. F. A. Smidt, Jr., J. A. Sprague, J. E. Westmoreland, and P. R. Malmberg, J. Nucl. Mater. 18, 302 (1972).
3. T. H. Blewitt, C. Sartain, T. L. Scott, and R. A. Conner, Jr., Proc. of the Am. Phys. Soc. Mtg., Denver, Colorado, March 31-April 3, 1975.
4. T. D. Ryan, Ph.D. Thesis, University of Michigan, 1975.
5. P. R. Okamoto and H. Wiedersich, J. Nucl. Mater. 53, 336 (1974).
6. R. A. Johnson and N. Q. Lam, to be published.
7. N. Q. Lam, private communication.

THE DEPENDENCE OF SWELLING ON VOID SURFACE REACTION RATE CONSTANTS

E. P. Simonen and J. L. Brimhall
Battelle-Pacific Northwest Laboratories
Richland, Washington 99352

ABSTRACT

Void growth data from ion bombarded molybdenum, nickel, and 316 stainless steel are analyzed with respect to dislocation bias and void surface kinetics. The strength of the surface kinetic influence is calculated and the absence of point defect bias at voids is discussed.

INTRODUCTION

Void formation in irradiated materials has been a subject of intense study for the past several years. The theory of void growth has been developed based on reaction rate theory and point defect diffusion to sinks[1]. Furthermore, the role of the void surface in the void growth process can be important[2]. The purpose of the present work is to incorporate in the Brailsford and Bullough[1] swelling model the surface kinetic influence of vacancies and interstitials. In addition, the changing role of void surface creation, surface kinetics and volume diffusion are calculated as a function of void size. Observed void growth rates in ion bombarded molybdenum[3], nickel[4], and 316 stainless steel[2] are used to determine surface kinetic constants and their associated activation energies.

VOID SINK STRENGTH

The void sink efficiency, k_v^2, is derived from the Brailsford and Bullough[1] model for finite surface transfer kinetics to obtain

$$k_v^2 = 4\pi r_v \rho_v / (1 + \frac{D}{\bar{K} r_v}). \quad (1)$$

r_v and ρ_v are the void radius and number density; D and $\bar{K}$ are the point defect diffusivity and transfer velocity, respectively. Measured void growth kinetics can be used to determine $\bar{K}$ if the other material and irradiation parameters in the model are known or assumed. In the present study the surface reaction constant, $\bar{K}$, was defined by the following relationship:

$$\bar{K} = \frac{D}{b} \exp\left(-\frac{\Delta E_m}{kT}\right); \quad (2)$$

where b is the jump distance and kT has its usual meaning. The activation energy ΔE_m describes the increase in the activation enthalpy for migration due to the presence of the void surface.

ANALYSIS

The ancillary data used for these calculations are shown in Table 1.

Table 1. Definition of Vacancy Diffusivity, D_v, Interstitial Diffusivity, D_i, and Equilibrium Vacancy Concentration, c_e

Material	E_m^v(a) eV	E_f^v(b) eV	E_m^i(c) eV	D_v^o(a) cm^2/sec	D_i^o(c) cm^2/sec	Comments
Mo	1.7	2.3	0.2	0.1	1.0	(a) $D_v = D_v^o \exp(-E_m^v/kT)$
Ni	1.4	1.4	1.1	0.1	0.1	(b) $c_e = \exp(-E_f^v/kT)$
316 SS	1.3	1.6	0.2	0.6	1.1	(c) $D_i = D_i^o \exp(-E_m^i/kT)$

The microstructural parameters were determined by linear interpolation of the experimental data for molybdenum[3] and nickel[4] and from best fit

straight lines through the experimental data for 316 stainless steel[2]. The void radius was calculated as a function of displacements per atom by calculating the void growth rate from the Brailsford and Bullough[1] model and allowing the radius to increase by one percent at that rate. A new growth rate was then calculated and the process repeated as often as necessary. The experimental displacements per atom have been corrected to be consistent with the recommended practice for calculating displacement damage[5].

The void growth model contains three unknown parameters, $\overline{K}_{vacancy}$, $\overline{K}_{interstitial}$, and the dislocation bias. Since there are three unknowns to compare with only one experimental known, r_v, it was necessary to place additional constraints on the unknowns to predict a unique growth rate. For this reason only special cases of surface kinetic influence were considered.

In the first case of interest the void growth data were compared with predicted kinetics based on chosen values for interstitial bias at dislocations and neglecting the void surface kinetic influence. The predicted void growth rates are consistent with a dislocation bias of 0.4% for molybdenum, 8% for nickel at 575°C, 20% for nickel at 625°C, and 1% for 316 stainless steel. In each instance it is noted in Fig. 1 that the predicted behavior is in good agreement with observed void growth; but, the predicted bias in molybdenum and stainless steel is much less than expected[6]. Larger dislocation biases, however, could be consistent with the data if void surface kinetics are retarding void growth.

With surface kinetic influence the void may be either a biased or unbiased sink. In the case of no void bias, the dislocation bias for interstitials must be assumed a priori and the value of ΔE_m determined. Unbiased surface kinetics retard void growth by reducing the arrival rates of both vacancies and interstitials at voids. To compensate for this reduced rate, larger dislocation biases must be assumed to maintain agreement with the growth data. A maximum realistic value of dislocation bias equal to 20% was chosen to obtain estimates of expected magnitudes for ΔE_m. With a dislocation bias of 20%, the corresponding increase in point defect migration activation energy at a void surface was 1.1 eV in

molybdenum, 0.6 eV in 316 stainless steel, 0.4 eV in nickel at 575°C, and no increase in nickel at 675°C. The large magnitudes of ΔE_m assumed in Fig. 1 indicate a dominant surface kinetic influence.

As a biased sink, voids show a preference for either interstitials or vacancies. Interstitial void bias decreases the growth rate by reducing the difference in the arrival rates of vacancies and interstitials at voids. Substantial reduction in growth rate due to interstitial bias is only observed for voids nearly equal to the critical size. This restriction on growth is difficult to justify in rationalizing larger choices for dislocation bias. On the other hand, vacancy bias at voids results in an increase in the void growth rate. Hence, vacancy bias also cannot be responsible for the small dislocation bias predicted by volume diffusion control.

The influence of surface kinetics on void growth is illustrated shematically in Fig. 2, where the relationships between the calculated vacancy concentrations are shown. The matrix concentration, c_v, minus the equilibrium vacancy concentration, c_e, represents the total supersaturation of vacancies in solution. This supersaturation in molybdenum is partitioned as indicated in Fig. 3 between volume diffusion, $\Delta C_{diffussion}$; surface kinetics, $\Delta C_{kinetics}$; and surface creation, $\Delta C_{creation}$. The results in Fig. 3 were obtained from the relationships given in Fig. 2. The sink efficiencies used to determine c_v were calculated assuming 2×10^9 dislocations per cm^2 with 0.4% bias and 10^{16} voids/cm^3 with ΔE_m equal to zero. Mutual competition between the mechanisms is observed with void sizes smaller than the critical size for growth, r_c; however, volume diffusion dominates for larger sizes as expected.

SUMMARY

The data for void growth in ion bombarded molybdenum, nickel, and 316 stainless steel can be rationalized with or without surface kinetic influence for different choices of dislocation bias. However, without surface kinetic influence the dislocation bias was found to be smaller than expected from independent calculations[6]. Using a dislocation bias

of 20%, the calculated increase in point defect migration activation energy at a void surface was found to be larger than might reasonably be expected. The void growth data and expected dislocation biases suggest that voids are unbiased sinks. This conclusion is surprising if indeed the surface kinetic influence is to alter the migration activation energy of vacancies and interstitials.

ACKNOWLEDGMENT

This paper is based on work performed under United States Energy Research and Development Administration Contract AT(45-1)-1830.

REFERENCES

1. A. D. Brailsford and R. Bullough, J. Nucl. Mater. 44, 121 (1972).
2. L. K. Mansur, P. R. Okamoto, A. Taylor, and Che-Yu Li in: Defects and Defect Clusters in B.C.C. Metals and Their Alloys, R. J. Arsenault (ed.), p. 509, Nuclear Metallurgy, vol. 18, Natl. Bureau of Standards, 1973.
3. J. L. Brimhall and E. P. Simonen, J. Nucl. Mater. 52, 323 (1974).
4. J. A. Sprague, P. R. Malmberg, and F. A. Smidt, Jr., in: Cooperative Radiation Effects Simulation Program, Semiannual Progress Report for the period 1 May - 31 October 1974, L. E. Steele and E. A. Wolicki (eds.), p. 24, NRL Memorandum Report 2998, 1974.
5. D. G. Doran, J. R. Beeler, Jr., N. D. Dudey, and M. J. Fluss, Report on the Working Group on Displacement Models and Procedures for Damage Calculations, HEDL-TME 73-76 (December 1973).
6. P. T. Heald, Phys. Rev. 31, 551 (1975).

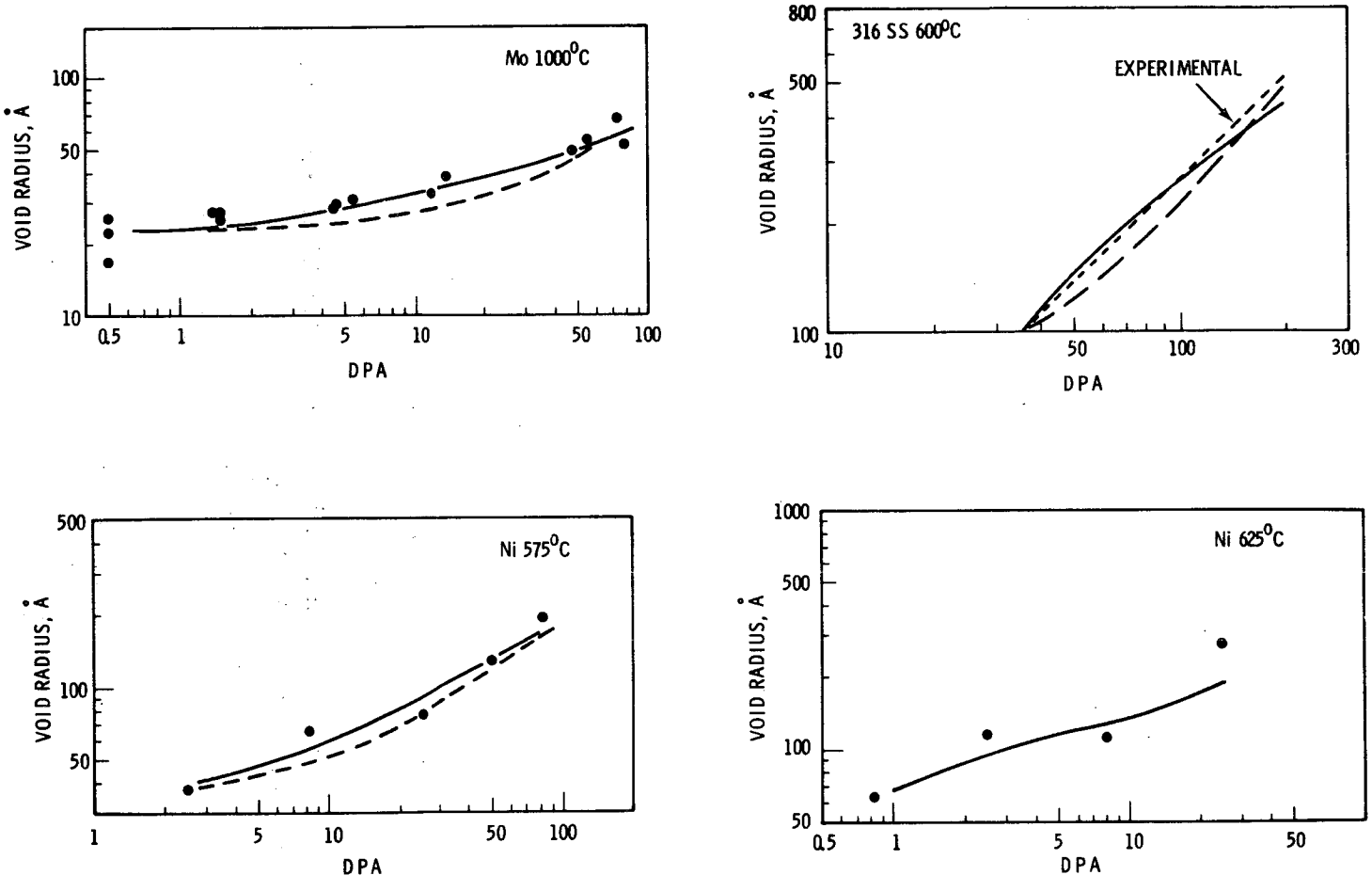


Fig. 1. Measured void radii vs. displacements per atom (DPA) compared with predictions based on no surface kinetic influence (solid line) and with surface kinetic influence (dashed line). Measured radii for 316 SS are represented by a best fit dotted line.

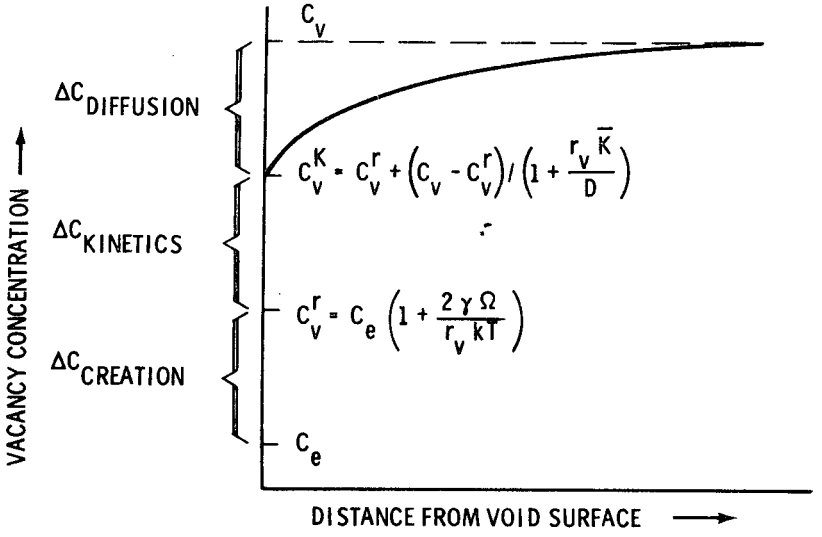


Fig. 2. Vacancy concentration vs. distance from the void surface. The surface concentration, C_v^K, is dependent on the vacancy transfer velocity, $\bar{K}$, and the surface energy, γ, assumed to be 1000 ergs/cm^2, Ω is atomic volume.

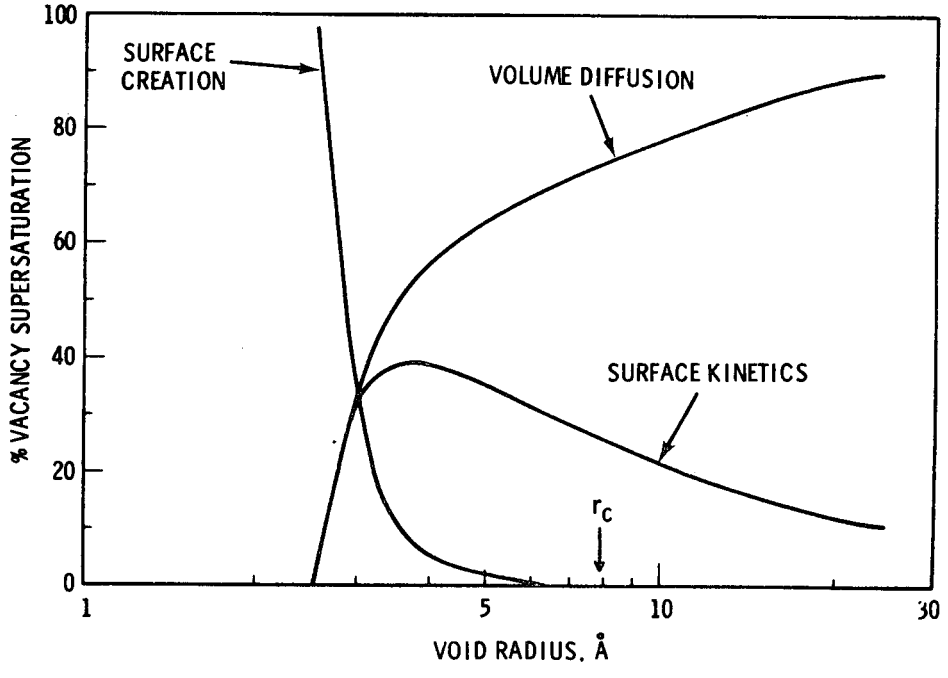


Fig. 3. The influence of void radius on partitioning of vacancy supersaturation as calculated in Fig. 2.

THE EFFECT OF SOLUTE CONTENT AND PRECIPITATE DISTRIBUTION ON FAST NEUTRON DAMAGE IN ALUMINUM-COPPER ALLOYS*

R. W. Carpenter and J. C. Ogle
Metals and Ceramics Division
Oak Ridge National Laboratory
Oak Ridge, Tennessee 37830 USA

INTRODUCTION

The presence of metallic solutes or second phases in a metal subjected to neutron irradiation can be expected to markedly influence the microstructural changes that occur. Farrell et al.[1] have shown that a commercial aluminum alloy containing Mg_2Si precipitate is much more resistant to swelling resulting from void nucleation and growth than elemental aluminum at a very high dose, $\sim 3 \times 10^{23}$ n/cm^2 (E > 0.1 MeV). Risbet et al.[2] have shown that Al–4% Cu alloys are more resistant to swelling than aluminum containing small amounts of metallic impurities at a low neutron dose ($\sim 5 \times 10^{20}$ n/cm^2, E > 0.1 MeV), and further, that the resistance to swelling was dependent on the precipitate distribution that existed prior to irradiation. In the present investigation two Al-Cu alloys having different copper concentrations were given various heat treatments to develop different precipitate morphologies and then irradiated at 55°C, along with high-purity aluminum specimens that served as reference materials. The object of this work was experimental evaluation, at a high neutron dose, of the effect of precipitate distribution on swelling in two similar alloys with differing solute content. In this way it is possible to gain a measure of the relative importance of solute content in the terminal solid solution and a metastable or equilibrium precipitate distribution on the irradiation response of the alloys.

---

*Research sponsored by the Energy Research and Development Administration under contract with the Union Carbide Corporation.

EXPERIMENTAL DETAILS

Specimen Materials

Two alloys, containing nominally 1.7 and 3.8 wt % Cu, were made from high-purity Al and Cu by induction melting in previously outgassed graphite crucibles. The furnace was evacuated to $\sim 10^{-6}$ torr during melting, and zone leveling techniques were used to prevent macrosegregation. The ingots were cold swaged to 2.5 mm diameter and homogenized at either 525 or 575°C. Aging heat treatments were performed in fused salt baths. All heat treatments were terminated by quenching the specimens into iced brine. Total metallic impurity content after homogenization was < 20 wt ppm. Chemical analysis for oxygen, nitrogen, and hydrogen after fabrication and homogenization showed the total content of these gases to be 0.0032 and 0.0008 wt % in the 3.8 and 1.7% Cu alloys, respectively. In both alloys the principal gaseous impurity was oxygen.

The aluminum used for both reference irradiation specimens and base constituent in the alloys was found by chemical analysis to contain < 8.1 wt ppm metallic impurities; the principal impurities were magnesium, copper, and iron. Analysis showed the total gas content to be 0.0078 wt %. Oxygen was the principal gaseous impurity.

Irradiation Procedure

The alloys, after being given various heat treatments described below, were irradiated in a High Flux Isotope Reactor peripheral target position, near the horizontal centerline. The specimens were in contact with the reactor cooling water throughout the irradiation; the specimen temperature during irradiation was 55 ± 5°C. The fast flux at the specimen position was 1.4×10^{15} n/cm^2 · sec ($E > 0.1$ MeV) and the total dose was 2.8×10^{22} n/cm^2.

Swelling measurements were made by the liquid displacement technique in the hot cell, using an identically heat treated but unirradiated specimen to determine a reference density.

EXPERIMENTAL OBSERVATIONS

The measured swelling that occurred in the specimens is listed in Table 1, together with the preirradiation heat treatments given each specimen. In Table 1 heat treatment H denotes solution treatment and quench.

Table 1. Measured Neutron Irradiation Induced Swelling

Alloy	Heat Treatment	Preirradiation Structure	Swelling (%)
Al	H	Single-phase α	12.4
Al–3.8% Cu	H	GPZ	0.07
Al–3.8% Cu	H + 1 hr at 169°C	GPZ + θ''	0.33
Al–3.8% Cu	H + 10 hr at 200°C	θ'	0.54
Al–3.8% Cu	H + 50 hr at 200°C	θ'	2.30
Al–1.7% Cu	H	GPZ	1.13
Al–1.7% Cu	H + 1 hr at 169°C	GP + θ''	0.77
Al–1.7% Cu	H + 10 hr at 200°C	θ'	0.68
Al–1.7% Cu	H + 10 hr at 240°C	θ'	--

The results show that all of the alloys swelled much less than the unalloyed aluminum. Alloys containing 3.8% Cu exhibited essentially no swelling when in the solution-treated and quenched state prior to irradiation. The microstructure of this alloy after irradiation is shown in Fig. 1a, and a corresponding symmetrical diffraction pattern in Fig. 1b. It is easy to see that strong strain contrast is associated with the disk-like particles that lie on {001} matrix planes near $\bar{s} = 0$ (Fig. 1a) and that diffuse streaks in ⟨100⟩ characteristic of small particle sizes exist in the diffraction pattern (Fig. 1b). No voids were observed in this specimen. Before irradiation this specimen contained fine GP zones and the diffraction pattern exhibited continuous ⟨100⟩ streaks without subsidiary maxima. The changes during irradiation correspond to a coarsening of the microstructure, but not loss of coherency, and a change in the zone crystallography indicated by the existence of the subsidiary

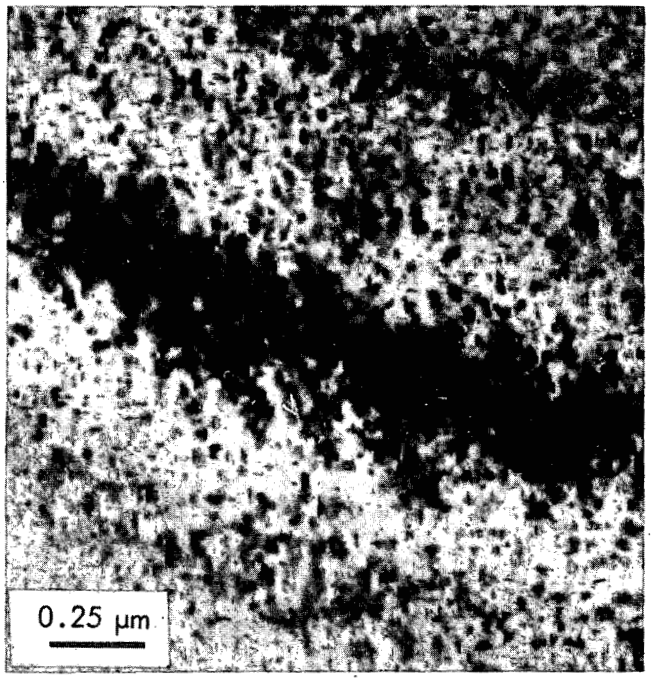


Fig. 1a. Al–3.8 wt % Cu Solution Treated and Quenched, then Neutron Irradiated to $\sim 3 \times 10^{22}$ n/cm^2 at 55°C. Foil plane near (001).

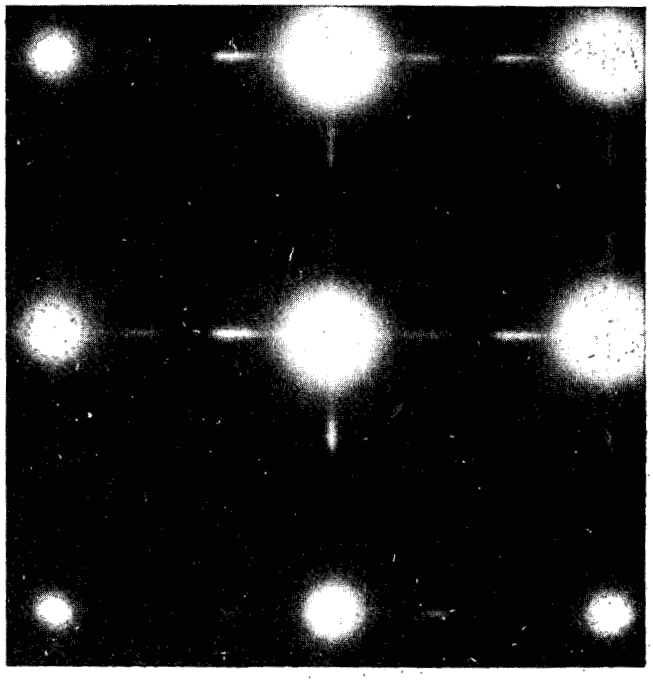


Fig. 1b. Selected Area Electron Diffraction Pattern from Specimen Shown in Fig. 1a, at Symmetrical (001) Orientation. Note maxima in ⟨100⟩ streaks and absence of diffuse intensity near {110} positions.

maxima in the ⟨100⟩ streaks. These diffraction effects are similar to those observed in unirradiated alloys containing θ″ or θ′ precipitate. In the present case there is very little diffracted intensity around the {110} positions in reciprocal space, therefore the structure of the coherent precipitates in the irradiated specimens probably corresponds more closely to θ″ than to θ′. When the 3.8% Cu alloy was aged to contain relatively large

θ' precipitate prior to irradiation a bimodal void size distribution was formed. An example of the bimodal void distribution is shown in Fig. 2a, taken in a thin region of the foil. The large voids are on the order of 600 Å and the small ones are $\sim$ 100 Å in size. The small voids are clearly visible only in thin foil regions and appear to be more or less homogeneously distributed except in regions close to θ' particles. The large voids are not homogeneously distributed, but rather are associated closely with the location of the previously formed θ' precipitates. An example of the association between the large voids and the θ' plates is shown in Fig. 2b, which is a thicker region of the same foil shown in Fig. 2a. When coarser θ' was formed in this alloy prior to irradiation the same general behavior occurred during irradiation, but the resulting voids were larger and faceting was more easily visible as shown in Fig. 3. The general behavior of the 3.8% Cu alloy then was maximum suppression of void formation in the solution-treated and quenched state. The swelling magnitude gradually increased when the metastable precipitate dispersion was coarsened by appropriate heat treatment of the specimens before irradiation.

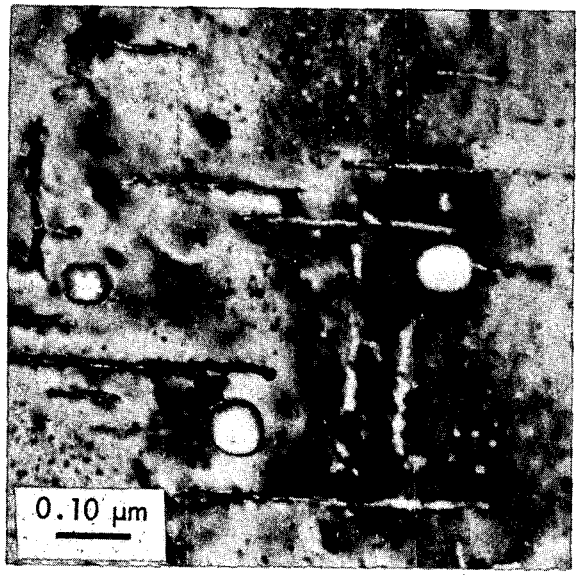


Fig. 2a. Al–3.8 wt % Cu Alloy Aged 10 hr at 200°C, then Neutron Irradiated to $\sim 3 \times 10^{22}$ n/cm^2 at 55°C. Note bimodal void size distribution was formed during irradiation. Foil plane near $(21\bar{3})$.

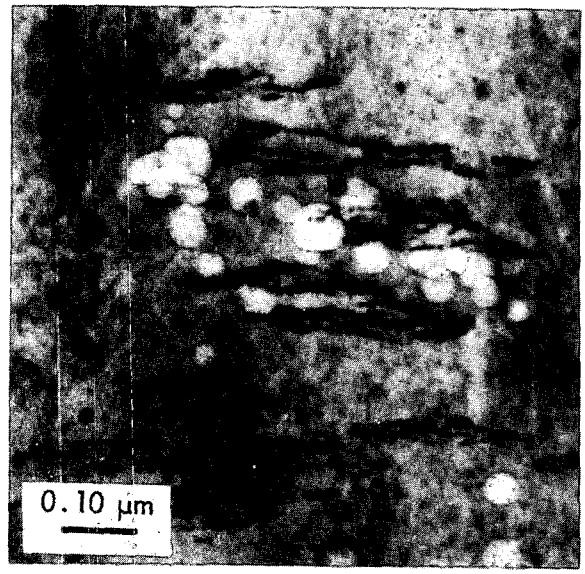


Fig. 2b. Thick Region of Specimen Shown in Fig. 2a. The large voids are distributed inhomogeneously and are associated with θ' interfaces.

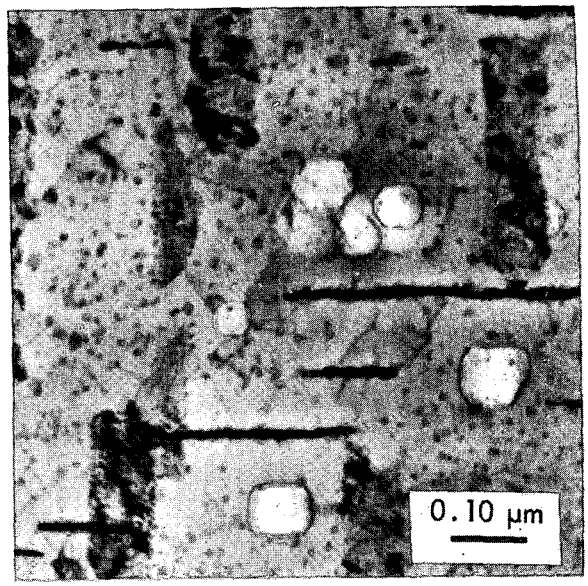


Fig. 3. Al–3.8 wt % Cu Alloy Aged 50 hr at 200°C Prior to Irradiation. Large faceted voids associated with θ′ particles and swelling increases with the scale of θ′. Foil plane near (011).

The 1.7% Cu alloy behaved in a similar manner, but there were some significant differences as shown in Table 1. When solution treated and quenched to form a fine homogeneous array of GP zones prior to irradiation this alloy did form voids during irradiation, as shown in Fig. 4. The void density is rather low and the size intermediate between the extremes of the bimodal void distribution. The appearance of the zones and associated diffraction effects (under the appropriate diffracting conditions) is similar to the appearance noted above for the identically treated 3.8% Cu alloy. When the 1.7% Cu alloy was aged to form θ′ plates prior to irradiation the swelling behavior was quite similar to the 3.8% Cu alloy, as shown in Table 1. An example of the association of large voids with the θ′ plates in this alloy is shown in Fig. 5.

DISCUSSION

It is clear from the data in Table 1 that the formation of various mestastable precipitates in the alloys prior to irradiation strongly surpressed the swelling expected as a result of the neutron irradiation, and that the magnitude of the swelling surpression depends on the type and size distribution of the precipitate. Further, metastable precipitates in these alloys appear to be relatively stable during irradiation, especially θ′. The swelling magnitude for the unalloyed aluminum in the

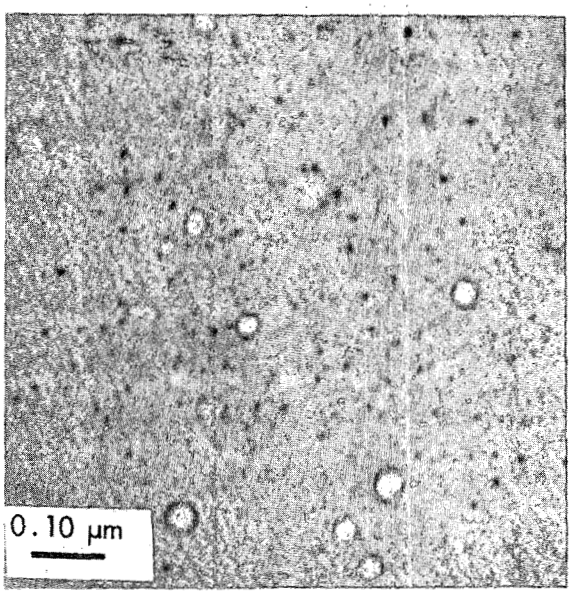


Fig. 4. Al–1.7 wt % Cu Alloy Solution Treated and Quenched, then Neutron Irradiated to ~3 x 10^{22} n/cm^2. Void size ~300 Å. Small dark spots are neutron induced silicon precipitate.* Foil plane near (001).

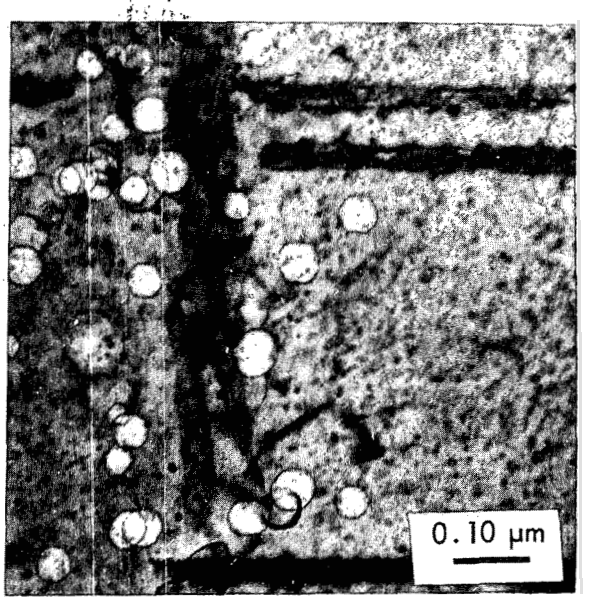


Fig. 5. Al–1.7 wt % Cu Aged 10 hr at 240°C Before Irradiation. Heterogeneous distribution of large voids, associated with θ′ particles. Foil plane near (2$\bar{1}\bar{5}$).

present work (12.4%) is in reasonable agreement with a linear extrapolation to the present neutron dose of the swelling observed for high purity aluminum by Risbet and Levy (see Al_I in Table 2 of ref. 2); the extrapolation yields 7.6% swelling. A linear dependence of swelling on dose has been observed in several metals, and is the most reasonable behavior to expect in the present case.[3] However, our results for swelling in the Al–3.8% Cu alloy show that minimum swelling is associated with an initial (i.e. preirradiation) GP zone array, and that swelling increases as the microstructure is coarsened prior to irradiation. These results are in disagreement with those of Risbet et al., who found for an Al–4% Cu alloy maximum swelling in the GP zone containing alloy and no swelling in the alloy when aged to contain the coarser precipitates θ′′, θ′ or θ prior to irradiation. The irradiation temperature of the two investigations was

*During the irradiation cycle in the reactor about 0.5 wt % Si was produced in the specimens by nuclear transmutation of some of the aluminum according to the reaction $^{27}Al(n,\gamma)^{28}Al$, $^{28}Al \rightarrow {}^{28}Si + \beta$ with the thermal component of the neutron spectrum; the silicon produced forms a fine precipitate dispersion visible in the background of all the micrographs.[6]

the same, but our total dose exceeded that of Risbet et al., by a factor of 50. In the case of alloys with the coarser preirradiation microstructures the explanation may be the higher dose used in the present work.

For alloys that contain metastable or stable second phases and exhibit resistance to swelling, the solute concentration in the solid solution that coexists with the second phase is of interest, since the origin of the swelling resistance could be the solid solution itself, the presence of the second phase, or both. For the case of Al–Cu alloys it is known that ~50 ppm Cu will reduce the swelling in high purity aluminum by about a factor of 2 at a dose of $\sim 5 \times 10^{20}$ nvt $(E > 0.1 \text{ MeV})^2$. Equilibrium solubility limit data for Cu in Al are available over the temperature range 550 to 250°C, and they show the solubility to be small.[7] Extrapolation of this data to 55°C, a rather large but necessary extrapolation, indicates that the amount of copper in the matrix solution at 55°C was <100 ppm. Based on this estimate we believe that Cu in solution in Al could reduce the swelling relative to pure Al by a factor of ~2, and that the metastable phases present during irradiation are more important to the swelling behavior. The swelling behavior of the Al–3.8% Cu alloy aged for two different times at 200°C prior to irradiation (see Table 1) supports this viewpoint; the amount of swelling differed by a factor of 4 for these two specimens containing the same metastable precipitate and thus the same copper concentration in the matrix solution. We recognize that the matrix copper concentration will vary somewhat depending on the particular coexisting metastable precipitate, however, in view of the large temperature extrapolations necessary to obtain solubility limits at 55°C we believe that 100 ppm is a reasonable estimate in general.

The probable origin of the void formation resistance for the present GP zone containing alloys is trapping of point defects caused by the irradiation and then recombination in the neighborhood of the zones. Bullough et al.[4] have discussed such a mechanism. The efficiency of the mechanism presumably depends on the coherent precipitate being a neutral (i.e., non-biased) sink for point defects, and the volume concentration of the precipitates. In the present case a high volume concentration

of coherent trapping centers was present in both alloys when solution treated and quenched prior to irradiation and they existed throughout the irradiation, though some coarsening occurred during the irradiation (see Fig. 1). However, the strain field associated with these zones has tetragonal rather than spherical symmetry; thus the recombination centers are biased. Apparently the critical point is that coherency is not lost at the zone, thus recombination is enhanced.

The origin of the large voids adjacent to θ' particles in the specimens aged appropriately prior to irradiation is directly related to the precipitate morphology. Two different mechanisms may contribute to the nucleation and growth of these voids. First, it is well known that these metastable precipitates lose coherency on their broad faces (on {100} matrix planes) when large, and develop an array of misfit dislocations there.[5] They may then appear to radiation-induced point defects as locally dense biased sinks. The resulting high vacancy concentration in the neighborhood of the broad faces would result in early nucleation of voids in this region, and subsequent growth. This concept requires misfit dislocations in the interfaces; larger θ' particles are more likely to be incoherent and to have a high population of misfit dislocations on their interfaces, in qualitative agreement with the observed increase in swelling associated with a coarser θ' dispersion. Second, it is probable that the matrix adjacent to θ' particles has a somewhat lower copper concentration than the particle-free matrix regions. Copper in solution in aluminum will reduce swelling, thus a reduced copper concentration near the interfaces will contribute to enhance swelling in those regions. The relative importance of these two effects is uncertain at present, however, in view of the restricted solubility of copper in aluminum below ~100°C the former mechanism is probably the most important.

REFERENCES

1. K. Farrell and A. E. Richt, Proc. ASTM Symp. on the Effects of Radiation on Structural Materials, Gatlinburg, Tenn., June 11–13, 1974.
2. A. Risbet and V. Levy, J. Nucl. Mater. 44, 113 (1972).
3. Y. Adda, Proc. Intern. Conf. on Radiation-Induced Voids in Metals, Albany, NY, p. 31, CONF-710601, USAEC Tech. Info. Center, 1972.
4. R. Bullough and R. C. Perrin, Proc. Intern. Conf. on Radiation-Induced Voids in Metals, Albany, NY, p. 769, CONF-710601, USAEC Tech. Info. Center, Oak Ridge, Tenn., 1972.
5. G. C. Weatherly and R. B. Nicholson, Phil. Mag. 17, 801 (1968).
6. K. Farrell, J. O. Stiegler, and R. E. Gehlbach, Metallography 3, 275 (1970).
7. M. Hansen and K. Anderko, Constitution of Binary Alloys, 2nd Edition, McGraw-Hill, p. 87 (1958).

SUPPRESSION OF VOID FORMATION IN NICKEL BY A DYNAMIC TRAPPING MECHANISM

S. M. Sorensen, Jr.* and C. W. Chen
Ames Laboratory-USERDA and Department
of Materials Science and Engineering
Iowa State University
Ames, Iowa 50010

ABSTRACT

The effect of carbon on void formation in high purity nickel under neutron irradiation to four fluences ranging from $4x10^{18}$ to $2x10^{20}$ n/cm^2 (E>0.1 MeV) at 500°C was investigated using transmission electron microscopy. In samples containing up to 84 wt ppm C, cubic voids were observed, and the void size tended to increase with increasing C content, while the void density decreased at much greater rates. Consequently, the associated swelling was seen to be steadily reduced. In samples containing 600 ppm C, void formation was completely suppressed, and an irradiation-induced dissolution of graphite precipitates occurred. The suppression of void formation in the irradiated Ni is attributed to an effective trapping mechanism associated with the interstitial C atoms in solution. Quantitative analyses on the size and density of voids reveal that the suppressing effect of C is mainly on void nucleation, not on growth. This trapping mechanism is considered to be dynamic in nature because the traps served by the C atoms can move through the lattice rapidly during irradiation until they are anchored in defect complexes.

It is now recognized that several different types of trapping mechanisms are effective in suppressing void formation in irradiated metals and alloys. Grain boundaries[1], dislocations[2], precipitates[3] and substitutional solute atoms[4] have all been shown to exert suppressing effects on void formation. These mechanisms display the common feature that the traps are static in nature because they remain essentially stationary in the lattice during irradiation. Recently we reported that a dynamic

---

*Now at the Inland Steel Research Center, East Chicago, Indiana 46312.

trapping mechanism is also capable of suppressing void formation in irradiated metals[5]. In the latter case, interstitial solute atoms of carbon were observed to suppress void formation in Ni which had been irradiated by neutrons to a fluence of 9×10^{19} n/cm^2 (E>0.1 MeV) at 710°C. The suppression was either partial or complete, depending on the carbon content.

Since 710°C is near the upper limit of the temperature range for void formation in Ni[6], the observed swelling at that temperature is extremely small, being less than 5×10^{-4}. To further confirm the suppressing effect of carbon and to explore its dependence on the temperature and fluence of irradiation, it is deemed necessary to irradiate the Ni-C alloys at lower temperatures and to various fluences. The present report describes the results obtained from a series of new experiments.

EXPERIMENTAL PROCEDURE

Sheet samples of high purity (>99.99 wt%) Ni were prepared with five different carbon concentrations (4, 16, 27, 84 and 600 wt ppm; carbon analysis performed by combustion chromotography). Prior to irradiation, all samples received a high-vacuum anneal at 1000°C for 24 hrs under a residual pressure $<2\times10^{-7}$ Torr. Four sets of samples were irradiated in the central thimble of the Ames Laboratory Research Reactor (ALRR) to fluences ranging from 4×10^{18} n/cm^2 to 0.26, 0.53, and 2.0×10^{20} n/cm^2 (E>0.1 MeV). Sample temperature was maintained at 500±10°C throughout the irradiations by Joule heating. The samples were examined by transmission electron microscopy (TEM) using a Hitachi 100 kV electron microscope. Voids produced at 500°C are cubic in shape, with little or no truncation. For such cubic voids, the edge length was used to characterize the void size, which was measured on the electron photomicrographs enlarged to 150,000x by a Zeiss particle-size analyzer. Foil thicknesses were determined by the slip-trace method, the extinction contour method, or (and) the method developed by Wolff[7].

RESULTS

Despite the variation of fluence by a factor of 50, the irradiation experiments yielded essentially the same results as far as void formation is concerned. Table 1 lists the results of quantitative analyses on the size and density of voids produced at 0.4 and 5.3×10^{19} n/cm^2 (E>0.1 MeV) fluences. In samples containing up to 84 ppm C, while the mean void size was observed to increase with increasing C content, the void density decreased at much greater rates. Consequently, the associated swelling decreased progressively with increasing C content. As might be expected, the maximum swelling increased steadily with fluence from 0.006% at 4×10^{18} n/cm^2 to 0.38% at 2×10^{20} n/cm^2. Typical examples of the induced cubic voids are shown in Fig. 1. Samples with 600 ppm C showed no voids at all four fluences, thus reconfirming the behavior previously observed[5] after irradiation at 710°C.

Because of the temperature dependence of the solubility limit for C in Ni, a related phenomenon was observed in the Ni-5 samples. The maximum solubility of C is about 600 ppm at 710°C but it is decreased to about 155 ppm at 500°C[8]. Thus, aging of the Ni-5 samples at 500°C for 100 hrs allowed carbon to be precipitated out in nodular form (Fig. 2A). The selected-area electron-diffraction patterns of the aged samples showed diffuse rings, indicating the amorphous structure of graphite in the precipitates consistent with the Ni-C phase diagram[9]. Upon irradiation, however, neither graphite precipitates nor voids were observed. Dislocations with heavy decorations of precipitates, presumably carbides, are the main defects in the irradiated lattices of Ni-5 samples (Fig. 2B).

DISCUSSION

The experimental results have confirmed that carbon is capable of suppressing void formation in Ni under neutron irradiation at 500°C as is at 710°C. The void suppression is only partial when the C content is relatively low; and the suppression becomes complete at the concentration of 600 ppm. Moreover, the same suppressing effect prevails in the fluence

range tested. It is therefore concluded that the effectiveness of the present method for the suppression of void formation is independent of the irradiation temperature and fluence up to at least 2×10^{20} n/cm^2 (E>0.1 MeV). Although this fluence is still a low value relative to the dosage expected for the core components of fast breeder reactors, nevertheless it is about three orders of magnitude higher than the critical fluence required for void formation in Ni[10].

To elucidate the trapping mechanism associated with the C atoms, we note that the void density decreased eventually to zero, but the void size increased with increasing C content. Thus, we further conclude that the effect of carbon is largely to suppress void nucleation, not void growth. A similar conclusion was reached in a recent study by Smidt et al.[4], who ascribed the suppressing effect of certain substitutional solutes on void formation in irradiated iron to a reduction of vacancy supersaturation, thereby making it difficult, and eventually impossible, for void nuclei to be formed. In this connection, it is pertinent to refer to another recent study by Makin and Walter[11], who examined the effect of C on the swelling of 316 - type stainless steel under 1 MeV electron irradiation in the temperature range 500-600^{o}C. They also found a reduction in swelling with increasing C content. However, they observed that carbon tended to increase the void density and to reduce the void growth rate. The latter observations are contrary to our results shown in Table 1. To reconcile the differences, it is important to realize that increasing the C content in 316-type stainless steel would also promote carbide precipitation, which is capable of reducing swelling through the formation of denuded zones around the carbide precipitates. This is in contrast to our Ni-5 samples, in which most of the carbon is in solution by virtue of the irradiation-induced dissolution of the graphite nodules. The dissolution effect of irradiation on graphite precipitates in Ni alloys was discussed by Nelson et al.[12].

To support the trapping capability of carbon atoms for vacancies, it was previously cited[5] that computer simulation studies have shown stable configurations of monovacancy-, divacancy-, and split interstitial-carbon atom complexes and,their binding energies are given at 0.30, 0.86, and

0.46 eV, respectively. The positive, relatively large binding energy for the divacancy-carbon atom complex implies that each carbon atom is capable of capturing at least two vacancies. It is not known at present whether or not the suppressing effect of carbon will eventually be saturated at high fluences. Additional experiments are needed to test this possibility.

The unique feature of this trapping mechanism is the dynamic behavior of the carbon atoms in solution. The jump frequency of C-atoms can be calculated applying the expression given in the previous paper[5]. Using the activation energy of 34.8 kcal/mole deduced by Berry[13] for the migration of C-atoms in Ni, and other appropriate constants, the jump frequency of C-atoms is calculated to be 3.5×10^7 jumps/s at 500°C. This jump frequency should be compared with 1.3×10^5 jumps/s for monovacancies in Ni at the same temperature. The comparison clearly shows that interstitial-carbon atoms are indeed highly mobile in the Ni lattice at 500°C.

In summary, we conclude that the presence of carbon atoms in the Ni lattice exerts a suppressing effect on void formation which is independent of the irradiation temperature and fluence up to 2×10^{20} n/cm^2 (E>0.1 MeV). The trapping mechanism associated with the C-atoms is characterized by the dynamic behavior of the interstitial-atom traps in contrast to the static nature of all other trapping mechanisms.

REFERENCES

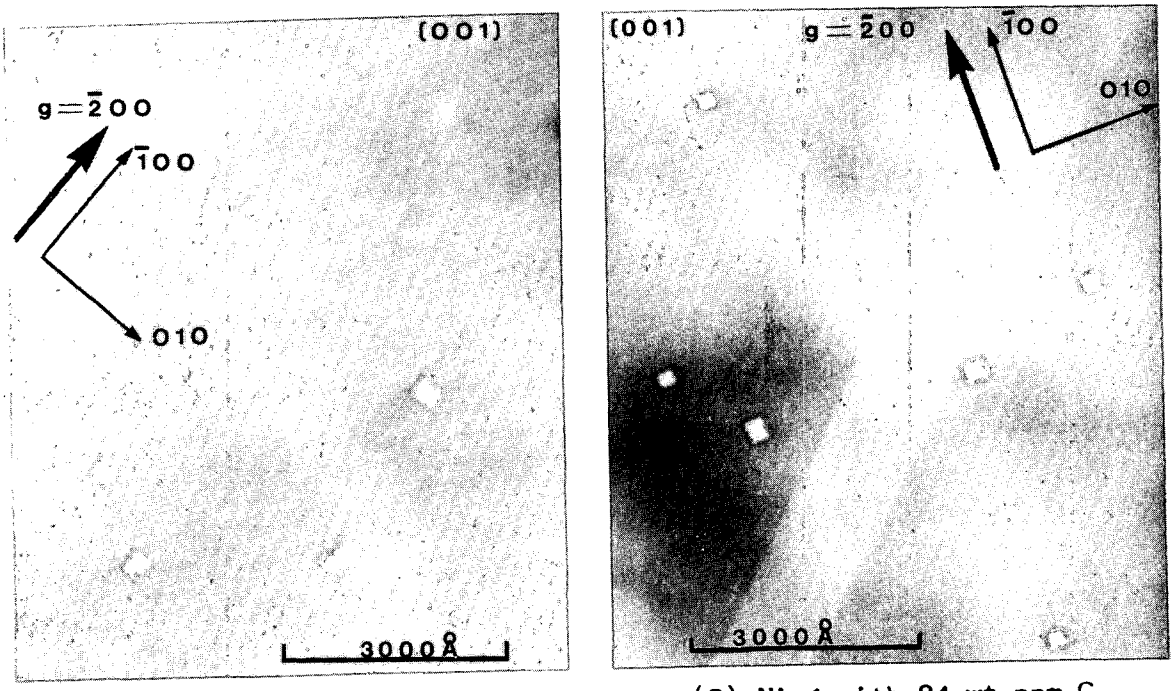
1. A. Wolfenden, K. Farrell and J. O. Stiegler, Electron Microscopy and Structure of Materials, p. 984, G. Thomas, R. M. Fulrath and R. M. Fisher (ed.) University of California Press, Berkeley, CA, 1972.
2. R. Bullough and R. C. Perrin, Irradiation Effects on Structural Alloys for Nuclear Reactor Applications, p. 317, ASTM STP 484, Am. Soc. for Testing and Materials, Philadelphia, PA, 1970.
3. J. J. Laidler, Radiation-Induced Voids in Metals, p. 174, J. W. Corbett and L. C. Ianniello (ed.), National Technical Information Service, Springfield, VA, 1972.
4. F. A. Smidt, Jr., J. A. Sprague, J. E. Westmoreland and P. R. Malmberg, Defect and Defect Clusters in BCC Metals and Their Alloys, p. 341,

R. J. Arsenault (ed.), National Bureau of Standards, Gaithersburg, MD, 1973.

5. S. M. Sorensen, Jr. and C. W. Chen, J. Nucl. Mat., to be published.
6. J. L. Brimhall and B. Mastel, Scripta Met. 4, 51 (1970).
7. U. E. Wolff, Metallography 2, 89 (1969).
8. K. Natesan and F. F. Kassner, Met. Trans. 4, 2557 (1973).
9. Metals Handbook, 8, Eighth Edition, p. 279, Metals Park, Ohio, 1973.
10. J. E. Harbottle and S. M. Dickerson, J. Nucl. Mat. 44, 313 (1972).
11. M. J. Makin and G. P. Walters, Consultant Symposium on the Physics of Irradiation Produced Voids, p. 299, AERE-R-7934, R. S. Nelson (ed.), AERE, Harwell, 1975.
12. R. S. Nelson, J. A. Hudson and D. J. Mazey, J. Nucl. Mat. 44, 318, (1972).
13. B. S. Berry, J. Appl. Phys., 44, 3792 (1973).

Table 1. Void formation data for high purity nickel irradiated in the ALRR to fluences of (I) 4.0×10^{18} and (II) 5.3×10^{19} n/cm^2 (E>0.1 MeV) at 500±10°C.

Sample Designation	Carbon Content, wt ppm	Mean Void Size, Å		Void Number Density, Voids/cm^3		Swelling (ΔV/V)	
		Fluence I	Fluence II	Fluence I	Fluence II	Fluence I	Fluence II
Ni-1	4	146	198	0.2×10^{14}	2.5×10^{14}	0.006%	0.19%
Ni-2	16	148	205	0.15×10^{14}	1.8×10^{14}	0.005%	0.15%
Ni-3	27	157	214	0.1×10^{14}	1.3×10^{14}	0.004%	0.13%
Ni-4	84	~200	247	$\sim 0.01 \times 10^{14}$	0.6×10^{14}	~0.001%	0.09%
Ni-5	600	NO VOIDS OBSERVED					



(A) Ni-1 with 4 wt ppm C. (B) Ni-4 with 84 wt ppm C.

Fig. 1. Cubic voids induced in high-purity nickel by neutron irradiation to the fluence of 5.3×10^{19} n/cm^2 (E > 0.1 MeV) at 500°C in the ALRR.

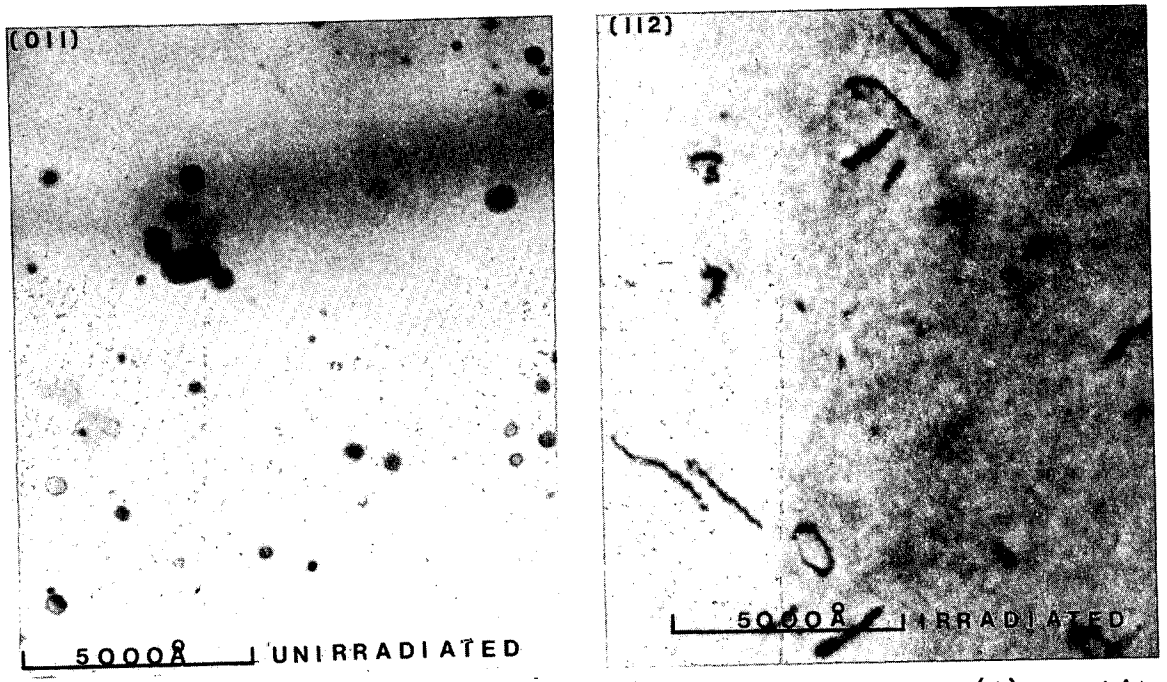


Fig. 2. Lattice defects observed in Ni-5 with 600 wt ppm C: (A) graphite nodules in a sample unirradiated but aged at 500°C for 100 hrs; (B) dislocations heavily decorated with precipitates in another sample irradiated to 5.3×10^{19} n/cm^2 (E > 0.1 MeV) at 500°C.

THE ORIGIN AND STABILITY OF DEFECT STRUCTURES: THE VOID LATTICE AND SIMILAR PHENOMENA

A.M. Stoneham
Theoretical Physics Division, AERE Harwell,
Oxon OX11 ORA United Kingdom

ABSTRACT

The void lattice is an impressive example of the many solid-state systems which show periodicity. The reasons for ordering and the factors determining the scale of the order are compared, giving a context within which the void lattice can be discussed. The reasons for the stability of the void lattice are summarised. Available information about the mechanism of formation is analysed, with emphasis on electron diffraction results.

---

1. PERIODICITY IN CONDENSED SYSTEMS

It is common knowledge that atoms order regularly on a microscopic scale to form crystals, and the macroscopic periodicities of man-made structures can be seen almost everywhere. But it still comes as a surprise to see periodicity on an intermediate scale - of a few hundred Angstroms, for example, as in the void lattice - or on a much larger scale, like convection cells in clouds. Yet there are many cases where intermediate periodicity is observed, with a wide range of reasons for it. This section surveys some of the known cases.

1.1. Classes of Periodic Structure

Broadly speaking, there are six main classes of regular array in which periodicity on an intermediate scale is seen:

A. Cases analogous to the void lattice, where the elastic interaction dominates:
- Void lattice and related bubble lattices[1]
- Ordering of shear planes in non-stoichiometric oxides[2]
- Interstitial alloys, e.g. $V_{16}N$, $Ta_{64}C$
- Ordered vacancy structures, e.g. V_6C_5 and related systems
- Ordered precipitates[3]
- Possibly ordered radiation-induced colloids in fluoride structures[4]

B. Domain structures, where the periodicity is usually the result of competition between two independent energy terms
- Nearly isotropic ferromagnets, with wall energy per unit volume $\sim D^{-1}$ (D≡wall spacing) and demagnetising field energy $\sim D^{+1}$
- Highly anisotropic ferromagnet, with wall energy $\sim D^{-1}$ and anisotropy energy $\sim D^{+1}$
- Ferroelectrics, where similar terms and elastic interactions associated with the domain-wall dislocations.

C. The Fluxoid Lattice in type II superconductors in a magnetic field[5]. Here there are filaments of normal metal in a superconducting matrix. If the penetration depth is much greater than the coherence length, there is a negative energy associated with the boundary. The detailed configuration is a compromise between this, magnetic field terms and a repulsion between the flux lines.

D. Ordering associated with electronic structure
- Long period alloys and cases where Fermi-surface geometry is important
- Charge-density waves; here the periodicity can be an irrational multiple of that of the underlying lattice.

E. Instability structures, where one starts from an unstable initial configuration and a periodicity emerges characteristic of the fastest-forming instability:
- Spinodal decomposition[6]
- Convection cells[7]
- Various premelting and solidification phenomena[8]

F. Miscellaneous forms which are less readily classified, e.g.:
- Vernier effects, when a slight mismatch between two simple periodic systems (e.g. ordinary crystal lattices) occurs
- Diffraction effects, e.g. the ripples on beaches caused by diffraction of water waves[9]
- Ordering in aqueous solution.[10]

These lists are far from complete, although they do indicate the rich diversity of these phenomena. Some of the common features are now analysed.

1.2 Characteristics of Periodic Structures

1.2.1 What determines the period?

Many of the structures involve a characteristic scale length, and the period is a multiple of that. Examples are:

System:	Scale length:
Void lattice	Void diameter
Shear plane structures	Repeat unit within single planes
Convection cells	Thickness of convection layer

In other cases there can be more than one scale length, and the period is related to them in a way which may be complex. Thus for the fluxoid lattice one has both a penetration depth and coherence length. In most of the systems discussed, the period is one which minimises the free energy. However, in instability structures, the period may be instead the one which gives the maximum initial rate of change of the free energy.

1.2.2 Does the structure align with the underlying lattice?

In some cases - all of class 1 (elasticity ordering) and some of class 2 (domains in very anisotropic ferromagnets), 4 (long period alloys) and 6 (Vernier structures) the mechanism leading to periodicity automatically

ensures alignment. In other cases, e.g. the fluxoid lattice, the alignment observed is the result of small terms which have little or no effect on the ordering[11]. In further cases still (e.g. domains in isotropic ferromagnets) the sample shape may be more important than its underlying structure.

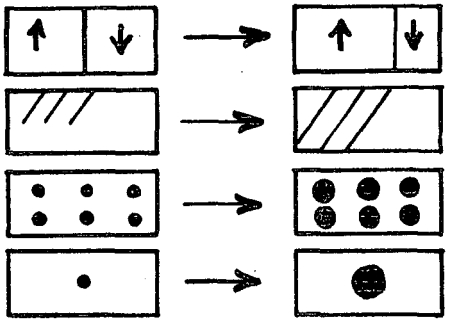
1.2.3 Can there be defects in the ordered structure?

In most cases the answer is yes. Particularly attractive examples of dislocations, interstitials, etc., have been seen in the void lattice and the fluxoid lattice. Disclinations are seen in the fluxoid case[5] and in domain structures in highly anisotropic ferromagnets[12]. In other cases, whilst the order is not perfect, it is hard to describe it in terms of a "defect" structure in an otherwise perfect array; the lack of order is closer to that in amorphous crystals, where short-range order may be maintained with reduced long-range order.

1.2.4 How can one change the ordered structure?

The simplest change is to try to alter either the relative sizes of the lattice parameter and the size of a basic unit(e.g. a void diameter) or to try to grow the lattice over a larger region. Various effects are found:

Growth on same sites → Examples are

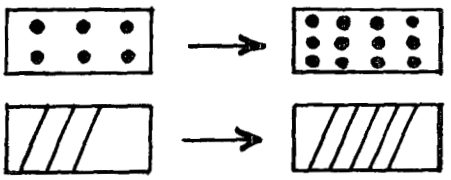


... Domain wall motion as field changes

. Shear plane extension

. BUT one simple case is NOT seen except in the (disordered) case of the interstitial-H liquid in Nb:H

More sites with components unaltered



Examples are

- Type II superconductors as field changes
- Shear planes as non-stoichiometry increases

Saturation: no growth or new sites



As in the void lattice, where vacancies stay in solution once the lattice has formed

1.2.5 Analogies with interactions in Crystals

The void lattice consists of an array of voids similar in broad structure to a crystal. Likewise (although in two dimensions) the fluxoid lattice is analogous to a crystal. How do the interactions between the units compare with the interactions between atoms?

The void-void interactions are relatively short-range, with a strong orientation dependence. The obvious analogues are the valence crystals like diamond and silicon. The interaction between flux lines, however, is purely repulsive and roughly isotropic- the lattice is stabilized by an interaction with a magnetic field which cannot be written as a sum of pairwise interactions. This is similar to simple metals, where repulsive interactions between cores are stabilized by non-pairwise interactions involving the electron gas.

1.3 General Aspects of Ordering: Diffraction Studies

The original void-lattice studies, and indeed those of most ordered systems, were made by direct microscopy. However, it became clear early on that diffraction methods had particular advantages because they could pick out just those periodicities which were developing long before they were directly visible. Moreover, the diffraction methods could be used for studying order of submicroscopic bubbles and voids, where direct observation is impractical.

1.3.1 Theories of Ordering

The exploitation of diffraction methods in studies of ordering (including spinodal decomposition and clustering) has been developed particularly by Hilliard and de Fontaine and their collaborators[13,6]. Their work, like that of Stoneham[14] and Tewary[15] for the void lattice, shows that there are advantages in working with a reciprocal-space theory too. The point is that the total energy can be written clearly and concisely in terms of the Fourier transforms of concentration fluctuations $[c_i(\underset{\sim}{r})-\bar{c}_i]$ and of lattice displacements $\underset{\sim}{u}(\underset{\sim}{r})$. From such energy expressions one can obtain (a) stability conditions, which may indicate ordering, and (b) eigenvalues and eigenvectors which indicate both how and how fast an instability develops.

In the case of the void lattice, the details are still rather too complex and obscure to apply the more sophisticated methods. But it must be stressed (i) that diffraction shows very clearly how order emerges, and (ii) the exploitation of periodicity allows a great simplification of much of the theory of the energetics of void lattices.

1.3.2 Electron Diffraction by Void and Bubble lattices

Electron diffraction by void and bubble lattices[16] has given results beyond the real-space observations:

(a) Order has been identified in cases where the dimensions were too small for direct microscopy and where the ordering was incomplete;

(b) Lattice parameters of ordered structures can be measured accurately, although it does not seem possible to discern[17] the shapes of the voids or the bubbles from spot intensities;

(c) The emergence of a void lattice from a "hard-sphere" gas of voids has been noted[18]. Here a ring of intensity is observed at first, evolving into spots as the lattice evolves.

(d) In some cases there are signs of extra, unexpected, spots appearing. Their origin is not clear, but they may be multiple reflections, analogous to those seen in grain-boundary diffraction[19].

2. ORDERING IN THE VOID LATTICE

2.1 Energies of Voids and competing clusters

Voids are not the only stable form of defect cluster, and it is well known that more stable structures exist for very large clusters. Since the competition between different clusters is important in itself as well as its possible relevance to ordering, rough values of the energies are quoted here[20]. Three basic energy parameters are the surface energy Γ, the stacking fault energy γ, and $E_o \equiv \frac{1}{2}$ (shear modulus) $b^2/(1-\nu)$, with ν = Poisson's ratio and b the Burgers' vector. It seems to be a rule that high stacking-fault energies (e.g. Mo, Ni) favour a void lattice.

Perfect hexagonal prismatic loop, radius R:

$$E_p \sim E_o \cdot \frac{R}{b} \{ \ln \frac{R}{b} + \frac{5}{3} \} \qquad \rightarrow N^{-\frac{1}{2}} \qquad (1)$$

Corresponding faulted loop, with stacking fault:

$$E_F \sim \frac{2}{3} E_p + \pi R^2 \gamma \qquad \rightarrow N^{o} \qquad (2)$$

Stacking fault tetrahedron with side L

$$E_s \sim \frac{1}{3\pi} E_o \frac{L}{b} \ln (\frac{2L}{b}) + \sqrt{3}\, L^2 \gamma \rightarrow N^{o} \qquad (3)$$

Void

$$E_v \sim 4\pi R^2 \Gamma \qquad \rightarrow N^{-1/3} \qquad (4)$$

The powers of N indicate the way the energy <u>per vacancy</u> changes with the number of vacancies for large clusters. However, in the cases relevant to the void lattice ($N \sim 1000$), the asymptotic form has not been reached, and either voids or stacking-fault tetrahedra are the most stable.

2.2 The Energetics of Ordering

2.2.1 General

Most of the contributions to the energy of void ordering were reviewed at the Harwell meeting[1]. The main conclusions were

I There was a substantial elastic interaction between the voids, and this was mainly responsible for the binding. The binding could be predicted accurately only if certain features were included specifically, namely

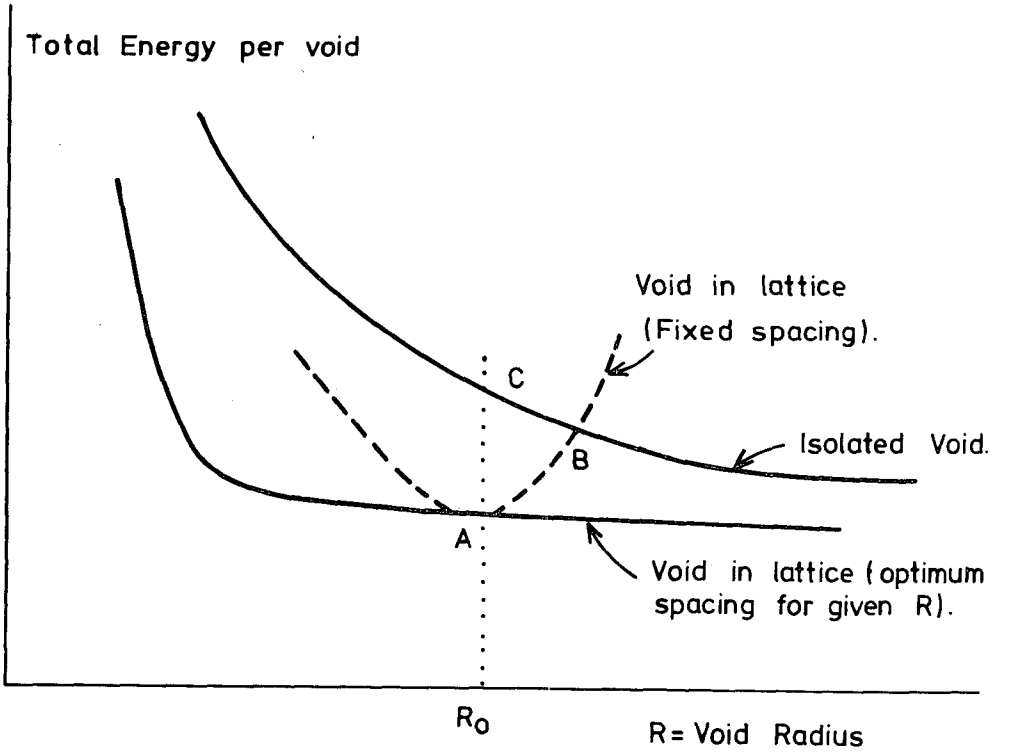
(a) The underlying atomic lattice structure

(b) The phonon dispersion of the host lattice

(c) The effects of the voids themselves on the elastic response of the host lattice.

II That the other mechanisms proposed for the binding of voids in the lattice, based on plasmon or anharmonic phonon contributions, seem neither necessary nor desirable, in that they tend to reduce the already-small predictions of lattice spacings.

III The energetic features - stability against loss of voids or void-lattice melting, stability against growth of all voids at constant lattice spacing, etc. - can be summarised in the figure. The stability against growth at constant spacing, which leads to saturation, depends on how fast curve II rises above point A, whereas stability against "melting" is determined by the energy (C-A) at constant void size, or by (B-A) when growth is allowed. Quantitative plots of this sort have been obtained in unpublished work of Stoneham and of Tewary.



IV All theories agree that the optimum void spacing L is roughly proportional to the void radius R, i.e. L/R depends only on the material to a good approximation. This seems to be confirmed by experiment, although without great consistency between different workers. The result means that, when a void lattice is formed, the fraction F of atomic sites in voids (≡ number of vacancies in voids/total sites) is a constant depending only on the material and not on predoping, form of radiation, temperature, etc. Moteff[21] has commented on another novel feature, namely that R and L can have a simple temperature dependence, and he notes that disordered voids tend to have a similar dependence of their mean radius and spacing.

2.2.2 Other Notions about Ordering

Some other proposals for void ordering have been made, none involving the known interaction between voids. Foreman's crowdion mechanism[22] was discussed previously, and its status seems the same: it appears capable of assisting in the tidying-up some of the void lattices with smaller lattice parameters. Other theories include some comments by Ashbee[23] and the two which follow:

Brown and Brown & Norris Model[24] Consider an array of voids, vacancies and interstitials. The total energy per atomic volume (which can be related to E_T, which is that per atom) is the sum of point-defect energies (proportional to their concentrations and formation energies) and the void surface energies (proportional to R^2 and to the surface energy). Interaction energies are ignored. If the void radius R and spacing L is fixed, then the steady-state point defect concentrations can be found from a diffusion equation. With the additional constraint of constant number of atoms, one can calculate $E_T(L,T)$. The conjecture is that $E_T(L,T)$ has a minimum for some value of L.

Brown & Norris show E_T does have such a minimum (unlike the original proposal), but conclude it is not related to either the void lattice or to the saturation of swelling.

Winter's Model Winter[25] suggested that all void lattices should be bcc because the vacancies have, on average, less far to go to the nearest void. His proposal is inconsistent with observation (fcc lattices are seen in Ni) and does not explain the alignment of the void and host crystal axes. There is no evidence that bulk vacancy motion is a serious limiting step, as assumed by Winter.

2.3 The Sequence of Void Ordering

At the 1974 Voids Symposium, the sequence of ordering thought most likely was this[1]:

I Initial formation of many small, randomly-distributed voids.

II Growth of voids, possibly with coarsening from the growth of large voids at the expense of small ones.

III Appearance of local ordered region where the void distribution is fortuitously favourable.

IV Spread of order to adjacent regions.

Some aspects of this rather superficial description need further comment.

2.3.1 Pre-ordering: Does any ordering occur in Stages I or II?

Are the initially-produced voids randomly distributed? And, if so, is there any underlying defect structure which is not random? There is no evidence for long-range order in the void distribution at first, and indeed order only appears to set in once the voids have reached a suitable size. But short-range order surely occurs: voids tend to avoid each other because they compete for vacancies in the metal around them. Indeed, the distribution of voids is rather like that in the "hard-sphere gas" model often used in the theory of liquids. The effective radius of the void relevant here is the radius of the region around it from which it takes vacancies, and not the geometric size of the void. The short-range order can be detected. In electron diffraction, rings are seen before any lattice spots are apparent, analogous to Debye-Scherrer rings[18]. If the voids order at constant density, the first ring should be at a scattering vector about 20% less than for the first spots.

2.3.2 Movement of Voids

Ordering requires adjustments in void positions. Is the behaviour consistent with known mechanisms of motion?

Motion over only small distances is needed for order at constant void density, for some short-range order appears to be present already. Since the spacing and void radius R are related, we may write a typical distance moved as $2\beta R$, with β of order unity. For voids of the sizes of interest, surface diffusion controls the rate. The void and surface diffusion constants are related by

$$D_{void} = \alpha N^{-4/3} D_s \qquad (5)$$

where N vacancies are assimilated into the void. Here α is of order unity, various slightly-different forms being given in the literature[26].

The characteristic time for voids to move a distance $2\beta R$ is

$$\tau = \gamma \frac{\Omega^{2/3}}{D_s} N^2 \qquad (6)$$

where Ω is the atomic volume and $\gamma=\gamma_R \equiv (1.54\ \beta^2/\alpha)$ for random motion, or $\gamma=\gamma_R\ \Theta/T$ when the motion is driven by a lattice stabilization energy $k\Theta$. Since observed lattices seem to have $H \sim 1500\text{-}2000^oK$, forced diffusion is somewhat faster. If the time of an experiment is τ_x, void motion can lead to lattice formation when $(D_S/\gamma) \geq \Omega^{2/3}N^2/\tau_x$. With $\gamma=10^{1/3}$, $\Omega=10^{-23}$ cc, τ_x = 1000 sec and N=1000, this means

$$D_S \geq 10^{-12}\ cm^2/sec \qquad (7)$$

There are many estimates of surface diffusion, with varying reliability and interpretation. Some experiments give a motion energy alone,[27,29] others probably give the sum of a motion and formation energy[28,29]. The results depend on which surface is involved, being fastest for the {110} faces believed to be the preferred facets in many cases. To give rough orders of magnitude, it seems clear that, if we can assume the formation energy part of the activation energy can be written off (for no thermal defect production is needed), then the criterion (7) is satisfied for Ta, W, Ni and Mo at least from 300^oC upwards. If one must include the formation energy factor, Mo must be taken to 700^oC or above. These numbers ignore both pinning and radiation-enhanced diffusion.

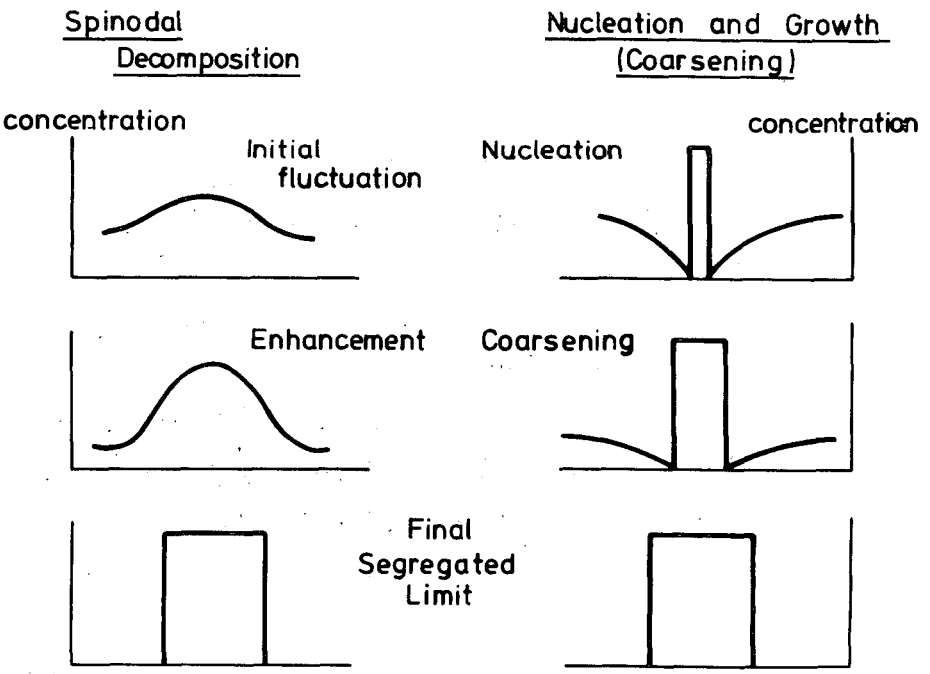
The conclusion is that voids move. They move neither fast nor far, but their motion is enough for lattice formation.

2.4 Comparison with other ordering mechanisms

The natural analogies to make are either with coarsening[3] and with spinodal decomposition[6]. Even here there are obvious differences, for for continued irradiation changing numbers of vacancies corresponds to changing concentrations in the alloy problem. But, since Evans has shown[30] that a specimen irradiated at low temperatures can form a lattice on annealing, we can assume that the kinetics of radiation damage are not important provided the damage is sufficient. We argue here that the void lattice resembles coarsening, and not spinodal decomposition.

The main features of coarsening are shown by Andell, Nicholson and Eshelby's study of aged Ni-Al. Here nucleation of precipitates ceases very early, and larger particles grow at the expense of small ones. The growth is diffusion-controlled and surface-energy driven. The ordering of precipitates occurs because of the elastic interaction between precipitates. This interaction does not affect the kinetics of coarsening, nor does it inhibit diffusion; it merely selects those particles favourably located for growth.

All these features (with a slight change of vocabulary) fit well with what is known of the void-lattice formation, although no corresponding kinetic studies have been made. By contrast, there seems no reasonable analogy with spinodal decomposition. In spinodal decomposition, a new phase forms by a continuous process, where a concentration fluctuation leads to the rapid formation of periodic clusters. The driving force is an interaction energy term which, for the void lattice, would require vacancies to tend to congregate even without void formation (i.e. vacancies would tend to move up a vacancy concentration gradient when the gradient is changing sufficiently rapidly). The main differences are indicated in the diagram (after ref. 6)



REFERENCES

1. A.M. Stoneham, Harwell Voids Symposium (AERE-R7934, ed. R.S. Nelson) p319 (1974).
2. A.M. Stoneham and P.J. Durham, J. Phys. Chem. Sol. 34 2127 (1973)
3. A.J. Andell and R.B. Nicholson Acta Met. 14 1295 (1966)
4. L.E. Murr, Science 183 206 (1974)
5. H. Traube & U Essmann, Phys.Stat.Sol. 18 813 (1966), 25, 373 (1968)
6. J.W. Cahn, Trans. Met. Soc. AIME 242 166 (1968) J.Appl.Phys. 39 4052(1968)
7. S. Chandresekhar, Hydrodynamics & Hydromagnetic Stability (Oxford University Press)
8. M. Hamalainen, J. Cryst. Growth 1 125 (1967), 2 131 (1968)
9. e.g. W. Bascom, Sci. Am., August 1959.
10. R.A. Howe, W.S. Howells & J.E. Enderby, J. Phys. C4 L (1972)
    G.W. Neilson, R.A. Howe & J.E. Enderby, Chem. Phys. Lett. 33 284 (1975)
11. H. Vilmaier, R. Zeller & P.H. Dederichs, Phys. Lett. 44A 331 (1973)
12. See, e.g. fig. 5.5, p109 of Craike & Tebble, Ferromagnetism & Ferromagnetic Domains
13. D. de Fontaine & H.E. Cook, Battelle Critical Phenomena Colloquium 257 (1970)
    D. de Fontaine, J. Phys. Chem. Sol. 33 297 (1972) and 34 1285 (1973)
14. A.M. Stoneham J. Phys. F1 778 (1971)
15. V.K. Tewary & R. Bullough, J. Phys. F2 L69 (1972)
16. S.L. Sass & B.L. Eyre Phil Mag. 27 1447 (1973)
    B.L. Eyre & A.F. Bartlett, J. Nucl. Mat. 47 143 (1973)
17. A.M. Stoneham, J. Phys. F4 1335 (1974)
18. D. Mazey, private communication
19. S.L. Sass, T.Y. Tann & R.W. Balluffi, Phil. Mag. 31 559 (1975)
20. J.A. Sigler & D. Kuhlmann-Wilsdorf, Harwell Clusters Symposium (AERE-R5269, ed. M.J. Makin) p.125 (1966)
21. J. Moteff, V.K. Sikka & H. Jang, Harwell Voids Symposium (AERE R-7934, ed. R.S. Nelson) p181 (1974)
22. A.J.E. Foreman, AERE R-7135 (1972)

23. K.H.G. Ashbee, Reactivity of Solids (ed. J.S. Anderson, M.W. Roberts, F.S. Stone; Chapman & Hall) p66 (1972)

24. L.M. Brown, Scripta Met. 6 387, 793 (1972)
D.N. Seidman & R.W. Balluffi, Scripta Met. 6 789 (1972)
D.I.R. Norris & L.M. Brown, Scripta Met. 8 1045 (1974)

25. A.T. Winter, Scripta Met. 7 49 (1973)

26. (a) E.E. Gruber, Albany Voids Meeting (ed. J.W. Corbett & L.C. Iannielo, U.S.A.E.C. Symposium 26) p665 (1972)
(b) Y.E. Geguzin & M.A. Krivoglaz, Migration of Macroscopic Inclusions in Solids, Consultants Bureau 1973.

27. W.R. Graham & G. Ehrlich, Phys. Rev. Lett. 31 1407 (1973) and Thin Sol. Films 25 85 (1975)
G. Ayrault & G. Ehrlich, J. Chem. Phys. 60 281 (1974)
T.T. Tsong, P. Cowan & G. Kellogg, Thin Sol. Films 25 97 (1975)

28. K. Singer & D. Tabor, Structure & Properties of Metal Surfaces, (CNRS 1970)
See also listings in Surfaces and Interfaces I (ed. J.J. Burke, N.L. Reed & V. Weiss; Syracuse University Press) p302 (1967) and Surface Phenomena of Metals (Society of Chemical Industry Monograph 28) p13 (1968)

29. The parameters taken from refs 28, 29 were the following:

System	D_{SO} cm^2/sec	Activation Energy (eV)	Motion Energy (eV)
Ni	300	1.7	-
Cu	650	1.9	-
Mo	0.8	3-3.4	0.92
Ta	-	2.0	0.78

Values given are for <110> where available, otherwise for unspecified surfaces.

30. J.H. Evans, Harwell Voids Symposium (AERE R-7934, ed. R.S. Nelson) p 95 (1974).

STABILITY OF VOID LATTICES UNDER IRRADIATION: A KINETIC MODEL

P. Benoist and G. Martin
DEDR and SRMP , CEN Saclay
BP n° 2, 91190 Gif/Yvette - FRANCE

ABSTRACT

Voids are imbedded in a homogeneous medium where point defects are uniformly created and annihilated. As shown by a perturbation calculation, the proportion of the defects which are lost on the cavities goes through a maximum, when the voids are arranged on a translation lattice.

If a void is displaced from ist lattice site, its growth rate becomes anisotropic and is larger in the direction of the vacant site.

The relative efficiency of BCC versus FCC void lattices for the capture of point defects is shown to depend on the relaxation length of the point defects in the surrounding medium.

It is shown that the rate of energy dissipation in the crystal under irradiation is maximum when the voids are ordered on the appropriate lattice.

INTRODUCTION

The existence of an instability threshold for a crystal under irradiation has been recently predicted [1,2]. Above a critical temperature dependent Point Defect (PD) generation rate, the crystal may undergo a transformation by broken spatial symmetry : the amplitude of certain PD concentration waves will then increase, resulting in a spatially periodical clustering of the PD. These PD clusters may then collapse into voids, loops, tetrahedra, etc ...

In the present work it is shown that, once a void lattice has been generated, the voids under irradiation are stabilized on their void

lattice sites by the overlapping of the diffusion fields of the PD around each cavity. Moreover, under reasonable assumptions, it is shown that the intensity of dissipation of the energy injected into the crystal by PD production is maximum when the voids are ordered on the appropriate translation lattice. Void lattices might therefore be examples of *dissipative structures*, the appearance of which is triggered by far from equilibrium conditions [3].

MUTUAL INFLUENCE OF GROWING CAVITIES

Fundamental equation

Let us consider a population of spherical cavities of uniform radius ρ, imbedded in a medium where PD are uniformly generated at a rate g. Under steady state conditions, the PD concentration $C_d(\vec{r})$ at a point $\vec{r}$ of the domain external to the cavities is governed by Eq. (1) :

$$D \nabla^2 C_d - \alpha C_d + g = 0 \qquad (1)$$

where D is the PD diffusion coefficient and αC_d is a linearized expression of the rate of PD annihilation in the medium around the cavities. As a boundary condition, it is assumed that $C_d(\vec{r})$ is equal to zero at the surface of every cavity. Eq. (1) may also be written :

$$D \nabla^2 C - \alpha C = 0 \qquad (2)$$

with the definition : $C(\vec{r}) = C_d(\vec{r}) - (g/\alpha)$, the value of C at the surface of the cavities being now $- g/\alpha$.

Let us now define the Green function $G(\vec{r}' - \vec{r})$ in an infinite homogeneous medium by :

$$D \nabla^2 G - \alpha G + \delta(\vec{r}' - \vec{r}) = 0 \qquad (3)$$

the function G being equal to zero at infinity.

Multiplying Eq. (2) by G, Eq. (3) by C, substracting and

integrating with the help of Green's theorem leads to * :

$$\int_{\sigma} G(\vec{r}' - \vec{r})\, j(\vec{r}')\, d^2 r' = \frac{g}{\alpha}\left[\frac{1}{2} - D \int_{\sigma} \frac{\partial G(\vec{r}' - \vec{r})}{\partial n'}\, d^2 \vec{r}'\right] \qquad (4)$$

where $\vec{r}$ and $\vec{r}'$ define points on the surface of the cavities; the integration is extended to the total surface of all the cavities (σ); $\frac{\partial}{\partial n'}$ is the normal derivative at point $\vec{r}'$, directed outward the cavity, and

$$j(\vec{r}') = D \frac{\partial C(\vec{r}')}{\partial n'} \qquad (5)$$

The function G is known to be

$$G(\vec{R}) = \frac{e^{-\kappa R}}{4\pi D R} \qquad (6)$$

where $R = |\vec{R}|$, $\vec{R} = \vec{r}' - \vec{r}$ and κ is the inverse of the relaxation length of the defects, in the medium between the cavities : $\kappa = \sqrt{\alpha/D}$.

Eq. (4) is a Fredholm equation of the first kind. It gives the flux $j(\vec{r}')$ of the defects entering the unit surface of the cavity at the point $\vec{r}'$, as a function of the parameters g, α, D and of the spatial distribution of the voids, which is defined by the set of all possible values of R.

Eq. (4) may be rewritten

$$|G|j> = |Q> \qquad (7)$$

where G is an operator. Eq. (7) is the basic equation of the model. It enables to solve the problem suggested recently by Winter [4].

Perturbation Calculation

Let us start with voids located at the sites of an infinite translation lattice, called the void lattice (VL). The unknown flux $j(\vec{r}')$ is invariant under the VL translations.

Let us now displace slightly one cavity, labelled o, from its VL site. The resulting variations in the operator G and the source

---

* the term 1/2 results from an additionnal contribution to the integral of the RHS of Eq. (4), when $\vec{r}' \to \vec{r}$ (non uniform convergence).

term Q in Eq. (7) are given to first order by :

$$|\delta G|j> + |G|\delta j> = |\delta Q> \tag{8}$$

Let us represent the integration over $\vec{r}$ on the total surface of all the cavities by $<1|$. Then from Eq. (8), one gets :

$$<1|G|\delta j> = <1|\delta Q> - <1|\delta G|j> \tag{9}$$

In this equation, $<1|G|$ and $|j>$ are functions of $\vec{r}'$. Since they refer to the unperturbed VL, they are invariant under the VL translations. Neglecting higher order harmonics, they may be replaced by their average values on the surface σ_l of any single cavity (l), which we note respectively $\frac{1}{\sigma l} <1|G|l>$ and $\bar{j}$. Therefore, from Eq. (9) :

$$<1|\delta j> = \frac{<1|\delta Q> - \bar{j} <1|\delta G|1>}{\frac{1}{\sigma_l} <1|G|l>} \tag{10}$$

$<1|\delta j>$ is the total variation of the flux of PD entering the cavities, induced by the displacement of one cavity from its lattice site. That $<1|\delta j>$ is *always negative* as claimed in the introduction can be proved as follows :

a) From Eq. (6), $\frac{1}{\sigma l} <1|G|l>$ is seen to be positive. The same is true for $\bar{j}$.

b) Let us rewrite $<1|\delta Q>$ and $<1|\delta G|1>$ as follows :

$$\begin{aligned} <1|\delta Q> &= -\frac{gD}{\alpha} \Sigma_k \Sigma_{l \neq k} \delta P'_{kl} \\ <1|\delta G|1> &= \Sigma_k \Sigma_{l \neq k} \delta P_{kl} \end{aligned} \tag{11}$$

where δP_{kl} and $\delta P'_{kl}$ are respectively the perturbation of $<l|G|k>$ and $<l|\frac{\partial G}{\partial n'}|k>$; k and l refer to the surfaces of cavities k and l.

From Eq. (6) one finds that, R_{kl} being the distance between the centres of the spheres k and l:

$P'_{kl} = \gamma' G(R_{kl})$ and $P_{kl} = \gamma G(R_{kl})$ with

$$\gamma' = (4\pi)^2 \frac{\rho^2}{\kappa} \text{ sh } \kappa\rho \ (\text{ch } \kappa\rho - \frac{\text{sh } \kappa\rho}{\kappa\rho})$$

$$\gamma = (4\pi)^2 \frac{\rho^2}{\kappa^2} \text{ sh}^2 \ \kappa\rho \qquad (12)$$

As shown by Eq. (12) γ and γ' are always positive. Since $k = 0$ labels the only cavity to have been displaced, the non vanishing terms in Eq. (11) are such that k or l is equal to zero. Therefore the numerator in Eq. (10) is given by :

$$- 2 \ (\frac{gD}{\alpha} \gamma' + \bar{j} \ \gamma) \ \Sigma_{k\neq 0} \ \delta G \ (R_{ko}) \qquad (13)$$

which is always negative provided that the summation over k is always positive. That this is true can be proved rigorously, but can be physically understood from the following : according to Eq. (3), $\Sigma_{k\neq 0} G \ (R_{ko})$ is the concentration at the site zero, created by a set of positive PD punctual sources, located at all the sites but the zeroth, of a translation lattice, in an homogeneous medium. At site zero, the absence of a PD source creates a dip in the PD concentration. Therefore the variation of this concentration in the vicinity of the zeroth site, $\Sigma_{k\neq 0} \ \delta G \ (R_{ko})$, is always positive.

As a summary, the PD elimination rate on cavities is maximum when these cavities are ordered on a translation lattice. A similar effect was noticed by Ham [5] in the problem of precipitation on dislocations.

CONSEQUENCES

Dynamical Stability of growing Cavities

If a cavity is slightly displaced from it's VL site, its growth rate becomes anisotropic : it is larger in the direction of the unoccupied VL site. This results from the dipolar term in $j(\vec{r})$ on the displaced cavity : the PD reach preferentially the cavity from the vacant VL site. This can be proved rigorously using the same formalism as above, but the following argument gives the physical mechanism : consider two cavities imbedded in the medium described by Eq. (1). If the cavities

are very far apart, the PD flux around each cavity has a spherical symmetry : the growth rate of each cavity is isotropic. On the other hand, if the two cavities are in contact, no PD will enter any of the cavities at the point of contact. Between these two limiting cases, less defects will reach the cavity from the direction which points to its neighbour. If surface diffusion effects are neglected, the cavity will *grow away* from its neighbour.

In other words, the overlapping of the diffusion fields of the PD around each cavity creates a repulsive "force" on the cavity. For reasons of symmetry, this force is zero when all cavities are on their VL site. This is the kinetic mechanism for VL stability.

The VL stability with respect to void radius fluctuations is under study.

Respective Capture Efficiencies of different Void Lattices

For which translation lattice is the PD elimination rate on cavities maximum ?

Let us come back to a perfect VL. As discussed above, $j(\vec{r}')$ may be replaced by its average value $\bar{j}$, calculated from Eq. (7). Integrating on $\vec{r}$ over the surface of the cavity l gives :

$$\bar{j} = \frac{\langle l|Q\rangle}{\langle l|G|1\rangle} = \frac{g/\alpha\ [\sigma_l/2 - D\ \Sigma_k\ P'_{kl}]}{\Sigma_k\ P_{kl}} \qquad (14)$$

From Eq. (12) :

$$\bar{j} = \frac{g\ \sigma_l}{2\ \alpha\ \gamma\ \Sigma_k\ G\ (R_{ko})} - \frac{g\ D\ \gamma'}{\alpha\ \gamma} \qquad (15)$$

Since $\bar{j}$ is always positive, the VL for which $\bar{j}$ is maximum is the one for which $f = \Sigma_k\ G\ (R_{ko})$ is minimum.

If the PD relaxation length is large compared to the nearest neighbour distance d in the void lattice ($\kappa d << 1$), the exponential in Eq. (6) is unity and one is left with the calculation of the lattice sums in different lattices for a given lattice points density.

As shown by Sholl [7] the lattice sum f is minimum in the BCC structure. Therefore, in the limit $\kappa d << 1$, $\bar{j}$ is maximum for the BCC

void lattice.

In the reverse case ($\kappa d >> 1$), the first nearest neighbours of the displaced cavity give the dominant contribution to f. For a given void density, the FCC lattice provides the largest nearest neighbour distance. It therefore minimizes f or equivalently maximizes $\bar{j}$.

Between these two limiting cases, there exists a critical value of κ which gives to the BCC and FCC void lattices the same PD capture efficiency.

VOID LATTICES AS DISSIPATIVE STRUCTURES

The physics of the preceeding sections may be summarized as follows : under irradiation, the overlapping of PD diffusion fields around the cavities produces a repulsive "force" on the cavities, which stabilizes them on the VL sites. For a given void population (number density N, radius ρ), BCC VL structure is the most absorbing, provided that the PD relaxation length between the cavities is large. As will be shown below, these facts are relevant to the energetics of the crystal under irradiation .

The generation of Frenkel pairs injects into the unit volume of the crystal the formation energy of these pairs at a rate proportional to g. Under quasi steady state conditions, part of this energy is stored as surface energy of the cavities, at a rate proportionnal to the rate of increase of the specific void area : $\dot{a}$. The remaining part is dissipated into heat : it can neither be stored as dislocation line tension since the dislocation density is known to saturate, nor as PD supersaturation since this supersaturation decreases as swelling proceeds.

As shown be the standard rate theory of swelling [7],

$$\dot{a} = \eta 4\pi N \frac{D_v \kappa_{di} - D_i \kappa_{dv}}{\kappa_{iv}} \left[-1+\sqrt{1+ \frac{4\, g\, \kappa_{iv}}{(\kappa_{dv}+\eta 4\pi N\rho D_v)\ (\kappa_{di}+\eta 4\pi N\rho D_i)}}\ \right] \qquad (16)$$

where κ_{iv}, κ_{id}, κ_{vd} are respectively the rate-constants for interstitial-vacancy, interstitial-dislocation, vacancy-dislocation reactions and η

a correction parameter which we introduce to account for the effect of the spatial distribution of voids on the rate of PD elimination on these voids; η may be calculated from Eq. (14) and is maximum for the appropriate VL.

As shown by Eq. (16), $\dot{a}$ decreases when η increases provided that $N\rho$ is large i.e. that the cavities contribute predominantly to the elimination of the PD. The presence of thermal vacancies which has been omitted in Eq. (16) does not alter this trend.

Therefore, for given values of g, N, and ρ, $\dot{a}$ is minimum when the cavities are located at the nodes of the appropriate lattice (η maximum). Thus the rate of energy dissipation is maximized by the formation of this void lattice. Void lattices might therefore be an example of *dissipative structures* in solids [8].

It therefore appears that intensive irradiation may trigger a restructuration of crystalline solids [1,2], the new structure being highly organized and quite stable. This is an illustration for crystalline solids of a general idea which encounters more and more success in physical chemistry [3]. That the PD clusters arrays which have been reported up to now [9-12] *are* examples of such structures, remains however to be proved by an appropriate experimentation and more realistic calculations, which in particular would take into account the interaction energy between the PD clusters [13].

Acknowledgements : We thank D^r Adda for his continuous interest in this work and P^r Gerl and D^r Soulé for usefull suggestions.

REFERENCES

1 . G. Martin, This issue.

2 . G. Martin, Phil. Mag., in the press

3 . I. Prigogine and R. Lefever, Adv. Chem. Phys., 29, 1 (1975)

4 . A.T. Winter, Scr. Metall., 7, 49 (1973)

5 . F.S. Ham, J. Appl. Phys., 30, 915 (1959)

6 . C.A. Sholl, Proc. Phys. Soc., 92, 434 (1967)

7 . M. Gomolinski and G. Brébec, J. Nucl. Mater., 43, 59 (1972)

8 . P. Glansdorff and I. prigogine, Structure Stabilité et Fluctuations, Masson, Paris, 1971.

9 . G.L. Kulcinski and J.L. Birmhall, Effect of radiation on substructure and mechanical properties of metals and alloys, p. 258, ASTM STP 529, Philadelphia, 1973.

10. D.J. Mazey, S. Francis and J.A. Hudson, J. Nucl. Mater., 47, 137 (1973)

11. M.O. Ruault and B. Jouffrey, Appl. Phys. Lett., 25, 265 (1974)

12. J.O. Stiegler and K. Farrell, Scr. Metall., 8, 651 (1974)

13. e.g. J.R. Willis, J. Mech. Phys. Solids, 23, 129 (1975)

VOID ORDERING IN O-DOPED Nb AND Nb-1 AT.% Zr INDUCED BY $^{58}Ni^{+}$ BOMBARDMENT

B. A. Loomis, A. Taylor, and S. B. Gerber
Materials Science Division
Argonne National Laboratory
Argonne, Illinois 60439

ABSTRACT

The experimental results show that void ordering does not occur in "pure" Nb or Nb-1 at.% Zr during irradiation with 3.2-MeV $^{58}Ni^{+}$. O impurity in Nb and Nb-1 at.% Zr can result in void ordering at irradiation temperatures of 750 to 1010°C. The minimum concentration of O in Nb that will result in void ordering is dependent on the irradiation temperature. The necessity for O (or N) impurity in Nb for the formation of an ordered void array tends to be substantiated by the observation that a Ti coating on O-doped Nb precludes the formation of an ordered void array. The experimental results suggest that a relation may exist between the oxide (or nitride) surface film with a "domain" structure and the ordered void array.

INTRODUCTION

A recent paper on the void swelling of pure Nb and Nb-1% Zr by Loomis et al.[1] reported that a high O concentration in Nb and Nb-1% Zr prior to $^{58}Ni^{+}$ irradiation leads to void ordering. In the present paper, we shall discuss the experimental results of an extensive study to determine the role of intrinsic O impurity in Nb that results in the formation of the ordered void array. We shall also present results that suggest a relation may exist between oxide (or nitride) films observed on O-doped Nb and the formation of the ordered void array. Finally, we shall present microstructural evidence that a Ti coating on O-doped Nb precludes the formation of an ordered array.

*Work supported by the U.S. Energy Research and Development Administration.

EXPERIMENTAL MATERIALS AND PROCEDURE

The preparation of high-purity Nb and Nb-1% Zr basic material used in the present study has been described.[1] The pure materials were doped with O by heating at 1200°C in O at 1 x 10^{-6} to 5 x 10^{-6} Torr for 5-15 min and then homogenized by annealing at 1200°C for 1 hr. This procedure yielded Nb and Nb-1% Zr containing O concentrations ranging from 0.05 to 0.85% O. Some of this material was subsequently coated with ∿1600 Å of Ti by vapor deposition.

Specimens of Nb, Nb-1% Zr, Nb-0.05 to 0.85% O, and Ti-coated material were irradiated at the Argonne Dynamitron facility with 3.3 ± 0.3-MeV $^{58}Ni^{+}$ at a nominal displacement rate of 5 x 10^{-3} dpa/s (atom displacements per atom per second). A more detailed account of the irradiation procedure has been presented.[1]

Following irradiation, a specimen for transmission-electron-microscopy (TEM) observation was perforated from the unbombarded surface by electrochemical polishing in a HNO_3-HF solution. The void distribution in the bombarded layer was determined by electrochemical removal of successive 2000-3000 Å sections from the bombarded surface in a 2.5% HF-5% H_2SO_4-92.5% MeOH solution. The TEM examination and evaluation of the data have been described.[1]

EXPERIMENTAL RESULTS

The ordered void array in $^{58}Ni^{+}$-irradiated Nb containing O impurity has a body-centered-cubic (bcc) superlattice that is superimposed on the host Nb bcc lattice. In Fig. 1, the superlattice of voids in Nb-0.52% O after irradition at 780°C to ∿50 dpa is shown in the <100>, <110>, or <111>.

The void microstructures in pure Nb and Nb that contain increasing concentrations of O impurity prior to irradiation at 780 and 828°C are shown in Fig. 2. It can be seen in Fig. 2 that the ordered void array is not formed in "pure" Nb, i.e., 0.006% O, 0.003% N, and 0.011% C. As can also be observed in Fig. 2, to obtain a more perfect void order, the

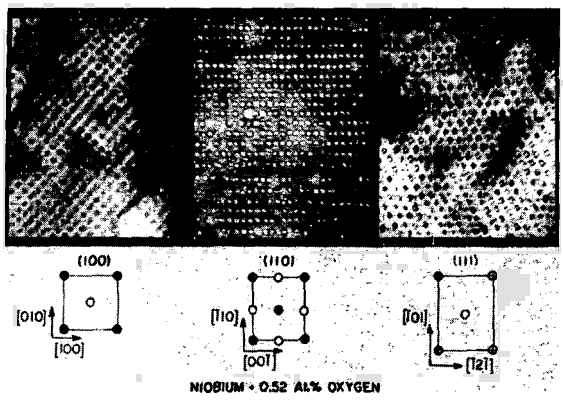


Fig. 1. Void lattice in Nb-0.52% O in <100>, <110>, or <111> after irradiation at 780°C to ∿50 dpa.

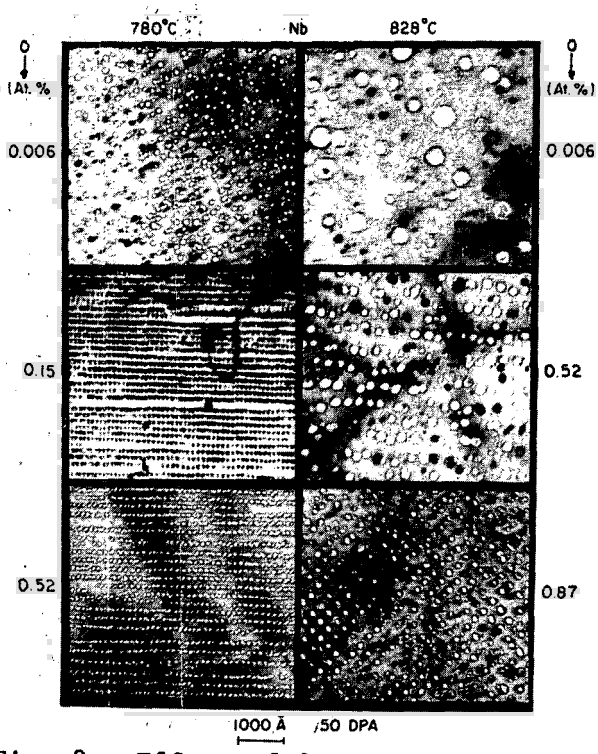


Fig. 2. Effect of O concentration on void lattice formation.

O concentration must be increased as the irradiation temperature increases. Void ordering is observed in Nb-0.5% O at irradiation temperatures between 750 and 1010°C. However, the perfection of the void order decreases substantially with an increase in temperature for Nb-0.5% O material. The decrease in perfection with an increase in temperature can be related to a corresponding increase in the void diameter and a decrease in void number density. Void ordering has not been observed in Nb-0.5% O material for irradiation temperatures below 750°C. Void ordering is also not observed in "pure" Nb-1% Zr but is observed in Nb-1% Zr-0.27% O.

The distribution of void size in Nb and Nb-0.5% O (ordered voids) after irradiation at 780 and 828°C to ∿50 dpa is shown in Fig. 3. The general observation, which is represented in Fig. 3, is that O doping of Nb results in a decreased average void size and an increased void number density.

The dependence on the irradiation temperature of the void lattice parameter, average void size, and the ratio of void lattice parameter

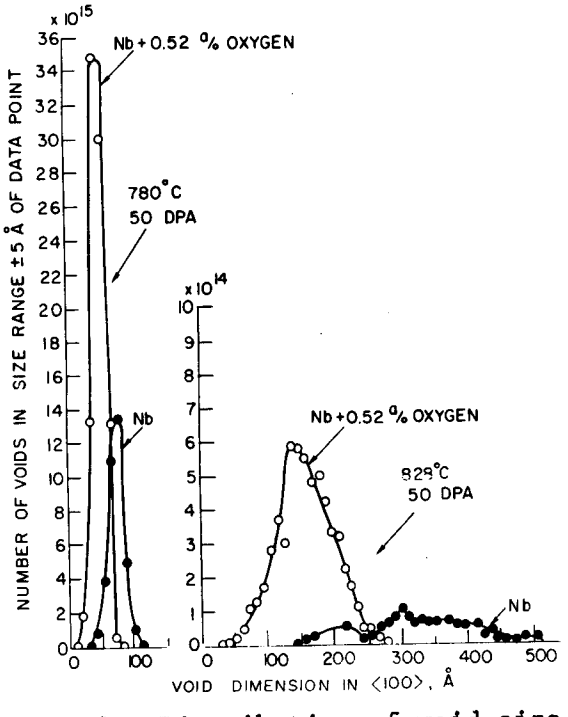


Fig. 3. Distribution of void size.

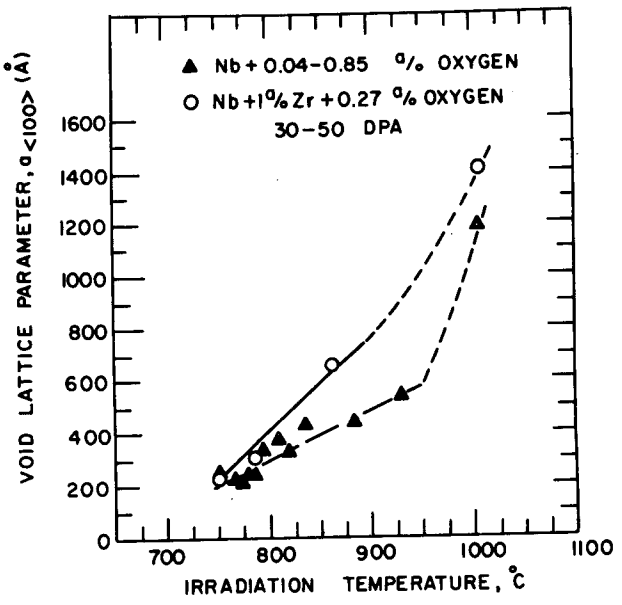


Fig. 4. Temperature dependence of void lattice parameter in O-doped Nb and Nb-1% Zr.

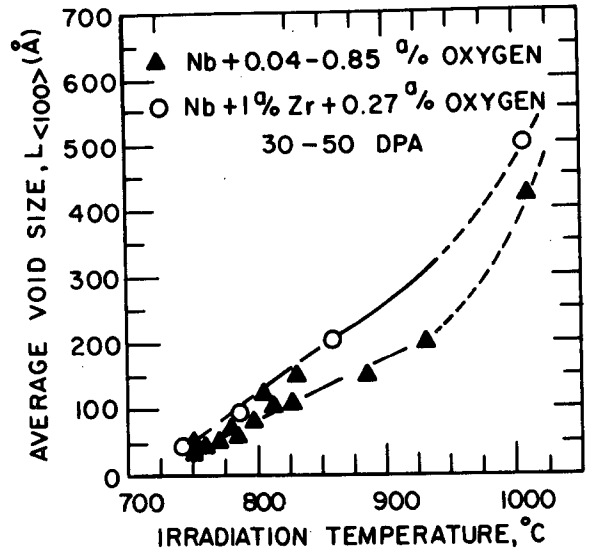


Fig. 5. Temperature dependence of average void size in O-doped Nb and Nb-1% Zr.

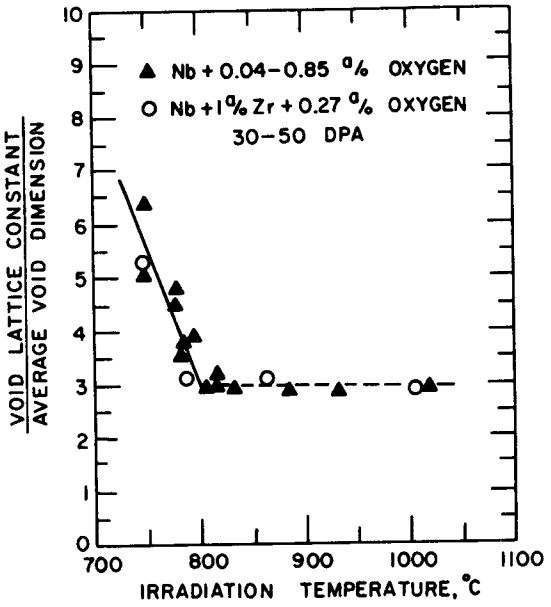


Fig. 6. Temperature dependence of ratio of lattice parameter to void size.

to average void size in O-doped Nb and Nb-1% Zr is shown in Figs. 4, 5, and 6, respectively. The ratio shown in Fig. 6 decreases from an extrapolated value of ∿8 at 700°C (void ordering is not observed below 750°C however) to ∿3 at 800°C, and the ratio has a constant value of ∿3 from 800 to 1010°C. The void lattice parameter (Fig. 4) and the average void dimension (Fig. 5) are larger in Nb-1% Zr-0.27% O than in O-doped Nb, whereas the ratio of these parameters (Fig. 6) is approximately the same in both materials. The lattice parameter of the void array in Nb containing 0.05 to 0.5% O irradiated at 780°C to ∿50 dpa is approximately independent of the O concentration.

The ordered void array can be produced in Nb doped with 0.25% N and irradiated with $^{58}Ni^{+}$ at 780°C. O-doped Nb has also been irradiated with V^{+}, and, to date, we have observed no significant difference in the void microstructure from the Ni^{+} irradiation results.

The TEM observations of $^{58}Ni^{+}$-irradiated specimens always reveal the presence of an oxide (or nitride) film on the bombarded surface. A film was also observed on Nb-0.85% O material (Fig. 7) that was annealed (but not irradiated) at 500°C for 1 hr in the same vacuum system used for irradiation. The microstructure of the annealed material shows a parallel "domain" structure in the oxide (or nitride) film. The spacing of the "domains" (∿275 Å in <110>) is approximately the same as the <110> void spacing in the same Nb-0.87% O material irradiated at 828°C to ∿50 dpa. We have not investigated this film structure on other annealed materials nor at higher annnealing temperatures. Aligned voids and oxide (or nitride) "domain" structure in Nb-0.14% O irradiated at 780°C are shown in Fig. 8. The presence of an oxide (or nitride) film is confirmed by selected area diffraction together with the undulating darkness of the parallel "domains." The voids are aligned where the boundary (light gray) of the "domains" is well defined. In regions in which the boundaries are

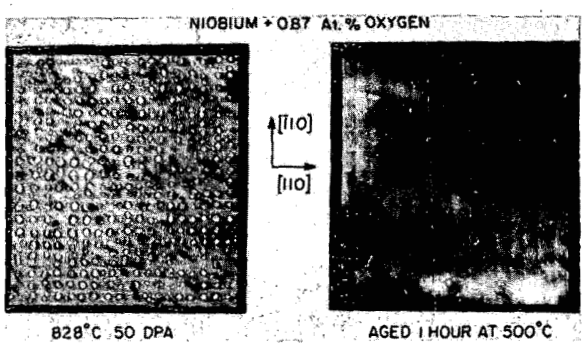


Fig. 7. Void lattice and oxide film in Nb-0.87% O.

not well defined, the voids appear to be much less ordered, and they appear to be completely absent in the immediate vicinity of the precipitate.

The effect of a ∿1600-Å Ti coating on the void microstructure in an Nb-0.05% O specimen irradiated at 780°C to ∿50 dpa is shown in Fig. 9. An ordered void array was observed in the uncoated material (Fig. 9b and d), whereas the voids appear to be random in the Ti-coated material (Fig. 9c). No voids were observed in the Ti layer (Fig. 9a). An x-ray analysis with a scanning-electron microscope at a section depth of 4900 Å showed no Ti present. A similar effect of a Ti-coating is observed for Nb-0.35% O material.

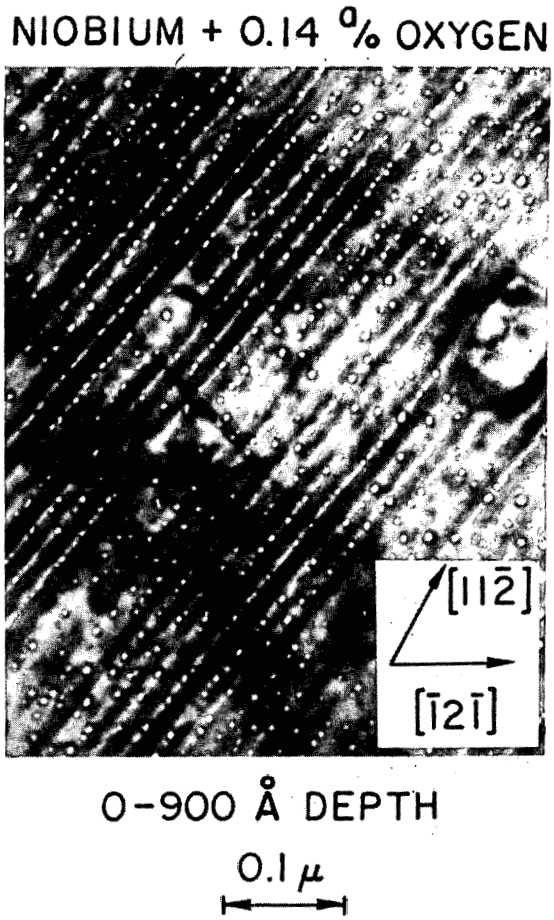


Fig. 8. Aligned voids on "domain" boundary.

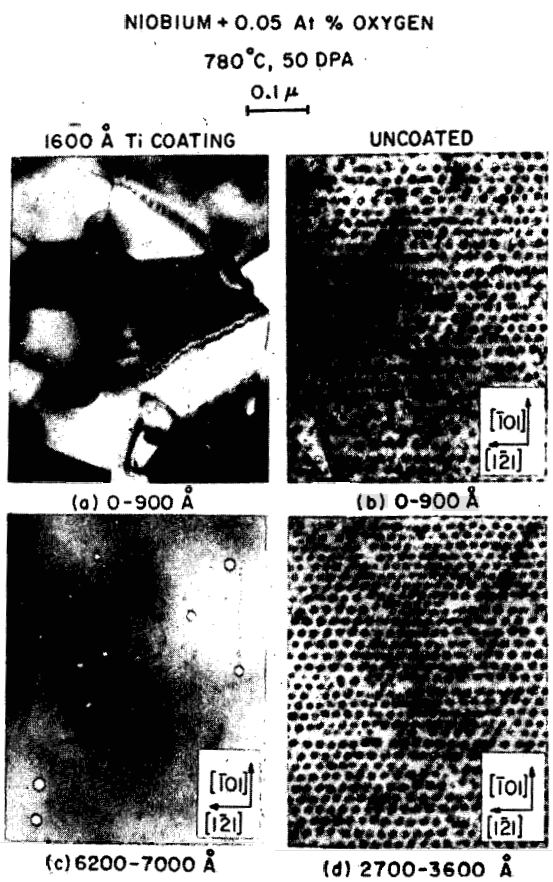


Fig. 9. Effect of Ti coating on void ordering.

DISCUSSION OF RESULTS

The experimental results obtained show that void ordering does not occur in "pure" Nb nor Nb-1% Zr during irradiation with 3.2-MeV $^{58}Ni^{+}$. Furthermore, the experimental results show that O impurity in Nb and Nb-1% Zr can result in void ordering during $^{58}Ni^{+}$ irradiation at temperatures of 750-1010°C. The minimum concentration of O in Nb that will result in void ordering is dependent on irradition temperature. The observed coincidence of the "domain" spacing in the oxide (or nitride) film and the void spacing in the ordered array is not believed to be fortuitous, but the role of the "domain" structure in void ordering is obscure at the present time. The necessity for O (or N) impurity in Nb for the formation of an ordered void array tends to be substantiated by the observation that a Ti coating on O-doped Nb precludes the formation of an ordered void array. The absence of an ordered void array in the Ti-coated material is attributed to the reduction of O (and N) concentration below the minimum level for ordering by Ti "gettering" of O (and N) in the irradiation damage layer.

Some theoretical efforts[2-4] to explain void superlattices assume that elastic interactions between voids are the primary cause of ordering and the elastic interactions arise as a result of surface-tension forces. Nolfi[5] also assumes elastic interactions are responsible for formation of void lattices, but he considers that the elastic interactions arise between "misfitting" void-solute (i.e., O or N) shell composites. Our experimental observations do not unequivocally support one or the other of these theories, but observations of realignment of voids in the vicinity of edge-dislocation type of void imperfections suggest the existence of void or void-solute shell composite interactions.

REFERENCES

1. B. A. Loomis, A. Taylor, and S. B. Gerber, J. Nucl. Mater. 56, 25 (1975).
2. A. M. Stoneham, Consultant Symposium-The Physics of Irradiation-Produced Voids, ed. R. S. Nelson, AERE Harwell Report R7934, p. 319 (1975).
3. J. H. Evans, R. Bullough, and A. M. Stoneham, Proc. 1971 Intl. Conf. on Radiation-Induced Voids in Metals, eds. J. W. Corbett and L. C. Ianniello, AEC Symp. Ser. 26, CONF-710601, p. 522 (1972).
4. V. K. Tewary, J. Phys. F: Metal Phys. 3, 1275(1973).
5. F. V. Nolfi, Jr., to be published in J. Appl. Phys.

ELASTIC INTERACTIONS BETWEEN "VOIDS" INDUCED BY SOLUTE SEGREGATION*

F. V. Nolfi, Jr.
Materials Science Division
Argonne National Laboratory
Argonne, Illinois 60439

ABSTRACT

Expressions are derived for the elastic interaction energy between void-solute shell composites. These composites consist of spherical void cores surrounded by spherically symmetric solute shells containing a uniform concentration of irradiation segregated solute. The solutes are assumed to be "misfitting" and the only sources of internal stress, the surface stress of the voids being taken to be zero. The elastic interaction energy between composites arises because of the so-called inhomogeneity interaction and has minimum values at certain composite separations and solute shell thickness. The calculations are compared with experimental investigations of void ordering in an Ni ion-irradiated Nb-1 Zr alloy containing 0.0038 atom fraction of oxygen as an impurity. Given experimentally determined void sizes and auxiliary data, the correct void lattice parameter is predicted when the solute shell thickness is ∿30% of the composite radius. In pure Nb, it is found that O, C, or N impurities are necessary for void ordering, which supports the main thesis of the present paper, viz., solutes/impurities are a primary cause of void ordering.

INTRODUCTION

Ordered arrays of voids have been observed in a wide variety of metals and alloys that have been subjected to certain conditions of temperature and displacement-producing radiation.[1] These ordered arrays, or void lattices, always possess the same "crystal structure" as the host metal or alloy, and the void lattice is always parallel

*Work supported by the U.S. Energy Research and Development Administration.

to the host lattice. Aside from phenomenological interest, void lattices have stirred investigations, since suspicion exists that swelling saturates after voids become ordered.

The most prominent theoretical efforts[1-3] to explain void lattices have assumed that elastic interactions between voids are the primary cause of ordering. These theories correlate the void lattice parameter with void spacings for which the elastic interaction energy of the system is a minimum and assume that the elastic interactions arise as a result of "surface tension forces."

Melan and Bullough[2] have considered the effects of elastic anisotropy. Their work neglects the fact that voids have zero elastic constants, but elastic anisotropy intrinsically seems capable of explaining the structure and orientation of the void lattice relative to the host material. However, void lattices have been observed in tungsten,[4] which is nearly isotropic elastically. Thus, it seems possible that elastic anisotropy may not be necessary for void ordering.

In the present paper, we also assume that elastic interactions are responsible for the formation of void lattices. However, we diverge substantially from previous theories in that we do not consider "surface tension forces" as the source of the elastic interactions. Rather, we consider the interactions that arise from stresses generated as a result of irradiation-induced segregation of misfitting solutes/impurities to voids.[5] This approach has the following advantages. First, we do not depend upon the existence of an intrinsic surface stress.* This is important since considerable theoretical and experimental evidence exists that suggests the surface stress of metals, especially closely packed metals, is near zero.[6] Second, even small bulk concentrations of solute/impurities produce stresses that give rise to elastic interaction energies an order of magnitude larger than surface stress forces give. Third,

*We note that τ_i is not to be equated with the surface tension γ. In solids, these two quantities are related but not necessarily equal.[6]

in support of segregation-induced interactions Loomis[7] reports that voids do not order in Nb unless a minimum amount of O, C, or N is present. Concentrations required are in the range of 60 to 200 ppm by weight.

In the present work we assume spherical void-solute shells in an infinite elastically isotropic medium. As will be shown, the origin of the interactions between these entities is the so-called inhomogeneity interaction.[8-12] It is well known[10] that this interaction always causes simple misfitting voids to be attracted to each other. However, the effect of segregated solutes is to cause complex interactions to develop between composites, and a "repulsive" component emerges. As a consequence, minima in the interaction energy between composites become possible.

THE ELASTIC INTERACTION ENERGY BETWEEN TWO MISFITTING VOID-SOLUTE COMPOSITES

We assume that spherical void-solute composites are embedded in an infinite matrix that is free of external stresses. A composite with radius r_c, shown schematically in Fig. 1, consists of a spherical void core of radius r_v surrounded by a spherically symmetric solute shell; the solute concentration in the shell is taken to be uniform. For interstitial or substitutional solutes with significant size differences from the solvent, this shell will be accompanied by an induced-stress state.[5]

What we desire to calculate is the interaction energy between two void-solute composites. This interaction energy varies with the relative positions of the composites, and we seek to find separations for which the energy is a minimum. Nolfi[13] has shown that for cases where the segregated solute does not change the elastic constants of the solute shell by more than 20%, the interaction energy between two composites may be approximated by

$$E_{int} \sim \frac{(e^T)^2 r_v^3}{\alpha^6}[2.48\delta\mu g(\alpha,\beta) - 6.98\mu(1-\alpha^3)f(\beta)] \quad (1)$$

where μ is the shear modulus of the matrix, $\alpha \equiv r_v/r_c$, $\beta \equiv R/r_v$ with R the center to center separation of the composites, e^T is the unrestrained volume change of a composite when solute is added and $\delta\mu$ is the change in

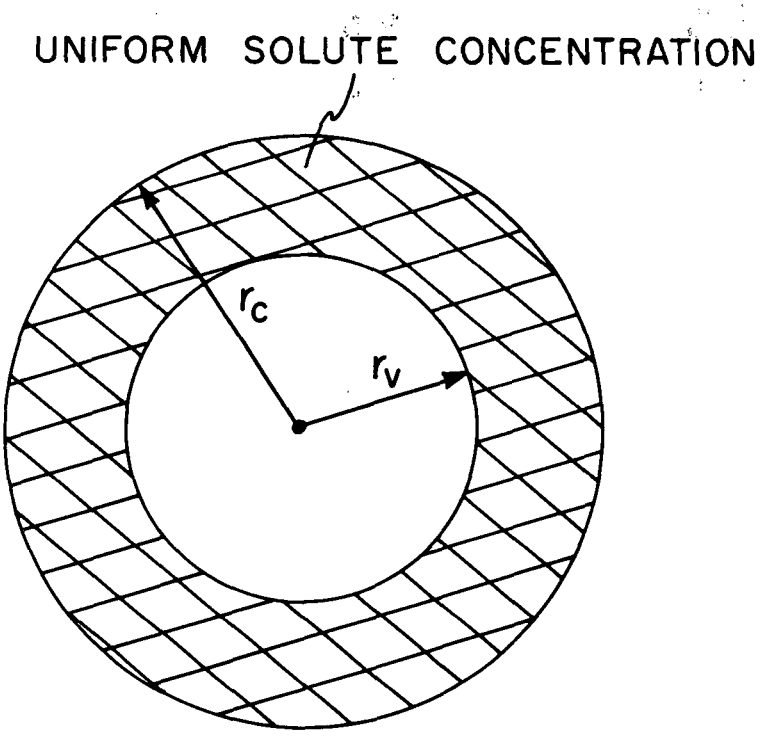


Fig. 1. Schematic diagram of void-solute shell composite. r_v is the void radius and r_c is the composite radius.

shear modulus in the region $r_v \leq r \leq r_c$ induced by the solute segregation. Here, $g(\alpha,\beta) \equiv \alpha^3/[(\alpha\beta)^2 - 1]^3 - 1/(\beta^2 - 1)^3$, $f(\beta) \sim 2/3\beta^6$, and $\alpha\beta \geq 2$ is a necessary condition in order to avoid composite overlap.

There are essentially two "mechanisms" by which Eq. (1) may achieve minimum values. First, if $\delta\mu$ in the region $r_v \leq r \leq r_c$ is significant and positive, say in the order of 0.2μ, then the left-hand term in brackets (I_2) is positive and represents a "repulsive component" in the interaction energy. The right-hand term (I_1) is always negative or "attractive", so that the two terms are opposed to each other. Hence, depending upon the values of α, which are determined by the void size and degree of solute segregation, Eq. (1) may have minima at certain β. In other words, the repulsive component in Eq. (1) arises because the "hard" solute shells repel each other and the attractive component arises because the "soft" voids attract each other. Minimum values are obtained when a proper balance is achieved.

The second mechanism for obtaining minima in Eq. (1) is best discussed by considering the following specific experimental conditions. Loomis[14]

has reported the existence of ordered voids in a Nb-1 Zr alloy irradiated with Ni ions at ∿1000°K; the alloy contained 0.38 at % oxygen as an impurity. The average and maximum void radii reported are 51 Å and 65 Å, respectively, and the void lattice (bcc) spacing is 307 Å. If it is assumed that the dimensions of the composites remain fixed during adjustments of the void lattice spacing, then a decrease in this spacing is equivalent to an increase in the number density of the composites and visa versa. Further, if the total amount of oxygen is distributed equally among all the composites on the lattice, then the oxygen concentration X (atom fraction) in the solute shells will depend upon the composite spacings according to the relation

$$X = \bar{X}/[\bar{X} + (1 - \alpha^3)/\alpha^3(\sqrt{3}\beta^3/3\pi - 1)] \qquad (2)$$

where $\bar{X}$ is the mean oxygen concentrations, and we have assumed a bcc void lattice. This relation shows that X, and hence e^T, increases with β as shown in Fig. 2.* Since the solubility of oxygen limits the maximum oxygen concentration to 2 at %, I_2 in Eq. (1) is ignorable. This obtains because such a concentration of oxygen has only a small effect on μ.[15] Under such conditions, $E_{int} \propto (e^T)^2 f(\beta)$ and in Fig. 3 we show that E_{int} generally has minima at certain values of β.

In Table 1 we present detailed calculations of E_{int}, corresponding to the specific experimental system under discussion. If we assume that the composite separation corresponds to the nearest neighbor distance in a bcc void lattice, then the correct void lattice spacing is obtained for $\alpha = 0.7$, $\beta = 4$, and the calculated interaction energy is -2.43 kT. It is important to emphasize, that were it not for the fact that e^T increases with β, then the theory would predict that E_{int} has no minimum values since $f(\beta) \propto \beta^{-6}$ is a monotonically decreasing function of β.

Summarizing, we have shown that by taking into account irradiation induced solute segregation, at least two possible mechanisms exist by which stable void lattices may be predicted. These results are obtainable using isotropic elasticity, and the theory does not depend upon the

*In Ref. 13, we show that e^T is a linear function of X.

existence of an intrinsic surface stress in the void surfaces. The theory seems to be able to correctly predict the experimental results, and is supported by the recent observations of Loomis[7] that minimum concentrations of O, C, or N are necessary in Nb if voids are to order.

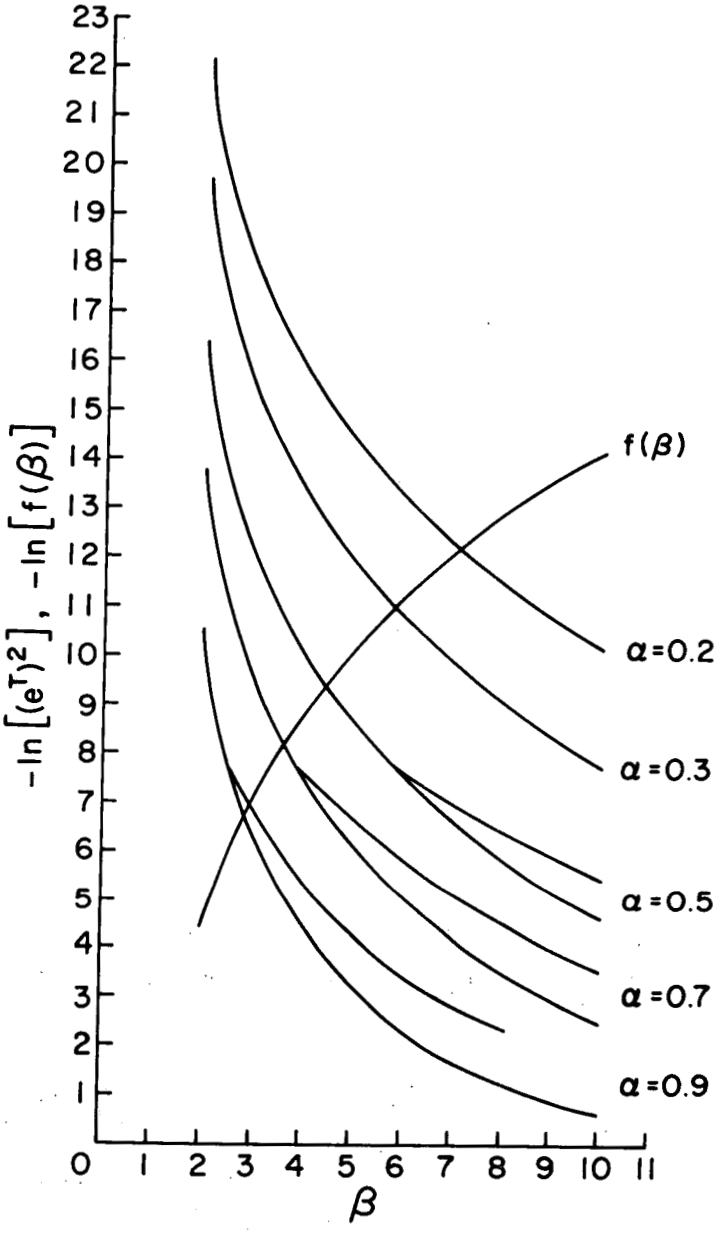


Fig. 2. Plots of $-\ell n(e^T)^2$ and $-\ell nf(\beta)$ versus β. Upper branches on curves for α=0.5, 0.7, and 0.9 reflect NbO precipitation occurring at X=0.02 (Oxygen solubility at T$\sim$1000°K).

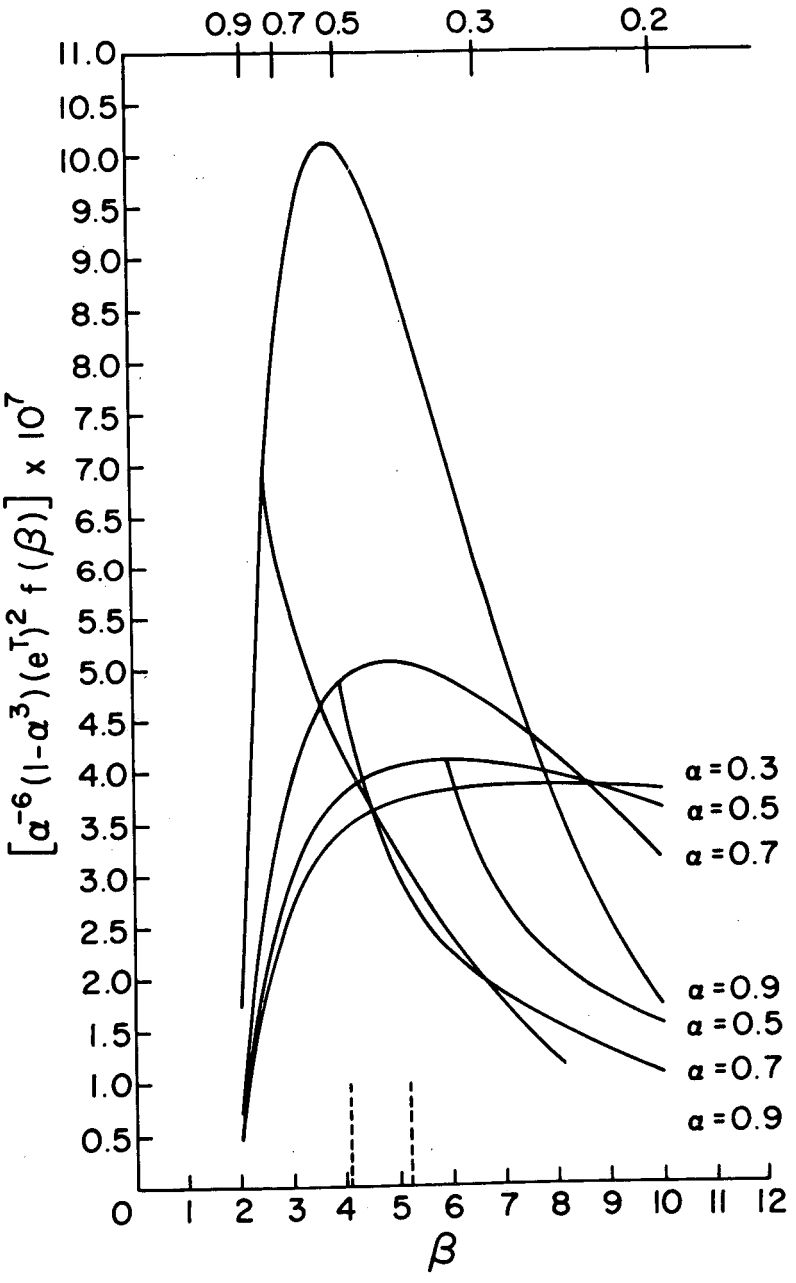


Fig. 3. Master plot of $-E_{int}(\nu=1/3)/6.98\mu r_v^3$ versus β. The lower branches of the curves for $\alpha=0.5$, 0.7, and 0.9 reflect NbO precipitation occurring at X=0.02 (Oxygen solubility at T$\sim$1000°K).

Table 1. Calculated Values of E_{int} Versus β for Indicated Parameters. $r_v = 65$ Å.

α	β	$X \cdot 10^2$	I_1[a]	I_2[a]	E_{int}[a]
0.5	4.00	0.58	-1.98	0.048	-1.94
↓	4.80	1.04	-2.09	0.067	-2.04
	5.60	1.67	-2.13	0.093	-2.05
	6.40	2.50	-1.76	0.083	-1.69
	7.20	3.54	-1.36	0.060	-1.31
	8.00	4.81	-1.12	0.047	-1.08
0.7	2.86	0.65	-1.92	0.020	-1.91
↓	3.43	1.26	-2.36	0.035	-2.34
	4.00	2.09	-2.45	0.049	-2.43
	4.57	3.18	-1.83	0.032	-1.81
	5.14	4.54	-1.47	0.024	-1.46
	5.71	6.20	-1.25	0.019	-1.24
0.9	2.22	1.03	-2.11	0.019	-2.11
↓	2.67	2.48	-3.28	0.040	-3.27
	3.11	4.43	-2.76	0.028	-2.75
	3.56	6.91	-2.42	0.021	-2.41
	4.00	9.91	-2.16	0.017	-2.15
	4.44	13.40	-1.93	0.015	-1.93

[a]The tabulated energies are normalized to kT.

Auxiliary Data: $X_{sol} = 0.02$

$\mu = 3.75 \times 10^{11}$ dynes·cm^{-2}

$\delta\mu(r_v \leq r \leq r_c) = 0.4X\mu$ where X is oxygen in solution.[15]

$\nu = 1/3$

$T = 1000°K$

REFERENCES

1. A. M. Stoneham, Consultant Symposium on "The Physics of Irradiation Produced Voids," R. S. Nelson, ed., AERE Harwell Report #R7934, 319 (1975).
2. J. H. Evans, R. Bullough, and A. M. Stoneham, Proceedings of the Albany Conference, "Radiation-Induced Voids in Metals," J. W. Corbett and L. C. Ianniello, eds., 522 (1972).
3. V. K. Tewary, J. Phys. F: Metal Phys., 3, 1275 (1973).
4. V. K. Sikka and J. Moteff, J. Appl. Phys., 43, 4942 (1972).
5. F. V. Nolfi, Jr., Scripta Met., 7, 1181 (1973).
6. F. V. Nolfi, Jr. and C. A. Johnson, Acta Met., 20, 769 (1972).
7. B. A. Loomis, to be published.
8. J. D. Eshelby, Proc. Royal Soc., A, 241, 376 (1957).
9. J. D. Eshelby, Progress in Solid Mechanics, 2, Chapter 3, North-Holland, Amsterdam, 89 (1961).
10. J. D. Eshelby, Acta Met., 14, 1295 (1966).
11. J. D. Eshelby, Acta Met., 3, 487 (1955).
12. J. D. Eshelby, Solid State Physics, 3, Academic Press Inc., 79 (1956).
13. F. V. Nolfi, Jr., J. Appl. Phys., accepted for publication.
14. B. A. Loomis, to be published.
15. E. S. Fisher, Phys. Stat. Sol. 28 (1975).

IRRADIATION CREEP AND EFFECTS OF STRESS ON SWELLING

R. Bullough
Theoretical Physics Division, A.E.R.E. Harwell
Nr. Didcot, Oxon, U.K.

ABSTRACT

A rate theoretical discussion of the various effects of stress on the migration, segregation and aggregation of irradiation produced point defects will be presented. The significance of the stress induced preferred migration to the irradiation and deformation produced dislocations will be highlighted and used to discuss the theory of irradiation creep. The influence of the onset of swelling on such irradiation creep will be considered together with the direct effects of stress on swelling at higher temperatures. A particular feature of the presentation will be the emphasis placed on the vacancy loops formed athermally from the vacancy rich regions of the displacement cascades.

---

1. INTRODUCTION

The cladding and structural components in the core of the fast reactor will be subjected to a variety of external stresses and therefore the choice of materials for such components and the various design tolerances are constrained by their response to such stresses. The present discussion of the stress dependent responses will be confined to the irradiation environment and thus conventional thermal creep processes, where the strain is caused by either glissile movement of dislocations or point defect diffusion, will only be discussed if they interfere with the irradiation controlled phenomena. Within the irradiation environment such stresses can lead to irradiation creep[1,2,3] and a direct modification of the swelling[4]. These effects, together with the possible interaction between swelling and irradiation creep, will be discussed in the present paper. Although the discussion will be also restricted to the irradiation

behaviour of cubic metals, there is no doubt that intrinsic growth processes as well as irradiation creep and swelling will be affected by applied stresses and thus the present discussion will have relevance to such materials.

It is apparent from the recent review[1] by Hesketh, in 1972, of irradiation creep that at the time of writing that review no satisfactory model of irradiation creep in non-fissile cubic metals had been formulated. To quote Hesketh "In the cubic materials, the effect of external stress on the thermal activation of dislocation loop nuclei still looks the best buy". The activated process envisaged involves the stress assisted unfaulting of interstitial loops[5]. Such a process yields an irradiation creep strain that can be comparable to the strain arising from the preferred nucleation of the interstitial loops themselves and furthermore its existence depends on the preferred nucleation process[6,7,8] actually *occuring*. Since the strain rate arising from the interstitial loop nucleation controlled process decreases inversely with increasing total dislocation density[6] the process cannot be the operative mechanism for cold worked metals, for it is observed that the irradiation creep rate is relatively insensitive to cold work. There are two conceptually very simple tests for the dominance of the preferred nucleation mechanism[1]. (i) If the loop nucleation is completed without stress then the loop nuclei will be randomly orientated and the subsequent application of a tensile stress will not change this distribution. No irradiation creep should then occur. Of course, if the temperature is high enough creep could occur by preferred vacancy emission leading to preferred growth of the aligned interstitial loops; however Brailsford and Bullough[6] have shown that this emission contribution is very small. (ii) If the applied stress is removed after the completion of loop nucleation then the material should continue creeping at the same rate. In fact the preferred nucleation process is simply stress induced growth. Of course, both these tests require that the final interstitial loop population is nucleated at a reasonably low dose. If this is not so, due to interstitial solute trapping etc., and continuous interstitial loop nucleation persists, then the stress sensitivity will also persist. In pure materials such

a definitive test should be possible however. Notwithstanding the result of such tests the failure of the interstitial loop nucleation model to explain the insensitivity of irradiation creep to cold work, together with the observed relative insensitivity to temperature, in complete contrast to the swelling phenomena, does suggest that another mechanism is responsible for the creep.

Such an alternative is the "stress induced preferred absorption" mechansim (henceforth referred to as SIPA), by which the irradiation produced point defects will suffer a preferential drift to different parts of the dislocation distribution. Thus the edge dislocations in the material with their extra planes oriented orthogonal to the stress axis will absorb slightly more interstitials than the edge dislocations with differing orientations; similarly these latter dislocations will absorb slightly more vacancies than the former orthogonally oriented dislocations. These induced point defect interactions with the dislocations arise because the interatomic force constants in the neighbourhood of the point defects will differ from the force constants in the perfect, defect free, matrix; the point defects thus have a different local linear response from the perfect matrix. Eshelby[9] has shown how the interactions between such point defects and an applied stress field can be analysed by representing the point defect as an inclusion with elastic constants that differ from the matrix elastic constants. The interactions between the point defects and the dislocations under an external stress can thus be obtained by replacing Eshelby's applied stress by the sum of the internal dislocation stress field and the external stress field. The suggestion that this SIPA mechanism could provide an explanation of irradiation creep in metals was first made by Heald and Speight[2]; subsequently Bullough and Willis[3] derived the accurate interaction energies which confirmed the viability of the mechanism and Bullough and Hayns[10] went on to use rate theory to derive the explicit expressions for the irradiation creep rate.

In the present paper we shall review the SIPA model of irradiation creep and, by describing it in close association with the general effects of stress on swelling together with other possible irradiation creep

mechanisms, we hope to put such stress effects into correct relative perspective. The general framework for our discussion is given in section 2 where particular emphasis will be put on the significance of the vacancy loops formed from high energy cascades. The general rate theory analysis will be presented in section 3. In section 4 we present certain limiting analytic results together with some numerical results and discuss some of their more intriguing features.

2. GENERAL FRAMEWORK

There are many defect features that must be included in a comprehensive description of the fast neutron damage process in metals. In this section we will simply list these and comment upon their significance to irradiation creep and swelling in the presence of a uniaxial tensile stress. The section is thus a brief introduction to the more mathematical rate theoretical content of the next section.

(1) The essential feature of the damage situation is that equal numbers of displacement vacancies and interstitials are produced in the presence of an existing dislocation network together with other structural defects such as grain boundaries, precipitates and impurity atoms[11].

(2) The interstitials are very mobile compared with the vacancies and rapidly form planar aggregates - interstitial dislocation loops. Under a uniaxial tension slightly more such interstitial loops will be nucleated in an aligned orientation than in a non-aligned orientation. The subsequent growth of such loops gives a contribution to the irradiation creep[6].

(3) The interstitials are more strongly attracted to dislocations than are the vacancies and there is thus a net interstitial flux at the dislocation (biassed) sinks[11].

(4) The vacancies also subsequently form aggregates which, in the presence of transmutation gases and other suitable nucleating agents, adopt a three dimensional morphology. These small equilibrium gas bubbles are essentially neutral (no bias for interstitials) but the preferential loss of interstitials to the dislocation sinks ensures that any point defect

flux into such neutral sinks must be vacancy in character. The gas bubbles will thus grow into voids and swelling will occur[11].

(5) If the temperature is high enough then preferred vacancy emission from the aligned interstitial loops will occur. The aligned interstitial loops will thus preferentially grow both by SIPA and by vacancy emission and both processes will contribute directly to irradiation creep. Of course, even without SIPA or vacancy emission the preferred nucleation[6] of such loops in the aligned orientation will give irradiation creep.

(6) Vacancy emission also yields a contribution to the irradiation creep from the random dislocation network since we expect roughly one third of the network dislocations to be sympathetically orientated relative to the stress axis[4].

(7) Such stress assisted vacancy emission will lead to enhanced swelling only at high temperatures (at or above the stress free peak swelling temperature)[4].

(8) The precise significance of such vacancy emission controlled irradiation creep is very difficult to be certain about since at such relatively high temperatures irradiation independent (thermal) creep processes are present and the applied driving stress can be rapidly relieved[4].

(9) In addition to the homogenous considerations cascade damage will produce an inhomogeneous distribution of vacancies and interstitials. In particular there is now unassailable evidence[12,13] to show that a significant number of the cascades collapse to form vacancy loops even over the temperatures at which voids form and grow. The, albeit transient, existence of such loops means that the number of vacancies available at any time to enhance the growth of voids is reduced; the vacancy loops are dislocation loops and therefore they preferentially attract interstitials and thus both further bias the system for void growth and increase the net loss of point defects by increasing the overall dislocation sink. Under a uniaxial tensile stress more vacancy loops should nucleate in the non-aligned orientations relative to the stress axis. The SIPA mechanism ensures that the aligned vacancy loops

will shrink faster than the non-aligned vacancy loops; in addition, if the temperature is high enough, preferred vacancy emission from the aligned vacancy loops will occur. Both these destruction processes contribute initially to irradiation creep. However, they both ultimately cause preferential loss of aligned vacancy loops which means that the aligned dislocation density from the vacancy loops will drop compared with the non-aligned and the resulting irradiation creep rate can fall. Of course it is unreasonable to maintain such loop asymmetries when the loop densities attain such high values that the loops will interact with each other and such asymmetry considerations for both the vacancy and interstitial loops are probably only important over a very limited temperature and irradiation dose range.

These remarks are intended to highlight some of the less controversial aspects of irradiation creep and swelling; further discussion will be given in the final section. In the next section we present a brief outline of the general rate theory required.

3. THE RATE THEORY OF IRRADIATION CREEP AND STRESS ASSISTED SWELLING

The notation of this section will follow Bullough and Hayns[10] with additions, where necessary, from Brailsford and Bullough[4] and Bullough, Eyre and Krishan[12]; these three works can usefully be used to supplement the present outline. For simplicity we will omit the presence of grain boundaries and precipitates; the extension to include these is trivial. The defect aggregates present are thus interstitial loops, vacancy loops, network dislocations and voids. The symbols used have the following significance*:

c_i, c_v : steady state interstitial and vacancy fractional concentrations.

c_v^e : equilibrium vacancy concentration in the perfect matrix.

D_i, D_v : interstitial and vacancy diffusion coefficients.

Z_i, Z_v : interstitial and vacancy bias parameters.

*Where appropriate the superscripts A and N on these quantities distinguish the aligned and non-aligned orientations relative to the applied stress axis.

r_{IL} : average interstitial loop radius

q_i : total number of interstitials in interstitial loops

N_{IL} : volume concentration of interstitial loops.

r_{VL} : average vacancy loop radius

N_{VL} : volume concentration of vacancy loops

R_{VL} : particular vacancy loop radius

q_v : total number of vacancies in vacancy loops

n_{VL} : fractional rate of formation of vacancy loops

K : fractional displacement rate

εK : fractional rate of vacancy deposition in vacancy loops[12]

$k_i^2 = k_{iV}^2 + k_{iD}^2$: total sink strength for interstitials

$k_{iV}^2 = 4\pi r_V C_V (1 + k_i r_V)$: void sink strength for interstitials, corrected to second order.[14]

C_V : volume concentration of voids

r_V : average void radius

$k_{iD}^2 = Z_i^A \rho_D^A + Z_i^N \rho_D^N$: dislocation sink strength for interstitials

$\rho_D = \rho_N + \rho_{VL} + \rho_{IL}$: total dislocation density where N → network, VL → vacancy loops and IL → interstitial loops.

$k_v^2 = k_{vV}^2 + k_{vD}^2$: total sink strengths for vacancies

$k_{vV}^2 = 4\pi r_V C_V (1 + k_v r_V)$: void sink strength for vacancies, corrected to second order[14]

$k_{vD}^2 = Z_v^A \rho_D^A + Z_v^N \rho_D^N$: dislocation sink strength for vacancies

$K^e = K_V + K_N + K_{IL} + K_{VL}$: total vacancy emission rate from voids, dislocation network, interstitial dislocation loops and vacancy dislocation loops

f_{IL} : excess fraction of total interstitial loops aligned perpendicular to the stress axis

f_{VL} : excess fraction of total vacancy loops in the two non-aligned orientations.

The steady state point defect concentrations c_i, c_v

These are given by the simultaneous quadratic equations[12]

$$\left.\begin{aligned} K - k_i^2 D_i c_i - \alpha c_i c_v &= 0 \\ K^e + (1-\varepsilon)K - k_v^2 D_v c_v - \alpha c_i c_v &= 0 \end{aligned}\right\} \quad (1)$$

where α is the recombination coefficient and the various components of the vacancy emission rate K^e have the explicit forms:

The rate of vacancy emission from the voids

$$K_V = k_{vV}^2 \bar{c}_v \quad (2)$$

where

$$\bar{c}_V = c_v^e \exp\left\{\left(\frac{2\gamma}{r_V} - p_g\right) b^3/kT\right\} \quad (3)$$

is the equilibrium vacancy concentration adjacent to a void and in $\bar{c}_V$ γ is the surface tension and the gas pressure

$$p_g = 3n_g kT/4\pi\left(r_V^3 - \frac{3b_v n_g}{4\pi}\right). \quad (4)$$

The van der Waal gas law has been assumed (b_v is van der Waals constant) and n_g is the number of gas atoms in the void with average radius r_V.

The rate of vacancy emission from the dislocation network

$$K_N = K_N^A + K_N^N = Z_v^A \rho_N^A D_v \bar{c}_N(\sigma) + Z_v^N \rho_N^N D_v \bar{c}_N(0) \quad (5)$$

where

$$\bar{c}_N = c_v^e \exp(\sigma b^3/kT) \quad (6)$$

is the equilibrium vacancy concentration adjacent to an edge dislocation in the network in the aligned* orientation relative to the applied tensile

*For simplicity three orthogonal edge dislocation orientations will be considered; the aligned orientation is such that the extra plane of the edge dislocation is orthogonal to the tensile stress axis and the non-aligned orientations are thus the two orthogonal orientations.

stress σ. The preferred emission and absorption by the network is assumed not to perturb its random nature and thus we may write

$$\left.\begin{aligned} \rho_N^A &= \frac{1}{3}\rho_N \\ \text{and} \quad \rho_N^N &= \frac{2}{3}\rho_N \end{aligned}\right\} \tag{7}$$

The rate of vacancy emission from the interstitial loops

$$\begin{aligned} K_{IL} &= K_{IL}^A + K_{IL}^N \\ &= Z_v^A \rho_{IL}^A D_v \bar{c}_{IL}(\sigma, r_{IL}^A) + Z_v^N \rho_{IL}^N D_v \bar{c}_{IL}(0, r_{IL}^N) \end{aligned} \tag{8}$$

where, if N_{IL} is the total concentration of interstitial loops,

$$\left.\begin{aligned} \rho_{IL}^A &= 2\pi r_{IL}^A \tfrac{1}{3}(1 + 2f_{IL})N_{IL} \\ \rho_{IL}^N &= 2\pi r_{IL}^N \tfrac{2}{3}(1 - f_{IL})N_{IL} \end{aligned}\right\} \tag{9}$$

$$\text{and } \bar{c}_{IL}(\sigma, r) = c_v^e \exp\left\{-\left[(\gamma_{SF} + F_{el}(r))b^2 - \sigma b^3\right]/kT\right\} \tag{10}$$

is the equilibrium vacancy concentration adjacent to an aligned interstitial loop of radius r. In expression (10) γ_{SF} is the stacking fault energy (relevant if the loop is faulted otherwise zero) and $F_{el}(r)$ is the elastic energy of a dislocation loop of radius r (its line tension). Note both these terms are resisting the emission of vacancies from the loop - an interstitial loops gets bigger when it emits vacancies.

The rate of vacancy emission from vacancy loops

$$\begin{aligned} K_{VL} &= K_{VL}^A + K_{VL}^N \\ &= Z^A \rho_{VL}^A D_v \bar{c}_{VL}(\sigma, r_{VL}^A) + Z_v^N \rho_{VL}^N D_v \bar{c}_{VL}(0, r_{VL}^N) \end{aligned} \tag{11}$$

where

$$\rho_{VL}^{A} = 2\pi r_{VL}^{A} N_{VL}^{A} \,, \qquad \rho_{VL}^{N} = 2\pi r_{VL}^{N} N_{VL}^{N} \tag{12}$$

and

$$\bar{c}_{VL}(\sigma,r) = c_v^{\,e} \exp\left\{\left[\left[(\gamma_{SF} + F_{el}(r)\,)b^2 + \sigma b^3 \right]/kT \right\}\right. \tag{13}$$

is the equilibrium vacancy concentration adjacent to an aligned vacancy loop of radius r. We now note that for vacancy loops the stacking fault energy and the dislocation line energy are both <u>assisting</u> the emission of vacancies from the loop - a vacancy loop gets smaller when it emits vacancies. Since the vacancy loops have a finite lifetime we have separate rate equations for N_{VL}^{A} and N_{VL}^{N} and the preferred nucleation fraction parameter f_{VL} appears in these rate equations rather than explicity relating the vacancy loop dislocation densities to the total loop concentrations as occurs for the interstitial loops in expression (9).

The analysis of Bullough, Eyre and Krishan[12] can now be slightly generalised to include the uniaxial tensile stress σ. The resulting seven rate equations can be written in the obvious notational form

<u>The rate of change of swelling</u>: $S = \frac{4}{3}\pi r_v^{\,3} C_V$:

$$\frac{dS}{dt} = k_{vV}^2 D_v c_v - k_{iV}^2 D_i c_i - K_V D_v \tag{14}$$

<u>The rate of growth of the interstitial loop radii</u>: r_{IL}^{A} and r_{IL}^{N}

$$\frac{dr_{IL}^{A}}{dt} = \frac{1}{b}\left[Z_i^{A} D_i c_i - Z_v^{A} D_v c_v + Z_v^{A} D_v \bar{c}_{IL}(\sigma, r_{IL}^{A}) \right] \tag{15}$$

$$\frac{dr_{IL}^{N}}{dt} = \frac{1}{b}\left[Z_i^{N} D_i c_i - Z_v^{N} D_v c_v + Z_v^{N} D_v \bar{c}_{IL}(0, r_{IL}^{N}) \right] \tag{16}$$

The vacancy loop equations[12,15]

(a) The rate of change of the numbers of vacancy loops: N_{VL}^{A} and N_{VL}^{N}

$$\frac{dN_{VL}^{A}}{dt} = \frac{1}{3}(1 - 2f_{VL})\frac{n_{VL}}{b^3} - \frac{N_{VL}^{A}}{R_{VL}(0)b}\left[Z_i^{A}D_i c_i - Z_v^{A}D_v c_v + Z_v^{A}D_v \bar{c}_{VL}(\sigma, R_{VL}(0))\right] \quad (17)$$

$$\frac{dN_{VL}^{N}}{dt} = \frac{2}{3}(1 + f_{VL})\frac{n_{VL}}{b^3} - \frac{N_{VL}^{N}}{R_{VL}(0)b}\left[Z_i^{N}D_i c_i - Z_v^{N}D_v c_v + Z_v^{N}D_v \bar{c}_{VL}(0, R_{VL}(0))\right] \quad (18)$$

(b) The rate of change of the number of vacancies in vacancy loops: q_v^{A} and q_v^{N}

$$\frac{dq_v^{A}}{dt} = \frac{1}{3}(1 - 2f_{VL})\varepsilon K - \left[\frac{4\pi q_v^{A} N_{VL}^{A}}{b}\right]^{\frac{1}{2}}\left[Z_i^{A}D_i c_i - Z_v^{A}D_v c_v + Z_v^{A}D_v \bar{c}_{VL}(\sigma, r_{VL}^{A})\right] \quad (19)$$

$$\frac{dq_v^{N}}{dt} = \frac{2}{3}(1 + f_{VL})\varepsilon K - \left[\frac{4\pi q_v^{N} N_{VL}^{N}}{b}\right]^{\frac{1}{2}}\left[Z_i^{N}D_i c_i - Z_v^{N}D_v c_v + Z_v^{N}D_v \bar{c}_{VL}(0, r_{VL}^{N})\right] \quad (20)$$

These rate equations can be numerically integrated subject to the initial conditions

$$S(0) = \frac{4}{3}\pi r_V^3(0)C_V \text{ with } r_V(0) = 10\ \text{Å},\ p_g(0) = 2\gamma/r_V(0) \quad (21)$$

$$r_{IL}^{A} = r_{IL}^{N} = \left[S(0)/\pi b N_{IL}\right]^{\frac{1}{2}} \quad (22)$$

$$N_{VL}^{A} = N_{VL}^{N} = 0 \quad (23)$$

and

$$q_v^{A} = q_v^{N} = 0 \quad (24)$$

Simultaneously with the stress dependent swelling S the dislocation network, interstitial loops and vacancy loops will all produce irradiation creep and the total creep strain ε_T may be thus written in obvious notation

$$\varepsilon_T = \varepsilon_N + \varepsilon_{IL} + \varepsilon_{VL} \quad (25)$$

where

1. Irradiation creep strain from the network, ε_N, given by the rate equation

$$\frac{d\varepsilon_N}{dt} = \frac{\rho_N}{3}\left[(Z_i^A - Z_i^N)D_i c_i + (Z_v^N - Z_v^A)D_v c_v\right]$$

$$+ \frac{\rho_N}{3}\left[Z_v^A D_v \bar{c}_N(\sigma) - Z_v^N D_v \bar{c}_N(0)\right] \qquad (26)$$

which should be integrated simultaneously with the previous seven rate equations (14)-(20).

2. Irradiation creep strain from the interstitial loops, ε_{IL}, given by

$$\varepsilon_{IL} = q_i^A - \tfrac{1}{2}q_i^N \qquad (27)$$

which may be written, in terms of r_{IL}^A and r_{IL}^N, as

$$\varepsilon_{IL} = \frac{\pi b}{3} N_{IL}\left[(1 + 2f_{IL})(r_{IL}^A)^2 - (1 - f_{IL})(r_{IL}^N)^2\right] \qquad (28)$$

In this case a strain rate equation analogous to (26) is not necessary but, if required, can be deduced by differentiating (28) and using equations (15) and (16).

3. Irradiation creep strain from the vacancy loops, ε_{VL}, given by

$$\varepsilon_{VL} = -\left[q_v^A - \tfrac{1}{2}q_v^N\right] \qquad (29)$$

which may be written in terms of r_{VL}^A, r_{VL}^N, N_{VL}^A and N_{VL}^N as

$$\varepsilon_{VL} = \frac{\pi b}{2}\left[(r_{VL}^N)^2 N_{VL}^N - 2(r_{VL}^A)^2 N_{VL}^A\right] \qquad (30)$$

The corresponding creep rate $d\varepsilon_{VL}/dt$ follows by differentiating (29) and using equations (19)and (20).

The complete rate equations and the resulting irradiation creep strains have been computed for the physical and irradiation parameters

relevant to M316 steel under fast neutron irradiation[15]. Some remarks on these results are presented in the next section and certain limiting forms for the irradiation creep will be presented that can be derived by systematically simplifying the general analysis presented above.

4. RESULTS AND GENERAL CONCLUSIONS

In this section we discuss certain analytic irradiation creep strain results that particularly demonstrate the effects of the onset of swelling on irradiation creep. In addition we shall comment on some of the general features of the total irradiation creep as deduced numerically from the analysis in section 2.

It is obvious that the irradiation creep by the SIPA mechanism will be a maximum when the only sinks for point defects are dislocations. Thus if voids begin to appear and grow the irradiation creep will always begin to fall[10]. This can be analytically demonstrated from the previous equations by assuming that only network dislocations and voids are present ($N_{VL} = 0$, $N_{IL} = 0$) and further assuming that ρ_N is so large that recombination may be neglected. At temperatures below the peak swelling temperature, we may neglect vacancy emission, $K^e \sim 0$, and (14) and (26) yield

$$\frac{dS}{dt} = k_{vV}^2(D_v c_v - D_i c_i) \tag{31}$$

and

$$\frac{d\varepsilon_N}{dt} = \frac{\rho_N}{3}\left[(Z_i^A - Z_i^N)D_i c_i + (Z_v^N - Z_v^A)D_v c_v\right] \tag{32}$$

These equations can be integrated with the aid of (1) and with the simpler first order void sink strengths

$$k_{vV} = k_{iV} = 4\pi r_V C_V \tag{33}$$

We obtain for the irradiation creep strain ε_N:

$$\varepsilon_N = \frac{1}{3}\left[\frac{(Z_i^A - Z_i^N)}{Z_i} + \frac{(Z_v^N - Z_v^A)}{Z_v}\right](Kt) - \frac{Z_i Z_v}{3(Z_i - Z_v)}\left[\frac{(Z_i^A - Z_i^N)}{Z_i^2} + \frac{(Z_v^N - Z_v^A)}{Z_v^2}\right]S \qquad (34)$$

where $Z_i = \frac{1}{3}(Z_i^A + 2Z_i^N)$, $Z_v = \frac{1}{3}(Z_v^A + 2Z_v^N)$

The first term is the SIPA contribution and the second term is the explicit negative term due to presence of voids. It should be noted that the first term is a good representation of the total irradiation creep, even when interstitial and vacancy loops are present, if the temperature is below the vacancy emission temperature - about 450°C in M316 steel - and if the material is cold worked.[10]

Bullough and Willis have derived expressions for the stress induced interaction energy between the edge dislocations and the interstitials and vacancies. By assuming a linear relation between the various Z_i, Z_v bias factors and the amplitudes of these interaction energies*, Bullough and Hayns[10] show that

$$Z_i^A - Z_i^N = \frac{45\, Z_i\, \sigma}{4\mu\, e_i^o} \frac{\Delta\mu_i}{(15 - 7\Delta\mu_i)} \qquad (35)$$

and

$$Z_v^N - Z_v^A = -\frac{45\, Z_v\, \sigma}{4\mu\, e_v^o} \frac{\Delta\mu_v}{(15 - 7\Delta\mu_v)} \qquad (36)$$

where e_i^o, e_v^o are the relaxation volume strains associated with the free interstitial and vacancy respectively, μ is the shear modulus of the matrix,

$$\Delta\mu_i = \frac{\mu - \mu_i}{\mu}, \qquad \Delta\mu_v = \frac{\mu - \mu_v}{\mu} \qquad (37)$$

*If a logarithmic variation with amplitude is assumed expressions (35) and (36) are modified by approximately a factor of two. The logarithmic form arises from the assumption of cylindrical cellular geometry associated with the dislocations; since vacancy loops are so important it seems likely that spherical geometry will be more relevant for each loop with the consequent loss of the logarithmic dependence.

and μ_i, μ_v are the shear moduli associated with the interstitial and vacancy*. These local moduli have been discussed by Bullough and Willis[3] and they conclude it is reasonable to take the limiting values $\mu_i = 0$, $\mu_v = \mu$; that is

and

$$\Delta\mu_i = 1$$
$$\Delta\mu_v = 0 \qquad (38)$$

With these values the simple SIPA (temperature independent) result is

$$\varepsilon = 0.47 \frac{\sigma}{\mu\, e_i^0} (Kt) \qquad (39)$$

This result is plotted in figure 1 together with the experimental results

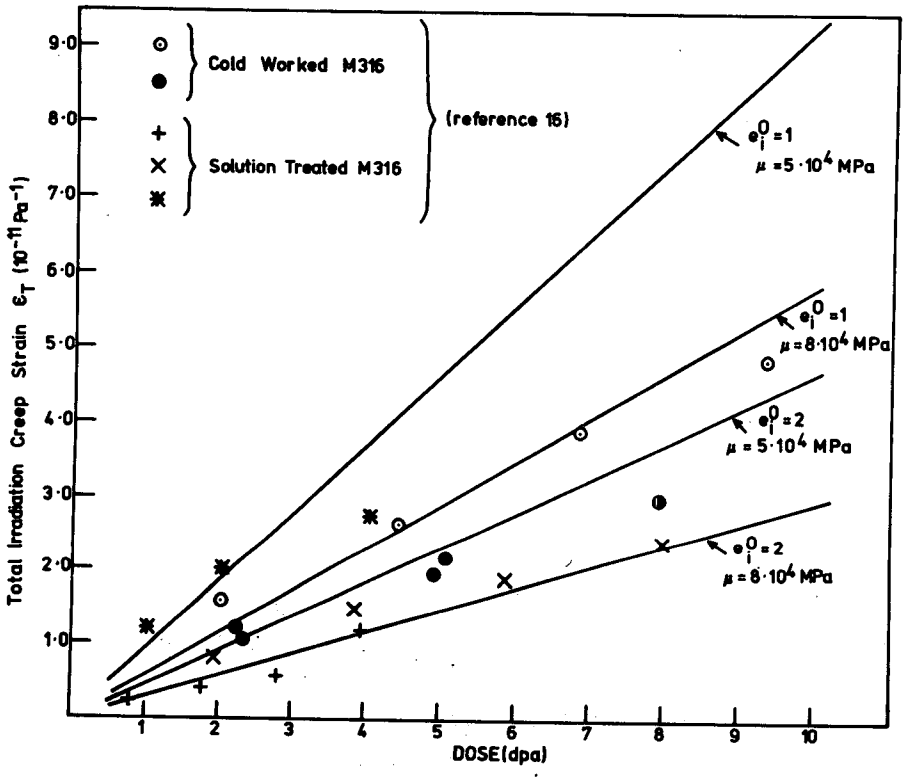


Figure 1

A plot of expression (39) for the low temperature irradiation creep due to the SIPA mechanism; the relevant experimental data on solution treated and cold worked M 316 steels is also given[16].

*The moduli of the effective elastic inclusion that represents the point defects[3].

of Mosedale et al[16] on cold worked and solution treated M316. The small range of possible e_i^o and μ values are quite sufficient to encompass these experimental results at 280°C.

The full numerical solution gives a total irradiation creep strain at 280°C that is quite indistinguishable from (39) and thus we feel confident that the SIPA mechanism provides an adequate explanation of the low temperature irradiation creep.

The thermal emission terms become relevant at higher temperatures and the numerical results thus far obtained[15] enable the following conclusions to be drawn for M316 steel.

1. Up to about 400°C there is only a negligible contribution to the irradiation creep from all the possible thermal emission terms. The SIPA mechanism is the dominant contribution to the irradiation creep and up to this temperature the expected irradiation creep is independent of temperature.

2. At 450°C the vacancy emission from the vacancy loops is important - it occurs at this relatively low temperature because of the high line tension driving force in (13). At this temperature in cold worked materials the expected creep strain rate is just over twice its low temperature value. The loop-loop interactions within the vacancy loop population become important at low doses ($\sim$ 0.03 dpa) and thus persistent asymmetry in the loop distributions should not occur at higher doses.

In solution treated material the total creep strain is reduced compared with cold worked material because the critical dose for loop-loop interaction and consequent removal of the asymmetry in the loop distribution, is increased.

3. At 500°C the asymmetry in the vacancy loop population persists to high doses and the vacancy emission contribution can become negative and virtually cancel the SIPA contribution from the vacancy loops. A large contribution in cold worked material comes from the thermal emission from the network, which when added to the SIPA creep from the network ensures that the irradiation creep rate in cold worked materials should

be about twice the low temperature value. In solution treated material the vacancy loop contribution cancels as for the cold worked material and there is no significant network or interstitial loop contribution. We expect the irradiation creep rate to be less by about a factor of two compared with cold worked material. Observations at 500°C on solution treated M316 would thus be most interesting. Of course at temperatures greater than 500°C substantial vacancy emission from all the relevant sources is expected and thus a significant thermal creep contribution could easily confuse the interpretation of such observations.

4. The applied stress can only affect the swelling at temperatures greater than the stress free peak swelling temperature ($\sim$ 450°C in M316). This conclusion is thus completely consistent with our earlier conclusion[4].

5. The irradiation creep is expected to decrease when voids appear and grow.

6. It is not reasonable to add a positive term proportional to swelling to an expression such as (39) and use the sum as a design criteria.

7. The precise inter-relation of the contributions from the network, vacancy loops and interstitials is complex but essential features of these contributions and the absolute magnitudes of the SIPA contributions strongly supports the contention that the SIPA mechanism is the dominant cause of irradiation creep.

I am most grateful to Dr. M.R. Hayns for the technical discussions and computational help.

REFERENCES

1. R.V. Hesketh, Irradiation Embrittlement and Creep in Fuel Cladding and Core Components, BNES Conf., London (9-10 Nov. 1972), p.221.
2. P.T. Heald and M.V. Speight, Phil. Mag. 29, 1075 (1974).
3. R. Bullough and J.R. Willis, Phil. Mag. 31, 875 (1975).
4. A.D. Brailsford and R. Bullough, J. Nucl. Mat. 48, 87 (1973).
5. G.W. Lewthwaite, Scripta Met. 7, 75 (1973).
6. A.D. Brailsford and R. Bullough, Phil. Mag. 27, 49 (1973).

7. A.D. Brailsford and R. Bullough, Irradiation Embrittlement and Creep in Fuel Cladding and Core Components, BNES Conf., London (9-10 Nov. 1972), p.267.
8. G. Lewthwaite, J. Nucl. Mat. 46, 324 (1973).
9. J.D. Eshelby, Proc. Roy. Soc. A241, 376 (1957).
10. R. Bullough and M.R. Hayns, J. Nucl. Mat. (1975) to be published. Also Harwell Res. Report TP 616,(1975).
11. A.D. Brailsford and R. Bullough, J. Nucl. Mat. 44, 121 (1972).
12. R. Bullough, B.L. Eyre and K. Krishan, Proc. Roy. Soc. (1975) to be published. Also Harwell Res. Report AERE-R 7952, (1975).
13. B.L. Eyre and C.A. English, Proc. of Conf. on "Physics of Voids", ed. R.S. Nelson, Harwell Report AERE-R7934 (1975).
14. A.D. Brailsford, R. Bullough and M.R. Hayns, (1975) to be published.
15. R. Bullough and M.R. Hayns, (1975) to be published.
16. D. Mosedale, G.W. Lewthwaite and I. Ramsay, Irradiation Embrittlement and Creep in Fuel Cladding and Core Components, BNES Conf. London (9-10 Nov. 1972) p.233

THE GROWTH OF GRAIN BOUNDARY CAVITIES UNDER APPLIED STRESS AND IRRADIATION

J. F. Mancuso, F. H. Huang and Che-Yu Li
Department of Materials Science and Engineering
Cornell University, Ithaca, N.Y. 14853

ABSTRACT

Grain boundary cavity growth under the simultaneous influence of irradiation and applied stress is considered. Recent data on grain boundary sliding in polycrystalline solids suggest that at the grain boundaries the normal stress, the driving force for grain boundary cavity growth, is relaxed. The kinetics of this process are formulated as a function of the normal stress and the rate limiting mechanisms for mass transport, which include bulk diffusion and defect-absorption reactions at the sink.

Introduction.--Grain boundary cavitation followed by intergranular fracture is a frequent mode of failure for structural materials at temperatures and stresses of practical interest. Extensive theoretical and experimental investigations have treated this phenomenon when it occurred without the influence of irradiation.[1] This phenomenon also can occur under irradiation. For example, the fuel element cladding has been observed to fail intergranularly in the experimental fast reactor. This work examines the kinetics of grain boundary cavity growth under the simultaneous influence of irradiation and stress.

In the present analysis, cavity growth by mass transport will be considered. The driving force for mass transport is the normal stress at the grain boundary.[2] Recent progress on grain boundary sliding suggests that the normal stress at the grain boundary can be relaxed.[3,4] This subject will be discussed in the next section. The section following treats out-pile cavity growth. This analysis differs from reported work in the boundary conditions adopted and the driving forces for mass transport.[1,5] The effects of irradiation will be discussed in the final section. During irradiation both grain boundaries and cavities are sinks

for irradiation produced defects. The annihilation of these defects can be controlled by either long range diffusion or reaction rates at the sinks.

Normal Stress at a Grain Boundary.--This section deals with the role of grain boundary sliding in plastic deformation and the possibility that the normal stress at the grain boundary can be relaxed.

The mechanism for cavity growth controlled by mass transport is similar to that for Herring-Nabarro creep where, in the absence of irradiation, the grain boundary is the source of vacancies and cavities are the sinks.[6,7] Without internal gas pressure, the driving force for cavity growth is the normal stress at the grain boundary. Out-of-pile experiments[8] show that cavity growth occurs predominately on grain boundaries transverse to the tensile axis. The normal stress calculated by a simple geometrical decomposition of the applied stress does not account for these observations.[8]

The contribution of grain boundary sliding to the plastic deformation of a polycrystalline solid can be illustrated by the data shown in Fig. 1,[9] which contains load relaxation data for type 316 stainless steel in the form of a log σ vs log $\dot{\varepsilon}$ plot. According to the phenomenological model of grain boundary sliding suggested by Hart,[4] the portion of the data at high stresses and high strain-rates (corresponding to the upper plateau) signifies that deformation is controlled by grain matrix processes. As the strain-rate decreases, the contribution of grain boundary sliding increases. In the lower plateau the grain boundary will offer little resistance to deformation and, again, the deformation will be controlled by processes in the grain matrix.

In the region of negligible grain boundary resistance the shear stress at the grain boundary will be relaxed.[4] This relaxation will be accompanied by shear stress concentrations at the grain boundary intersection. These stress concentrations will have a component of stress in the direction of the applied stress. Since the integral of the stress in the tensile direction should equal the applied load, the stress concentrations will lead to reduced stresses in the tensile direction at

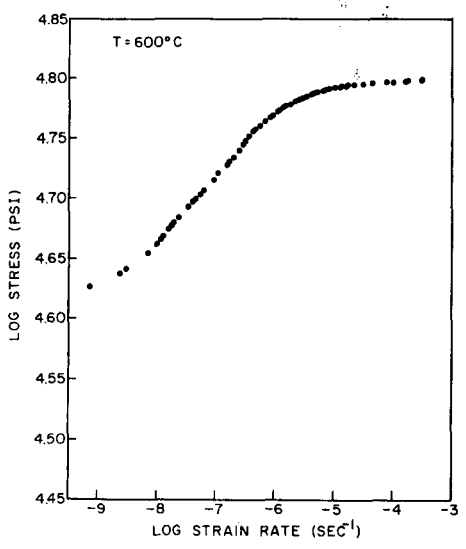


Fig. 1: Load relaxation data of type 316 stainless steel in the form of a logσ-log$\dot{\epsilon}$ plot.

the sliding grain boundaries. The normal stresses at these grain boundaries will be relaxed. Cavities on grain boundaries transverse to the applied stress axis will not be affected by grain boundary sliding. For the data in Fig. 1, the shear stress at an average grain boundary has been calculated as a function of strain rates in Fig. 2 to show the region where relaxation is important. Under irradiation, the $\log \sigma - \log \dot{\epsilon}$ relationship will be altered such that the possibility of relaxing the stress at the grain boundary can be enhanced. For LMFBR and CTR applications, this possibility will favor cavity growth on grain boundaries transverse to the applied stress axis and can reduce the probability of failure.

Out-of-Pile Cavity Growth.--The two fundamental processes proposed in the literature for grain boundary cavity growth are grain boundary sliding and stress induced mass transport.[1,10] The radial growth rates for grain boundary cavities in, for example, type 316 stainless steel are 10^{-10}-10^{-8}cm/sec under low stresses. The calculated grain boundary sliding velocities in Fig. 3 suggest that grain boundary sliding does not contribute significantly to cavity growth. This paper treats cavity growth controlled by mass transport only.

The system to be analyzed is a planar grain boundary under uniaxial tension containing an array of identical hexagonal cells with a center-to-center spacing, a_o and a cavity of radius r_o. The location of the cavities is sufficiently far from the grain intersections that edge effects can be ignored. Mass transport is assumed to be predominately along the grain boundary. The quasi-steady-state, mass balance equation at any point on the grain boundary can be represented as:[6] $(\delta B/\Omega)\nabla^2(\mu-\mu_v) = G$, where $\mu-\mu_v$ is the difference in chemical potential

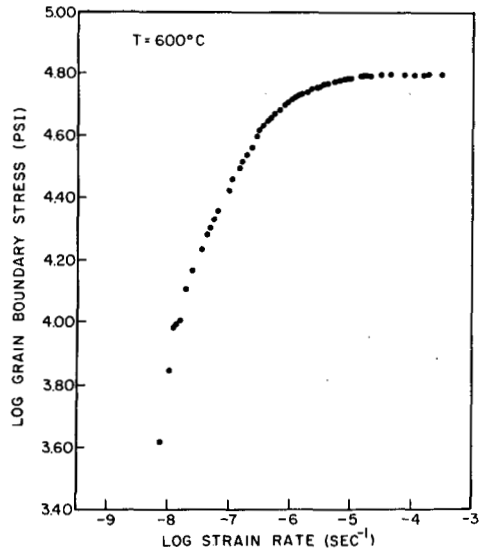


Fig. 2: Grain boundary shear stress as a function of the plastic strain rate calculated from the data in Fig. 1 and the parallel model in Ref. 4. The grain matrix $\log\sigma$-$\log\dot{\varepsilon}$ curve used has the form $\log(\sigma^*/\sigma)=(\dot{\varepsilon}^*/\dot{\varepsilon})^{\lambda}$ with $\lambda=.15$, $\log\sigma^*=4.810$ and $\log\dot{\varepsilon}^*=-14.519$. Grain boundary sliding behavior is assumed non-Newtonian.

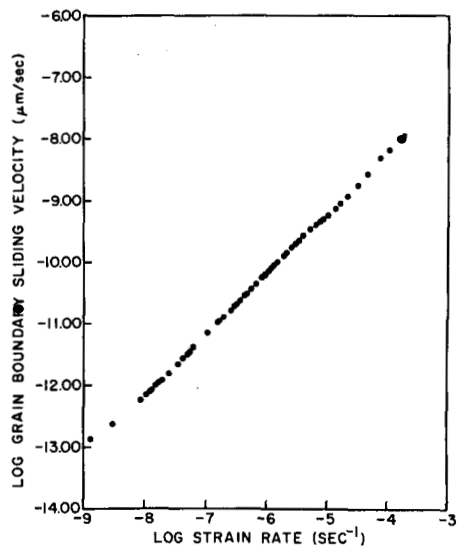


Fig. 3: Grain boundary sliding velocity as a function of total strain rate from the data in Fig. 1 and the model used for Fig. 2.

of the atom and the vacancy in the immediate vicinity of the grain boundary; G is the vacancy generation rate at the grain boundary; B is the atomic mobility in the grain boundary; Ω is the atomic volume; and δ is the grain boundary thickness. $\mu-\mu_v$ at the grain boundary is related to the normal stress, σ_n,[6] as: $\mu-\mu_v = -\sigma_n\Omega$.

The mass balance equation becomes: $-\delta B \nabla^2\sigma_n = G$. The following boundary conditions are used: 1) $\mu-\mu_v = -2\gamma\Omega/r_o$ at the cavity surface, where γ is surface tension, 2) the mass flux is zero at $r=a_o/2$, 3) G = constant and 4) the average normal stress, σ_{avg}, at the grain boundary containing cavities equals that calculated without cavities. The cylindrically symmetrical, general solution of the mass balance equation is $\sigma_n(r) = -Gr^2/(4\gamma b) + \alpha\ln r + \beta$ where σ_n is normal stress and r is distance and $\alpha = Ga_o^2/8\gamma B$ and $\beta = 2\gamma/r + G/4\gamma B\,[a_o^2\ln r_o/2 - r_o^2]$. The parameter G can be found from boundary condition 4). The radial growth rate, dr_o/dt, is related to the mass flux, $-\delta B\nabla(\mu-\mu_v)/2r_o$, at cavity surface such that

$$dr_o/dt = \frac{\Omega\delta B\{\sigma_{avg} - 2\gamma/r_o[1-(2r_o/a_o)^2]\}(1-a_o^2/4r_o^2)}{2a_o^2[3/4+1/4(2r_o/a_o)^4+\ln(2r_o/a_o)+(2r_o/a_o)^2]} \qquad (1)$$

where σ_{avg}, the average normal stress, depends on grain boundary orientation and the extent of grain boundary sliding. These aspects have not been considered in the reported work.[5] Numerically equation (1) leads to a radial growth rate proportional to $(\text{time})^{.4}$.

Nucleation of cavities is assumed to be an easy process because small amounts of sliding result in copious nucleation of cavities. For an in-reactor system, the collection of helium atoms at the grain boundary will enhance cavity nucleation.

Under tensile-compressive, cyclic loading the present analysis, in which the chemical potential is used as the driving force for cavity growth, predicts that cavities of finite initial size will shrink as a function of time according to equation (1). This conclusion is different from that of Weertman and Skelton.[5,11]

Cavity Growth Under Irradiation.--Both grain boundaries and grain boundary cavities act as sinks for point defects[12,13] created in the grain matrix during irradiation. If the annihilation of these point defects is controlled by long range diffusion, local equilibrium will be maintained between the point defects and the sinks. The analysis presented in the previous section will remain applicable and the stress induced growth rate will be exactly the same. When annihilation of point defects is controlled by reaction rates at the sinks, local equilibrium will no longer be maintained at the sinks and the formulation given in Section III will have to be modified. Under the assumption of a quasi-steady-state, the concentration of point defects at the sink can be evaluated by the application of the condition of mass-balance. Under the same quasi-steady-state assumption the gradient of the concentration can be taken as the driving force for mass transport. At the grain boundary, the mass-balance between the vacancy flux coming from the bulk and the rate of absorption is[12,13,14]

$$K[C_v^{gb}-C_v^e] = D^b[C_v^b-C_v^{gb}]/L \text{ or } C_v^{gb} = [-KC_v^e+D^bC_v^b/L]/[K+D^b/L] \qquad (2)$$

The left hand side of the first equation represents the net vacancy absorption rate at the grain boundary where K is the reaction-rate constant at the grain boundary. C_v^{gb} is the vacancy concentration at the grain boundary and C_v^e is the concentration at thermal equilibrium. The right hand side of the first equation represents the diffusing flux from the bulk; where D^b is the bulk diffusion constant, L is the characteristic diffusion length, and C_v^b is the vacancy concentration in the bulk.

At the grain boundary, the thermal equilibrium concentration of vacancies is $C_o \exp[\sigma_n \Omega/kT]$, where C_o is the equilibrium concentration at zero stress. The thermal equilibrium concentration of interstitials is negligible. The flux of atoms along the grain boundary, J, due to the existance of a gradient in C_v^{gb} is $(\delta BkT/\Omega C_v^{gb})\nabla C_v^{gb}$. From equation (2), J becomes $\delta B[K/(K+D^b/L)]\nabla\sigma_n$. If the mobility is not strongly influenced by irradiation and if $K/(K+D_v/L) \ll 1$, the flux along the grain boundary under irradiation is much less than the flux at a boundary under the same applied stress but without the influence of irradiation. Equation (2) reduces to the bulk diffusion controlled case when the factor $K/(K+D_v^b/L)$ approaches unity. The possibility of reaction rate controlled point defect annihilation was neglected by Weertman.[5]

A mass balance equation corresponding to the out-of-pile case can be written as $-\delta B[K/(K+D_v^b/L)]\nabla^2\sigma_n = G$. The boundary conditions 2), 3) and 4) of the previous section apply here without modification. Boundary condition 1), however, is replaced by the condition that C_v^{gb} at r_o equals the vacancy concentration at the cavity surface. C_v at the cavity surface can be calculated by balancing the vacancy currents from the bulk with the absorption rate there. For the purpose of demonstrating the physical consequence of the present analysis, the parameters K and L in equation (2) are assumed to be the same for both the cavity and the grain boundary. The same procedure used in the previous section yields a radial growth rate, which is a factor $(K/(K+D^b/L)$ smaller than that predicted by equation (1). Thus, for a given applied stress, the growth is reduced from that expected for the case where point defect annihilation is controlled by bulk diffusion, if the mobility is not influenced by irradiation.

The hoop stress of the fuel element cladding in the experimental LMFBR has been estimated to be typically 15 ksi.[15,16] For an average cladding temperature of 650°C, annealed, type 316 stainless steel at this strsss will fail in 15 days out-of-pile.[17] Cladding at similar conditions in a fast reactor maintains its integrity for more than 200 days.[15,16] This result can be used to support the possibility that point defect annihilation controlled by reaction rates at the sinks may reduce the rate of cavity growth.

ACKNOWLEDGEMENT

The work is supported by the U.S. Energy Research and Development Administration.

REFERENCES

1. F. Garofalo, Fundamentals of Creep and Creep-Rupture in Metals, p. 241, MacMillan, 1965.
2. D. Hull and D. E. Rimmer, Phil. Mag., 1959, 4, 673.
3. G. L. Wire, H. Yamada, and Che-Yu Li, Acta Met., 1974, 22, 505.
4. E. W. Hart, Acta Met., 1967, 15, 1545.
5. J. Weertman, Met. Trans., 1974, 5, 1743.
6. C. Herring, J. Appl. Phys., 1950, 21, 437.
7. R. W. Balluffi and L. L. Seigle, Acta Met., 1957, 449.
8. B. J. Cane, Ph.D. Thesis, Univ. of Sheffied, October 1972.
9. Che-Yu Li, Progress Report COO-2172-11, ERDA Contract E(11-1)2172, Cornell University, 1975.
10. H. E. Evans, Phil. Mag., 1971, 23, 1101.
11. R. P. Skelton, Phil. Mag., 1966, 14, 563.
12. L. K. Mansur, P. R. Okamoto, A. Taylor and Che-Yu Li, "Surface Reaction Limited Void Growth," to be published in the Proc. of the 7th ASTM Symposium on Rad. Eff. Str. Mat. in Gatlinburg, Tenn., 1974.
13. S. P. Harkness and Che-Yu Li, Met. Trans., 1971, 2, 1457.
14. J. F. Mancuso, J. L. Straalsund, and Che-Yu Li, "Steady-State Dis-

dislocatin-Void Configuration Under Irradiation," to be published in J. Nue. Mat.

15. V. Z. Jankus, Nucl. Eng. Design, 1972, 18, 83.
16. M. C. Billone, private communication.
17. F. L. Yaggee and Che-Yu Li, Report No. ANL-7805, Argonne Nat. Lab., Dec. 1972.

RADIATION DAMAGE SIMULATION EXPERIMENTS IN ZIRCONIUM

D. Faulkner and M. P. Puls
Materials Science Branch
Atomic Energy of Canada Limited
Whiteshell Nuclear Research Establishment
Pinawa, Manitoba, Canada

ABSTRACT

The structural changes observed in zirconium during irradiation with high energy electrons or ions are described. The development of a dislocation structure as a function of displacement level and of temperature is analysed for the case of zirconium irradiated with 100 keV He^+ ions. The influence of the induced dislocation structure and of insoluble gases on void nucleation is discussed.

INTRODUCTION

The use of high energy electrons or ions to produce atomic displacements under controlled conditions provides a convenient means of simulating the processes which occur as a result of irradiation by fast neutrons. Electron or ion irradiations offer considerable advantages over in-reactor irradiations in terms of both cost, time savings and experimental control.

Zirconium, in contrast to most other metals, appears to be extremely resistant to void formation during neutron irradiation[1] and it has been suggested that this situation may arise either as a result of insufficient nuclei in the form of insoluble gases[1,2,3], or the lack of a suitable dislocation structure[1,4]. In this paper, the effects of pre-injected gases and the development of a radiation-induced dislocation structure are discussed in relation to void nucleation in zirconium. High energy electrons and ions are used to provide atomic displacements.

EXPERIMENTAL

Polycrystalline crystal bar zirconium supplied either by the Materials Research Corp. (MRC) or by A. D. McKay Ltd. (ADM) was used for

the majority of the experiments. The impurity content of the two materials is summarised in Table 1. One single crystal specimen of MRC purity was also irradiated.

Table 1. Manufacturer's Analysis for Crystal Bar Zirconium

Element	MRC (ppm-wt)	ADM (ppm-wt)
O	39	80
H	16	25
N	<1	7
Fe	30	172
Hf	200	84
Ta	<10	200
Cr	2	16
C	<5	35

Electron irradiations were performed in an AEI EM7 High Voltage Electron Microscope (HVEM) operating at 1 MV. Irradiations were confined to temperatures in the range 400-500°C, and the beam current was adjusted to give a displacement rate of $\sim 3 \times 10^{-3}$ dpa.s^{-1}.

Inert gas ion irradiations were performed over the temperature range 300-500°C. Helium^{+} ions of 100 keV were used for most of the irradiations and a beam current density of 2×10^{14} ions.cm^{-2}.s^{-1} was chosen to give a displacement rate of $\sim 4 \times 10^{-3}$ dpa.s^{-1}. Irradiation times ranged from 50 s (0.2 dpa*) to 1250 s (5 dpa). For comparative purposes, a limited number of specimens were irradiated using 100 keV C^{+}, Ne^{+} or Ar^{+} ions.

Two selected experiments were performed using the Harwell Variable Energy Cyclotron (VEC). A 46.5 MeV beam of Ni^{6+} ions, providing a displacement rate of $\sim 1 \times 10^{-3}$ dpa.s^{-1}, was chosen for these experiments: (1) A sample of MRC zirconium containing 1×10^{-5} atoms/atom He was irradiated at 465°C to a maximum displacement level of $\sim$ 38 dpa. The target was not rocked, and the damage peak occurred $\sim$ 8 μm from the irradiated surface. (2) A similar sample of MRC zirconium, together with a single crystal of the same purity, both containing $\sim 2.5 \times 10^{-5}$ atoms/atom He, were irradiated at 475°C to a maximum displacement level of $\sim$ 45 dpa. In this experiment, the target was rocked during the irradiation to provide a uniformly damaged region 5-8 μm from the irradiated surface.

* All of the dpa values cited in this paper were calculated using the EDEP-1 program of Manning and Mueller[5] assuming a Kinchin-Pease scaling factor of 0.8 and E_d = 24 eV.

He implantation for the above experiments was performed using the VEC rocked target holder to provide a uniform distribution of implanted gas. A number of specimens for electron irradiation or 100 keV C^+ ion irradiation were pre-injected with $\sim 1.5 \times 10^{-5}$ atoms/atom Ne using a 100 keV beam of Ne^+ ions. The distribution of inert gas in these samples is likely to be less uniform than in the He implanted samples.

Apart from those specimens examined during irradiation in the HVEM, the majority of specimens were examined in a JEOL 200B electron microscope operating at 200 kV. In situ observations of defect formation during ion irradiation were also made for a number of specimens using the Harwell accelerator/microscope link.

All specimens for electron microscopy were prepared by electropolishing in a solution of 10% perchloric acid in ethanol. A potential of 30 V was applied to the cell, and the electrolyte was kept at $\sim -60°C$ in order to minimise oxide and hydride formation. Specimens irradiated with 100 keV ions were back-thinned to the irradiated surface, whilst the VEC specimens were first polished down to the required depth and subsequently back-thinned in the same manner. Specimens for irradiation in the HVEM and in the accelerator/microscope link were prepared by conventionally thinning from both sides.

RESULTS

Void Formation in Zirconium

Voids were observed only in specimens of ADM zirconium containing $\sim 1.5 \times 10^{-5}$ atoms/atom Ne and irradiated in the HVEM. Fig. 1 shows the dislocation structure developed after irradiation to ~ 5 dpa at 430°C, whilst Fig. 2 shows the presence of voids after irradiation to 9 dpa at the same temperature. Voids were also observed in the same material irradiated at 495°C. No voids were observed in MRC material similarly pre-injected with Ne, or in either ADM or MRC zirconium which had not been pre-injected with Ne. A specimen of ADM zirconium doped with 1.5×10^{-5} atoms/atom Ne was irradiated at 520°C with 100 keV C^+ to a dose of

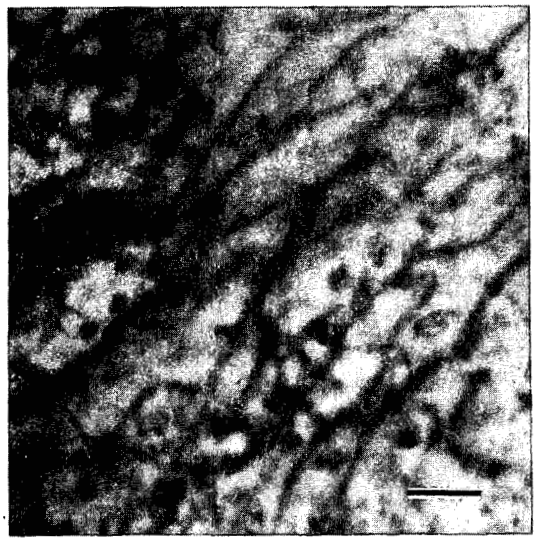


Fig. 1. Damage structure at 5 dpa and 430°C (HVEM).

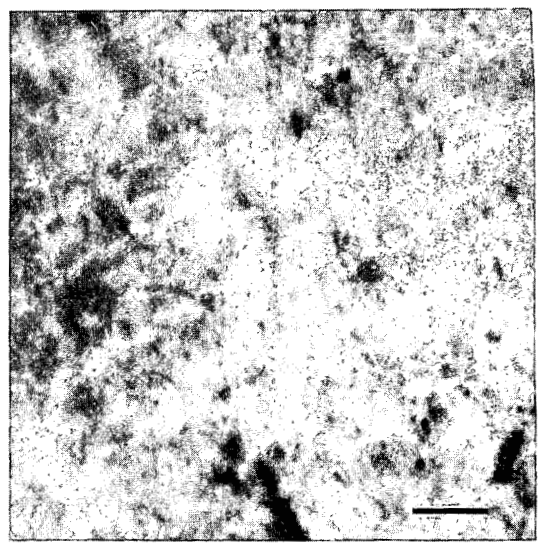


Fig. 2. Voids formed at 9 dpa and 430°C (HVEM).

(scale bar on all micrographs represents 0.1 μm)

∿ 22 dpa. The dislocation structure developed is illustrated in Fig. 3, but unlike the electron-irradiated material, no voids were observed. Similarly, no voids were observed in MRC zirconium pre-injected with up to 2.5×10^{-5} atoms/atom He and irradiated with 46.5 MeV Ni^{6+} ions.

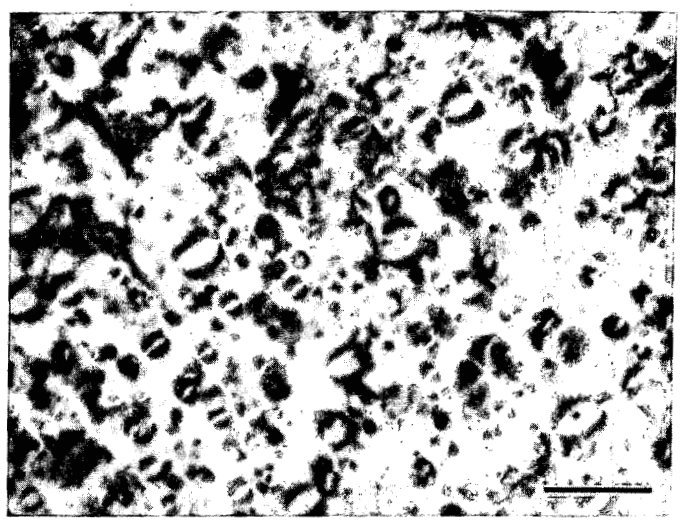


Fig. 3. Damage structure after 22 dpa 100 keV C^{+} irradiation at 520°C.

The Development of a Dislocation Structure in Zirconium

The development of a dislocation structure at low doses was investigated using 100 keV He^+ ions as the bombarding particle. The general trends indicate the formation of small (< 100 Å diameter) defect clusters or loops at low temperatures (350°C), larger, well defined loops, up to 300 Å in diameter, at intermediate temperatures (400°C) and large loops (up to 600 Å in diameter) at higher temperatures (up to 500°C). Figs. 4 and 5 show the structures observed after irradiation to 0.2 dpa at 400 and 450°C, respectively. The measured defect densities under these conditions are $\sim 1.3 \times 10^{21}/m^3$ and $6 \times 10^{20}/m^3$ respectively. The loop density increases with dose up to $\sim$ 1 dpa where it appears to saturate. Figs. 6 and 7 illustrate the structures observed at 400 and 450°C after irradiation to 0.5 dpa. Analysis of the loops indicates that the loop plane normals lie near $\langle 10\bar{1}0 \rangle$. There is no evidence of loops having c-component Burgers vectors, and all observations are consistent with loops having Burgers vectors of the type $1/3\langle 11\bar{2}0 \rangle$. It is not clear whether the observed saturation is a true effect or whether the situation is confused by the presence of helium gas bubbles. The development of the dislocation structure during ion irradiation differs from that observed during electron

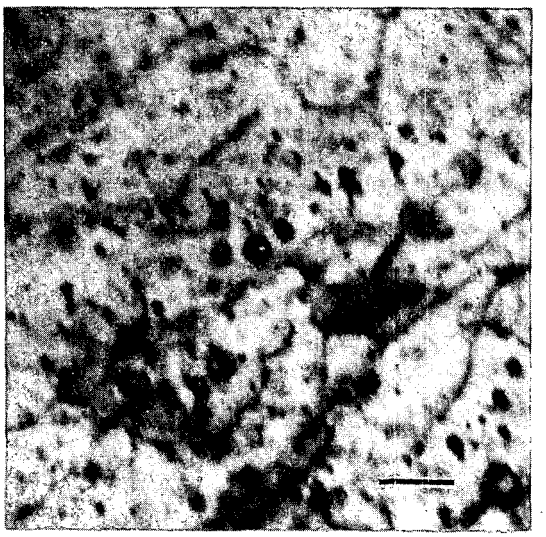


Fig. 4. Damage structure from 100 keV He^+ irradiation at 400°C (0.2 dpa).

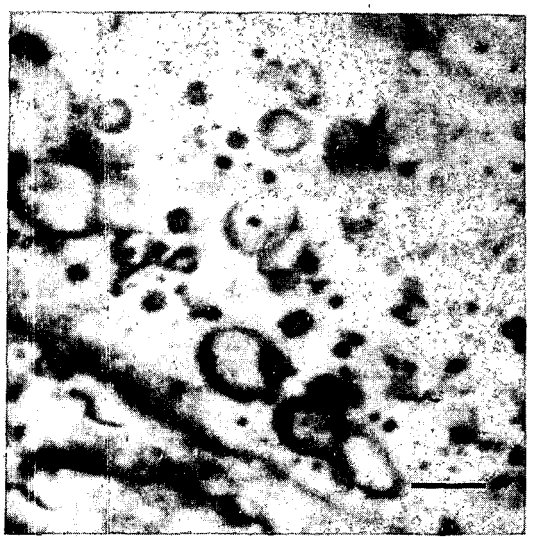


Fig. 5. Damage structure from 100 keV He^+ irradiation at 450°C (0.2 dpa).

irradiation in that there is less evidence of dislocation loop interactions and a tendency for the loops to remain quite small. These observations are also valid for 100 keV C^+, Ne^+ and Ar^+ irradiations where the implanted ions should have less influence on the induced structure.

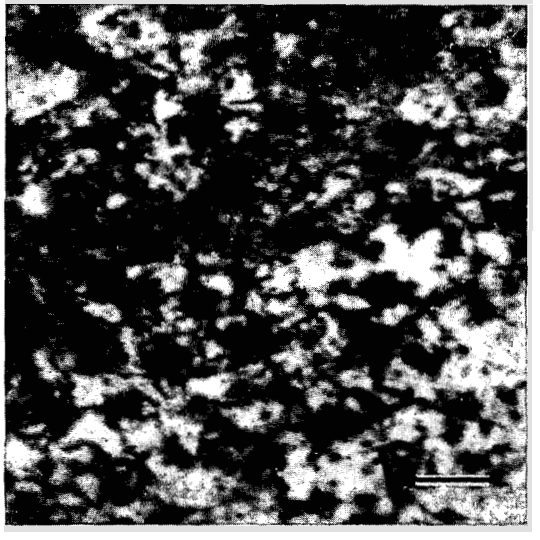


Fig. 6. Damage structure from 100 keV He^+ irradiation at 400°C (0.5 dpa).

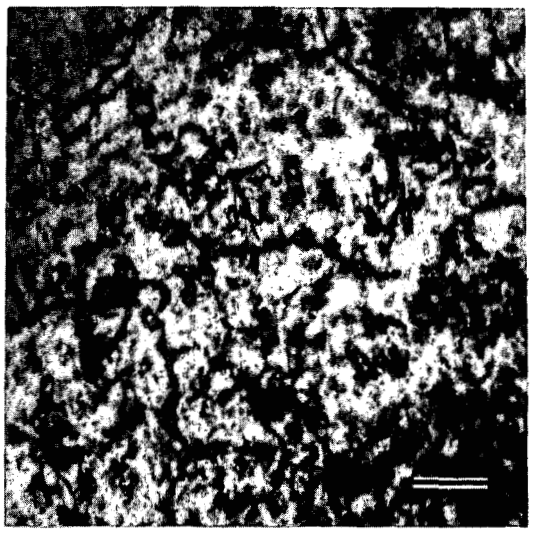


Fig. 7. Damage structure from 100 keV He^+ irradiation at 450°C (0.5 dpa).

DISCUSSION AND CONCLUSIONS

In agreement with previous work[1,2,6], it is clear from the present investigation that zirconium is extremely resistant to void formation. Nevertheless, HVEM irradiation experiments have shown that, given the right conditions, voids will form in zirconium[3,7]. In the present study voids were observed only in material pre-injected with insoluble neon prior to irradiation in the HVEM. This is in agreement with the observations of Carpenter[3], but differs from the results of Buckley and Manthorpe[7], who have observed void formation in the absence of pre-injected gas. The influence of insoluble gases is obviously to aid the nucleation of voids. However, the presence of an insoluble gas is not a sufficient condition to promote void formation. This fact is born out by the observations made on the two grades of zirconium used in this investigation. Voids were observed only in ADM material and not in the "purer" MRC grade

zirconium, even though both materials were pre-injected with the same amount of gas. This would indicate that other factors, such as impurities, play an important role in affecting the nucleation and/or growth process.

Significantly, a specimen identical to that in which voids were produced in the HVEM, did not produce voids during 100 keV C^+ ion irradiation, nor were voids observed in 46.5 MeV Ni^{6+} irradiated specimens containing up to 2.5×10^{-5} atoms/atom He. Recent analysis of neutron irradiated Zr-2.5wt% Nb[8] has revealed that the He content is about an order of magnitude higher than might be expected using available cross-section data for zirconium[9]. An extrapolation of the results[8] would indicate that neutron irradiation to a fluence of 5×10^{25} n/m^2 ($E > 1$ MeV) should produce $\sim 1.2 \times 10^{-6}$ atoms/atom He. This concentration is generally found adequate to stabilise voids in steels. Consequently, it is not simply the lack of insoluble gases which limits void formation in zirconium.

It is now well established that the formation of voids is dependent on the presence of a biased interstitial sink so as to provide an excess of vacancies. This biased sink is generally considered to be the edge dislocation. In an annealed metal, dislocations may be produced during irradiation as a result of point defect migration and clustering. The collapse of these clusters to form dislocation loops, and the subsequent growth of these loops to produce a dislocation network generally provides the necessary sinks. The degree of biasing at a dislocation should remain constant provided dislocation climb is not impeded. It will however be reduced if climb is prohibited.

In the course of this investigation it was noted that loop interactions and dislocation climb were more prevalent during electron than during ion irradiation. No saturation effect was noted during HVEM irradiations up to displacement levels of 15 dpa. Direct observations of damage processes in the accelerator/microscope link indicated structural saturation at damage levels in excess of $\sim$ 30 dpa, whilst in the thicker ion-irradiated samples, saturation occurred at much lower levels. Low dose ion irradiations indicate that there is little growth of loops to greater than $\sim$ 600 Å even at 450°C, and no well defined dislocation

network is established. We believe that it is this apparent lack of dislocation climb which causes zirconium to be resistant to void formation. The most probable explanation for these observations is that dislocation motion is restricted by impurity pinning. However, in addition to this effect, impurities might also affect Frenkel recombination kinetics or may directly influence the relative probability for the formation of either voids or vacancy dislocation loops.

Recent results[10] show that an increase in metallic impurities or an increase in oxygen in the range $1.5 - 6 \times 10^{-4}$ atoms/atom only marginally affects the annealing kinetics of low temperature neutron-irradiated Zr. This suggests that Frenkel recombination kinetics are little affected by impurities. There still remains the question as to whether impurities may influence, directly, the relative probabilities for the nucleation of voids or the collapse of vacancy clusters to produce vacancy dislocation loops. Evidence for an impurity effect on nucleation can be found both in our HVEM irradiations and in the vacancy quenching experiments of Carpenter and Watters[11]. In both cases, there is an indication that the formation of voids or vacancy loops is inhibited in higher-purity materials. Thus, in such materials, nucleation may be a problem. However, the fact still remains, that the primary influence of impurities is likely to be in the restriction of dislocation motion by pinning. Further evidence for this impurity effect was obtained by Buckley and Manthorpe. Thus, in their HVEM irradiations, when the hot stage vacuum was poor, loop growth and interaction (forming tangles) stopped after a certain irradiation time.

Our analysis is complicated by the additional unknown factor introduced through the difference in the initial Frenkel defect distribution between electron and ion irradiations. Although ion irradiations were carried out at an almost identical dose rate to HVEM irradiations ($\sim 10^{-3}$ dpa.s^{-1}), the lack of voids in the former suggests that the damage cascade may play an important part in influencing the nucleation efficiency of voids.

We conclude that impurity-dislocation loop interaction, by inhibiting loop growth, is probably the most significant factor in limiting the

development of a mobile dislocation structure and hence void formation. However, the less uniform Frenkel defect distribution produced by ion or neutron irradiations combined with the influence of impurities on the nucleation process may, in addition, favour the nucleation of vacancy dislocation loops over voids.

ACKNOWLEDGEMENT

The authors acknowledge the cooperation of AERE Harwell for the provision of accelerator facilities.

REFERENCES

1. A. Wolfenden and K. Farrell, Scripta Met. 6, 127 (1972).
2. D.O. Northwood and R.W. Gilbert, Rad. Eff. 22, 139 (1974).
3. G.J.C. Carpenter, Rad. Eff. 19, 189 (1973).
4. M.J. Makin, Phil. Mag. 25, 761 (1972).
5. I. Manning and G.P. Mueller, Computer Phys. Comm. 1, 85 (1974).
6. R.B. Adamson, W.L. Bell and D. Lee, Zirconium in Nuclear Applications, ASTM STP551 (1974).
7. S.N. Buckley and S.A. Manthorpe, Paper presented at International Conference on Physical Metallurgy of Reactor Fuel Elements, Berkeley Nuclear Laboratories, Sept. 2-7, 1973.
8. D. Faulkner, unpublished work (1974).
9. W.N. McElroy and H. Farrar IV, Radiation Induced Voids in Metals, J.W. Corbett and L.C. Ianiello, eds., U.S.A.E.C. Symposium Series No. 26, p. 187 (1972).
10. P. Vialaret, F. Moreau, A. Bessis, C. Dimitrov and O. Dimitrov, J. Nucl. Mat. 55, 83 (1975).
11. G.J.C. Carpenter and J.F. Watters, Acta Met. 21, 1207 (1973).

AUTHOR INDEX

Abe, H. 977
Adda, Y. 1169
Antesberger, G. 561, 575, 657
Arko, A. J. 846
Arsenault, R. J. 1018
Aspeling, J. 545, 553
Averback, R. S. 127, 1048

Bajaj, R. 1010
Balluffi, R. W. 852
Beck, C. A. 1077
Beeler, J. R., Jr. 21, 28
Beeler, M. F. 21, 28
Benedek, R. 207
Benoist, P. 1236
Bentley, J. 925
Bernas, H. 134
Biget, M. 66
Birtcher, R. C. 138, 405, 1150
Blewitt, T. H. 138, 152, 1150
Böning, K. 80, 88
Borg, R. J. 532
Bounaud, J. Y. 790
Bressers, J. 1018
Breuer, N. 227
Brice, D. K. 35
Brimhall, J. L. 568, 1196
Brown, B. S. 138, 1150
Brown, L. M. 775
Bullough, R. 1261
Butler, W. H. 804
Butteweg, D. 463

Carpenter, G.J.C. 782
Carpenter, R. W. 1203
Chambron, W. 261
Chang. Y. K. 846
Chaplin, R. L. 561
Chaumont, J. 134
Chen, C. W. 1213
Cherns, D. 178
Choi, Y. H. 1181
Coltman, R. R., Jr. 214, 431, 445
561, 657
Conner, R. A., Jr. 171
Cost, J. 1055
Coussement, R. 325
Crabtree, G. W. 846

Dander, W. 463
Das, G. 73
Dausinger, F. 438
Dedek, U. 411, 575
Dederichs, P. H. 187, 220, 227
Diehl, J. 629, 663, 715, 1136
Dienes, G. J. 1045
Dimitrov, C. 80, 608
Dimitrov, O. 80
Dworschak, F. 601, 615

Ehrhart, P. 295, 302, 470, 839
Eldrup, M. 1127
English, C. A. 910, 918
Evans, J. H. 1127
Eyre, B. L. 729, 910, 918, 925

Faber, K. H. 459
Faulkner, D. 1287
Fikus, J. H. 875
Fischer, H. 715
Flament, J. L. 1169
Frank, W. 553
Fritsch, G. 405
Fujita, H. 882
Furukawa, K. 622

Gauster, W. B. 1143
Gerber, S. B. 1245
Glowinski, L. 1169
Goland, A. N. 1107
Gomez, C. 715
Gonzalez, H. 1055
Gösele, U. 539
Granato, A. V. 932
Grilhé, J. 636, 896
Guérard, B. von 287, 309
Guinan, M. W. 532, 970

Halbwachs, M. 1055
Hasiguti, R. R. 643
Haubold, H.-G. 268
Hayns, M. R. 764
Hertz, W. 405
Higgins, R. J. 846
Hillairet, J. 1055
Hirano, H. 622
Hoff, H. A. 1092
Howe, L. M. 316
Huang, F. H. 1279

Igata, N. 797
Ikeuchi, K. 622
Isebeck, K. 545

Jackson, J. J. 452
Jenkins, M. L. 113
Johnson, R. A. 875
Jouffrey, B. 134, 722
Jung, P. 418, 424

Karasawa, T. 643
Katerbau, K.-H. 113
Katoh, S. 1155
Kenik, E. A. 73
Ketterson, J. B. 846
Kiritani, M. 695, 889
Kirk, M. A. 152, 171
Kissinger, H. E. 568
Kitajima, K. 977
Klabunde, C. E. 431, 445, 561, 657
Koehler, J. S. 397
Kosel, T. 903
Koyama, A. 643
Kubin, L. 722

Lam, N. Q. 1077
Lanore, J. M. 1169
Larson, B. C. 820
Lauzier, J. 957, 963
Lehmann, C. 227
Leibfried, G. 227
Lennartz, R. 411, 601
Lessmann, E. 333
Leteurtre, J. 790
Levy, V. 1169
Li, C.-Y. 1279
Loomis, B. A. 1245
Loretto, M. H. 925
Lucasson, A. 66
Lucasson, P. 42, 66

Maehara, Y. 889
Mancuso, J. F. 1279
Mansel, W. 349
Mansur, L. K. 804
Mantl, S. 1122, 1143
Martin, G. 1084, 1236
Mauer, W. 88
Maury, F. 66
Mayer, R. M. 775
Merbold, U. 629
Merkle, K. L. 127, 1048

Meshii, M. 984
Meurer, H. P. 615
Minier, C. 957, 963
Minter, F. J. 178
Mitchell, T. E. 73
Mogensen, O. E. 1127
Monsau, Th. 601
Moser, P. 261, 957
Murakami, H. 797
Myers, S. M. 1063

Nakata, K. 622
Narayan, J. 90, 120
Nelson, R. S. 178
Nicklow, R. M. 214
Nielsen, C. H. 373
Nishimoto, M. 1155
Noggle, T. S. 90
Nolfi, F. V., Jr. 1252
Northwood, D. O. 782
Nowicki, L. J. 1077

Odeurs, J. 325
Oen, O. S. 90
Ogle, J. C. 1203
Ohr, S. M. 650
Okada, T. 1155
Okamoto, P. R. 1188
Okuda, S. 361, 977
Oleownik, G. 341

Parkin, D. M. 1162
Pattyn, H. 325
Peisl, J. 287, 309
Pfändner, K. 88
Piani, C.S.B. 545
Poerschke, R. 1070
Potter, D. I. 1092
Pronko, P. P. 145
Puls, M. P. 1287

Quenneville, A. F. 316

Redman, J. K. 445
Regnier, P. 1169
Rehn, L. E. 234, 240
Risbet, A. 1169
Rivière, J. P. 636
Roberto, J. B. 120
Robinson, M. T. 1
Robrock, K.-H. 234, 240

Rocher, A. 722
Rosner, P. 80, 88
Rothman, S. J. 1070
Ruault, M. O. 134, 722
Rühle, M. 715
Russell, K. C. 1181

Sakairi, H. 643
Sato, A. 984
Sawada, A. 882
Schaefer, H. E. 463
Schilling, W. 470
Schlagheck, U. 839
Schober, H. R. 220
Schober, T. 418, 1143
Scholz, A. 227
Scholz, R. 333
Schroeder, H. 411, 575
Schroeder, K. 525
Schüle, W. 333, 341
Schultz, H. 438, 459
Schweikhardt, J. 459
Scott, T. L. 138, 152
Sechard, A. 247
Seeger, A. 493, 539, 553
Segura, E. 295
Seidman, D. N. 373
Seiffert, S. L. 963
Seshan, K. 896
Simonen, E. P. 568, 1196
Snead, C. L., Jr. 1162
Sonnenberg, K. 470, 561, 575, 657
Sorensen, S. M., Jr. 1213
Sosin, A. 518
Spirić, V. 234, 240
Sprague, J. A. 1181
Stathopoulos, A. Y. 918
Stebut, J. von 247
Stoneham, A. M. 1221
Stuart, R. N. 532
Sumida, N. 882
Summers, J. 910
Swanson, M. L. 316

Takahashi, H. 1100
Takamura, J. 622
Takamura, S. 977
Takata, H. 889
Takemoto, K. 882
Takeyama, T. 1100
Taylor, A. 1188, 1245

Tewary, V. K. 220
Triftshäuser, W. 1122, 1136, 1143
Trinkaus, H. 254
Tsubakihara, H. 1155

Urban, K. 675

Vajda, P. 66
Van Konynenburg, R. A. 970
Verdone, J. 261
Vogl, G. 349

Wadley, H. 910, 918
Washburn, J. 896, 903
Watari, F. 797
Watson, J. E. 405
Wechsler, M. S. 991, 1010
Weller, M. 629, 1136
Wiedersich, H. 1188
Wienhold, P. 561, 657
Wilkens, M. 98, 113
Williams, J. M. 431, 561, 657
Wilson, K. L. 373
Wilson, W. D. 1025
Windmiller, L. R. 846
Wolfer, W. G. 812
Wollenberger, H. 582, 601, 615, 1070
Wood, R. F. 214
Wozniak, D. G. 1150

Yagi, E. 643
Yoo, M. H. 804
Yoshida, N. 889
Young, F. W., Jr. 214, 846

*U.S. GOVERNMENT PRINTING OFFICE: 1976-648-370/10270 Region No. 4